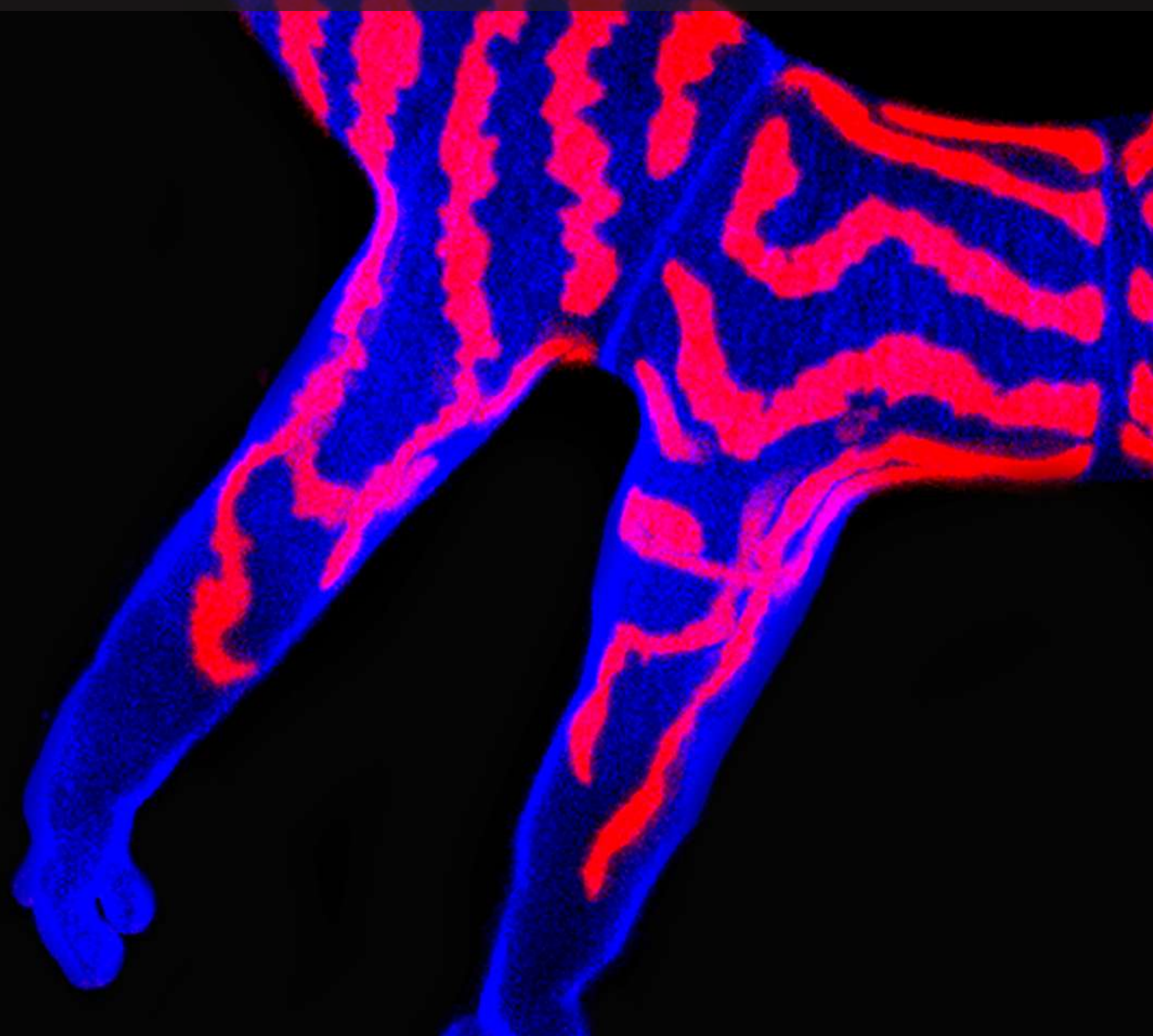
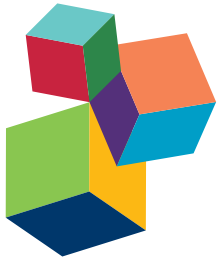


CHAROPHYTES: EVOLUTIONARY ANCESTORS OF PLANTS AND EMERGING MODELS FOR PLANT RESEARCH

EDITED BY: David S. Domozych, Zoë A. Popper and Iben Sørensen

PUBLISHED IN: Frontiers in Plant Science





Frontiers Copyright Statement

© Copyright 2007-2017 Frontiers Media SA. All rights reserved.

All content included on this site, such as text, graphics, logos, button icons, images, video/audio clips, downloads, data compilations and software, is the property of or is licensed to Frontiers Media SA ("Frontiers") or its licensees and/or subcontractors. The copyright in the text of individual articles is the property of their respective authors, subject to a license granted to Frontiers.

The compilation of articles constituting this e-book, wherever published, as well as the compilation of all other content on this site, is the exclusive property of Frontiers. For the conditions for downloading and copying of e-books from Frontiers' website, please see the Terms for Website Use. If purchasing Frontiers e-books from other websites or sources, the conditions of the website concerned apply.

Images and graphics not forming part of user-contributed materials may not be downloaded or copied without permission.

Individual articles may be downloaded and reproduced in accordance with the principles of the CC-BY licence subject to any copyright or other notices. They may not be re-sold as an e-book.

As author or other contributor you grant a CC-BY licence to others to reproduce your articles, including any graphics and third-party materials supplied by you, in accordance with the Conditions for Website Use and subject to any copyright notices which you include in connection with your articles and materials.

All copyright, and all rights therein, are protected by national and international copyright laws.

The above represents a summary only. For the full conditions see the Conditions for Authors and the Conditions for Website Use.

ISSN 1664-8714

ISBN 978-2-88945-164-7

DOI 10.3389/978-2-88945-164-7

About Frontiers

Frontiers is more than just an open-access publisher of scholarly articles: it is a pioneering approach to the world of academia, radically improving the way scholarly research is managed. The grand vision of Frontiers is a world where all people have an equal opportunity to seek, share and generate knowledge. Frontiers provides immediate and permanent online open access to all its publications, but this alone is not enough to realize our grand goals.

Frontiers Journal Series

The Frontiers Journal Series is a multi-tier and interdisciplinary set of open-access, online journals, promising a paradigm shift from the current review, selection and dissemination processes in academic publishing. All Frontiers journals are driven by researchers for researchers; therefore, they constitute a service to the scholarly community. At the same time, the Frontiers Journal Series operates on a revolutionary invention, the tiered publishing system, initially addressing specific communities of scholars, and gradually climbing up to broader public understanding, thus serving the interests of the lay society, too.

Dedication to Quality

Each Frontiers article is a landmark of the highest quality, thanks to genuinely collaborative interactions between authors and review editors, who include some of the world's best academicians. Research must be certified by peers before entering a stream of knowledge that may eventually reach the public - and shape society; therefore, Frontiers only applies the most rigorous and unbiased reviews.

Frontiers revolutionizes research publishing by freely delivering the most outstanding research, evaluated with no bias from both the academic and social point of view.

By applying the most advanced information technologies, Frontiers is catapulting scholarly publishing into a new generation.

What are Frontiers Research Topics?

Frontiers Research Topics are very popular trademarks of the Frontiers Journals Series: they are collections of at least ten articles, all centered on a particular subject. With their unique mix of varied contributions from Original Research to Review Articles, Frontiers Research Topics unify the most influential researchers, the latest key findings and historical advances in a hot research area! Find out more on how to host your own Frontiers Research Topic or contribute to one as an author by contacting the Frontiers Editorial Office: researchtopics@frontiersin.org

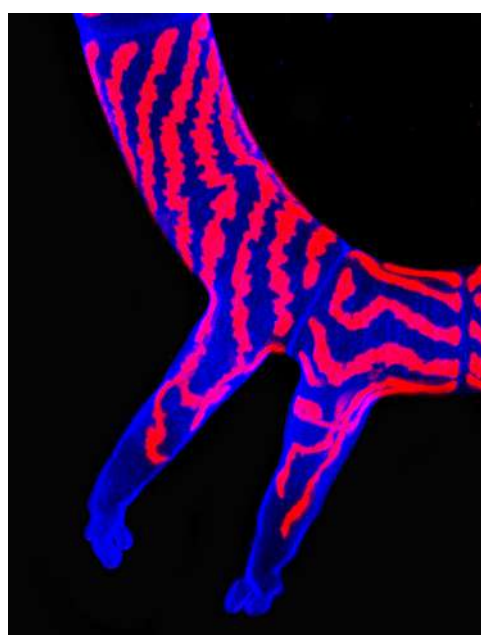
CHAROPHYTES: EVOLUTIONARY ANCESTORS OF PLANTS AND EMERGING MODELS FOR PLANT RESEARCH

Topic Editors:

David S. Domozych, Skidmore College, USA

Zoë A. Popper, National University of Ireland, Galway, Ireland

Iben Sørensen, Cornell University, USA



The wound response and Calcofluor labeling of the charophyte, *Spirogyra*. When filaments are wounded by excision, small arm-like rhizoids emerge from individual cells and are used for attachment to adjacent substrates. The labeled cell wall (blue) and chloroplast (red) are visible.

Image by David S. Domozych

The charophytes are the group of green algae that are ancestral and most closely related to land plants. Today, these organisms are not only important in evolutionary studies but have become outstanding model organisms for plant research.

Citation: Domozych, D. S., Popper, Z. A., Sørensen, I., eds. (2017). Charophytes: Evolutionary Ancestors of Plants and Emerging Models for Plant Research. Lausanne: Frontiers Media.
doi: 10.3389/978-2-88945-164-7

Table of Contents

- 04 Editorial: Charophytes: Evolutionary Ancestors of Plants and Emerging Models for Plant Research**
David Domozych, Iben Sørensen and Zoë A. Popper
- 06 Charophytes: Evolutionary Giants and Emerging Model Organisms**
David S. Domozych, Zoë A. Popper and Iben Sørensen
- 14 Micrasterias as a Model System in Plant Cell Biology**
Ursula Lütz-Meindl
- 35 Comparative Chloroplast Genome Analyses of Streptophyte Green Algae Uncover Major Structural Alterations in the Klebsormidiophyceae, Coleochaetophyceae and Zygnematophyceae**
Claude Lemieux, Christian Otis and Monique Turmel
- 59 Primitive Extracellular Lipid Components on the Surface of the Charophytic Alga Klebsormidium flaccidum and Their Possible Biosynthetic Pathways as Deduced from the Genome Sequence**
Satoshi Kondo, Koichi Hori, Yuko Sasaki-Sekimoto, Atsuko Kobayashi, Tsubasa Kato, Naoko Yuno-Ohta, Takashi Nobusawa, Kinuka Ohtaka, Mie Shimojima and Hiroyuki Ohta
- 74 Abiotic Stress Tolerance of Charophyte Green Algae: New Challenges for Omics Techniques**
Andreas Holzinger and Martina Pichrtová
- 91 Multi-Scale Characean Experimental System: From Electrophysiology of Membrane Transporters to Cell-to-Cell Connectivity, Cytoplasmic Streaming and Auxin Metabolism**
Mary J. Beilby
- 111 Is Wortmannin-Induced Reorganization of the trans-Golgi Network the Key to Explain Charosome Formation?**
Ilse Foissner, Aniela Sommer, Margit Hoeftberger, Marion C. Hoepflinger and Marketa Absolonova
- 128 Concanavalin A Disrupts the Release of Fibrous Material Necessary for Zygote Formation of a Unicellular Charophycean Alga, Closterium peracerosum-strigosum-littorale Complex**
Jun Abe, Sachie Hori, Mamiko Sato and Hiroyuki Sekimoto
- 136 Enzyme-Less Growth in Chara and Terrestrial Plants**
John S. Boyer



Editorial: Charophytes: Evolutionary Ancestors of Plants and Emerging Models for Plant Research

David Domozych^{1*}, Iben Sørensen² and Zoë A. Popper³

¹ Department of Biology, Skidmore Microscopy Imaging Center, Skidmore College, New York, NY, USA, ² Plant Biology Section, School of Integrative Plant Sciences, Cornell University, Ithaca, NY, USA, ³ Botany and Plant Sciences, School of Natural Science, National University of Ireland, Galway, Ireland

Keywords: charophytes, model, evolution, streptophytes, algae

Editorial on the Research Topic

Charophytes: Evolutionary Ancestors of Plants and Emerging Models for Plant Research

Approximately 450–500 million years ago, an ancient freshwater green alga successfully colonized land. From this profoundly important event in our planet's natural history, the spectacular diversity of plants that now occupy most of our terrestrial ecosystems arose. Essentially, the planet's atmosphere and biogeochemistry dramatically changed to yield conditions that support our biota. Land plant evolution also directed the origin and development of human civilization as it ultimately served as the basis of agriculture, clothing, building and medicines, to name just a few. The Charophycean Green Algae or charophytes (also known as streptophyte algae) are the group of green algae that are ancestral to land plants. Extant charophyte taxa also share a large number of features that are found in modern land plants. Over the past half century, studies of charophytes have been inspired by this evolutionary significance. Yet as we have learned more about the intricacies of their biology, charophyte research has notably expanded and several inclusive taxa have become important “tools” in understanding the foundations of plant life. This has been further complemented by many advantageous experimental attributes of charophytes including their small size, their efficacious accommodation to molecular and high resolution imaging technologies and their relative ease in experimental manipulation. Many, in fact, have become or are becoming important model organisms in several areas of basic plant biology (Domozych et al.). The Frontiers in Plant Science series, “Charophytes: Evolutionary ancestors of plants and emerging models for plant research” provides a collection of reports and reviews that demonstrate the ever growing importance of charophytes in plant research.

One of most well-known and studied charophytes is the unicellular desmid, *Micrasterias*, whose spectacular morphology and associated cellular morphogenesis make it ideal for elucidating the subcellular foundations of cell development and physiology. In this series on charophytes, Lütz-Meindl provides a detailed summary of past and current research efforts that have focused on *Micrasterias*. Though cell expansion, subcellular dynamics and cell wall development have been important focal points of previous study, this alga is now benefitting ecophysiological analyses especially in the elucidation of adaptations to various stresses. Other desmids as well have contributed to foundational areas of biological research. For example, species of *Closterium* provide excellent models for studying reproductive biology. In this series, Abe et al. demonstrate this using lectin cytochemistry and electron microscopy to describe putative molecules required for gamete release during sexual reproduction.

Desmids are not sole “stars” of charophyte-based research. The stoneworts (e.g., *Chara* and *Nitella*) have long been important to plant research. These algae produce exceptionally large

OPEN ACCESS

Edited and reviewed by:

Neelima Roy Sinha,
University of California, Davis, USA

*Correspondence:

David Domozych
ddomoz@skidmore.edu

Specialty section:

This article was submitted to
Plant Evolution and Development,
a section of the journal
Frontiers in Plant Science

Received: 21 December 2016

Accepted: 27 February 2017

Published: 14 March 2017

Citation:

Domozych D, Sørensen I and
Popper ZA (2017) Editorial:
Charophytes: Evolutionary Ancestors
of Plants and Emerging Models for
Plant Research.
Front. Plant Sci. 8:338.
doi: 10.3389/fpls.2017.00338

internodal cells that are uniquely valuable to various cellular studies. Belby describes the distinct features of these algae and specifically reports on the diverse methodologies that have been used and key results that have been obtained in studies dealing with electrophysiology, auxin dynamics and membrane transporters. Central to the physiology of any plant cell including *Chara* is endomembrane dynamics especially the coordinated balance between exo- and endocytosis in the membrane trafficking network. Foissner et al. describe membrane dynamics in the internodal cells of *Chara* when treated with the fungal metabolite, wortmannin. Using immunofluorescence and transmission electron microscopy-based imaging they demonstrate significant reorganization of the trans Golgi network (TGN) and changes to the unique membranous charasomes. Ultimately, the expansion and development of the cells of *Chara*, as in all plants, is controlled by turgor and the structural dynamics of the cell wall. Pectins represent the largest domain of the wall matrix polysaccharides that are critical to cell development. Boyer elegantly describes the distinctive pectin-Ca²⁺ cycle in the *Chara* cell wall that allows for controlled wall expansion and possible implications for plant cells in general.

Charophytes are now also becoming important organism in studies focused on stress-induced adaptations of plant cells. These studies are not only important in understanding survival mechanisms of plants under various stresses but also provide insight into the evolutionary processes that may have led to colonization of land by ancient charophytes. Holzinger and Pichrtova explore various adaptive mechanisms including biochemical, structural and physiological processes that extant charophytes employ for survival on land. Additionally, they describe the molecular machinery that modulates when these algae are under particular pressures such as exposure to UV light and desiccation. In the same vein, Kondo et al. used genomic sequence analysis and biochemistry to identify a lipid-

like aliphatic component in the early divergent charophyte, *Klebsormidum*. The authors discuss the existence of cutin-like substances that may function under stress in a similar way to the cuticular waxes of land plants.

The study of charophytes is still in an early but exciting phase of discovery with much yet to be resolved. Areas that will require extensive research efforts are the molecular phylogeny and taxonomy of the diverse taxa within this algal group. Lemieux et al. employ chloroplast genome analyses to decipher major structural alterations amongst three groups of charophytes, specifically focusing on the large inverted repeat sequence encoding the rRNA operon.

This series on charophytes serves as only a brief sampling of the intriguing biology of these algae. It is hoped that this will encourage and enthuse many more plant scientists to incorporate these algae in their research.

AUTHOR CONTRIBUTIONS

All authors listed, have made substantial, direct and intellectual contribution to the work, and approved it for publication.

FUNDING

This work was funded by NSF-MCB grant 1517345.

Conflict of Interest Statement: The authors declare that the research was conducted in the absence of any commercial or financial relationships that could be construed as a potential conflict of interest.

Copyright © 2017 Domozych, Sørensen and Popper. This is an open-access article distributed under the terms of the Creative Commons Attribution License (CC BY). The use, distribution or reproduction in other forums is permitted, provided the original author(s) or licensor are credited and that the original publication in this journal is cited, in accordance with accepted academic practice. No use, distribution or reproduction is permitted which does not comply with these terms.



Charophytes: Evolutionary Giants and Emerging Model Organisms

David S. Domozych^{1*}, Zoë A. Popper² and Iben Sørensen³

¹ Department of Biology, Skidmore College, Saratoga Springs, NY, USA, ² Botany and Plant Science, School of Natural Science, National University of Ireland, Galway, Ireland, ³ Plant Biology Section, School of Integrative Plant Science, Cornell University, Ithaca, NY, USA

Charophytes are the group of green algae whose ancestral lineage gave rise to land plants in what resulted in a profoundly transformative event in the natural history of the planet. Extant charophytes exhibit many features that are similar to those found in land plants and their relatively simple phenotypes make them efficacious organisms for the study of many fundamental biological phenomena. Several taxa including *Micrasterias*, *Penium*, *Chara*, and *Coleochaete* are valuable model organisms for the study of cell biology, development, physiology and ecology of plants. New and rapidly expanding molecular studies are increasing the use of charophytes that in turn, will dramatically enhance our understanding of the evolution of plants and the adaptations that allowed for survival on land. The *Frontiers in Plant Science* series on “Charophytes” provides an assortment of new research reports and reviews on charophytes and their emerging significance as model plants.

OPEN ACCESS

Edited by:

Stefan A. Rensing,
University of Marburg, Germany

Reviewed by:

Burkhard Becker,
University of Cologne, Germany
Holger Breuninger,
University of Oxford, UK

*Correspondence:

David S. Domozych
ddomoz@skidmore.edu

Specialty section:

This article was submitted to
Plant Evolution and Development,
a section of the journal
Frontiers in Plant Science

Received: 19 July 2016

Accepted: 15 September 2016

Published: 10 October 2016

Citation:

Domozych DS, Popper ZA and Sørensen I (2016) Charophytes: Evolutionary Giants and Emerging Model Organisms. *Front. Plant Sci.* 7:1470.
doi: 10.3389/fpls.2016.01470

INTRODUCTION

Charophytes or basal Streptophytes; (Becker and Marin, 2009; Leliaert et al., 2012) constitute a diverse taxonomic assortment of extant freshwater and terrestrial green algae that display a wide array of unicellular, filamentous, and “parenchymatous” forms (Graham, 1993; Lewis and McCourt, 2004). An ancestral lineage of charophytes emerged onto and colonized land 450–500 million years ago. These organisms adapted to terrestrial conditions, became capable of surviving and reproducing when fully exposed to the atmosphere, and some members ultimately evolved into land plants (Zhong et al., 2013; Delwiche and Cooper, 2015). This “terrestrialization” of green plants represented a keystone biological event that forever changed the biogeochemistry and natural history of the planet. The subsequent proliferation of land plants changed atmospheric and further altered soil conditions and allowed for the emergence of other diverse life forms onto land. Land plant evolution also transformed human history most significantly through the innovation of agriculture and the consequential creation of modern human civilization. Partly due to their evolutionary significance, charophytes have received significant attention from plant biologists over the past decades (Pickett-Heaps and Marchant, 1972; Pickett-Heaps, 1975; Mattox and Stewart, 1984; Becker and Marin, 2009; Harholt et al., 2016). However, as additional new data has been gathered regarding the biology of these algae, they have become important models for understanding basic phenomena in biochemistry, cell biology, developmental biology, ecology and increasingly, molecular biology (Delwiche and Cooper, 2015; Lemieux et al., 2016). The *Frontiers in Plant Science* series on “Charophytes” illustrates the importance of these organisms in several specific areas of plant biology research. This mini-review highlights the attributes of charophytes as model organisms

in diverse areas of research. It also will hopefully provide encouragement for a new generation of scientists to expand the use of these algae in basic research and to initiate screening of other taxa that, in turn, may lead to the identification and use of new model charophytes.

THE “LINE-UP” OF CHAROPHYTES

During the 1970s and 1980s, ultrastructural (e.g., cell division mechanism, flagellar apparatus substructure) and biochemical (e.g., enzyme profiles) data were the main criteria for the inclusion of a green alga in the charophyte lineage (Mattox and Stewart, 1984; Lewis and McCourt, 2004; Leliaert et al., 2012). From the 1990s to today, studies focused on molecular analyses of chloroplast and nuclear genomes and transcriptomes have reaffirmed and refined earlier taxonomic and phylogenetic schemes (Timme et al., 2012; Delwiche and Cooper, 2015). This has further been supplemented by detailed biochemical, immunological and cell biology-based analyses of charophyte cell walls and hormone biosynthetic and signaling pathways (Popper and Fry, 2003; Popper, 2008; Sørensen et al., 2010, 2011, 2012; Zhang and van Duijn, 2014; Ju et al., 2015; O’Rourke et al., 2015). Extant charophytes display a relatively low percentage of diversity in comparison with other green algal taxa and encompass 13 families and 122 genera (Becker and Marin, 2009; Leliaert et al.,

2012). Current phylogenetic opinion places the charophytes in six classes (**Figure 1**; Delwiche and Cooper, 2015). The basal class, the Mesostigmatophyceae, is represented by a single known genus, *Mesostigma*. This alga is a unicellular biflagellate with a unique asymmetric shape (i.e., like a flattened lifeboat) and is covered by layers of ornately designed scales (Manton and Ettl, 1965; Becker et al., 1991; Domozych et al., 1991, 1992). The second class, the Chlorokybophyceae, also consists of a single known type, *Chlorokybus atmophyticus*. This rare alga forms a sarcinoid packet of cells surrounded by a thick gel-like covering (Rogers et al., 1980). It should be noted that alternative phylogenies place *Mesostigma* and *Chlorokybus* as sister lineages that together are sister to all other Streptophytes (Rodríguez-Ezpeleta et al., 2007). In the six class phylogeny, the third class, the Klebsormidiophyceae, consists of three genera that form simple unbranched filaments (Sluiman et al., 2008) that often are members of “biological crusts” growing upon surfaces of various terrestrial habitats. Several species in this class can even withstand significant desiccation stress when part of desert crusts (Mikhailuk et al., 2008, 2014; Holzinger and Karsten, 2013); others are tolerant to the desiccation stresses associated with low temperature environments (Stamenkovic et al., 2014; Herburger and Holzinger, 2015). These first three classes constitute the “early divergent” charophytes. The “late divergent” lineage also includes three classes. The Charophyceae, or stoneworts, are commonly found in freshwater ecosystems

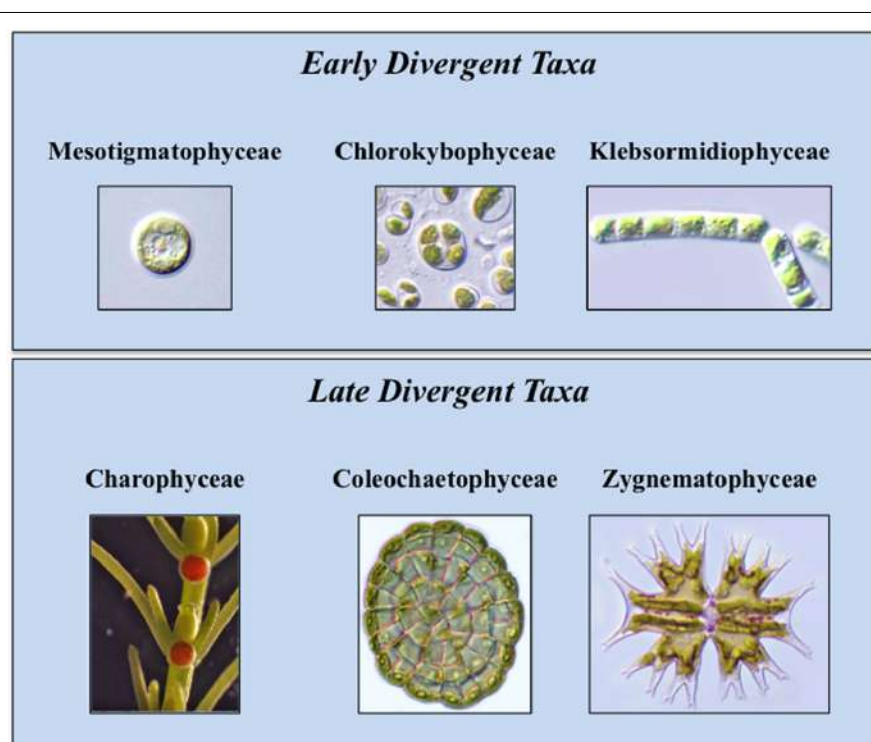


FIGURE 1 | Extant Charophytes. Extant Charophytes are divided into early and late diverging taxa. The early diverging taxa include the Mesostigmatophyceae, the Chlorokybophyceae, and the Klebsormidiophyceae and the late diverging taxa include the Charophyceae, the Coleochaetophyceae, and the Zygnematophyceae. Representatives of each group are *Mesostigma* (Mesostigmatophyceae), *Chlorokybus atmophyticus* (Chlorokybophyceae), *Klebsormidium flaccidum* (Klebsormidiophyceae), *Chara* (Charophyceae), *Coleochaete scutata* (Coleochaetophyceae), and *Micrasterias* (Zygnematophyceae).

and possess macroscopic multicellular thalli consisting of aggregations of branched filaments made of exceptionally elongate cells (Lewis and McCourt, 2004). Members of this group exhibit oogamy-based sexual reproduction that includes motile sperm and non-motile eggs both produced in multicelled gametangia. The Coleochaetophyceae consist of taxa that have multicellular thalli made of branched filamentous or parenchyma-like thalli (Graham, 1993; Delwiche et al., 2002). These organisms also display distinct oogamy-based sexual reproduction. The Coleochaetophyceae are typically found at the interface of freshwater and terrestrial habitats, often as epiphytes. Finally, the largest and most diverse group of charophytes, the Zygnematophyceae, consists of unicells and unbranched filaments (Gontcharov et al., 2003; Guiry, 2013). The distinguishing feature of this group is the presence of conjugation-based sexual reproduction that requires complex cell-cell signaling and adhesion (Abe et al., 2016). The zygnematophycean algae are common inhabitants of freshwater habitats, sometimes occurring in spectacular ephemeral blooms, as well as in moist terrestrial substrates.

CHAROPHYTES AS MODEL ORGANISMS

Several charophytes have been used extensively as model organisms in the study of basic biological processes. Their small and simple thalli (i.e., when compared to land plants) and ease in experimental manipulation are just two of their attributes that make them attractive model organisms. Recent evidence has also demonstrated that many charophytes have several remarkably similar features to those of land plants including the presence of biosynthetic pathways for many growth regulators (Figure 2; Boot et al., 2012; Hori et al., 2014; Wang et al., 2014, 2015; Holzinger and Becker, 2015; Ju et al., 2015) and multiple cell wall polymers (Popper, 2008; Sørensen et al., 2010, 2011, 2012; Mikkelsen et al., 2014). These two characteristics have made charophytes efficacious in such areas of study as plant molecular development and stress physiology. While many charophytes have been used in a wide array of biological studies, the following taxa are most notable for their extensive use in multiple areas of study as models:

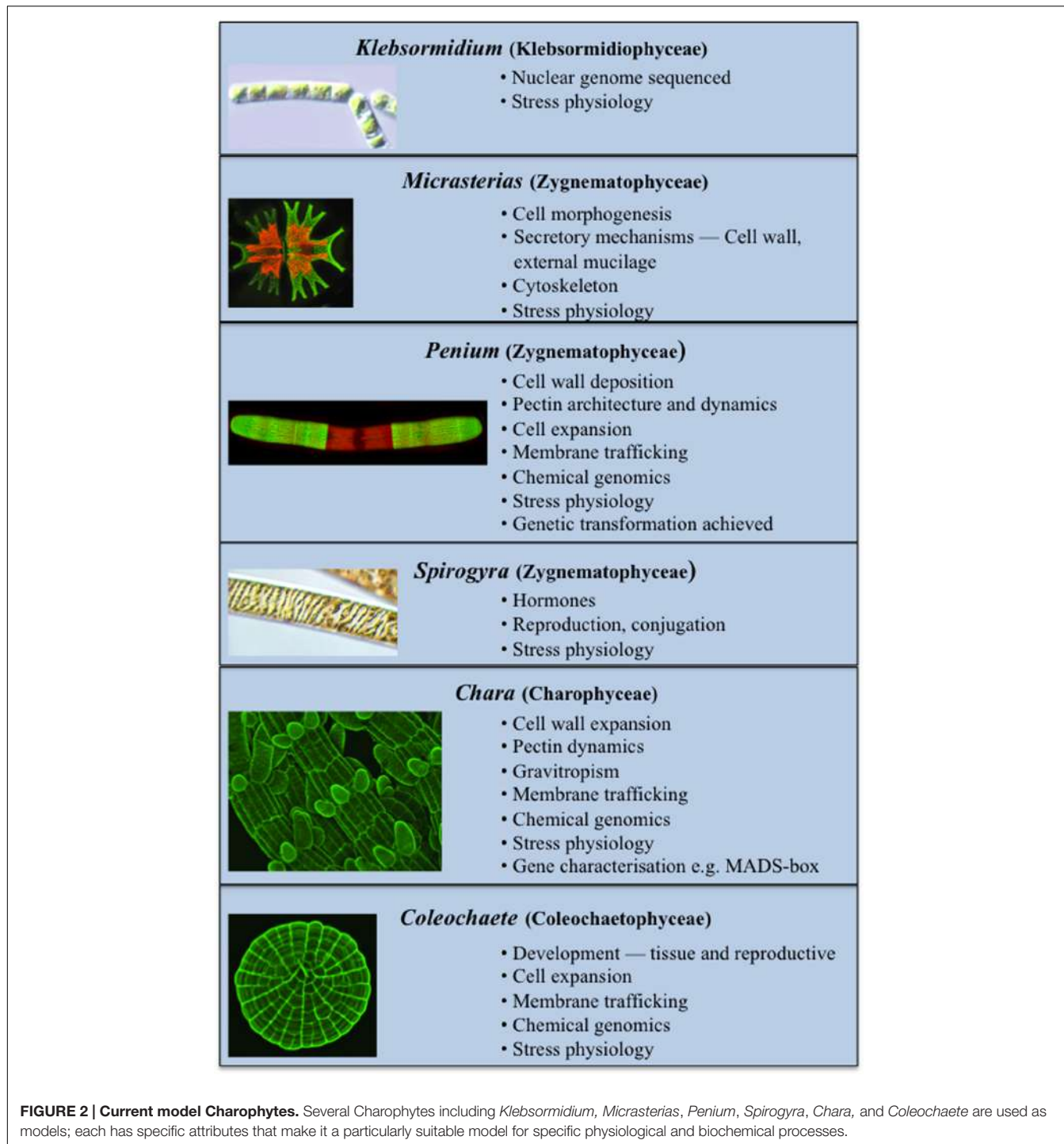
Desmids: The Symmetrical Models

The Zygnematophyceae have recently been shown to most likely be the closest living ancestors of land plants (Wodniok et al., 2011; Delwiche and Cooper, 2015). Unicellular members of the inclusive placoderm desmid group have become important models for elucidating many fundamental principles of plant cell biology and development. Large cell size, notable symmetry/shape, distinct cell wall architecture and elaborate endomembrane/cytoskeletal systems are just a few of the characteristics that make them excellent cell systems for studying cell physiology and development. The recent establishment of stable transformed lines and soon-to-be sequenced genomes/transcriptomes of select desmids have further enhanced their value in botanical studies. Two taxa,

Micrasterias and *Penium*, have emerged as the most well studied of the desmids.

Micrasterias has been the most popular desmid for cell biology research for the past 50 years due to its unique features (Meindl, 1993; Lutz-Meindl, 2016). The *Micrasterias* cell exhibits a bilateral symmetry that is often highlighted by a spectacularly dissected (i.e., multilobed) periphery. New daughter semicells produced by cell division do not have this complex morphology but rather are spherical in shape. A complex post-cytokinetic developmental program that employs multiple sets of highly coordinated subcellular mechanisms subsequently generates the multilobed phenotype during daughter semicell expansion. This program also is responsible for deposition of polymers for the production of both a primary and secondary cell wall. These events are centered on a large network of Golgi bodies and associated vesicles that yield a complex secretory mechanism. This process, in turn, is targeted to specific cell surface sites that generate a multipolar cell expansion and the concurrent secretion of cell wall macromolecules and extracellular mucilage (Kim et al., 1996; Lutz-Meindl and Brosch-Salomon, 2000; Oertel et al., 2004; Aichinger and Lutz-Meindl, 2005). The delivery of secretory components to precise cell surface loci requires an elaborate actinomyosin-based cytomotile system and is controlled by several signal transduction cascades (Meindl et al., 1994; Oertel et al., 2003). Furthermore, cell morphogenesis is highly sensitive to external stress (e.g., oxidative stress, salinity, heavy metals) that leads to major changes in cell differentiation (Darehshouri et al., 2008; Affenzeller et al., 2009; Andosch et al., 2012). *Micrasterias* is an outstanding organism for analyzing these subcellular features as it is easy to maintain and manipulate in the laboratory and it lends itself especially well for acquisition of high resolution imaging using light and electron microscopy including immunocytochemistry, Focused Ion Beam-Scanning Electron Microscopy (FIB-SEM) and Electron Energy Loss Spectroscopy (EELS) imaging (Lutz-Meindl, 2007; Eder and Lutz-Meindl, 2008, 2010; Wanner et al., 2013; Lutz-Meindl et al., 2015). Furthermore, initial molecular analyses including the production of transformed cell lines have further enhanced the use of *Micrasterias* especially in the molecular dynamics of cell wall processing (Vannerum et al., 2010, 2011, 2012).

Over the past decade, the desmid, *Penium margaritaceum*, has also become a valuable model organism (Domozych et al., 2009, 2014; Sørensen et al., 2014; Rydahl et al., 2015; Worden et al., 2015). Unlike *Micrasterias*, *Penium* has a simple cylindrical shape, possesses only a primary cell wall and deposits wall polymers at two specific loci of the cell surface during expansion (Domozych et al., 2011). This relative simplicity is highly attractive for elucidating fundamental principles of plant cell development including cell wall development, cell expansion and secretion dynamics (Domozych et al., 2005, 2014; Ochs et al., 2014). One of its main attributes is that it has wall polymers similar to those present in many land plants (e.g., cellulose, pectins, hemicelluloses) and that these polymers can be labeled with monoclonal antibodies. After labeling of live cells, these can be returned to culture where subsequent cell expansion and wall deposition events can be monitored (Domozych et al., 2009; Rydahl et al., 2015). *Penium* is also easily maintained in the



laboratory and its fast growth rate under precisely controlled conditions makes it an excellent specimen for large-scale concurrent microarray screenings of many chemical agents (by growth in multi-well plates) and for assessment of their specific effects on expansion/wall development (Worden et al., 2015). This significantly aids in revealing the role of specific subcellular components and processes in the expansion/differentiation. Recently, the isolation of stable transformed lines (Sørensen et al.,

2014) has further enhanced the potential of this alga in future plant cell studies.

Chara and Nitella: Cellular Giants for Plant Physiology

Species of *Chara* and *Nitella* (Charophyceae) have long been used as specimens for a variety of biological investigations

especially those dealing with cellular dynamics, expansion and cytoplasmic streaming (Green, 1954; Probine and Preston, 1962). Their macroscopic thalli are distinguished by nodes, where branches and gametangia arise, and internodal regions that consist of exceptionally elongate cells. Internodal cells exhibit a clearly notable stratification of subcellular components whereby helical-oriented chloroplasts define a stationary cortex that surrounds an endoplasm where the fastest recorded actinomyosin-generated cytoplasmic streaming occurs. The cytoplasm contains diverse endomembrane components that participate in dynamic membrane trafficking networks (e.g., endocytosis and exocytosis) that are controlled by complex signal transduction cascades (Foissner and Wastenys, 2000, 2012, 2014; Sommer et al., 2015; Foissner et al., 2016). The internodal cells possess cell walls rich in cellulose and the pectin, homogalacturonan (HG). Turgor is the main driving force for expansion and pectin is most likely the load-bearing component controlling wall expansion. Cyclic, non-enzymatic modulation and concurrent calcium complexing of the HG is the mechanism responsible for controlling wall modulations that lead to cell expansion (Proseus and Boyer, 2007, 2008, 2012; Boyer, 2016). One of the technical advantages of *Chara* and *Nitella* in cellular research is that internodal cells can be individually removed; endoplasm and cell walls can be “dissected out” and then used as acellular systems for experimental manipulation.

Other thallus components like rhizoids have organized polar organization of the cytoplasm. These cells contain sedimentable, mineral-rich statoliths located at the apex that function in gravity perception (Hodick et al., 1998; Braun, 2002; Braun and Limbach, 2006). This feature has made *Chara* the first charophyte in space. During TEXUS rocket parabolic flights, it was shown that the statoliths exert tensional forces on actin filaments. A balance of forces (i.e., gravity and the counteracting force of actin filaments) is responsible for the correct positioning of the statoliths in the rhizoid that, in turn, guarantee the ability to respond to the gravity vector (Braun and Limbach, 2006). The use of laser tweezers and slow rotating centrifuge microscopy has demonstrated that statolith sedimentation is not sufficient to cause gravitropic bending of the rhizoid tip. Rather, the mineral-rich statoliths must settle onto specific regions of the plasma membrane for gravitropic morphological effects to proceed (Braun, 2002). *Chara* has also been used to study other phenomena including electrophysiology and the role and movement of hormones (Belby, 2016).

Coleochaete for Developmental Studies and Pattern Development

The formation of a multicellular thallus (i.e., tissue, organ) of a plant requires precise, spatially regulated cell division planes that are controlled by multiple sets of genes expressed at specific points during development (Besson and Dumais, 2011; Umen, 2014). Directed in both 3-dimensional space and time, thallus morphogenesis also modulates in response to external stress factors. In plants, these developmental programs are made even more complex by the presence of cell walls that do not allow for cell migration or tissue flexibility. The elucidation of the

specific events that are central to the manifestation of thallus shape and size is often difficult to decipher in land plants where resolution of specific cell behaviors are often poorly resolved when embedded in highly complex and expansive tissues/organs. The use of organisms with simpler thallus designs has been advantageous for understanding basic developmental phenomena and the charophyte genus *Coleochaete* is one such example. Certain species (e.g., *C. orbicularis*, *C. scutatum*) produce a parenchymatous discoid thallus that grows outward by a combination of anti- or peri-clinal cell divisions and subsequent expansion of its outermost cells (Brown et al., 1994; Cook, 2004). The plane of division of any cell follows simple rules that are based upon cell size, cell shape and geographic location in the thallus (Dupuy et al., 2010; Besson and Dumais, 2011). This characteristic allows for the construction of mathematical models that can then be used to interpret multicellular morphogenesis (Domozych and Domozych, 2014; Umen, 2014) and yield critical insight into the evolution, biomechanics and physiology of organs and whole organisms. Furthermore, some *Coleochaete* species have been extensively studied to determine the structural and functional modulations that occur to a thallus under desiccation conditions (Graham et al., 2012), i.e., key features in understanding early land plant evolution and plant growth dynamics during droughts.

Insights from Genomic and Gene Studies

Similarly to many other technologies, molecular tools have the ability to impart new information of importance for many areas of research, including physiology and development. For example members of the MADS-box gene family have been isolated and characterized from three charophytes, *Chara globularis*, *Coleochaete scutata*, and *Closterium peracerosum-strigosum-littorale* (Tanabe et al., 2005). The expression pattern of the MADS-box genes in the charophytes suggests that they play a role in haploid development and reproduction (Tanabe et al., 2005). They are thought to have been recruited into the diploid generation, and their roles in development further diversified, during land plant evolution (Tanabe et al., 2005). To date *Klebsormidium flaccidum* is the only charophyte for which a near complete nuclear genome is available (Hori et al., 2014); although chloroplast and mitochondrial genomes have been sequenced for representatives of each of the six classes of charophytes and ESTs (expressed sequence tags) are available for some charophytes (Delwiche, 2016). The *Klebsormidium* genome has already revealed the presence of genes for the synthesis of several plant hormones and signaling intermediates, mechanisms for protection against high light intensity (Hori et al., 2014), and the presence of Group IIb WRKY transcription factors that were previously thought to have first appeared in mosses (Rinerson et al., 2015). Several charophyte genome sequencing projects are currently underway (Delwiche, 2016) and will enable more detailed comparative analyses including a larger number of charophytes and potentially give new insight into the evolutionary relationships between species and genes. The unique position of charophytes as the earliest diverging group of Streptophytes makes them a particularly powerful tool for evolutionary-developmental studies and emerging technologies

such as the recent achievement of stable transformation in *Penium* (Sørensen et al., 2014) will enable the function of specific genes to be explored.

FUTURE USES OF CHAROPHYTES AS MODEL ORGANISMS

A critical next step in charophyte research is the analysis of the genomes of inclusive taxa and comparative studies with those of land plants. Not only will this work yield key insight into the adaptive mechanisms that charophytes evolved when emerging onto, and successfully colonizing, terrestrial habitats but will further refine and expand the use of current model organisms in fundamental plant research. Although molecular studies will support many areas of research, two areas that will immediately benefit will be cell wall biology and the dynamics of growth regulators in growth and development. In the former, charophytes could provide clarification to many basic yet poorly resolved phenomena including pectin- and cell wall protein- biosynthesis, the controlled secretion, deposition and post-secretory modulations of wall polymers and the specific, interactive membrane trafficking networks in plant cells. In the

latter, charophyte models would help decipher the molecular signaling, cell biology and developmental dynamics of growth and development associated with hormones like ethylene and auxin. Recent ecophysiological studies with charophytes also offer a potential bonanza of critical data in determining how plant cells adapt to stress, including desiccation and salt tolerance (Holzinger and Karsten, 2013; Pichrtová et al., 2014; Herburger et al., 2015; Holzinger and Becker, 2015; Holzinger and Pichrtová, 2016; Kondo et al., 2016). The future of charophyte research is indeed very bright and will consequentially become a boon for all of plant biology.

AUTHOR CONTRIBUTIONS

All authors listed, have made substantial, direct and intellectual contribution to the work, and approved it for publication.

ACKNOWLEDGMENT

This work was supported by NSF (USA) MCB collaborative grants 1517345 and 1517546.

REFERENCES

- Abe, J., Hori, S., Sato, M., and Sekimoto, H. (2016). Concanavalin A-binding molecule on conjugation papillae is essential for release of gametes in a unicellular charophycean alga, *Cladophora peracerosum-strigosum-littoralis* complex. *Front. Plant Sci.* 7:1040. doi: 10.3389/fpls.2016.01040
- Affenzeller, M. J., Darezshouri, A., Andosch, A., Lutz, C., and Lutz-Meindl, U. (2009). Salt stress-induced cell death in the unicellular green alga *Micrasterias denticulata*. *J. Exp. Bot.* 60, 939–954. doi: 10.1093/jxb/ern348
- Aichinger, N., and Lutz-Meindl, U. (2005). Organelle interactions and possible degradation pathways visualized in high pressure frozen algal cells. *J. Microsc.* 219, 86–94. doi: 10.1111/j.1365-2818.2005.01496.x
- Andosch, A., Affenzeller, M. J., Lutz, C., and Lutz-Meindl, U. (2012). A freshwater green alga under cadmium stress: ameliorating calcium effects on ultrastructure and photosynthesis in the unicellular model *Micrasterias*. *J. Plant Physiol.* 169, 1489–1500. doi: 10.1016/j.jplph.2012.06.002
- Becker, B., Becker, D., Kammerling, J. P., and Melkonian, M. (1991). 2-keto-sugar acids in green flagellates — a chemical marker for prasinophycean scales. *J. Phycol.* 27, 498–504. doi: 10.1111/j.0022-3646.1991.00498.x
- Becker, B., and Marin, B. (2009). Streptophyte algae and the origin of embryophytes. *Ann. Bot.* 103, 999–1004. doi: 10.1093/aob/mcp044
- Belby, M. J. (2016). Multi-scale characean experimental system: from electrophysiology of membrane transporters to cell-to-cell connectivity, cytoplasmic streaming and auxin metabolism. *Front. Plant Sci.* 7:1052. doi: 10.3389/fpls.2016.01052
- Besson, S., and Dumais, J. (2011). Universal rule for the symmetric division of plant cells. *Proc. Natl. Acad. Sci. U.S.A.* 108, 6294–6299.
- Boot, K. J. M., Libbenga, K. R., Hille, S. C., Offringa, R., and van Duijn, B. (2012). Polar auxin transport: an early invention. *J. Expt. Bot.* 63, 4213–4218. doi: 10.1093/jxb/ers106
- Boyer, J. (2016). Enzyme-less growth in *Chara* and terrestrial plants. *Front. Plant Sci.* 7:866. doi: 10.3389/fpls.2016.00866
- Braun, M. (2002). Gravity perception requires statoliths settled on specific plasma membrane areas in characean rhizoids and protonemata. *Protoplasma* 219, 150–159. doi: 10.1007/s007090200016
- Braun, M., and Limbach, C. (2006). Rhizoids and protonemata of characean algae: model cells for research on polarized growth and plant gravity sensing. *Protoplasma* 229, 133–142. doi: 10.1007/s00709-006-0208-9
- Brown, R. C., Lemmon, B. E., and Graham, L. E. (1994). Morphogenetic plastid migration and microtubule arrays in mitosis and cytokinesis in the green alga *Coleochaete orbicularis*. *Am. J. Bot.* 81, 127–133. doi: 10.2307/2445625
- Cook, M. E. (2004). Cytokinesis in *Coleochaete orbicularis* (Charophyceae): an ancestral mechanism inherited in plants. *Am. J. Bot.* 91, 313–320. doi: 10.3732/ajb.91.3.313
- Darezshouri, A., Affenzeller, M., and Lutz-Meindl, U. (2008). Cell death upon H₂O₂ induction in the unicellular green alga *Micrasterias*. *Plant Biol.* 10, 732–745. doi: 10.1111/j.1438-8677.2008.00078.x
- Delwiche, C. F. (2016). The genomes of charophyte green algae. *Adv. Bot. Res.* 78, 255–270. doi: 10.1016/bs.abr.2016.02.002
- Delwiche, C. F., and Cooper, E. D. (2015). The evolutionary origin of a terrestrial flora. *Curr. Biol.* 25, R899–R910. doi: 10.1016/j.cub.2015.08.029
- Delwiche, C. F., Karol, K. G., Cimino, M. T., and Sytsma, K. J. (2002). Phylogeny of the genus *Coleochaete* and related taxa based on the chloroplast gene rbcL. *J. Phycol.* 38, 394–403. doi: 10.1046/j.1529-8817.2002.01174.x
- Domozych, D. S., Brechka, H., Britton, A., and Toso, M. (2011). Cell wall growth and modulation dynamics in a model unicellular green alga — *Penium margaritaceum*: live cell labeling with monoclonal antibodies. *J. Bot.* 2011:8. doi: 10.1155/2011/632165
- Domozych, D. S., and Domozych, C. E. (2014). Multicellularity in green algae: upsizing in a walled complex. *Front. Plant Sci.* 5:649. doi: 10.3389/fpls.201400649
- Domozych, D. S., Kort, S., Benton, S., and Yu, T. (2005). The extracellular polymeric substance of the green alga *Penium margaritaceum* and its role in biofilm formation. *Biofilms* 2, 129–144. doi: 10.1017/S1479050500181X
- Domozych, D. S., Lambisse, L., Kiemele, S. N., and Gretz, M. R. (2009). Cell-wall development and bipolar growth in the desmid *Penium margaritaceum* (Zygnematophyceae, Streptophyta), asymmetry in a symmetric world. *J. Phycol.* 45, 879–893. doi: 10.1111/j.1529-8817.2009.00713.x
- Domozych, D. S., Shaw, B., and Shaw, P. J. (1992). Scale biogenesis in the green alga, *Mesostigma viride*. *Protoplasma* 167, 19–22. doi: 10.1007/BF01353577
- Domozych, D. S., Sørensen, I., Popper, Z. A., Ochs, J., Andreas, A., Fang, J. U., et al. (2014). Pectin metabolism and assembly in the cell wall of the charophyte green alga *Penium margaritaceum*. *Plant Physiol.* 165, 105–118. doi: 10.1104/pp.114.236257

- Domozych, D. S., Wells, B., and Shaw, P. J. (1991). The basket scales of the green alga *Mesostigma viridae*: chemistry, immunology and ultrastructure. *J. Cell Sci.* 100, 397–407.
- Dupuy, L., Mackenzie, J., and Haseloff, J. (2010). Coordination of plant cell division and expansion in a simple morphogenetic system. *Proc. Natl. Acad. Sci. U.S.A.* 107, 2711–2716. doi: 10.1073/pnas.0906322107
- Eder, M., and Lutz-Meindl, U. (2008). Pectin-like carbohydrates in the green alga *Micrasterias* characterized by cytochemical analysis and energy filtering TEM. *J. Microsc.* 231, 201–214. doi: 10.1111/j.1365-2818.2008.02036.x
- Eder, M., and Lutz-Meindl, U. (2010). Analyses and localization of pectin-like carbohydrates in cell wall and mucilage of the green alga *Netrium digitus*. *Protoplasma* 243, 25–38. doi: 10.1007/s00709-009-0040-0
- Foissner, I., Sommer, A., Hoeftberger, M., Hoepflinger, M. C., and Absolonova, M. (2016). Is Wormannin-induced reorganization of the trans-Golgi network the key to understanding charasome formation. *Front. Plant Sci.* 7:756. doi: 10.3389/fpls.2016.00756
- Foissner, I., and Wastenys, G. O. (2000). “Actin in characean intermodal cells,” in *Actin: A Dynamic Framework for Multiple Plant Cell Functions*, eds C. Staiger, D. F. Baluska, D. Volkmann, and P. Barlow (Dordrecht: Kluwer Academic Publisher), 259–274.
- Foissner, I., and Wastenys, G. O. (2012). The characean intermodal cell as a model system for studying wound healing. *J. Microsc.* 247, 10–22. doi: 10.1111/j.1365-2818.2011.03572.x
- Foissner, I., and Wastenys, G. O. (2014). “Characean intermodal cells as a model system for the study of cell organization,” in *International Review of Cell and Molecular Biology*, ed. W. J. Kwang (New York, NY: Academic Press), 307–364.
- Gontcharov, A. A., Marin, B. A., and Melkonian, M. A. (2003). Molecular phylogeny of conjugating green algae (Zygnemophyceae, Streptophyta) inferred from SSU rDNA sequence comparisons. *J. Mol. Evol.* 56, 89–104. doi: 10.1007/s00239-002-2383-4
- Graham, L. E. (1993). Origin of Land Plants. New York, NY: John Wiley & Sons, 287.
- Graham, L. E., Arancibia-Avila, P., Taylor, W. A., Strother, P. K., and Cook, M. (2012). Aeroterrestrial Coleochaete (Streptophyta, Coleochaetales) models early plant adaptation to land. *Am. J. Bot.* 99, 130–144. doi: 10.3732/ajb.1100245
- Green, P. B. (1954). The spiral growth pattern of the cell wall in *Nettella axillaries*. *Am. J. Bot.* 41, 403–409. doi: 10.2307/2438730
- Guiry, M. D. (2013). Taxonomy and nomenclature of the Conjugatophyceae (=Zygnemophyceae). *Algae* 28, 1–29. doi: 10.4490/algae.2013.28.1.001
- Harholt, J., Moestrup, O., and Ulvskov, P. (2016). Why Plants were terrestrial from the beginning. *Trends Plant Sci.* 21, 96–101. doi: 10.1016/j.tplants.2015.11.010
- Herburger, K., and Holzinger, A. (2015). Localization and quantification of callose in the Streptophyte green algae *Zygnuma* and *Klebsormidium*: correlation with desiccation tolerance. *Plant Cell Physiol.* 56, 2259–2270. doi: 10.1093/pcp/pcv139
- Herburger, K., Lewis, L. A., and Holzinger, A. (2015). Photosynthetic efficiency, desiccation tolerance and ultrastructure in two phylogenetically distinct strains of alpine *Zygnuma* sp. (Zygnemophyceae, Streptophyta): role of pre-akinete formation. *Protoplasma* 252, 571–589. doi: 10.1007/s00709-014-0703-3
- Hodick, D., Buchen, B., and Sievers, A. (1998). Statolith positioning by microfilaments in *Chara* rhizoids and protonemata. *Adv. Space Res.* 21, 1183–1189. doi: 10.1016/S0273-1177(97)00633-9
- Holzinger, A., and Becker, B. (2015). Desiccation tolerance in the streptophyte green alga *Klebsormidium*: the role of phytohormones. *Commun. Integr. Biol.* 8:e1059978. doi: 10.1080/19420889.2015.1059978
- Holzinger, A., and Karsten, U. (2013). Desiccation stress and tolerance in green algae: consequences for ultrastructure, physiological, and molecular mechanisms. *Front. Plant Sci.* 4:327. doi: 10.3389/fpls.2013.00327
- Holzinger, A., and Pichrtová, M. (2016). Abiotic stress tolerance of charophyte green algae: new challenges for omics techniques. *Front. Plant Sci.* 7:678. doi: 10.3389/fpls.2016.00678
- Hori, K., Maruyama, F., Fujisawa, T., Togashi, T., Yamamoto, N., Seo, M., et al. (2014). *Klebsormidium flaccidum* genome reveals primary factors for plant terrestrial adaptation. *Nat. Commun.* 5:3978. doi: 10.1038/ncomm3978
- Ju, C., Van de Poel, B., Cooper, E. D., Thierer, J. H., Gibbons, T. R., Delwiche, C. F., et al. (2015). Conservation of ethylene as a plant hormone over 450 million years of evolution. *Nat. Plants* 1:14004. doi: 10.1038/NPLANTS.2014.4
- Kim, N.-H., Herth, W., Vuong, R., and Chanzy, H. (1996). The cellulose system in the cell wall of *Micrasterias*. *J. Struct. Biol.* 117, 195–203. doi: 10.1006/jsb1.1996.0083
- Kondo, S., Hori, K., Sasaki-Sekimoto, Y., Kobayashi, A., Kto, T., Yun-Ohta, N., et al. (2016). Primitive extracellular lipid components on the surface of the charophytic alga *Klebsormidium flaccidum* and their possible biosynthetic pathways as deduced from the genome sequence. *Front. Plant Sci.* 7:952. doi: 10.3389/fpls.2016.00952
- Leliaert, F., Smith, D. R., Moreau, H., Herron, M. H., Verbruggen, H., Delwiche, C. F., et al. (2012). Phylogeny and molecular evolution of the green algae. *Crit. Rev. Plant Sci.* 31, 1–46. doi: 10.1080/07352689.2011.615705
- Lemieux, C., Otis, C., and Turmel, M. (2016). Comparative chloroplast genome analyses of streptophyte green algae uncover major structural alterations in the *Klebsormidiophyceae*, *Coleochaetophyceae* and *Zygnematophyceae*. *Front. Plant Sci.* 7:697. doi: 10.3389/fpls.2016.00697
- Lewis, L. A., and McCourt, R. M. (2004). Green algae and the origin of land plants. *Am. J. Bot.* 91, 1535–1556. doi: 10.3732/ajb.91.10.1535
- Lutz-Meindl, U. (2007). Use of energy filtering transmission electron microscopy for image generation and element analysis in plant organisms. *Micron* 38, 181–196. doi: 10.1016/j.micron.2006.03.017
- Lutz-Meindl, U. (2016). *Micrasterias* as a model system in plant cell biology. *Front. Plant Sci.* 7:999. doi: 10.3389/fpls.2016.00999
- Lutz-Meindl, U., and Brosch-Salomon, S. (2000). Cell wall secretion in the green alga *Micrasterias*. *J. Microsc.* 198, 208–217. doi: 10.1046/j.1365-2818.2000.00699.x
- Lutz-Meindl, U., Luckner, M., Andosch, A., and Wanner, G. (2015). Structural stress responses and degradation of dictyosomes in algae analysed by TEM and FIB-SEM tomography. *J. Microsc.* 263, 129–141. doi: 10.1111/jmi.12369
- Manton, I., and Ettl, H. (1965). Observations on fine structure of *Mesostigma viride* Lauterborn. *J. Linn. Soc. (Bot.)* 59, 175–184. doi: 10.1111/j.1095-8339.1965.tb00056.x
- Mattox, K. R., and Stewart, K. D. (1984). “Classification of the green algae: a concept based on comparative cytology,” in *The Systematics of Green Algae*, eds D. E. G. Irvine and D. M. Johns (London: Academic Press), 29–72.
- Meindl, U. (1993). *Micrasterias* cells as a model system for research on morphogenesis. *Microbiol. Rev.* 57, 415–433.
- Meindl, U., Zhang, D., and Hepler, P. K. (1994). Actin microfilaments are associated with the migrating nucleus and cell cortex in the green alga *Micrasterias*, Studies on living cells. *J. Cell Sci.* 107, 1929–1934.
- Mikhailyuk, T., Holzinger, A., Massalski, A., and Karsten, U. (2014). Morphological and ultrastructural aspects of *Interfilum* and *Klebsormidium* (*Klebsormidiophyceae*, *Streptophyta*) with special reference to cell division and thallus formation. *Eur. J. Phycol.* 49, 395–412. doi: 10.1080/09670262.2014.949308
- Mikhailyuk, T. I., Sluiman, H. J., Massalski, A., Mudimu, O., Demchenko, E. M., Kondratyuk, S. Y., et al. (2008). New streptophyte green algae from terrestrial habitats and an assessment of the genus *Interfilum* (*Klebsormidiophyceae*, *Streptophyta*). *J. Phycol.* 44, 1586–1603. doi: 10.1111/j.1529-8817.2008.00606.x
- Mikkelsen, M. D., Harholt, J., Ulvskov, P., Johansen, I. E., Fangel, J. U., Doblin, M. S., et al. (2014). Evidence for land plant cell wall biosynthetic mechanisms in charophyte green algae. *Ann. Bot.* 114, 1217–1236. doi: 10.1093/aob/mcu171
- Ochs, J., LaRue, T., Tinaz, B., Yongue, C., and Domozych, D. S. (2014). The cortical cytoskeletal network and cell-wall dynamics in the unicellular charophycean green alga *Penium margaritaceum*. *Ann. Bot.* 114, 1237–1249. doi: 10.1093/aob/mcu013
- Oertel, A., Aichinger, N., Hochreiter, R., Thalhamer, J., and Lutz-Meindl, U. (2004). Analysis of mucilage secretion and excretion in *Micrasterias* (Chlorophyta) by means of immunoelectron microscopy and digital time lapse video microscopy. *J. Phycol.* 40, 711–720. doi: 10.1111/j.1529-8817.2004.03222.x
- Oertel, A., Holzinger, A., and Lutz-Meindl, U. (2003). Involvement of myosin in intracellular motility and cytomorphogenesis in *Micrasterias*. *Cell Biol. Int.* 27, 977–986. doi: 10.1016/j.cellbi.2003.07.004
- O'Rourke, C., Gregson, T., Murray, L., Sadler, I. H., and Fry, S. C. (2015). Sugar composition of the pectic polysaccharides of charophytes, the closest algal relatives of land-plants: presence of 3-O-methyl-D-galactose residues. *Ann. Bot.* 116, 225–236. doi: 10.1093/aob/mcv089
- Pichrtová, M., Kulichová, J., and Holzinger, A. (2014). Nitrogen limitation and slow drying induce desiccation tolerance in conjugating green algae

- (Zygnematophyceae, Streptophyta) from polar habitats. *PLoS ONE* 9:e113137. doi: 10.1371/journal.pone.0113137
- Pickett-Heaps, J. D. (1975). *Green Algae: Structure, Reproduction and Evolution in Selected Genera*. Sunderland, MA: Sinauer.
- Pickett-Heaps, J. D., and Marchant, H. J. (1972). The phylogeny of green algae: a new proposal. *Cytobios* 6, 255–264.
- Popper, Z. A. (2008). Evolution and diversity of green plant cell walls. *Curr. Opin. Plant Biol.* 11, 286–292. doi: 10.1016/j.pbi.2008.02.012
- Popper, Z. A., and Fry, S. C. (2003). Primary cell wall composition of bryophytes and charophytes. *Ann. Bot.* 91, 1–12. doi: 10.1093/aob/mcg013
- Probine, M. C., and Preston, R. D. (1962). Cell growth and the structure and mechanical properties of the wall in internodal cells of *Nitella opaca* II. Mechanical properties of the walls. *J. Exp. Bot.* 13, 111–127. doi: 10.1093/jxb/13.1.111
- Proseus, T. E., and Boyer, J. S. (2007). Tension required for pectate chemistry to control growth in *Chara corallina*. *J. Exp. Bot.* 58, 4283–4292. doi: 10.1093/jxb/erm318
- Proseus, T. E., and Boyer, J. S. (2008). Calcium pectate chemistry causes growth to be stored in *Chara corallina*: a test of the pectate cycle. *Plant Cell Environ.* 31, 1147–1155. doi: 10.1111/j.1365-3040.2008.01829.x
- Proseus, T. E., and Boyer, J. S. (2012). Calcium deprivation disrupts enlargement of *Chara corallina* cells: further evidence for the calcium pectate cycle. *J. Exp. Bot.* 63, 3953–3958. doi: 10.1093/jxb/ers089
- Rinerson, C. I., Rabata, R. C., Tripathi, P., Shen, Q. J., and Rushton, P. J. (2015). The evolution of WRKY transcription factors. *BMC Plant Biol.* 15:66. doi: 10.1186/s12870-015-0456-y
- Rodríguez-Ezpeleta, N., Philippe, H., Brinkmann, H., Becker, B., and Melkonian, M. (2007). Phylogenetic analyses of nuclear, mitochondrial and plastid multi-gene datasets support the placement of *Mesostigma* in the Streptophyta. *Mol. Biol. Evol.* 24, 723–731. doi: 10.1093/molbev/msl200
- Rogers, C. E., Mattox, K. R., and Stewart, K. D. (1980). The zoospore of *Chlorokybus atmophyticus*, a charophyte with sarcinoid growth habit. *Am. J. Bot.* 67, 774–783. doi: 10.2307/2442669
- Rydahl, M. G., Fangel, J. U., Mikkelsen, M. D., Johansen, I. E., Andreas, A., Harholt, J., et al. (2015). “*Penium margaritaceum* as a model organism for cell wall analysis of expanding plant cells,” in *Plant Cell Expansion. Methods in Molecular Biology* 1242, ed. J. M. Estevez (New York, NY: Humana Press), 1–22.
- Sluiman, H. J., Guihal, C., and Mudimu, O. (2008). Assessing phylogenetic affinities and species delimitations in *Klebsormidiales* (Streptophyta): nuclear-encoded rDNA phylogenies and ITS secondary structure models in *Klebsormidium*, *Hormidiella*, and *Entransia*. *J. Phycol.* 44, 183–195. doi: 10.1111/j.1529-8817.2007.00442.x
- Sommer, A., Hoeftberger, M., Hoepflinger, S., Bulychev, A., and Foissner, I. (2015). Convoluted plasma membrane domains in the green alga *Chara* are depleted of microtubules and actin filaments. *Plant Cell Physiol.* 56, 1981–1996. doi: 10.1093/pcp/pcv119
- Sørensen, I., Domozych, D., and Willats, W. G. T. (2010). How have plant cell walls evolved? *Plant Physiol.* 153, 366–372. doi: 10.1104/pp.110.154427
- Sørensen, I., Fei, Z., Andreas, A., Willats, W. G. T., Domozych, D. S., Rose, J. K. C., et al. (2014). Stable transformation and reverse genetic analysis of *Penium margaritaceum*: a platform for studies of charophyte green algae, the immediate ancestors of land plants. *Plant J.* 77, 339–351. doi: 10.1111/tpj.12375
- Sørensen, I., Pettolino, F., Bacic, A., Ralph, J., Lu, F., O’Neill, M., et al. (2011). The Charophycean green algae provide insights into the early origins of plant cell walls. *Plant J.* 68, 201–211. doi: 10.1111/j.1365-313X.2011.04686.x
- Sørensen, I., Rose, J. K. C., Doyle, J. J., Domozych, D. S., and Willats, W. G. T. (2012). The Charophycean green algae as model systems to study plant cell walls and other evolutionary adaptations that gave rise to land plant. *Plant Signal. Behav.* 7, 1–3. doi: 10.4161/psb.7.1.18574
- Stamenkovic, M., Woelken, E., and Hanelt, D. (2014). Ultrastructure of *Cosmarium* strains (Zygnematophyceae, Streptophyta) collected from various geographic locations shows species-specific differences both at optimal and stress temperatures. *Protoplasma* 251, 1491–1509.
- Tanabe, Y., Hasebe, M., Sekimoto, H., Nishiyama, T., Kitani, M., Henshel, K., et al. (2005). Characterization of MADS-box genes in charophycean green algae and its implication for the evolution of MADS-box genes. *Proc. Natl. Acad. Sci. U.S.A.* 102, 2436–2441. doi: 10.1073/pnas.0409860102
- Timme, R. E., Bachvaroff, T. R., and Delwiche, C. F. (2012). Broad phylogenomic sampling and the sister lineage of land plants. *PLoS ONE* 7:e29696. doi: 10.1371/journal.pone.0029696
- Umen, J. G. (2014). Green algae and the origins of multicellularity in the plant kingdom. *Cold Spring Harb. Perspect. Biol.* 2014:a016170. doi: 10.1101/cshperspect.a016170
- Vannerum, K., Abe, J., Sekimoto, H., Inze, D., and Vyverman, W. (2010). Intracellular localization of an endogenous cellulose synthase of *Micrasterias denticulata* (Desmidiales, Chlorophyta) by means of transient genetic transformation. *J. Phycol.* 46, 839–845. doi: 10.1111/j.1529-8817.2010.00867.x
- Vannerum, K., De Rycke, R., Pollier, J., Goossens, A., Inzé, D., and Vyverman, W. (2012). Characterization of a RABE (RAS gene from rat brain E) GTPase expressed during morphogenesis in the unicellular green alga *Micrasterias denticulata* (Zygnematophyceae, Streptophyta). *J. Phycol.* 48, 682–692. doi: 10.1111/j.1529-8817.2012.01170.x
- Vannerum, K., Huysman, M. J. J., De Rycke, R., Vuylsteke, M., Leliaert, F., Pollier, J., et al. (2011). Transcriptional analysis of cell growth and morphogenesis in the unicellular green alga *Micrasterias* (Streptophyta), with emphasis on the role of expansin. *BMC Plant Biol.* 11:128. doi: 10.1186/1471-2229-11-128
- Wang, C., Liu, Y., Li, S.-S., and Han, G.-Z. (2014). Origin of plant auxin biosynthesis in charophyte algae. *Trends Plant Sci.* 19, 741–743. doi: 10.1016/j.tplants.2014.10.004
- Wang, C., Liu, Y., Li, S.-S., and Han, G.-Z. (2015). Insights into the origin and evolution of the plant hormone signaling machinery. *Plant Physiol.* 167, 872–886. doi: 10.1104/pp.114.247403
- Wanner, G., Schaefer, T., and Lutz-Meindl, U. (2013). 3-D analysis of dictyosomes and multivesicular bodies in the green alga *Micrasterias denticulata* by FIB/SEM tomography. *J. Struct. Biol.* 184, 203–211. doi: 10.1016/j.jsb.2013.10.003
- Wodniok, S., Brinkmann, H., Glockner, G., Heidel, A. J., Phillippe, H., Melkonian, M., et al. (2011). Origin of land plants: do conjugating green algae hold the key? *BMC Evol. Biol.* 11:104. doi: 10.1186/1471-2148-11-104
- Worden, N., Esteve Esteve, V., Domozych, D. S. and Drakakaki, G. (2015) “Using chemical genomics to study cell wall formation and cell growth in *Arabidopsis thaliana* and *Penium margaritaceum*,” in *Plant Cell Expansion. Methods in Molecular Biology* 1242, ed. J. M. Estevez (New York, NY: Humana Press), 23–40.
- Zhang, S., and van Duijn, B. (2014). Cellular auxin transport in algae. *Plant* 3, 58–69. doi: 10.3390/plants3010058
- Zhong, B., Liu, L., Yan, Z., and Penny, D. (2013). Origin of land plants using the multispecies coalescence model. *Trends Plant Sci.* 18, 492–495. doi: 10.1016/j.tplants.2013.04.009

Conflict of Interest Statement: The authors declare that the research was conducted in the absence of any commercial or financial relationships that could be construed as a potential conflict of interest.

Copyright © 2016 Domozych, Popper and Sørensen. This is an open-access article distributed under the terms of the Creative Commons Attribution License (CC BY). The use, distribution or reproduction in other forums is permitted, provided the original author(s) or licensor are credited and that the original publication in this journal is cited, in accordance with accepted academic practice. No use, distribution or reproduction is permitted which does not comply with these terms.



***Micrasterias* as a Model System in Plant Cell Biology**

Ursula Lütz-Meindl*

Plant Physiology Division, Cell Biology Department, University of Salzburg, Salzburg, Austria

The unicellular freshwater alga *Micrasterias denticulata* is an exceptional organism due to its complex star-shaped, highly symmetric morphology and has thus attracted the interest of researchers for many decades. As a member of the Streptophyta, *Micrasterias* is not only genetically closely related to higher land plants but shares common features with them in many physiological and cell biological aspects. These facts, together with its considerable cell size of about 200 µm, its modest cultivation conditions and the uncomplicated accessibility particularly to any microscopic techniques, make *Micrasterias* a very well suited cell biological plant model system. The review focuses particularly on cell wall formation and composition, dictyosomal structure and function, cytoskeleton control of growth and morphogenesis as well as on ionic regulation and signal transduction. It has been also shown in the recent years that *Micrasterias* is a highly sensitive indicator for environmental stress impact such as heavy metals, high salinity, oxidative stress or starvation. Stress induced organelle degradation, autophagy, adaption and detoxification mechanisms have moved in the center of interest and have been investigated with modern microscopic techniques such as 3-D- and analytical electron microscopy as well as with biochemical, physiological and molecular approaches. This review is intended to summarize and discuss the most important results obtained in *Micrasterias* in the last 20 years and to compare the results to similar processes in higher plant cells.

OPEN ACCESS

Edited by:

David Domozych,
Skidmore College, USA

Reviewed by:

Sven B. Gould,
Heinrich Heine University, Germany

Eric Roberts,
Rhode Island College, USA

***Correspondence:**

Ursula Lütz-Meindl
ursula.meindl@sbg.ac.at

Specialty section:

This article was submitted to
Plant Evolution and Development,
a section of the journal
Frontiers in Plant Science

Received: 21 March 2016

Accepted: 24 June 2016

Published: 12 July 2016

Citation:

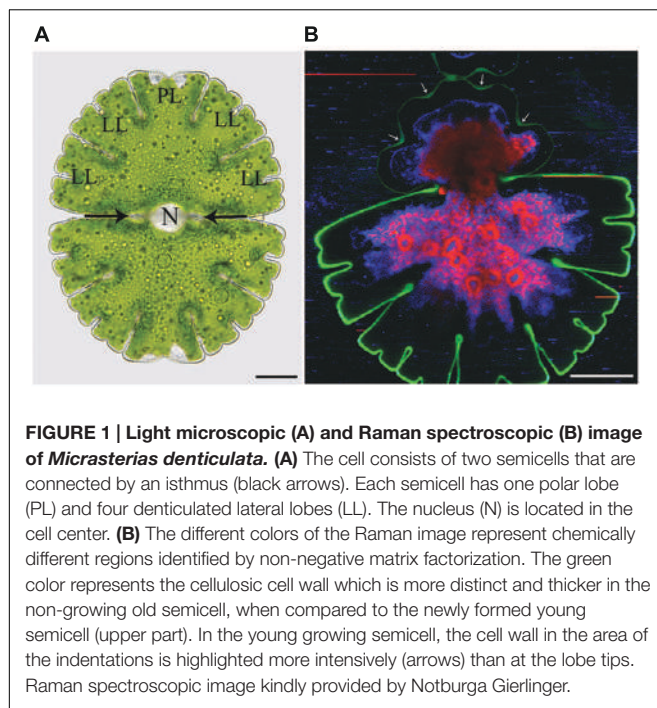
Lütz-Meindl U (2016) *Micrasterias* as a Model System in Plant Cell Biology.
Front. Plant Sci. 7:999.

doi: 10.3389/fpls.2016.00999

INTRODUCTION

Among the placoderm desmids the genus *Micrasterias* has an exceptional position due to its highly ornamented, star-shaped morphology with deep indentations and furcated lobe tips (**Figure 1A**). By their beauty, their high symmetry and their flat, disk-shaped cell architecture facilitating any microscopic analysis as well as their close relationship to higher plants (Wodniok et al., 2011; Leliaert et al., 2012) *Micrasterias* cells have lent themselves as excellent model systems for studying plant cell morphogenesis. In many aspects results obtained in *Micrasterias* cells are applicable to higher plants and comparison with them additionally provides information on the evolution of cellular processes.

Early investigations around the turn of the 19th century have already focused on cell shape formation of this extraordinary organism (Hauptfleisch, 1888; Lütkemüller, 1902) and the implementation of an appropriate nutrient solution for their easy cultivation (Pringsheim, 1930; Waris, 1950a) represented the basis for numerous further studies. Whereas the very early



investigations were intended to find an inner “cytoplasmic framework” for the morphology of *Micrasterias* (Waris, 1950b) subsequent studies focused on the peripheral cytoplasm (Teiling, 1950) and the nucleus (Waris and Kallio, 1964) as shape determining units. At a time where genetic control of cellular processes was far from being understood these studies (Kallio, 1949; Kallio and Heikkilä, 1972; Kallio and Lehtonen, 1981) provided interesting insight into cytomorphogenesis by showing that a three-lobed pre-stage of a young semicell of *Micrasterias* can be formed even when the nucleus is physically removed. Further differentiation into lobe tips and indentations, however, requires continuous nuclear control. An increase in ploidy increases the complexity of the cell pattern and leads to triradiate or quadriradiate *Micrasterias* cells (for summary see Kallio and Lehtonen, 1981).

Kiermayer (1964) who tested several *Micrasterias* species for their suitability as cell biological model system in respect to growth and reproduction properties and their sensitivity to experimental and environmental impact, was the one who selected the species *Micrasterias denticulata* and defined its developmental stages in 15 min intervals. This represented the basis for his first investigations on ultrastructural details during morphogenesis (Kiermayer, 1968, 1970a) and for numerous other studies on cell physiology, cell wall formation, secretion, cytoskeleton function, and environmental impact in *M. denticulata* in the last decades (for references see below).

The most important insights into cytomorphogenesis arising from Kiermayer’s studies and summarized by Kiermayer (1981), Kiermayer and Meindl (1984), and Meindl (1993) were that the large dictyosomes of a *Micrasterias* cell consist of a constant number of 11 cisternae throughout the cell cycle and that they switch a several times during morphogenesis

to form the different vesicle populations that contain cell wall precursors for septum-, primary- and secondary wall formation. These results obtained by standard chemical fixation were confirmed in a later study on high pressure frozen *Micrasterias* cells (Meindl et al., 1992). The contents of the different vesicle populations observed by Kiermayer were defined by immuno-transmission electron microscopy (TEM) and immunofluorescence experiments in the confocal laser scanning microscope (CLSM) using antibodies against cell wall constituents such as, pectins, different hemicelluloses and arabinogalactane proteins (AGP; Lütz-Meindl and Brosch-Salomon, 2000; Eder and Lütz-Meindl, 2008; Eder et al., 2008 see also below). Additionally, by simple turgor reduction experiments Kiermayer’s studies (Kiermayer, 1964, 1967, 1981) demonstrated impressively that the plasma membrane contains a pre-pattern for morphogenesis in form of “membrane recognition areas” for the cell wall delivering vesicles and thus plays the major role in cell shaping of *Micrasterias*. The “membrane recognition areas” postulated by Kiermayer were later shown to be zones of continuously changing, local calcium influx at the respective lobe tips during development of the cell pattern (Meindl, 1982a,b; Troxell et al., 1986; Troxell, 1989; Troxell and Scheffey, 1991). They correspond to the fusion sites of primary wall material delivering Golgi vesicles as shown by means of autoradiography (Lacalli, 1975) and by TEM in high pressure frozen developmental stages (Meindl et al., 1992).

Doberstein and Kiermayer (1972) were the first who described hexagonally ordered “rosette” complexes inside of a particular Golgi vesicle population, the flat vesicles, which are delivered to the plasma membrane, where they are responsible for formation of cellulose fibrils. *M. denticulata* was thus the first plant cell in which cellulose formation was discovered. By Kimura et al. (1999) it was proven in vascular plants by means of immuno labeling and freeze fracture technique in TEM that the rosette terminal complexes are the sites of cellulose formation. In *Micrasterias* an endogenous cellulose synthase was localized many years later by means of transient genetic transformation (Vannerum et al., 2010).

Another finding that goes back to Kiermayer and gives information on the basics of growth and morphogenesis in *Micrasterias* is the perception that continuous protein synthesis is required throughout its morphogenesis and that any experimental interruption by employment of different RNA or protein synthesis inhibitors is reflected in characteristic cellular reactions summarized as “anuclear type of development” (ATD) syndrome (Kiermayer and Meindl, 1980, 1986). Its typical morphological appearance is a reduction of the cell pattern to three to five cylindrical lobes which lack further differentiation. As such shape malformations have so far only been found in *Micrasterias* cells that grow without nuclear control (summarized by Kallio and Lehtonen, 1981) and are not inducible by any of the numerous drugs and inhibitors that have been tested on *Micrasterias* the term “ATD” syndrome was invented for it. Besides the characteristic cell shape malformation the ATD syndrome comprises prolonged extension of the primary wall from 5 h in controls up to 24 h. Consequently the cells burst due to a lack of secondary wall formation. Additionally the structure

of the primary wall is altered and the number of dictyosomes is reduced. Knowledge on the characteristics of this syndrome allows easy detection of any impairment of protein biosynthesis in *Micrasterias*, e.g., by experimental or environmental influence.

Kiermayer's, (1968) excellent TEM images on microtubule distribution around the nucleus in growing and non-growing *Micrasterias* cells also inspired further research on the involvement of the cytoskeleton in intracellular organelle migration. During growth the large nucleus moves from its position in the central constriction of a *Micrasterias* cell, called isthmus (**Figure 1A**), into the expanding semicell and returns to the cell center at the end of morphogenesis. Coincidentally the chloroplast which has duplicated before mitosis, expands itself into the growing semicell. Its shape copies the outer cell shape at the end of development. Both organelle movements are cytoskeleton dependent (Kiermayer, 1970b; Meindl and Kiermayer, 1982; Meindl, 1983, 1992; for summary see Meindl, 1993; Lütz-Meindl and Menzel, 2000). During its migration the nucleus is surrounded by a basket-shaped microtubule system that also contains actin filaments (Meindl et al., 1994). It originates from a distinct microtubule center and stays in contact with the cell center by a continuously elongating microtubule band during nuclear migration into the growing semicell. Along this band the nucleus moves back into the isthmus where it is anchored by a ring shaped microtubule band after morphogenesis. This band corresponds to the pre-prophase band of higher plant cells (Pickett-Heaps and Northcote, 1966; Karahara et al., 2009). Any physical or chemical disruption of microtubules during growth of *Micrasterias* leads to an abnormal dislocation of the nucleus into the cell periphery and prevents further cell divisions (Meindl, 1983; Holzinger et al., 2002). Several studies indicated that the actin binding protein profilin, myosins and kinesis-like proteins are involved in regulation and/or achievement of nuclear and chloroplast migration in growing *Micrasterias* cells (Holzinger et al., 2000; Holzinger and Lütz-Meindl, 2002; Oertel et al., 2003). As the nucleus of *M. denticulata* measures about 30 μm in diameter and is thus easily detectable even with a dissecting microscope, the alga is a perfect system for identifying activity of anti-microtubule drugs in a plant cell by a simple methodological approach (Meindl and Kiermayer, 1981). Any dislocation of the nucleus indicates a dysfunction of the microtubule system.

Whereas cell shaping and intracellular regulators of growth and cytomorphogenesis have been in the center of research on *Micrasterias* for several decades, the suitability of this alga as sensitive model for studying environmental impact has gained importance in the recent years. *Micrasterias* and other members of the family Desmidiaceae mostly inhabit acid peat bogs all over the world, from tropic climates to Polar Regions and from sea level up to more than 3000 m altitudes (see also Brook, 1981). Their natural habitats are shallow bog ponds that may be exposed to rapidly changing environmental conditions and may face extreme parameters such as intense sun light, high UV irradiation, drought, increasing salinity, very low, but also high temperature as well as impact of man-made pollutants such as heavy metals, pesticides or fertilizers.

Based on earlier results briefly outlined in the Section "Introduction" and on a more detailed survey on results obtained in the last 20 years, this review aims to provide an overview on our present knowledge on the cell biological basis for growth and cell shape formation as well as on responses of *Micrasterias* to different abiotic stress scenarios. Recent results on dictyosomal function, cell wall composition, the cytoskeletal and ionic regulation of growth, stress-induced organelle degradation, occurrence and induction of autophagy and programmed cell death as well as on accompanying physiological parameters will be in the focus of this review. Comparison to similar processes in closely related higher land plants will be drawn in each chapter and an outlook on future research topics on *Micrasterias* will complete this work.

CELL BIOLOGICAL BASIS OF GROWTH AND SHAPE FORMATION

Cell Wall Development and Function of Dictyosomes

Cell development and pattern formation of *M. denticulata* (summarized by Meindl, 1993) starts with the formation of a thin, fragile septum wall at the overlapping zone of the two parental secondary cell walls in the isthmus during late mitosis. The two halves of a *Micrasterias* cell are separated when the septum closes like a diaphragm. The septum consists mainly of high-methyl esterified pectins that are delivered to the growing septum by a particular "septum vesicle" population as shown by immunogold labeling with JIM antibodies (Lütz-Meindl and Brosch-Salomon, 2000). Septum formation lasts about 15 min and is followed by the process of primary wall formation and shaping. According to our present knowledge shaping of *Micrasterias* cells is regarded as a temporal and spatial sequence of repeated growth cessation at particular, symmetrically arranged points at the cell periphery. While the first bulge that develops from the parental semicells grows uniformly in the main plane of the cell, cessation of growth at two symmetrical points after about 75 min leads to the formation of the first two indentations that develop to the deepest at the final cell shape. They define the species specific morphology of a *M. denticulata* cell. Subsequent formation of the residual indentations follows the same principle. In the areas between the growth cessation points, deposition of primary wall material and expansion is continued. Growing and non-growing zones alternate during shape formation and the number of both increases with proceeding development. In early stages the single lobes perform tip growth which from its course resembles tip growth of pollen tubes, root hairs or moss protonemata (Vidali and Bezanilla, 2012; Gu and Nielsen, 2013; Rounds and Bezanilla, 2013). However, several tips of a *Micrasterias* cell grow at the same time. This process has been defined as "multipolar tip growth" (Kiermayer and Meindl, 1989; Lütz-Meindl and Menzel, 2000), an unique phenomenon that represents an enormous demand for a single cell. Finally the outer cell shape of *M. denticulata* is completed about 5 h after mitosis by furcation of the lobe tips. Underneath the primary wall a thick

cellulose rich secondary wall is deposited that contains pores. The primary wall is finally pushed off by a sudden onset of mucilage production through the secondary wall and its pores (for details see Oertel et al., 2004).

Achievement of the complex cell pattern of a *Micrasterias* cell requires particular physical properties of the primary cell wall that allow intussusception of wall material on the one hand and stiffening and growth arrest on the other hand. Recent Raman spectroscopic investigations (**Figure 1B**) clearly show that the cellulose content of the primary wall of the outgrowing lobes is much lower than that of the indentations in which the cell wall is thicker and less extensible. This technique also demonstrates unambiguously the considerable difference in thickness and cellulose content between the growing primary and the non-growing secondary cell wall. The degree of pectin esterification which determines the calcium-binding capacity accounts for the flexibility of the cell wall during primary wall growth. A combination of immuno TEM, immuno fluorescence, de-esterification studies and calcium measurements by TEM-coupled electron energy loss spectroscopy (EELS) has shown (Lütz-Meindl and Brosch-Salomon, 2000; Eder and Lütz-Meindl, 2008) that pectic polysaccharides are transported to the cell wall in a de-esterified form inside of a particular Golgi vesicle population (D-vesicles according to Kiermayer, 1970a,b; Meindl et al., 1992; Lütz-Meindl and Brosch-Salomon, 2000) and become methyl-esterified at the inner side of the developing primary wall (Eder and Lütz-Meindl, 2008). This allows flexibility and integration of new wall material. While they are translocated toward the outer side of the wall they become again de-esterified (see also Lütz-Meindl and Brosch-Salomon, 2000) and are thus able to bind high amounts of calcium (**Figures 2A,B**) which leads to wall stiffening and growth cessation. Enzyme activity assays provided evidence for the existence of a pectin-desterifying enzyme in *M. denticulata*. Moreover, enhanced desterification by experimental addition of a pectin methylesterase that de-esterifies pectins in higher plants, resulted in growth inhibition and shape

malformation of *Micrasterias* (Eder and Lütz-Meindl, 2008). This indicates that as in higher plant cells (Carpita and Gibeaut, 1993; Goldberg et al., 2001; Bosch et al., 2005; Bosch and Hepler, 2005) the de-esterification process and its regulation is crucial for morphogenesis and growth of *Micrasterias* (Eder and Lütz-Meindl, 2008). Though it is likely, there is so far no indication that the degree of esterification is different in the areas of the forming indentations in comparison to the zones of the outgrowing lobes.

The existence of pectins and particularly of homogalacturonans as dominant polysaccharide in growing cell walls has been also demonstrated in other members of Desmidiaeae such as *Closterium* and *Penium* (Baylson et al., 2001; Domozych et al., 2007) as well as in other green algae (Popper and Fry, 2003). By extraction of isolated cell walls of *Penium* a particular homogalacturonan was identified that was partially esterified and was equivalent to that of land plants. As in *Micrasterias*, the cell wall of *Penium* was recognized by the antibodies JIM 5 and JIM7 and the degree of de-esterification increased with the distance from the isthmus region (Domozych et al., 2006; Domozych et al., 2007). The degree of methyl-esterification in the growing primary wall of *Micrasterias* corresponds well to findings in higher plants (Bush and McCann, 1999). However, the detailed structure of pectins in desmids is not yet known. There are some indications that algae contain higher contents of galacturonic and glucuronic acid than higher plants (Popper and Fry, 2003).

Mucilage vesicles of *Micrasterias* reveal the highest calcium-binding capacity among all cytoplasmic components measured by EELS indicating a high amount of low-methyl-esterified pectins in the mucilage during its transport to the cell periphery (**Figures 2A,B**; Eder and Lütz-Meindl, 2008). As soon as they are excreted through the cell wall or the pores (Oertel et al., 2004) their calcium-binding capacity diminishes either by enzymatic activity or by changing pH (Eder and Lütz-Meindl, 2008). This allows uptake of water and swelling, which is responsible for generating the force for directed movement of desmids with respect to light (Domozych and Rogers-Domozych, 1993) but

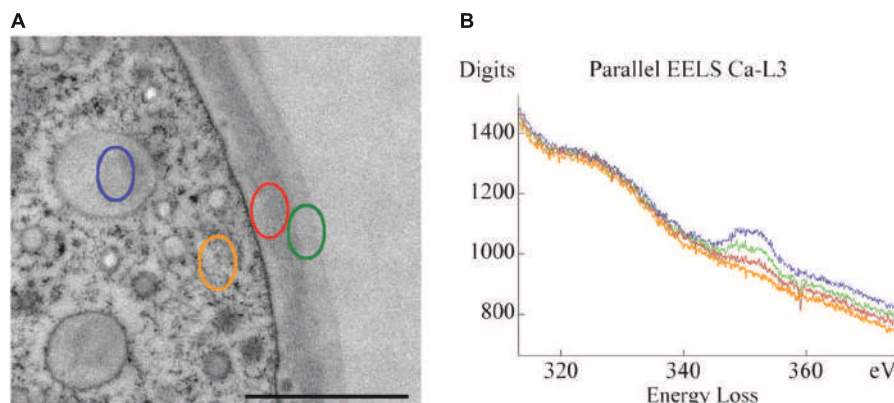


FIGURE 2 | Transmission electron microscopy (TEM) micrograph (A) of cell periphery and primary cell wall of *M. denticulata* with highlighted measurement sites of EEL spectra (scale bar is 1 μm). (B) EEL spectra acquired at the Ca L_{2,3}-edge, indicating calcium binding capacities of different cell components after doping with calcium acetate. Outer side of primary wall (green) has higher calcium binding capacity than inner side (red). Mucilage vesicle (blue) reveal highest calcium binding capacity, the cytoplasm (orange) lowest. Reprinted with permission from Eder and Lütz-Meindl (2008), Copyright[®] 2008 Royal Microscopical Society.

also for protecting the cells against unfavorable environmental conditions (Oertel et al., 2004).

Additional components of the primary cell wall of *Micrasterias* that may be involved in regulation and achievement of growth and morphogenesis are AGPs and hemicelluloses. AGPs are hydroxyproline-rich proteoglycans that have been identified in the plasma membrane and in plant cell walls (Serpé and Nothnagel, 1999) and are involved in growth, development and differentiation of higher plant cells (Knox et al., 1989; Majewska-Sawka and Nothnagel, 2000; Seifert and Roberts, 2007). In *Micrasterias* AGPs have been located in the primary cell wall, in D-vesicles, in parts of the dictyosomes and along the plasma membrane of the non-growing semicell by means of antibodies specific to higher plant AGPs (Lütz-Meindl and Brosch-Salomon, 2000; Eder et al., 2008). Their presence exclusively along the plasma membrane of the non-growing semicell may indicate a regulatory role in growth. As cell wall material containing vesicles are produced at dictyosomes all over the cell and are also transported to the periphery of the non-growing semicell, a barrier function of AGPs as postulated by Kreuger and van Holst (1996) may prevent their fusion in the non-growing part of a *Micrasterias* cell.

The labeling pattern of AGPs by the antibodies JIM8, JIM13 and JIM14 both by immunofluorescence in CLSM and by immunogold labeling in TEM (**Figures 3A,B**) in the primary cell wall suggests an involvement of the recognized AGP type 2 proteoglycans (see Knox et al., 1991; Yates et al., 1996) in cell development of *Micrasterias* (Eder et al., 2008). However, their distribution did not correlate with the cell pattern. The properties of the epitopes recognized at immunodot- and Western blots suggest a similar molecular weight of the AGPs in *Micrasterias* as those of higher plants (Eder et al., 2008). They are rich in galactose and xylose but in contrast to higher plants do not bind to a synthetic glycoside, the β -GlcY reagent (Yariv et al., 1962, 1967) which is generally used for their identification.

The growing primary wall of *Micrasterias* also contains xyloglucans (Eder et al., 2008) similar to those of higher land plants as indicated by fluorescence labeling (**Figures 4A–E**) by an antibody directed against higher plant epitopes (Lynch and Staehelin, 1992). Immuno TEM experiments showed that some of these epitopes are also present in the secondary wall. Binding of this antibody at the *trans*-side and in primary wall material containing vesicles (D-vesicles) suggests that these xyloglucans are secreted in *Micrasterias* similar to higher plant cells. Interestingly the secondary wall of *Micrasterias* (**Figure 4F**) but not the primary wall also contains mixed-linked glucans [(1-3, 1-4)- β -D-glucans; Eder et al., 2008] that belong to the major polysaccharide component of the cell wall of grasses (Gibeaut and Carpita, 1993; Meikle et al., 1994; Trethewey et al., 2005). Similar glucans have also been identified in the alga *Ulva lactuca* and in the liverwort *Lophocolea bidentata* by (1-3, 1-4)- β -D-glucanase digestion (Popper and Fry, 2003).

Analyses of genome-wide transcript expression of synchronized cultures with high percentages of growing cells of *M. denticulata* provided evidence for a role of Rab and SNARE cycles in vesicle fusions and for AGP-like proteins in growth and cell pattern formation (Vannerum

et al., 2011). Additionally the xyloglucan-modifying enzymes xyloglucan endotransglycosylase/hydrolase (XET/XTH), class-III-peroxidases and expansins have been identified as growth and cell shape formation relevant constituents among the 107 genes identified. Phylogenetic analysis suggested that four of the identified genes showed high similarity to the expansin A family of higher plants, although their domain organization was divergent. Overexpression of one of these genes (MdEXP2) resulted in cell shape aberrations. Unfortunately so far only transient transformation is possible in *Micrasterias* (Vannerum et al., 2010). A recent study on the closely related alga *Penium margaritaceum*, however, reporting on a successful stable transformation and reverse genetic analysis (Sorensen et al., 2014) are encouraging also for future studies in *Micrasterias* in this respect.

All these results show that similar to recent results in *Penium* (Domozych et al., 2014) the cell wall of *Micrasterias* generally corresponds to that of higher land plants. However it differs in details, which is of evolutionary interest as these differences may have been crucial for the colonization of terrestrial habitats. For further discussion and additional aspects on the evolution of cell walls and on terrestrialization of Streptophyta see the reviews by Graham et al. (2000), Sorensen et al. (2010, 2012), Domozych et al. (2012), Delwiche and Cooper (2015), Harholt et al. (2016).

Formation of the patterned cell wall in *Micrasterias* requires temporally orchestrated production and precise deposition of cell wall material during development. Timely supply with cell wall material is achieved by highly regulated and synchronized switching of the dictyosomes for producing vesicle populations with different contents as shown by several earlier investigations (for literature see Introduction). Thus precise definition of a developmental stage of *Micrasterias* is easily possible by a TEM image of just a few Golgi bodies and their associated vesicles. As mucilage vesicles are delivered from the dictyosomes consistently, also in non-growing cells (Oertel et al., 2004) dictyosomal activity in *Micrasterias* is maintained continuously during the cell's life cycle. This is contrary to most other plant cells where dictyosomal secretion ceases when growth is completed.

Various cell physiological studies using inhibitors that target different steps of product formation gave insight into the reaction of the secretory machinery and have revealed similarities to higher plant cells. Disturbance of N- or O-linked glycosylations in dictyosomes by tunicamycin and brefeldin A had drastic consequences on Golgi morphology and secretion (Höftberger et al., 1995; Salomon and Meindl, 1996). As in higher plant cells (Satiat-Jeunemaitre et al., 1996) brefeldin A leading to dissociation of COP1 proteins from Golgi membranes (Nebenführ et al., 2002) resulted in a reversible reduction in the number of dictyosomes in favor of the ER in *Micrasterias* (Salomon and Meindl, 1996). In a similar way as thapsigargin (see below), the Ca-ATPase inhibitor cyclopiazonic acid prevented product supply from the ER leading to dilatations of ER cisternae and a reduction on the number of dictyosomal *cis*-cisternae (Höftberger et al., 1995) indicating the importance of calcium for proper secretion. Experimental release of nitric oxide (NO) by donors such as S-nitroso-N-acetyl-DL-penicillamine (SNAP) or sodium nitroprusside (SNP) selectively suppressed secondary

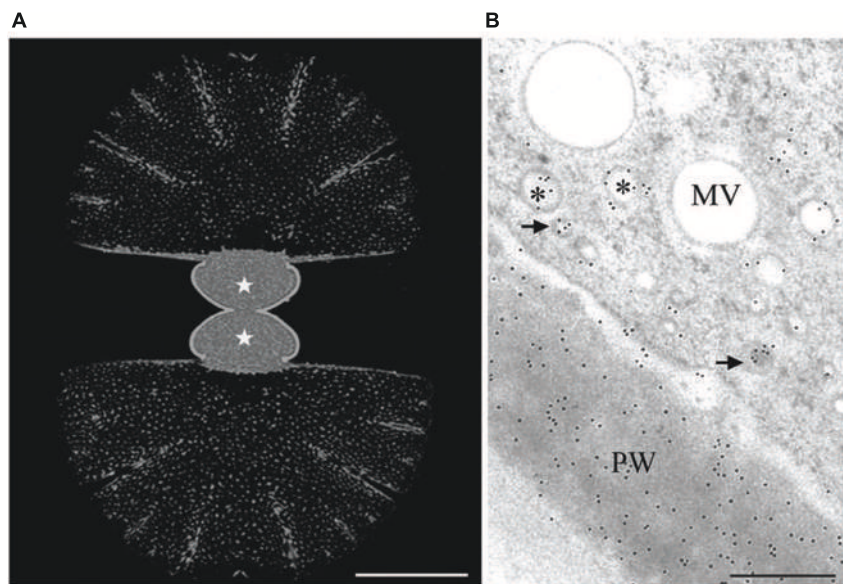


FIGURE 3 | Immuno labeling of growing *Micrasterias* cells by monoclonal anti-AGP antibody JIM13. **(A)** Labeling of the primary wall of both growing semicells (asterisks) visualized in CLSM. The non-growing secondary walls of the old semicells (upper and lower part are not labeled). Scale bar is 50 μm . **(B)** TEM micrograph showing labeling of primary wall (PW) and two different vesicle populations indicated by asterisks and arrows (scale bar is 0.5 μm). Reprinted with permission from Eder et al. (2008), Copyright[©] 2008 Phycological Society of America.

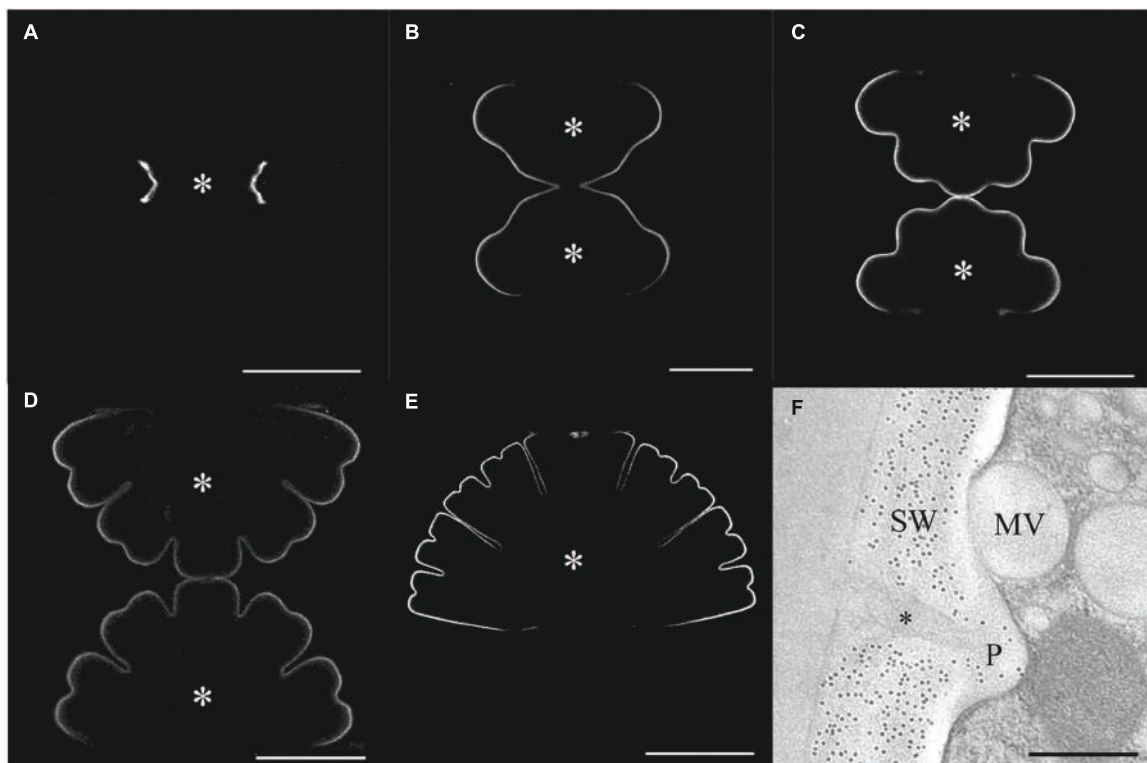


FIGURE 4 | Immuno labeling of the cell wall of developing stages of *Micrasterias*. **(A–E)** Primary wall of different developing stages of *Micrasterias* labeled by polyclonal anti-xyloglucan antibody. Asterisks indicate growing semicells (scale bars are 50 μm). **(F)** Immunogold labeling of the non-growing secondary wall by BG1 antibody recognizing (1-3, 1-4)- β -D-glucans. Mucilage (asterisk) in cell wall pore (P) and mucilage vesicle are not labeled (scale bar is 0.5 μm). Reprinted with permission from Eder et al. (2008), Copyright[©] 2008 Phycological Society of America.

wall formation in *Micrasterias* (Lehner et al., 2009) and impaired dictyosomal function probably via inhibition of enzymes such as glyceraldehyde-3-phosphate-dehydrogenase (GAPDH).

Dictyosomes of *Micrasterias* are unique organelles measuring 2–3 μm in diameter and revealing a constant number of 11 cisternae independent from the stage of the cell cycle. They are thus many times larger than in higher plant cells or in other algae (see also Lütz-Meindl et al., 2015). In growing cells they are located in great number around the nucleus and along the chloroplast membrane. Like in higher plant cells (see e.g., Hawes and Satiat-Jeunemaitre, 2005) they have been shown to be associated with a *cis*-located ER cisternae in TEM. A recent study using focused ion beam milling and block face imaging by field emission scanning electron microscopy (FIB-SEM) has yielded first information on the 3-D architecture of Golgi stacks in *M. denticulata* (Wanner et al., 2013). This method allows 3-D reconstruction of large cytoplasmic volumes up to several hundred μm^3 by 5–10 nm serial slicing. FIB-SEM series and 3-D reconstruction of high pressure frozen and cryo-substituted *Micrasterias* cells showed that the dictyosomes are not only associated with a *cis*-ER cisternae but are surrounded by a huge *trans*-side located ER sheath leading to an almost entire ER envelope around them (**Figures 5A,B**).

Membranes of *trans*-Golgi cisternae were found to be in contact with these *trans*-ER cisternae. This finding is particularly interesting as “*trans*-ER” systems are well known from mammalian cells (for review see Mogelsvang et al., 2004) but not from higher plant cells. It opens new insight into functional interactions between the ER and the Golgi system. Additionally this study indicates that multivesicular bodies regarded as components of the endocytic pathway are in close spatial contact not only with membranes of *trans*-Golgi compartments as postulated in higher plants (see for example Otegui and Spitzer, 2008; Robinson et al., 2008) but also with the *trans*-ER. This may indicate that both membrane systems participate in their formation in *Micrasterias*. Interconnections between dictyosomal cisternae were visualized by FIB-SEM tomography and it was shown that the Golgi stacks consist of flat unfenestrated cisternae with slightly lacerated rims (Wanner et al., 2013).

In summary this section shows that timely coordinated function of the exceptionally large and highly organized dictyosomes of a *M. denticulata* cell, in tight cooperation with its surrounding ER envelope represents a basis for morphogenesis. The products they deliver into the growing primary wall correspond essentially to that of higher plants.

Involvement of the Cytoskeleton in Growth and Morphogenesis

The multi-lobed symmetric morphology of a *Micrasterias* cell may suggest the existence of internal fibrillary axes that provide the basis for shape generation. Early investigators postulated a “cytoplasmic framework” (Waris, 1950b) that has never been verified. Although randomly oriented microtubules have been reported in the cortical cytoplasm of growing *M. denticulata* (Kiermayer, 1968) and *M. pinnatifida* cells by TEM, it has soon

turned out that chemical destruction of these microtubules neither influences growth and cell pattern formation (for summary see Kiermayer, 1981; Meindl, 1993; Lütz-Meindl and Menzel, 2000) nor alters the patterned distribution of cellulose microfibrils in the secondary wall (Schmid and Meindl, 1992). This is contrasting to findings in numerous higher plant cells (e.g., Lloyd and Chan, 2008) and also to results in the closely related desmids *Closterium* (Hogetsu, 1992) and *Penium* (Domozych et al., 2014) both growing at one distinct tip only. It is supposed that the cortical microtubules in *Micrasterias* only represent a cytoplasmic reinforcement of the cell wall (Schmid and Meindl, 1992), while the more centrally located microtubules participate in chloroplast expansion during growth (Meindl and Kiermayer, 1982).

The actin system of *M. denticulata* was visualized by means of microinjection of fluorescently labeled phalloidin into growing cells (Meindl et al., 1994), as well as by phalloidin staining of glutaraldehyde/formaldehyde fixed unembedded cells or by actin-antibody labeling of methyl-methacrylate embedded cells (Pflügl-Haill et al., 2000). While only single actin filaments are present during early developmental stages, a distinct, dense actin filament network extending from the chloroplast surface toward the plasma membrane pervades the growing semicells as soon as cell differentiation starts. The actin cables of this network show high dynamics when labeled with fluorescent phalloidin, but no preferential cell pattern related orientation in growing cells (Meindl et al., 1994). Involvement of the actin cytoskeleton in growth and cell pattern formation in *Micrasterias* is indicated by numerous results. Primary wall material containing D-vesicles are lined up in front of their fusion sites at the lobe tips in high pressure frozen developmental stages indicating a regulatory role of filamentous structures (Meindl et al., 1992). Disturbance of the balance between filamentous actin and its globular subunits (G-Actin) by experimental injection of small amounts of the G-actin-binding protein profilin leads to retardation of growth (Holzinger et al., 1997). Immuno TEM and immuno blot studies have provided evidence for the presence of the actin-binding protein spectrin in the desmids *M. denticulata*, *Closterium lunula* and *Euastrum oblongum* (Holzinger et al., 1999). Additionally spectrins are known to cross-link actin filaments and to accomplish F-actin membrane interactions (for references see Holzinger et al., 1999). In growing *M. denticulata* cells this regulatory protein was found at membranes of different secretory vesicle populations and also on membranes of primary wall material containing D-vesicles. This indicates an involvement of spectrin in actin dependent vesicle transport representing the basis for growth.

Several studies in *M. denticulata* but also in other desmids have clearly indicated that any disruption of the actin filament system causes dose-dependent growth inhibition and severe cell shape malformations up to a complete loss of cell symmetry (summarized in Lütz-Meindl and Menzel, 2000). Coincidentally a breakdown of the actin network in *M. denticulata* has been visualized in CLSM as consequence of incubation with the actin disorganizing drugs latrunculin B and cytochalasin D. Only clusters of non-filamentous actin and short actin filaments

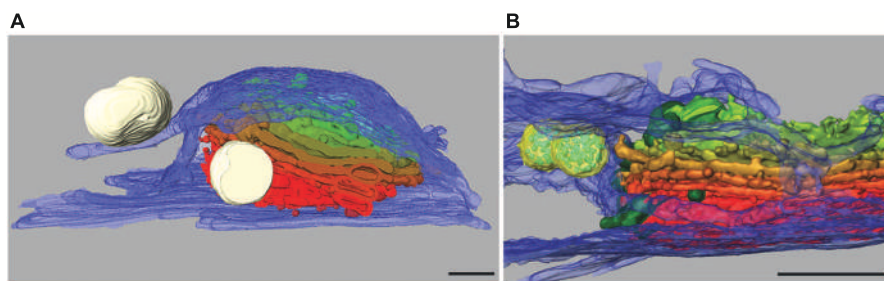


FIGURE 5 | 3-D reconstruction of *Micrasterias* dictyosomes from FIB-SEM series. *Cis*-side in red, *trans*-side in green. **(A)** The entire dictyosome is enwrapped by ER envelope (blue) (scale bar is 1 μm). **(B)** Detail of another dictyosome showing the close spatial interaction between dictyosomal cisternae and the ER. Mucilage vesicles in white, multivesicular bodies in yellow (scale bar is 1 μm). Reprinted with permission from Lütz-Meindl et al. (2015), **(A)** Copyright[®] 2015 Royal Microscopical Society and from Wanner et al. (2013) **(B)**, Copyright[®] 2013 Elsevier Inc.

remained visible after this experimental procedure (Pflügl-Haill et al., 2000). On the other hand also over-stabilization of the actin cytoskeleton in growing *Micrasterias* cells by jasplakinolide (Holzinger and Meindl, 1997) and chondramides (Holzinger and Lütz-Meindl, 2001) results in retardation of cell growth and in severe cell shape aberration in a similar way as induced by the actin depolymerizing agents (see above). In case of jasplakinolide the cells are filled with abnormal aggregations of actin filaments as shown by TEM, while chondramides induce abnormal F-actin lumps or dense F-actin batches in a time dependent manner as visualized by immuno fluorescence or phalloidin labeling. Additionally the internal structural organization of the *Micrasterias* cell is lost and organelles are displaced.

All these studies strongly indicate a regulatory role of the actin system in morphogenesis of *Micrasterias* (see also Lütz-Meindl and Menzel, 2000). Actin filaments are involved in transport of cell wall material containing vesicles to the plasma membrane that is achieved by cytoplasmic streaming. However, inhibition of cytoplasmic streaming induced by any impact on the polymerization status of the F-actin system cannot account for the formation cell shape aberrations, but would only result in retardation or inhibition of growth. The severe cell shape malformations that occur independently from the mode of the F-actin impairment indicate that a functioning F-actin dynamics is indispensable for morphogenesis in *Micrasterias*. These results also emphasize how important it is to have model systems in which growth and morphogenesis can be easily distinguished as it is the case in *Micrasterias*.

Ionic Regulation and Signal Transduction

Early studies have revealed that a local influx of calcium at the growing lobe tips of *Micrasterias* accompanies cell differentiation (Meindl, 1982a). This is in good agreement with findings in tip growing higher plant cells such as pollen tubes or root hairs where the zone of calcium influx corresponds to the area of cell wall expansion (e.g., Hepler and Winship, 2010). During oscillating pollen tube growth stretch-activated calcium channels open and an intracellular tip-focused gradient of cytosolic calcium is established. In *Micrasterias* calcium influx is clearly correlated to cell pattern formation (Meindl, 1982a, 1985; Troxell and Scheffey, 1991; see also Meindl, 1993). When the first pair of indentations

is formed, calcium influx can be found at four symmetrically arranged zones that develop to the four main lateral lobes during the subsequent growth step. As soon as these four lateral lobes, as well as the polar lobe that lags behind slightly, have reached a particular size, the calcium influx pattern splits again and the lobe tips become bifurcated. Due to relative slow growth velocity in comparison to, e.g., pollen tubes, it is not possible in *Micrasterias* to determine whether calcium influxes follow or precede cell wall growth.

Besides the occurrence of multipolar growth and the corresponding simultaneous calcium influxes at several sites, another difference in calcium regulation in *Micrasterias* is apparent when compared to tip growing higher plant cells. Ratio imaging by the calcium indicator fura-2 dextran revealed that no measurable intracellular calcium gradient is established during the outgrowth of the lobes of *Micrasterias* (Holzinger et al., 1995). This result was further corroborated by experimental perturbation of the intracellular calcium level by either injection of BAPTA-type buffers known to dissipate intracellular calcium gradients. As these experiments had no influence on cell growth and pattern formation in *Micrasterias* it was concluded that calcium is only important at the outermost growth zones in the area of the plasma membrane, possibly for fusion of the secretory vesicles. In contrast to tip growing higher plant cells such as pollen tubes (Holdaway-Clarke and Hepler, 2003) cytoplasmic calcium gradients do not seem to be involved in growth and cell shaping of *Micrasterias*.

That local calcium influx is correlated to cell pattern formation was demonstrated in a uniradiate variation of *M. thomasiana* (*Micrasterias thomasiana uniradiata*) in which the cell pattern is only expressed at one half of the cell. Only at the patterned side of the cell calcium influxes were measured or visualized by fluorescent markers, whereas at the non-patterned side no fluorescent signals were visible and outward directed currents were measured (Meindl, 1985; Troxell and Scheffey, 1991). Moreover experiments with ionophores, chelators or calcium channel blockers clearly showed a correlation between the intracellularly available calcium level and cell growth (for references see above and also McNally et al., 1983; Meindl, 1993). It was also demonstrated (Meindl, 1990) that formation of abnormal cell patterns as for example induced by elevated

temperature is accompanied by a shift in the calcium distribution at the plasma membrane suggesting calcium influxes not at the lobe tips but at abnormally growing areas in between (see also below).

Nitric oxide (NO) which is regarded as key molecule for intracellular signaling and is involved in developmental and growth processes of higher plants but also in programmed cell death and defense mechanisms (see e.g., Murgia et al., 2004; An et al., 2005) has been shown to inhibit growth but not morphogenesis in *Micrasterias* (Lehner et al., 2009). The NO donors SNAP and SNP both arrest cell development, impaired dictyosomal function and prevented secondary wall formation. As the NO scavenger cPTIO (2-(4-carboxyphenyl)-4,4,5,5-tetramethylimidazoline-1-oxyl-3-oxide, potassium salt) abrogated SNP induced effects, it was concluded that growth inhibition was due to NO. It was hypothesized that NO inactivates enzymes of the secretory pathway such as GAPDH and thus provokes growth inhibition by preventing supply of cell wall material (Lehner et al., 2009). This indicates that a well-balanced level of NO is required for normal growth of *Micrasterias* cells.

Acetylcholine, one of the best investigated neurotransmitter in animal cells which has also been detected in moss, ferns and higher plants (Miura and Shih, 1984; Tretyan and Kendrick, 1991) has been also shown to be involved in growth and differentiation of *Micrasterias* (Schiechl et al., 2008). *Micrasterias* was the first unicellular alga in which a light-dependent production of acetylcholine has been proved by HPLC-coupled mass spectrometry. Both, cholinergic agonists (carbachol, nicotine) and antagonists (*D*-tubocurarine, hexamethonium) inhibited cell growth and evoked substantial cell shape aberrations when applied to early developmental stages (Figures 6A,B). Particularly the classic acetylcholine-receptor agonist nicotine additionally suppressed formation of the secondary cell wall. The presence of cholinergic receptors in *Micrasterias* was concluded from these results. They are obviously involved in growth of this alga and thus, like in higher plant cells, represent a basis for light induced differentiation (Schiechl et al., 2008).

To finalize this section it must be noted that our understanding of ionic regulation and signal transduction during of cell differentiation in *Micrasterias* is still in its infancy and that further studies will be required to obtain a more comprehensive insight.

STRESS RESPONSES AND ADAPTATION

Temperature

Due to their worldwide distribution from tropical zones up to Polar Regions and high altitude mountains (Brook, 1981) desmids such as *Micrasterias* are generally well adapted to a wide range of water temperatures. On the other hand, even under moderate climatic conditions the small bog ponds the algae inhabit and that usually are not shaded by higher plants, can be exposed to rapidly changing seasonal and diurnal temperature conditions. The cells may face deep frost conditions in winter but also temperatures higher than 30°C during continuing heat periods in summer. While non-growing *Micrasterias* cells are better adapted, developing cells react highly sensitive to temperature changes with respect to growth and morphogenesis (Meindl, 1990; Weiss and Lütz-Meindl, 1999; Weiss et al., 1999).

Low temperature between 3 and 9°C generally retards growth and development in *M. denticulata* cells that were pre-cultivated at 20°C (Meindl, 1990). When exposed in early developmental stages shortly after mitosis, temperatures lower than 3°C inhibit growth of *Micrasterias* cells completely and lead to cell death within 4 h. A temperature range between 4° and 9°C allows growth, but within the 5 h required for normal differentiation at 20°C, only an undifferentiated bulb is formed. Primary wall growth under these low temperature conditions is continued up to 24 h and frequently cell shape malformations arise. They are mostly characterized by a simplification of the cell pattern, yet the basic symmetry of the cell is maintained. Cytoskeleton dependent processes like spreading of the chloroplast and migration of the nucleus back to its central position are retarded.

Temperatures up to 30°C only slightly accelerate the developmental process in *Micrasterias* but have no consequences on cell pattern formation (Meindl, 1990). When the cells are exposed to temperatures between 30 and 33°C the resulting size and cell pattern is clearly reduced. In a range between 33 and 36°C severe shape formations occur. Depending on the precise temperature and on the developmental stage at the beginning of treatment, the malformations are expressed in either a simplification of the cell pattern, or in formation of bizarre asymmetric cell shapes, or in development of multi-lobed cells with a higher number of lobes when compared to shapes formed at 20°C. The shape malformations go along with changes in patterned calcium distribution as indicated by a fluorescent marker (Meindl, 1990). Variations in cell size and pattern formation due to elevated temperature was also found in *M. rotata* indicating high temperature-related phenotypic plasticity (Neustupa et al., 2008).

In *M. denticulata* large areas of heat shock granules surrounded by ER cisternae are frequently found in the cytoplasm during elevated temperature (Meindl, 1990). The heat shock

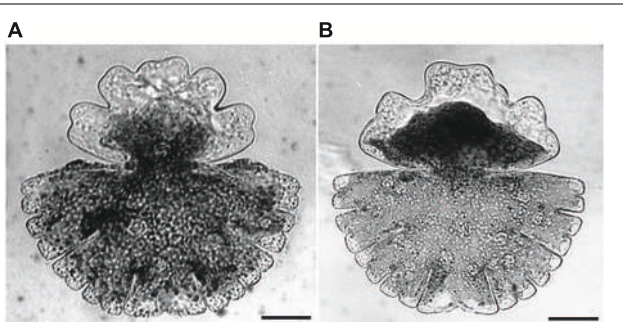


FIGURE 6 | Cell shape malformations of growing *Micrasterias* cells treated with the cholinergic antagonist *D*-tubocurarine (A) and with the agonist nicotine (B) during growth (scale bars are 30 μm). Reprinted with permission from Schiechl et al. (2008), Copyright© 2008 Elsevier Ireland Ltd.

proteins hsp70 and BiP (binding protein) were detected by immuno-blotting. Hsp70 was found to be increasingly expressed after continuous or repeated experimental heat exposure (Weiss and Lütz-Meindl, 1999). Heat induced *de novo* synthesis of hsp70 reached its maximum after 9 h continuous heat exposure which corresponds well to findings in higher plant cells (see e.g., Ougham and Howarth, 1988). Within a certain temperature range (15 – 39°C), the intensity of the heat response in *Micrasterias* depends on the preceding cultivation temperature and on the duration of the heat exposure. Cells cultivated at 25°C generally react much weaker to heat than those grown at 15 or 20°C, indicating their distinct adaptive abilities (Weiss et al., 1999). Heat induced disturbance of cell shape formation is more pronounced after pre-cultivation at 15 and 20°C than at 25°C. In contrast, cell division rates are reduced more severely by heat after pre-cultivation at 25°C than after 20 or 15°C. Independent from the cultivation temperature, photosynthetic activity and respiration measured by polarographic oxygen production/consumption increase continuously and reach a peak in a range between 30 and 32°C. Thereafter photosynthesis drops to zero at 40°C after pre-cultivation at 15° but declines less distinctly after pre-cultivation at 20 or 25°C. These results show that the optimum temperature for photosynthesis in *Micrasterias* is similar to that determined in higher plants of temperate areas (Larcher, 2001) and that primary energy balancing processes such as photosynthesis and respiration are less affected by elevated temperature than cell division rates and cell shaping (Weiss et al., 1999). This fact may represent an important strategy for survival of the cells in their natural habitats. Good adaptation to different temperature regimes with respect to photosynthetic activity was also shown in closely related desmids collected at different climate zones (see for example Stamenkovic and Hanelt, 2013).

UV Irradiation

Micrasterias denticulata cells show surprising high tolerance against experimental UV irradiation down to cut-off wavelength of 284 nm when exposed in the presence of white light in a sun simulator (Meindl and Lütz, 1996). Even in the sensitive stage of cell development, growth and pattern formation as well as cytoplasmic streaming are not affected by a 5 h treatment. When UV exposure is extended or the cut-off wavelength is lowered to 280 nm or 275 nm cell growth and differentiation are inhibited, cytoplasmic streaming is retarded, vacuoles are formed and the distribution of the large chloroplast that fills each semicell is disturbed. Drastic alterations of chloroplast structure ending up in more or less complete disintegration of grana and stroma thylakoids were observed (Lütz et al., 1997). These ultrastructural changes are reflected in a continuous decrease of photosystem II (PSII) activity as measured by fast chlorophyll fluorescence. The ratio between variable and maximum fluorescence (Fv/Fm ratio) reached very low levels around 0.1 after 1 h exposure to 280 nm or 275 nm UV cut-off wavelength, whereas untreated controls at culture conditions reached an averaged Fv/Fm value of 0.76. Photosynthetic oxygen production is maintained even at high UV irradiation with cut-off wavelengths of 275 nm for 15 min, but is completely suppressed upon prolonged treatment (Lütz et al., 1997).

In addition to the breakdown of chloroplast structure and photosynthesis the endomembrane system reacts distinctly to irradiation with low UV cut-off wavelengths. As a typical hallmark for stress (see below) the dictyosomes become involute, the number of their cisternae decreases and vesicle production is either reduced or completely inhibited (Meindl and Lütz, 1996). Abnormally large sheets of ER cisternae pervade the cytoplasm and microtubule re-polymerization during nuclear migration is prevented.

In summary these results show that like other desmids (see e.g., Holzinger and Lütz, 2006; Holzinger et al., 2009) *Micrasterias* is highly adapted to UV-B irradiation, which may explain the worldwide distribution and the presence of this group of algae even in high mountain areas or Polar Regions. It remains to be investigated how the considerable UV-B resistance of *Micrasterias* is achieved. As in other algae, a protecting function of the surrounding mucilage envelope or of the thick secondary cell wall, absorbance by particular metabolites and/or a very well developed physiological repair system may account for it (Oertel et al., 2004; Remias et al., 2012; Kitzing et al., 2014).

Oxidative Stress

Unfavorable environmental conditions such as UV irradiation, high light intensities, drought, salinity or man-made entry of heavy metals by traffic or agricultural practices, as well as compounds like herbicides may cause oxidative stress in higher plants but also in aquatic photosynthetic organisms. Among the different reactive oxygen species (ROS) hydrogen peroxide (H_2O_2) represents a key molecule in biotic and abiotic stress and induces programmed cell death (PCD) in plant and animal cells.

Experimental application of H_2O_2 causes severe ultrastructural and physiological alterations in *M. denticulata* (Darehshouri et al., 2008). Swelling of mitochondria with simultaneous reduction of cristae, increase in the volume of ER as well as bending of dictyosomes associated with a bulging of their *cis*-cisternae and inhibition of vesicle production at the *trans*-side are the most pronounced structural effects of short-term H_2O_2 exposure. Photosynthetic activity measured by fast chlorophyll fluorescence decreased in these cells to Fv/Fm values of around 0.3 (see above). As the activity of caspase-like proteins known to be involved in PCD of plant cells (van Doorn and Woltering, 2005) increases in *Micrasterias* during H_2O_2 impact, it is likely that the cells undergo PCD. This is also corroborated by the fact that cell vitality is maintained, chromatin is slightly condensed and the increase in caspase-like activity is abrogated by a “classical” caspase-3-inhibitor (Darehshouri et al., 2008). Although molecular participants in PCD are not yet known these results clearly point toward the capability of *Micrasterias* to undergo PCD. This is in good agreement with studies on other unicellular algae such as *Dunaliella* (Segovia and Berges, 2005) or *Chlorella* (Zuppini et al., 2007) but represents the first report on PCD in a desmid. The physiological importance of PCD in *Micrasterias* may be explained by “altruistic cell death” (see also Lee et al., 2002). Under unfavorable environmental conditions PCD of a large number of cells may be beneficial for the survival of the population at their natural habitat. The surviving cells may use dead cells and the mucilage obtained from them for

protection against further environmental impact (Darehshouri et al., 2008).

Oxidative stress following different kinetics of increased ROS production is also evoked in *Micrasterias* as consequence of experimentally elevated salinity, osmotic stress and by exposure to different heavy metal solutions (see below).

High Salinity

In the small bog ponds that desmids like *Micrasterias* inhabit, the algae may face rapidly changing osmolarities of their surroundings water by evaporation during high temperature periods as well as by dilution during rain. Additionally the cells are endangered by increase in salinity which may occur due to agricultural practices such as fertilization or to road salt. In contrast to salt tolerant green algae such as *Dunaliella*, *Chlamydomonas* or *Chlorella* that have developed metabolic strategies to cope with elevated salinity (Peláez et al., 2004; Yoshida et al., 2004; Takagi et al., 2006; Goyal, 2007) particularly large-cell desmid such as *Micrasterias* usually growing only in rain-supplied acid bogs, are not at all adapted to increasing salt concentrations. This means that high salinity may represent a severe danger to the population.

In an early study (Meindl et al., 1989) it was demonstrated that the osmolarity of the nutrient solution markedly influences cell division rates of *M. denticulata*. An experimental increase in the osmolarity of the nutrient solution from the usual level (lower than 2 mosm/kg) up to 26 mosm/kg results in a steady decrease of the cell number as indicated by a particular cell division assay (Meindl et al., 1989). It ends up in a complete arrest of cell divisions at the highest osmolarity. *Micrasterias* cells that are not able to divide under these circumstances accumulate high amounts of starch grains, plastoglobules and oil bodies in their chloroplasts. Vacuoles of these cells appear highly electron dense in TEM indicating high salt accumulation. All together the appearance of these cells corresponds to storage stages that are also found at their natural habitats in winter or early spring (for further discussion and literature see Meindl et al., 1989). Interestingly cells kept at high osmolarity start dividing within 1 day when osmolarity is diminished in recovery experiments. This indicates that changes in osmolarity of the surrounding medium are important for switching off the cells from an inactive storage to an active division stage. The fact that during winter or other unfavorable environmental conditions such as drought, cell division is arrested, guarantees survival of the population by maintaining their energy balance. Dilution of the surrounding medium by rain immediately induces cell divisions.

Experimental addition of KCl or NaCl to the culture medium leads to severe ultrastructural and physiological changes in *M. denticulata* that can be clearly distinguished from changes induced by osmotic stress (Affenzeller et al., 2009a,b). KCl (200 mM) caused the most pronounced effects by inducing foam-like vacuolization of the cytoplasm and severe morphological changes of mitochondria even after 3 h incubation. The outer membrane of all mitochondria showed balloon-like protrusions and their matrix appeared condensed indicating a kind of shrinkage induced by KCl induced intra-organelle osmotic changes (Figure 7A). Similar structural alterations

of mitochondria are known from higher plant cells under anoxic conditions (Virolainen et al., 2002) and also from nerve cell during PCD (Muriel et al., 2000). Interestingly the severe structural changes did not influence their function in *Micrasterias*. Respiration in KCl exposed cells was not decreased (Affenzeller et al., 2009b).

In contrast, function of the endomembrane system was considerably impaired. ER cisternae were swollen and dramatically increased in number, whereas the cisternal number per Golgi stack decreased. Single dictyosomal cisternae were detached from the stack, both at the *cis*- and the *trans*-side. The remaining dictyosomal cisternae were completely inoperable as vesicles were no longer found in their proximity (Affenzeller et al., 2009b). When KCl treatment was continued for up to 24 h, degrading dictyosomes consisting of only two or three coiled cisternae were frequently found in contact with large ER compartments. 3-D analyses by FIB-SEM tomography provided evidence for the dictyosomal degradation process that occurred as consequence of KCl stress (Figure 8; Lütz-Meindl et al., 2015). Dictyosomal degradation starts with detachment of single cisternae from a stack. These cisternae form balls that may contain other cisternae of the same stack (Figures 7B,C). They increase in size by fusion with ER compartments and are finally absorbed by huge ER cisternae that pervade the cytoplasm. In contrast to our earlier assumptions (Affenzeller et al., 2009a,b) dictyosomes in *Micrasterias* are not disintegrated via autophagy. Although detailed studies on stress-induced dictyosomal disintegration are still missing there is also no evidence in the literature for autophagic degradation of dictyosomes in higher plant cells. Comprehensive articles that summarize selective autophagy in plants (Michaeli and Galili, 2014) report on autophagy of ER, mitochondria, plastids and peroxisomes, but not of dictyosomes.

Nevertheless structural hallmarks for autophagy do occur in salt stress *Micrasterias* cells. Both in NaCl and KCl exposed cells double membranes deriving from the ER partially surround or completely engulf peroxisomes indicating pexophagy (Affenzeller et al., 2009b). It seems that this autophagic process accompanies salt stress induced PCD. After both treatments cell vitality drops after 12 h exposure and is reduced to about 10% of controls after 48 h KCl incubation. DNA of NaCl and KCl treated *Micrasterias* cells fragments into discrete pieces of about 180 bp, a process referred to as DNA laddering and regarded as hallmark for PCD both in plant and animal cells (for discussion see Affenzeller et al., 2009a,b). DNA laddering occurs only after NaCl and KCl stress in *Micrasterias* but not after iso-osmotic sorbitol stress indicating that the ionic rather than the osmotic component of salt stress induces PCD. This is also reflected in the kinetics of ROS production. Like in higher plant cells (Zhu, 2001, 2002) salt stress in *Micrasterias* also causes enhanced ROS formation. Whereas the ROS level increases continuously within 3 h during osmotic sorbitol stress in *Micrasterias* it rises dramatically within 5 min during KCl and NaCl stress and then drops down to control level within 3 h (Affenzeller et al., 2009b). Because ROS are known as regulatory signals in cellular defense including PCD in higher plant cells (Lin et al., 2006) these different kinetics may be crucial for the induction of PCD. That cell death provoked by

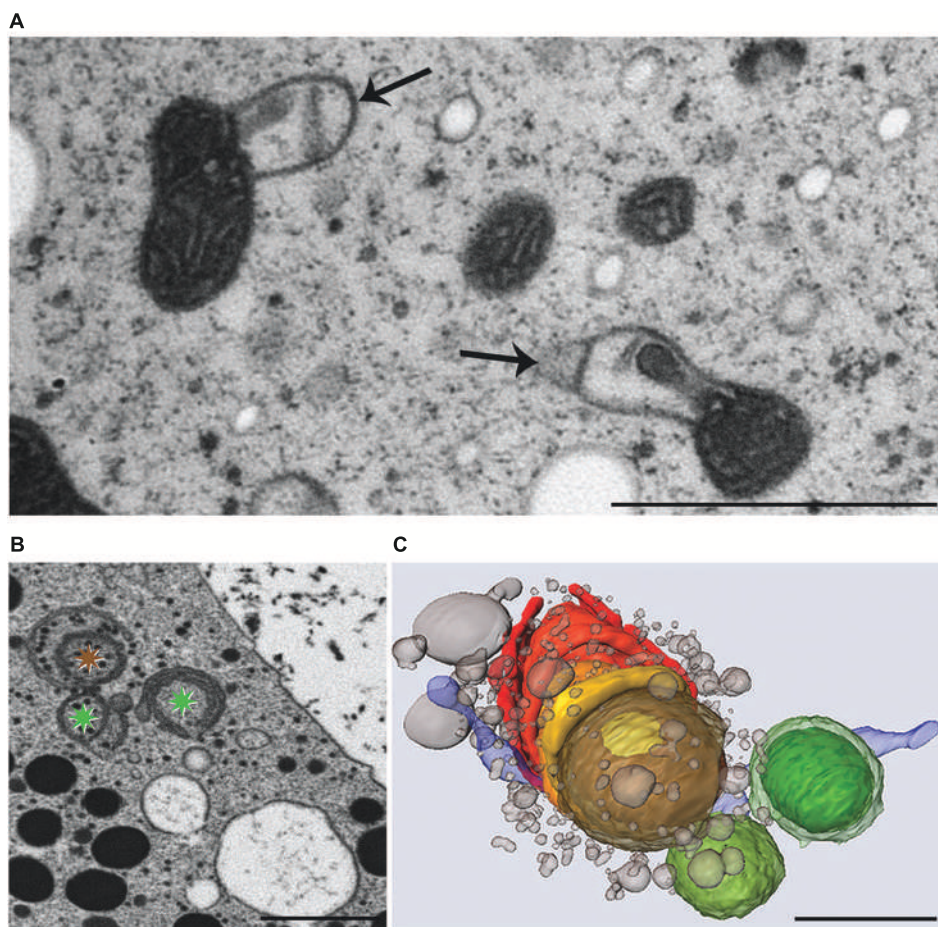


FIGURE 7 | Transmission electron microscopy micrographs of mitochondria (A), FIB-SEM image of degrading dictyosome (B) and 3-D reconstruction of degrading dictyosome from FIB-SEM series (C) after exposure of *Micrasterias* to KCl. (A) Mitochondria with balloon-like protrusions of outer membrane and condensed matrix. (B) The colored asterisks indicate parts of the dictyosome that are reconstructed in (C). (C) The reconstruction shows that the dictyosomal cisternae form balls during degradation. Remnants of dictyosomal cisternae in red, ER in blue, small vesicles represent degradation products of cisternae. Scale bars are 1 μ m. (B,C) Reprinted with permission from Lütz-Meindl et al. (2015), Copyright[©] 2015 Royal Microscopical Society.

salt stress in *Micrasterias* is an active process indicated by the fact that all structural alterations as well as DNA laddering occur at a point of time when metabolism is still unaffected. This is indicated by measurements of respiration, photosynthetic activity and plastid pigment composition.

By means of TEM-coupled EELS and statistical analyses, the chloroplast was determined as the main site of ROS, respectively H₂O₂ production in salt stress exposed *Micrasterias* cells (Darehshouri and Lütz-Meindl, 2010). Precipitation with cerium chloride also showed increased H₂O₂ levels in mitochondria, the cytoplasm and at the plasma membrane. The latter indicates an activation of the plasma membrane associated NADPH oxidase by salt stress, whereas the high values in the cytoplasm may result from ROS release by chloroplast and mitochondria (Darehshouri and Lütz-Meindl, 2010).

In summary, these studies show that imbalance of ionic homeostasis induced by salt stress, as in higher plant cells and yeast (Huh et al., 2002) triggers PCD in the theoretically “immortal” alga *Micrasterias*. By comparison to cell death events

evoked by oxidative stress (see above) it becomes evident that one and the same organism is capable of performing different PCD pathways. This suggests that different stress inducers may activate different cellular reactions. An increase in caspase-3-like activity as found after oxidative stress in *Micrasterias* (Darehshouri et al., 2008) cannot be measured during salt stress (Affenzeller et al., 2009b). In contrast, DNA laddering accompanying cell death after salt stress does not take place during oxidative stress.

Heavy Metal Impact

Increasing environmental pollution due to progressive traffic and industrial as well as agricultural production leads to the release of heavy metals into air, soil and water. Particularly aerosols generated by burning fossil fuels may enter ecosystems with high humidity such as peat bogs. It was demonstrated in several studies (e.g., Syrovetsnik et al., 2004) that metals such as zinc, copper and cadmium may exceed the maximum permissible concentration in peat bogs by a factor of three or even higher.

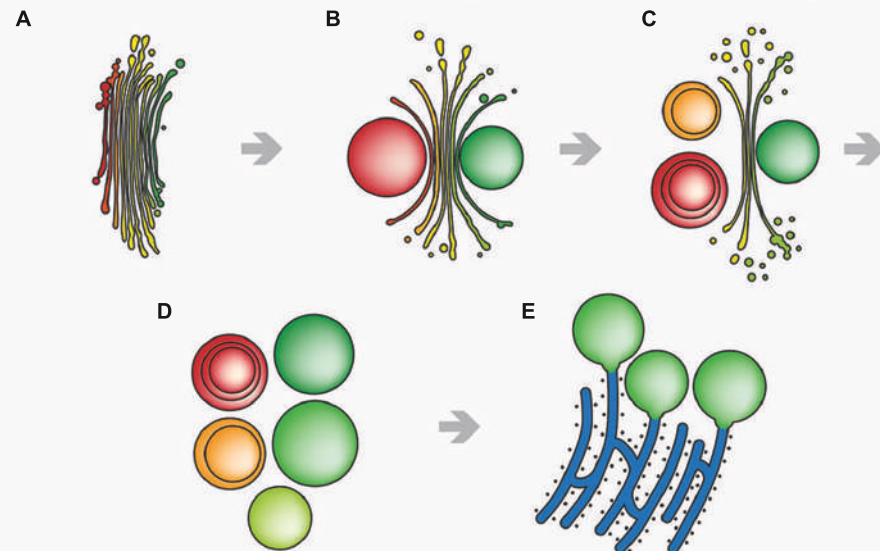


FIGURE 8 | Schematic drawing of stress-induced degradation of dictyosomes in *Micrasterias*. (A) Control dictyosome with 11 cisternae (cis-side in red). (B) Beginning degradation, outermost cis- and trans-cisternae form balls. (C) Proceeding degradation and reduction of cisternal number. Cisternal balls include other cisternal balls. Numerous degradation products are visible close to the degrading dictyosome. (D) Dictyosome has completely disintegrated into balls. (E) The cisternal balls fuse with long, stress-induced ER cisternae. Reprinted with permission from Lütz-Meindl et al. (2015), Copyright © 2015 Royal Microscopical Society.

The low pH characteristic for peat bogs and ranging between 3.5 and 6.8 may increase the solubility of metals and thus enhances the threat to the ecosystem via accumulation of metals. Large-celled desmids such as *Micrasterias* growing exclusively under oligotrophic conditions are extremely sensitive to any contamination (Lenzenweger, 1996), particularly during their development.

Morphogenesis and cell development of *M. denticulata* are negatively affected by Zn, Al, Cd, Cr and Pb when applied at the highest concentrations that still allowed cell growth and decrease cell division rates in long-term experiments (Volland et al., 2011, 2012, 2014; Andosch et al., 2012). Correspondingly, photosynthetic activity measured by means of oxygen production and by fast chlorophyll fluorescence is reduced by almost all metals or completely abolished as in the case of CrVI. It reveals even negative values by application of low concentrated Cd (0.6 µM). Respiration in *Micrasterias* is markedly stimulated by every metal stress with highest values in Cu treated samples. This is not surprising as the repair and defense mechanisms induced by metal stress require high amounts of ATP. A similar increase in respiration during stress has been identified in *Micrasterias* during other stress scenarios (see above) and is also well known from stress response in higher plant cells (Larcher, 2001).

Plant cells and particular algae have different possibilities to cope with metal pollutants (see for example Rai and Gaur, 2001). In order to limit cytoplasmic metal concentrations they may attach metals to the extracellular matrix (cell wall and/or mucilage layer), actively excrete them into their surroundings or they may compartmentalize them in vacuoles or other

storage compartments which frequently occurs by complexation by phytochelatines, metallothioneins or strong chelators. To understand cellular metal detoxification and tolerance mechanisms it is thus important to determine intracellular targets of metals and to localize metals intracellularly. By means of TEM analyses and EELS (see above) that allows identification and semi-quantitative determination of element concentrations at highest possible spatial and energy resolution (see Lütz-Meindl, 2007) intracellular metal effects and sites of metal sequestration were determined in *M. denticulata*. It was shown that **aluminum** is only bound to the cell wall of *Micrasterias* when applied in long-term experiments. It was not found intracellularly but it induces abnormal depositions of primary material when applied during growth. This indicates that its binding to the cell wall matrix changes physical properties of the wall that account for the abnormal depositions and also for the shape malformations that are induced (for details and further discussion see Volland et al., 2011).

Similar results have been obtained after incubation of *Micrasterias* cells with **lead** that leads to severe cell shape malformation but is neither found in the cell wall nor in any intracellular compartment. It does not evoke any ultrastructural changes nor does it influence photosynthetic activity (Volland et al., 2014). It is therefore suggested as with Al, that Pb effects in *Micrasterias* are due to replacement of pectin-bound Ca²⁺ by the metal and that the arising changes in primary wall plasticity are responsible for the disturbed cell pattern formation. In fact Pb effects on cell shaping of *Micrasterias* could be almost completely abrogated by addition of Ca or Gd. The effects of inorganic lead in *Micrasterias* described above are in good agreement with

findings of an earlier study where it was shown that PbCl_2 caused bursting of the cells without any visible ultrastructural changes (Meindl and Röderer, 1990). In contrast, organic triethyl lead which was used as antiknock additive in fuels, evoked severe disturbance of the endomembrane system and of secondary cell wall formation.

High Ca^{2+} -binding abilities of cell wall pectins have been shown for Al in *Micrasterias* (Volland et al., 2011) and have been suggested for Pb for example in moss (Krzesowska et al., 2004). In this way the cell wall may act as a kind of filter by accumulating the metals thus preventing more severe intracellular damage. The result that Pb does not enter *Micrasterias* cells does not correspond to findings in higher plants, where Pb was frequently found to be taken up into the cytoplasm and to affect intracellular components (e.g., Jiang and Liu, 2010). It must be mentioned, however, that the considerable energy loss at the Pb $\text{M}_{4,5}$ edge that was taken for identification of Pb by EELS and that induces unfavorable signal to noise ratios, may have prevented detection of low Pb amounts in *Micrasterias* cells (for discussion see Volland et al., 2014).

Zinc and copper were identified in cell wall precipitations of *Micrasterias* after long-term exposure (Volland et al., 2011). Additionally, both metals were found in mucilage vesicles which are secreted steadily in *Micrasterias*. Elimination of metals from the cytoplasm by using mucilage vesicles as fast vehicles seems to represent an important detoxification mechanism in *Micrasterias*. Increased mucilage production has been frequently observed in this alga under different stress scenarios. An increased number of structural interactions between mucilage vesicles and different cellular compartments are generally found in *Micrasterias* cells during stress. In lower number they are also visible in untreated high-pressure frozen *Micrasterias* cells in TEM (Aichinger and Lütz-Meindl, 2005) and have been interpreted as degradation and/or detoxification mechanisms for maintaining normal cellular turnover.

Zn is additionally compartmentalized in vacuoles of *Micrasterias* which become electron dense upon continuing Zn influence. Along with elevated oxygen levels in the same areas, a sequestration of Zn as oxide is indicated. A crucial role of the vacuole in metal detoxification has been frequently demonstrated in higher plants. In the metal-tolerant plants *Cardaminopsis* and *Armeria* (Neumann and zur Nieden, 2001; Heumann, 2002) as well as in *Zea* (Jiang et al., 2007) the vacuole was shown to be the main depot for Zn. In *Micrasterias* the relatively high tolerance to Zn concentrations up to $30 \mu\text{M}$ is probably due to the ability of the cell to compartmentalize the metal in the cell wall and in vacuoles and to excrete it via mucilage production (Volland et al., 2011). In its ability to survive relatively high Zn concentrations at least for a limited period of time *Micrasterias* corresponds to the Zn-tolerant green alga *Stigeoclonium* growing in polluted mining water and producing high amounts of phytochelatine-related peptides (Pawlak-Skowronska, 2003).

Among all metals investigated Cu is compartmentalized the best in *Micrasterias*. Besides sequestration in the cell wall and in mucilage vesicles Cu was also found as precipitates in starch

grains where it may help to avoid toxic effects as long as starch is not catabolized (Volland et al., 2011). Long-term experiments revealed that non-growing *Micrasterias* cells can cope with low concentrated Cu for a limited period of time of 3 weeks as indicated by an only slight reduction of both photosynthetic efficiency and cell division rates. Nevertheless, as in other algae such as diatoms or the green algae *Chlorella* and *Chlamydomonas* (Nassiri et al., 1997; Mehta and Gaur, 1999; Franklin et al., 2000) Cu induces severe toxic effects in *Micrasterias* and leads to cell death in concentrations above $0.4 \mu\text{M}$. The high redox potential of Cu ions may cause its extreme toxicity to algae that led to its use as algicide.

Chromium widely used in industry and existing in two oxidative states has severe inhibitory effects on *M. denticulata* (Volland et al., 2012). Whereas cell development and pattern formation is almost completely suppressed by 1 mM solutions of both CrIII and CrVI, only CrVI evoked a complete arrest of cell divisions even when applied in the low concentration $5 \mu\text{M}$ for 3 weeks. Increased vacuolization, condensed cytoplasm, swollen mitochondria and involute dictyosomes were the main ultrastructural alterations after exposure of *Micrasterias* to CrVI. They are regarded as general stress hallmarks (see also salt- or other metal stress). Additionally and more specifically, electron dense precipitations in bag-like structures were found in random distribution along the inner side of the cell wall under CrVI impact. The latter structures contained Cr as measured by EELS along with elevated levels of iron and oxygen. As these Cr containing bags were located outside of the plasma membrane these results indicate that Cr is extruded from the *Micrasterias* cell in form of an iron-oxygen compound (Volland et al., 2012).

By means of atomic emission spectroscopy it was found that untreated *Micrasterias* control cells contain considerable amounts of about 1.3 g Fe/kg dry weight whereas the Cr content ranged around 5.8 mg/kg dry weight. When the cells are exposed to $10 \mu\text{M}$ CrVI, the Cr:Fe ratio shifted in favor of chromium from 1:200 to 1:1.5 after only 1 week. This implies that Cr in *Micrasterias* is taken up instead of Fe, which is also corroborated by the fact that divalent ions of Fe, Zn and Ca are able to diminish effects of Cr in *Micrasterias* (Volland et al., 2014). A similar competition between Cr, Fe, S and P for carrier uptake is also known from higher plant cells (Shanker et al., 2005) and Cr was shown to displace other metals and particularly Fe from reaction centers (Pandey and Sharma, 2003). In *Micrasterias* Cr uptake was decreased when the cells were treated with Fe prior to Cr exposure and Cr accumulations in "bags" were no longer measurable by EELS under these conditions. Cr also triggered rapid ROS formation in *Micrasterias*. Interestingly the induced ROS kinetics in *Micrasterias* followed a double peak, which is known to be indicative for oxidative burst known as defense mechanism in higher plants particularly as consequence of pathogen attack leading to PCD around the infection site (e.g., Mandal et al., 2011).

These investigations show that Cr in both oxidative states is readily taken up into the alga *Micrasterias* although Cr represents an unessential nutrient. Like in higher plant cells the highly water soluble anion CrVI is more toxic in *Micrasterias* than the

cation CrIII. CrVI induces severe impact on ultrastructure and physiology of *Micrasterias* and interferes with Fe homeostasis.

Among all metals tested on *Micrasterias* **cadmium** was the only one that, though extremely toxic to physiology and ultrastructure of the cells, was not compartmentalized intracellularly at all (Volland et al., 2011; Andosch et al., 2012). Cd is highly water soluble and enters aquatic ecosystems and soils mainly as consequence of anthropogenic activities such as disposal of electronic components. It represents a severe threat to human health by getting into the food chain via accumulation by plants (Templeton and Liu, 2010). Besides its severe negative implications on cell pattern formation, growth, photosynthetic activity and cell division (see above) it induces dictyosomal disintegration and autophagy in *Micrasterias* in concentrations of 150 μM (Andosch et al., 2012). Even a 1 h exposure to Cd resulted in a dramatic disturbance of ultrastructure, morphology and function of dictyosomes. The 11 cisternae of a control Golgi stack of *Micrasterias* were reduced to a maximum of 4 on the one hand, whereas on the other hand dictyosomal clusters that have completely lost their *cis-trans*-polarity (**Figure 9**) were found in Cd exposed cells. Vesicles were no longer found at the cisternal rims or in surrounding of the dictyosomes indicating a loss in secretion activity. The remaining inoperable dictyosomes consisted of only a few ring-shaped cisternae that were frequently surrounded by dilated ER cisternae (Andosch et al., 2012). Different stages of autophagosomes and autophagic vacuoles enclosing organelles, cytoplasmic portions or mucilage vesicles were present. Although cell viability was not affected, prolonged treatment with Cd for 1 day resulted in an almost complete depletion of dictyosomes in *Micrasterias*.

Similar to the results obtained during KCl stress, evidence was provided for a non-autophagic degradation of dictyosomes by means of FIB-SEM tomography also in Cd treated cells (Lütz-Meindl et al., 2015). **Figures 10A–E** show TEM images and a 3-D reconstruction of a dictyosome during beginning disintegration. Both at the *cis*- and the *trans*-side detached cisternae form balls whereas the remaining middle cisternae of a stack appear bent

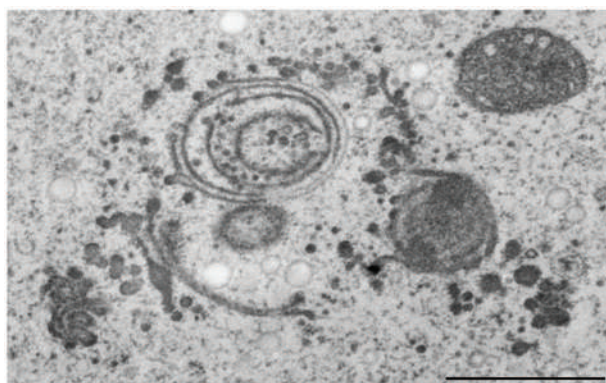


FIGURE 9 | Transmission electron microscopy micrograph of abnormal cluster of dictyosomes induced by treatment of *Micrasterias* with CdSO_4 . Scale bar 1 μm .

and their rims are markedly lacerated. This indicates that stress induced dictyosomal degradation follows the same way after salt stress and Cd exposure (see also **Figure 8**). Also the kinetics of ROS production during Cd exposure of *Micrasterias* corresponds to that during salt stress (Andosch et al., 2012). ROS production increases by a factor 7 within the first 30 min of Cd stress and drops down almost to control level after 4 days.

There are several indications that Cd exerts its negative effects on cell development, physiology and ultrastructure of *Micrasterias* by disturbing Ca homeostasis (Andosch et al., 2012). For example, Cd induced disturbance of structural and functional integrity of dictyosomes in *Micrasterias* can be mimicked by thapsigargin an inhibitor of plant and animal Ca^{2+} -ATPase. This corresponds to results obtained in yeast where it was shown that Cd may affect Ca dependent Golgi ATPases (Lauer et al., 2008) that are also present in plant Golgi membranes (Ordenes et al., 2002). Abnormal cluster formation of dictyosomes during Cd exposure (see above) suggests a disturbing effect on the actin cytoskeleton that positions the Golgi bodies in desmids (see e.g., Url et al., 1993), via disturbance of Ca levels. Moreover addition of Ca to the culture medium prior to Cd exposure has been shown to prevent adverse Cd effects both on chloroplast structure and on photosynthetic activity in *Micrasterias* (Andosch et al., 2012). Also, the calcium channel blocker Gd was able to almost completely reverse negative impact of Cd on developing *Micrasterias* cells (Volland et al., 2014).

The ameliorating effects of Ca on Cd induced ultrastructural and physiological disturbances in *Micrasterias* are not surprising because of the ionic similarities between Ca and Cd. This implies that Cd may substitute Ca in essential metabolic pathways and may for example also bind to calmodulin. In case of its photosynthesis inhibiting effect, it obviously displaces Ca from the catalytic core of the photosystem II-water-oxidizing complex as shown in higher plants (Bartlett et al., 2008). Addition of Ca to the culture medium may then reactivate photosynthesis by preventing Cd uptake and binding (see also Volland et al., 2014). As similar ameliorating effects were observed after addition of Fe it was concluded that uptake of Cd is mediated in *Micrasterias* cells via both Ca and Fe plasma membrane channels (Volland et al., 2014).

By means of UPLC-mass spectrometry it was shown that Cd induces formation of phytochelatins in *Micrasterias* (Volland et al., 2013). Phytochelatins are known to be involved in detoxification of metals in higher plants (Ernst et al., 2008), fungi (Krauss et al., 2011) and green algae such as *Chlamydomonas* (Bräutigam et al., 2009) and others. Identification of PC₂, PC₃, and PC₄ after 3 weeks exposure to Cd was the first proof of phytochelatins in an alga of the division Streptophyta (Volland et al., 2013). As the glutathione level of Cd treated cells was not significantly elevated it is assumed that glutathione required for phytochelatin biosynthesis is constantly supplied. It remains to be investigated in which way phytochelatins are involved in Cd detoxification in *Micrasterias*. Phytochelatines were neither detected in control cells nor in Cu exposed *Micrasterias* cells.

In summary these results show that physiological reactions of *Micrasterias* to different metals are similar, comprising

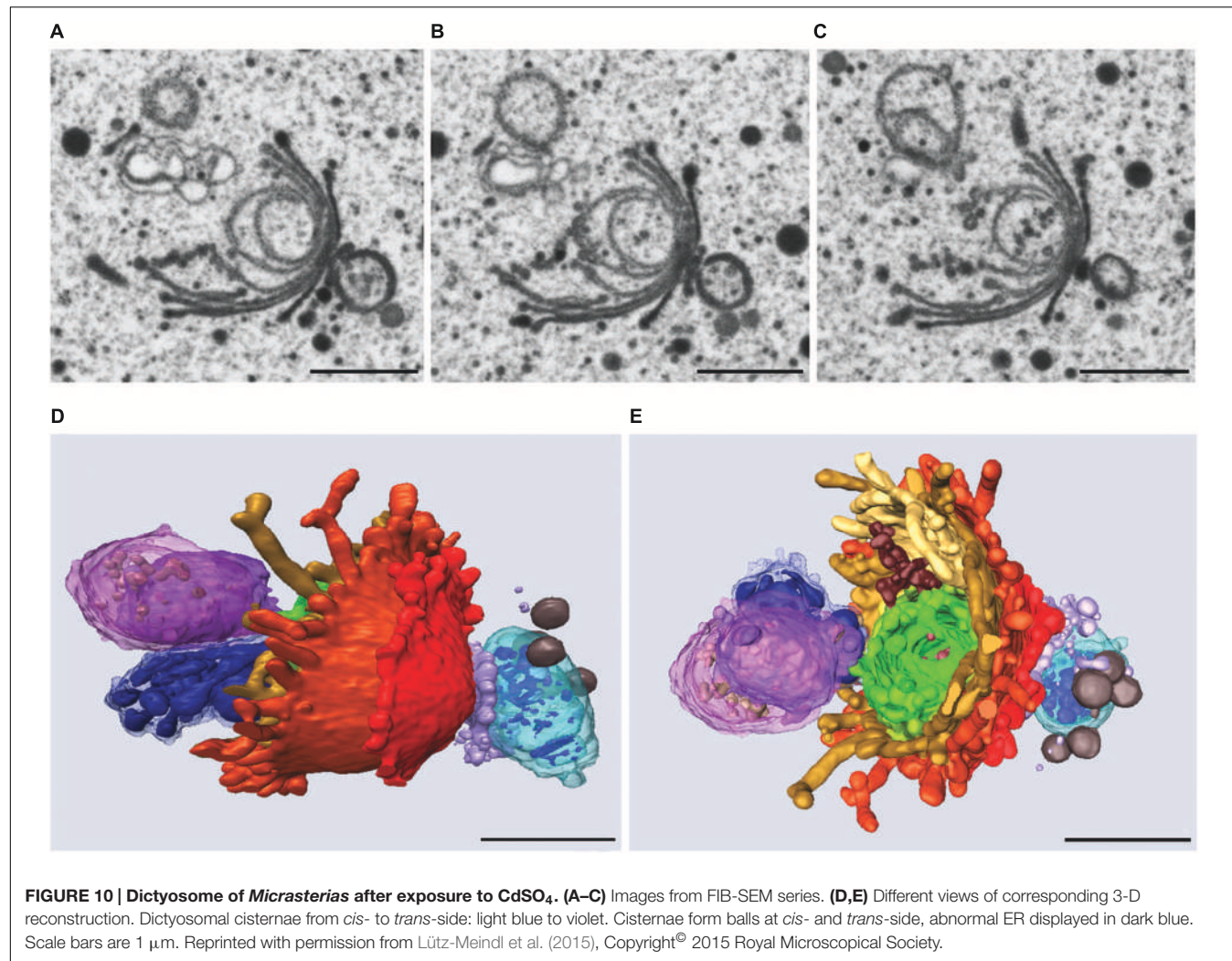


FIGURE 10 | Dictyosome of *Micrasterias* after exposure to CdSO_4 . (A–C) Images from FIB-SEM series. (D,E) Different views of corresponding 3-D reconstruction. Dictyosomal cisternae from *cis*- to *trans*-side: light blue to violet. Cisternae form balls at *cis*- and *trans*-side, abnormal ER displayed in dark blue. Scale bars are 1 μm . Reprinted with permission from Lütz-Meindl et al. (2015), Copyright[®] 2015 Royal Microscopical Society.

decrease in photosynthetic activity and cell division rates, ROS production and increased respiration thus corresponding essentially to those of higher plants. At an ultrastructural level, chloroplast structure as well as morphology and activity of the endomembrane system seem to be the main metal targets. Filtering by the extraplasmonic matrix (mucilage and/or cell wall), excretion by mucilage vesicles and intracellular compartmentalization seem to be the most important detoxification strategies of *Micrasterias* that allow survival of the cells at least within certain concentration and duration limits.

CONCLUSION AND OUTLOOK

This review shows that the alga *Micrasterias* is well suited as model system in plant cell biology for multiple reasons. The alga reveals an exceptional multipolar tip growth with several lobes developing simultaneously at the same plane. The continuously changing growing and non-growing zones of the primary cell wall allow for studying growth regulation in directly adjacent

areas within one and the same cell and has high potential for providing insight into involvement of the cytoskeleton or ionic components in growth and cell shape formation. The alga develops two distinctly distinguishable cell walls that in their composition both resemble that of higher plant cells. The flexible highly pectic primary wall of *Micrasterias* is similar to cell walls in tip growing plant cells such as pollen tubes or root hairs and the protective thick cellulose-rich secondary wall corresponds to walls of non-growing higher plant parenchymatic cells. The extremely large dictyosomes that correspond to the large cell size provide excellent possibilities for investigating their function. They are enveloped by a huge ER sheath, consist of a constant number of 11 cisternae during the entire cell cycle and produce vesicle continuously even in non-growing periods. As most of their products are already well defined they lend themselves not only for basic cell biological studies on the function of the secretory machinery but represent also highly sensitive indicators for any kind of stress. Experimental or environmental impact on *Micrasterias* is easily recognizable not only by cell shape malformations but also by characteristic structural and functional reactions of the dictyosomes. They occur during high salinity or

oxidative stress in the same way as during impact by different metal or herbicide pollutants indicating that dictyosomes in *Micrasterias* are highly sensitive stress sensors. Also degradation of dictyosomes under severe stress, achieved by detachment of single cisternae at both side of a Golgi stack occurs similarly during different stress scenarios. Degraded dictyosomes are absorbed by ER cisternae reflecting the high similarity between Golgi and ER membranes as also known from higher plant cells.

Despite their natural adaptation to oligotrophic, low salt-concentrated waters, *Micrasterias* cells are capable of coping with environmental pollution to a considerable degree. This is accomplished by an obvious physiological flexibility as well as by the capability of the *Micrasterias* cell of performing autophagy, and of compartmentalizing pollutants in cell walls and vacuoles, respectively, by excreting them via constant mucilage production. The molecular players that are involved in these processes as well as a possible regulation by signal molecules such as phytohormones remains to be investigated. Further establishment of molecular tools and sequencing of essential regulators combined with employment of high resolution 3-D microscopic techniques will enable the next steps for elucidating cell shape formation and for understanding intracellular stress response regulation. By its exceptional features and its close

relation to higher land plants *Micrasterias* may help in detecting plant specific cellular processes and pathways that would remain undiscovered when only using “classical” model system such as *Arabidopsis*.

AUTHOR CONTRIBUTIONS

The author confirms being the sole contributor of this work and approved it for publication.

ACKNOWLEDGMENTS

The author wishes to thank all former and present collaboration partners and coworkers for their highly estimated input on the studies on *Micrasterias* and particularly Prof. Dr. Gerhard Wanner for the 3-D FIB-SEM images. The valuable and competent help of Mag. Ancuela Andosch in preparing this manuscript is gratefully acknowledged. The studies on *Micrasterias* were financially supported by the Austrian Science Fund, projects P15849 BIO, P18869-B16 and P21035-B16 to UL-M.

REFERENCES

- Affenzeller, M. J., Darezshouri, A., Andosch, A., Lütz, C., and Lütz-Meindl, U. (2009a). PCD and autophagy in the unicellular green alga *Micrasterias denticulata*. *Autophagy* 5, 854–855. doi: 10.4161/auto.8791
- Affenzeller, M. J., Darezshouri, A., Andosch, A., Lütz, C., and Lütz-Meindl, U. (2009b). Salt stress-induced cell death in the unicellular green alga *Micrasterias denticulata*. *J. Exp. Bot.* 60, 939–954. doi: 10.1093/jxb/ern348
- Aichinger, N., and Lütz-Meindl, U. (2005). Organelle interactions and possible degradation pathways visualized in high-pressure frozen algal cells. *J. Microsc.* 219, 86–94. doi: 10.1111/j.1365-2818.2005.01496.x
- An, L., Liu, Y., Zhang, M., Chen, T., and Wang, X. (2005). Effects of nitric oxide on growth of maize seed leaves in the presence or absence of ultraviolet-B radiation. *J. Plant Physiol.* 162, 317–326. doi: 10.1016/j.jplph.2004.07.004
- Andosch, A., Affenzeller, M. J., Lütz, C., and Lütz-Meindl, U. (2012). A freshwater green alga under cadmium stress: ameliorating calcium effects on ultrastructure and photosynthesis in the unicellular model *Micrasterias*. *J. Plant Physiol.* 169, 1489–1500. doi: 10.1016/j.jplph.2012.06.002
- Bartlett, J. E., Baranov, S. V., Ananyev, G. M., and Dismukes, G. C. (2008). Calcium controls the assembly of the photosynthetic water-oxidizing complex: a cadmium(II) inorganic mutant of the Mn₄Ca core. *Philos. Trans. R. Soc. Lond. B Biol. Sci.* 363, 1253–1261. doi: 10.1098/rstb.2007.2222
- Baylson, F. A., Stevens, B. W., and Domozych, D. S. (2001). Composition and synthesis of the pectin and protein components of the cell wall of *Closterium acerosum* (Chlorophyta). *J. Phycol.* 37, 796–809. doi: 10.1046/j.1529-8817.2001.00179.x
- Bosch, M., Cheung, A. Y., and Hepler, P. K. (2005). Pectin methylesterase, a regulator of pollen tube growth. *Plant Physiol.* 138, 1334–1346. doi: 10.1104/pp.105.059865
- Bosch, M., and Hepler, P. K. (2005). Pectin methylesterases and pectin dynamics in pollen tubes. *Plant Cell* 17, 3219–3226. doi: 10.1105/tpc.105.037473
- Bräutigam, A., Schaumlöffel, D., Krauss, G. J., and Wesenberg, D. (2009). Analytical approach for characterization of cadmium-induced thiol peptides—a case study using *Chlamydomonas reinhardtii*. *Anal. Bioanal. Chem.* 395, 1737–1747. doi: 10.1007/s00216-009-2921-7
- Brook, A. J. (1981). “The biology of desmids,” in *Botanical Monographs*, eds J. H. Burnett, H. G. Baker, H. Beevers, and F. R. Whatley (Oxford: Blackwell Scientific).
- Bush, M. S., and McCann, M. C. (1999). Pectic epitopes are differentially distributed in the cell walls of potato (*Solanum tuberosum*) tubers. *Physiol. Plant.* 107, 201–213. doi: 10.1034/j.1399-3054.1999.100208.x
- Carpita, N. C., and Gibeaut, D. M. (1993). Structural models of primary cell walls in flowering plants: consistency of molecular structure with the physical properties of the walls during growth. *Plant J.* 3, 1–30. doi: 10.1111/j.1365-313X.1993.tb00007.x
- Darezshouri, A., Affenzeller, M., and Lütz-Meindl, U. (2008). Cell death upon H₂O₂ induction in the unicellular green alga *Micrasterias*. *Plant Biol.* 10, 732–745. doi: 10.1111/j.1438-8677.2008.00078.x
- Darezshouri, A., and Lütz-Meindl, U. (2010). H₂O₂ localization in the green alga *Micrasterias* after salt and osmotic stress by TEM-coupled electron energy loss spectroscopy. *Protoplasma* 239, 49–56. doi: 10.1007/s00709-009-0081-4
- Delwiche, C. F., and Cooper, E. D. (2015). The evolutionary origin of a terrestrial flora. *Curr. Biol.* 25, R899–R910. doi: 10.1016/j.cub.2015.08.029
- Dobberstein, B., and Kiermayer, O. (1972). Das Aufreten eines besonderen Typs von Golgivesikeln während der Sekundärwandbildung von *Micrasterias denticulata*. *Breb. Protoplasma* 75, 185–194. doi: 10.1007/BF01279403
- Domozych, D. S., Ciancia, M., Fangel, J. U., Mikkelsen, M. D., Ulvskov, P., and Willats, W. G. T. (2012). The cell walls of green algae: a journey through evolution and diversity. *Front. Plant Sci.* 3:82. doi: 10.3389/fpls.2012.00082
- Domozych, D. S., Kiemle, S., Domozych, C. E., and Gretz, M. R. (2006). How symmetrical are desmids? Cell wall chemistry and development in *Penium margaritaceum*. *J. Phycol.* 42(Suppl. 1), 47.
- Domozych, D. S., and Rogers-Domozych, C. (1993). Mucilage processing and secretion in the green alga *Closterium*. II. Ultrastructure and immunocytochemistry. *J. Phycol.* 29, 659–667. doi: 10.1111/j.0022-3646.1993.00659.x
- Domozych, D. S., Serfis, A., Kiemle, S. N., and Gretz, M. R. (2007). The structure and biochemistry of charophycean cell walls: I. Pectins of *Penium margaritaceum*. *Protoplasma* 230, 99–115. doi: 10.1007/s00709-006-0197-8
- Domozych, D. S., Sorensen, I., Sacks, C., Brechka, H., Andreas, A., Fangel, J. U., et al. (2014). Disruption of the microtubule network alters cellulose deposition and causes major changes in pectin distribution in the cell wall of the green alga, *Penium margaritaceum*. *J. Exp. Bot.* 65, 465–479. doi: 10.1093/jxb/ert390
- Eder, M., and Lütz-Meindl, U. (2008). Pectin-like carbohydrates in the green alga *Micrasterias* characterized by cytochemical analysis and energy filtering TEM. *J. Microsc.* 231, 201–214. doi: 10.1111/j.1365-2818.2008.02036.x

- Eder, M., Tenhaken, R., Driouich, A., and Lütz-Meindl, U. (2008). Occurrence and characterization of arabinogalactan-like proteins and hemicelluloses in *Micrasterias* (Streptophyta). *J. Phycol.* 44, 1221–1234. doi: 10.1111/j.1529-8817.2008.00576.x
- Ernst, W. H. O., Krauss, G.-J., Verkleij, J. A. C., and Wesenberg, D. (2008). Interaction of heavy metals with the sulphur metabolism in angiosperms from an ecological point of view. *Plant Cell Environ.* 31, 123–143.
- Franklin, N. M., Stauber, J. L., Markich, S. J., and Lim, R. P. (2000). pH-dependent toxicity of copper and uranium to a tropical freshwater alga (*Chlorella* sp.). *Aquat. Toxicol.* 48, 275–289. doi: 10.1016/S0166-445X(99)00042-9
- Gibeaut, D. M., and Carpita, N. C. (1993). Synthesis of (1→3), (1→4)-beta-D-glucan in the Golgi apparatus of maize coleoptiles. *Proc. Natl. Acad. Sci. U.S.A.* 90, 3850–3854. doi: 10.1073/pnas.90.9.3850
- Goldberg, R., Pierron, M., Bordenave, M., Breton, C., Morvan, C., and Du Penhoat, C. H. (2001). Control of mung bean pectinmethyltransferase isoform activities – Influence of pH and carboxyl group distribution along the pectic chains. *J. Biol. Chem.* 276, 8841–8847. doi: 10.1074/jbc.M001791200
- Goyal, A. (2007). Osmoregulation in *Dunaliella*. Part II: photosynthesis and starch contribute carbon for glycerol synthesis during a salt stress in *Dunaliella tertiolecta*. *Plant Physiol. Biochem.* 45, 705–710. doi: 10.1016/j.plaphy.2007.05.009
- Graham, L. E., Cook, M. E., and Busse, J. S. (2000). The origin of plants: body plan changes contributing to a major evolutionary radiation. *Proc. Natl. Acad. Sci. U.S.A.* 25, 4535–4540. doi: 10.1073/pnas.97.9.4535
- Gu, F., and Nielsen, E. (2013). Targeting and regulation of cell wall synthesis during tip growth in plants. *J. Integr. Plant Biol.* 55, 835–846. doi: 10.1111/jipb.12077
- Hartholt, J., Moestrup, O., and Ulvskov, P. (2016). Why plants were terrestrial from the beginning. *Trends Plant Sci.* 21, 96–101. doi: 10.1016/j.tplants.2015.11.010
- Hauptfleisch, P. (1888). Zellmembran und Hüllgallerte der Desmidiae. *Mit. Naturwiss. Ver. Neuvorpommern Rügen Greifswald Berlin* 20, 59–136.
- Hawes, C., and Satiat-Jeunemaitre, B. (2005). The plant Golgi apparatus—going with the flow. *Biochim. Biophys. Acta* 1744, 466–480. doi: 10.1016/j.bbamcr.2005.03.009
- Hepler, P. K., and Winship, L. J. (2010). Calcium at the cell wall-cytoplasm interface. *J. Integr. Plant Biol.* 52, 147–160. doi: 10.1111/j.1744-7909.2010.00923.x
- Heumann, H.-G. (2002). Ultrastructural localization of zinc in zinc-tolerant *Armeria maritima* ssp. *halleri* by autometallography. *J. Plant Physiol.* 159, 191–203. doi: 10.1078/0176-1617-00553
- Höftberger, M., Url, T., and Meindl, U. (1995). The ionophore nigericin prevents the stopping mechanism of the microtubule-dependent nuclear migration in desmids. *Cryptogamic Bot.* 5, 5–13.
- Hogetsu, T. (1992). “The cytoskeleton in Desmidiales – cell morphogenesis,” in *The Cytoskeleton of the Algae*, ed. D. Menzel (Boca Raton, FL: CRC Press), 133–147.
- Holdaway-Clarke, T. L., and Hepler, P. K. (2003). Control of pollen tube growth: role of ion gradients and fluxes. *New Phytol.* 159, 539–563. doi: 10.1046/j.1469-8137.2003.00847.x
- Holzinger, A., Callaham, D. A., Hepler, P. K., and Meindl, U. (1995). Free calcium in *Micrasterias*: local gradients are not detected in growing lobes. *Eur. J. Cell Biol.* 67, 363–371.
- Holzinger, A., De Ruijter, N., Emons, A. M., and Lütz-Meindl, U. (1999). Spectrin-like proteins in green algae (Desmidiae). *Cell Biol. Int.* 23, 335–344. doi: 10.1006/cbir.1999.0365
- Holzinger, A., and Lütz, C. (2006). Algae and UV irradiation: effects on ultrastructure and related metabolic functions. *Micron* 37, 190–207. doi: 10.1016/j.micron.2005.10.015
- Holzinger, A., and Lütz-Meindl, U. (2001). Chondramides, novel cyclodepsipeptides from myxobacteria, influence cell development and induce actin filament polymerization in the green alga *Micrasterias*. *Cell Motil. Cytoskeleton* 48, 87–95. doi: 10.1002/1097-0169(200102)48:2<87::AID-CM1000>3.0.CO;2-C
- Holzinger, A., and Lütz-Meindl, U. (2002). Kinesin-like proteins are involved in postmitotic nuclear migration of the unicellular green alga *Micrasterias denticulata*. *Cell Biol. Int.* 26, 689–697. doi: 10.1006/cbir.2002.0920
- Holzinger, A., and Meindl, U. (1997). Jasplakinolide, a novel actin targeting peptide, inhibits cell growth and induces actin filament polymerization in the green alga *Micrasterias*. *Cell Motil. Cytoskeleton* 38, 365–372. doi: 10.1002/(SICI)1097-0169(1997)38:4<365::AID-CM6>3.3.CO;2-P
- Holzinger, A., Mittermann, I., Laffer, S., Valenta, R., and Meindl, U. (1997). Microinjection of profilins from different sources into the green alga *Micrasterias* causes transient inhibition of cell growth. *Protoplasma* 199, 124–134. doi: 10.1007/BF01294501
- Holzinger, A., Monajebiashi, S., Greulich, K. O., and Lütz-Meindl, U. (2002). Impairment of cytoskeleton-dependent vesicle and organelle translocation in green algae: combined use of a microfocused infrared laser as microbeam and optical tweezers. *J. Microsc.* 208, 77–83. doi: 10.1046/j.1365-2818.2002.01069.x
- Holzinger, A., Roleda, M. Y., and Lütz, C. (2009). The vegetative arctic freshwater green alga *Zygnema* is insensitive to experimental UV exposure. *Micron* 40, 831–838. doi: 10.1016/j.micron.2009.06.008
- Holzinger, A., Valenta, R., and Lütz-Meindl, U. (2000). Profilin is localized in the nucleus-associated microtubule and actin system and is evenly distributed in the cytoplasm of the green alga *Micrasterias denticulata*. *Protoplasma* 212, 197–205. doi: 10.1007/BF01282920
- Huh, G.-H., Damsz, B., Matsumoto, T. K., Reddy, M. P., Rus, A. M., Ibeas, J. I., et al. (2002). Salt causes ion disequilibrium-induced programmed cell death in yeast and plants. *Plant J.* 29, 649–659. doi: 10.1046/j.0960-7412.2001.01247.x
- Jiang, H. M., Yang, J. C., and Zhang, J. F. (2007). Effects of external phosphorus on the cell ultrastructure and the chlorophyll content of maize under cadmium and zinc stress. *Environ. Pollut.* 147, 750–756. doi: 10.1016/j.envpol.2006.09.006
- Jiang, W., and Liu, D. (2010). Pb-induced cellular defense system in the root meristematic cells of *Allium sativum* L. *BMC Plant Biol.* 10:40. doi: 10.1186/1471-2229-10-40
- Kallio, P. (1949). Artificially produced binuclear, diploid and anuclear desmids. *Arch. Soc. Vanamo* 24, 1–120.
- Kallio, P., and Heikkilä, H. (1972). “On the effect of elimination of nuclear control in *Micrasterias*,” in *Plant Cells*, eds S. Bonotto, R. Goutier, K. Kirchmann, and J. R. Maisin (New York, NY: Academic Press Inc.), 167–192.
- Kallio, P., and Lehtonen, J. (1981). “Nuclear control of morphogenesis in *Micrasterias*,” in *Cytomorphogenesis in Plants*, ed. O. Kiermayer (Vienna: Springer-Verlag KG), 191–213.
- Karahara, I., Suda, J., Tahara, H., Yokota, E., Shimmen, T., Misaki, K., et al. (2009). The preprophase band is a localized center of clathrin-mediated endocytosis in late prophase cells of the onion cotyledon epidermis. *Plant J.* 57, 819–831. doi: 10.1111/j.1365-313X.2008.03725.x
- Kiermayer, O. (1964). Untersuchungen über die Morphogenese und Zellwandbildung bei *Micrasterias denticulata* Breb. Allgemeiner Überblick. *Protoplasma* 59, 382–420. doi: 10.1007/BF01247857
- Kiermayer, O. (1967). Das Septum-Initialmuster von *Micrasterias denticulata* und seine Bildung. *Protoplasma* 64, 481–484. doi: 10.1007/BF01666545
- Kiermayer, O. (1968). The distribution of microtubules in differentiating cells of *Micrasterias denticulata*. *Planta* 83, 223–236. doi: 10.1007/BF00385332
- Kiermayer, O. (1970a). Elektronenmikroskopische Untersuchungen zum Problem der Cytomorphogenese von *Micrasterias denticulata* Bréb. *Protoplasma* 69, 97–132. doi: 10.1007/BF01276654
- Kiermayer, O. (1970b). Causal aspects of cytomorphogenesis in *Micrasterias*. *Ann. N. Y. Acad. Sci.* 175, 686–701. doi: 10.1111/j.1749-6632.1970.tb45185.x
- Kiermayer, O. (1981). “Cytoplasmic basis of morphogenesis in *Micrasterias*,” in *Cytomorphogenesis in Plants*, ed. O. Kiermayer (Vienna: Springer-Verlag KG), 147–189.
- Kiermayer, O., and Meindl, U. (1980). Elektronenmikroskopische Untersuchungen zum Problem der Cytomorphogenese von *Micrasterias denticulata* Bréb. III. Einfluss von Cycloheximid auf die Bildung und Ultrastruktur der Primärwand. *Protoplasma* 103, 169–177. doi: 10.1007/BF01276674
- Kiermayer, O., and Meindl, U. (1984). “Interaction of the golgi apparatus and the plasmalemma in the cytomorphogenesis of *Micrasterias*,” in *Compartments in Algal Cells and Their Interaction*, eds W. Wiessner, D. Robinson, and R. C. Starr (Berlin: Springer-Verlag KG), 175–182.
- Kiermayer, O., and Meindl, U. (1986). Das “Anuclear type of development” (ATD)-Phänomen hervorgerufen durch Hemmung der Proteinsynthese bei verschiedenen Desmidiae. *Ber. Nat. Med. Ver. Salzburg* 8, 101–114.
- Kiermayer, O., and Meindl, U. (1989). “Cellular morphogenesis: the desmid (Chlorophyceae) system,” in *Algae as Experimental System. Plant Cell Biology*, eds A. W. Coleman, L. J. Goff, and J. R. Stein-Taylor (New York, NY: Alan R. Liss, Inc.), 149–168.
- Kimura, S., Laosinchai, W., Itoh, T., Cui, X., Linder, C. R., and Brown, R. M. Jr. (1999). Immunogold labeling of rosette terminal cellulose-synthesizing

- complexes in the vascular plant *Vigna angularis*. *Plant Cell* 11, 2075–2086. doi: 10.2307/3871010
- Kitzing, C., Proeschold, T., and Karsten, U. (2014). UV-induced effects on growth, photosynthetic performance and sunscreen contents in different populations of the green alga *Klebsormidium fluitans* (Streptophyta) from alpine soil crusts. *Microbiol. Ecol.* 67, 327–340. doi: 10.1007/s00248-013-0317-x
- Knox, J. P., Day, S., and Roberts, K. (1989). A set of cell surface glycoproteins forms an early marker of cell position but not cell type in the root apical meristem of *Daucus carota L.* *Development* 106, 47–56.
- Knox, J. P., Linstead, P. J., Peart, J., Cooper, C., and Roberts, K. (1991). Developmentally regulated epitopes of cell surface arabinogalactan proteins and their relation to root tissue pattern formation. *Plant J.* 1, 317–326. doi: 10.1046/j.1365-313X.1991.t01-9-00999.x
- Krauss, G.-J., Sole, M., Krauss, G., Schlosser, D., Wesenberg, D., and Baerlocher, F. (2011). Fungi in freshwater: ecology, physiology and biochemical potential. *FEMS Microbiol. Rev.* 35, 620–651. doi: 10.1111/j.1574-6976.2011.00266.x
- Kreuger, M., and van Holst, G. J. (1996). Arabinogalactan proteins and plant differentiation. *Plant Mol. Biol.* 30, 1077–1086. doi: 10.1007/BF00019543
- Krzeslowska, M., Wozny, A., and Konieczna-Koperska, J. (2004). Calcium ameliorates effects of lead in protonema of *Funaria hygrometrica* Hedw. *Biol. Plant.* 48, 569–574. doi: 10.1023/B:BIOP.0000047154.16119.32
- Lacalli, T. C. (1975). Morphogenesis in *Micrasterias*. I. Tip growth. *J. Embryol. Exp. Morphol.* 33, 95–115.
- Larcher, W. (2001). *Ökophysiologie der Pflanzen*. Stuttgart: Eugen Ulmer.
- Lauer, C. M. Jr., Bonatto, D., Mielniczki-Pereira, A. A., Schuch, A. Z., Dias, J. F., Yoneama, M. L., et al. (2008). The Pmr1 protein, the major yeast Ca²⁺-ATPase in the Golgi, regulates intracellular levels of the cadmium ion. *FEMS Microbiol. Lett.* 285, 79–88. doi: 10.1111/j.1574-6968.2008.01214.x
- Lee, N., Bertholet, S., Debrabant, A., Muller, J., Duncan, R., and Nakhasi, H. L. (2002) Programmed cell death in the unicellular protozoan parasite *Leishmania*. *Cell Death Differ.* 9, 53–64. doi: 10.1038/sj/cdd/4400952
- Lechner, C., Kerschbaum, H. H., and Lütz-Meindl, U. (2009). Nitric oxide suppresses growth and development in the unicellular green alga *Micrasterias denticulata*. *J. Plant Physiol.* 166, 117–127. doi: 10.1016/j.jplph.2008.02.012
- Leliaert, F., Smith, D. R., Moreau, H., Herron, M. D., Verbruggen, H., Delwiche, C. F., et al. (2012). Phylogeny and molecular evolution of the green algae. *Crit. Rev. Plant Sci.* 31, 1–46. doi: 10.1080/07352689.2011.615705
- Lenzenweger, R. (1996). *Desmidaceenflora von Österreich-Teil 1*. Berlin: J. Cramer in der Gebrüder Bornträger Verlagsbuchhandlung.
- Lin, J., Wang, Y., and Wang, G. (2006). Salt stress-induced programmed cell death in tobacco protoplasts is mediated by reactive oxygen species and mitochondrial permeability transition pore status. *J. Plant Physiol.* 163, 731–739. doi: 10.1016/j.jplph.2005.06.016
- Lloyd, C., and Chan, J. (2008). The parallel lives of microtubules and cellulose microfibrils. *Curr. Opin. Plant Biol.* 11, 641–646. doi: 10.1016/j.pbi.2008.10.007
- Lütkenmüller, J. (1902). Die Zellmembran der Desmidaceen. *Beitr. Biol. Pfl. Breslau* 8, 347–414.
- Lütz, C., Seidlitz, H. K., and Meindl, U. (1997). Physiological and structural changes in the chloroplast of the green alga *Micrasterias denticulata* induced by UV-B simulation. *Plant Ecol.* 128, 54–64.
- Lütz-Meindl, U. (2007). Use of energy filtering transmission electron microscopy for image generation and element analysis in plant organisms. *Micron* 38, 181–196. doi: 10.1016/j.micron.2006.03.017
- Lütz-Meindl, U., and Brosch-Salomon, S. (2000). Cell wall secretion in the green alga *Micrasterias*. *J. Microsc.* 198, 208–217. doi: 10.1046/j.1365-2818.2000.00699.x
- Lütz-Meindl, U., Luckner, M., Andosch, A., and Wanner, G. (2015). Structural stress responses and degradation of dictyosomes in algae analysed by TEM and FIB-SEM tomography. *J. Microsc.* doi: 10.1111/jmi.12369 [Epub ahead of print].
- Lütz-Meindl, U., and Menzel, D. (2000). “Actin and cytomorphogenesis in the giant, single-celled green algae *Acetabularia* and *Micrasterias*,” in *Actin: A Dynamic Framework for Multiple Plant Cell Functions*, eds C. J. Staiger, F. Baluska, D. Volkmann, and P. Barlow (Dordrecht: Kluwer Academic Publishers), 213–236.
- Lynch, M. A., and Staehelin, L. A. (1992). Domain-specific and cell type-specific localization of two types of cell wall matrix polysaccharides in the clover root tip. *J. Cell Biol.* 118, 467–479. doi: 10.1083/jcb.118.2.467
- Majewska-Sawka, A., and Nothnagel, E. A. (2000). The multiple roles of arabinogalactan proteins in plant development. *Plant Physiol.* 122, 3–10. doi: 10.1104/pp.122.1.3
- Mandal, S., Das, R. K., and Mishra, S. (2011). Differential occurrence of oxidative burst and antioxidative mechanism in compatible and incompatible interactions of *Solanum lycopersicum* and *Ralstonia solanacearum*. *Plant Physiol. Biochem.* 49, 117–123. doi: 10.1016/j.plaphy.2010.10.006
- McNally, J. G., Cowan, J. D., and Swift, H. (1983). The effects of the ionophore A23187 on pattern formation in the alga *Micrasterias*. *Dev. Biol.* 97, 137–145. doi: 10.1016/0012-1606(83)90071-4
- Mehta, S. K., and Gaur, J. P. (1999). Heavy-metal-induced proline accumulation and its role in ameliorating metal toxicity in *Chlorella vulgaris*. *New Phytol.* 143, 253–259. doi: 10.1046/j.1469-8137.1999.00447.x
- Meikle, P. J., Hoogenraad, N. J., Bonig, I., Clarke, A. E., and Stone, B. A. (1994). A (1-->3,1-->4)-beta-glucan-specific monoclonal antibody and its use in the quantitation and immunocytochemical location of (1-->3,1-->4)-beta-glucans. *Plant J.* 5, 1–9. doi: 10.1046/j.1365-313X.1994.5010001.x
- Meindl, U. (1982a). Local accumulation of membrane associated calcium according to cell pattern formation in *Micrasterias denticulata* visualized by chlortetracycline fluorescence. *Protoplasma* 110, 143–146. doi: 10.1007/BF01281541
- Meindl, U. (1982b). Patterned distribution of membrane associated calcium during pore formation in *Micrasterias denticulata*. *Protoplasma* 112, 138–141. doi: 10.1007/BF01280225
- Meindl, U. (1983). Cytoskeletal control of nuclear migration and anchoring in developing cells of *Micrasterias denticulata* and the change caused by the anti-microtubular herbicide amiprofos-methyl (APM). *Protoplasma* 118, 75–90. doi: 10.1007/BF01284749
- Meindl, U. (1985). Experimental and ultrastructural studies on cell shape formation in the defect mutant cell *Micrasterias thomasiana* f uniradiata. *Protoplasma* 129, 74–87. doi: 10.1007/BF01282307
- Meindl, U. (1990). Effects of temperature on cytomorphogenesis and ultrastructure of *Micrasterias denticulata* Breb. *Protoplasma* 157, 3–18. doi: 10.1007/BF01322635
- Meindl, U. (1992). “Cytoskeleton-based nuclear translocation in desmids,” in *The Cytoskeleton of Algae*, ed. D. Menzel (Boca Raton, FL: CRC Press, Inc.), 138–147.
- Meindl, U. (1993). *Micrasterias* cells as a model system for research on morphogenesis. *Microbiol. Rev.* 57, 415–433.
- Meindl, U., and Kiermayer, O. (1981). Biologischer Test zur Bestimmung der Antimikrotubuli-Wirkung verschiedener Stoffe mit Hilfe der Grünalge *Micrasterias denticulata*. *Mikroskopie* 38, 325–336.
- Meindl, U., and Kiermayer, O. (1982). Über die Kern- und Chloroplastenmigration von *Micrasterias denticulata* Breb. II. Die Chloroplastenmigration und ihre Veränderung durch verschiedene Stoffe. *Phyton* 22, 213–231.
- Meindl, U., Lancelle, S., and Hepler, P. (1992). Vesicle production and fusion during lobe formation in *Micrasterias* visualized by high-pressure freeze fixation. *Protoplasma* 170, 104–114. doi: 10.1007/BF01378786
- Meindl, U., and Lütz, C. (1996). Effects of UV irradiation on cell development and ultrastructure of the green alga *Micrasterias*. *J. Photochem. Photobiol. B Biol.* 36, 285–292. doi: 10.1016/S1011-1344(96)07395-2
- Meindl, U., and Röderer, G. (1990). Influence of inorganic and triethyl lead on nuclear migration and ultrastructure of *Micrasterias*. *Ecotoxicol. Environ. Saf.* 19, 192–203. doi: 10.1016/0147-6513(90)90067-F
- Meindl, U., Wittmann-Pinegger, D., and Kiermayer, O. (1989). Cell multiplication and ultrastructure of *Micrasterias denticulata* Desmidiaeae grown under salt stress. *Plant Syst. Evol.* 164, 197–208. doi: 10.1007/BF00940437
- Meindl, U., Zhang, D., and Hepler, P. K. (1994). Actin microfilaments are associated with the migrating nucleus and the cell cortex in the green alga *Micrasterias*. Studies on living cells. *J. Cell Sci.* 107, 1929–1934.
- Michaeli, S., and Galili, G. (2014). Degradation of organelles or specific organelle components via selective autophagy in plant cells. *Int. J. Mol. Sci.* 15, 7624–7638. doi: 10.3390/ijms15057624
- Miura, G. A., and Shih, T. M. (1984). Cholinergic constituents in plants: characterization and distribution of acetylcholine and choline. *Physiol. Plant.* 61, 417–421. doi: 10.1111/j.1399-3054.1984.tb06349.x

- Mogelsvang, S., Marsh, B. J., Ladinsky, M. S., and Howell, K. E. (2004). Predicting function from structure: 3D structure studies of the mammalian Golgi complex. *Traffic* 5, 338–345. doi: 10.1111/j.1398-9219.2004.00186.x
- Murgia, I., De Pinto, M. C., Delledonne, M., Soave, C., and De Gara, L. (2004). Comparative effects of various nitric oxide donors on ferritin regulation, programmed cell death, and cell redox state in plant cells. *J. Plant Physiol.* 161, 777–783. doi: 10.1016/j.jplph.2003.12.004
- Muriel, M.-P., Lambeng, N., Darios, F., Michel, P. P., Hirsch, E. C., Agid, Y., et al. (2000). Mitochondrial free calcium levels (Rhod-2 fluorescence) and ultrastructural alterations in neuronally differentiated PC12 cells during ceramide-dependent cell death. *J. Comp. Neurol.* 426, 297–315. doi: 10.1002/1096-9861(20001016)426:2<297::AID-CNE10>3.0.CO;2-O
- Nassiri, Y., Mansot, J. L., Wery, J., Ginsburger-Vogel, T., and Amiard, J. C. (1997). Ultrastructural and electron energy loss spectroscopy studies of sequestration mechanisms of Cd and Cu in the marine diatom *Skeletonema costatum*. *Arch. Environ. Contam. Toxicol.* 33, 147–155. doi: 10.1007/s002449900236
- Nebenführ, A., Ritzenthaler, C., and Robinson, D. G. (2002). Brefeldin A: deciphering an enigmatic inhibitor of secretion. *Plant Physiol.* 130, 1102–1108. doi: 10.1104/pp.011569
- Neumann, D., and zur Nieden, U. (2001). Silicon and heavy metal tolerance of higher plants. *Phytochemistry* 56, 685–692. doi: 10.1016/S0031-9422(00)00472-6
- Neustupa, J., Stastny, J., and Hodac, L. (2008). Temperature-related phenotypic plasticity in the green microalga *Micrasterias rotata*. *Aquat. Microbiol. Ecol.* 51, 77–86. doi: 10.3354/ame01184
- Oertel, A., Aichinger, N., Hochreiter, R., Thalhamer, J., and Lütz-Meindl, U. (2004). Analysis of mucilage secretion and excretion in *Micrasterias* (Chlorophyta) by means of immunoelectron microscopy and digital time lapse video microscopy. *J. Phycol.* 40, 711–720. doi: 10.1111/j.1529-8817.2004.03222.x
- Oertel, A., Holzinger, A., and Lütz-Meindl, U. (2003). Involvement of myosin in intracellular motility and cytomorphogenesis in *Micrasterias*. *Cell Biol. Int.* 27, 977–986. doi: 10.1016/j.cellbi.2003.07.004
- Ordenes, V. R., Reyes, F. C., Wolff, D., and Orellana, A. (2002). A thapsigargin-sensitive Ca²⁺ pump is present in the pea Golgi apparatus membrane. *Plant Physiol.* 129, 1820–1828. doi: 10.1104/pp.002055
- Otegui, M. S., and Spitzer, C. (2008). Endosomal functions in plants. *Traffic* 9, 1589–1598. doi: 10.1111/j.1600-0854.2008.00787.x
- Ougham, H. J., and Howarth, C. J. (1988). Temperature shock proteins in plants. *Symp. Soc. Exp. Biol.* 42, 259–280.
- Pandey, N., and Sharma, C. P. (2003). Chromium interference in iron nutrition and water relations of cabbage. *Environ. Exp. Bot.* 49, 195–200. doi: 10.1016/S0098-8472(02)00088-6
- Pawlak-Skowronska, B. (2003). When adapted to high zinc concentrations the periphytic green alga *Stigeoclonium tenuie* produces high amounts of novel phytochelin-related peptides. *Aquat. Toxicol.* 62, 155–163. doi: 10.1016/S0166-445X(02)00080-2
- Pelah, D., Sintov, A., and Cohen, E. (2004). The effect of salt stress on the production of canthaxanthin and astaxanthin by *Chlorella zoefingiensis* grown under limited light intensity. *World J. Microbiol. Biotechnol.* 20, 483–486. doi: 10.1023/B:WIBI.0000040398.93103.21
- Pflügl-Haill, M., Vidali, L., Vos, J. W., Hepler, P. K., and Lütz-Meindl, U. (2000). Changes of the actin filament system in the green alga *Micrasterias denticulata* induced by different cytoskeleton inhibitors. *Protoplasma* 212, 206–216. doi: 10.1007/BF01282921
- Pickett-Heaps, J. D., and Northcote, D. H. (1966). Organization of microtubules and endoplasmic reticulum during mitosis and cytokinesis in wheat meristems. *J. Cell Sci.* 1, 109–120.
- Popper, Z. A., and Fry, S. C. (2003). Primary cell wall composition of bryophytes and charophytes. *Ann. Bot.* 91, 1–12. doi: 10.1093/aob/mcg013
- Pringsheim, E. G. (1930). Die Kultur von *Micrasterias* und *Volvox*. *Arch. Protistenkd.* 72, 1–48.
- Rai, L. C., and Gaur, J. P. (2001). “Algal adaptation to environmental stresses,” in *Physiological, Biochemical and Molecular Mechanisms*, eds L. C. Rai and J. P. Gaur (Heidelberg: Springer Verlag), 1–421.
- Remias, D., Schwaiger, S., Aigner, S., Leya, T., Stuppner, H., and Lütz, C. (2012). Characterization of an UV- and VIS-absorbing, purpurogallin-derived secondary pigment new to algae and highly abundant in *Mesotaenium berggrenii* (Zygnematophyceae, Chlorophyta), an extremophile living on glaciers. *FEMS Microbiol. Ecol.* 79, 638–648. doi: 10.1111/j.1574-6941.2011.01245.x
- Robinson, D. G., Jiang, L., and Schumacher, K. (2008). The endosomal system of plants: charting new and familiar territories. *Plant Physiol.* 147, 1482–1492. doi: 10.1104/pp.108.120105
- Rounds, C. M., and Bezanilla, M. (2013). Growth mechanisms in tip-growing plant cells. *Annu. Rev. Plant Biol.* 64, 243–265. doi: 10.1146/annurev-arplant-050312-120150
- Salomon, S., and Meindl, U. (1996). Brefeldin A induces reversible dissociation of the Golgi apparatus in the green alga *Micrasterias*. *Protoplasma* 194, 231–242. doi: 10.1007/BF01882030
- Satiat-Jeunemaitre, B., Cole, L., Bourett, T., Howard, R., and Hawes, C. (1996). Brefeldin A effects in plant and fungal cells: something new about vesicle trafficking? *J. Microsc.* 181, 162–177. doi: 10.1046/j.1365-2818.1996.112393.x
- Schiechl, G., Himmelsbach, M., Buchberger, W., Kerschbaum, H. H., and Lütz-Meindl, U. (2008). Identification of acetylcholine and impact of cholinomimetic drugs on cell differentiation and growth in the unicellular green alga *Micrasterias denticulata*. *Plant Sci.* 175, 262–266. doi: 10.1016/j.plantsci.2008.04.006
- Schmid, V. H. R., and Meindl, U. (1992). Microtubules do not control orientation of secondary cell wall microfibril deposition in *Micrasterias*. *Protoplasma* 169, 148–154. doi: 10.1007/BF01323614
- Segovia, M., and Berges, J. A. (2005). Effect of inhibitors of protein synthesis and DNA replication on the induction of proteolytic activities, caspase-like activities and cell death in the unicellular chlorophyte *Dunaliella tertiolecta*. *Eur. J. Phycol.* 40, 21–30. doi: 10.1080/09670260400019774
- Seifert, G. J., and Roberts, K. (2007). The biology of arabinogalactan proteins. *Annu. Rev. Plant Biol.* 58, 137–161. doi: 10.1146/annurev.arplant.58.032806.103801
- Serpé, M. D., and Nothnagel, E. A. (1999). “Arabinogalactan-proteins in the multiple domains of the plant cell surface,” in *Advances in Botanical Research*, ed. J. A. Callow (Cambridge, MA: Academic Press Limited), 207–289.
- Shanker, A. K., Cervantes, C., Loza-Távara, H., and Avudainayagam, S. (2005). Chromium toxicity in plants. *Environ. Int.* 31, 739–753. doi: 10.1016/j.envint.2005.02.003
- Sorensen, I., Domozych, D., and Willats, W. G. T. (2010). How have plant cell walls evolved? *Plant Physiol.* 153, 366–372. doi: 10.1104/pp.110.154427
- Sorensen, I., Fei, Z., Andreas, A., Willats, W. G. T., Domozych, D. S., and Rose, J. K. C. (2014). Stable transformation and reverse genetic analysis of *Penium margaritaceum*: a platform for studies of charophyte green algae, the immediate ancestors of land plants. *Plant J.* 77, 339–351. doi: 10.1111/tpj.12375
- Sorensen, I., Rose, J. K., Doyle, J. J., Domozych, D. S., and Willats, W. G. (2012). The Charophycean green algae as model systems to study plant cell walls and other evolutionary adaptations that gave rise to land plants. *Plant Signal. Behav.* 7, 1–3. doi: 10.4161/psb.7.1.18574
- Stamenkovic, M., and Hanelt, D. (2013). Adaptation of growth and photosynthesis to certain temperature regimes is an indicator for the geographical distribution of *Cosmarium* strains (Zygnematophyceae, Streptophyta). *Eur. J. Phycol.* 48, 116–127. doi: 10.1080/09670262.2013.772657
- Syrovetnik, K., Puura, E., and Neretnieks, I. (2004). Accumulation of heavy metals in Oostriku peat bog, Estonia: site description, conceptual modelling and geochemical modelling of the source of the metals. *Environ. Geol.* 45, 731–740. doi: 10.1007/s00254-003-0931-x
- Takagi, M., Karseno, and Yoshida, T. (2006). Effect of salt concentration on intracellular accumulation of lipids and triacylglyceride in marine microalgae *Dunaliella* cells. *J. Biosci. Bioeng.* 101, 223–226. doi: 10.1263/jbb.101.223
- Teiling, E. (1950). Radiation of desmids, its origin and its consequence as regards taxonomy and nomenclature. *Protoplasma* 150, 299–327.
- Templeton, D. M., and Liu, Y. (2010). Multiple roles of cadmium in cell death and survival. *Chem. Biol. Interact.* 188, 267–275. doi: 10.1016/j.cbi.2010.03.040
- Trethewey, J. A., Campbell, L. M., and Harris, P. J. (2005). (1- > 3),(1- > 4)-{beta}-d-Glucans in the cell walls of the Poales (sensu lato): an immunogold labeling study using a monoclonal antibody. *Am. J. Bot.* 92, 1660–1674. doi: 10.3732/ajb.92.10.1660
- Tretyn, A., and Kendrick, R. E. (1991). Acetylcholine in plants: presence metabolism and mechanism of action. *Bot. Rev.* 57, 33–73. doi: 10.1007/BF02858764

- Troxell, C. L. (1989). Transcellular ionic currents during primary wall morphogenesis in *Micrasterias* and *Closterium*. *Biol. Bull.* 176, 36–40. doi: 10.2307/1541646
- Troxell, C. L., and Scheffey, C. (1991). Ionic currents flow through *Micrasterias* and *Closterium* cells during expansion of the primary cell wall. *Planta* 184, 218–225. doi: 10.1007/BF00197950
- Troxell, C. L., Scheffey, C., and Pickett-Heaps, J. D. (1986). “Ionic currents during wall morphogenesis in *Micrasterias* and *Closterium*,” in *Ionic Currents in Development*, ed. R. Nuccitelli (New York, NY: Alan R. Liss, Inc.), 105–112.
- Url, T., Höftberger, M., and Meindl, U. (1993). Cytochalasin B influences dictyosomal vesicle production and morphogenesis in the desmid Euastrum. *J. Phycol.* 29, 667–674. doi: 10.1111/j.0022-3646.1993.00667.x
- van Doorn, W. G., and Woltering, E. J. (2005). Many ways to exit? Cell death categories in plants. *Trends Plant Sci.* 10, 117–122. doi: 10.1016/j.tplants.2005.01.006
- Vannerum, K., Abe, J., Sekimoto, H., Inze, D., and Vyverman, W. (2010). Intracellular localization of an endogenous cellulose synthase of *Micrasterias denticulata* (Desmidiales, Chlorophyta) by means of transient genetic transformation. *J. Phycol.* 46, 839–845. doi: 10.1111/j.1529-8817.2010.00867.x
- Vannerum, K., Huysman, M. J. J., De Rycke, R., Vuylsteke, M., Leliaert, F., Pollier, J., et al. (2011). Transcriptional analysis of cell growth and morphogenesis in the unicellular green alga *Micrasterias* (Streptophyta), with emphasis on the role of expansin. *BMC Plant Biol.* 11:128. doi: 10.1186/1471-2229-11-128
- Vidali, L., and Bezanilla, M. (2012). Physcomitrella patens: a model for tip cell growth and differentiation. *Curr. Opin. Plant Biol.* 15, 625–631. doi: 10.1016/j.pbi.2012.09.008
- Virolainen, E., Blokhina, O., and Fagerstedt, K. (2002). Ca²⁺-induced high amplitude swelling and cytochrome c release from wheat (*Triticum aestivum* L.) mitochondria under anoxic stress. *Ann. Bot.* 90, 509–516. doi: 10.1093/aob/mcf221
- Volland, S., Andosch, A., Milla, M., Stöger, B., Lütz, C., and Lütz-Meindl, U. (2011). Intracellular metal compartmentalization in the green algal model system *Micrasterias denticulata* (Streptophyta) measured by transmission electron microscopy-coupled electron energy loss spectroscopy. *J. Phycol.* 47, 565–579. doi: 10.1111/j.1529-8817.2011.00988.x
- Volland, S., Bayer, E., Baumgartner, V., Andosch, A., Lütz, C., Sima, E., et al. (2014). Rescue of heavy metal effects on cell physiology of the algal model system *Micrasterias* by divalent ions. *J. Plant Physiol.* 171, 154–163. doi: 10.1016/j.jplph.2013.10.002
- Volland, S., Lütz, C., Michalke, B., and Lütz-Meindl, U. (2012). Intracellular chromium localization and cell physiological response in the unicellular alga *Micrasterias*. *Aquat. Toxicol.* 109, 59–69. doi: 10.1016/j.aquatox.2011.11.013
- Volland, S., Schaumloffel, D., Dobritzsch, D., Krauss, G. J., and Lütz-Meindl, U. (2013). Identification of phytochelatins in the cadmium-stressed conjugating green alga *Micrasterias denticulata*. *Chemosphere* 91, 448–454. doi: 10.1016/j.chemosphere.2012.11.064
- Wanner, G., Schaefer, T., and Lütz-Meindl, U. (2013). 3-D analysis of dictyosomes and multivesicular bodies in the green alga *Micrasterias denticulata* by FIB/SEM tomography. *J. Struct. Biol.* 184, 203–211. doi: 10.1016/j.jsb.2013.10.003
- Waris, H. (1950a). Cytophysiological studies on *Micrasterias*. I. Nuclear and cell division. *Physiol. Plant.* 3, 1–16.
- Waris, H. (1950b). Cytophysiological studies on *Micrasterias*. II. The cytoplasmic framework and its mutation. *Physiol. Plant.* 3, 236–247.
- Waris, H., and Kallio, P. (1964). Morphogenesis in *Micrasterias*. *Adv. Morphog.* 4, 45–80. doi: 10.1016/B978-1-4831-9951-1.50005-X
- Weiss, D., Lütz, C., and Lütz-Meindl, U. (1999). Photosynthesis and heat response of the green alga *Micrasterias denticulata* (Desmidiae). *Z. Naturforsch.* 54c, 508–516.
- Weiss, D., and Lütz-Meindl, U. (1999). Heat response in the green alga *Micrasterias denticulata* (Desmidiae): immunodetection and localization of BiP and heat shock protein 70. *Nova Hedwig.* 69, 217–228.
- Wodniok, S., Brinkmann, H., Glöckner, G., Heidel, A. J., Philippe, H., Melkonian, M., et al. (2011). Origin of land plants: do conjugating green algae hold the key? *BMC Evol. Biol.* 11:104. doi: 10.1186/1471-2148-11-104
- Yariv, J., Lis, H., and Katchalski, E. (1967). Precipitation of arabic acid and some seed polysaccharides by glycosylphenylazo dyes. *Biochem. J.* 105, 1C–2C. doi: 10.1042/bj1050001C
- Yariv, J., Rapport, M. M., and Graf, L. (1962). The interaction of glycosides and saccharides with antibody to the corresponding phenylazo glycosides. *Biochem. J.* 85, 383–388. doi: 10.1042/bj0850383
- Yates, E. A., Valdor, J. F., Haslam, S. M., Morris, H. R., Dell, A., Mackie, W., et al. (1996). Characterization of carbohydrate structural features recognized by anti-arabinogalactan-protein monoclonal antibodies. *Glycobiology* 6, 131–139. doi: 10.1093/glycob/6.2.131
- Yoshida, K., Igarashi, E., Wakatsuki, E., Miyamoto, K., and Hirata, K. (2004). Mitigation of osmotic and salt stresses by abscisic acid through reduction of stress-derived oxidative damage in *Chlamydomonas reinhardtii*. *Plant Sci.* 167, 1335–1341. doi: 10.1016/j.plantsci.2004.07.002
- Zhu, J. K. (2001). Plant salt tolerance. *Trends Plant Sci.* 6, 66–71. doi: 10.1016/S1360-1385(00)01838-0
- Zhu, J. K. (2002). Salt and drought stress signal transduction in plants. *Annu. Rev. Plant Biol.* 53, 247–273. doi: 10.1146/annurev.arplant.53.091401.143329
- Zuppini, A., Andreoli, C., and Baldan, B. (2007). Heat stress: an inducer of programmed cell death in *Chlorella saccharophila*. *Plant Cell Physiol.* 48, 1000–1009. doi: 10.1093/pcp/pcm070

Conflict of Interest Statement: The author declares that the research was conducted in the absence of any commercial or financial relationships that could be construed as a potential conflict of interest.

Copyright © 2016 Lütz-Meindl. This is an open-access article distributed under the terms of the Creative Commons Attribution License (CC BY). The use, distribution or reproduction in other forums is permitted, provided the original author(s) or licensor are credited and that the original publication in this journal is cited, in accordance with accepted academic practice. No use, distribution or reproduction is permitted which does not comply with these terms.



Comparative Chloroplast Genome Analyses of Streptophyte Green Algae Uncover Major Structural Alterations in the Klebsormidiophyceae, Coleochaetophyceae and Zygnematophyceae

Claude Lemieux*, Christian Otis and Monique Turmel

Institut de Biologie Intégrative et des Systèmes, Département de Biochimie, de Microbiologie et de Bio-informatique, Université Laval, Québec, QC, Canada

OPEN ACCESS

Edited by:

David Domozych,
Skidmore College, USA

Reviewed by:

David Roy Smith,
University of Western Ontario, Canada

Burkhard Becker,
University of Cologne, Germany

Robert K. Jansen,
The University of Texas at Austin, USA

***Correspondence:**

Claude Lemieux
claude.lemieux@bcm.ulaval.ca

Specialty section:

This article was submitted to
Plant Evolution and Development,
a section of the journal
Frontiers in Plant Science

Received: 25 February 2016

Accepted: 06 May 2016

Published: 24 May 2016

Citation:

Lemieux C, Otis C and Turmel M (2016) Comparative Chloroplast Genome Analyses of Streptophyte Green Algae Uncover Major Structural Alterations in the Klebsormidiophyceae, Coleochaetophyceae and Zygnematophyceae. *Front. Plant Sci.* 7:697.
doi: 10.3389/fpls.2016.00697

The Streptophyta comprises all land plants and six main lineages of freshwater green algae: Mesostigmatophyceae, Chlorokybophyceae, Klebsormidiophyceae, Charophyceae, Coleochaetophyceae and Zygnematophyceae. Previous comparisons of the chloroplast genome from nine streptophyte algae (including four zygnematophyceans) revealed that, although land plant chloroplast DNAs (cpDNAs) inherited most of their highly conserved structural features from green algal ancestors, considerable cpDNA changes took place during the evolution of the Zygnematophyceae, the sister group of land plants. To gain deeper insights into the evolutionary dynamics of the chloroplast genome in streptophyte algae, we sequenced the cpDNAs of nine additional taxa: two klebsormidiophyceans (*Entransia fimbriata* and *Klebsormidium* sp. SAG 51.86), one coleocheatophycean (*Coleochaete scutata*) and six zygnematophyceans (*Cylindrocystis brebissonii*, *Netrium digitus*, *Roya obtusa*, *Spirogyra maxima*, *Cosmarium botrytis* and *Cladophoraceum baillyanum*). Our comparative analyses of these genomes with their streptophyte algal counterparts indicate that the large inverted repeat (IR) encoding the rDNA operon experienced loss or expansion/contraction in all three sampled classes and that genes were extensively shuffled in both the Klebsormidiophyceae and Zygnematophyceae. The klebsormidiophycean genomes boast greatly expanded IRs, with the *Entransia* 60,590-bp IR being the largest known among green algae. The 206,025-bp *Entransia* cpDNA, which is one of the largest genome among streptophytes, encodes 118 standard genes, i.e., four additional genes compared to its *Klebsormidium flaccidum* homolog. We inferred that seven of the 21 group II introns usually found in land plants were already present in the common ancestor of the Klebsormidiophyceae and its sister lineages. At 107,236 bp and with 117 standard genes, the *Coleochaete* IR-less genome is both the smallest and most compact among the streptophyte algal cpDNAs analyzed thus far; it

lacks eight genes relative to its *Chaetosphaeridium globosum* homolog, four of which represent unique events in the evolutionary scenario of gene losses we reconstructed for streptophyte algae. The 10 compared zygnematophycean cpDNAs display tremendous variations at all levels, except gene content. During zygnematophycean evolution, the IR disappeared a minimum of five times, the rDNA operon was broken at four distinct sites, group II introns were lost on at least 43 occasions, and putative foreign genes, mainly of phage/viral origin, were gained.

Keywords: Streptophyta, charophytes, phylogenomics, plastid DNA, large inverted repeat, chloroplast genome evolution, genome rearrangements, group II introns

INTRODUCTION

The green plants, also referred to as Viridiplantae or Chloroplastida, split early (1200–700 Mya) into two main clades, the Chlorophyta and Streptophyta (Lewis and McCourt, 2004; Leliaert et al., 2012; Becker, 2013), and about 470 Mya, green algae from the Streptophyta gave rise to all land plants (Gensel, 2008; Becker and Marin, 2009; Kenrick et al., 2012). The streptophyte green algae, also called charophyte algae, inhabit freshwater environments and display a variety of cellular organizations, ranging from unicellular (e.g., *Mesostigma viride*, the only species of the Mesostigmatophyceae and some species of the Zygnetophyceae), to packets of cells (*Chlorokybus atmophyticus*) or filaments (Klebsormidiophyceae and Zygnetophyceae), and to multicellular organization (Cleocheotophyceae and Charophyceae) (Graham et al., 2000; McCourt et al., 2004; Umen, 2014). Identifying which of the six main lineages of streptophyte algae is the closest to land plants proved to be challenging (Karol et al., 2001; Turmel et al., 2006, 2007, 2013; Laurin-Lemay et al., 2012; Zhong et al., 2013); but there is now solid evidence based on both nuclear (Wodniok et al., 2011; Laurin-Lemay et al., 2012; Timme et al., 2012; Zhong et al., 2013; Wickett et al., 2014) and chloroplast phylogenomic studies that the Zygnetophyceae is sister to all land plants (Turmel et al., 2006; Turmel et al., 2007; Civan et al., 2014; Zhong et al., 2014). This morphologically diverse group comprises all green algae that reproduce sexually by conjugation and is the only streptophyte algal class that displays substantial diversity (at least 4000 species) (Gerrath, 2003), with several major lineages identified on the basis of the nuclear-encoded small subunit (SSU) rDNA and chloroplast-encoded *rbcL* gene sequences (Gontcharov et al., 2003, 2004), or on the basis of the chloroplast and mitochondrial *psaA*, *rbcL* and *cox3* genes (Hall et al., 2008). Based on the structure of the cell wall, the Zygnetophyceae has been divided into two orders: the Zygnematales feature a smooth cell wall (the ancestral trait) and the Desmidiales an ornamented and segmented cell wall (McCourt et al., 2000; Gerrath, 2003). Cell division in the three earliest-diverging lineages of the Streptophyta, the Mesostigmatophyceae, Chlorokybophyceae and Klebsormidiophyceae, occurs by furrowing, but as in land plants, the morphologically more complex Charophyceae and Cleocheotophyceae use a mechanism of cell division involving a phragmoplast and possess cell walls with plasmodesmata (Graham et al., 2000; McCourt et al., 2004).

To date, only nine chloroplast genome sequences of streptophyte algae are available in public databases: four for the Zygnetophyceae and a single genome for each of the remaining streptophyte algal lineages (Lemieux et al., 2000; Turmel et al., 2002, 2005, 2006; Lemieux et al., 2007; Civan et al., 2014). From their gene contents, which vary from 114 to 138 standard genes (i.e., genes whose orthologs are usually found in the chloroplast of photosynthetic eukaryotes), it was predicted that 144 unique standard genes were present in the common ancestor of all streptophytes (Turmel et al., 2006). Comparisons of streptophyte algal genomes with their land plant counterparts revealed that a large fraction of the structural features typically conserved in land plant chloroplast DNAs (cpDNAs) were inherited from streptophyte green algae occupying early diverging lineages (Turmel et al., 2006, 2007; Civan et al., 2014). For instance, 15 of the 21 group II introns found in land plants arose before the emergence of the Klebsormidiophyceae or during the evolutionary interval separating the latter lineage from the Charophyceae (Turmel et al., 2006, 2007; Civan et al., 2014). It was also inferred that the chloroplast genome remained unchanged or mostly unchanged in terms of gene content, gene order, and intron content during the transition from streptophyte algae to land plants (Turmel et al., 2006, 2007). In contrast, extensive gene shuffling and substantial structural alterations, including multiple intron losses, took place within the Zygnetophyceae (Turmel et al., 2005; Civan et al., 2014). The highly conserved quadripartite structure of green plant cpDNAs — a structure characterized by two copies of a large inverted repeat (IR) sequence encoding the rRNA operon, which are separated from one another by small and large single-copy (SSC and LSC) regions — was found in only one of the analyzed zygnematophyceans (*Roya anglica*); however, this IR contains a broken rRNA operon and two open reading frames (ORFs) not previously reported in other streptophyte IRs (Civan et al., 2014). This observation led Civan et al. (2014) to propose that either the IR was lost on three independent occurrences during the evolution of the Zygnetophyceae or that it arose *de novo* from an ancestor lacking an IR. In *Klebsormidium flaccidum*, the IR is also unusual with regards to its exceptionally large size and its apparent lack of the 4.5S and 5S rRNA genes from the rRNA operon (Civan et al., 2014).

Sampling of additional streptophyte algal taxa is required to better understand the evolutionary history of the chloroplast genome in the Zygnetophyceae and its evolutionary dynamics

in other classes. Toward these goals, we sequenced the chloroplast genomes of the klebsormidiophyceans *Entransia fimbriata* and *Klebsormidium* spec. SAG 51.86, the coleochaetophycean *Coleochaete scutata*, and six zygnematophyceans that were selected to represent distinct lineages in the SSU rDNA and *rbcL* phylogenies reported by Gontcharov et al. (2004): *Cylindrocystis brebissonii*, *Netrium digitus*, *Roya obtusa* and *Spirogyra maxima* belong to the Zygnematales, while *Cosmarium botrytis* and *Cladophora bailyanum* represent the Desmidiales. Our comparative analyses of these genomes with their previously described streptophyte green algal counterparts indicate that the large IR was involved in major structural changes (IR losses or expansion/contraction) in all three sampled classes and that genes underwent extensive shuffling in both the Klebsormidiophyceae and the Zygnematophyceae.

MATERIALS AND METHODS

Strains and Culture Conditions

Strains of *Klebsormidium* sp. SAG 51.86, *Coleochaete scutata* SAG 110.80M, *Cladophora bailyanum* SAG 50.89, *Cylindrocystis brebissonii* SAG 615-1, and *Roya obtusa* SAG 168.80 were obtained from the culture collection of algae at the University of Goettingen¹, whereas *Entransia fimbriata* UTEX LB 2353, *Cosmarium botrytis* UTEX 175, *Netrium digitus* UTEX LB 561, and *Spirogyra maxima* UTEX LB 2495 originated from the culture collection of algae at the University of Texas in Austin². All strains were grown in medium C (Andersen, 2005) at 18°C under alternating 12-h light/dark periods.

Genome Assemblies and Sequence Analyses

For all strains, except *Cosmarium* and *Cylindrocystis*, total cellular DNA was extracted as described (Turmel et al., 1999a) and A + T-rich organellar DNA was separated from nuclear DNA by CsCl-bisbenzimidazole isopycnic centrifugation (Lemieux et al., 2014). Total cellular DNA from *Cosmarium* and *Cylindrocystis* was isolated using the EZNA HP Plant Mini Kit of Omega Bio-Tek (Norcross, GA, USA).

For Illumina sequencing of the *Cladophora*, *Cosmarium*, and *Cylindrocystis* chloroplast genomes, libraries of 700-bp fragments were constructed using the TrueSeq DNA Sample Prep Kit (Illumina, San Diego, CA, USA) and paired-end reads were generated on the Illumina HiSeq 2000 (100-bp reads) or the MiSeq (300-bp reads) sequencing platforms by the Innovation Centre of McGill University and Génome Québec³ and the “Plateforme d’Analyses Génomiques de l’Université Laval⁴”, respectively. Reads were assembled using Ray v2.3.1 (Boisvert et al., 2010) and contigs were visualized, linked and edited using CONSED v22 (Gordon et al., 1998). Contigs of chloroplast origin were identified by BLAST searches against a local database of

organellar genomes. Regions spanning gaps in cpDNA assemblies were amplified by polymerase chain reaction (PCR) with primers specific to the flanking sequences. Purified PCR products were sequenced using Sanger chemistry with the PRISM BigDye Terminator Ready Reaction Cycle Sequencing Kit (Applied Biosystems, Foster City, CA, USA) on ABI model 373 or 377 DNA sequencers (Applied Biosystems).

For 454 sequencing of the *Entransia*, *Netrium*, *Roya* and *Spirogyra* chloroplast genomes, shotgun libraries (700-bp fragments) of A + T-rich DNA fractions were constructed using the GS-FLX Titanium Rapid Library Preparation Kit of Roche 454 Life Sciences (Branford, CT, USA). Library construction and 454 GS-FLX DNA Titanium pyrosequencing were carried out by the “Plateforme d’Analyses Génomiques de l’Université Laval⁵.” Reads were assembled using Newbler v2.5 (Margulies et al., 2005) with default parameters, and contigs were visualized, linked and edited using CONSED v22 (Gordon et al., 1998). Identification of cpDNA contigs and gap filling were performed as described above for Illumina sequence assemblies.

For Sanger sequencing of the *Klebsormidium* and *Coleochaete* chloroplast genomes, random clone libraries were prepared from 1500 to 2000-bp fragments derived from A + T rich DNA fractions using the pSMART-HCKan (Lucigen Corporation, Middleton, WI, USA) plasmid. Positive clones were selected by hybridization of each plasmid library with the original DNA used for cloning. DNA templates were amplified using the Illustra TempliPhi Amplification Kit (GE Healthcare, Baie d’Urfé, Canada) and sequenced with the PRISM BigDye terminator cycle sequencing ready reaction kit (Applied Biosystems) on ABI model 373 or 377 DNA sequencers (Applied Biosystems), using SR2 and SL1 primers as well as oligonucleotides complementary to internal regions of the plasmid DNA inserts. The resulting sequences were edited and assembled using Sequencher v5.1 (Gene Codes Corporation, Ann Arbor, MI, USA). Genomic regions not represented in the sequence assemblies or plasmid clones were directly sequenced from PCR-amplified fragments using primers specific to the flanking contigs.

Genes and ORFs were identified on the final assemblies using a custom-built suite of bioinformatics tools as described previously (Turmel et al., 2006). tRNA genes were localized using tRNAscan-SE v1.3.1 (Lowe and Eddy, 1997). Intron boundaries were determined by modeling intron secondary structures (Michel et al., 1989; Michel and Westhof, 1990) and by comparing intron-containing genes with intronless homologs. Circular genome maps were drawn with OGDraw v1.2 (Lohse et al., 2007). Genome-scale sequence comparisons of the pairs of *Roya* and *Klebsormidium* species were carried out with LAST v7.1.4 (Frith et al., 2010). For all compared genomes, G + C contents of a set of 88 protein-coding genes were determined at the three codon positions using DAMBE v5 (Xia, 2013).

To estimate the proportion of small repeated sequences, repeats ≥ 30 bp were retrieved using REPFIND of the REPuter v2.74 program (Kurtz et al., 2001) with the options –f –p –l –allmax and were then masked on the genome sequences using

¹<http://www.uni-goettingen.de/de/184982.html>

²<http://utex.org/>

³<http://gqinnovationcenter.com/index.aspx>

⁴<http://pag.ibis.ulaval.ca/seq/en/>

⁵<http://pag.ibis.ulaval.ca/seq/en/>

RepeatMasker⁶ running under the Crossmatch search engine⁷. The G+C contents of the repeated and unique sequences were calculated from the outputs of RepeatMasker that were generated with the -xsmall option (under this option the repeat regions are returned in lower case and non-repetitive regions in capitals in the masked file).

Phylogenetic Analyses

The chloroplast genomes of 28 streptophyte taxa were used to generate the analyzed amino acid (PCG-AA) and nucleotide (PCG12) data sets. The latter were assembled from the following 88 protein-coding genes: *accD*, *atpA*, *B*, *E*, *F*, *H*, *I*, *ccsA*, *cemA*, *chlB*, *I*, *L*, *N*, *clpP*, *ftsH*, *infA*, *ndhA*, *B*, *C*, *D*, *E*, *F*, *G*, *H*, *I*, *J*, *K*, *odpB*, *petA*, *B*, *D*, *G*, *L*, *N*, *psaA*, *B*, *C*, *I*, *J*, *M*, *psbA*, *B*, *C*, *D*, *E*, *F*, *H*, *I*, *J*, *K*, *L*, *M*, *N*, *T*, *Z*, *rbcL*, *rpl2*, *14*, *16*, *20*, *21*, *22*, *23*, *32*, *33*, *36*, *rpoA*, *B*, *C1*, *C2*, *rps2*, *3*, *4*, *7*, *8*, *11*, *12*, *14*, *15*, *16*, *18*, *19*, *ycf1*, *3*, *4*, *12*, *62*, *66*.

The PCG-AA data set was prepared as follows: the deduced amino acid sequences from the 88 individual genes were aligned using MUSCLE v3.7 (Edgar, 2004), the ambiguously aligned regions in each alignment were removed using TrimAl v1.3 (Capella-Gutierrez et al., 2009) with the options block = 6, gt = 0.7, st = 0.005 and sw = 3, and the protein alignments were concatenated using Phyutility v2.2.6 (Smith and Dunn, 2008). Phylogenies were inferred from the PCG-AA data set using the maximum likelihood (ML) and Bayesian methods. ML analyses were carried out using RAxML v8.2.3 (Stamatakis, 2014) and the GTR + Γ4 model of sequence evolution; in these analyses, the data set was partitioned by gene, with the model applied to each partition. Confidence of branch points was estimated by fast-bootstrap analysis ($f = a$) with 100 replicates. Bayesian analyses were performed with PhyloBayes v4.1 (Lartillot et al., 2009) using the site-heterogeneous CATGTR + Γ4 model (Lartillot and Philippe, 2004). Five independent chains were run for 2,000 cycles and consensus topologies were calculated from the saved trees using the BPCOMP program of PhyloBayes after a burn-in of 500 cycles. Under these conditions, the largest discrepancy observed across all bipartitions in the consensus topologies (maxdiff) was 0.0007, indicating that convergence between the chains was achieved.

The PCG12 nucleotide data set (first and second codon positions) was prepared as follows. The multiple sequence alignment of each protein was converted into a codon alignment, the poorly aligned and divergent regions in each codon alignment were excluded using Gblocks v0.91b (Castresana, 2000) with the $-t = c$, $-b3 = 5$, $-b4 = 5$ and $-b5 = \text{half}$ options, and the individual gene alignments were concatenated using Phyutility v2.2.6 (Smith and Dunn, 2008). The third codon positions of the resulting PCG123 alignment were then excluded using Mesquite v3.04 (Maddison and Maddison, 2015) to produce the PCG12 data set. ML analysis of the PCG12 data set was carried out using RAxML v8.2.3 (Stamatakis, 2014) and the GTR + Γ4 model of sequence evolution. This data set was partitioned into gene groups, with the model applied to each partition. Confidence of

branch points was estimated by fast-bootstrap analysis ($f = a$) with 100 replicates.

dN, dS and dN/dS trees were inferred from a *tufA* codon alignment prepared as described above using PAML v4.8a (Yang, 2007) and the F3X4 codon frequencies model implemented in codeml. Positive selection was tested across the *tufA* sequences using the PARRIS module implemented in Datamonkey (Delport et al., 2010).

Analyses of Gene Order and Reconstruction of Genomic Character Evolution

Syntenic regions in pairwise genome comparisons were identified using a custom-built program and the number of gene reversals between the compared genomes was estimated with GRIMM v2.01 (Tesler, 2002). The same custom-built program was employed to convert gene order to all possible pairs of signed genes (i.e., taking into account gene polarity); the gene pairs conserved in three or more genomes were visualized using Mesquite v3.04 (Maddison and Maddison, 2015). Gains and/or losses of genomic characters (standard genes, introns and gene pairs) were mapped on the streptophyte tree topology inferred in this study using MacClade v4.08 (Maddison and Maddison, 2000) and the Dollo principle of parsimony.

A ML tree based on gene adjacency was inferred using the phylogeny reconstruction option of the MLGO web server (Hu et al., 2014) and a gene order matrix containing all standard genes (including all copies of duplicated genes). Confidence of branch points was estimated by 1000 bootstrap replications. A gene reversal tree with the same topology as the MLGO tree was also computed; branch lengths were estimated using the $-t$ option of MGR v2.03 (Bourque and Pevzner, 2002) and a gene order matrix of the 89 genes shared by all compared genomes; because MGR cannot handle duplicated genes, only one copy of the IR and of each duplicated gene was included in this analysis.

Availability of Supporting Data

The chloroplast genome sequences generated in this study are available in the GenBank database under the accession numbers KU646489-KU646497. The data sets supporting the results of this article are available in the TreeBASE repository (Study ID 19085).

RESULTS

General Features

The chloroplast genomes of the nine sampled taxa, except that of *Klebsormidium* sp. SAG 51.86, were entirely sequenced and assembled as circular-mapping molecules (Figures 1–4). Although these genomes assembled as circles, it is possible that they exist *in vivo* as multi-genomic, linear-branched structures, as reported for land plant cpDNAs (Bendich, 2004). Their sizes range from 107 (for *Coleochaete*) to 208 kb (for *Cosmarium*) (Figures 1–4). Genome size variation is also important among lineages of the same class, in particular within the Zygnematophyceae where the variation is 1.6-fold (from

⁶<http://www.repeatmasker.org/>

⁷<http://www.phrap.org/>

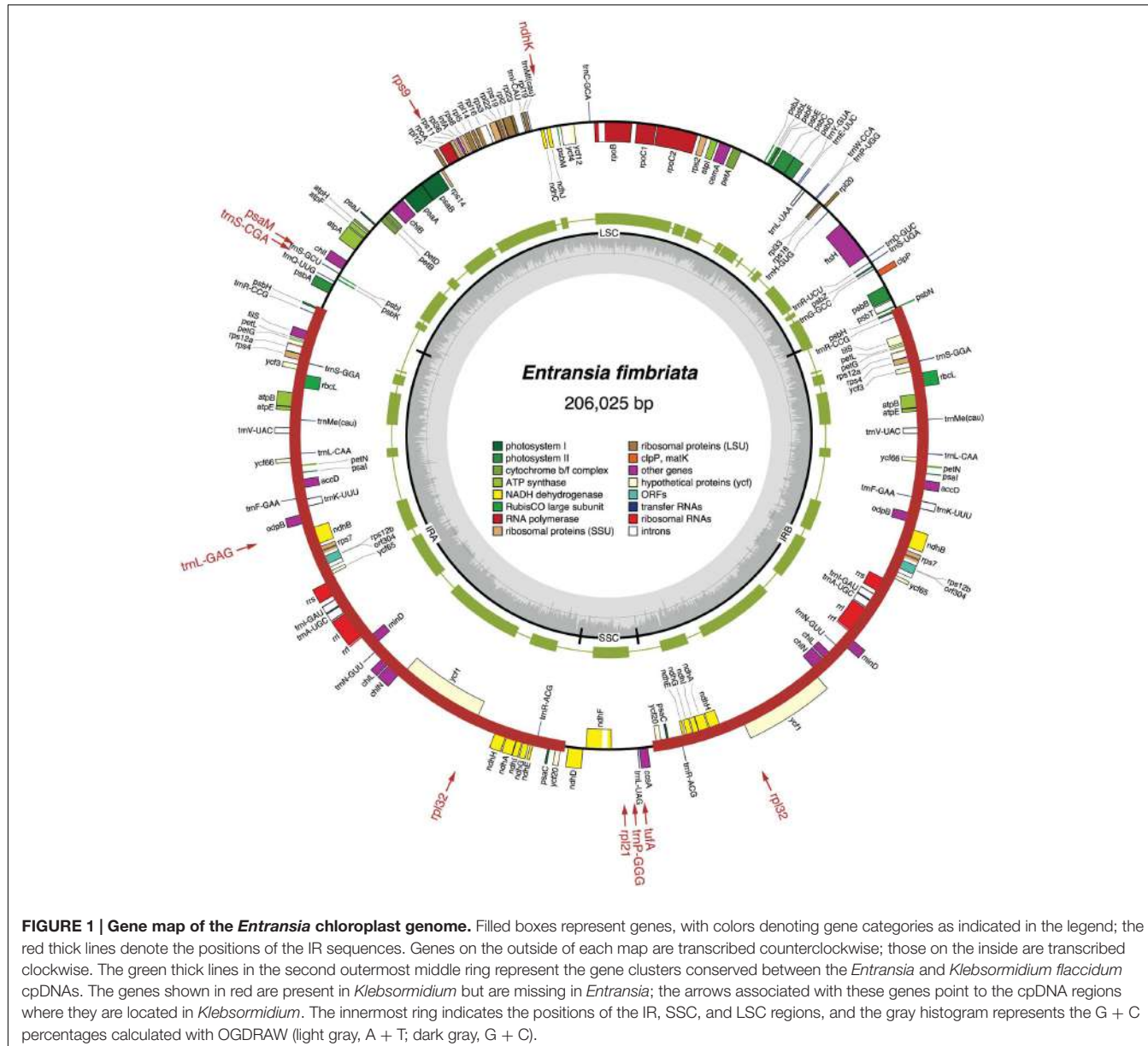
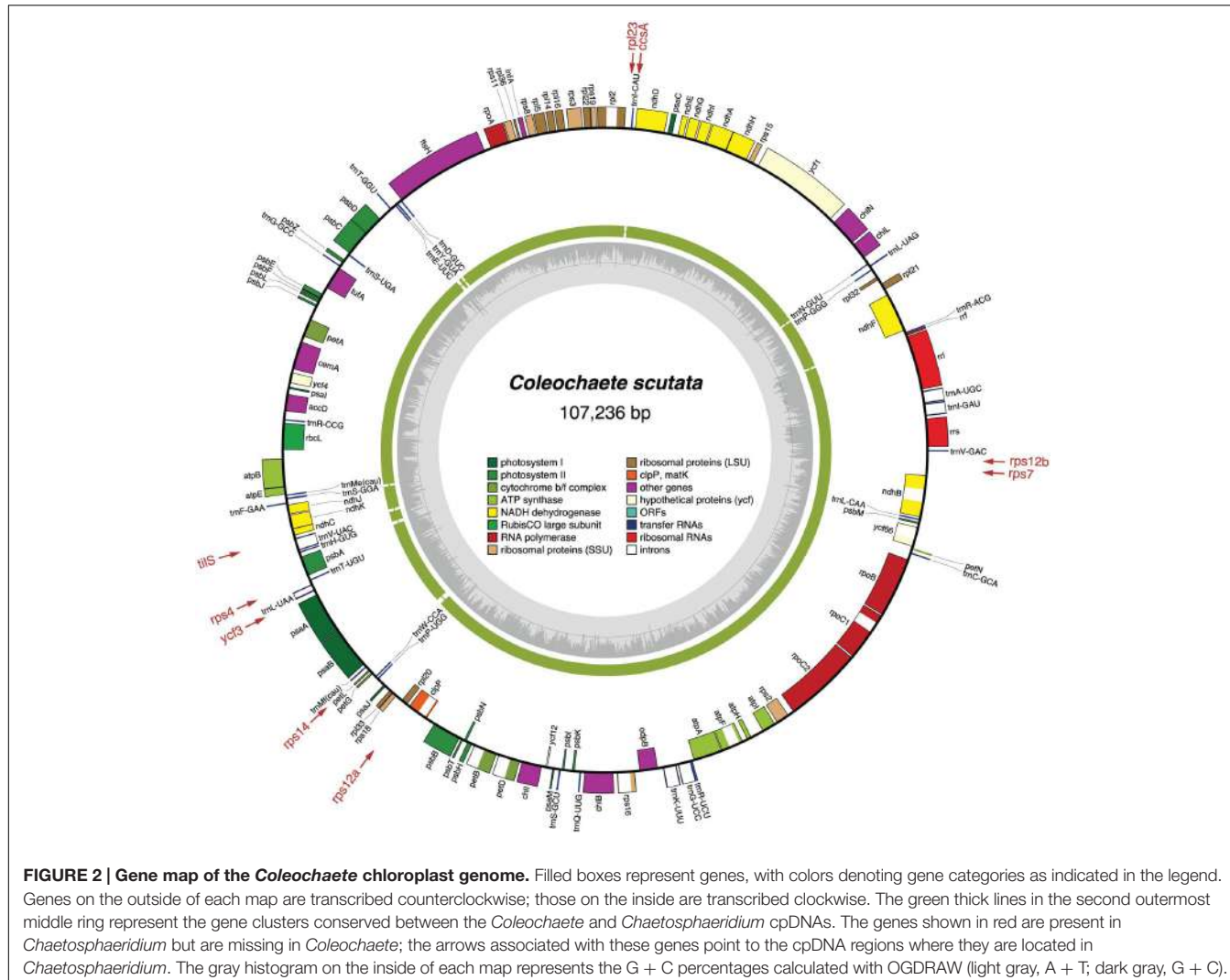


FIGURE 1 | Gene map of the *Entransia* chloroplast genome. Filled boxes represent genes, with colors denoting gene categories as indicated in the legend; the red thick lines denote the positions of the IR sequences. Genes on the outside of each map are transcribed counterclockwise; those on the inside are transcribed clockwise. The green thick lines in the second outermost middle ring represent the gene clusters conserved between the *Entransia* and *Klebsormidium flaccidum* cpDNAs. The genes shown in red are present in *Klebsormidium* but are missing in *Entransia*; the arrows associated with these genes point to the cpDNA regions where they are located in *Klebsormidium*. The innermost ring indicates the positions of the IR, SSC, and LSC regions, and the gray histogram represents the G + C percentages calculated with OGDRAW (light gray, A + T; dark gray, G + C).

130 kb in *Spirogyra* to 208 kb in *Cosmarium*). Within the Klebsormidiophyceae, differences in IR size, intron content, and lengths of intergenic regions essentially account for the increased size of the *Entransia* genome (206 kb) compared to that of *Klebsormidium flaccidum* (177 kb) (Table 1; Figure 5). Note that we detected an IR in the partially sequenced *Klebsormidium* sp. SAG 51.86 genome but were unable to identify the IR/SSC junction; 91% of this 130,962-kb genome sequence could be aligned with the *Klebsormidium flaccidum* genome in a strictly colinear fashion, highlighting the absence of just two genes [*trnN(guu)* and *ccsA*] and a total of 7,551 divergent positions, i.e., 6.3% of the aligned sequence. Within the Coleochaetophyceae, the 24-kb difference between the *Chaetosphaeridium* and *Coleochaete* genomes is largely due to the absence of the IR and of eight genes, as well as to shorter intergenic regions in

Coleochaete (Table 1; Figure 5). For the Zygnematophyceae, the observed genome size variation is attributable to combinations of all the abovementioned factors (Table 1; Figure 5). Only half of the six newly sequenced zygnematophycean genomes display an IR: the 12.6-kb IR of *Roya obtusa* is about two-fold smaller than those of *Closterium* and *Cosmarium*, but is about the same size as that found in the coleochaetophycean *Chaetosphaeridium*. The newly sequenced zygnematophycean genomes also differ greatly in intron content. For instance, the *Closterium* and *Cosmarium* genomes, which are the largest among the examined zygnematophyceans, display the lowest and highest numbers of introns, respectively; moreover, they exhibit the highest proportion of repeats ≥ 30 bp (Table 1). Note that the alignment of the *Roya obtusa* and *Roya anglica* cpDNAs revealed that these genomes are colinear over their entire length and that



their sequences diverge at only 74 sites (i.e., 0.05% divergence), 12 of which are indels of 1, 2, or 4 nucleotides.

G + C content at the genome level varies from 26.2 to 42.2%, and at the high end of this range are found the cpDNAs of *Chlorokybus*, *Klebsormidium flaccidum* and of the zygnematophyceans *Mesotaenium*, *Cladophora* and *Cosmarium* (**Table 1**). Although coding regions have generally a higher G + C content than introns and intergeneric regions, the *Cosmarium* genome harbors an excess of guanines and cytosines in its intergenic regions compared to the rest of the genome sequence (Supplementary Figure S1A). The *Klebsormidium flaccidum* and *Mesotaenium* coding regions display the highest G + C content at the first, second and third codon positions (Supplementary Figure S1B). The dispersed repeats present in both the *Cladophora* and *Cosmarium* genomes are richer in G + C than unique sequences (52.5 and 60.7% versus 38.6 and 38.5%, respectively).

Phylogenomic Analyses

Before moving on to other comparative genome analyses, we provide here the phylogenetic context that will be necessary to

interpret the results of these analyses. We analyzed an amino acid data set (PCG-AA, 18,646 sites) and a nucleotide data set (PCG12, 38,354 sites), both derived from the same set of 88 chloroplast protein-coding genes from 28 streptophytes — 18 algae and ten selected land plants — using the Bayesian and/or ML methods (**Figure 6**). Missing data account for only 5.2% of each data set. Regardless of the data set or the reconstruction method used, identical relationships were recovered for the streptophyte algae, with the Zygnematophyceae being sister to land plants. In the latter algal class, *Mesotaenium* represents the earliest-diverging lineage and is followed by the clade formed by *Zygnema* and *Cylindrocystis*, and next by the *Spirogyra* and *Netrium* lineages. The two *Roya* species, which also belong to the Zygnematales order, are sister to the desmidalean clade uniting *Cladophora* with *Cosmarium* and *Staurastrum*. All the nodes associated with the streptophyte algal lineages received strong statistical support in the ML protein tree, except the inner node subtending the branch leading to *Spirogyra* and its sister lineages. The protein and gene phylogenies differed only with respect to the branching order of the bryophyte lineages.

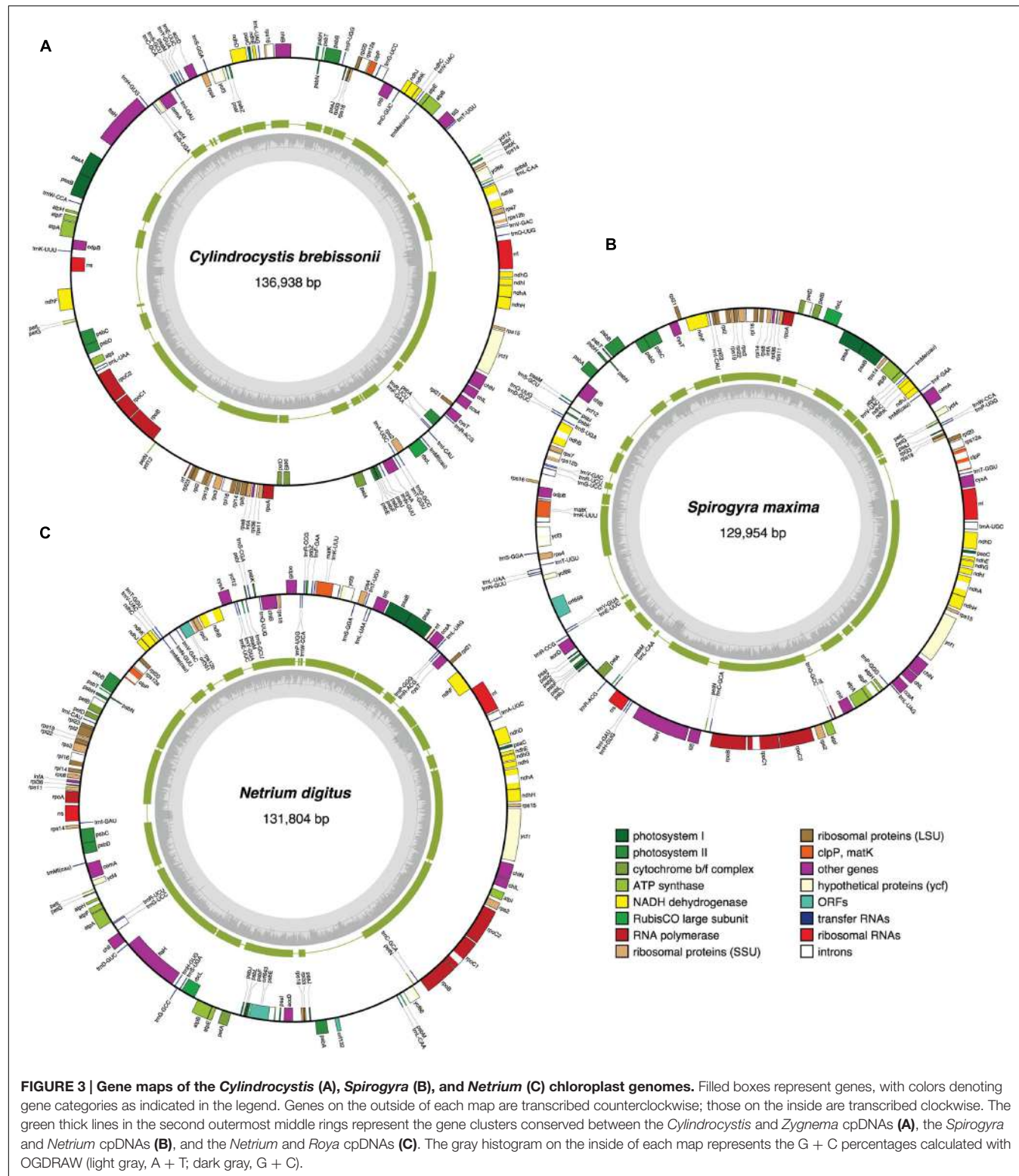


FIGURE 3 | Gene maps of the *Cylindrocystis* (A), *Spirogyra* (B), and *Netrium* (C) chloroplast genomes. Filled boxes represent genes, with colors denoting gene categories as indicated in the legend. Genes on the outside of each map are transcribed counterclockwise; those on the inside are transcribed clockwise. The green thick lines in the second outermost middle rings represent the gene clusters conserved between the *Cylindrocystis* and *Zygnema* cpDNAs (A), the *Spirogyra* and *Netrium* cpDNAs (B), and the *Netrium* and *Roya* cpDNAs (C). The gray histogram on the inside of each map represents the G + C percentages calculated with OGDRAW (light gray, A + T; dark gray, G + C).

Gene Content

Standard Genes

All compared genomes share a set of 90 genes coding for three rRNAs (*rrs*, *rnl* and *rrf*), 24 tRNAs, and 63 proteins (see legend of

Figure 7). Therefore, of the 144 standard genes predicted to have been present in the common ancestor of all streptophytes, 54 (42 protein-coding genes, 11 tRNA genes and the *ssrA* gene coding for tmRNA) experienced losses from the chloroplast during

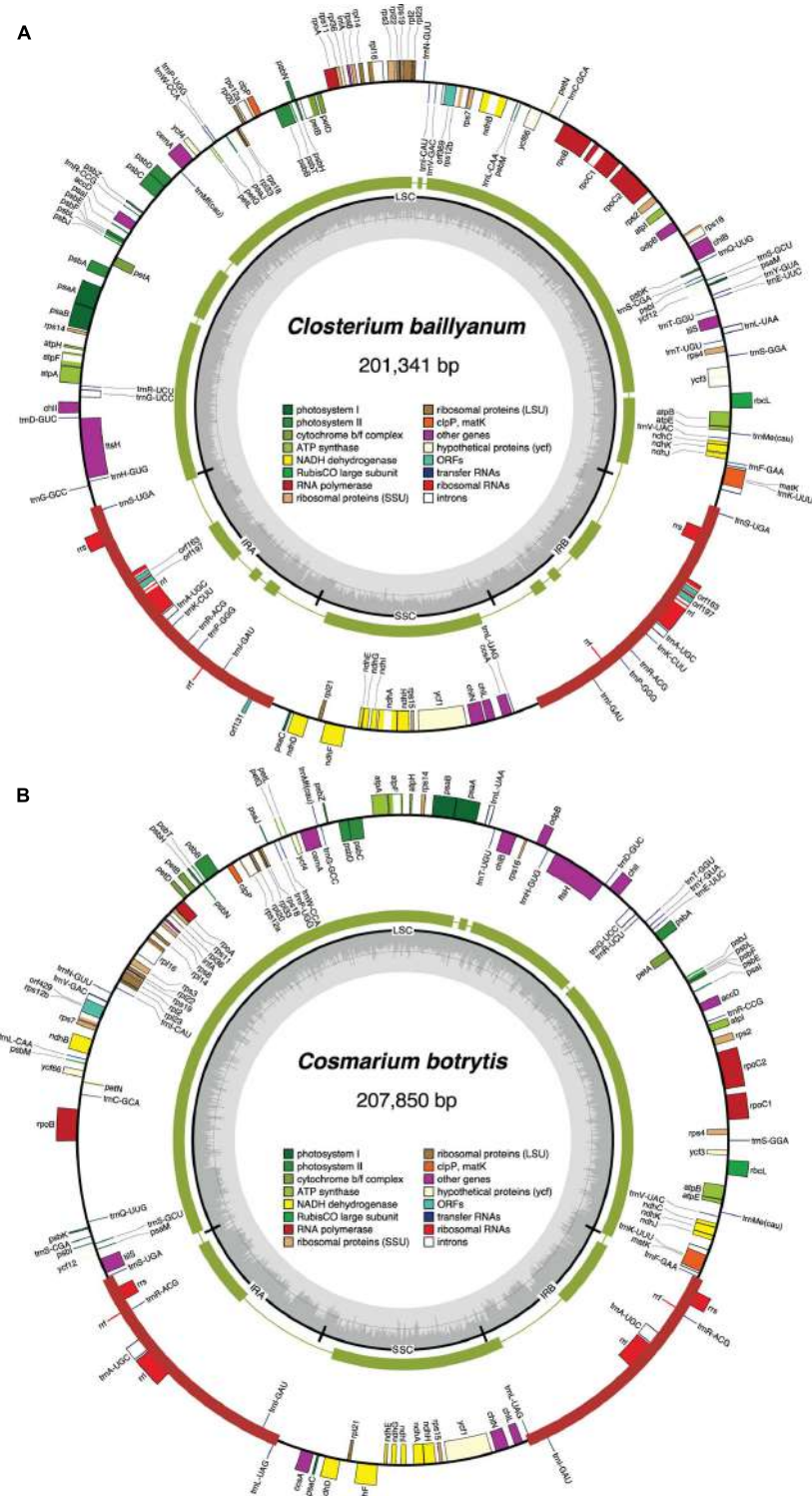
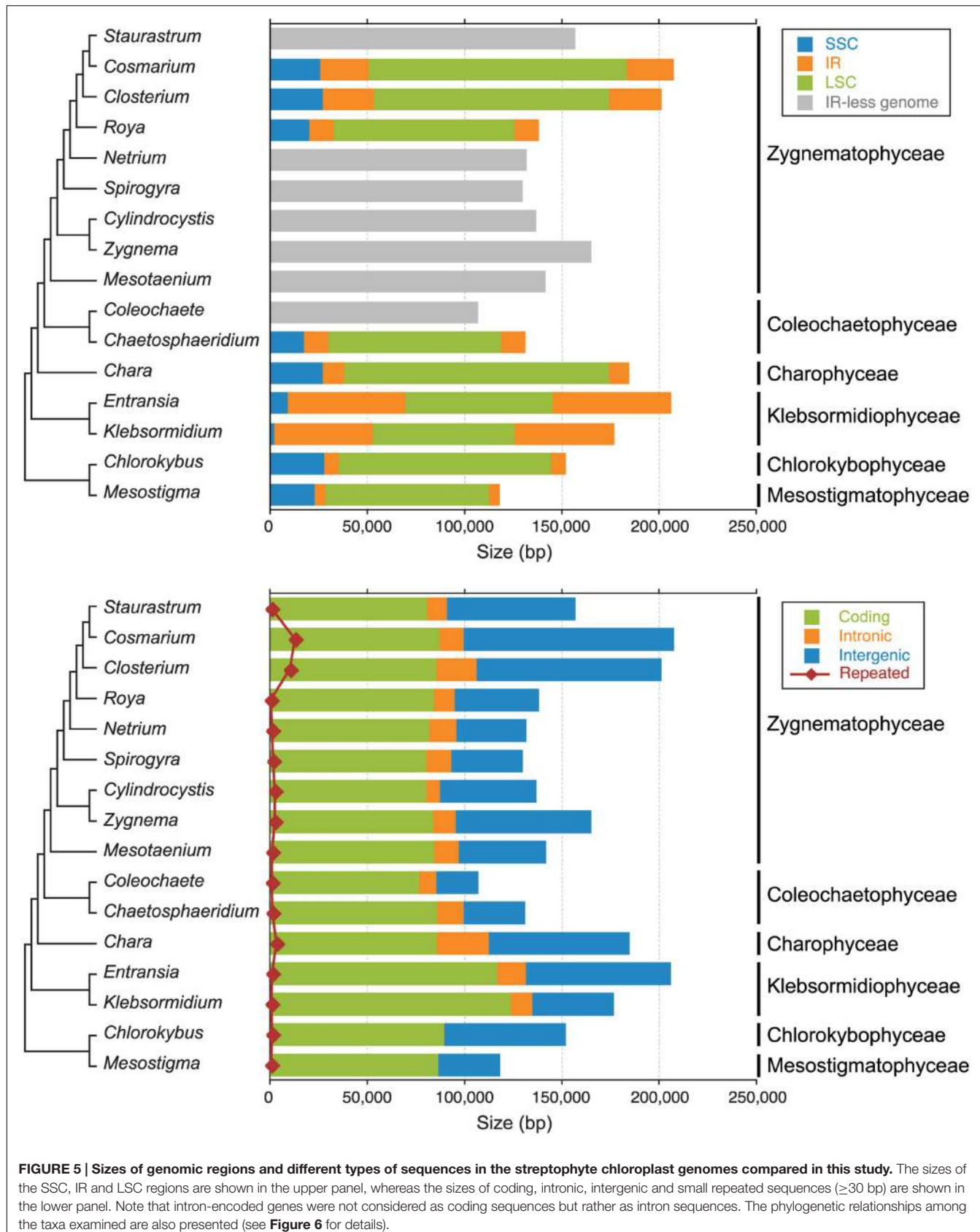


FIGURE 4 | Gene maps of the *Closterium* (A) and *Cosmarium* (B) chloroplast genomes. Filled boxes represent genes, with colors denoting gene categories as indicated in the legend; the red thick lines denote the positions of the IR sequences. Genes on the outside of each map are transcribed counterclockwise; those on the inside are transcribed clockwise. The green thick lines in the second outermost middle rings represent the gene clusters conserved between the *Closterium* and *Roya* cpDNAs (A) and the *Cosmarium* and *Staurastrum* cpDNAs (B). The innermost ring indicates the positions of the IR, SSC and LSC regions. The innermost ring indicates the positions of the IR, SSC and LSC regions, and the gray histogram represents the G + C percentages calculated with OGDRAW (light gray, A + T; dark gray, G + C).

TABLE 1 | General features of the streptophyte green algal chloroplast genomes compared in this study.

Taxon	Accession no. ^a	Size (bp)			G+C (%)		Genes		Introns (no.)		Repeats ^b (%)
		Total	IR	LSC	SSC	No. ^c	% genome ^d	Group I	Group II ^e		
Mesostigmatophyceae											
<i>Mesostigma viride</i> NIES 296	NC_002186	118,360	6,057	83,627	22,619	30.1	137	73.2			0.2
Chlorokybophyceae											
<i>Chlorokybus atmophyticus</i> SAG 48.80	NC_008822	152,254	7,640	109,098	27,876	38.2	138	58.8	1		0.5
Klebsormidophyceae											
<i>Klebsormidium</i> sp. SAG 51.86 ^f	KU646497*	>130,962 ^g									
<i>Klebsormidium flaccidum</i> SAG 121.8	NC_024167	176,832	51,118	72,779	1,817	40.6	112	67.7	12 (2)		0
<i>Entransia fimbriata</i> UTEX LB 2353	KU646490*	206,025	60,590	75,629	9,216	33.0	118	64.4	12 (2)		0.2
Charophyceae											
<i>Chara vulgaris</i>	NC_008097	184,933	10,919	135,815	27,280	26.2	127	60.9	2	16 (1)	1.6
Coleochaetophyceae											
<i>Chaetosphaeridium globosum</i> M1311	NC_004115	131,183	12,431	88,682	17,639	29.6	125	76.9	1	17 (1)	0.7
<i>Coleochaete scutata</i> SAG 110.80M	KU646493*	107,236				27.6	117	79.9	1	14 (0)	0.6
Zygnematophyceae											
<i>Mesotaenium endlicherianum</i> SAG 12.97	NC_024169	142,017				42.2	124	68.4	1	16 (1)	0.6
<i>Zygneria circumcarinatum</i> SAG 698-1a	NC_008117	165,372				31.1	125	57.8	1	12 (1)	1.2
<i>Cylindrocystis brebissonii</i> SAG 615-1	KU646495*	136,938				29.8	122	63.8	1	9 (1)	1.5
<i>Spirogyra maxima</i> UTEX LB 2495	KU646489*	129,954				30.1	124	73.3	1	16 (1)	1.0
<i>Netrium digitus</i> UTEX LB 561	KU646491*	131,804				31.4	125	74.5	1	13 (1)	0.5
<i>Roya anglica</i> AC01 799	NC_024168	138,275	12,568	92,926	20,213	33.1	122	69.7	1	9 (1)	0.1
<i>Roya obtusa</i> SAG 168.80	KU646496*	138,272	12,568	92,924	20,212	33.1	122	69.9	1	9 (1)	0.1
<i>Cladophora bailyanum</i> SAG 50.89	KU646494*	201,341	26,784	120,746	27,027	39.3	124	53.1	4	15 (1)	4.9
<i>Cosmarium batovi</i> UTEX 175	KU646492*	207,850	24,465	132,863	26,057	39.8	122	47.9	1	6 (1)	6.0
<i>Staurastrum punctulatum</i> SAG 679-1	NC_008116	157,089				32.5	122 ^h	58.4	1	7 (1)	0.3

^aThe asterisks denote the nine genomes described here for the first time. ^bNon-overlapping repeat elements were mapped on each genome with RepeatMasker using the repeats ≥ 30 bp identified with REPuter as input sequences. ^cOnly standard genes conserved in green plant chloroplast genomes are included in these values. Duplicated genes were counted only once. ^dThese values include the sequences of standard genes and ORFs coding for proteins of known functions. The first value provides the total number of group I introns; the number of trans-spliced introns is given in parentheses. ^eThis species was formerly called *Microspora stagnorum* (Mikhail'yuk et al., 2008). ^fThe exact size of the *Klebsormidium* sp. SAG 51.86 genome could not be determined because the IR/SSC junction was not identified. The features of this genome were estimated from the partial sequence. ^gThis value includes the *trnS(cga)* pseudogene found in the *Staurastrum* genome (Turmel et al., 2005).



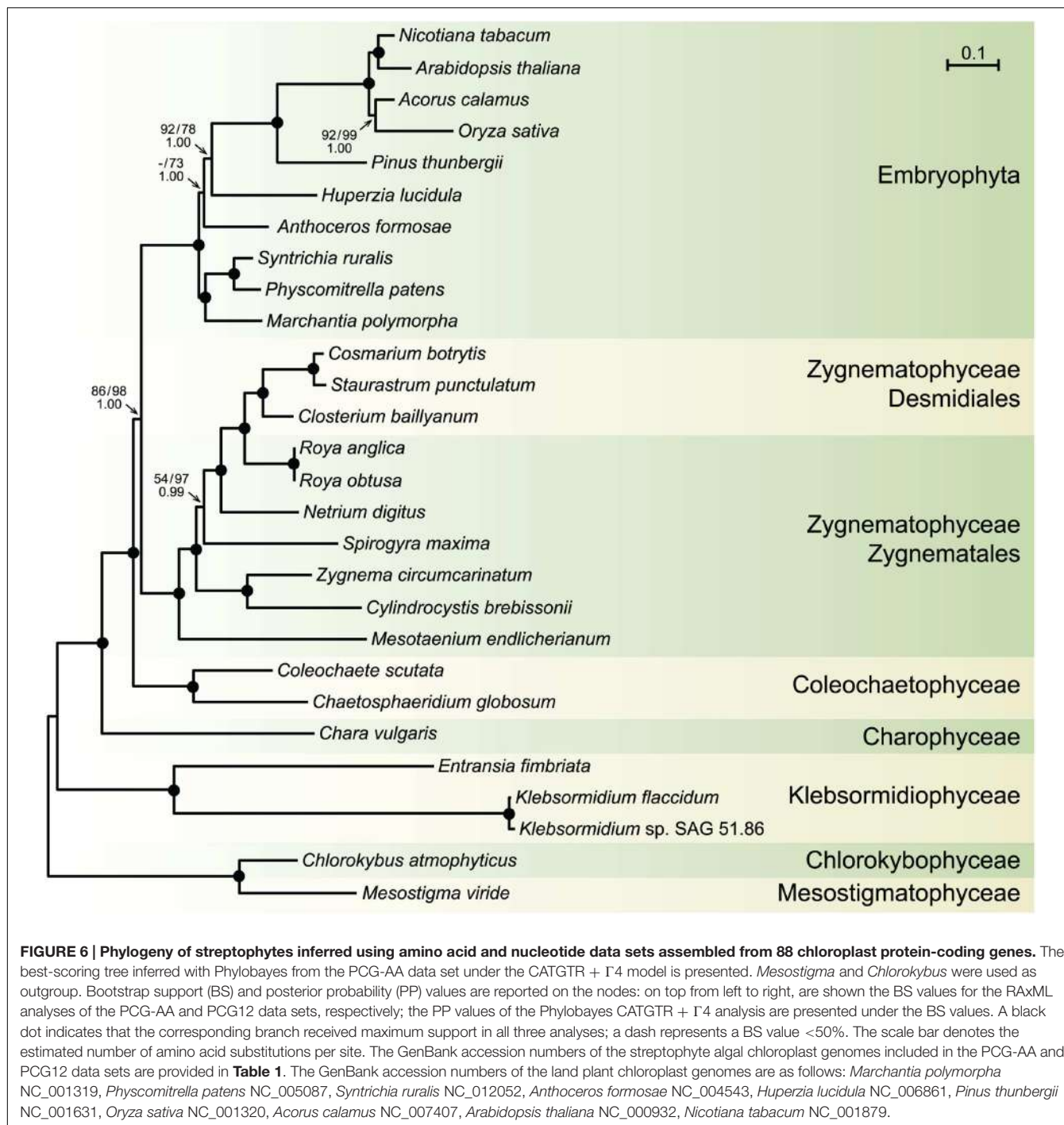
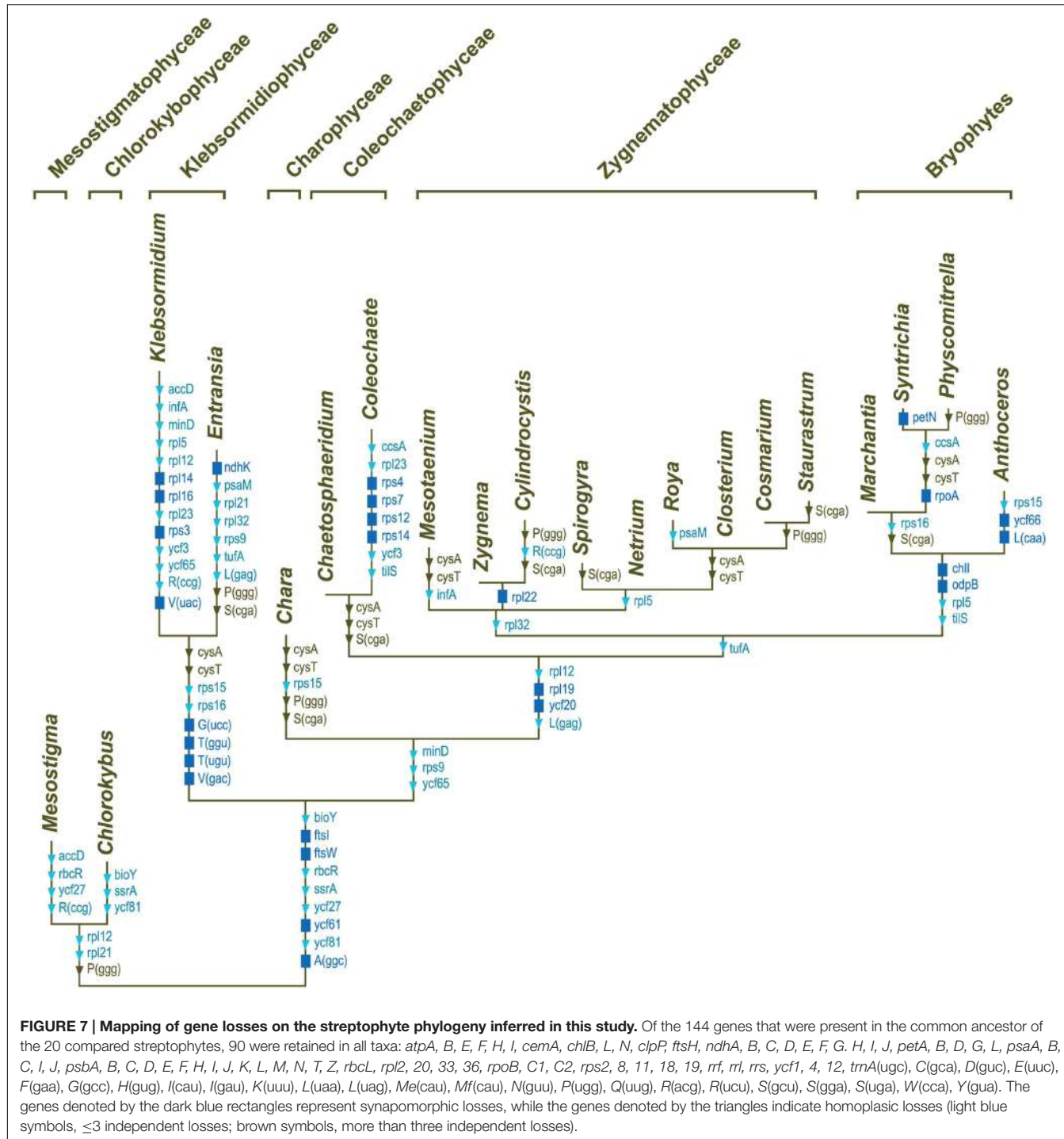


FIGURE 6 | Phylogeny of streptophytes inferred using amino acid and nucleotide data sets assembled from 88 chloroplast protein-coding genes. The best-scoring tree inferred with Phylobayes from the PCG-AA data set under the CATGTR + Γ4 model is presented. *Mesostigma* and *Chlorokybus* were used as outgroup. Bootstrap support (BS) and posterior probability (PP) values are reported on the nodes: on top from left to right, are shown the BS values for the RAxML analyses of the PCG-AA and PCG12 data sets, respectively; the PP values of the Phylobayes CATGTR + Γ4 analysis are presented under the BS values. A black dot indicates that the corresponding branch received maximum support in all three analyses; a dash represents a BS value <50%. The scale bar denotes the estimated number of amino acid substitutions per site. The GenBank accession numbers of the streptophyte algal chloroplast genomes included in the PCG-AA and PCG12 data sets are provided in Table 1. The GenBank accession numbers of the land plant chloroplast genomes are as follows: *Marchantia polymorpha* NC_001319, *Physcomitrella patens* NC_005087, *Syntrichia ruralis* NC_012052, *Anthoceros formosae* NC_004543, *Huperzia lucidula* NC_006861, *Pinus thunbergii* NC_001631, *Oryza sativa* NC_001320, *Acorus calamus* NC_007407, *Arabidopsis thaliana* NC_000932, *Nicotiana tabacum* NC_001879.

diversification of streptophyte algae (Figure 7). A total of 103 gene losses was inferred by mapping these genes on the phylogeny shown in Figure 6. Only 26 of these events occurred once, many of which represent signatures uniting different streptophyte classes or divergent lineages belonging to the same class.

Subsequent to the losses of three genes during the evolutionary period preceding the emergence of the common ancestor of *Chaetosphaeridium* and *Coleochaete*, eight genes disappeared in the lineage leading to *Coleochaete*. The reduced number of genes

in klebsormidiophyceans is the result of eight gene losses that occurred during the interval leading to the common ancestor of the *Klebsormidium* and *Entransia* genera and of 22 gene losses that occurred in the lineages leading to *Klebsormidium* and *Entransia*. Note that the *rrf* gene encoding the 5S rRNA is not included in the list of *Klebsormidium* losses; Civan et al. (2014) failed to identify this gene in [GenBank:NC_024167] but we discovered its highly divergent sequence at coordinate positions 92980–93102 and 156632–156510 during the course of



this study. We also found the 3' *rrl* sequence that was reported to be missing in the same alga (Civan et al., 2014); this sequence corresponds to the 4.5S rRNA that is part of the land plant large-subunit rRNA. The complete *rrl* gene spans coordinate positions 89958–92857 and 159654–156755 in the *Klebsormidium* genome [GenBank:NC_024167].

Of the 123 genes predicted to have been present in the common ancestor of all land plants, fewer than five are

missing in the Zygnematophyceae. *Netrium* is missing *rpl32*, and in addition to the latter gene, *Zygnema* is missing *rpl22* and *Spirogyra trnS(cga)*. The *cysA* and *cysT* genes encoding components of the sulfate transport system are found in early-diverging lineages of the Zygnematophyceae (*Zygnema*, *Cylindrocystis*, *Spirogyra* and *Netrium*) but are missing in all other streptophyte lineages, except in the basal Mesostigmatophyceae and Chlorokybophyceae.

The gene loss scenario discussed above does not include *trnK(cuu)*, a tRNA gene found exclusively in the zygnematophytes *Mesotaenium* and *Cladophora*. BlastN similarity searches against the non-redundant database of NCBI indicated that this gene arose from duplication and subsequent sequence divergence of *trnN(guu)*. Prior to our study, the trebouxiophycean *Stichococcus bacillaris* was the only known green alga carrying *trnK(cuu)* in its chloroplast; however, it was found to originate from duplication of *trnK(uuu)* (Turmel et al., 2015).

Increased Mutation Rates of *tufA* in the Coleochaetophyceae

The *Coleochaete scutata* *tufA* gene encoding the protein synthesis factor Tu has retained an intact open reading frame but like its *Chaetosphaeridium* and *Coleochaete orbicularis* counterparts, it is highly divergent in sequence compared to the corresponding genes found in *Mesostigma*, *Chlorokybus* and *Chara*. Our alignment of streptophyte *tufA* sequences also revealed a marked G + C bias at the third codon positions of the *Klebsormidium* sequence. We calculated dN, dS and dN/dS branch lengths for *tufA* based on the relationships we inferred in Figure 6 and found that the dN branches subtending and within the *Coleochaete* + *Chaetosphaeridium* clade are very long compared to all other examined streptophyte algae (Figure 8). The long branch subtending the *Coleochaete* + *Chaetosphaeridium* clade in the dN/dS tree might suggest that *tufA* experienced positive selection during early evolution of coleochaetophyceans. However, no evidence for positive selection across the *tufA* sequence ($P < 0.1$) was obtained in the likelihood ratio test implemented in the PARRIS module of Datamonkey (Delpont et al., 2010).

Non-standard Genes

Freestanding ORFs showing similarities (*E*-value threshold of 1e-08) with recognized protein domains were identified in zygnematophycean chloroplast genomes (Table 2). They encode type II intron maturases (MatK), a phage DNA primase and DNA breaking-rejoining enzymes (recombinase/integrase).

The *Roya obtusa* genome contains an ORF (*orf230*, coordinates 102713-103405 in GenBank:KU646496) that is similar to chloroplast ORFs present in *Roya anglica* and two ferns of the Ophioglossaceae, *Mankyua chejuensis* and *Ophioglossum californicum*. In addition, the *psbJ-petA* intergenic regions of *Netrium*, *Roya obtusa*, *Cladophora*, and *Cosmarium* display an ORF encoding a hypothetical protein resembling those encoded at the same genomic locations in *Zygnema*, *Roya anglica*, and *Staurastrum*. The alignment of these hypothetical proteins indicates that the N-terminal portion is the most conserved (Supplementary Figure S2); however, given the small size and close proximity of this region to the 3' end of *petA*, the corresponding DNA sequence possibly represents a conserved regulatory sequence.

In *Klebsormidium* sp. SAG 51.86 cpDNA, *orf453* encodes a protein with reverse transcriptase (RT) and intron maturase domains that is highly similar to a freestanding ORF annotated as *matK* in the corresponding sequence of the *Klebsormidium flaccidum* genome. This coding sequence is more likely to be part

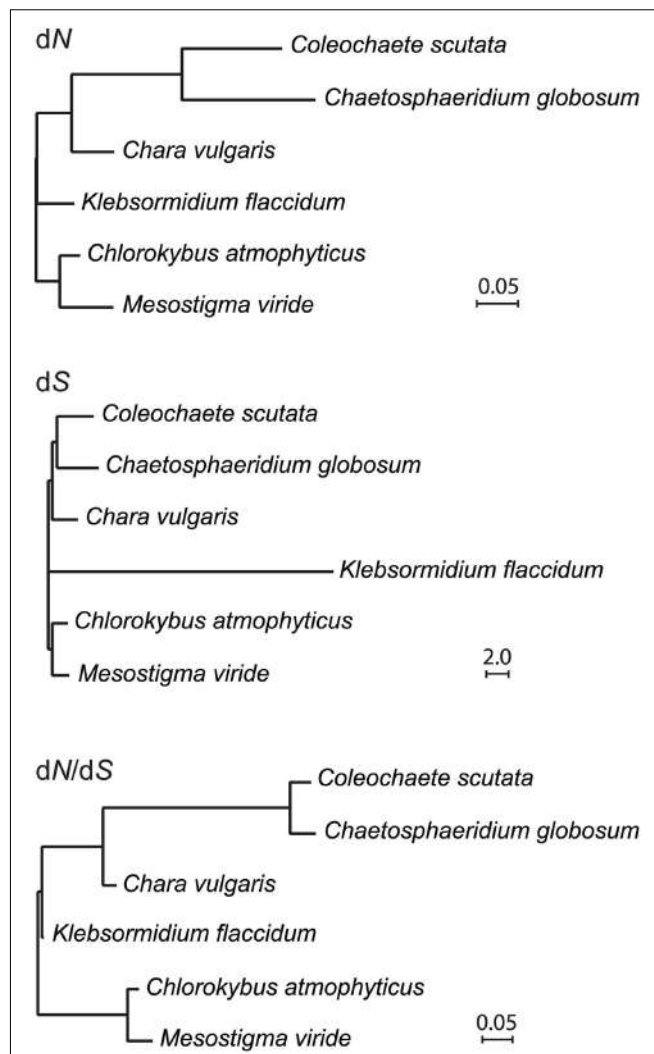


FIGURE 8 | Accelerated evolution of *tufA* in the Coleochaetophyceae. dN, dS and dN/dS branch lengths were calculated using PAML v4.8a and the streptophyte tree topology inferred in this study.

of the group II intron fragment linked with *psbA* exon 1, and consistent with this view, it shows less similarity to the *matK* genes encoded by *trnK(uuu)* introns than with the ORFs encoded by other group II introns (e.g., those in *Pyramimonas parkeae* *atpB*, *Tydemania expeditionis* *psbC* and *Jenufa minuta* *psbB*).

Intron Distribution

Introns in streptophyte algal cpDNAs are inserted at 38 distinct sites, 22 of which are shared with most land plants [21 group II intron sites and the *trnL(uaa)_35* group I intron site]. Only four sites hold group I introns (*rrl_2449*, *rrl_2500*, *rrl_2593*, and *trnL(uaa)_35*). Figure 9 shows the scenario of chloroplast intron gains and losses that we reconstructed by mapping the presence/absence of introns on the phylogeny inferred in this study. All streptophyte algal genomes, except *Mesostigma* and *Klebsormidium* cpDNAs, contain the *trnL(uaa)_35* intron. Group II introns shared with land plants were acquired during four

TABLE 2 | Non-standard genes identified as freestanding ORFs in the chloroplast genomes compared in this study.

Taxon	ORF ^a	Coordinates ^b	Conserved domain
<i>Mesotaenium endlicherianum</i>	519	108900–110459	Type II intron maturase MatK (CHL00002)
<i>Zygnema circumcarinatum</i>	531	66206–67801	Type II intron maturase MatK (CHL00002)
<i>Spirogyra maxima</i>	659	72632–74611	Phage integrase family (pfam00589) and integrase core domain (pfam00665)
<i>Netrium digitus</i>	132	102944–103342	Phage integrase family (pfam00589)
<i>Roya obtusa / Roya anglica</i>	268	96776–97582	Phage integrase family (pfam00589)
<i>Staurastrum punctulatum</i>	108	142226–142552	Phage DNA primase, D5 N terminal like domain (pfam08706)

^aReported here are the freestanding ORFs larger than 100 codons that revealed similarity (*E*-value threshold of 1e-08) with recognized protein domains in BlastP searches. Each ORF is identified by the number of amino acid residues in the encoded protein. ^bGenomic coordinates of the ORFs in the GenBank accessions provided in Table 1.

distinct evolutionary intervals (these branches are denoted by roman numerals in Figure 9), but most of these introns were later lost on one or more occasions. Within the Zygnematophyceae, 43 events of intron losses involving 18 sites were recorded; only the *trans*-spliced *rps12_114* and the *cis*-spliced *rpl16_9* and *trnG(ucc)_23* introns were spared from losses. The *trnI(gau)_39* and *trnV(uac)_37* introns were lost before the emergence of this clade.

The only ORF-containing group II introns that streptophyte algae share with land plants are the *trnK(uuu)_37* and *trans*-spliced *rps12_114* introns, but the ORF is not conserved in all algal taxa carrying these introns. The ORF encoding the intron maturase MatK is missing from the *trnK(uuu)_37* introns of *Coleochaete* and the Klebsormidiophyceae, and there is no *trnK(uuu)_37* intron in the early diverging zygnematophyceans *Mesotaenium*, *Cylindrocystis* and *Zygnema*; however, the *matK* ORF is freestanding in both *Mesotaenium* and *Zygnema* (Table 2). An ORF is also absent from the *trans*-spliced *rps12_114* intron in *Klebsormidium*, *Chara*, *Spirogyra*, and the three zygnematophyceans just mentioned.

The group II introns that are not shared with land plants occur in *Klebsormidium* (sites 3, 4, 6, 10, 12, 15, and 20), *Entransia* (sites 11, 17, 21, and 33), *Chara* (site 1) and *Netrium* (site 16) (Figure 9). Only two of these lineage-specific introns (the *Klebsormidium psbA* and *Netrium psbE* introns) harbor an ORF coding for a putative protein with RT and/or maturase domains. The group I introns that are not shared with land plants are found in *Chara* (site 36) and *Closterium* (sites 35, 36, and 37).

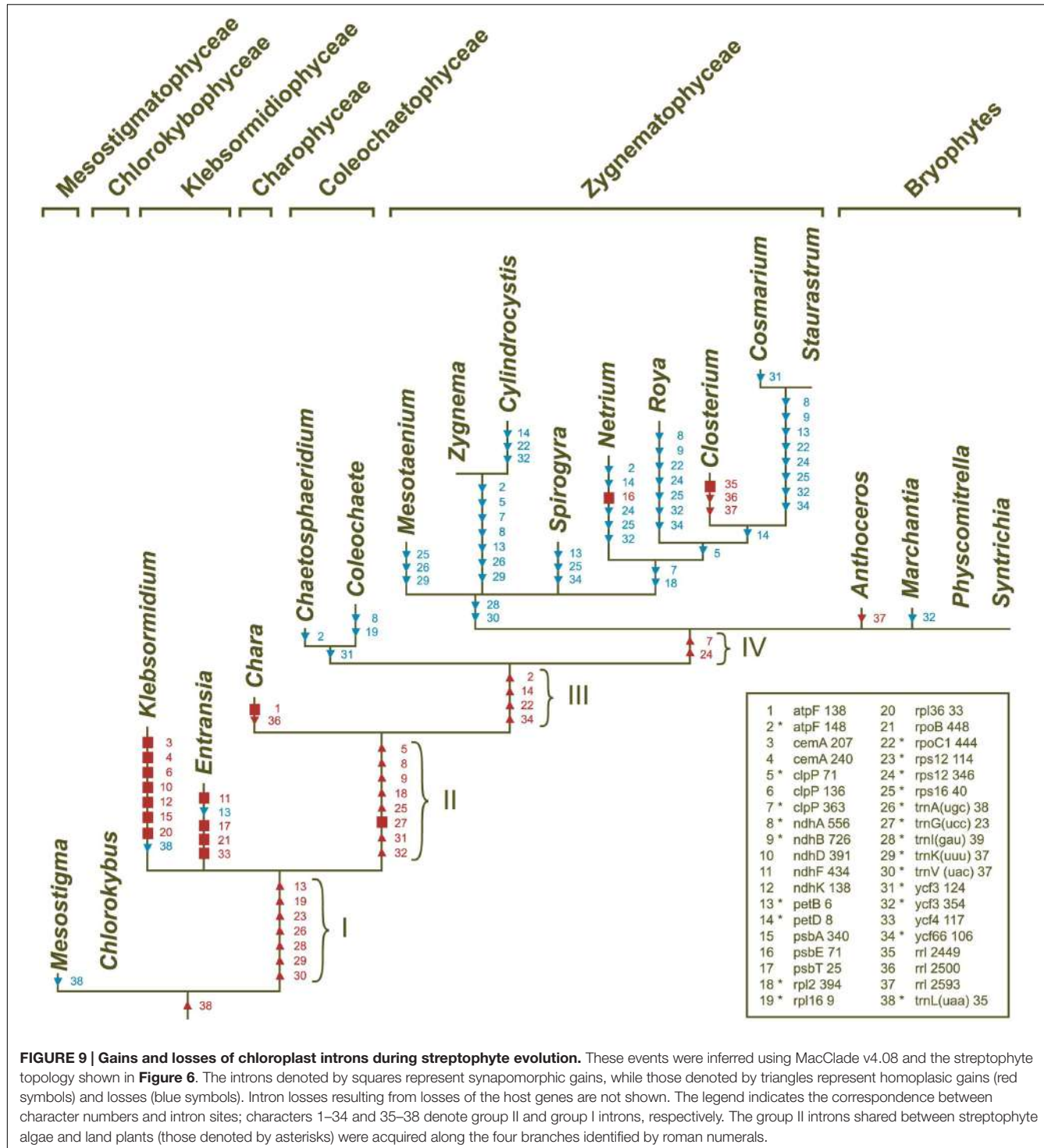
Gene Organization

Comparative analyses of gene organization were carried out using four complementary approaches. First, syntetic regions were identified in pairwise genome comparisons (Figures 1–4). Second, we compared the gene partitioning patterns of the IR-containing genomes and examined whether the genes found in the IR, SSC and LSC are also clustered in IR-lacking genomes (Figure 10). Third, phylogenetic trees based on gene order were inferred using the MLGO web server (Hu et al., 2014) and MGR v2.03 (Bourque and Pevzner, 2002): MLGO reconstructs ML phylogenies based on gene adjacency, whereas MGR estimates the number of reversals required to interconvert gene order in pairs of genomes and construct tree topologies based on rearrangement distance (Figure 11). The data set analyzed with MLGO contained all standard genes in each genome (including

both copies of duplicated genes), while the data set analyzed with MGR was restricted to the 89 genes common to all compared genomes. Finally, the presence/absence of signed gene pairs in three or more genomes (Figure 12) were coded as binary Dollo characters and the gene pairs representing synapomorphic gains and losses were mapped on the streptophyte phylogeny reported in this study using MacClade v4.08 (Figure 13). The Dollo principle assumes that characters can be lost independently in several evolutionary lineages but cannot be regained. Because inversion endpoints have been shown to be reutilized multiple times in land plant chloroplast genomes experiencing frequent rearrangements (Jansen and Ruhlman, 2012), coding of gene pairs as Dollo characters might not be fully justified. For this reason, we have also coded gene pairs as unordered (Fitch parsimony) or ordered (Wagner parsimony) characters and found no difference in the evolutionary scenarios we inferred.

Although gene order is highly variable among streptophyte algal genomes, the branching order inferred with MLGO is entirely congruent with the phylogeny based on gene and protein sequences (Figures 6 and 11). The reversal distances estimated by MGR reveal that the chloroplast genomes of the bryophytes, Coleochaetophyceae and especially *Chara* are the least rearranged relative to those of *Mesostigma* and *Chlorokybus*, and that they are followed closely by the klebsormidiophycean genomes. By comparison, the Zygnematophyceae display very long branches indicative of massive gene shuffling. Of the examined zygnematophyceans, the representative of the earliest-diverging lineage (*Mesotaenium*) boasts the least rearranged genome.

The *Coleochaete* and *Chaetosphaeridium* cpDNAs share nine blocks of sequences containing 116 of their 117 and 125 conserved genes, respectively (Figure 2). Only eight reversals are required to interconvert the gene order of these two genomes. Following the loss of the IR in the *Coleochaete* lineage, the partitioning of genes between the SSC and LSC regions has been barely affected (Figure 10); in other words, the genes corresponding to those located 5' and 3' of the rRNA operon in the *Chaetosphaeridium* genome have largely remained clustered in *Coleochaete*. Three of the eight genes missing in *Coleochaete* (*rps14*, *tilS* and *ccsA*) correspond to breakpoints between syntetic blocks while the remaining, which are all part of ribosomal protein operons, have been cleanly excised from internal regions of syntetic blocks (Figures 2 and 12).



The *Klebsormidium flaccidum* and *Entransia* genomes display 26 syntenic blocks containing 85 of their 114 and 118 conserved genes, respectively (**Figure 1**). The vastly expanded IRs of these algae differ considerably from one another and from streptophyte IRs displaying an ancestral organization (i.e., those of *Mesostigma*, *Chlorokybus*, *Chara*, coleochaetophyceans and bryophytes) with respect to gene content (**Figure 10**). Of the 32

and 44 genes present in the *Klebsormidium* and *Entransia* IRs, respectively, only 14 are shared besides the five genes making up the rRNA operon; however, all genes typically found 5' and 3' of the rRNA operon in ancestral IR-containing genomes, except for *tufA* in *Klebsormidium*, have remained ancestrally segregated. Eight of the 22 genes lost in the lineages leading to *Klebsormidium* and *Entransia* [*accD*, *minD*, *psaM*, *rpl12*, *rpl32*, *tufA*, *trnV(uac)*

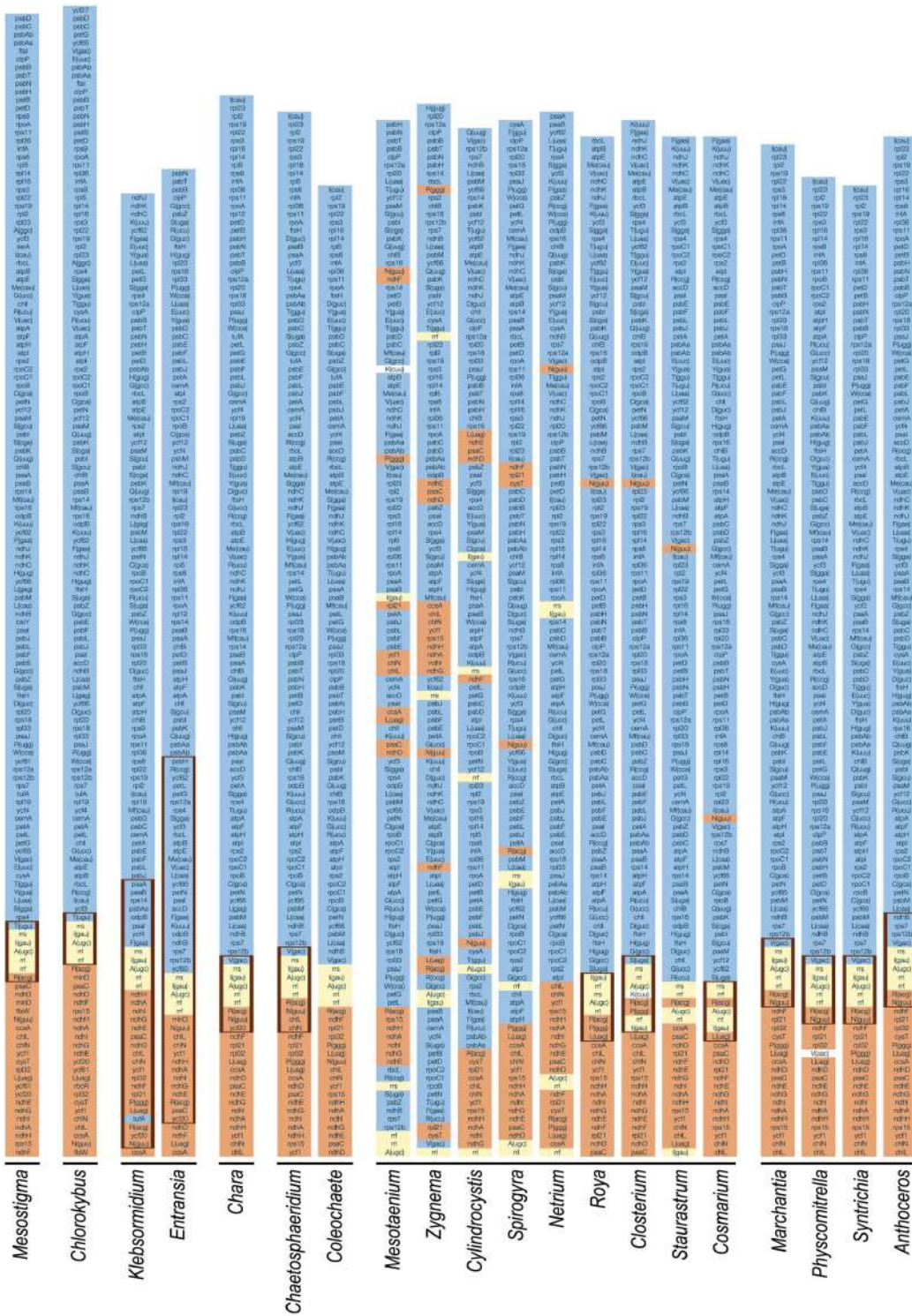
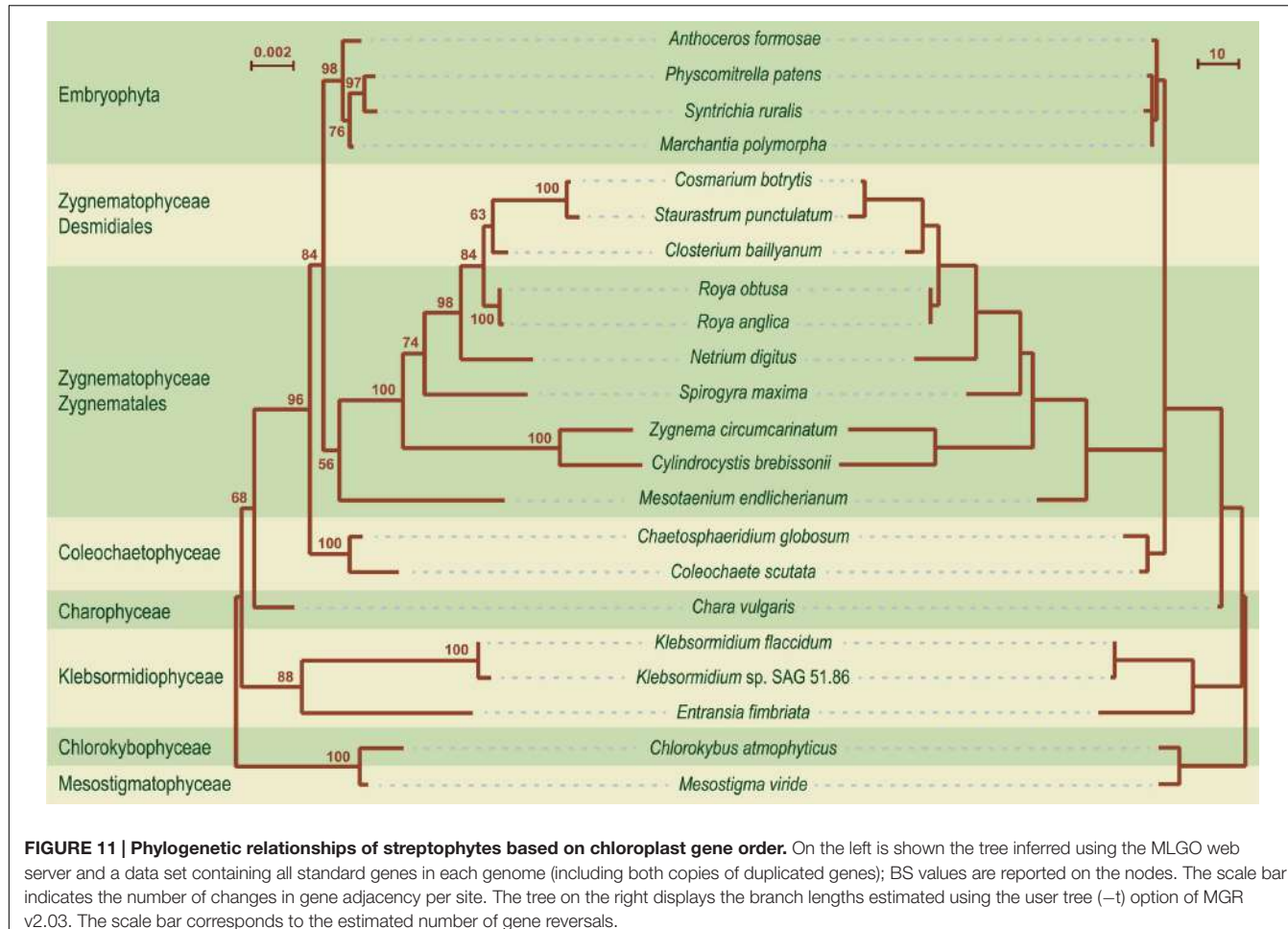


FIGURE 10 | Gene partitioning patterns of streptophyte chloroplast genomes. For each genome, one copy of the IR (thick vertical lines) and the entire SSC and LSC regions are represented. The five genes composing the rDNA operon are highlighted in yellow. The color assigned to each of the remaining genes is dependent upon the position of the corresponding gene relative to the rDNA operon in the cpDNA of the streptophyte alga *Mesostigma viride*, a genome displaying an ancestral gene partitioning pattern. The genes highlighted in orange are found within or near the SSC region in this streptophyte genome (downstream of the rDNA operon), whereas those highlighted in blue are found within or near the LSC region (upstream of the rDNA operon). To simplify the comparison of gene order, some genomes are represented in their alternative isomeric forms relative to the genome sequences deposited in GenBank. Note that the *trnK*(cuu) genes of *Mesotaenium* and *Closterium*, and the *tmV*(aac) gene of *Physcomitrella* were not color-coded because their evolutionary origins are unclear.



and *ycf65*] correspond to breakpoints between synteny blocks, while the others have been cleanly excised from internal regions of synteny blocks (Figures 1 and 12). Gene rearrangements have disrupted some ancestral gene clusters, e.g., *rpoC2* is no longer adjacent to *rps2* and *atpI* is no longer beside *atpH* (Figure 12).

The chloroplast genomes of the Zygnematophyceae exhibit a wide range of divergence at the gene order level (Figure 11). The *Cosmarium* and *Staurastrum* genomes are the most similar, with six syntenic blocks containing all 122 encoded genes except *trnS(uga)* (Figure 4). All investigated zygnematophycean genomes feature a disrupted rRNA operon; two, three or four breakage sites are observed depending on the species (Figure 12). Like the IRs of the *Roya* species, those of *Cosmarium* and *Closterium* harbor two to four tRNA genes in addition to the genes composing the rRNA operon (Figure 10). Of these tRNA genes, only *trnR(acg)* is shared with the IRs of streptophyte algal cpDNAs having an ancestral partitioning pattern. All the genes ancestrally located in the SSC and LSC regions, with the single exception of *trnN(guu)*, still form ancestrally segregated groups in the *Roya*, *Cosmarium*, and *Closterium* genomes (Figure 10). In contrast, reshuffling of gene order in the *Mesotaenium*, *Zygnema* + *Cylindrocystis* and *Spirogyra* lineages led to extensive dispersal, throughout the genome, of the IR-encoded genes and of

the genes typically found in the SSC and LSC regions of ancestral streptophyte IR-containing cpDNAs (Figure 10).

Several gene pairs representing synapomorphic signatures of distinct lineages were lost or acquired before the Klebsormidiophyceae, Coleochaetophyceae and bryophyte lineage each arose. But just a single synapomorphy, corresponding to loss of linkage between the *trnI(gau)* and *trnA(ugc)* genes in the rDNA operon, unites the Zygnematophyceae (Figure 13). Following the emergence of the *Mesotaenium* lineage, two additional gene rearrangements occurred in the common ancestor of the remaining zygnematophyceans: the rDNA operon was broken at a second site (between *rrl* and *rrf*) and the ancestral pair 5'psbZ-5'*trnS(uga)* was lost. Reversal of the *ycf1* gene in the ancestral 3'*chlN*-3'*ycf1* pair is a unique gene rearrangement shared by all Coleochaetophyceae, Zygnematophyceae and bryophytes. In contrast, no synapomorphic loss of gene pairs accompanied the emergence of the Charophyceae.

DISCUSSION

The comparative analyses presented in this study, which include a sampling of nine additional chloroplast genomes

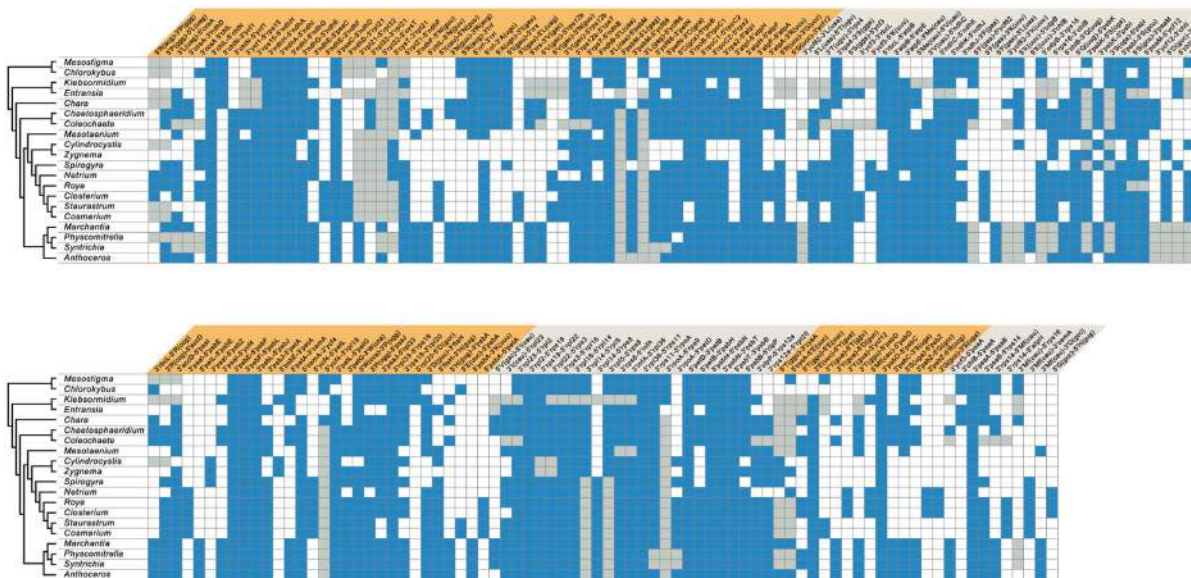


FIGURE 12 | Shared gene pairs in streptophyte chloroplast genomes. The gene pairs shared by at least three taxa were identified among all possible signed gene pairs in the compared genomes. The presence of a gene pair is denoted by a blue box; a gray box refers to a gene pair in which at least one gene is missing due to gene loss. Gene pairs are organized in blocks of contiguous gene pairs (shown as alternating colors) to facilitate the identification of conserved gene clusters.

from the Klebsormidiophyceae, Coleochaetophyceae and Zygnematophyceae, alter markedly our view of chloroplast genome evolution in streptophytes. Our results clearly indicate that the chloroplast genome is evolving in a dynamic fashion not only in the Zygnematophyceae but also in the Klebsormidiophyceae and Coleochaetophyceae. The diversity of genomic structures and organizations found in these three classes is reminiscent of the diversity that has recently been reported for various classes of the Chlorophyta (Brouard et al., 2010; Lemieux et al., 2014; Leliaert and Lopez-Bautista, 2015; Turmel et al., 2015), and contrasts with the extremely conservative evolutionary trend observed in most land plants (Wickett et al., 2011; Jansen and Ruhlman, 2012; Ruhlman and Jansen, 2014). In the following sections, we highlight the evolutionary trends observed in each streptophyte algal class.

The phylogenies we inferred from 88 chloroplast protein-coding genes and proteins are congruent with recent phylogenomic studies indicating that the Zygnematophyceae is sister to land plants (Wodniok et al., 2011; Laurin-Lemay et al., 2012; Timme et al., 2012; Zhong et al., 2013; Wickett et al., 2014). The relationships among the members of the Zygnematophyceae are consistent with the phylogeny reported by Gontcharov et al. (2004). Moreover, the differences in branching order of the bryophyte lineages between the protein and gene trees are in agreement with previously reported phylogenomic studies (Cox et al., 2014; Wickett et al., 2014).

Mesostigmatophyceae and Chlorokybophyceae

The *Mesostigma* and *Chlorokybus* chloroplast genomes are the most rich in ancestral traits among the Viridiplantae (Lemieux

et al., 2000, 2007). They feature the most extensive gene content, are almost devoid of introns, contain many operons typically found in cyanobacteria, and have retained a quadripartite architecture with a pattern of gene partitioning that closely resembles those found in early diverging members of the Chlorophyta (e.g., *Nephroselmis*; Turmel et al., 1999b; Lemieux et al., 2014 and *Pyramimonas*; Turmel et al., 2009) (Table 1; Figure 10). These ancestral features mirror the deep-branching positions of *Mesostigma* and *Chlorokybus* and illustrate the great structural stability of the chloroplast genome in the clade uniting these algae.

Klebsormidiophyceae

The *Entransia* and *Klebsormidium flaccidum* chloroplast genomes have retained a quadripartite architecture, but their IRs are greatly enlarged and include many genes typically found in the SSC and LSC regions (Figures 1, 5, and 10). Reconstruction of the ancestral genome reveals that the IR underwent considerable expansion toward the SSC region before the split of the two klebsormidiophycean lineages and that it expanded predominantly toward the LSC region following this divergence. At 61 kb, the *Entransia* IR is the largest known among the green algae examined so far. Compared to the *Klebsormidium flaccidum* IR, it contains twice as many genes of LSC origin but fewer genes of SSC origin, suggesting that shifts of both the IR/SSC and IR/LSC junctions are on-going events in the Klebsormidiophyceae. Sampling of additional taxa from this class should provide more information on the directionality and extent of these shifts in various lineages. Like klebsormidiophycean cpDNAs, the chloroplast genomes of the chlorodendrophyccean green algae *Scherffelia* and *Tetraselmis* feature enlarged IRs with a rich gene content, but the ancestral

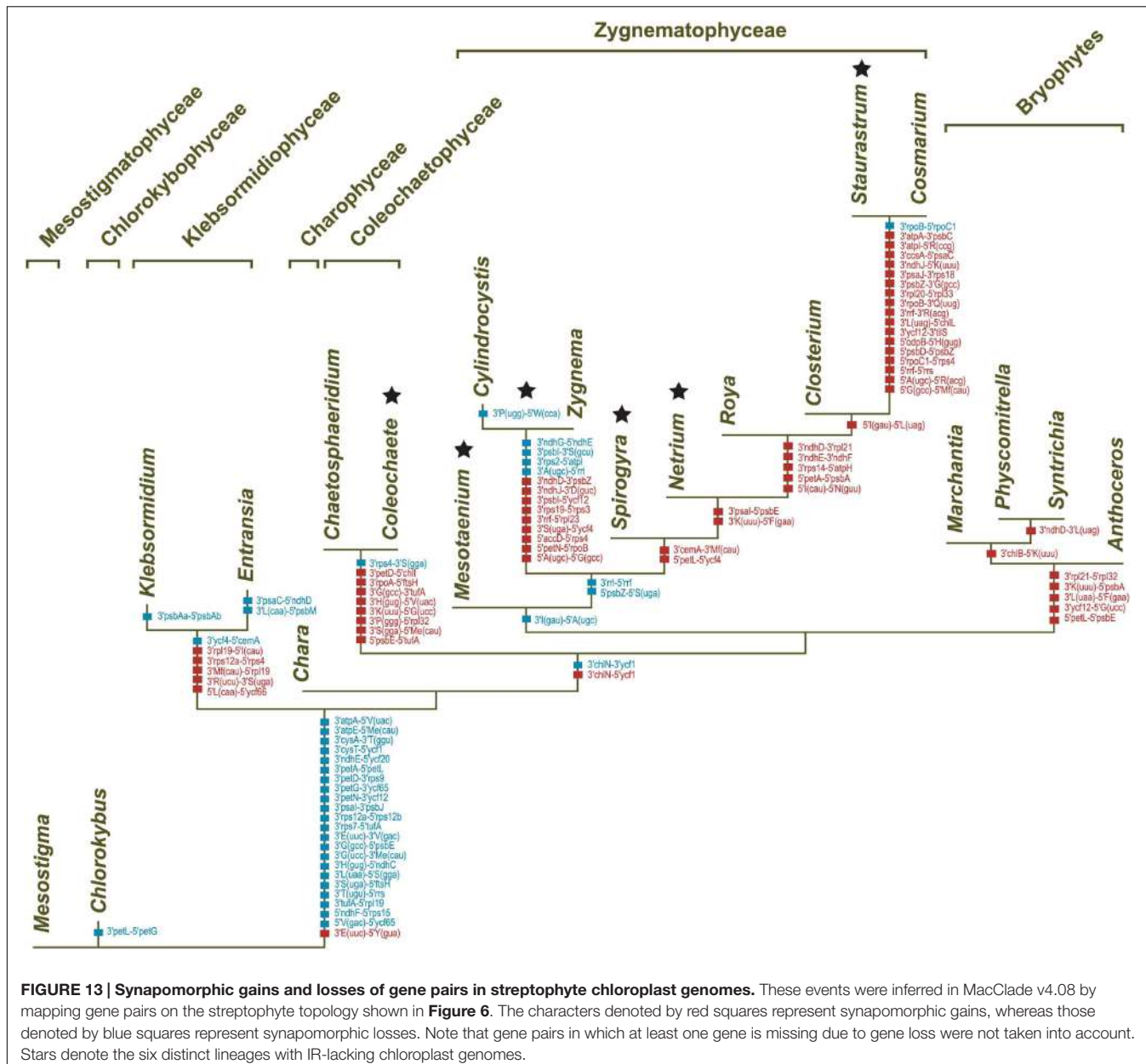


FIGURE 13 | Synapomorphic gains and losses of gene pairs in streptophyte chloroplast genomes. These events were inferred in MacClade v4.08 by mapping gene pairs on the streptophyte topology shown in Figure 6. The characters denoted by red squares represent synapomorphic gains, whereas those denoted by blue squares represent synapomorphic losses. Note that gene pairs in which at least one gene is missing due to gene loss were not taken into account. Stars denote the six distinct lineages with IR-lacking chloroplast genomes.

partitioning pattern has not been maintained (Turmel et al., 2016).

Thirty standard chloroplast genes were lost during the evolution of the Klebsormidiophyceae; losses of *ndhK*, *rpl14*, *rpl16*, *rps3*, *trnG(ucc)*, *trnT(ggu)*, *trnT(ugu)*, *trnV(gac)* and *trnV(uac)*, in particular, are unique among streptophyte algae (Figure 7). As a consequence of the substantial losses of *trn* gene, the complement of tRNAs encoded in klebsormidiophycean chloroplast genomes is not sufficient to decode the entire set of codons found in these genomes. For example, there is no chloroplast-encoded tRNA^{Thr} in *Klebsormidium* and *Entransia*, and no chloroplast-encoded tRNA^{Val} in *Klebsormidium*. It thus appears that these missing tRNAs are imported from the cytosol into the chloroplast. Import of nuclear-encoded tRNAs into

plastids has previously been suggested for non-photosynthetic land plants (Wicke et al., 2011).

Klebsormidiophycean chloroplast genomes contain an abundance of introns. Civan et al. (2014) previously inferred that the common ancestor of the Klebsormidiophyceae and its sister lineages (branch I in Figure 9) shared five group II introns with extant land plants. To this set of early acquired introns, we must now add the *rpl16_9* and *trnV(uac)_37* introns, which we identified in the *Entransia* genome. Although the *Klebsormidium flaccidum* and *Entransia* chloroplast genomes contain a large number of lineage-specific group II introns (seven are unique to *Klebsormidium* and four are unique to *Entransia*), they have no intron insertion sites in common other than those shared with land plants, thus suggesting that the lineage-specific introns were

mostly acquired through intragenomic proliferation of founding introns.

It is intriguing that the *tufA* gene resides in the SSC region rather than in the LSC region in the *Klebsormidium* chloroplast genome and that it is entirely missing in the *Entransia* genome. In *Mesostigma*, *Chlorokybus* and most chlorophyte cpDNAs, *tufA* is part of the *str* operon, which also comprises *rps12* and *rps7* (transcription order is 5'-*rps12*-*rps7*-*tufA*-3'). It appears that breakage of this operon through the acquisition of a *trans*-spliced group II intron at site 114 of *rps12* soon after the divergence of the *Mesostigma* + *Chlorokybus* clade led to relocation of *rps12* exon 1 outside the operon and ultimately to loss of linkage between *rps7* and *tufA*, which resulted in transfer of *tufA* to the SSC region in *Klebsormidium* and to the complete loss of this gene in *Entransia*. There is also no linkage between *rps7* and *tufA* in the *Chara* and *Chaetosphaeridium* genomes, and both *rps12* and *rps7* are completely missing in *Coleochaete*.

Charophyceae

Only the chloroplast genome sequence of *Chara vulgaris* is currently available for the Charophyceae (Turmel et al., 2006). Remarkably, this alga has retained the largest degree of ancestral traits among the streptophytes that diverged after the *Mesostigma* + *Chlorokybus* clade. This highly conservative evolutionary trend is apparent at all levels, including overall architecture, gene content, gene partitioning, and gene organization (Figure 10). The *Chara* genome is clearly the least rearranged relative to the *Mesostigma* and *Chlorokybus* cpDNAs, as revealed by the short branch length separating these taxa in the MGR tree shown in Figure 11. It will be interesting to see if sampling of additional taxa from the Charophyceae will support the notion that the chloroplast genome is evolving at a very slow rate in this class. In this context, it is noteworthy that the mitochondrial genomes of the distantly related charophycean algae *Chara vulgaris* and *Nitella hyalina* contain the same gene complement and display exactly the same gene order (Turmel et al., 2013).

Coleochaetophyceae

Our chloroplast genome analyses of a second representative of the Coleochaetophyceae unveiled a less conservative evolutionary history than previously thought for this class. Genome streamlining appears to be the main evolutionary force in the lineage leading to *Coleochaete*. The *Coleochaete* genome is both the smallest and most compact among the streptophyte algal cpDNAs investigated so far (Table 1). Unlike the *Chaetosphaeridium* cpDNA (Turmel et al., 2002), it lacks an IR and several standard genes. Notably, losses of four ribosomal protein-coding genes (*rps4*, *rps7*, *rps12*, and *rps14*) represent unique events in the evolutionary scenario we inferred for streptophyte algae (Figure 7). Otherwise, gene organization has been highly preserved in *Coleochaete* and *Chaetosphaeridium* and the genes usually present in the IR, SSC and LSC regions have retained an ancestral partitioning pattern in the *Coleochaete* genome (Figures 10 and 11).

The *tufA* gene is evolving at a fast pace in the Coleochaetophyceae (Figure 8). Considering that this gene

has completely disappeared from the chloroplast genome and is most probably nuclear-encoded in all streptophyte lineages that evolved after the divergence of the Coleochaetophyceae (Figure 7), it is possible that the chloroplast *tufA* sequences identified in the Coleochaetophyceae do not encode the functional elongation factor EF-Tu; instead, a nuclear gene product might play this role in protein synthesis. This hypothesis was proposed earlier by Baldauf et al. (1990) who reported that the chloroplast *tufA* sequence of *Coleochaete orbicularis* is unusually divergent and differs considerably at what was otherwise conserved amino acid positions. These authors speculated that, despite the presence of numerous mutations, long-term maintenance of an intact ORF at the *Coleochaete tufA* locus might be the result of selection to retain less constrained subsets of the original EF-Tu functions. This hypothesis is attractive, considering that EF-Tu has been shown to play an important role in cell shape maintenance in *Bacillus subtilis* through direct interaction with MreB (Defeu Soufo et al., 2010), a protein involved in septum synthesis and cell division (Fenton and Gerdes, 2013); however, it is not supported by our finding that there was no positive selection across the *tufA* sequence in the Coleochaetophyceae. Putative nuclear copies of *tufA* were detected in *Coleochaete orbicularis* by Southern blot analysis (Baldauf et al., 1990), and our BLASP searches against the 1000 Plants (oneKP) database⁸ using the *Chara* chloroplast *tufA* sequence as query identified highly similar sequences (*E*-value threshold of 0.0) that contain all functional domains of EF-Tu in the RNA-seq assemblies of *Coleochaete scutata* (VQBJ-2010477), *Coleochaete irregularis* (QPDY-2029449) and *Chaetosphaeridium globosum* (DRGY-2007378). Taken together, these observations support the notion that the nucleus houses the functional coding sequence for the chloroplast EF-Tu and that the divergent *tufA* sequence in the chloroplast genome is undergoing pseudogenization.

Zygnematophyceae

Previous studies revealed that the zygnematophycean chloroplast genome is highly variable in overall structure, gene order and intron content (Turmel et al., 2005, 2007; Civan et al., 2014). The comparative genome analyses reported here, which include six additional taxa sampled from the Zygnematales and Desmidiales, underscore the exceptionally dynamic evolution of this genome.

To account for the presence of an IR in one of the four zygnematophycean taxa they examined (*Roya*), Civan et al. (2014) proposed that the IR was either lost three times or gained once *de novo* during the diversification of the Zygnematophyceae. Our finding that the cpDNAs of the desmidaleans *Closterium* and *Cosmarium* also have an IR suggests that the IR was lost a minimum of five times (Figures 5 and 13). It is unlikely that the IR was acquired *de novo* on one or more independent occasions because the ancestral gene partitioning pattern has been retained in late-diverging zygnematophyceans with IR-less chloroplast genomes (*Staurastrum* and *Netrium*). Indeed,

⁸<https://www.bioinfodata.org/Blast4OneKP/home>

considering that the genes originally present in the IR and SSC regions were dispersed throughout the genome as a result of high frequency gene rearrangements in early diverging lineages of the Zygnematophyceae (**Figure 10**), it is difficult to envision that the region containing all the genes encoded by the rDNA operon became duplicated at exactly the same site as the ancestral LSC/SSC junction in the common ancestor of *Roya*, *Closterium*, *Staurastrum*, and *Cosmarium* and that the ancestral gene partitions were restored concomitantly (**Figure 6**). The notion that the quadripartite structure was eliminated multiple times in the Zygnematophyceae predicts that future studies with a broader taxon sampling of this class will uncover early diverging taxa harboring IR-containing chloroplast genomes. Independent losses of the IR also took place in other lineages of the Viridiplantae, including land plants (Wicke et al., 2011; Jansen and Ruhlman, 2012; Ruhlman and Jansen, 2014). The quadripartite structure was eliminated at least four times in prasinophytes (Turmel et al., 2009; Lemieux et al., 2014), seven times in the Trebouxiophyceae (de Cambiaire et al., 2007; Turmel et al., 2015), twice in the Ulvophyceae (Lu et al., 2011; Leliaert and Lopez-Bautista, 2015; Melton et al., 2015) and once in the Chlorophyceae (Bélanger et al., 2006; Brouard et al., 2010, 2011). In the case of the Chlorophyceae, the reported loss unites two major lineages of the OCC clade: the Chaetophorales and Chaetopeltidales (Brouard et al., 2010).

The long branches leading to the zygnematophycean taxa in the MGR tree (**Figure 11**) indicate that the chloroplast genome underwent more extensive gene scrambling in the Zygnematophyceae than in any other streptophyte algal classes. These gene rearrangements were accompanied by the disruption of several ancestral clusters, including the rDNA operon (**Figure 13**). The latter operon was broken at four distinct sites, three of which are associated with synapomorphic losses of gene pairs: (1) the *trnI(gau)*-*trnA(ugc)* pair in the common ancestor of all zygnematophyceans, (2) the *rnl-rnf* pair following the divergence of *Mesotaenium* and (3) the *rnl-rnf* pair in the common ancestor of *Zygnema* and *Cylindrocystis*. The fourth site, located between *rrs* and *trnI(gau)*, was disrupted along the branches leading to *Mesotaenium*, to the common ancestor of *Zygnema* and *Cylindrocystis*, and to the common ancestor of *Netrium* and its sister clade. Disruptions of the chloroplast rDNA operon are rare events among viridiplants but have been reported in some chlorophyte lineages featuring highly rearranged genomes (de Cambiaire et al., 2007; Turmel et al., 2009, 2015; Lu et al., 2011; Lemieux et al., 2014; Leliaert and Lopez-Bautista, 2015).

In land plants, IR loss and/or acquisition of short dispersed repeats have been associated with an increased rate of genome rearrangements (Palmer, 1991; Wicke et al., 2011; Jansen and Ruhlman, 2012; Weng et al., 2014), but these factors are unlikely to be the main force driving genome rearrangements in zygnematophyceans. Although gene order in the *Zygnema* and *Cylindrocystis* IR-less genomes was reconfigured at a faster rate compared to their IR-containing homologs, this is not the case for other zygnematophycean lineages (*Mesotaenium*, *Spirogyra*, and *Netrium*) that also feature IR-less genomes

but much shorter branches (**Figure 11**). Similarly, the extent of gene rearrangements and repeat contents are weakly correlated; zygnematophycean genomes are generally poor in short dispersed repeats and those having the highest proportion of these elements (*Cosmarium* and *Closterium* cpDNAs) show minor differences in gene rearrangements (**Figure 11**) compared to their closest relatives having much fewer repeats (*Staurastrum* and *Roya*).

In agreement with the study of Civan et al. (2014), we inferred that the common ancestor of zygnematophyceans harbored all the 21 group II introns usually present in land plant genomes, except those in *trnI(gau)*, a gene that was part of the ancestral rDNA operon, and in *trnV(uac)*. Just three introns — *rpl16_9*, *rps12_114* and *trnG(ccc)_23* — were retained in all ten examined taxa. While Civan et al. (2014) predicted 20 independent events of intron loss in the Zygnematophyceae, we scored 43 losses in our study (**Figure 9**). Two introns were lost only once (those at sites 18 and 31 in **Figure 9**), six were lost twice (sites 2, 5, 7, 9, 26, 29), and the remaining introns on three, four or five occasions. The underlying cause of this intron instability remains unclear. It has been previously speculated that intron losses could be the result of retroposition events (reverse transcription of a spliced RNA copy, followed by recombination-dependent insertion into the genome) and that the protein encoded by the *trans-spliced* *rps12_114* intron in several zygnematophycean lineages could provide the RT activity required for these events (Turmel et al., 2005; Civan et al., 2014). Although RT-mediated intron loss is a mechanism that is very efficient in removing introns (Cohen et al., 2012), very few zygnematophycean genomes actually encode a protein with this activity. Our BLAST analyses of group II intron-encoded ORFs revealed that only the *orf643* in the *psbE_71* group II intron of *Netrium* (an intron unique to this alga) codes for a putative RT; all other intron-encoded ORFs were found to contain an intron maturase domain, including the *Staurastrum orf404* that we incorrectly annotated as a RT gene in a previous report (Turmel et al., 2005). These observations, however, do not necessarily invalidate the retroposition hypothesis for intron removal in the Zygnematophyceae, as RT genes might have been present in ancestral chloroplast genomes. Alternatively, RT activities of mitochondrial or nuclear origin might also be invoked to support this hypothesis. The finding of a group II intron-encoded RT in the mitochondrial *cox2* gene of *Closterium baillyanum* is consistent with this idea (Turmel et al., 2013).

Putative gains of foreign genes by the chloroplast genome have been documented for several green algal lineages: prasinophytes (Turmel et al., 2009; Lemieux et al., 2014), Trebouxiophyceae (Turmel et al., 2015), Ulvophyceae (Leliaert and Lopez-Bautista, 2015), Chlorophyceae (Brouard et al., 2008) and streptophyte algae (Civan et al., 2014). Here we report further evidence that genes encoding integrases/recombinases (Int) and DNA primases of phage/viral origin were transferred to the chloroplast during the evolution of the Zygnematophyceae (**Table 2**). Putative Int-encoding genes have been also identified in the mitochondrial genomes of various streptophytes: *Klebsormidium flaccidum* (*orf374* in GenBank:KP165386), *Chaetosphaeridium globosum*

(Turmel et al., 2002), *Roya obtusa* (Turmel et al., 2013) and the lycophyte *Phlegmariurus squarrosum* (*orf233* in GenBank JQ002659). Inter-organellar gene transfers might account for the presence of these genes in both the chloroplast and mitochondria.

Early insertions of viral genes in the IR of the zygnematophycean chloroplast genome might have contributed to the instability of the IR. Civan et al. (2014) proposed that both cpDNA-encoded RT and Int activities have shaped this genome. Given that these activities are essential components of the replicative machinery of retroelements, they speculated that invasion of retroviruses and/or retrotransposons in the chloroplasts of early diverging zygnematophyceans triggered massive genome rearrangements. However, this scenario is not consistent with the findings that the chloroplast-encoded Int sequences uncovered in the zygnematophyceans investigated so far more likely originate from phages/viruses than retroelements and that only *Netrium* carries a chloroplast-encoded RT. As proposed for other streptophyte lineages with unusually rearranged chloroplast genomes (Weng et al., 2014; Zhang et al., 2016), it appears more likely that nuclear-encoded, plastid-targeted genes involved in DNA replication, recombination, and repair (and also perhaps in reverse transcription) played a major important

role in reshuffling the zygnematophycean chloroplast genome.

AUTHOR CONTRIBUTIONS

CL and MT conceived and designed the research. CL and CO performed the research. CL, CO, and MT analyzed the data. MT and CL wrote the paper.

FUNDING

This work was supported by the Natural Sciences and Engineering Research Council of Canada (http://www.nserc-crsng.gc.ca/index_eng.asp) (Grant No. 2830-2007 to MT and CL).

SUPPLEMENTARY MATERIAL

The Supplementary Material for this article can be found online at: <http://journal.frontiersin.org/article/10.3389/fpls.2016.00697>

REFERENCES

- Andersen, R. A. (2005). *Algal Culturing Techniques*. Boston, MA: Elsevier.
- Baldauf, S. L., Manhart, J. R., and Palmer, J. D. (1990). Different fates of the chloroplast tufA gene following its transfer to the nucleus in green algae. *Proc. Natl. Acad. Sci. U.S.A.* 87, 5317–5321. doi: 10.1073/pnas.87.14.5317
- Becker, B. (2013). Snow ball earth and the split of Streptophyta and Chlorophyta. *Trends Plant Sci.* 18, 180–183. doi: 10.1016/j.tplants.2012.09.010
- Becker, B., and Marin, B. (2009). Streptophyte algae and the origin of embryophytes. *Ann. Bot.* 103, 999–1004. doi: 10.1093/aob/mcp044
- Bélanger, A. S., Brouard, J. S., Charlebois, P., Otis, C., Lemieux, C., and Turmel, M. (2006). Distinctive architecture of the chloroplast genome in the chlorophycean green alga *Stigeoclonium helveticum*. *Mol. Genet. Genomics* 276, 464–477. doi: 10.1007/s00438-006-0156-2
- Bendich, A. J. (2004). Circular chloroplast chromosomes: the grand illusion. *Plant Cell* 16, 1661–1666. doi: 10.1105/tpc.160771
- Boisvert, S., Laviolette, F., and Corbeil, J. (2010). Ray: simultaneous assembly of reads from a mix of high-throughput sequencing technologies. *J. Comput. Biol.* 17, 1519–1533. doi: 10.1089/cmb.2009.0238
- Bourque, G., and Pevzner, P. A. (2002). Genome-scale evolution: reconstructing gene orders in the ancestral species. *Genome Res.* 12, 26–36.
- Brouard, J. S., Otis, C., Lemieux, C., and Turmel, M. (2008). Chloroplast DNA sequence of the green alga *Oedogonium cardiacum* (Chlorophyceae): unique genome architecture, derived characters shared with the Chaetophorales and novel genes acquired through horizontal transfer. *BMC Genomics* 9:290. doi: 10.1186/1471-2164-9-290
- Brouard, J. S., Otis, C., Lemieux, C., and Turmel, M. (2010). The exceptionally large chloroplast genome of the green alga *Floydiella terrestris* illuminates the evolutionary history of the Chlorophyceae. *Genome Biol. Evol.* 2, 240–256. doi: 10.1093/gbe/evq014
- Brouard, J. S., Otis, C., Lemieux, C., and Turmel, M. (2011). The chloroplast genome of the green alga *Schizomeris leibleinii* (Chlorophyceae) provides evidence for bidirectional DNA replication from a single origin in the Chaetophorales. *Genome Biol. Evol.* 3, 505–515. doi: 10.1093/gbe/evr037
- Capella-Gutierrez, S., Silla-Martinez, J. M., and Gabaldon, T. (2009). trimAl: a tool for automated alignment trimming in large-scale phylogenetic analyses. *Bioinformatics* 25, 1972–1973. doi: 10.1093/bioinformatics/btp348
- Castresana, J. (2000). Selection of conserved blocks from multiple alignments for their use in phylogenetic analysis. *Mol. Biol. Evol.* 17, 540–552. doi: 10.1093/oxfordjournals.molbev.a026334
- Civan, P., Foster, P. G., Embley, M. T., Seneca, A., and Cox, C. J. (2014). Analyses of charophyte chloroplast genomes help characterize the ancestral chloroplast genome of land plants. *Genome Biol. Evol.* 6, 897–911. doi: 10.1093/gbe/evu061
- Cohen, N. E., Shen, R., and Carmel, L. (2012). The role of reverse transcriptase in intron gain and loss mechanisms. *Mol. Biol. Evol.* 29, 179–186. doi: 10.1093/molbev/msr192
- Cox, C. J., Li, B., Foster, P. G., Embley, T. M., and Civan, P. (2014). Conflicting phylogenies for early land plants are caused by composition biases among synonymous substitutions. *Syst. Biol.* 63, 272–279. doi: 10.1093/sysbio/syt109
- de Cambaire, J. C., Otis, C., Turmel, M., and Lemieux, C. (2007). The chloroplast genome sequence of the green alga *Leptosira terrestris*: multiple losses of the inverted repeat and extensive genome rearrangements within the Trebouxiophyceae. *BMC Genomics* 8:213. doi: 10.1186/1471-2164-8-213
- Defeu Soufo, H. J., Reimold, C., Linne, U., Knust, T., Gescher, J., and Graumann, P. L. (2010). Bacterial translation elongation factor EF-Tu interacts and colocalizes with actin-like MreB protein. *Proc. Natl. Acad. Sci. U.S.A.* 107, 3163–3168. doi: 10.1073/pnas.0911979107
- Delport, W., Poon, A. F., Frost, S. D., and Kosakovsky Pond, S. L. (2010). Datamonitor 2010: a suite of phylogenetic analysis tools for evolutionary biology. *Bioinformatics* 26, 2455–2457. doi: 10.1093/bioinformatics/btq429
- Edgar, R. C. (2004). MUSCLE: multiple sequence alignment with high accuracy and high throughput. *Nucleic Acids Res.* 32, 1792–1797. doi: 10.1093/nar/gkh340
- Fenton, A. K., and Gerdes, K. (2013). Direct interaction of FtsZ and MreB is required for septum synthesis and cell division in *Escherichia coli*. *EMBO J.* 32, 1953–1965. doi: 10.1038/embj.2013.129
- Frith, M. C., Hamada, M., and Horton, P. (2010). Parameters for accurate genome alignment. *BMC Bioinformatics* 11:80. doi: 10.1186/1471-2105-11-80
- Gensel, P. G. (2008). The earliest land plants. *Annu. Rev. Ecol. Evol. Syst.* 39, 459–477. doi: 10.1146/annurev.Ecolsys.39.110707.173526
- Gerrath, J. F. (2003). “Conjugating green algae and desmids,” in *Freshwater Algae of North America: Ecology and Classification*, eds J. D. Wehr and R. G. Sheath (San Diego: Academic Press), 353–381.
- Gontcharov, A. A., Marin, B., and Melkonian, M. (2003). Molecular phylogeny of conjugating green algae (Zygnemophyceae, Streptophyta) inferred from SSU

- rDNA sequence comparisons. *J. Mol. Evol.* 56, 89–104. doi: 10.1007/s00239-002-2383-4
- Gontcharov, A. A., Marin, B., and Melkonian, M. (2004). Are combined analyses better than single gene phylogenies? A case study using SSU rDNA and rbcL sequence comparisons in the Zygnematophyceae (Streptophyta). *Mol. Biol. Evol.* 21, 612–624. doi: 10.1093/molbev/msh052
- Gordon, D., Abajian, C., and Green, P. (1998). Consed: a graphical tool for sequence finishing. *Genome Res.* 8, 195–202. doi: 10.1101/gr.8.3.195
- Graham, L. E., Cook, M. E., and Busse, J. S. (2000). The origin of plants: body plan changes contributing to a major evolutionary radiation. *Proc. Natl. Acad. Sci. U.S.A.* 97, 4535–4540. doi: 10.1073/pnas.97.9.4535
- Hall, J. D., Karol, K. G., McCourt, R. M., and Delwiche, C. F. (2008). Phylogeny of the conjugating green algae based on chloroplast and mitochondrial nucleotide sequence data. *J. Phycol.* 44, 467–477. doi: 10.1111/j.1529-8817.2008.00485.X
- Hu, F., Lin, Y., and Tang, J. (2014). MLGO: phylogeny reconstruction and ancestral inference from gene-order data. *BMC Bioinformatics* 15:354. doi: 10.1186/s12859-014-0354-6
- Jansen, R. K., and Ruhrlman, T. A. (2012). “Plastid genomes of seed plants,” in *Genomics of Chloroplasts and Mitochondria*, eds R. Bock and V. Knoop (Berlin: Springer), 103–126.
- Karol, K. G., McCourt, R. M., Cimino, M. T., and Delwiche, C. F. (2001). The closest living relatives of land plants. *Science* 294, 2351–2353. doi: 10.1126/science.1065156
- Kenrick, P., Wellman, C. H., Schneider, H., and Edgecombe, G. D. (2012). A timeline for terrestrialization: consequences for the carbon cycle in the Palaeozoic. *Philos. Trans. R. Soc. Lond. B Biol. Sci.* 367, 519–536. doi: 10.1098/rstb.2011.0271
- Kurtz, S., Choudhuri, J. V., Ohlebusch, E., Schleiermacher, C., Stoye, J., and Giegerich, R. (2001). REPuter: the manifold applications of repeat analysis on a genomic scale. *Nucleic Acids Res.* 29, 4633–4642. doi: 10.1093/nar/29.22.4633
- Lartillot, N., Lepage, T., and Blanquart, S. (2009). PhyloBayes 3: a Bayesian software package for phylogenetic reconstruction and molecular dating. *Bioinformatics* 25, 2286–2288. doi: 10.1093/bioinformatics/btp368
- Lartillot, N., and Philippe, H. (2004). A Bayesian mixture model for across-site heterogeneities in the amino-acid replacement process. *Mol. Biol. Evol.* 21, 1095–1109. doi: 10.1093/molbev/msh112
- Laurin-Lemay, S., Brinkmann, H., and Philippe, H. (2012). Origin of land plants revisited in the light of sequence contamination and missing data. *Curr. Biol.* 22, R593–R594. doi: 10.1016/j.cub.2012.06.013
- Leliaert, F., and Lopez-Bautista, J. M. (2015). The chloroplast genomes of *Bryopsis plumosa* and *Tydemania* expeditions (Bryopsidales, Chlorophyta): compact genomes and genes of bacterial origin. *BMC Genomics* 16:204. doi: 10.1186/s12864-015-1418-3
- Leliaert, F., Smith, D. R., Moreau, H., Herron, M. D., Verbruggen, H., Delwiche, C. F., et al. (2012). Phylogeny and molecular evolution of the green algae. *CRC Crit. Rev. Plant Sci.* 31, 1–46. doi: 10.1080/07352689.2011.615705
- Lemieux, C., Otis, C., and Turmel, M. (2000). Ancestral chloroplast genome in *Mesostigma viride* reveals an early branch of green plant evolution. *Nature* 403, 649–652. doi: 10.1038/35001059
- Lemieux, C., Otis, C., and Turmel, M. (2007). A clade uniting the green algae *Mesostigma viride* and *Chlorokybus atmophyticus* represents the deepest branch of the Streptophyta in chloroplast genome-based phylogenies. *BMC Biol.* 5:2. doi: 10.1186/1741-7007-5-2
- Lemieux, C., Otis, C., and Turmel, M. (2014). Six newly sequenced chloroplast genomes from prasinophyte green algae provide insights into the relationships among prasinophyte lineages and the diversity of streamlined genome architecture in picoplanktonic species. *BMC Genomics* 15:857. doi: 10.1186/1471-2164-15-857
- Lewis, L. A., and McCourt, R. M. (2004). Green algae and the origin of land plants. *Am. J. Bot.* 91, 1535–1556. doi: 10.3732/ajb.91.10.1535
- Lohse, M., Drechsel, O., and Bock, R. (2007). OrganellarGenomeDRAW (OGDRAW): a tool for the easy generation of high-quality custom graphical maps of plastid and mitochondrial genomes. *Curr. Genet.* 52, 267–274. doi: 10.1007/s00294-007-0161-y
- Lowe, T. M., and Eddy, S. R. (1997). tRNAscan-SE: a program for improved detection of transfer RNA genes in genomic sequence. *Nucleic Acids Res.* 25, 955–964. doi: 10.1093/nar/25.5.0955
- Lu, F., Xu, W., Tian, C., Wang, G., Niu, J., Pan, G., et al. (2011). The *Bryopsis hypnoides* plastid genome: multimeric forms and complete nucleotide sequence. *PLoS ONE* 6:e14663. doi: 10.1371/journal.pone.0014663
- Maddison, D. R., and Maddison, W. P. (2000). *MacClade 4: Analysis of Phylogeny and Character Evolution*. Sunderland, MA: Sinauer Associates.
- Maddison, W. P., and Maddison, D. R. (2015). *Mesquite: a Modular System for Evolutionary Analysis*. Version 3.04. Available at: <http://mesquitemproject.org/>
- Margulies, M., Egholm, M., Altman, W. E., Attiya, S., Bader, J. S., Bemben, L. A., et al. (2005). Genome sequencing in microfabricated high-density picolitre reactors. *Nature* 437, 376–380. doi: 10.1038/Nature03959
- McCourt, R. M., Delwiche, C. F., and Karol, K. G. (2004). Charophyte algae and land plant origins. *Trends Ecol. Evol.* 19, 661–666. doi: 10.1016/j.tree.2004.09.013
- McCourt, R. M., Karol, K. G., Bell, J., Helm-Bychowski, K. M., Grajewska, A., Wojciechowski, M. F., et al. (2000). Phylogeny of the conjugating green algae (Zygnematophyceae) based on rbcL sequences. *J. Phycol.* 36, 747–758. doi: 10.1046/j.1529-8817.2000.99106.X
- Melton, J. T. III, Leliaert, F., Tronholm, A., and Lopez-Bautista, J. M. (2015). The complete chloroplast and mitochondrial genomes of the green macroalga *Ulva* sp. UNA00071828 (Ulvophyceae, Chlorophyta). *PLoS ONE* 10:e0121020. doi: 10.1371/journal.pone.0121020
- Michel, F., Umesono, K., and Ozeki, H. (1989). Comparative and functional anatomy of group II catalytic introns - a review. *Gene* 82, 5–30. doi: 10.1016/0378-1119(89)90026-7
- Michel, F., and Westhof, E. (1990). Modelling of the three-dimensional architecture of group I catalytic introns based on comparative sequence analysis. *J. Mol. Biol.* 216, 585–610. doi: 10.1016/0022-2836(90)90386-Z
- Mikhailuk, T. I., Sluiman, H. J., Massalski, A., Mudimu, O., Demchenko, E. M., Kondratyuk, S. Y., et al. (2008). New streptophyte green algae from terrestrial habitats and an assessment of the genus *Interfilum* (Klebsormidiophyceae, Streptophyta). *J. Phycol.* 44, 1586–1603. doi: 10.1111/j.1529-8817.2008.00606.X
- Palmer, J. D. (1991). “Plastid chromosomes: structure and evolution,” in *The Molecular Biology of Plastids*, ed. I. K. Vasil (Cambridge: Academic Press), 5–53.
- Ruhrlman, T. A., and Jansen, R. K. (2014). “The plastid genomes of flowering plants,” in *Chloroplast Biotechnology*, ed. P. Maliga (New York City, NY: Humana Press), 3–38.
- Smith, S. A., and Dunn, C. W. (2008). Phyutility: a phyloinformatics tool for trees, alignments and molecular data. *Bioinformatics* 24, 715–716. doi: 10.1093/bioinformatics/btm619
- Stamatakis, A. (2014). RAxML version 8: a tool for phylogenetic analysis and post-analysis of large phylogenies. *Bioinformatics* 30, 1312–1313. doi: 10.1093/bioinformatics/btu033
- Tesler, G. (2002). GRIMM: genome rearrangements web server. *Bioinformatics* 18, 492–493. doi: 10.1093/bioinformatics/18.3.492
- Timme, R. E., Bachvaroff, T. R., and Delwiche, C. F. (2012). Broad phylogenomic sampling and the sister lineage of land plants. *PLoS ONE* 7:e29696. doi: 10.1371/journal.pone.0029696
- Turmel, M., de Cambiaire, J. C., Otis, C., and Lemieux, C. (2016). Distinctive architecture of the chloroplast genome in the chlorodendrophycean green algae *Scherffelia dubia* and *Tetraselmis* sp. CCMP 881. *PLoS ONE* 11:e0148934. doi: 10.1371/journal.pone.0148934
- Turmel, M., Gagnon, M. C., O’Kelly, C. J., Otis, C., and Lemieux, C. (2009). The chloroplast genomes of the green algae Pyramimonas, Monomastix, and Pycnococcus shed new light on the evolutionary history of prasinophytes and the origin of the secondary chloroplasts of euglenids. *Mol. Biol. Evol.* 26, 631–648. doi: 10.1093/molbev/msn285
- Turmel, M., Lemieux, C., Burger, G., Lang, B. F., Otis, C., Plante, I., et al. (1999a). The complete mitochondrial DNA sequences of *Nephroselmis olivacea* and *Pedinomonas minor*. Two radically different evolutionary patterns within green algae. *Plant Cell* 11, 1717–1730. doi: 10.2307/3871049
- Turmel, M., Otis, C., and Lemieux, C. (1999b). The complete chloroplast DNA sequence of the green alga *Nephroselmis olivacea*: insights into the architecture of ancestral chloroplast genomes. *Proc. Natl. Acad. Sci. U.S.A.* 96, 10248–10253. doi: 10.1073/pnas.96.18.10248
- Turmel, M., Otis, C., and Lemieux, C. (2002). The chloroplast and mitochondrial genome sequences of the charophyte *Chaetosphaeridium globosum*: insights into the timing of the events that restructured organelle DNAs within the

- green algal lineage that led to land plants. *Proc. Natl. Acad. Sci. U.S.A.* 99, 11275–11280. doi: 10.1073/pnas.162203299
- Turmel, M., Otis, C. and Lemieux, C. (2005). The complete chloroplast DNA sequences of the charophycean green algae *Staurastrum* and *Zygnema* reveal that the chloroplast genome underwent extensive changes during the evolution of the Zygnematales. *BMC Biol.* 3:22. doi: 10.1186/1741-7007-3-22
- Turmel, M., Otis, C., and Lemieux, C. (2006). The chloroplast genome sequence of *Chara vulgaris* sheds new light into the closest green algal relatives of land plants. *Mol. Biol. Evol.* 23, 1324–1338. doi: 10.1093/molbev/msk018
- Turmel, M., Otis, C., and Lemieux, C. (2013). Tracing the evolution of streptophyte algae and their mitochondrial genome. *Genome Biol. Evol.* 5, 1817–1835. doi: 10.1093/gbe/evt135
- Turmel, M., Otis, C., and Lemieux, C. (2015). Dynamic evolution of the chloroplast genome in the green algal classes *Pedinophyceae* and *Trebouxiophyceae*. *Genome Biol. Evol.* 7, 2062–2082. doi: 10.1093/gbe/evw130
- Turmel, M., Pombert, J. F., Charlebois, P., Otis, C., and Lemieux, C. (2007). The green algal ancestry of land plants as revealed by the chloroplast genome. *Int. J. Plant Sci.* 168, 679–689. doi: 10.1086/513470
- Umen, J. G. (2014). Green algae and the origins of multicellularity in the plant kingdom. *Cold Spring Harb. Perspect. Biol.* 6:a016170. doi: 10.1101/cshperspect.a016170
- Weng, M. L., Blazier, J. C., Govindu, M., and Jansen, R. K. (2014). Reconstruction of the ancestral plastid genome in Geraniaceae reveals a correlation between genome rearrangements, repeats, and nucleotide substitution rates. *Mol. Biol. Evol.* 31, 645–659. doi: 10.1093/molbev/mst257
- Wicke, S., Schneeweiss, G. M., dePamphilis, C. W., Muller, K. F., and Quandt, D. (2011). The evolution of the plastid chromosome in land plants: gene content, gene order, gene function. *Plant Mol. Biol.* 76, 273–297. doi: 10.1007/s11103-011-9762-4
- Wickett, N. J., Mirarab, S., Nguyen, N., Warnow, T., Carpenter, E., Matasci, N., et al. (2014). Phylogenomic analysis of the origin and early diversification of land plants. *Proc. Natl. Acad. Sci. U.S.A.* 111, E4859–E4868. doi: 10.1073/pnas.1323926111
- Wodniok, S., Brinkmann, H., Glockner, G., Heidel, A. J., Philippe, H., Melkonian, M., et al. (2011). Origin of land plants: do conjugating green algae hold the key? *BMC Evol. Biol.* 11:104. doi: 10.1186/1471-2148-11-104
- Xia, X. (2013). DAMBE5: a comprehensive software package for data analysis in molecular biology and evolution. *Mol. Biol. Evol.* 30, 1720–1728. doi: 10.1093/molbev/mst064
- Yang, Z. (2007). PAML 4: phylogenetic analysis by maximum likelihood. *Mol. Biol. Evol.* 24, 1586–1591. doi: 10.1093/molbev/msm088
- Zhang, J., Ruhlman, T. A., Sabir, J. S., Blazier, J. C., Weng, M. L., Park, S., et al. (2016). Coevolution between nuclear-encoded DNA replication, recombination, and repair genes and plastid genome complexity. *Genome Biol. Evol.* 8, 622–634. doi: 10.1093/gbe/evw033
- Zhong, B., Liu, L., Yan, Z., and Penny, D. (2013). Origin of land plants using the multispecies coalescent model. *Trends Plant Sci.* 18, 492–495. doi: 10.1016/j.tplants.2013.04.009
- Zhong, B., Xi, Z., Goremykin, V. V., Fong, R., McLenaghan, P. A., Novis, P. M., et al. (2014). Streptophyte algae and the origin of land plants revisited using heterogeneous models with three new algal chloroplast genomes. *Mol. Biol. Evol.* 31, 177–183. doi: 10.1093/molbev/mst200

Conflict of Interest Statement: The authors declare that the research was conducted in the absence of any commercial or financial relationships that could be construed as a potential conflict of interest.

Copyright © 2016 Lemieux, Otis and Turmel. This is an open-access article distributed under the terms of the Creative Commons Attribution License (CC BY). The use, distribution or reproduction in other forums is permitted, provided the original author(s) or licensor are credited and that the original publication in this journal is cited, in accordance with accepted academic practice. No use, distribution or reproduction is permitted which does not comply with these terms.



Primitive Extracellular Lipid Components on the Surface of the Charophytic Alga *Klebsormidium flaccidum* and Their Possible Biosynthetic Pathways as Deduced from the Genome Sequence

Satoshi Kondo¹, Koichi Hori^{2,3}, Yuko Sasaki-Sekimoto^{2,3}, Atsuko Kobayashi⁴, Tsubasa Kato⁵, Naoko Yuno-Ohta⁵, Takashi Nobusawa^{2,3}, Kinuka Ohtaka¹, Mie Shimojima^{1,2} and Hiroyuki Ohta^{1,2,3,4*}

OPEN ACCESS

Edited by:

David Domozych,
Skidmore College, USA

Reviewed by:

Mi Chung Suh,
Chonnam National University,
South Korea
Sandra Cristina Raimundo,
Skidmore College, USA

*Correspondence:

Hiroyuki Ohta
ohta.h.ab@m.titech.ac.jp

Specialty section:

This article was submitted to
Plant Evolution and Development,
a section of the journal
Frontiers in Plant Science

Received: 24 March 2016

Accepted: 15 June 2016

Published: 30 June 2016

Citation:

Kondo S, Hori K, Sasaki-Sekimoto Y, Kobayashi A, Kato T, Yuno-Ohta N, Nobusawa T, Ohtaka K, Shimojima M and Ohta H (2016) Primitive Extracellular Lipid Components on the Surface of the Charophytic Alga *Klebsormidium flaccidum* and Their Possible Biosynthetic Pathways as Deduced from the Genome Sequence. *Front. Plant Sci.* 7:952.
doi: 10.3389/fpls.2016.00952

Klebsormidium flaccidum is a charophytic alga living in terrestrial and semiaquatic environments. *K. flaccidum* grows in various habitats, such as low-temperature areas and under desiccated conditions, because of its ability to tolerate harsh environments. Wax and cuticle polymers that contribute to the cuticle layer of plants are important for the survival of land plants, as they protect against those harsh environmental conditions and were probably critical for the transition from aquatic microorganism to land plants. Bryophytes, non-vascular land plants, have similar, but simpler, extracellular waxes and polyester backbones than those of vascular plants. The presence of waxes in terrestrial algae, especially in charophytes, which are the closest algae to land plants, could provide clues in elucidating the mechanism of land colonization by plants. Here, we compared genes involved in the lipid biosynthetic pathways of *Arabidopsis thaliana* to the *K. flaccidum* and the *Chlamydomonas reinhardtii* genomes, and identified wax-related genes in both algae. A simple and easy extraction method was developed for the recovery of the surface lipids from *K. flaccidum* and *C. reinhardtii*. Although these algae have wax components, their surface lipids were largely different from those of land plants. We also investigated aliphatic substances in the cell wall fraction of *K. flaccidum* and *C. reinhardtii*. Many of the fatty acids were determined to be lipophilic monomers in *K. flaccidum*, and a Fourier transform infrared spectroscopic analysis revealed that their possible binding mode was distinct from that of *A. thaliana*. Thus, we propose that *K. flaccidum* has a cuticle-like hydrophobic layer composed of lipids and glycoproteins, with a different composition from the cutin polymer typically found in land plant cuticles.

Keywords: *Klebsormidium flaccidum*, *Chlamydomonas reinhardtii*, *Arabidopsis thaliana*, extracellular lipids, polyester backbone, wax, cuticle

INTRODUCTION

The aerial epidermis of land plants is covered by a cuticle layer that has critical roles in protecting the plants from ultraviolet irradiation (Barnes et al., 1998), in controlling non-stomatal water loss (Riederer and Schreiber, 2001), and in guarding plants from pathogens and insect herbivores (Müller and Riederer, 2005; Skamnioti and Gurr, 2007), as well as in preventing organ fusion during development (Lolle et al., 1998; Sieber et al., 2000). The cuticle in higher plants is composed of three layers, the cuticular layer, which is anchored to the cell wall by oligosaccharides; the cuticle proper, consisting of intracuticular waxes located above the cuticular layer; and the outermost epicuticular wax (Pollard et al., 2008).

Most research on the molecular components of the epicuticular wax has been undertaken using *Arabidopsis thaliana*. Alkanes, ketones, aldehydes, primary and secondary alcohols, and very-long-chain fatty acids are included in wax (Kunst and Samuels, 2003; Samuels et al., 2008; Lee and Suh, 2015). These lipid classes are made up of very-long-chain fatty acyl moieties with more than 20 carbon atoms. Deficiencies in wax components leads to detrimental phenotypes: *eceriferum1-1* (*cer1-1*), a mutant of cuticular wax synthesis, reduces alkane coverage (Bernard et al., 2012) and pollen fertility under low-humidity conditions (Aarts et al., 1995); the loss of CUTICULAR1 activity results in dysfunctional pollen grains (Millar et al., 1999); and *cer7-3* results in reduced seed viability (Hooker et al., 2007). Thus, wax plays various important roles in *A. thaliana*. Epicuticular wax has also been analyzed from Bryophytes, such as *Andreaea* and *Polygonatum* species (Haas, 1982). In this report, the outer lipids of these Bryophytes are composed of alkanes, wax esters, aldehydes, primary alcohols, and fatty acids.

Constituents of the cuticle, including the cuticle proper and cuticular layer, were also investigated in *A. thaliana* (Graça et al., 2002; Franke et al., 2005; Molina et al., 2006). The cuticle of shoots is composed of aliphatic polymers, such as cutin and cutan. The former can be depolymerized by acid or alkaline hydrolysis, whereas the latter is difficult to break down using either acidic or alkaline reagents. Cutin obtained from the hydrolysis of delipidated *Arabidopsis* leaves or stems has been analyzed, and various fatty acid derivatives, such as ω -hydroxy fatty acids, α,ω -dicarboxylic acids, polyhydroxy fatty acids, and glycerol, were found. These monomers form an aliphatic network via primary or secondary ester bonds, producing vigorous structures and interspaces filled with waxes on the plant surface. A null mutant of long-chain acyl-CoA synthetase2 (LACS2) exhibits a decrease in the cutin layer thickness on the abaxial surface of its leaves, and its growth is inhibited in *A. thaliana* (Schnurr et al., 2004). Furthermore, *Oryza sativa* that lacks the cytochrome P450 superfamily gene CYP704B2 displays reduced growth, male sterility, aborted pollen grains and undeveloped anther cuticles (Li et al., 2010). The *desperado-3* (*dso-3*) mutant in *A. thaliana*, which lacks the ABCG transporter gene, displays a reduced amount of both wax and cutin monomers. Root branching and growth

inhibition have also been observed in *dso-3* (Panikashvili et al., 2007).

As lipophilic outer layers are necessary for land plants, it is of great interest to determine whether terrestrial algae also have these outer lipids. Rindi et al. (2008) analyzed *Klebsormidium* species and speculated that some of them have an outer layer, called the “superficial hydro-repellent layer,” which is formed in a liquid medium. However, there is no chemical evidence supporting the presence of a superficial hydro-repellent layer in some microalgae.

The genus *Klebsormidium* belongs to the Klebsormidiales, one of the basal groups of the Charophycean Green Algae (CGA), the extant algal group as a model of ancestors of land plants, that typically have multicellular and non-branching filaments without differentiated cells (Hori et al., 2014). It is one of the most common genera of terrestrial algae and includes a few species of green algae that occur in subaerial and semiaquatic environments worldwide, such as the northernmost habitat of Ny-Ålesund, Norway (Kaštovská et al., 2005), southern Africa (Karsten et al., 2015), the European Alps (Karsten et al., 2010), and Japan. The survival of these algae may be attributed to their high tolerance to desiccation (Herburger and Holzinger, 2015; Karsten et al., 2015), low temperature (Nagao et al., 2008), and osmotic stress (Kaplan et al., 2012).

It is generally accepted that the ancestor(s) of land plants was closely related to modern charophytes (Lewis and McCourt, 2004; Becker and Marin, 2009; Popper et al., 2011; Leliaert et al., 2012; Timme et al., 2012). Initial land colonization has been proposed to be carried out by aquatic algae adapting to a terrestrial environment. Therefore, *Klebsormidium* is an important genus for evolutionary studies. Recently, the draft genome sequence of *Klebsormidium flaccidum* strain NIES-2285 was completed (Hori et al., 2014). Thus, investigating the extracellular lipid components of this alga could be helpful for elucidating details of plant terrestrialization.

Here, we identified the genes encoded by the *K. flaccidum* genome that are homologous to those involved in the wax and cutin synthesis pathways of *A. thaliana*. Because genes related to lipid synthesis were found, we tried to confirm the existence of the extracellular lipids on the surface of *K. flaccidum* using a simple and easy extraction method and analyzed those that were present. In addition, we studied the contents and binding patterns of cutin monomers using gas chromatography-mass spectrometry (GC-MS) and attenuated total reflectance (ATR) Fourier transform infrared spectroscopy (FTIR). Our results demonstrated that the components of the extracellular lipids of *K. flaccidum*, dominated by alkanes and triacylglycerols (TAGs), were similar to those of *Chlamydomonas reinhardtii*, which belongs to the Chlorophyceae, and different from those of *A. thaliana*. *K. flaccidum* likely does not have aliphatic polymers on its cell walls, unlike *A. thaliana*; however, a great amount of fatty acids was covalently attached to the delipidated cell wall fraction, providing a primitive cuticle layer-like structure that may be filled with surface lipids, such as alkanes and TAGs.

MATERIALS AND METHODS

Plant Materials

Arabidopsis thaliana ecotype Columbia was grown in soil under continuous light ($40\text{--}50 \mu\text{mol photons m}^{-2} \text{ s}^{-1}$) at 22°C for 42 days. *K. flaccidum* strain NIES-2285 was cultured on a nitrocellulose membrane placed on an agar plate of NIES-C medium (Ichimura, 1971) in a Petri dish under continuous light ($10 \mu\text{mol photons m}^{-2} \text{ s}^{-1}$) at 23°C for 28 or 42 days. *C. reinhardtii* was cultured on a nitrocellulose membrane placed on an agar plate containing Tris-acetate-phosphate medium under the same conditions as *K. flaccidum* for 14 days. Both nitrocellulose membranes and agar powder were delipidated three times with more than 15 fold amount by weight of chloroform before the cultivation of algae.

Reagents

Phytol, stigmasterol, and β -sitosterol containing campesterol and the fatty acids including linoleic and linolenic acids, myristoyl, palmitoyl, stearoyl, oleoyl chlorides, and N, O-bis(trimethylsilyl) trifluoroacetamide with 1% trimethylchlorosilane (BSTFA-TMCS, for the trimethylsilyl derivatization) were purchased from Tokyo Chemical Industry Co, Ltd., (TCI). Primuline (for lipid detection) and other organic solvents were purchased from Wako Pure Chemical Industries, Ltd., and silica gel 60 thin-layer chromatography (TLC) plates were purchased from Merck Millipore.

Synthesis of Steryl and Phytol Esters

Steryl and phytol esters carrying specific fatty acids were synthesized by reacting fatty acyl chlorides with sterols or phytol, respectively (Wisnieski et al., 1973; Terzaghi, 1986). Fatty acyl chlorides were prepared by reacting linoleic or linolenic acid as a free fatty acid with an excess of oxalyl chloride in the presence of sodium carbonate (2 mol per mol of fatty acid) in dichloromethane. The reaction mixture was stirred for 6 h at room temperature and then heated for 60 min under reflux at 80°C . Excess oxalyl chloride was removed under vacuum, and then the acyl chloride was dissolved in dichloromethane and added to an equimolar quantity of campesterol plus sitosterol, stigmasterol, or phytol dissolved in dichloromethane with sodium carbonate (2 mol per mol of fatty acid). Pyridine ($0.1 \text{ ml g acyl chloride}^{-1}$) was added dropwise, and the mixture was stirred for 12 h at room temperature. After the reaction mixture was filtered through sintered glass, the solvent was removed using a rotary evaporator, and sterol or phytol esters were purified by silica gel TLC with hexane/diethyl ether/acetic acid (80:20:1, v/v/v).

Scanning Electron Microscopy (SEM)

Klebsormidium flaccidum was transferred to a fresh agar medium or liquid medium. Three days after subculturing, algal cells were collected on 1.5% (w/v) agar medium and fixed with 2% (v/v) glutaraldehyde in 0.1 M phosphate buffer. Samples were dehydrated in a graded series of ethanol and t-butyl alcohol, and then dried by using a vacuum evaporator (VFD-21S, Vacuum

Device Inc.). The samples mounted on an aluminum stub were sputter-coated with osmium using an osmium coater (Neoc-Pro, Meiwafosis). SEM observations were performed using an S-3400 microscope (Hitachi) at 10 kV.

Extracellular Lipid Extraction

Chloroform Extraction of Extracellular Lipids

Klebsormidium flaccidum was cultured for 28 days or *C. reinhardtii* was cultured for 14 days on a nitrocellulose membrane placed on an agar plate. First, to determine an appropriate extraction time to isolate lipids, we immersed the entire membrane with *K. flaccidum* in 5 ml chloroform at room temperature in a glass Petri dish (Figure 1A). The solvent was recovered at predetermined time intervals of 10, 20, 30, 60, 120, 240, 480, and 1920 s. At each sampling time, the solvent was retrieved and then 5 ml of fresh chloroform was immediately added to the Petri dish for the next time point. The chloroform extracts were filtered and combined from 2 cultures, and then the solvent was removed with a gentle stream of nitrogen while heating to 30°C . The remaining lipids were weighed and subsequently dissolved in chloroform at $20 \text{ mg lipids ml}^{-1}$. After the final extraction, a portion of alga was dried for measuring the weight, and total lipids were extracted from aliquot as described by Bligh and Dyer (Bligh and Dyer, 1959) to determine the amounts of triacylglycerol (TAG) and monogalactosyldiacylglycerol (MGDG). As the protocol for chemical analysis, 30 s was employed as the extraction time, and the extracellular lipids were collected from 7 cultures.

Silica Gel Plate Extraction of Extracellular Lipids

Klebsormidium flaccidum was grown on nitrocellulose membranes as described above but for 42 days. Each membrane on which *K. flaccidum* cells were growing was then placed growing surface down on a silica gel 60 TLC plate (Merck Millipore) without any force for 30 s, 1, 2.5, 5, 10, and 20 min (Figure 1B), during which time point the extracellular lipids secreted from cells were transferred to the plate. After the membrane with the cells was carefully removed, the silica gel plate was dried in a fume hood at room temperature for 30 min. Lipids were detected using primuline under ultraviolet light (see below) and recovered from the silica gel plate by scraping the surface lipids into chloroform. The same process was used with *C. reinhardtii* after subculturing for 14 days. Wax was also extracted from *A. thaliana* by pressing it to a silica gel plate at approximate 100 g cm^{-1} by hand.

Extracellular Lipid Separation and Derivatization

The lipids were separated by TLC before the GC-MS analysis. The extracts were applied to silica gel 60 TLC plates and developed using the following solvent systems sequentially: (1) to a height of 20 cm with hexane; (2) to a height of 20 cm with toluene; and, (3) to a height of 10 cm with hexane/diethyl ether/acetic acid (70:30:1, v/v/v) (Yamashiro et al., 2001). To determine the extraction time, TAG and MGDG were separated on a TLC plate by using the following sequential two-part development system: (1) to a height of 20 cm with hexane/diethyl ether/acetic acid (70:30:1, v/v/v) and, (2) to a height of 10 cm

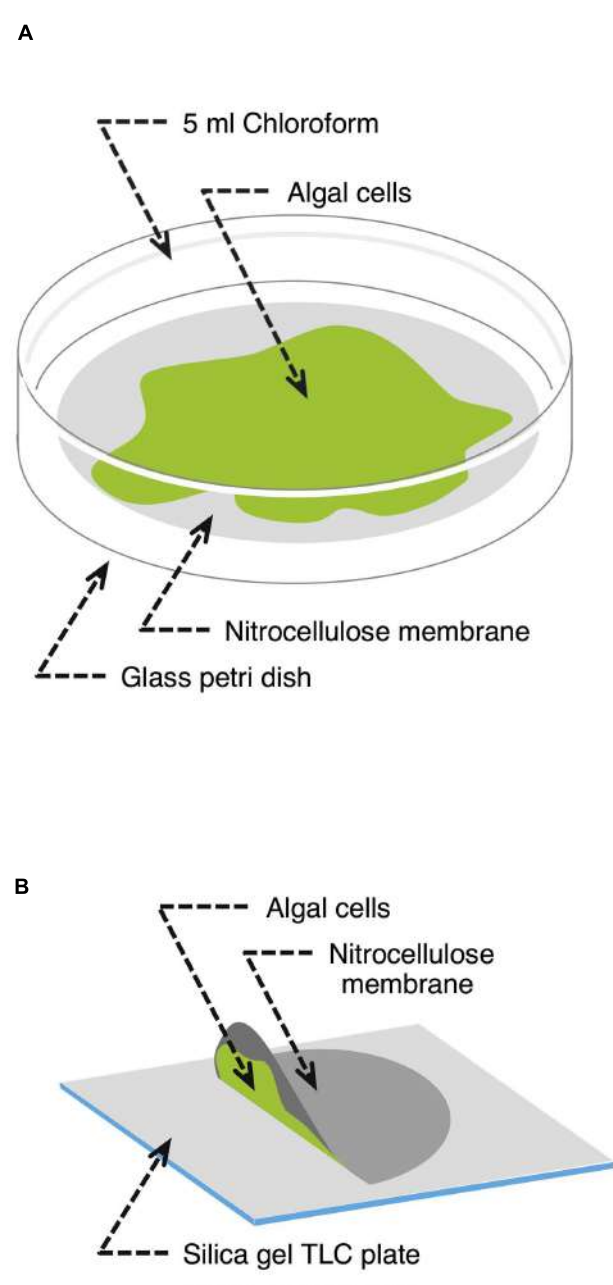


FIGURE 1 | Schematic representation of the lipid extraction methodologies used. (A) Chloroform extraction. Alga grown on a nitrocellulose membrane was transferred to a glass Petri dish containing 5 ml chloroform. After a predefined time, the chloroform was recovered and the algal cells were harvested to determine their dry weight. **(B)** Silica gel plate extraction. A nitrocellulose membrane covered with algal cells was placed on a silica gel plate culture facing down without any force for a predetermined period.

with acetone/toluene/water (91:30:8, v/v/v). All of the lipids on the TLC plates were visualized under ultraviolet light after the plates were sprayed with 0.01% (w/v) primuline in 80% (v/v)

acetone. The sterol lipid fraction was derivatized with 20 μ l BSTFA-TMCS and 20 μ l pyridine for 60 min at 80°C to transform all of the hydroxyl-containing groups into their corresponding trimethylsilyl derivatives. Fatty acid methyl esters were obtained from the TAG fraction by methanolysis with 350 μ l of 5% hydrochloric acid in methanol for 60 min at 80°C in a screw-capped test tube. The lipids corresponding to steryl esters were hydrolyzed by 1 ml of 2 M sodium methoxide solution in methanol at 80°C for 60 min. The resultant fatty acids and sterols were derivatized by 20 μ l BSTFA-TMCS and 20 μ l pyridine for 60 min at 70°C. Alkanes and phytol esters were analyzed without derivatization. For all of the classes, the lipids were characterized by GC-MS and quantified by GC-flame ionization detection (FID).

Lipid Characterization by GC-MS and GC-FID

The ratios of the lipids that corresponded to steryl esters, wax esters, and sterols were further identified using capillary gas chromatography (GC) connected to a electron ionization mass spectrometric detector (EI-MS; GC-2010 equipped with GCMS-TQ8030, Shimadzu) with a 30-m DB-5 column (0.25-mm i.d.; film thickness, 0.25 μ m; Agilent) with He. The carrier gas inlet pressure was regulated for a constant flow of 1.4 ml min⁻¹. GC was carried out with a temperature-programmed injection as follows: 50°C for 2 min, then raised by 40°C min⁻¹ to 200°C, held for 2 min at 200°C, raised by 3°C min⁻¹ to 320°C, and finally held for 30 min at 320°C. Alkanes were determined by GC-MS with the same conditions as above, except for the oven temperature program, which was as follows: 50°C for 2 min, increased by 10°C min⁻¹ to 220°C, then raised by 2°C min⁻¹ to 260°C, and finally held for 50 min. Both the ion source and the injection port were held at 250°C. The quantitative analysis was carried out using a capillary GC with a flame ionization detector (GC-2014, Shimadzu) under the same conditions as the GC-MS analysis. To determine the fatty acid composition of TAG, fatty acid methyl esters were prepared as described above and analyzed using GC-FID with the following oven temperature program: 180°C for 15 min, and then increased by 2°C min⁻¹ to 220°C.

Phylogenetic Analysis of Surface Lipid Biosynthesis-Related Proteins in *K. flaccidum*

The predicted protein sequences of *K. flaccidum* are available at http://www.plantmorphogenesis.bio.titech.ac.jp/~algae_genome_project/klebsormidium/index.html. Proteins of nine algae, *Chondrus crispus*, *Ectocarpus siliculosus*, *Phaeodactylum tricornutum*, *Cyanidioschyzon merolae*, *Micromonas* strain RCC299, *Ostreococcus tauri*, *Chlorella variabilis* NC64A, *Volvox carteri* f. *nagariensis*, and *C. reinhardtii*, and of five land plants, *Physcomitrella patens* subsp. *patens*, *Selaginella moellendorffii*, *O. sativa* subsp. *japonica*, *Populus trichocarpa*, and *A. thaliana*, were compared with those of *K. flaccidum* according to Hori et al. (2014). Based on the protein sequences involved in the biosynthesis of waxes, neutral lipids and cutin monomers in *A. thaliana*, searches using the BLASTP algorithm were carried out using the datasets from these 14 species (e-value < 10⁻³).

After removing inadequate sequences that were too short, of low quality, or had large deletions from the phylogenetic analysis, sequences were aligned using the MUSCLE program (Edgar, 2004). Alignments were edited using the G-Blocks program (Talavera and Castresana, 2007) to select the most-conserved sites, and to eliminate both highly variable and/or ambiguous portions of the alignments. The maximum likelihood analyses of all of the datasets were performed with MEGA6.0 (Tamura et al., 2013) using the appropriate models (Le and Gascuel, 2008). Bootstrap analyses with 500 replicates were carried out to estimate the support for internal nodes. These sequences were also studied with InterPro for predicting domains and important sites.

Cutin Monomer Analysis

Aliphatic components were derived from algal cells or plant according to Bonaventure et al. (2004) with slight modification (Li-Beisson et al., 2013). Approximately 100 mg of algal cells or plant was submerged in hot 2-propanol at 80°C for 10 min. After cooling to room temperature, the tissue was ground with a mortar and pestle and vortexed in the 2-propanol for 1 h to allow complete extraction of whole lipids. After centrifugation at 1,500 g for 5 min, the supernatant was discarded and fresh 2-propanol was added to the pellet. The pellet was then re-extracted for 1 h. After centrifugation at 1,500 g for 5 min, the supernatant was discarded. The pellet was delipidated sequentially by chloroform/methanol (2:1, v/v; 1 h), chloroform/methanol (1:2, v/v; 1 h), methanol (1 h) for all species. For further delipidation of algae, water (1 h), 2 M NaCl (1 h), water (1 h), methanol (1 h), chloroform/methanol (1:2, v/v; 1 h), chloroform/methanol (2:1, v/v; 1 h) and methanol (1 h) was used as described above. After the delipidation, the solvent was removed under a gentle stream of nitrogen gas, and pellets were lyophilized for 24 h.

To prepare aliphatic monomers, 2 ml of reaction medium, consisting of methanol/methyl acetate/28% sodium methoxide (12:3:5, v/v/v), was added to the delipidated pellets and heated at 60°C for 2 h. After cooling to room temperature, 4 ml dichloromethane, 0.5 ml glacial acetic acid, and 1 ml of buffer [100 mM Tris-HCl (pH 8.0), 0.9% (w/v) NaCl] were added. Phases were separated by centrifugation at 1,500 g for 2 min. The lower organic phase was collected, washed with 2 ml of buffer, and dehydrated over anhydrous sodium sulfate. The supernatant was dried under a gentle stream of nitrogen gas. Then, 20 µl of anhydrous pyridine and 20 µl of BSTFA-TMCS were added, and the mixture was vortexed for 10 s and then heated at 70°C for 60 min. After the derivatization, solvents were removed under a gentle stream of nitrogen gas, and lipids were analyzed by GC-MS and GC-FID.

ATR-FTIR Analysis

Cell wall was extracted as previously described with some modification (Carpita et al., 2001; Moller et al., 2007; Pattathil et al., 2012). Shortly, the pellets lyophilized after delipidation were pre-treated with the following agents: 100 mM 1,2-cyclohexylenedinitrilotetraacetic acid (CDTA) for 1 h at room temperature to remove pectic polysaccharides, 0.34 M NaClO₂ in 65 mM acetic acid for 1 h at 65°C, 0.1 M NaOH for 1 h at room

temperature, or hot water for 1 h at 80°C. Treated pellets were washed with water and then lyophilized for 24 h.

IR spectra were recorded by a Spectrum Two (PerkinElmer Japan Co. Ltd.) with universal attenuated total reflection (UATR) using a single reflection accessory fitted with a diamond prism (incident angle 45°). Dehumidification of inside FTIR system was kept using desiccant (molecular sieve). Pieces of each pellet were mounted on the top of ATR crystal and pressed using pressure arm with check which has 3 mm diameter. For background measurements, the same ATR prism was used without any solution (air only). Spectral measurements were carried out from 4,000 and 450 cm⁻¹ at a resolution of 4 cm⁻¹ and 24 ± 1°C. Interferograms from 4 scans were averaged to obtain each spectrum. A power spectrum was calculated from the interferogram (both side) using apodization of a Norton-Beer. Obtained original spectra were treated with an ATR correction.

RESULTS

SEM Observations

Before investigating surface lipids and their synthesis, surface structure of *K. flaccidum* cells was observed with SEM, 3 days after being transferred to fresh liquid or solid medium. Algal cells transferred to liquid medium had smooth surfaces (**Figures 2A,B**), whereas the surfaces of algae transferred to solid medium were strikingly different and seemed to be coated with frequently disrupted film-like structures (**Figures 2C,D**).

Phylogenetic Analyses of Surface Lipid Biosynthesis-Related Proteins in *K. flaccidum* and *C. reinhardtii*

We searched protein sequences from *K. flaccidum* and *C. reinhardtii* genomes by BLASTP program on the basis of

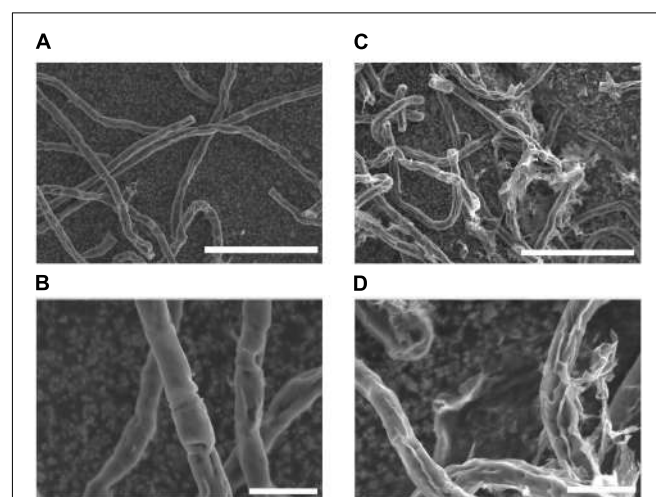


FIGURE 2 | Scanning electron microscopy pictures of *K. flaccidum* 3 days after transfer to a liquid or solid medium. SEM pictures of *K. flaccidum* 3 days after transfer to liquid (A,B) or solid (C,D) medium. Scale bars (A,C) = 50 µm, (B,D) = 10 µm.

the protein sequences involved in wax and cutin monomers biosynthesis pathways of *A. thaliana*. These sequences were aligned and curated by ClustalW, MUSCLE and G-Blocks.

Wax Biosynthesis

In *A. thaliana*, the biosynthesis of almost all of the surface waxes begins with very-long-chain fatty acids (VLCFAs) that typically have \geq C20. Based on a BLAST analysis across genomes, *K. flaccidum* has the counterparts to a set of enzymes involved in the elongation of fatty acids up to C24 in *A. thaliana*. Nevertheless, it is not clear whether *K. flaccidum* is able to synthesize VLCFAs since *A. thaliana* KCS4 could not rescue the yeast Δ elo2 Δ elo3 double mutant (Paul et al., 2006). *K. flaccidum* does not appear to contain homologs of ECERIFERUM2 (CER2) or ECERIFERUM6 (CER6), which are required for the synthesis of fatty acids containing \geq C28 (Figure 3A). CUTI/CER6/KCS6

catalyze the synthesis of VLCFAs with longer aliphatic chains than C24, which are cuticular wax components or precursors (Millar et al., 1999; Todd et al., 1999). CER2 and CER2-like genes are involved in the elongation of C28 to C34 VLCFAs (Haslam et al., 2012, 2015; Pascal et al., 2013). For alkane biosynthesis, there are counterparts to both ECERIFERUM3 (CER3) and ECERIFERUM7 (CER7) in *K. flaccidum* that work indirectly in the decarbonylation pathway. For *C. reinhardtii*, homologs involving fatty acid elongation, namely ketoacyl-CoA synthase (KCS), ketoacyl-CoA reductase (KCR), hydroxyacyl-CoA dehydrogenase (HACD), and enoyl-CoA reductase (ECR), were identified. No counterpart to ECERIFERUM1 (CER1), which produces alkanes, was clearly identified. Midchain alkane hydroxylase1 (MAH1) is involved in two steps in *A. thaliana*, the oxidation of alkane to a secondary alcohol, followed by the oxidation of the secondary alcohol to a ketone (Greer et al., 2007). *K. flaccidum* does not appear to have a MAH1 homolog. *A. thaliana* fatty acid reductase (FAR) protein sequences, when queried against the *K. flaccidum* genome using the BLASTP algorithm, produced no significant hits. However, only one gene encoding wax ester synthase/acyl-coenzyme A: diacylglycerol acyltransferase1-like (WSD1-like) was found in *K. flaccidum*. In case of *C. reinhardtii*, only a CER7 homolog was found in alkane biosynthesis, and no counterpart to WSD1-like proteins or FAR was identified in wax ester biosynthesis.

ABCG Transporters

In *A. thaliana*, some ABCG transporters are responsible for the transportation of wax precursors (Bird et al., 2007; Panikashvili et al., 2007; Panikashvili and Aharoni, 2008). *K. flaccidum* appears to contain homologs of ABCG transporters (Figure 3B). These ABCG transporters work as dimers, for example, DESPERADO (DSO)/ABCG11 and CER5/ABCG12 form heterodimers for transporting the wax precursors to the epicuticular wax layer. In the *K. flaccidum* and *C. reinhardtii* genomes, only counterparts to DSO were found.

Qualitative Analysis of Extracts by Immersion in Chloroform

After the identification of several genes related to surface lipid biosynthesis in *K. flaccidum* genome, we used two different methods to extract surface lipids from both *K. flaccidum* and *C. reinhardtii*. First, we applied the chloroform submergence method for extracting wax from plants (Li et al., 2008). In the initial assessment, immersion time points were studied using *K. flaccidum*. From 10 to 30 s, the lipid recovery rose sharply and then gradually increased until 1,920 s (Figure 4). Thus, algal lipids were extracted with chloroform for 30 s. We note that the lipid yield at 1,920 s contained \sim 40% of the total amount of TAG and 7.6% of the total amount of MGDG obtained by the Bligh and Dyer method (Figure 4). After extraction, lipids were separated on a TLC plate, identified by GC-MS, and quantified by GC-FID. According to the TLC images, the lipid composition of *K. flaccidum* was different from that of *A. thaliana* (Figure 5A). The fractions were identified as alkanes, sterol esters, phytol esters, TAGs, and sterols; however, ketones,

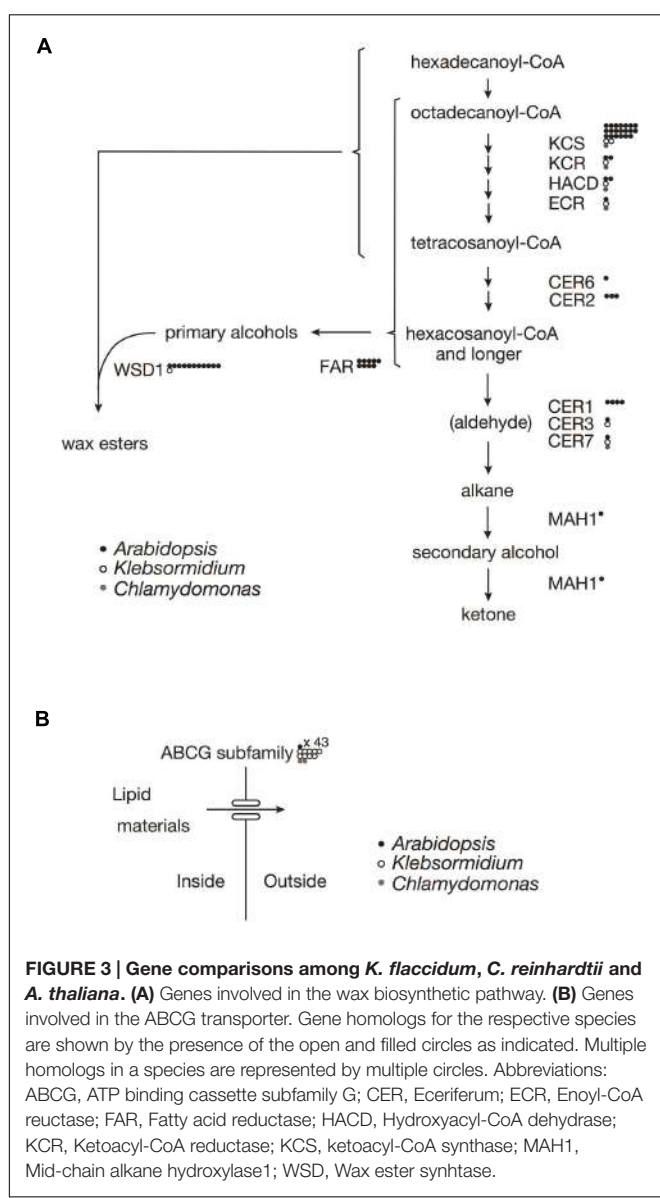


FIGURE 3 | Gene comparisons among *K. flaccidum*, *C. reinhardtii* and *A. thaliana*. (A) Genes involved in the wax biosynthetic pathway. (B) Genes involved in the ABCG transporter. Gene homologs for the respective species are shown by the presence of the open and filled circles as indicated. Multiple homologs in a species are represented by multiple circles. Abbreviations: ABCG, ATP binding cassette subfamily G; CER, Eceriferum; ECR, Enoyl-CoA reductase; FAR, Fatty acid reductase; HACD, Hydroxyacyl-CoA dehydratase; KCR, Ketoacyl-CoA reductase; KCS, ketoacyl-CoA synthase; MAH1, Mid-chain alkane hydroxylase1; WSD, Wax ester synthase.

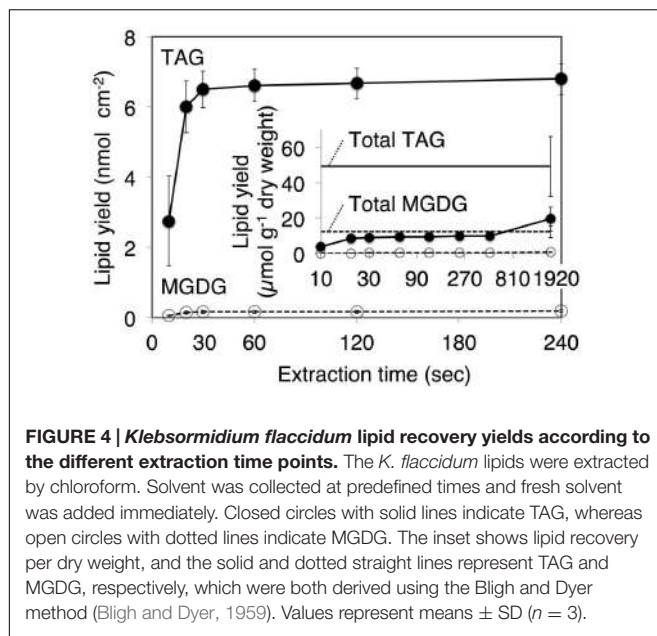


FIGURE 4 | *Klebsormidium flaccidum* lipid recovery yields according to the different extraction time points. The *K. flaccidum* lipids were extracted by chloroform. Solvent was collected at predefined times and fresh solvent was added immediately. Closed circles with solid lines indicate TAG, whereas open circles with dotted lines indicate MGDG. The inset shows lipid recovery per dry weight, and the solid and dotted straight lines represent TAG and MGDG, respectively, which were both derived using the Bligh and Dyer method (Bligh and Dyer, 1959). Values represent means \pm SD ($n = 3$).

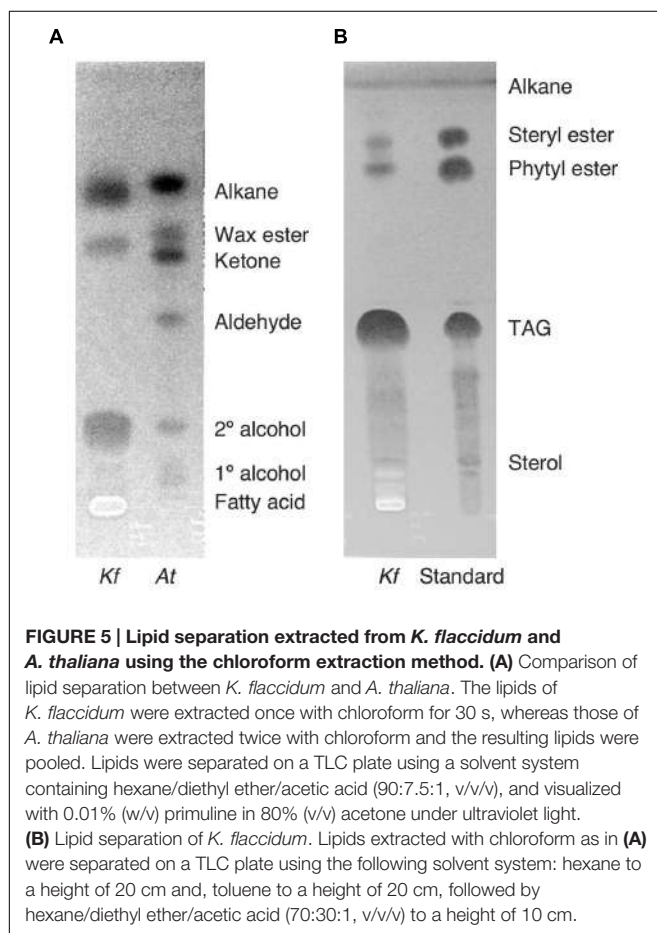


FIGURE 5 | Lipid separation extracted from *K. flaccidum* and *A. thaliana* using the chloroform extraction method. (A) Comparison of lipid separation between *K. flaccidum* and *A. thaliana*. The lipids of *K. flaccidum* were extracted once with chloroform for 30 s, whereas those of *A. thaliana* were extracted twice with chloroform and the resulting lipids were pooled. Lipids were separated on a TLC plate using a solvent system containing hexane/diethyl ether/acetic acid (90:7.5:1, v/v/v), and visualized with 0.01% (w/v) primuline in 80% (v/v) acetone under ultraviolet light. (B) Lipid separation of *K. flaccidum*. Lipids extracted with chloroform as in (A) were separated on a TLC plate using the following solvent system: hexane to a height of 20 cm and, toluene to a height of 20 cm, followed by hexane/diethyl ether/acetic acid (70:30:1, v/v/v) to a height of 10 cm.

aldehydes, and primary and secondary alcohols were not detected (Figures 5A,B). To determine their compositions, lipids were extracted from spots and analyzed by GC-MS after hydrolysis

with sodium methoxide and/or derivatization to trimethylsilyl ethers if necessary. Both *K. flaccidum* and *C. reinhardtii* included only docosane in their alkane fractions in which odd-numbered alkanes were absent according to the GC-FID chromatograms (Figure 6A) and GC-MS spectra (Figure 6B). Steryl esters, which included phytosterols, campesterol, β -sitosterol, and stigmasterol as the sterol moiety, were found only in *K. flaccidum* (Supplementary Figures S1A–D and S2A). Although *K. flaccidum* had an alkyl ester, its alcohol moiety consisted of phytol instead of fatty alcohol. The composition of the phytol ester was very simple, as only a single ester, phytol palmitate, was found in the GC-FID chromatogram (Supplementary Figure S1E). GC-MS spectra corroborated that the ester contained a phytol moiety (Supplementary Figure S1F). The abundant fatty acids in the TAG were linoleic acid (18:2) and oleic acid (18:1) in

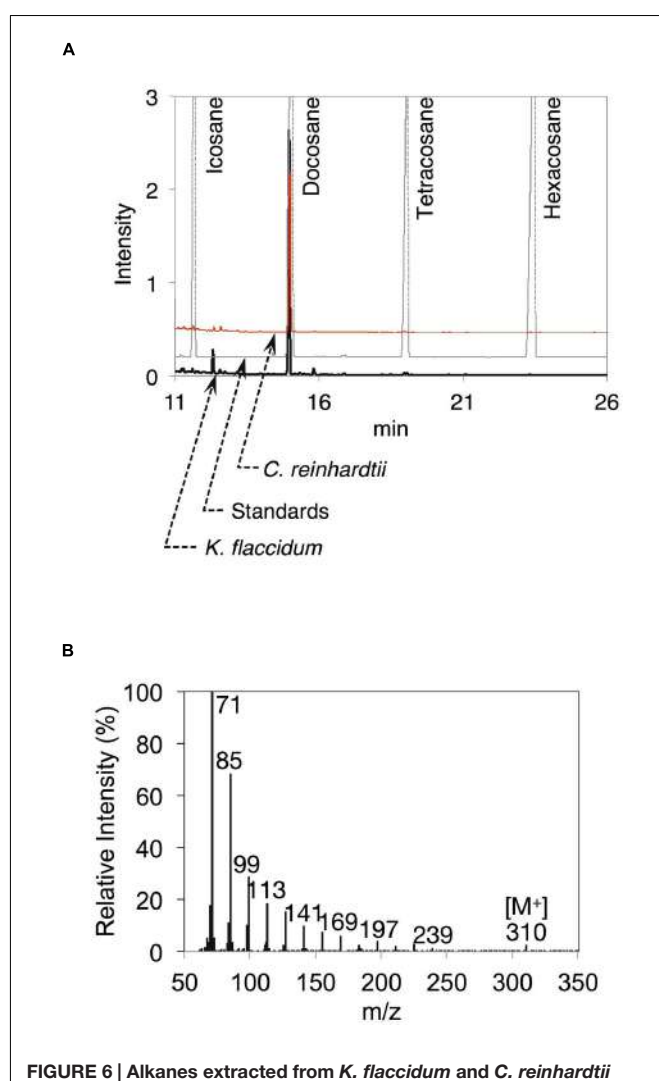


FIGURE 6 | Alkanes extracted from *K. flaccidum* and *C. reinhardtii* using the chloroform extraction method. (A) GC-FID chromatogram of the alkane fraction of *K. flaccidum* extracted with chloroform. Lipids were compared with commercially available standard alkanes. Black line: *K. flaccidum*. Red line: *C. reinhardtii*. Gray line: standards. (B) EI-MS spectrum of docosane obtained from *K. flaccidum*.

K. flaccidum and *C. reinhardtii*, respectively (Supplementary Figure S2C). The fatty acid composition of TAG corresponded with that of the inner TAG in *K. flaccidum* (Supplementary Figure S2C), whereas the composition was similar to that of the inner TAG in *C. reinhardtii* grown under nitrogen starvation conditions (Iwai et al., 2014). The final members of the algal surface lipids were the sterols, which reflected the composition of steryl esters in *K. flaccidum* (Supplementary Figures S1G and S2B).

Qualitative Analysis of Surface Lipids Obtained by Exposure to Silica Gel Plates

Because we cannot exclude the possibility that exposure to chloroform, even for a short period of time, could result in the extraction of intracellular lipids from *K. flaccidum* and *C. reinhardtii*, we tried to establish an alternative extraction method for these microorganisms by briefly placing them on a silica gel plate. We also applied this method, with slight modification, including contact with gentle pressure, to the acquisition of wax from *A. thaliana* (Supplementary Figure S3). Wax separation on a TLC plate indicated that the silica gel extraction method could be applied to *A. thaliana* since seven neutral lipids were extracted to the same extent as chloroform extraction (Supplementary Figure S3B). To determine the appropriate contact time, *K. flaccidum* (cultured for 42 days) grown on a nitrocellulose membrane was laid culture side down on a TLC plate for predetermined times from 30 s to 20 min. MGDG was not detected even after 20 min. Supplementary Figure S4 shows that 5 min was necessary and sufficient for the lipid extraction and, therefore, 5 min was used as the contact time for lipid extraction by silica gel plates. We also determined the appropriate culture time for *K. flaccidum* for the lipid extraction. Pale patches, indicative of lipid fluorescence, were observed in the primuline image of *K. flaccidum* cultured for 28 days (Figure 7A), but, by comparison, a darker and broader fluorescence was found from algae cultured for 42 days (Figure 7A). Therefore, algae cultured for 42 days were used for the lipid analyses. The same extraction method was applied to *C. reinhardtii* cultured for 14 days. Although the fluorescence intensity was weaker than that of *K. flaccidum* cultured for 42 days, lipids were also obtained from *C. reinhardtii* using this method (Figure 7A). In both algae, the lipids obtained by the silica gel plate method consisted of similar classes as those from the chloroform extracts. More specifically, lipids from the silica gel plate extractions included alkanes and TAGs; however, steryl esters, phytol esters, and sterols were not found (Figure 7B). All of the constituents of the lipids acquired by silica gel extraction were included in those acquired by chloroform, and no additional lipid classes were detected.

Comparison of the Lipid Contents Isolated with the Two Extraction Methods

Figure 8A shows the lipid composition of each lipid class of algae and plant extracted using the chloroform and silica gel methods.

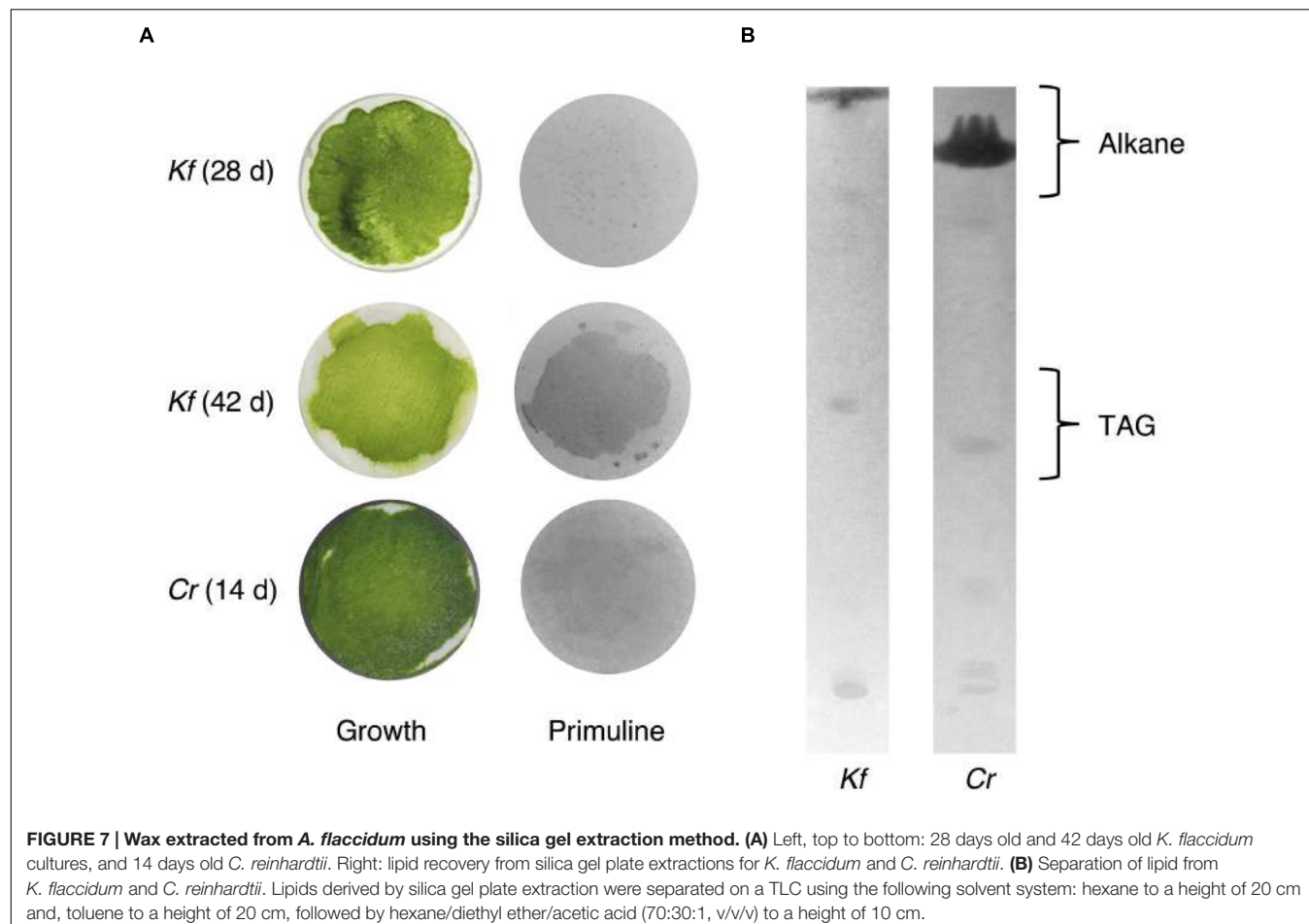
The docosane content for both *K. flaccidum* and *C. reinhardtii* was higher when using the silica gel plate extraction method compared to the chloroform extraction.

The fatty acid content of the TAG fraction from *K. flaccidum* seemed to differ depending on the extraction method. Figure 8B shows that hexadecanoic acid (16:0) was the major component extracted by the silica gel plate method, whereas octadecadienoic acid (18:2) was the most abundant component in the chloroform extract. Furthermore, the molar ratios of tetradecanoic acid (14:0) and octadecanoic acid (18:0) in the silica gel plate extraction were higher than those in the chloroform extraction. The same trend was observed in *C. reinhardtii*. In the silica gel plate extraction of *C. reinhardtii*, the molar ratios of tetradecanoic acid and hexadecanoic acid were higher than those in the chloroform extraction, and only octadecenoic acid (18:1) was detected in C18 fatty acids.

The amounts of surface lipids in the three organisms obtained by different extraction methods are shown in Figure 8C. The lipid content extracted from *K. flaccidum* with chloroform was $12.2 \text{ nmol cm}^{-2}$, which was ~ 120 times higher than the amount obtained by silica gel plate extraction. In contrast, the amount of lipids obtained from *C. reinhardtii* by chloroform extraction was slightly less, at $0.09 \text{ nmol cm}^{-2}$, than that obtained by silica gel plate extraction, at $0.13 \text{ nmol cm}^{-2}$. The wax load derived from *A. thaliana* was 5.1 nmol cm^{-2} , which was the highest value among all of the surface lipids, except for the wax load of *K. flaccidum* obtained by chloroform extraction.

Analysis of Aliphatic Cell Wall Components in Algae

Based on the method for analyzing cutin in *A. thaliana*, aliphatic components included in the delipidated algal residues were analyzed after alkaline hydrolysis followed by the appropriate derivatization. Figure 9A shows the total monomer contents of *K. flaccidum*, *C. reinhardtii*, and *A. thaliana*. Surprisingly, *K. flaccidum* had a considerable amount of fatty acid, ~ 30 -fold higher than that of *A. thaliana*. The amount of aliphatic monomers in *C. reinhardtii* was quite low compared with those of *K. flaccidum* and *A. thaliana*. Figure 9B shows the composition of the aliphatic components in the three organisms. Contrary to *A. thaliana*, which contains ω -hydroxy acid, 10,16-dihydroxy palmitic acid, and α,ω -dicarboxylic acid, key components of the cuticular network in higher plants (Yeats and Rose, 2013), *K. flaccidum* and *C. reinhardtii* contain only simple linear carbon chain fatty acids as aliphatic constituents that attach to cell wall components. No other fatty acid derivatives, like those in *A. thaliana*, were found in *K. flaccidum* or *C. reinhardtii*. In *K. flaccidum*, octadecadienoic acid (18:2) was the most abundant monomer, followed by hexadecanoic acid (16:0) and octadecenoic acid (18:1), and the contents of other fatty acids were very low. In *C. reinhardtii*, hexadecanoic acid was the most abundant component, followed, in decreasing order, by octadecadienoic acid (18:2), octadecenoic acid (18:1), hexadecenoic acid (16:1), and octadecanoic acid (18:0).



ATR-FTIR Analyses of Delipidated Cell Wall Residues

Because we found a large amount of fatty acid monomers that were covalently attached to the delipidated cell wall fraction in *K. flaccidum*, we analyzed the ATR-FTIR spectra of these fractions to determine how the fatty acids were attached to the cell wall. As shown in Figure 10C for *A. thaliana*, a peak at 1735 cm^{-1} was observed after the hot water treatment and then lost after the 0.1 M NaOH treatment. This peak probably represented C = O stretching and, therefore, the ester bond originating from the cuticle layer may have been largely removed by the NaOH treatment in *A. thaliana*. However, the corresponding peaks were originally much weaker in *K. flaccidum* and *C. reinhardtii*, and no change was observed after the same treatments (Figures 10A,B). Instead, two amide peaks at 1645 and $1529\text{--}1545\text{ cm}^{-1}$ were obvious, indicating that the represented proteins are major components of the cell wall fractions.

DISCUSSION

Only a few studies on the extracellular lipids of microorganisms have been reported. Conidiospores of *Alternaria tenuis*, *Botrytis fabae*, and *Neurospora crassa*, and sporangiospores of *Rhizopus*

stolonifer, were shown to have extracellular lipids (Fisher et al., 1978). In that study, the immersion of fungal conidiospores and sporangiospores in an organic solvent was used to extract lipids from the spore surface, but it was not clear whether lipids were derived only from the surface. To further understand the extracellular lipids of microorganisms, we tried to develop a new methodology for the extraction of outer lipids from algae using a silica gel plate instead of an organic solvent. Our approach was based on a previous study that used silica gel particles in the extraction of lipids from insects (Choe et al., 2012). For algae, it is difficult to separate silica gel particles from algal cells because of the fineness of the particles. Hence, we used a silica gel plate for lipid extraction from *K. flaccidum* and *C. reinhardtii*. Lipid extraction using a silica gel plate appeared to be useful in analyzing surface lipids of microalgae in comparison to the chloroform extraction method. However, all of the extracellular lipids might not have been recovered by this method. The compositions of the lipid classes were different between the extraction methods. We speculate that the differences between these methods reflect how lipids exist on the surface of the cells. Alkanes, sterols, steryl esters, phytol esters, and TAGs were isolated by chloroform extraction, whereas only alkanes and TAGs were detected following silica gel plate extraction from *K. flaccidum*. The amount of alkanes found was similar to that of

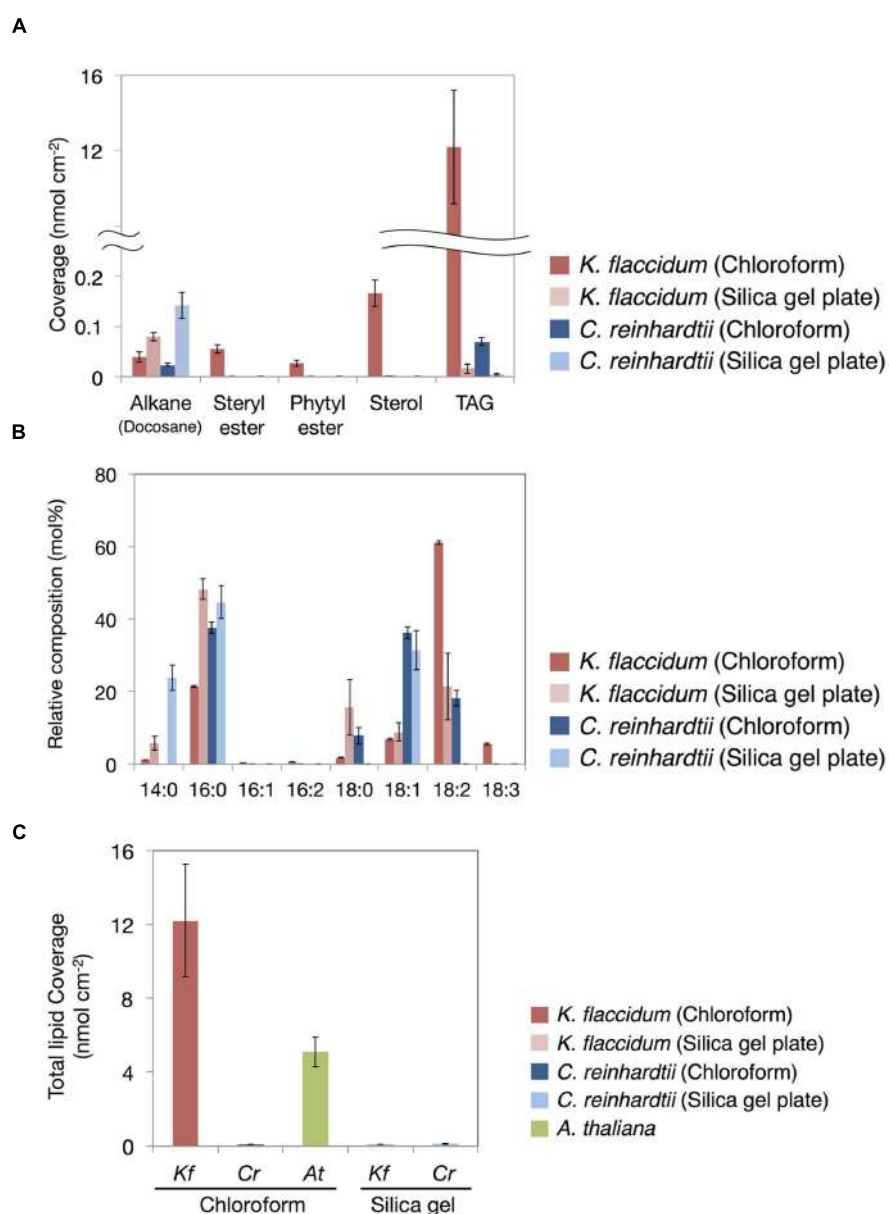


FIGURE 8 | Waxes from *K. flaccidum*, *C. reinhardtii*, and *A. thaliana*. **(A)** Comparison of the composition of waxes extracted from *K. flaccidum* and *C. reinhardtii* using different extraction methods. Waxes were separated by TLC, and appropriately derivatized and characterized by GC-FID. **(B)** Comparison of the composition of TAG fatty acids extracted from *K. flaccidum* and *C. reinhardtii* using different extraction methods. **(C)** Comparison of the total content of waxes from *K. flaccidum*, *C. reinhardtii*, and *A. thaliana* using different extraction methods. Values represent means \pm SD ($n = 4$).

steryl esters and phytol esters and was lower than that of sterols by chloroform extraction. The alkane yield was higher in the silica gel plate extraction than in the chloroform extraction in both *K. flaccidum* and *C. reinhardtii*. Silica gel plate extraction probably favors alkanes over other lipids, resulting in the higher alkane yield compared with other lipid yields.

Comprehensive genomic homology searches suggested that *K. flaccidum* and *C. reinhardtii* do not produce VLCFAs of more than 28 carbons (Figure 3A). Likewise, very-long-chain fatty alcohols might not be formed in these organisms because of the

absence of fatty acid reductase genes. Thus, we speculated that wax esters with long-chain fatty acids and fatty alcohols are not present in *K. flaccidum* in spite of the presence of a WSD1-like counterpart. This was supported by our subsequent surface lipid analysis, which indicated that these plant-like wax components were not found and that the surface lipid components were much more primitive, being mainly composed of alkanes and TAGs. These components, particularly a large proportion of TAGs, are probably embedded in the primitive cuticle layer, which is composed of cell wall-attached single fatty acyl chains.

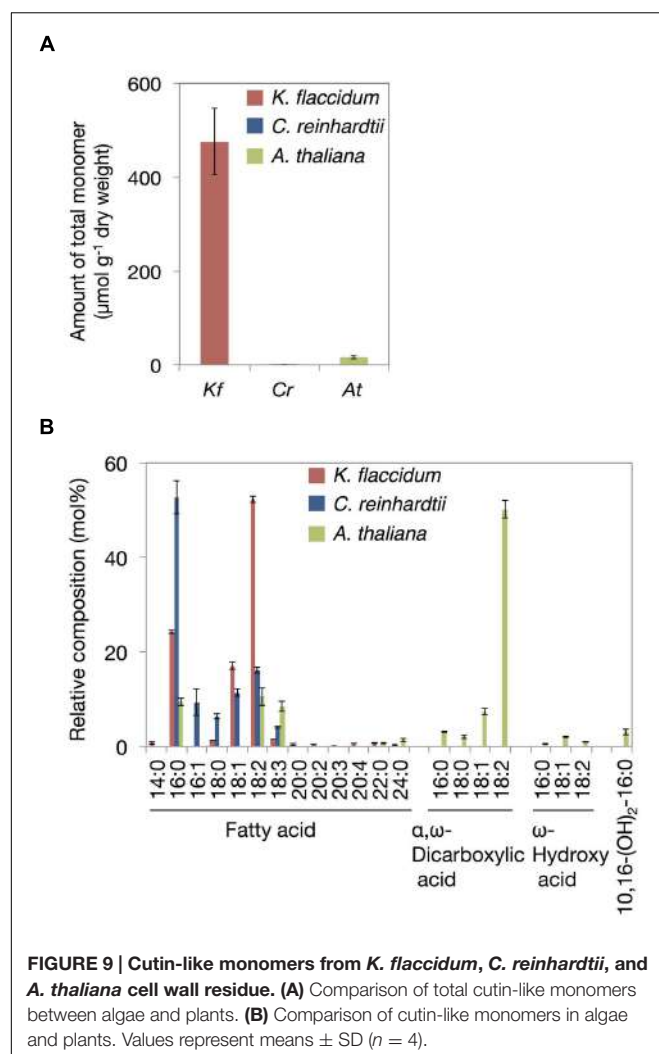


FIGURE 9 | Cutin-like monomers from *K. flaccidum*, *C. reinhardtii*, and *A. thaliana* cell wall residue. **(A)** Comparison of total cutin-like monomers between algae and plants. **(B)** Comparison of cutin-like monomers in algae and plants. Values represent means \pm SD ($n = 4$).

Arabidopsis thaliana surface lipids contain alkanes composed of odd-numbered chains, such as nonacosane and hentriacontane (Supplementary Figure S5), whereas *K. flaccidum* and *C. reinhardtii* surface lipids contain an even-numbered chain alkane, docosane (Figures 6A,B). The presence of even-numbered chain alkanes is not unusual, as they are found in several organisms, including the yeast *Saccharomyces oviformis*, the fungus *Trichoderma viride* (Ladygina et al., 2006), and the bacterium *Vibrio furnissii* M1 (Park, 2005). In *A. thaliana*, odd-numbered chain alkanes are synthesized through the decarbonylation pathway from VLCFAs (Kunst and Samuels, 2009). In contrast, even-numbered chain alkanes are proposed to be synthesized by the reduction of primary alcohols via aldehydes in *V. furnissii* (Park, 2005). Although *K. flaccidum* appears to contain counterparts to *A. thaliana* CER3 and CER7, which are involved in alkane biosynthesis, CER1, another important factor in this pathway, has not been found. CER3 and CER7 work indirectly and CER1 is necessary for alkane synthesis (Bourdenx et al., 2011; Bernard et al., 2012). It is not clear whether CER3 and CER7 are involved in the formation of docosane. The assumed

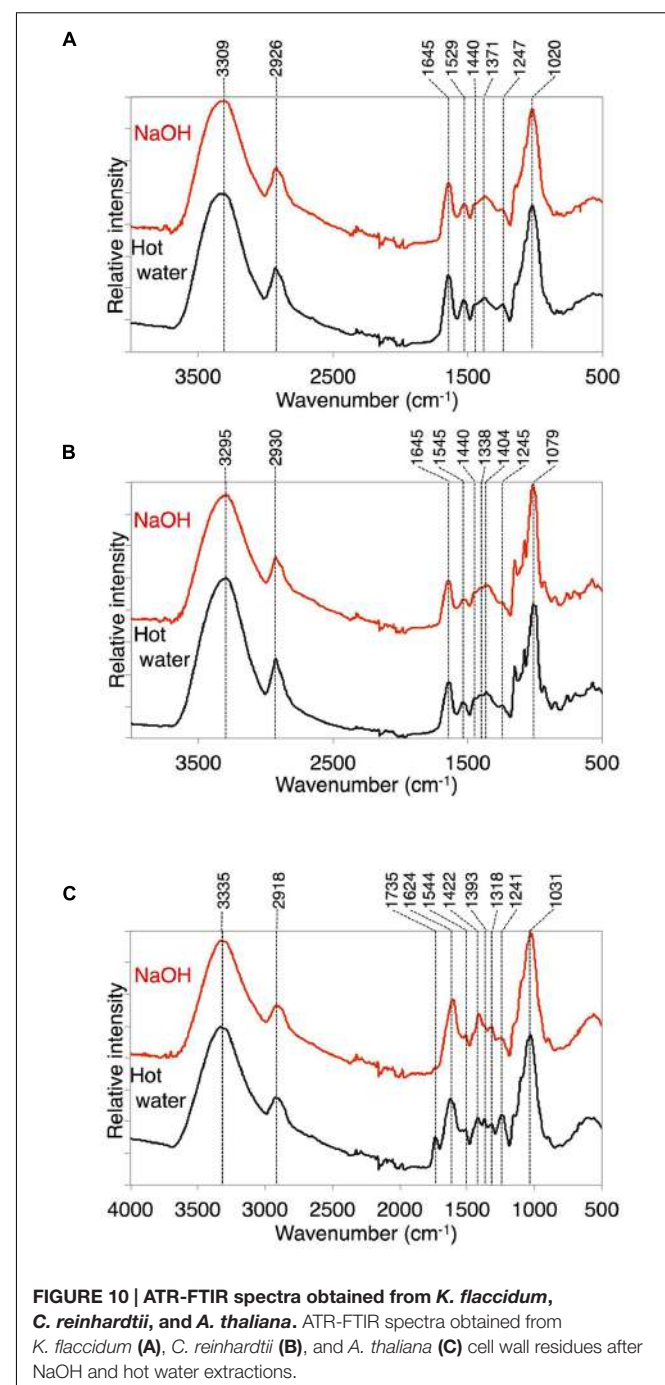
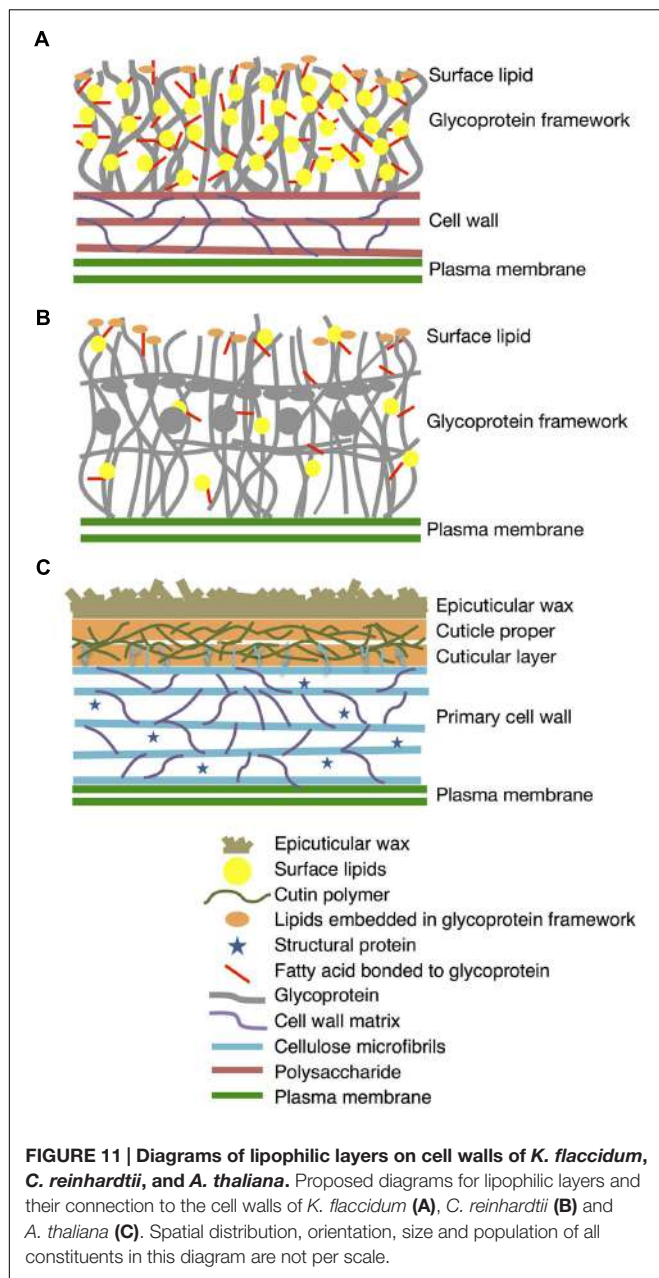


FIGURE 10 | ATR-FTIR spectra obtained from *K. flaccidum*, *C. reinhardtii*, and *A. thaliana*. ATR-FTIR spectra obtained from *K. flaccidum* **(A)**, *C. reinhardtii* **(B)**, and *A. thaliana* **(C)** cell wall residues after NaOH and hot water extractions.

proteins involved in phytol esters and steryl esters syntheses in *K. flaccidum* were shown in Supplementary Figures S6 and S7, respectively.

Comparison of the TAG Composition between Extraction Methods

It is interesting that the fatty acid composition of TAGs recovered by silica gel plate extraction was distinct from that recovered by chloroform extraction (Figure 8B). The former was



composed of more saturated fatty acids than the latter from both *K. flaccidum* and *C. reinhardtii*. This result could be expected, as unsaturated fatty acids are auto-oxidized more readily than saturated fatty acids under aerobic conditions (Porter et al., 1995). Indeed, many terrestrial plants have waxes composed of saturated fatty acid derivatives. Furthermore, the differences in the fatty acid constituents from intracellular TAGs are likely to demonstrate the existence of extracellular TAG in addition to the intracellular TAG fraction. Supplementary Figure S8 shows a proposed pathway for TAG biosynthesis in *K. flaccidum* and the candidate genes involved. Even though the *K. flaccidum* genome has a low number of gene paralogs in general (Hori et al., 2014), when compared with *A. thaliana*, *K. flaccidum*

contains the minimum set of enzymes required to assemble TAG. Moreover, *K. flaccidum* might carry a counterpart to diacylglycerol acyltransferase 1 (DGAT1), which catalyzes the final step of TAG formation and is proposed to play a role in sequestering the fatty acids of galactolipids released during chloroplast senescence (Kaup et al., 2002). Hence, a similar mechanism for salvaging fatty acids from galactolipids may occur in *K. flaccidum* and *C. reinhardtii* during some stress responses.

Recently, it was reported that Bayberry fruit contained a unique surface wax composed of major amounts of DAG and TAG, and minor amounts of MAG, all of which included only saturated fatty acids (Simpson and Ohlrogge, 2016). In their report, TAG was thought to be synthesized from DAG as an acyl acceptor and MAG as a donor outside the cell via unknown pathway. Three cutin-associated acyltransferases, *sn*-2 GPATs (Li et al., 2007a,b; Yang et al., 2010), an HXXD-motif acyltransferase closely related to *Arabidopsis* DEFECTIVE IN CUTICULAR RIDGES (DCR) (Panikashvili et al., 2009) and GDSL-motif lipase/transacylases related to tomato CUTIN DEFICIENT 1 (CD1) (Yeats et al., 2012), seem to involve in the TAG synthesis in Bayberry. Although *K. flaccidum* does not appear to have the counterparts to *sn*-2 GPAT or DCR, the counterparts to close homolog of CD1 from *A. thaliana*, Cutin synthase-like protein(LTL1/AtCUS1) (Yeats et al., 2014) and GDSL-MOTIF LIPASE5 (GLIP5) (Oh et al., 2005), were found (Supplementary Table S1). Other counterparts to HXXD-motif acyltransferases analyzed biologically in *A. thaliana* were not identified in *K. flaccidum*. It is possible that the counterparts to LTL1/AtCUS1 or GLIP5 might involve in the surface TAG synthesis in *K. flaccidum* in a similar fashion to that in Bayberry fruit, however, the pathway is still unclear since our data are insufficient because of the lack of their biochemical analyses.

Aliphatic Monomers Derived from the Cell Wall Fraction

When *K. flaccidum* was transferred to a solid medium, film-like structures were observed on the surface (Figures 2C,D); these structures were absent when the alga was cultured in liquid medium (Figures 2A,B). The film-like structures may have resulted from the drier growth conditions. Barberousse et al. (2006) described structures in *K. flaccidum* that were made from polysaccharides absorbed in higher amounts on hydrophobic than on hydrophilic materials. This alga may enwrap itself in more aliphatic substances than only polysaccharides, and these films may contain secreted surface lipid components that prevent water loss. In fact, appreciable amounts of fatty acids were detected in the *K. flaccidum* cell wall residue (Figures 9A,B and Supplementary Figure S9). Although *C. reinhardtii* includes hydroxyproline-rich glycoproteins on the cell wall (Goodenough and Heuser, 1985), it also has small amounts of fatty acids in its cell wall residue.

In both *K. flaccidum* and *C. reinhardtii*, the FTIR spectra for hot water, chlorite, and CDTA treatments were similar to each other (Supplementary Figure S10), which reflects the absence

of a plant-like hemicellulose-like polymers in *K. flaccidum*, as indicated in a previous study (Sørensen et al., 2011). The differences in FTIR spectra (**Figure 10C**) between hot water and 0.1 N NaOH treatments in *A. thaliana* indicated that the peak at 1735 cm⁻¹ corresponded to ester bonds binding to the wall matrix. Given that *K. flaccidum* has few ester bonds, similar to *C. reinhardtii*, according to its FTIR spectrum (**Figures 10A,B**), a large proportion of fatty acids is likely to bind to cell wall components, such as the lysine residues of cell wall proteins, via amide bonds. Indeed, two amide peaks, at 1645 and 1529–1545 cm⁻¹, which probably correspond to amide I and amide II, respectively, were found in both *K. flaccidum* and *C. reinhardtii*. Because the cell walls of *C. reinhardtii* seem to lack cellulose, and are largely composed of extracellular glycoproteins (Roberts, 1974), these amide bonds in *K. flaccidum* may be due to cell wall glycoproteins. Very small peaks corresponding to ester bonds in algae demonstrated that there was little contamination by TAGs or other esters in these fractions. Thus, the aliphatic moieties in the *K. flaccidum* cell wall seem to be in the form of single fatty acyl chains, and, therefore, most TAGs, sterols, steryl esters, and phytol esters may be embedded in the cell wall through their hydrophobic interactions with the fatty acyl moieties of the cell wall. The level of TAG obtained by chloroform extraction was ~730-fold higher than that obtained by silica gel plate extraction in *K. flaccidum*. However, the level of TAG obtained by chloroform extraction was only 14-fold higher than that obtained by silica gel plate extraction in *C. reinhardtii*. Thus, the amount of TAG embedded in the cell wall of *C. reinhardtii* is probably much less than that of *K. flaccidum*.

Weak, pale fluorescence was observed from *K. flaccidum* cultured for 28 days, whereas a stronger fluorescence was observed at 42 days, which indicated that the amount of lipids excreted to the surface increased with aging (**Figure 7**). Three of the five lipids detected in the chloroform extraction from *K. flaccidum* were esters (**Figure 8A**), which also play a role in the detoxification of fatty acid and alcohol (Turkish et al., 2005; Bouvier-Navé et al., 2010; Lippold et al., 2012). Thus, extracellular lipids are likely to be secreted as waste products and might function as defensive

REFERENCES

- Aarts, M. G., Keijzer, C. J., Stiekema, W. J., and Pereira, A. (1995). Molecular characterization of the CER1 gene of *Arabidopsis* involved in epicuticular wax biosynthesis and pollen fertility. *Plant Cell* 7, 2115–2127. doi: 10.1105/tpc.7.12.2115
- Barberousse, H., Ruiz, G., Gloaguen, V., Lombardo, R. J., Djediat, C., Mascarell, G., et al. (2006). Capsular polysaccharides secreted by building façade colonisers: characterisation and adsorption to surfaces. *Biofouling* 22, 361–370. doi: 10.1080/08927010601035803
- Barnes, J. D., Percy, K. E., Paul, N. D., Jones, P., McLaughlin, C. K., Mullineaux, P. M., et al. (1998). The influence of UV-B radiation on the physicochemical nature of Tobacco (*Nicotiana tabacum* L.) leaf surfaces. *J. Exp Bot.* 47, 99–109. doi: 10.1093/jxb/47.1.99
- Becker, B., and Marin, B. (2009). Streptophyte algae and the origin of embryophytes. *Ann. Bot.* 103, 999–1004. doi: 10.1093/aob/mcp044
- Bernard, A., Domergue, F., Pascal, S., Jetter, R., Renne, C., Faure, J. D., et al. (2012). Reconstitution of plant alkane biosynthesis in yeast demonstrates that

substances on the surface and within the acylated cell walls of *K. flaccidum*.

In this work, we present for the first time that *K. flaccidum* has lipophilic layers distinct from those of *A. thaliana* that contain a rather primitive wax layer and an alternative lipid-protein complex rather than a cutin polymer (**Figure 11**). *K. flaccidum* most likely has a glycoprotein framework with acyl side chains on its cell wall, with some lipids embedded in this framework. *C. reinhardtii* might also possess glycoproteins with acyl side chains, but the quantities of side chains and lipids in the framework are relatively small. Although the system to protect against stress conditions is more primitive than that in land plants, these aliphatic layers likely enable the algae to survive under terrestrial conditions.

AUTHOR CONTRIBUTIONS

SK performed GC-FID, GC-MS, and computational analysis. KH prepared samples of *K. flaccidum* strain NIES-2285 *C. reinhardtii*, and *A. thaliana*. KH helped in computational analysis. YS-S helped in GC-MS analysis. AK performed SEM analysis. TK and NY-O performed ATR-FTIR analysis. TN helped in lipid preparation. KO helped in cultivation of *K. flaccidum*. SK and HO wrote the manuscript and all authors contributed to the manuscript revision. MS and HO planned the project.

ACKNOWLEDGMENTS

This work was supported in part by a Grant-in-Aid for Scientific Research on Priority Areas (No. 15H04393, No. 23119506, No. 25119708, and No. 24580091) and JST CREST from the Ministry of Education, Sports, Science, and Culture in Japan.

SUPPLEMENTARY MATERIAL

The Supplementary Material for this article can be found online at: <http://journal.frontiersin.org/article/10.3389/fpls.2016.00952>

- Arabidopsis* ECERIFERUM1 and ECERIFERUM3 are core components of a very-long-chain alkane synthesis complex. *Plant Cell* 24, 3106–3118. doi: 10.1105/tpc.112.099796
- Bird, D., Beisson, F., Brigham, A., Shin, J., Greer, S., Jetter, R., et al. (2007). Characterization of *Arabidopsis* ABCG11/WBC11, an ATP binding cassette (ABC) transporter that is required for cuticular lipid secretion. *Plant J.* 52, 485–498. doi: 10.1111/j.1365-313X.2007.03252.x
- Bligh, E. G., and Dyer, W. J. (1959). A rapid method of total lipid extraction and purification. *Can. J. Biochem. Physiol.* 37, 911–917. doi: 10.1139/o59-099
- Bonaventure, G., Beisson, F., Ohlroge, J., and Pollard, M. (2004). Analysis of the aliphatic monomer composition of polyesters associated with *Arabidopsis* epidermis: occurrence of octadeca-cis-6, cis-9-diene-1,18-dioate as the major component. *Plant J.* 40, 920–930. doi: 10.1111/j.1365-313X.2004.02258.x
- Bourdenx, B., Bernard, A., Domergue, F., Pascal, S., Léger, A., Roby, D., et al. (2011). Overexpression of *Arabidopsis* ECERIFERUM1 promotes wax very-long-chain alkane biosynthesis and influences plant response to biotic and abiotic stresses. *Plant Physiol.* 156, 29–45. doi: 10.1104/pp.111.172320

- Bouvier-Navé, P., Berna, A., Noiri, A., Compagnon, V., Carlsson, A. S., Banas, A., et al. (2010). Involvement of the phospholipid sterol acyltransferase1 in plant sterol homeostasis and leaf senescence. *Plant Physiol.* 152, 107–119. doi: 10.1104/pp.109.145672
- Carpita, N. C., Defernez, M., Findlay, K., Wells, B., Shoue, D. A., Catchpole, G., et al. (2001). Cell wall architecture of the elongating maize coleoptile. *Plant Physiol.* 127, 551–565. doi: 10.1104/pp.010146
- Choe, D. H., Ramírez, S. R., and Tsutsui, N. D. (2012). A silica gel based method for extracting insect surface hydrocarbons. *J. Chem. Ecol.* 38, 176–187. doi: 10.1007/s10886-012-0074-1
- Edgar, R. C. (2004). MUSCLE, multiple sequence alignment with high accuracy and high throughput. *Nucleic Acids Res.* 32, 1792–1797. doi: 10.1093/nar/gkh340
- Fisher, D. J., Brown, G. A., and Holloway, P. J. (1978). Influence of growth medium on surface and wall lipid of fungal spores. *Phytochemistry* 17, 85–89. doi: 10.1016/S0031-9422(00)89685-5
- Franke, R., Briesen, I., Wojciechowski, T., Faust, A., Yaephremov, A., Nawrath, C., et al. (2005). Apoplastic polyesters in *Arabidopsis* surface tissues – A typical suberin and a particular cutin. *Phytochemistry* 66, 2643–2658. doi: 10.1016/j.phytochem.2005.09.027
- Goodenough, U., and Heuser, J. E. (1985). The *Chlamydomonas* cell wall and its constituent glycoproteins analyzed by the quick-freeze, deep-etch technique. *J. Cell Biol.* 101, 1550–1568. doi: 10.1083/jcb.101.4.1550
- Graça, J., Schreiber, L., Rodrigues, J., and Pereira, H. (2002). Glycerol and glyceryl esters of ω -hydroxyacids in cutins. *Phytochemistry* 61, 205–215. doi: 10.1016/S0031-9422(02)00212-1
- Greer, S., Wen, M., Bird, D., Wu, X., Samuels, L., Kunst, L., et al. (2007). The cytochrome p450 enzyme CYP96A15 is the midchain alkane hydroxylase responsible for formation of secondary alcohols and ketones in stem cuticular wax of *Arabidopsis*. *Plant Physiol.* 145, 653–667. doi: 10.1104/pp.107.107300
- Haas, K. (1982). Surface wax of *Andreaea* and *Pogonatum* species. *Phytochemistry* 21, 657–659. doi: 10.1016/0031-9422(82)83159-2
- Haslam, T. M., Fernández, A. M., Zhao, L., and Kunst, L. (2012). *Arabidopsis* ECERIFERUM2 is a component of the fatty acid elongation machinery required for fatty acid extension to exceptional lengths. *Plant Physiol.* 160, 1164–1174. doi: 10.1104/pp.112.201640
- Haslam, T. M., Haslam, R., Thoraval, D., Pascal, S., Delude, C., Domergue, F., et al. (2015). ECERIFERUM2-LIKE proteins have unique biochemical and physiological functions in very-long-chain fatty acid elongation. *Plant Physiol.* 167, 682–692. doi: 10.1104/pp.114.253195
- Herburger, K., and Holzinger, A. (2015). Localization and quantification of callose in the Streptophyte green algae *Zygnema* and *Klebsormidium*: correlation with desiccation tolerance. *Plant Cell Physiol.* 56, 2259–2270. doi: 10.1093/pcp/pcv139
- Hoover, T. S., Lam, P., Zheng, H., and Kunst, L. (2007). A core subunit of the RNA-processing/degrading exosome specifically influences cuticular wax biosynthesis in *Arabidopsis*. *Plant Cell* 19, 904–913. doi: 10.1105/tpc.106.049304
- Hori, K., Maruyama, F., Fujisawa, T., Togashi, T., Yamamoto, N., Seo, M., et al. (2014). *Klebsormidium flaccidum* genome reveals primary factors for plant terrestrial adaptation. *Nat. Commun.* 5:3978. doi: 10.1038/ncomms4978
- Ichimura, T. (1971). “Sexual cell division and conjugation-papilla formation in sexual reproduction of *Cladophora strigosum*,” in *Proceedings of the Seventh International Seaweed Symposium*, (Tokyo: University of Tokyo Press), 208–214.
- Iwai, M., Ikeda, K., Shimojima, M., and Ohta, O. (2014). Enhancement of extraplastidic oil synthesis in *Chlamydomonas reinhardtii* using a type-2 diacylglycerol acyltransferase with a phosphorus starvation-inducible promoter. *Plant Biotechnol. J.* 12, 808–819. doi: 10.1111/pbi.12210
- Kaplan, F., Lewis, L. A., Wastian, J., and Holzinger, A. (2012). Plasmolysis effects and osmotic potential of two phylogenetically distinct alpine strains of *Klebsormidium* (Streptophyta). *Protoplasma* 249, 789–804. doi: 10.1007/s00709-011-0324-z
- Karsten, U., Herburger, K., and Holzinger, A. (2015). Living in biological soil crust communities of African deserts-Physiological traits of green algal *Klebsormidium* species (Streptophyta) to cope with desiccation, light and temperature gradients. *J. Plant Physiol.* 194, 2–12. doi: 10.1016/j.jplph.2015.09.002
- Karsten, U., Lutz, C., and Holzinger, A. (2010). Ecophysiological performance of the aeroterrestrial green alga *Klebsormidium crenulatum* (Charophyceae, Streptophyta) isolated from an Alpine soil crust with an emphasis on desiccation stress. *J. Phycol.* 46, 1187–1197. doi: 10.1111/j.1529-887.2010.00921
- Kaštovská, K., Elster, J., Stibal, M., and Santrůčková, H. (2005). Microbial assemblages in soil microbial succession after glacial retreat in Svalbard (High Arctic). *Microbial. Ecol.* 50, 396–407. doi: 10.1007/s00248-005-0246-4
- Kaup, M. T., Froese, C. D., and Thompson, J. E. (2002). A role for diacylglycerol acyltransferase during leaf senescence. *Plant Physiol.* 129, 1616–1626. doi: 10.1104/pp.003087
- Kunst, L., and Samuels, A. L. (2003). Biosynthesis and secretion of plant cuticular wax. *Prog. Lipid Res.* 42, 51–80. doi: 10.1016/S0163-7827(02)00045-0
- Kunst, L., and Samuels, L. (2009). Plant cuticles shine: advances in wax biosynthesis and export. *Curr. Opin. Plant Biol.* 12, 721–727. doi: 10.1016/j.pbi.2009.09.009
- Ladygina, N., Dedyukhina, E. G., and Vainshtein, M. B. (2006). A review on microbial synthesis of hydrocarbon. *Process Biochem.* 41, 1001–1014. doi: 10.1016/j.procbio.2005.12.007
- Le, S. Q., and Gascuel, O. (2008). An improved general amino acid replacement matrix. *Mol. Biol. Evol.* 25, 1307–1320. doi: 10.1093/molbev/msn067
- Lee, S. B., and Suh, M. C. (2015). Advances in the understanding of cuticular waxes in *Arabidopsis thaliana* and crop species. *Plant Cell Rep.* 34, 557–572. doi: 10.1007/s00299-015-1772-2
- Leliaert, F., Smith, D. R., Moreau, H., Herron, M. D., Verbruggen, H., Delwiche, C. F., et al. (2012). Phylogeny and molecular evolution of the green algae. *Crit. Rev. Plant Sci.* 31, 1–46. doi: 10.1080/07352689.2011.615705
- Lewis, L. A., and McCourt, R. M. (2004). Green algae and the origin of land plants. *Am. J. Bot.* 91, 1535–1556. doi: 10.3732/ajb.91.10.1535
- Li, F., Wu, X., Lam, P., Bird, D., Zheng, H., Samuels, L., et al. (2008). Identification of the wax ester synthase/acyl-coenzyme A: diacylglycerol acyltransferase WSD1 required for stem wax ester biosynthesis in *Arabidopsis*. *Plant Physiol.* 148, 97–107. doi: 10.1104/pp.108.123471
- Li, H., Pinot, F., Sauveplane, V., Werck-Reichhart, D., Diehl, P., Schareiber, L., et al. (2010). Cytochrome P450 family member CYP704B2 catalyzes the ω -hydroxylation of fatty acids and is required for anther cutin biosynthesis and pollen exine formation in rice. *Plant Cell* 22, 173–190. doi: 10.1105/tpc.109.070326
- Li, Y., Beisson, F., Koo, A. J. K., Molina, I., Pollard, M., and Ohlrogge, J. (2007a). Identification of acyltransferases required for cutin biosynthesis and production of cutin with suberin-like monomers. *Proc. Natl. Acad. Sci. U.S.A.* 104, 18339–18344. doi: 10.1073/pnas.0706984104
- Li, Y., Beisson, F., Ohlrogge, J., and Pollard, M. (2007b). Monoacylglycerols are components of root waxes and can be produced in the aerial cuticle by ectopic expression of a suberin-associated acyltransferase. *Plant Physiol.* 144, 1267–1277. doi: 10.1104/pp.107.099432
- Li-Beisson, Y., Shorrosh, B., Beisson, F., Andersson, M. X., Arondel, V., Bates, P. D., et al. (2013). Acyl-lipid metabolism. *Arabidopsis Book* 11:e0161. doi: 10.1199/tab.0161
- Lippold, F., vom Dorp, K., Abraham, M., Hözl, G., Wewer, V., Yilmaz, J. L., et al. (2012). Fatty acid phytol ester synthesis in Chloroplasts of *Arabidopsis*. *Plant Cell* 24, 2001–2014. doi: 10.1105/tpc.112.095588
- Lolle, S. J., Hsu, W., and Pruitt, R. E. (1998). Genetic analysis of organ fusion in *Arabidopsis thaliana*. *Genetics* 149, 607–619.
- Millar, A. A., Clemens, S., Zachgo, S., Giblin, E. M., Taylor, D. C., and Kunst, L. (1999). CUT1, an *Arabidopsis* gene required for cuticular wax biosynthesis and pollen fertility, encodes a very-long-chain fatty acid condensing enzyme. *Plant Cell* 11, 825–838. doi: 10.1105/tpc.11.5.825
- Molina, I., Bonaventure, G., Ohlrogge, J., and Pollard, M. (2006). The lipid polyester composition of *Arabidopsis thaliana* and *Brassica napus* seeds. *Phytochemistry* 67, 2597–2610. doi: 10.1016/j.phytochem.2006.09.011
- Moller, I., Sørensen, I., Bernal, A. J., Blaukopf, C., Lee, K., Øbro, J., et al. (2007). High-throughput mapping of cell-wall polymers within and between plants using novel microarrays. *Plant J.* 50, 1118–1128. doi: 10.1111/j.1365-313X.2007.03114.x
- Müller, C., and Riederer, M. (2005). Plant surface properties in chemical ecology. *J. Chem. Ecol.* 31, 2621–2651. doi: 10.1007/s10886-005-7617-7

- Nagao, M., Matsui, K., and Uemura, M. (2008). *Klebsormidium flaccidum*, a charophycean green alga, exhibits cold acclimation that is closely associated with compatible solute accumulation and ultrastructural changes. *Plant Cell Environ.* 31, 872–885. doi: 10.1111/j.1365-3040.2008.01804.x
- Oh, I. S., Park, A. R., Bae, M. S., Kwon, S. J., Kim, Y. S., Lee, J. E., et al. (2005). Secretome analysis reveals an *Arabidopsis* lipase involved in defense against *Alternaria brassicicola*. *Plant Cell* 17, 2832–2847. doi: 10.1105/tpc.105.034819
- Panikashvili, D., and Aharoni, A. (2008). ABC-type transporters and cuticle assembly. *Plant Signal. Behav.* 3, 806–809. doi: 10.1104/pp.107.105676
- Panikashvili, D., Savaldi-Goldstein, S., Mandel, T., Yifhar, T., Franke, R. B., Hofer, R., et al. (2007). The *Arabidopsis* DESPERADO/AtWBC11 transporter is required for cutin and wax secretion. *Plant Physiol.* 145, 1345–1360. doi: 10.1104/pp.107.105676
- Panikashvili, D., Shi, J. X., Schreiber, L., and Aharoni, A. (2009). The *Arabidopsis* DCR encoding a soluble BAHD acyltransferase is required for cutin polyester formation and seed hydration properties. *Plant Physiol.* 151, 1773–1789. doi: 10.1104/pp.109.143388
- Park, M.-O. (2005). New pathway for long-chain *n*-alkane synthesis via 1-alcohol in *Vibrio furnissii* M1. *J. Bacteriol.* 187, 1426–1429. doi: 10.1128/JB.187.4.1426-1429.2005
- Pascal, S., Bernard, A., Sorel, M., Pervent, M., Vile, D., Haslam, R. P., et al. (2013). The *Arabidopsis* cer26 mutant, like the cer2 mutant, is specifically affected in the very long chain fatty acid elongation process. *Plant J.* 73, 733–746. doi: 10.1111/tpj.12060
- Pattathil, S., Avci, U., Miller, J. S., and Hahn, M. G. (2012). “Immunological approaches to plant cell wall and biomass characterization: glycome profiling,” in *Biomass Conversion: Methods and Protocols*, ed. M. E. Himmel (New York, NY: Humana Press), 61–72.
- Paul, S., Gable, K., Beaudoin, F., Cahoon, E., Jaworski, J., Napier, J. A., et al. (2006). Members of the *Arabidopsis* FAE1-like 3-ketoacyl-CoA synthase gene family substitute for the EloP proteins of *Saccharomyces cerevisiae*. *J. Biol. Chem.* 281, 9018–9029. doi: 10.1074/jbc.M507723200
- Pollard, M., Beisson, F., Li, Y., and Ohlrogge, J. B. (2008). Building lipid barriers: biosynthesis of cutin and suberin. *Trends Plant Sci.* 13, 236–246. doi: 10.1016/j.tplants.2008.03.003
- Popper, Z. A., Michel, G., Hervé, C., Domozych, D. S., Willats, W. G. T., Tuohy, M. G., et al. (2011). Evolution and diversity of plant cell walls: from algae to flowering plants. *Annu. Rev. Plant Biol.* 62, 567–590. doi: 10.1146/annurev-arplant-042110-103809
- Porter, N. A., Caldwell, S. E., and Mills, K. A. (1995). Mechanisms of free radical oxidation of unsaturated lipids. *Lipids* 30, 277–290. doi: 10.1007/BF02536034
- Riederer, M., and Schreiber, L. (2001). Protecting against water loss, analysis of the barrier properties of plant cuticles. *J. Exp. Bot.* 52, 2023–2032. doi: 10.1093/jexbot/52.363.2023
- Rindi, F., Guiry, M. D., and López-Bautista, J. M. (2008). Distribution, morphology, and phylogeny of *Klebsormidium* (*Klebsormidiales*, Charophyceae) in urban environments in Europe. *J. Phycol.* 44, 1529–1540. doi: 10.1111/j.1529-887.2008.00593.x
- Roberts, K. (1974). Crystalline glycoprotein cell walls of algae: their structure, composition and assembly. *Philos. Trans. R. Lond. B Biol. Sci.* 268, 129–146. doi: 10.1088/rstb.1974.0021
- Samuels, L., Kunst, L., and Jetter, R. (2008). Sealing plant surfaces: cuticular wax formation by epidermal cells. *Annu. Rev. Plant Biol.* 59, 638–707. doi: 10.1146/annurev.arplant.59.103006.093219
- Schnurr, J., Shockley, J., and Browse, J. (2004). The acyl-CoA synthetase encoded by LACS2 is essential for normal cuticle development in *Arabidopsis*. *Plant Cell* 16, 629–642. doi: 10.1105/tpc.017608
- Sieber, P., Schorderet, M., Ryser, U., Buchala, A., Kolattukudy, P., Méraux, J. P., et al. (2000). Transgenic *Arabidopsis* plants expressing a fungal cutinase show alterations in the structure and properties of the cuticle and postgenital organ fusions. *Plant Cell* 12, 721–737. doi: 10.1105/tpc.12.5.721
- Simpson, J. P., and Ohlrogge, J. B. (2016). A novel pathway for triacylglycerol biosynthesis is responsible for the accumulation of massive quantities of glycerolipids in the surface wax of Bayberry (*Myrica pensylvanica*) fruit. *Plant Cell* 28, 248–264. doi: 10.1105/tpc.15.00900
- Skamnioti, P., and Gurr, S. J. (2007). *Magnaporthe grisea* Cutinase2 mediates appressorium differentiation and host penetration and is required for full virulence. *Plant Cell* 19, 2674–2689. doi: 10.1105/tpc.107.051219
- Sørensen, I., Pettolino, F. A., Bacic, A., Ralph, J., Lu, F., O'Neill, M. A., et al. (2011). The charophycean green algae provide insights into the early origins of plant cell walls. *Plant J.* 68, 201–211. doi: 10.1111/j.1365-313X.2011.04686.x
- Talavera, G., and Castresana, J. (2007). Improvement of phylogenies after removing divergent and ambiguously aligned blocks from protein sequence alignments. *Syst. Biol.* 56, 564–577. doi: 10.1080/10635150701472164
- Tamura, K., Stecher, G., Peterson, D., Filipski, A., and Kumar, S. (2013). MEGA6, molecular evolutionary genetics analysis version 6.0. *Mol. Biol. Evol.* 30, 2725–2729. doi: 10.1093/molbev/mst197
- Terzaghi, W. B. (1986). A system for manipulating the membrane fatty acid composition of soybean cell cultures by adding tween-fatty acid esters to their growth medium. *Plant Physiol.* 82, 771–779. doi: 10.1104/pp.82.3.771
- Timme, R. E., Bachvaroff, T. R., and Delwiche, C. F. (2012). Broad phylogenomic sampling and the sister lineage of land plants. *PLoS ONE* 7:e29696. doi: 10.1371/journal.pone.0029696
- Todd, J., Post-Beittermiller, D., and Jaworski, J. G. (1999). KCS1 encodes a fatty acid elongase 3-ketoacyl-CoA Synthase affecting wax biosynthesis in *Arabidopsis thaliana*. *Plant J.* 17, 119–130. doi: 10.1046/j.1365-313X.1999.00352.x
- Turkish, A. R., Henneberry, A. L., Cromley, D., Padamsee, M., Oelkers, P., Bazzi, H., et al. (2005). Identification of two novel human acyl-CoA wax alcohol acyltransferases. *J. Biol. Chem.* 280, 14755–14764. doi: 10.1074/jbc.M500025200
- Wisnieski, B. J., Williams, R. E., and Fox, C. F. (1973). Manipulation of fatty acid composition in animal cells grown in culture. *Proc. Natl. Acad. Sci. U.S.A.* 70, 3669–3673. doi: 10.1073/pnas.70.12.3669
- Yamashiro, H., Oku, H., Onaga, K., Iwasaki, H., and Takara, K. (2001). Coral tumors store reduced level of lipids. *J. Exp. Mar. Biol. Ecol.* 265, 171–179. doi: 10.1016/S0022-0981(01)00333-1
- Yang, W. L., Pollard, M., Li-Beisson, Y., Beisson, F., Feig, M., and Ohlrogge, J. (2010). A distinct type of glycerol-3-phosphate acyltransferase with sn-2 preference and phosphatase activity producing 2-monoacylglycerol. *Proc. Natl. Acad. Sci. U.S.A.* 107, 12040–12045. doi: 10.1073/pnas.0914149107
- Yeats, T. H., Huang, W., Chatterjee, S., Viart, H. M. F., Clausen, M. H., Stark, R. E., et al. (2014). Tomato Cutin Deficient 1 (CD1) and putative orthologs comprise an ancient family of cutin synthase-like (CUS) proteins that are conserved among land plants. *Plant J.* 77, 667–675. doi: 10.1111/tpj.12422
- Yeats, T. H., Martin, L. B., Viart, H. M., Isaacson, T., He, Y., Zhao, L., et al. (2012). The identification of cutin synthase: formation of the plant polyester cutin. *Nat. Chem. Biol.* 8, 609–611. doi: 10.1038/nchembio.960
- Yeats, T. H., and Rose, J. K. C. (2013). The formation and function of plant cuticles. *Plant Physiol.* 163, 5–20. doi: 10.1104/pp.113.222737

Conflict of Interest Statement: The authors declare that the research was conducted in the absence of any commercial or financial relationships that could be construed as a potential conflict of interest.

The reviewer SR and handling Editor declared their shared affiliation, and the handling Editor states that the process nevertheless met the standards of a fair and objective review.

Copyright © 2016 Kondo, Hori, Sasaki-Sekimoto, Kobayashi, Kato, Yun-Ohta, Nobusawa, Ohtaka, Shimojima and Ohta. This is an open-access article distributed under the terms of the Creative Commons Attribution License (CC BY). The use, distribution or reproduction in other forums is permitted, provided the original author(s) or licensor are credited and that the original publication in this journal is cited, in accordance with accepted academic practice. No use, distribution or reproduction is permitted which does not comply with these terms.



Abiotic Stress Tolerance of Charophyte Green Algae: New Challenges for Omics Techniques

Andreas Holzinger^{1*} and Martina Pichrtová²

¹ Unit of Functional Plant Biology, Institute of Botany, University of Innsbruck, Innsbruck, Austria, ² Department of Botany, Faculty of Science, Charles University in Prague, Prague, Czech Republic

OPEN ACCESS

Edited by:

Zoë A. Popper,
National University of Ireland, Ireland

Reviewed by:

John Moore,
Stellenbosch University, South Africa
Sven B. Gould,
Heinrich-Heine-Universität Düsseldorf,
Germany

***Correspondence:**

Andreas Holzinger
andreas.holzinger@uibk.ac.at

Specialty section:

This article was submitted to
Plant Evolution and Development,
a section of the journal
Frontiers in Plant Science

Received: 24 March 2016

Accepted: 02 May 2016

Published: 20 May 2016

Citation:

Holzinger A and Pichrtová M (2016)
Abiotic Stress Tolerance
of Charophyte Green Algae: New
Challenges for Omics Techniques.
Front. Plant Sci. 7:678.
doi: 10.3389/fpls.2016.00678

Charophyte green algae are a paraphyletic group of freshwater and terrestrial green algae, comprising the classes of Chlorokybophyceae, Coleochaetophyceae, Klebsormidiophyceae, Zygnematophyceae, Mesostigmatophyceae, and Charophyceae. Zygnematophyceae (Conjugating green algae) are considered to be closest algal relatives to land plants (Embryophyta). Therefore, they are ideal model organisms for studying stress tolerance mechanisms connected with transition to land, one of the most important events in plant evolution and the Earth's history. In Zygnematophyceae, but also in Coleochaetophyceae, Chlorokybophyceae, and Klebsormidiophyceae terrestrial members are found which are frequently exposed to naturally occurring abiotic stress scenarios like desiccation, freezing and high photosynthetically active (PAR) as well as ultraviolet (UV) irradiation. Here, we summarize current knowledge about various stress tolerance mechanisms including insight provided by pioneer transcriptomic and proteomic studies. While formation of dormant spores is a typical strategy of freshwater classes, true terrestrial groups are stress tolerant in vegetative state. Aggregation of cells, flexible cell walls, mucilage production and accumulation of osmotically active compounds are the most common desiccation tolerance strategies. In addition, high photophysiological plasticity and accumulation of UV-screening compounds are important protective mechanisms in conditions with high irradiation. Now a shift from classical chemical analysis to next-generation genome sequencing, gene reconstruction and annotation, genome-scale molecular analysis using omics technologies followed by computer-assisted analysis will give new insights in a systems biology approach. For example, changes in transcriptome and role of phytohormone signaling in *Klebsormidium* during desiccation were recently described. Application of these modern approaches will deeply enhance our understanding of stress reactions in an unbiased non-targeted view in an evolutionary context.

Keywords: transcriptomics, proteomics, metabolomics, UV irradiation, desiccation, phylogenomic analysis

CHAROPHYTE ALGAE IN TERRESTRIAL ENVIRONMENTS

Charophyte green algae are a diverse paraphyletic assemblage of strictly freshwater algae (Leliaert et al., 2012) comprising about 100 genera. We can distinguish 'advanced charophytes' (Zygnematophyceae, Coleochaetophyceae, Charophyceae) recently designated as ZCC clade (de Vries et al., 2016) and 'basal charophytes' (Klebsormidiophyceae, Chlorokybophyceae,

Mesostigmatophyceae), designated as KCM clade (de Vries et al., 2016). However, charophyte green algae are not only restricted to aquatic habitats. Terrestrial forms occur in the classes Chlorokybophyceae (Lewis and McCourt, 2004), the Klebsormidiophyceae (e.g., Karsten et al., 2010; Karsten and Holzinger, 2012), the Zygnematophyceae (e.g., Lewis and McCourt, 2004; Holzinger et al., 2009, 2010) and the Coleochaetophyceae (Graham et al., 2012, 2013) and viable airborne cells of various charophyte algae were also reported (Sharma et al., 2007).

Colonization of moderately moist habitats in the proximity of water by the charophyte algal ancestor of land plants and its gradual transition to drylands has been suggested by Becker and Marin (2009). Recently, several reports have demonstrated the close relationship of land plants and Zygnematophyceae that are currently viewed as sister lineages (Becker and Marin, 2009; Wodniok et al., 2011; Timme et al., 2012; Becker, 2013; Zhong et al., 2014, 2015; Delaux et al., 2015). At present, Zygnematophyceae dominate in various stressful habitats. For example, desmids are typically found in acidic bogs (Štástný, 2010), *Zygogonium ericetorum* is a common member of temperate biological soil crust (Hoppert et al., 2004) and *Mesotaenium berggrenii* and *Ancylonema nordenskiöldii* live on the surface of glaciers on bare ice (Remias et al., 2009, 2012a,b).

Transition to terrestrial habitats is connected with frequent exposure to naturally occurring abiotic stress scenarios like desiccation, freezing and high PAR and UV radiation. The effects of these stresses on ultrastructure, photosynthesis and ecology in green algae have recently been reviewed (Holzinger and Lütz, 2006; Holzinger and Karsten, 2013; Karsten and Holzinger, 2014). In the present review, we mainly focus on the current knowledge about abiotic stress tolerance mechanisms known in terrestrial members of the charophyte algae as model systems to study terrestrialization events. We include important classical studies based on traditional methods as well as new understanding derived from recent transcriptomic and genomic datasets. In general, stress tolerance strategies are summarized in a simplified schema (**Figure 1**).

SELF-PROTECTION

The morphologically most complex group of charophyte algae, the class Charophyceae, is restricted solely to aquatic environment (Leliaert et al., 2012). On the other hand, terrestrial charophytes are characterized by a very simple thallus, unicellular or filamentous which, however, usually aggregate into colonies, multi-layered mats or biofilms. This growth pattern belongs to common stress avoidance strategies and provides protection from multiple stresses at the same time. While the outer layers are fully exposed to the environment and susceptible to damage, at the same time they efficiently protect the cells underneath by their water-holding and screening capacity. In addition, aeroterrestrial algae are also components of biological soil crusts, microecosystems containing also bacteria, Cyanobacteria, fungi, lichens, mosses, and anorganic particles where the whole community can profit from protection

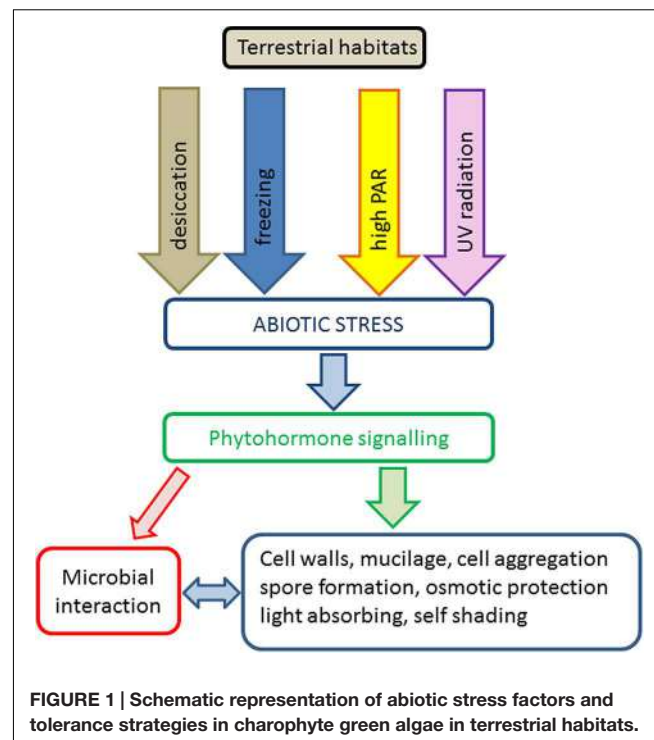


FIGURE 1 | Schematic representation of abiotic stress factors and tolerance strategies in charophyte green algae in terrestrial habitats.

provided by an individual member (Belnap and Lange, 2001).

Chlorokybus atmophyticus, the only known member of the class Chlorokybophyceae, occurs in subaerial habitats and is characterized by sarcinoid colonies with groups of cells embedded in soft mucilage (Škaloud, 2009).

Freshwater *Coleochaete* usually forms flat epiphytic disk or cushion-like thalli, composed by densely branched filaments. However, when grown in aero-terrestrial conditions, namely on agar or sand, it markedly changes its morphology and growth habitus. It forms multistratose clusters of thick walled cells with acetolysis resistant autofluorescent cell wall components (Graham et al., 2012).

Aeroterrestrial members of the class Klebsormidiophyceae form multi-layered biofilms on soil or other aeroterrestrial substrata (Karsten and Rindi, 2010; Karsten et al., 2013). This provides above all self-shading and photoprotection of individual filaments inside the mat which can be even enhanced by soil particles interwoven within the mats (Karsten and Holzinger, 2012; Karsten et al., 2013). The importance of self-shading is reflected by generally low light requirements for photosynthesis in *Klebsormidium* that were repeatedly shown (Karsten and Rindi, 2010; Karsten et al., 2013).

Mat-forming growth is also typical for filamentous Zygnematophyceae. Filaments usually start to grow at the bottom of a pool and when enough biomass is produced, oxygen bubbles trapped within it carry the mat to the surface of the pool (Graham et al., 1995). The top layers are then fully exposed to solar radiation which leads to their bleaching. Berry and Lembi (2000) measured irradiance below the *Spirogyra* mat to be more

than 30 times lower than at the mat surface. Moreover, the photosynthetic rate measured under experimental conditions was higher at lower irradiance showing that underlying filaments were exposed to more optimal irradiances (Berry and Lembí, 2000). Similarly, the low light adaptation in *Zygnema* is also usually explained by photoprotection provided by multi-layered mats (Holzinger et al., 2009; Herburger et al., 2015).

Spirogyra mats were even shown to be able of phototactic movement at low light conditions. The filaments align toward the light source and when they touch other filaments, they glide along each other, form bundles and move toward the light source by repeated rolling and stretching (Kim et al., 2005).

The differentiation of mat layers is best developed in terrestrial filamentous conjugating green alga *Z. ericetorum*. *Zygogonium ericetorum* produces two types of cells termed green and purple morphs (Figures 2A,B), (Aigner et al., 2013). The purple morph of the top layers is better protected from high irradiation and helps to shade the green morph underneath which is in turn less sensitive to desiccation (Holzinger et al., 2010; Aigner et al., 2013).

FORMATION OF SPECIALIZED CELLS

Formation of specialized stress-tolerant cells as a part of the life cycle is a widespread strategy for survival of unfavorable conditions and is widely known from many different groups of algae and other protists.

The first type of stress tolerant cells are dormant zygotes, i.e., resting cells that are developed as a result of sexual reproduction. Within Charophyta, such cells have been described in Coleochaetophyceae, Charophyceae, and Zygnematophyceae. Dormant zygotes usually require a period of dormancy before germination. Dormancy can be broken by a change in environmental conditions (temperature, light) or by addition of gibberellic acid (Sederias and Colman, 2007; Agrawal, 2009). Possible roles in phytohormone stress sensing and signal transduction are discussed below.

In Charophyceae, the dormant zygotes are termed oospores. Oospores are the overwintering stages that can survive anoxic conditions on lake bottoms. They are the only desiccation tolerant stages in the life cycle of Charophyceae and thus guarantee their survival in habitats that dry out for several years (Proctor, 1967; Leliaert et al., 2012). The young zygote secretes a thick cell wall and the inner walls of cortical cells thicken and become encrusted with lime. Calcified envelopes of the zygotes are known as “gyrogonites” (Leliaert et al., 2012).

Dormant zygotes, termed zygosporcs, that contain acetolysis resistant material are typical feature of the life cycle of Coleochaetophyceae (Delwiche et al., 1989) and Zygnematophyceae (e.g., *Zygnema* sp.: Stancheva et al., 2012, *Spirogyra* sp.: Stancheva et al., 2013 and *Z. ericetorum*: Stancheva et al., 2016). Cell walls of Zygnematophyceae zygosporcs consist of three major layers. Endospore is the colorless inner layer. The middle layer, termed mesospore, is crucial for stress tolerance as it contains enzyme- and acetolysis-resistant sporopollenin-like material. Exospore is at least partially enzyme-soluble, colorless

and sometimes also sculptured (Ashraf and Godward, 1980). Zygospores can be spherical, ellipsoid, rectangular, or lenticular and may be colored yellow, brown, purple, blue, or black (Kadlubowska, 1984). Most of the morphological characters important for traditional species determination are on the mesospore, where a blue vs. brown mesospores were suggested to separate different phylogenetic clades (Stancheva et al., 2012).

The other type of specialized cells is not formed during the sexual process, even though morphologically they can be very similar to the sexual spores. In Zygnematophyceae, mostly in filamentous Zygnematales, several such cell types were described. Parthenospores result from incomplete conjugation; they form directly from gametes that failed to find a compatible sexual partner (Kadlubowska, 1984). They are smaller and more rounded than zygospores (Poulíčková et al., 2007). Aplanospores are formed inside vegetative cells when protoplasts shrink and are enclosed by a complete new cell wall, independent of the original wall (Kadlubowska, 1984). Their formation was recently described in *Z. ericetorum* (Figures 2C–F), (Stancheva et al., 2014). Finally, akinetes develop directly from vegetative cells by thickening of the cell wall by deposition of wall material at the inner surface of the vegetative cell wall (Kadlubowska, 1984). In some species of *Zygnema*, the cell walls of mature akinetes can have a similar structure, ornamentation, and coloration to that of the zygospores (Kadlubowska, 1984). For morphology and light microscopy images of zygospores and akinetes, see Stancheva et al. (2012).

In contrast, many algae from stressful environments do not form any specialized stages and survive environmental stresses in vegetative state (Agrawal, 2009). Such cells are not dormant, so they can resume their physiological activity and growth immediately under restoring of favorable conditions (Agrawal, 2009). Nevertheless, vegetative cells in natural or experimentally induced stressful conditions differ from growing, non-stressed vegetative cells in many ways. They are usually characterized by storage product accumulation, thick cell wall, reduced physiological activity and ceased cellular division. Traditionally, such cells were sometimes termed ‘akinetes’ or even ‘winter forms’ in *Micrasterias* (Meindl et al., 1989). To avoid the confusion with ‘akinetes’ in *Zygnema* which are true specialized cells with zygospore-like cell walls, the term ‘pre-akinete’ or ‘mature cell’ has also been introduced by some authors for these hardened, stress tolerant vegetative cells (Fuller, 2013; Pichrtová et al., 2014a,b, 2016a; Herburger et al., 2015). The term ‘mature cell’ refers to the typical occurrence of such cells in old, starved cultures.

Mature cells (pre-akinetes) are key elements for survival of *Zygnema* in stressful environment where sexual reproduction and zygospore formation is very rare. Pre-akinetes of Arctic and Antarctic *Zygnema* survived when exposed to osmotic stress (Pichrtová et al., 2014a), desiccation (Pichrtová et al., 2014b), UV radiation (Holzinger et al., 2009), freezing (Hawes, 1990), and they were even observed to be the overwintering stages (Pichrtová et al., 2016b). Formation of mature cells (pre-akinetes) during aging of the cultures was tracked in cultures of Alpine strains of *Zygnema* (Figure 3), (Herburger et al., 2015); old

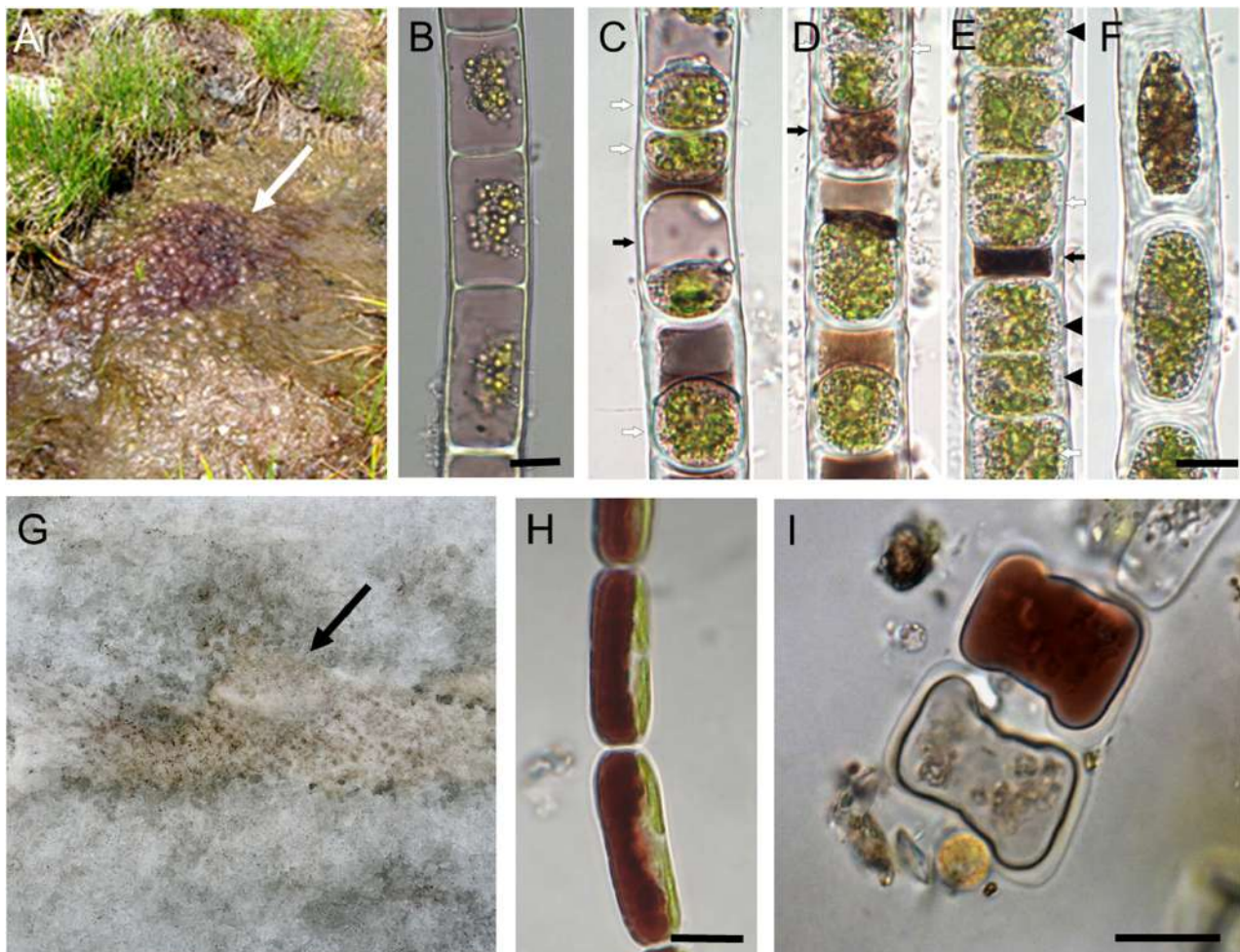


FIGURE 2 | Zygnematophyceae with purple vacuolar pigmentation. (A–F) *Zygogonium ericetorum*; **(G–I)** *Ancylonema nordenskiöldii*. **(A)** Habitat showing purple coloration (arrow). **(B)** vegetative filament. **(C–E)** aplanospore formation; white arrows indicate enlarged aplanospores with cell wall cleavage, black arrows point to compacted brownish residues; black arrowheads illustrate germinated aplanospores. **(F)** thick walled akinetes. **(G)** habitat on the surface of a glacier; arrow indicates coloration by algae. **(H)** vegetative filament with purple coloration of the vacuole. **(I)** conjugation stage. Bars **(B–F,H,I)** 10 µm. **(A,B)** Reprinted from Aigner et al. (2013), **(C–F)** reprinted from Stancheva et al. (2014), **(G–I)** reprinted from Remias et al. (2012a) with permission of Springer Business Media.

cultures survived desiccation at 84% RH and had in general lower rETR_{max} (Herburger et al., 2015). However, only after previous acclimation by slow desiccation (induced either by controlled desiccation at high relative humidity or by pre-cultivation on agar), the pre-akinetes were able to survive rapid desiccation in air at a relative humidity of 10% (Pichrtová et al., 2014b).

Glacier surface belongs to the most extreme habitats on Earth and it is interesting that the only eukaryotic algae that live there belong to the class Zygnematophyceae. Field populations of these algae, namely species *A. nordenskioeldii* (Figures 2G–I), (Remias et al., 2012a) and *M. berggrenii*, are also composed of vegetative cells; in the field no spores or cysts are produced even for overwintering (Remias et al., 2009, 2012a), however, conjugation has been observed in *A. nordenskioeldii* in field collected samples that were transferred to the laboratory (Figure 2I).

Members of the class Klebsormidiophyceae are also stress tolerant in their vegetative cells. Morison and Sheath (1985) showed a change in cellular morphology in desiccation tolerant *K. rivulare* resembling pre-akinete formation in *Zygnema*. Upon desiccation, carbohydrate and lipid contents increased and protein content decreased (Morison and Sheath, 1985). Many papers have recently been published that investigated various strains of *Klebsormidium*, *Interfilum*, *Hormidiella*, and *Entransia* in relation to desiccation stress (Karsten et al., 2010, 2013, 2014; Karsten and Holzinger, 2012; Herburger et al., 2016a). All species investigated were able to survive experimental desiccation and even the aquatic *Entransia* coped with low water availability better than other freshwater algae (Herburger et al., 2016a). Alpine strains of *Klebsormidium* were also markedly resistant to osmotic stress (Kaplan et al., 2012). Moreover, most of the investigated *Klebsormidium* sp. strains also survived freezing at -40°C (Elster et al., 2008).

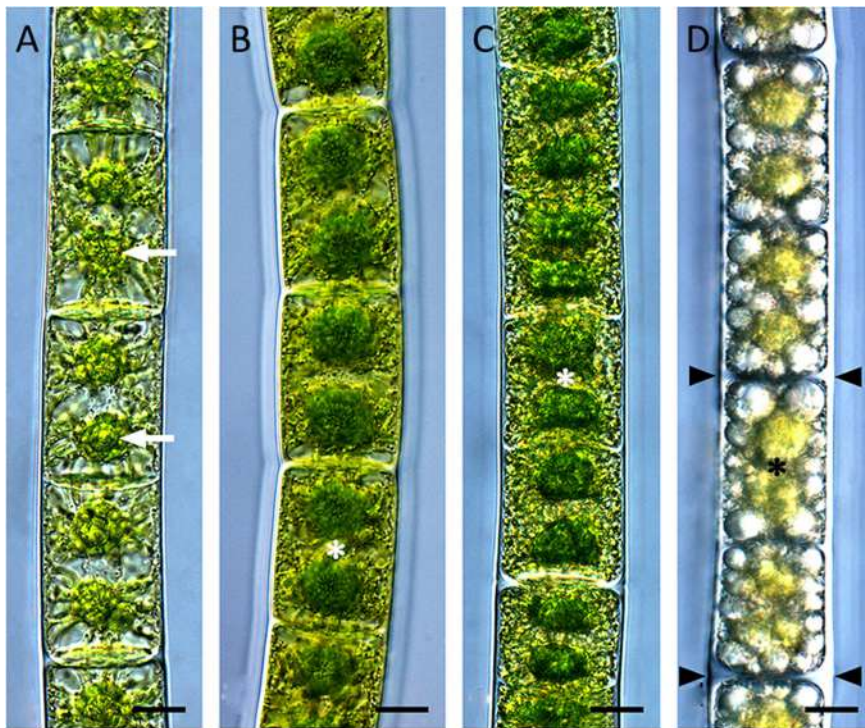


FIGURE 3 | Pre-akinete formation in *Zygnema* sp. Saalach. **(A)** 1 month, **(B)** 6 months, **(C)** 9 months, **(D)** 15 months old cultures. Arrows: pyrenoids, asterisks: nuclei, arrowheads: thickened cell walls. Bars 10 μm . Reprinted from Herburger et al. (2015).

CELL WALL STRUCTURE AND COMPOSITION IN RELATION TO STRESS TOLERANCE

Cell wall composition of charophyte green algae has recently been investigated extensively, particularly before the background that they are thought to be closest living relatives to land plants (Mikkelsen et al., 2014). Charophyte green algae have cell walls containing polymers with remarkable similarity to cellulose, pectins, hemicelluloses, arabinogalactan proteins (AGPs), extensin, and lignin present in embryophyte walls (Sørensen et al., 2011; Domozych et al., 2012). Charophyte green algae contain orthologous genes in the cellulose synthetase (*cesA*) family, as well as in the *cesA*-like families *cslC* and *cslD* as analyzed by a survey of genomes and transcriptomes (Yin et al., 2014). Recent review articles summarize cell wall composition of charophytes (Popper and Tuohy, 2010; Popper et al., 2011, 2014; Domozych et al., 2012; Sørensen et al., 2012; Domozych and Domozych, 2014). We will focus on the cell wall components that are involved in desiccation and irradiation stress tolerance. The cell walls of streptophytic green algae have been suggested to be a defining structure that enabled green algal ancestors to colonize land (Mikkelsen et al., 2014). However, what are the traits that enabled this colonization? All charophyte green algae are poikilohydric organisms, they equilibrate with the surrounding relative air humidity, and do not have mechanisms that protect from desiccation. However, some cell wall components might

have the sole function of prolonging the water holding capacities for algae that were exposed to desiccating conditions.

One of the major differences in early-divergent chlorophyte and prasinophyte algae genomes is the occurrence of a low number of glycosyl transferases (GTs), whereas land plants contain hundreds of GTs. Now there is genetic evidence that many of the core cell wall polysaccharides have their origin in charophyte green algae (Domozych et al., 2012). These include mannan, xyloglucan, xylan, pectin, and arabino-galactan proteins (Mikkelsen et al., 2014). Most important for stress tolerance are pectic proteins, which have been extensively studied in the mesotaeniaceae *Netrium* and the desmidiaeans green algae *Closterium*, *Penium*, and *Micrasterias* (e.g., Domozych and Rogers-Domozych, 1993; Brosch-Salomon et al., 1998; Domozych et al., 2007; Eder et al., 2008; Eder and Lütt-Meindl, 2010). While the chemical structure of the detected homogalacturonans (α -D-1,4-galacturonic acid) might vary in the degree of methyl esterification, relevant for the function of these compounds during developmental processes. When incorporated into mucilage, particularly the water holding capacities of these layers are ecologically relevant in habitats with fluctuating water regimes. Formation of mucilage layers is widespread in Zygnematophyceae. For example, in *Zygnema irregularare* formation of secondary pectic layers was observed during prolonged cultivation on solid medium (Fuller, 2013). In the desmid *Micrasterias denticulata* mucilage layers have been described and characterized (e.g., Oertel et al., 2004; Wanner et al., 2013). Additionally, pectic layers have another

great benefit in charophyte green algae – allowing to form multicellular organisms, a clear prerequisite of success for plants on land (Domozych and Domozych, 2014). Moreover, a mucilage layer has also been suggested to play a significant role in UV protection (Lütz et al., 1997), however, UV screening compounds have not directly been identified in the mucilage. Recently, homogalacturonans have been described as ancient streptophyte feature, albeit secondarily lost in *Klebsormidium* (O'Rourke et al., 2015). Members of the Klebsormidiales have indeed many differences concerning their cell walls (Mikhailuk et al., 2014), when compared to later branching charophytes.

The localization and function of callose, a β -D-1,3-glucan has been investigated in *Klebsormidium* and *Zygnema* (Herburger and Holzinger, 2015). Callose as a cell wall flexibilizing compound can protect cell walls from desiccation induced damage, when they follow the shrinkage of the protoplasts. It was previously shown by biochemical methods, that a high abundance of this compound was found in the early branching charophyte *Klebsormidium* (Sørensen et al., 2011). Upon localization this flexibilizing compound is predominately found in mechanically strained areas of the cell wall (Herburger and Holzinger, 2015). In *Klebsormidium* the absolute content of callose is significantly increased upon desiccation stress applied for up to 3 h. Localization of callose in *Klebsormidium* demonstrated that particularly the cross cell walls and the cell walls of the terminal cells contain high amounts of this compound, and thus can fold and follow the desiccation induced volume reduction (**Figures 4A–F**) (Herburger and Holzinger, 2015). In contrast, the later branching *Zygnema*, did not change the callose content upon desiccation stress. However, callose can still be localized in the cell walls of *Zygnema*, particularly in the cell corners, that are exposed to the most severe strain upon desiccation stress (**Figures 4G–L**). Desiccation induced volume changes have recently been investigated in *Klebsormidium* and *Zygnema* at different relative humidities, where *Zygnema* showed a more drastic volume reduction at the lowest RH tested (Lajos et al., 2016). Interestingly the more rigid, cellulose-rich secondary walls of *Zygnema* tolerate this stress without being damaged.

The occurrence of fossilizable biomacromolecules resistant to chemical processes in spores of charophyte green algae has been reported repeatedly (Versteegh and Blokker, 2004). The green autofluorescence of *Zygnematophyceae* zygospores is characteristic for sporopollenin-like material (algaenan) that differs from true sporopollenin of pollen grains in chemical composition and in biochemical pathway leading to its production (Versteegh and Blokker, 2004; Pouličková et al., 2007). While sporopollenin is synthesized in phenylpropanoid pathway, the acetate-malate pathway leads to algaenans (Versteegh and Blokker, 2004). Similarly, in *Coleochaete* the inner zygote cell wall layers have been described to contain material similar in ultrastructural appearance and chemistry to sporopollenin (Delwiche et al., 1989; Kroken et al., 1996). Sporopollenin is polymerized from hydroxylated fatty acids and phenolics, its occurrence predated lignin (summarized in Weng and Chapple, 2010). Sporopollenin and algaenans in the cell walls provides protection from both desiccation and UV radiation. The occurrence of 'lignin-like' phenolic compounds were described

in walls of vegetative cells of *Coleochaete* (Delwiche et al., 1989). However, many of these early findings were based on crude detection methods and have to be discussed critically (Weng and Chapple, 2010).

PHYSIOLOGICAL PROTECTION OF THE PHOTOSYNTHETIC APPARATUS

One of the key targets of radiation (high PAR and UV) as well as desiccation and temperature stress is photosynthesis. The effects of desiccation on photosynthesis of green algae were recently summarized (Holzinger and Karsten, 2013; Karsten and Holzinger, 2014). Photosynthetic strategies of desiccation tolerant organisms were recently summarized by Fernandez-Marin et al. (2016). It has been shown, that dehydration directly affects the electron transport chains in the thylakoid membranes. The loss of water in the presence of light increases the risk of chlorophyll overexcitation, which can in turn generate oxygen radicals and reactive oxygen species (ROS). These compounds have various negative effects that will not be further discussed in this review. To compensate these effects, tolerant organisms up-regulate photoprotection mechanisms (Fernandez-Marin et al., 2016). The regulation of the photosynthetic electron transport rates and protection through photoinhibition is crucial for survival (e.g., Roach and Krieger-Liszkay, 2014). UV-B radiation has been shown to induce similar photo-oxidative stress in charophyte green algae (Germ et al., 2009; Karsten and Holzinger, 2014). The shift from LHCSR (light-harvesting complex stress-related) in chlorophytes to PSBS (photosystem II subunit S)-dependent non-photochemical quenching (NPQ) in charophytes has been demonstrated in ZCC-clade genera (*Chara*, *Zygnema*, and *Cosmarium*; Gerotto and Morosinotto, 2013). While *Zygnema* and *Cosmarium* showed a fast NPQ induction upon light exposure, *Klebsormidium* and *Interfilum* as representatives of the KCM-clade had a much slower induction. The only exception was *Mesotaenium*, where little NPQ induction was found (Gerotto and Morosinotto, 2013), however, in this genus different strategies like abundant protection by phenolic compounds are established (see below).

Numerous publications have investigated photosynthetic performance under laboratory controlled conditions in *Klebsormidiophyceae* (Karsten et al., 2010, 2013, 2014, 2015; Karsten and Holzinger, 2012) and in *Zygnematophyceae* (Pichrtová et al., 2013, 2014b; Herburger et al., 2015). Some information on photosynthesis parameters and light acclimation are available in Characeae (Küster et al., 2000; Vieira and Necchi, 2003). In contrast, little is known on other charophyte green algae according their photosynthetic performance.

Many physiological data are available for the genus *Klebsormidium* (Karsten et al., 2010, 2013, 2015; Karsten and Holzinger, 2012). Regardless of strain and clade, *Klebsormidium* shows a broad light amplitude, the relative electron transport rate did not show photoinhibition up to $500 \mu\text{mol photons m}^{-2} \text{s}^{-1}$ in *Klebsormidium crenulatum* (**Figure 5A**), (Karsten et al., 2010). Very low light compensation points in the range $1.8\text{--}5.7 \mu\text{mol photons m}^{-2} \text{s}^{-1}$ were found for different *Klebsormidium*

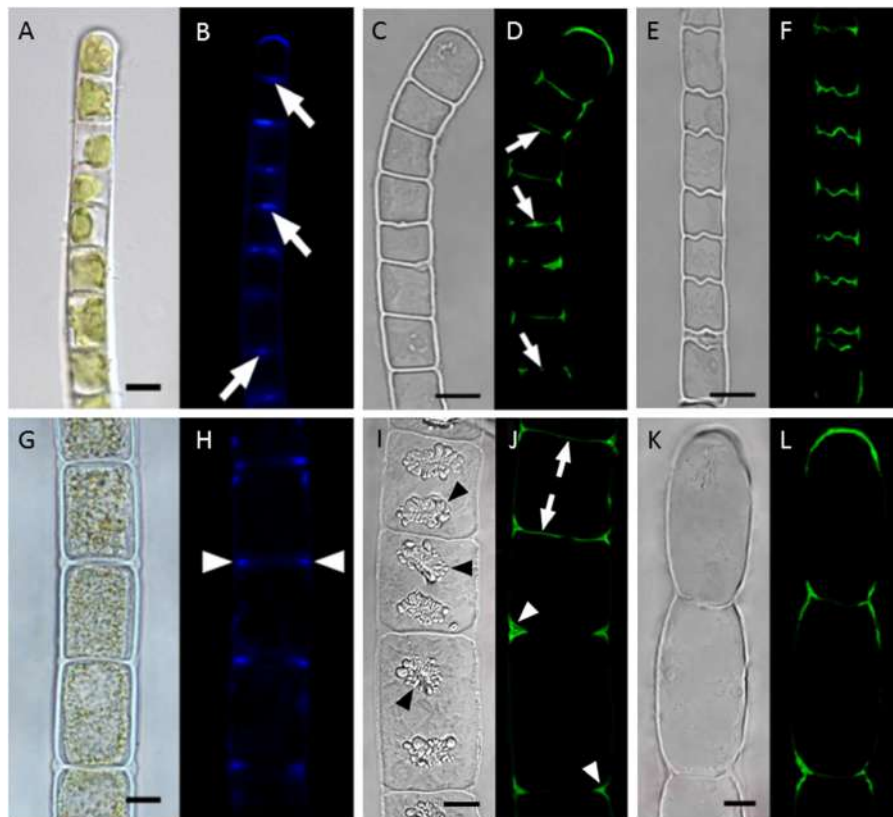


FIGURE 4 | Localization of callose in cell walls of *Klebsormidium crenulatum* (A–F) and *Zygnema* sp. *Saalach* (G,H). (A,B) Aniline blue staining, **(C,D)** staining of turgescence cell with antibody 400-2, **(E,F)** staining of desiccated cells with antibody 400-2, **(G,H)** aniline blue staining, **(I,J)** staining of turgescence cells with antibody 400-2, **(K,L)** staining of desiccated cell with antibody 400-2. Arrows: cross walls, arrowheads: cell corners. Bars 10 μm . reprinted from Herburger and Holzinger (2015).

species (Karsten et al., 2010; Karsten and Holzinger, 2012). The maximum photosynthetic oxygen production ranged from $37.9 \mu\text{mol O}_2 \text{ h}^{-1} \text{ mg}^{-1} \text{ chl a}$ in *K. crenulatum* (Karsten et al., 2010), $75.9 \mu\text{mol O}_2 \text{ h}^{-1} \text{ mg}^{-1} \text{ chl a}$ in *K. flaccidum* (Karsten et al., 2013) to $87.0 \mu\text{mol O}_2 \text{ h}^{-1} \text{ mg}^{-1} \text{ chl a}$ in *K. dissectum*.

The Klebsormidiophyceae genus *Interfilum* showed different kinetics of decrease in effective quantum yield under desiccation conditions in relation to their morphological characteristics (Karsten et al., 2014). While single celled strains exhibited a faster desiccation rate, cell packet forming strains showed slower desiccation rates (Karsten et al., 2014). In general, all investigated *Interfilum* strains exhibited optimum photosynthesis under low photon fluence rates, with no signs of photoinhibition under high light conditions up to $1500 \mu\text{mol photons m}^{-2} \text{ s}^{-1}$ (Figure 5B), (Karsten et al., 2014). In the additionally investigated Klebsormidiophyceae genera *Entransia* and *Hormidiella* similar reactions to desiccation were observed (Figure 5C), (Herburger et al., 2016a). All these data suggest that Klebsormidiophyceae have low light requirements, coupled with no photoinhibition under higher irradiation, corroborating a high photophysiological plasticity.

In contrast, in Zygnematophyceae rETR curves show much higher initial saturation irradiance (I_k values). In the

desmidiaeae *Cosmarium* (Stamenković and Hanelt, 2011), in the range of $1200 \mu\text{mol photons m}^{-2} \text{ s}^{-1}$ for tropical and cosmopolitan strains, somewhat lower in polar taxons (around $700 \mu\text{mol photons m}^{-2} \text{ s}^{-1}$). In a polar strain of *Zygnema* I_k values around $450 \mu\text{mol photons m}^{-2} \text{ s}^{-1}$ were observed (Holzinger et al., 2009). I_k values of *Zygnema* sp. collected in the Austrian Alps ($\sim 150 \mu\text{mol photons m}^{-2} \text{ s}^{-1}$) and in a lowland strain of *Zygnema* at $\sim 450 \mu\text{mol photons m}^{-2} \text{ s}^{-1}$ (Herburger et al., 2015). The rETR curves showed significant difference in relation to the culture age, where the oldest cultures had a significant drop in the maximum electron transport rate (rETR_{max}; Figure 5D), (Herburger et al., 2015). Signs of photoinhibition were observed in arctic and Antarctic *Zygnema* sp. strains, and the rETR_{max} values were drastically reduced upon osmotic stress (Figures 5E,F), (Kaplan et al., 2013). However, in general, the values determined for Zygnematophyceae point toward a higher light adaptation, and moreover remarkable resistance against UV irradiation has been observed (summarized in Holzinger and Lütz, 2006). How can this adaptation be realized?

The xanthophyll cycle pool size may contribute substantially to a well-developed photo protection process, in this way dissipating excessive irradiation (Stamenković et al., 2014).

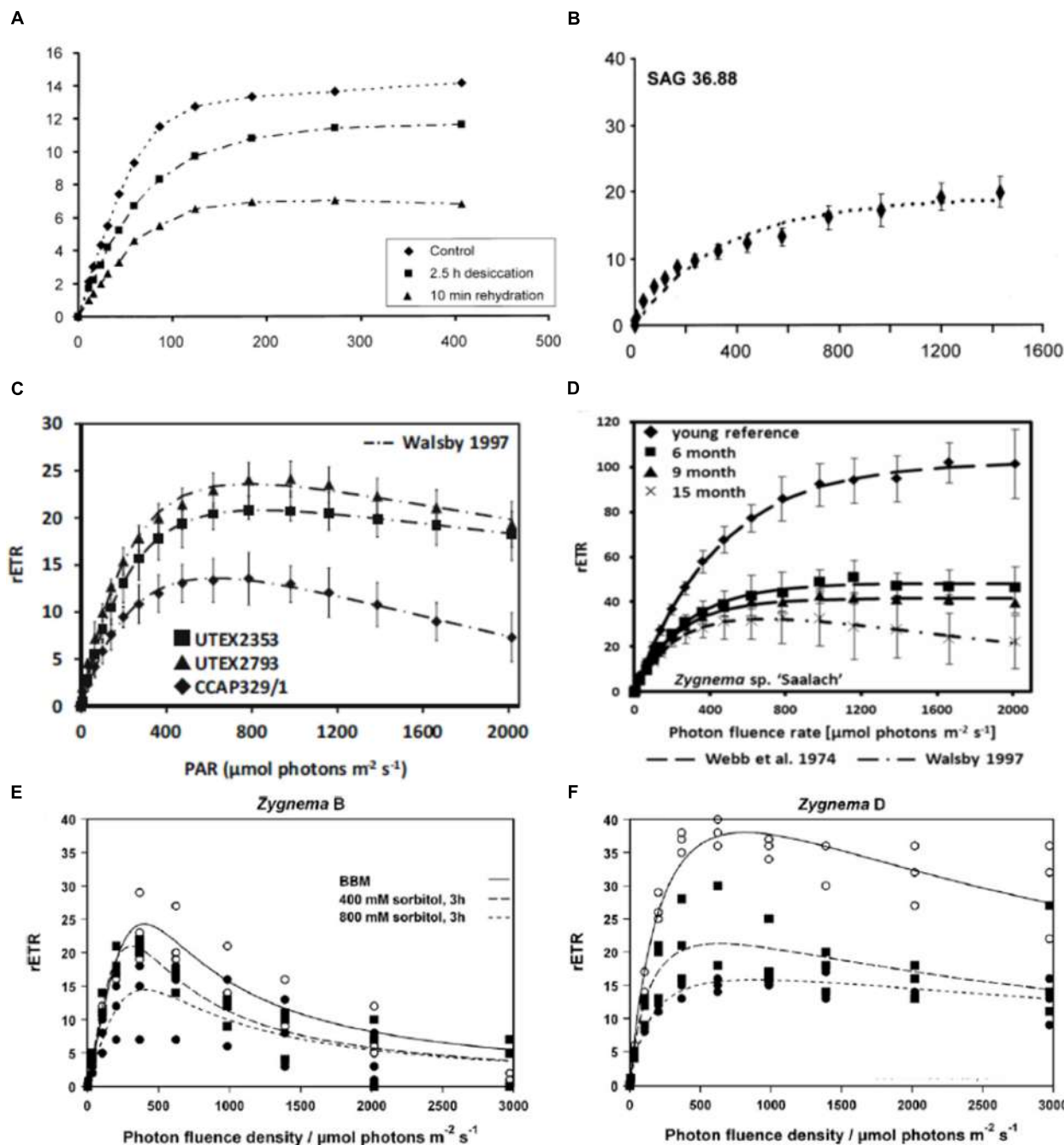


FIGURE 5 | Relative electron transport rates in different charophyte green algae. **(A)** *Klebsormidium crenulatum*, (SAG 2415, desiccation and rehydration, reprinted from Karsten et al., 2010 with permission of Wiley and Sons.), **(B)** *Interfilum* (SAG 36.88), reprinted from Karsten et al. (2014), **(C)** *Entransia fimbriata* (UTEX2353, UTEX2793) and *Hormidiella attenuata* (CCAP329/1) reprinted from Herburger et al. (2016a), **(D)** *Zygnema* sp. 'Saalach' (SAG 2419, various culture ages, reprinted from Herburger et al., 2015), **(E)** arctic *Zygnema* sp. 'B' (CCALA976, **(F)** Antarctic *Zygnema* sp. 'D' (**E,F**) reprinted from Kaplan et al. (2013).

There is evidence for the increase in zeaxanthin content of the PS II antenna in high light tolerating *Cosmarium* strains (Stamenković et al., 2014). In *Zygnema* strains from arctic and Antarctic habitats, a considerable amount of antheraxanthin and zeaxanthin was found (Pichrtová et al., 2013). The highest de-epoxidation state was found

in an arctic strain, which went along with the highest concentration of phenolic compounds (Pichrtová et al., 2013).

These studies match well with the findings of high resistance to photoinhibition in an Antarctic strain of *Zygnema* sp. (Thangaraj, 2016). In this study the cells have been exposed to 400, 1400,

2100, and 3500 μmol photons $\text{m}^{-2} \text{s}^{-1}$. After an initial drop of the F_v/F_m value, the cells showed a rapid tendency to recover, even after unrealistically high irradiation. The authors claim some constitutive and genetically fixed preservation mechanisms responsible for the high tolerance in the Antarctic *Zygnuma* sp. strain. Interestingly, dF_o did not recover to pre-treatment values, which indicated rearrangements of the LHC II complex.

Zygnematophyceae have shown remarkable stress tolerance to experimental UV radiation (Meindl and Lütz, 1996; Lütz et al., 1997). UV-effects in algae were summarized in Holzinger and Lütz (2006). In a study with field collected samples of *Zygnuma* sp. from Svalbard, virtually no effect on the ultrastructure but a significant decrease of the F_v/F_m value after 24 h UV A, but not after UV AB exposures was found (Holzinger et al., 2009). Similar results were gained by Pichrtová et al. (2013), albeit significant reduction in F_v/F_m were observed in an arctic and an Antarctic strain of *Zygnuma* sp. after a predominant UV A treatment for 8 days. Germ et al. (2009) did not find a decrease in F_v/F_m after UV B exposure in an arctic *Zygnuma* strain. In *Cosmarium* UV A radiation caused a twofold larger depression of F_v/F_m when compared to that under PAR irradiation (Stamenković and Hanelt, 2014). The observation that in several of the investigated *Zygnematophyceae* UV A lead to more pronounced photoinhibition, might be ecologically relevant, as in natural sunlight the proportion of UVA is at least ten times higher than UV B, and moreover this waveband is not blocked by the ozone layer.

PRODUCTION OF PROTECTIVE SUBSTANCES

Algae produce a vast spectrum of metabolites that help them to protect the cells against environmental stress. Some are produced as a result of stress but some are also produced constitutively. Precise classification according to their function is difficult, because very often one substance is involved in various processes. Here, we focus on two major protective mechanisms provided by accumulated compounds – osmotic acclimation, which is important for tolerating limiting water availability and UV (PAR) screening that protects exposed cells.

Accumulation of Organic Osmolytes

Preventing water loss and maintaining homeostasis under stress conditions is essential for normal cellular function. Increasing salinity, desiccation, and freezing lead to osmotic dehydration and a reduced cellular water potential (Bisson and Kirst, 1995). Therefore, the physiological effects of these stresses are similar and the acclimation during exposure to an individual stress can result in resistance to other stresses (Morison and Sheath, 1985; Welsh, 2000; Vilumbrales et al., 2013). Nevertheless, these stresses are complex and components other than osmotic dehydration play a role in their effects (e.g., ionic component of the salt stress, Darehshouri and Lütz-Meindl, 2010). Recently osmotic stress induced ultrastructural changes leading to degradation of dictyosomes were investigated by TEM and FIB-SEM tomography in the charophyte green algae *Micrasterias*

and *Nitella* (Lütz-Meindl et al., 2015). During the osmotic acclimation in response to long term hyperosmotic conditions, algae synthesize and accumulate various substances that increase the cellular osmotic value, leading to a negative osmotic potential (Bisson and Kirst, 1995). Organic osmolytes also play other roles in cellular protection. They can act as compatible solutes that are highly soluble, accumulate to high concentrations without interacting with cellular functions, protect proteins and stabilize membranes (Bisson and Kirst, 1995; Yancey, 2005). They can also act as antioxidants, cryoprotectants and heat protectants and can be rapidly degraded and used as respiratory substrates (Welsh, 2000; Yancey, 2005). Organic osmolytes are chemically diverse, comprising sugars, polyols, amino acids, and their derivatives (Welsh, 2000; Yancey, 2005).

Several studies reported osmolyte accumulation in various species of *Klebsormidium*. Sucrose and glutamic acid were detected as major osmoregulatory compounds of *K. flaccidum* and *K. sterile* subjected to osmotic stress in artificial seawater (Brown and Hellebust, 1980). *K. flaccidum* was capable to increase freezing tolerance during cold acclimation in a similar way to higher land plants (Nagao et al., 2008). The authors showed accumulation of sugars (mainly sucrose and glucose), but also of other compounds, such as amino acids and an unknown glycoside (Nagao et al., 2008). Kaplan et al. (2012) detected various soluble carbohydrates in two species of *Klebsormidium* (Table 1). The major proportion of oligosaccharides remained unidentified, the rest was dominated by raffinose, sucrose, glucose, xylose, galactose, mannose, inositol, fructose, glycerol, mannitol, and sorbitol (Kaplan et al., 2012). However, the total content of soluble carbohydrates was only approximately 1.2% of the dry weight (Kaplan et al., 2012). Karsten and Rindi (2010) reported sucrose as the major organic osmolyte of *Klebsormidium* sp. isolated from an urban wall in Germany. Sucrose accumulated in the cells with increasing salinity, in the highest salinity levels tested, however, the sucrose content and maximum quantum yield of PSII rapidly declined. This rather stenohaline response can be explained by the inability of Streptophyta to accumulate polyols as organic osmolytes (in contrast to most aeroterrestrial Chlorophyta, e.g., Gustavs et al., 2010), because sucrose cannot be accumulated to such a high content (Karsten and Rindi, 2010; Karsten et al., 2010). The only known report of sorbitol accumulation to high cellular concentrations by *K. marinum* (Brown and Hellebust, 1980) has to be viewed critically as molecular phylogenetic analyses revealed its position under Chlorophyta which resulted in its reclassification as *Stichococcus deasonii* (Neustupa et al., 2007).

Recent transcriptomic study of *K. crenulatum* showed up-regulation of sucrose synthase and sucrose phosphate synthase after desiccation stress (Holzinger et al., 2014) even though this enzyme has a different structure than in plants (Nagao and Uemura, 2012). In addition, several enzymes involved in the biosynthesis of the raffinose family of oligosaccharides were also up-regulated (Holzinger et al., 2014).

Low cellular osmotic potentials (-0.8 to -1.67 MPa) and tolerance to osmotic stress was also reported in arctic and Antarctic *Zygnuma* spp. (Kaplan et al., 2013; Pichrtová et al.,

2014a). Soluble sugars accounted for $9.9 \pm 0.8\%$ ash-free dry weight of field collected Antarctic *Zygnema* and 95% of the extracted sugars were identified as sucrose, with traces of glucose, fructose, and mannitol (Hawes, 1990). However, the author argued that this concentration is still too low to significantly depress the freezing point of the cell contents (Hawes, 1990).

Even though many streptophytes were shown to tolerate osmotic, desiccation and freezing stress, production of organic osmolytes within this group remains largely unknown or it seems that the detected organic osmolytes do not accumulate to high concentrations enough to fully explain the alga's stress tolerance (Hawes, 1990; Kaplan et al., 2012). Therefore, it seems that accumulation of soluble carbohydrates alone cannot explain the high osmotic values and water stress tolerance of aeroterrestrial streptophytic algae.

UV (and PAR) Screening Compounds

Strictly freshwater Charophyceae were found to be sensitive to UV B radiation, but at the same time they do not produce any UV absorbing compounds. They have to rely on natural UV attenuation provided by water and substances dissolved within (de Bakker et al., 2005).

Mycosporine-like amino acids (MAAs) are the most widespread compounds with UV screening function, commonly accumulating in many groups of algae and other organisms. They are colorless, water-soluble substances with peak absorbances between 310 and 360 nm (Cockell and Knowland, 1999; Shick and Dunlap, 2002). They can function also as antioxidants (Coba et al., 2009; Carreto and Carignan, 2011) and are involved in osmotic regulation (Shick and Dunlap, 2002; Oren, 2007). Within Charophyta, their production has been so far proven only in Klebsormidiophyceae. *K. fluitans* was shown to synthesize a so far unidentified MAA with absorption maximum at 324 nm (Table 1). After UV exposure, this compound was accumulated up to more than 1% DW (Kitzing et al., 2014). A closely related genus *Hormidiella* that occurs in similar habitats as *Klebsormidium* contains the same compound, while this compound was not present in *Entrania*, an aquatic genus from the same class. *Entrania* occurs in peat bogs and humic lakes where UV screening is provided by

dissolved organic carbon of the water (Kitzing and Karsten, 2015).

Another group of substances with UV screening function are phenolic substances. They are produced by only few algal classes and within charophytes their production has been so far proven only in Zygnematophyceae (Table 1), which chemotaxonically support their close relationship to land plants. Like MAAs, phenolics are water soluble and natural UV screens because of their aromatic groups. In addition, some phenolic substances cause strong pigmentation of the vacuoles and so they protect photosynthetic apparatus also from excessive PAR irradiation in a similar way as secondary carotenoids of some chlorophyte algae. In contrast to MAAs they do not contain nitrogen which makes their synthesis "cheaper" and therefore advantageous in extreme habitats with nutrient deficiency (Carreto and Carignan, 2011). This is probably the main reason why Zygnematophyceae are able to thrive in extreme environments like glacier surface where strong irradiation is coupled with very oligotrophic conditions. Phenolics also act as antioxidants and may play a role also against herbivores or parasites. Antibacterial activity of methanol extract of *Spirogyra varians* is also attributed to phenolics (Cannell et al., 1988).

Ancylonema nordenskioeldii and *M. berggrenii*, common zygnematophytes of both Alpine and Arctic glaciers, have dark purple brownish peripheral vacuoles containing phenolic pigments (Figures 2H,I). Phenolic compounds of *M. berggrenii* were determined as purpurogallin derivates (Remias et al., 2009, 2012b). The pigments cause even macroscopically visible coloration that significantly decreases the albedo of the ice and thus potentially promotes the melting of the glacier, with consequences for the whole ecosystem and global climate (Stibal et al., 2012).

Purple morph of *Z. ericetorum* similarly accumulates several unusual phenolic substances in vacuoles (Figures 2B–F), (Aigner et al., 2013). These components are mainly gallic acid derivatives, and their structure has recently been investigated (Newsome et al., 2013). In this way, *Zygogonium* has gained a high tolerance to iron, as well as aluminum (Herburger et al., 2016b). Various gallotannins were also detected in a *Spirogyra* sp. (Nishizawa et al., 1985). *Spirogyra pratensis* was able to produce purple

TABLE 1 | Summary of protective substances avoiding abiotic stress in charophyte green algae.

Charophyte Genus	Organic osmolytes	MAA	Phenolic compounds	Reference
<i>Klebsormidium</i> , <i>Hormidiella</i>		MAA 324 nm		Kitzing et al., 2014; Kitzing and Karsten, 2015
<i>Klebsormidium</i>	Sucrose, glucose, raffinose, xylose, galactose			Nagao et al., 2008; Karsten and Rindi, 2010; Kaplan et al., 2012
<i>Zygnema</i>	Sucrose, traces of glucose, fructose, mannitol			Hawes, 1990
<i>Ancylonema</i>		Purple vacuolar pigment		Remias et al., 2012a
<i>Mesotaenium</i>		Purpurogallin derivates		Remias et al., 2009, 2012b
<i>Zygogonium</i>		Glycosylated gallic acid derivatives, complexed with iron		Aigner et al., 2013; Newsome et al., 2013; Herburger et al., 2016b
<i>Spirogyra</i>		Gallotannins		Nishizawa et al., 1985
<i>Zygnemopsis</i>		Unspecified		Figueroa et al., 2009
<i>Zygnema</i>		Unspecified		Pichrtová et al., 2013

pigmentation in the presence of iron (Allen and Alston, 1959). A whole range of unspecified, phenolics with UV screening ability but lacking typical dark color were detected also in other zygnematophytes, such as *Zygnuma* (Pichrtová et al., 2013) and *Zygnemopsis* (Figueroa et al., 2009).

MOLECULAR INVESTIGATIONS OF STRESS RELATED PROCESSES

At the moment, only a few publications are available using 'omics' techniques to address the molecular pathways behind stress tolerance and adaptation in charophytes. Comparisons of plant molecular processes between the charophyte green algae *Coleochaete orbicularis* and *Spirogyra pratensis* were performed and revealed a closer similarity to *Arabidopsis thaliana* than to the chlorophyte *Chlamydomonas reinhardtii* (Timme and Delwiche, 2010). The authors used a list of genes identified by Graham et al. (2000) to be important for colonization of land and found solid hits and even true orthologs in *Coleochaete* and *Spirogyra* including, e.g., cellulosic cell walls and cytokinetic phragmoplasts. According to the body plan no hit for asymmetric cell division was found in *Spirogyra*, but two hits were obtained in *Coleochaete* (Timme and Delwiche, 2010). A transcriptomic study of severe desiccation stress in *K. crenulatum* demonstrated that most of the highest upregulated transcripts do not show any similarity to known proteins (Holzinger et al., 2014). Major physiological shifts upon desiccation were the up-regulation of transcripts for photosynthesis, energy production and ROS metabolism (Holzinger et al., 2014). Classical desiccation responses, like late embryogenesis abundant proteins (LEA) or proteins involved in early response to desiccation (ERD) as well as osmolyte production (raffinose family oligosaccharides RFO) were upregulated. In contrast, transcripts of cell division, DNA replication, cofactor biosynthesis, and amino acid biosynthesis were strictly down-regulated as a consequence of desiccation stress (Holzinger et al., 2014).

Recently the effect of ionizing radiation was investigated in an arctic strain of *Zygnuma* sp. (Choi et al., 2015). The photosynthetic efficiency markedly decreased with a 5 kGy dose, and the cells showed serious damage. However, an increase in DPPH radical scavenging activity was found in gamma-irradiated cells. The study is insofar interesting, as changes in the protein expression levels were investigated by a proteomics approach (Choi et al., 2015). Photosynthesis related proteins were up- or down-regulated, confirming the impact of gamma irradiation on the photosynthetic process. Proteins related to DNA repair, quinone oxidoreductase, regulation of microtubules and cell wall biogenesis were found to be upregulated. This means, that arctic *Zygnuma* cells showed the capacity to actively repair damages to DNA, which is likely an effect of ionizing radiation. The ubiquinone oxidoreductase 13-kD-like subunit was also upregulated upon gamma irradiation. This protein is a coenzyme of the mitochondrial NADP-dehydrogenase, essential for NAPH oxidation. Interestingly, the regulation of cytoskeletal elements, in the particular case through an armadillo repeat-containing kinesin protein, that is involved in the ATP-binding

mechanism (Choi et al., 2015). This might interact with organelle positioning and cell wall deposition.

In contrast, energy metabolism, isoprene biosynthesis and protein biosynthesis related proteins were down-regulated with the applied gamma-irradiation (Choi et al., 2015). This can be considered as a protection mechanism.

ALGAE AND MICROBE INTERACTION

There is increasing knowledge that charophytes serve as hosts for microbial communities that occur within surface mucilage matrices (Knack et al., 2015). These microbial associations were suggested to nurture the earliest plants and influence their biogeochemical roles. Microbiomes are known to be closely related to host organisms from certain lineages, it is hypothesized that microbiomes of early-diverging modern bryophytes and closely related charophyte green algae have commonalities reflecting the ancestral traits (Knack et al., 2015). Metagenomic sequence data were used from the late-diverging charophytes *Chaetosphaeridium* and *Coleochaete*, as well as the liverwort *Conocephalum* to infer bacteria and fungi for comparisons with the microbiome of an outgroup chlorophytic green alga *Cladophora*. It was found that the streptophyte (charophyte green algae and liverwort) microbiomes contained N-fixing cyanobacteria (*NifH* genes indicating nitrogen fixation), methanotrophs (*pMMo* genes indicating methane oxidation) and early diverging fungi. They were much more similar to each other than to the *Cladophora* microbiota (Knack et al., 2015).

Symbiotic interactions were also tested in a large scale transcriptomic analysis comparing 259 transcriptomes (10 green algal and basal land plant genomes) and were suggested to be involved in colonizing land by plants (Delaux et al., 2015). The appearance of a key regulator, a calcium and calmodulin-dependent protein kinase, suggested as symbiotic signaling pathway predated the conquering of land (Delaux et al., 2015). In their study, they tested the newly generated deep transcriptomes of the charophyte complex *Closterium peracerosum-strigosum-littorale* and the draft genome of *Spirogyra* sp. as well as transcriptomes of liverworts, mosses and hornworts. They report, that potential homologs of DMI1 and CCaMK ('symbiotic genes' belonging to the signaling module) were found in charophytes and even in chlorophytes (Delaux et al., 2015). This is insofar not surprising, as virtually all lichen forming algae (besides cyanophyta) belong to the chlorophytic lineage. Despite being very successful on land by tolerating extreme desiccation (e.g., Kranner et al., 2008), lichens did not give rise to further phylogenetic developments on land like the charophytes. The mutualistic fungal partners (Mucoromycotina/Glomeromycota), acting in some sort of primitive mycorrhizal symbiosis in early land plants, have recently been reviewed by Field et al. (2015).

FUNCTION OF PLANT HORMONES

Phytohormones play a critical role in signal transduction upon stress reactions. Recently transcriptomic and genomic

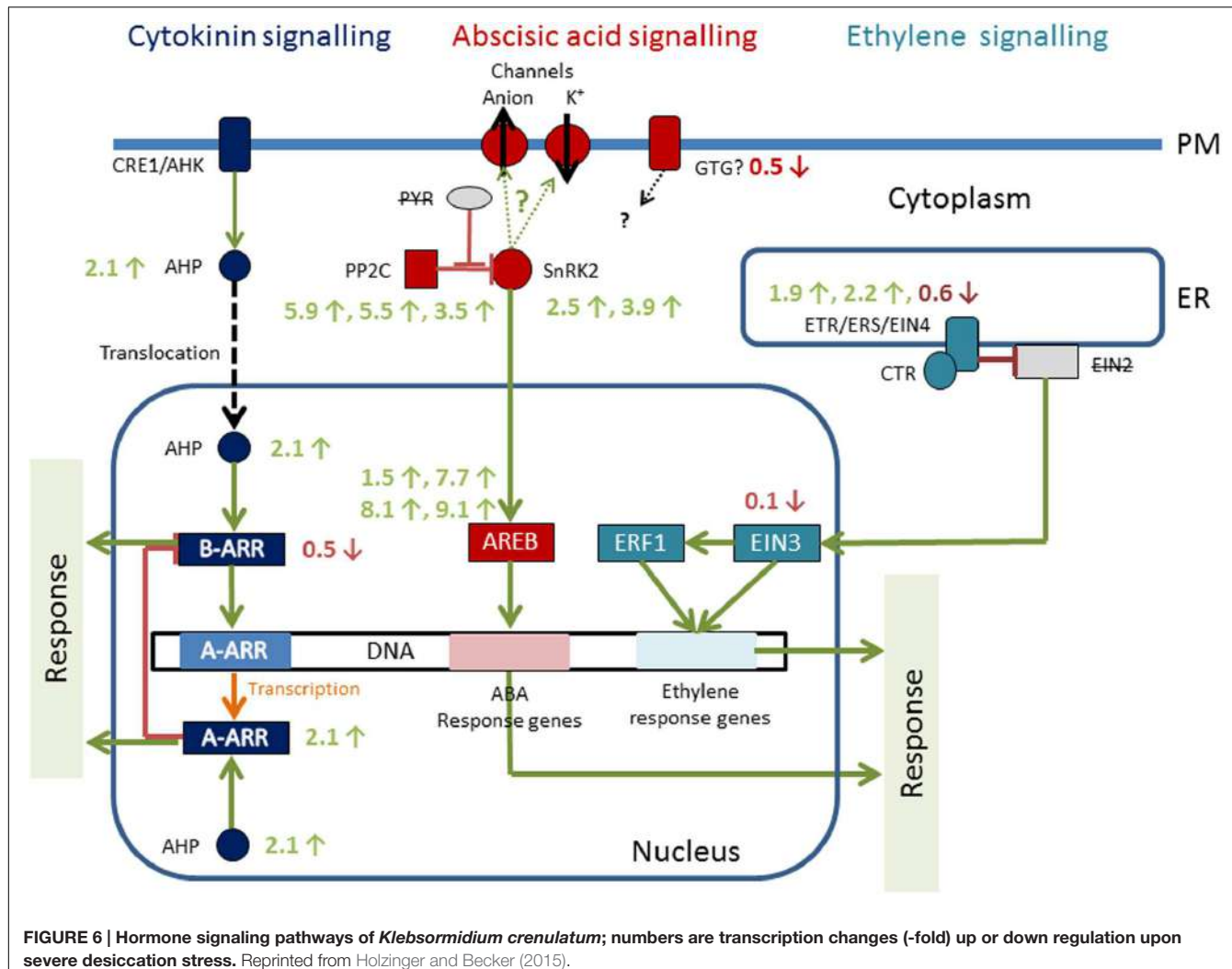


FIGURE 6 | Hormone signaling pathways of *Klebsormidium crenulatum*; numbers are transcription changes (-fold) up or down regulation upon severe desiccation stress. Reprinted from Holzinger and Becker (2015).

datasets became available in the early branching *Klebsormidium* (Holzinger et al., 2014; Hori et al., 2014), which allow to analyze the role of phytohormones in stress sensing (Figure 6). With the KEGG pathway reconstruction tool, almost complete pathways were found for cytokinin signaling, abscisic acid (ABA) signaling and ethylene response in *K. crenulatum* (Holzinger and Becker, 2015). In the draft sequence of *K. flaccidum* genome, signaling pathways for auxin, ABA, cytokinin, salicylic acid, and JA were found (Hori et al., 2014). Particularly the ABA response is well known in abiotic stress reactions. When *K. crenulatum* cells are exposed to severe desiccation stress ABA signaling components PP2C and SnRK2 were significantly increased, together with the nuclear AREB protein (Holzinger and Becker, 2015). There is a 70% overlap in differential gene expression profiles between plants that have been stressed with desiccation and high light, and it has to be stated that the majority of the ABA is synthesized in the plastids itself (de Vries et al., 2016). However, experimental ABA application did not change cold tolerance in *K. flaccidum* (Nagao et al., 2008). Also,

orthologs for the cytokinin receptors CRE1/AHK (in the plasma membrane), cytosolic AHP and the transcription factor A-ARP were upregulated as a consequence of desiccation stress in *K. crenulatum* (Holzinger and Becker, 2015). The abiotic stress of severe desiccation regulates the expression of three classical phytohormone pathways in *K. crenulatum*, corroborating that these early branching charophyte algae have the prerequisites for living on land (Holzinger and Becker, 2015). For successful terrestrialization, mechanisms to sense the external environment are crucial.

First evidence for ethylene biosynthesis and pathway genes in charophyte green algae have been given by Timme and Delwiche (2010). Ethylene response appears to be highly conserved as a plant hormone for the past 450 mio years (Ju et al., 2015). It was shown, that *Spirogyra* ethylene-signaling homologs have the capacity to partially rescue *Arabidopsis* defective mutants, indicating homologous ethylene-signaling pathways, implying that the common aquatic ancestor possessed this pathway already prior to the colonization of land (Ju et al., 2015).

STRATEGIES IN AN EVOLUTIONARY POINT OF VIEW

In a recent review, Delwiche and Cooper (2015) give an outstanding overview on the evolutionary background of the origin of the terrestrial flora. The discrepancy between single-gene and morphological analysis and genome-scale phylogenetic analysis are discussed, the latter clearly indicating the Zygnematophyceae as sister taxon to land plants (Timme and Delwiche, 2010; Wodniok et al., 2011; Timme et al., 2012; Wickett et al., 2014; Zhong et al., 2014, 2015). Recently this view has additionally been supported by analysis of plastid evolution (de Vries et al., 2016). While many prerequisites for the terrestrial life-style are common in several groups of charophytes, only zygnematophycean algae share with land plants the transfer of a few plastid genes to the nucleus (de Vries et al. (2016)). Chloroplasts became more submissive to nuclear control by key genes involved in the organelle division machinery (de Vries et al., 2016). Only basal charophyta (and some chlorophyta) possess the plastid division genes *ftsI*, *ftsW*, and *minD*. In contrast, ZCC-clade algae transferred these genes to the nucleus or lost them (de Vries et al., 2016). Interestingly, only the genus *Zygnuma* possess *cysA* and *cysT* (encoding components in the sulfate ABC transporter system). These genes were not observed in any other zygnematophycean plastid genomes. Thus, the *Zygnuma* plastid genome coding capacity was considered most similar to the hypothetical land plant ancestor (de Vries et al., 2016).

The link to understand evolution of terrestrial organisms from aquatic ones is to remember that life remains a fundamentally aquatic process (Delwiche and Cooper, 2015). The ancestral habitat for all charophyte lineages is freshwater, so terrestrial and semi-terrestrial environments are intermittently available to freshwater organisms. With the unpredictable changes of water availability organisms conquering land require desiccation tolerance mechanisms. Harholt et al. (2016) go even a step further, hypothesizing that charophycean green algal ancestors were already living on land for some time before the emergence of land plants. Their hypothesis is based on the idea that ancestral charophytes evolved their cell walls in response to the terrestrial selection pressure. However, this has to be seen critically, as strictly aquatic algae including chlorophytes have also evolved a complex cell wall modification machinery (e.g., Domozych et al., 2012). The occurrence of complex cell walls can thus not only be seen in connection with terrestrialization. Moreover, terrestrialization is not unique for charophytes evolutionary close to land plants, but also phylogenetic basal lineages contain terrestrial forms (e.g., chlorophytes like *Stichococcus*, *Trentepohlia*, *Apatococcus*, *Prasiola*).

Ecological differentiation has been suggested to trigger the formation of cryptic species in Klebsormidiales (Škaloud and Rindi, 2013). In this study, 14 lineages could be resolved based on

concatenated ITS rDNA + *rbcL* data sets with clear preferences for either natural subaerial substrata, artificial subaerial substrata or aquatic habitats. These results were interpreted as an evidence for the existence of a high number of cryptic species within morphospecies (Škaloud and Rindi, 2013). These investigations were expanded to a global scale study in the same genus, where in addition to the global ubiquity strong biogeographic patterns were revealed on a local scale (Ryšánek et al., 2015). Again, for the local fine-scale structuring of the genotypes habitat differentiation was suggested. In a recent study by Ryšánek et al. (2016) one of these ecological factors – the pH value (pH 4 to pH 8) of the substrate was investigated, and hypothesized as a potential important factor for sympatric speciation.

Survival in vegetative state, e.g., in form of ‘pre-akinetes’ in *Zygnuma* (Holzinger et al., 2009; Pichrtová et al., 2014a; Herburger et al., 2015) is important prerequisite for terrestrial life style. But also morphological features support this survival; One example is the holdfast of *Spirogyra* cells, which is preceded by callose deposition at the tip of developing rhizoids (Yamada et al., 2003). Branching is common in *Z. ericerorum* (Stancheva et al., 2014), and more complex morphologies can be observed in *Coleochaete*, still having the advantage of a small thallus (Leliaert et al., 2012). Structural simplicity might be advantageous in shallow and transient aquatic habitats, because even a thin film of water can provide enough room for coverage (Delwiche and Cooper, 2015). In addition, many species produce large amounts of mucilage with water holding capacities. The ultimate adaptation strategy to a terrestrial lifestyle is the sexual reproduction of Zygnematophyceae, which completely lacks flagellate stages and in the conjugation tube only gliding motility is necessary (Ikegaya et al., 2012).

In the present review, knowledge about stress tolerance mechanisms in Charophyta connected with life in terrestrial environment was summarized. We aimed to include insights derived from recent studies using omics techniques to investigate charophyte stress responses. A combination of methods will in future help to elucidate the stress tolerance that allows survival of this algal group under unfavorable conditions, and which key elements were responsible for the final transition to land.

AUTHOR CONTRIBUTIONS

All authors listed, have substantial, direct and intellectual contribution to the work, and approved it for publication.

ACKNOWLEDGMENT

This review article was supported by Austrian Science Fund (FWF) Project P 24242-B16 and FWF project I 1951-B16 to AH and by The Czech Science Foundation grant 15-34645 L to MP.

REFERENCES

- Agrawal, S. C. (2009). Factors affecting spore germination in algae - review. *Folia Microbiol.* 54, 273–302. doi: 10.1007/s12223-009-0047-0
- Aigner, S., Remias, D., Karsten, U., and Holzinger, A. (2013). Unusual phenolic compounds contribute to the ecophysiological performance in the purple-colored green alga *Zygogonium ericetorum* (Zygnematophyceae, Streptophyta) from a high-alpine habitat. *J. Phycol.* 49, 648–660. doi: 10.1111/jpy.12075
- Allen, A., and Alston, R. E. (1959). Formation of purple pigment in *Spirogyra pratensis* cultures. *Nature* 183, 1064–1065. doi: 10.1038/1831064b0
- Ashraf, M., and Godward, M. B. E. (1980). Ultrastructure and chemistry of the zygospore wall of *Spirogyra*. *Ann. Bot.* 46, 485–487.
- Becker, B. (2013). Snowball earth and the split of Streptophyta and Chlorophyta. *Trends Plant Sci.* 18, 180–183. doi: 10.1016/j.tplants.2012.09.010
- Becker, B., and Marin, B. (2009). Streptophyte algae and the origin of embryophytes. *Ann. Bot.* 103, 999–1004. doi: 10.1093/aob/mcp044
- Belnap, J., and Lange, O. L. (2001). *Biological Soil Crusts: Structure, Function and Management*. Berlin: Springer.
- Berry, H. A., and Lembi, C. A. (2000). Effects of temperature and irradiance on the seasonal variation of a *Spirogyra* (Chlorophyta) population in a midwestern lake (U.S.A.). *J. Phycol.* 36, 841–851. doi: 10.1046/j.1529-8817.2000.99138.x
- Bisson, M. A., and Kirst, G. O. (1995). Osmotic acclimation and turgor pressure regulation in algae. *Naturwissenschaften* 82, 461–471. doi: 10.1007/BF01131597
- Brosch-Salomon, S., Höftberger, M., Holzinger, A., and Lütz-Meindl, U. (1998). Ultrastructural localization of polysaccharides and N-acetyl-D-galactosamine in the secondary pathway of green algae (Desmidiaeae). *J. Exp. Bot.* 49, 145–153. doi: 10.1093/jxb/49.319.145
- Brown, L. M., and Hellebust, J. A. (1980). The contribution of organic solutes to osmotic balance in some green and eustigmatophyte algae. *J. Phycol.* 16, 265–270. doi: 10.1111/j.0022-3646.1980.00265.x
- Cannell, R. J., Farmer, P., and Walker, J. M. (1988). Purification and characterization of pentagalloylglucose, and alpha-glucosidase inhibitor/antibiotic from the freshwater green alga *Spirogyra varians*. *Biochem. J.* 255, 937–941. doi: 10.1042/bj2550937
- Carreto, J. I., and Carignan, M. O. (2011). Mycosporine-like amino acids: relevant secondary metabolites. Chemical and ecological aspects. *Marine Drugs* 9, 387–446. doi: 10.3390/med9030387
- Choi, J.-I., Yoon, M., Lim, S., Kim, G. H., and Park, H. (2015). Effect of gamma irradiation on physiological and proteomic changes of arctic *Zygnea* sp. (Chlorophyta, Zygnematales). *Phycologia* 54, 333–341. doi: 10.2216/14-106.1
- Coba, F., Aguilera, J., Figueroa, F. L., Gálvez, M. V., and Herrera, E. (2009). Antioxidant activity of mycosporine-like amino acids isolated from three red macroalgae and one marine lichen. *J. Appl. Phycol.* 21, 161–169. doi: 10.1007/s10811-008-9345-1
- Cockell, C. S., and Knowland, J. (1999). Ultraviolet radiation screening compounds. *Biol. Rev.* 74, 311–345. doi: 10.1111/j.1469-185X.1999.tb00189.x
- Darehshouri, A., and Lütz-Meindl, U. (2010). H₂O₂ localization in the green alga *Micrasterias* after salt and osmotic stress by TEM-coupled electron energy loss spectroscopy. *Protoplasma* 239, 49–56. doi: 10.1007/s00709-009-0081-4
- de Bakker, N. V. J., van Bodegom, P. M., van de Poll, W. H., Boelen, P., Nat, E., Rozema, J., et al. (2005). Is UV-B radiation affecting charophycean algae in shallow freshwater systems? *New Phytol.* 166, 957–966. doi: 10.1111/j.1469-8137.2005.01377.x
- de Vries, J., Stanton, A., Archibald, J. M., and Gould, S. B. (2016). Streptophyte terrestrialization in light of plastid evolution. *Trends Plant Sci.* doi: 10.1016/j.tplants.2016.01.021 [Epub ahead of print].
- Delaux, P.-M., Radhakrishnan, G. V., Jayaraman, D., Cheema, J., Malbreil, M., Volkenning, J. D., et al. (2015). Algal ancestors of land plants was prepared for symbiosis. *Proc. Natl. Acad. Sci. U.S.A.* 112, 13390–13395. doi: 10.1073/pnas.1515426112
- Delwiche, C. F., and Cooper, E. D. (2015). The evolutionary origin of a terrestrial flora. *Curr. Biol.* 25, R899–R910. doi: 10.1016/j.cub.2015.08.029
- Delwiche, C. F., Graham, L. E., and Thomson, N. (1989). Lignin-like compounds and sporopollenin in *Coleochaete*, an algal model for land plant ancestry. *Science* 245, 399–401. doi: 10.1126/science.245.4916.399
- Domozych, D. S., Ciancia, M., Fangel, J. U., Mikkelsen, M. D., Ulvskov, P., and Willats, W. G. T. (2012). The cell walls of green algae: a journey through evolution and diversity. *Front. Plant Sci.* 3:82. doi: 10.3389/fpls.2012.0008210.3389/fpls.2012.00082
- Domozych, D. S., and Domozych, C. E. (2014). Multicellularity in green algae: upsizing in a walled complex. *Front. Plant Sci.* 5:649. doi: 10.3389/fpls.2014.00649
- Domozych, D. S., and Rogers-Domozych, C. (1993). Mucilage processing and secretion in the green alga *Cladophora* II. Ultrastructure and immunocytochemistry. *J. Phycol.* 29, 659–667. doi: 10.1111/j.0022-3646.1993.00659.x
- Domozych, D. S., Serfis, A., Kiemle, S. N., and Gretz, M. R. (2007). The structure and biochemistry of charophycean cell walls. I. Pectins of *Pennium margaritaceum*. *Protoplasma* 230, 99–115. doi: 10.1007/s00709-006-0197-8
- Eder, M., and Lütz-Meindl, U. (2010). Analyses and localization of pectin-like carbohydrates in cell wall and mucilage of the green alga *Netrium digitus*. *Protoplasma* 243, 25–38. doi: 10.1007/s00709-009-0040-0
- Eder, M., Tenhaken, R., Driouch, A., and Lütz-Meindl, U. (2008). Occurrence and characterization of arabinogalactan-like proteins and hemicelluloses in *Micrasterias* (Streptophyta). *J. Phycol.* 44, 1221–1234. doi: 10.1111/j.1529-8817.2008.00576.x
- Elster, J., Degma, P., Kovacik, L., Valentova, L., Sramkova, K., and Pereira, B. (2008). Freezing and desiccation injury resistance in the filamentous green alga *Klebsormidium* from Antarctic, Arctic Slovakia. *Biologie* 63, 839–847.
- Fernandez-Marin, B., Holzinger, A., and Garcia-Plazaola, J. I. (2016). “Photosynthetic strategies of desiccation-tolerant organisms,” in *Handbook of Photosynthesis*, 3rd Edn, Chap. 38, ed. M. Pessarakli (Boca Raton, FL: CRC Press), 719–737.
- Field, K. J., Pressel, S., Duckett, J. G., Rimington, W. R., and Bidartondo, M. I. (2015). Symbiotic options for the conquest of land. *Trends Ecol. Evol.* 30, 477–486. doi: 10.1016/j.tree.2015.05.007
- Figueroa, F. L., Korbee, N., Carillo, P., Medina-Sanchez, J. M., Mata, M., Bonomi, J., et al. (2009). The effects of UV radiation on photosynthesis estimated as chlorophyll fluorescence in *Zygneropsis decussata* (Chlorophyta) growing in a high mountain lake (Sierra Nevada, Southern Spain). *J. Limnol.* 68, 206–216.
- Fuller, C. (2013). *Examining Morphological and Physiological Changes in Zygnea Irregular During A Desiccation and Recovery Period*. Master's thesis, California State University, San Marcos CA.
- Germ, M., Kreft, I., and Gaberščík, A. (2009). UV-B radiation and selenium affected energy availability in green alga *Zygnea*. *Biologia* 64, 676–679. doi: 10.2478/s11756-009-0062-2
- Gerotto, C., and Morosinotto, T. (2013). Evolution of photoprotection mechanisms upon land colonization: evidences of PSBS dependent NPQ in late Streptophyte algae. *Physiol. Plant* 149, 583–598. doi: 10.1111/ppl.12070
- Graham, J. M., Lembi, C. A., Adrian, H. L., and Spencer, D. F. (1995). Physiological responses to temperature and irradiance in *Spirogyra* (Zygnematales, Charophyceae). *J. Phycol.* 31, 531–540. doi: 10.1111/j.1529-8817.1995.tb02546.x
- Graham, L. E., Arancibia-Avila, P., Taylor, W. A., Strother, P. K., and Cook, M. E. (2012). Aeroterrestrial *Coleochaete* (Streptophyta, Coleochaetales) models early plant adaptation to land. *Am. J. Bot.* 99, 130–144. doi: 10.3732/ajb.1100245
- Graham, L. E., Cook, M. E., and Busse, J. S. (2000). The origin of plants: body plan changes contributing to a major evolutionary radiation. *Proc. Natl. Acad. Sci. U.S.A.* 97, 4535–4540. doi: 10.1073/pnas.97.9.4535
- Graham, L. E., Lewis, L. A., Taylor, W., Wellman, C., and Cook, M. E. (2013). “Early terrestrialization: transition from algal to bryophyte grade,” in *Advances in Photosynthesis and Respiration*, eds Hanson and S. Rice (Dordrecht: Springer), 9–28.
- Gustavs, L., Eggert, A., Michalik, D., and Karsten, U. (2010). Physiological and biochemical responses of green microalgae from different habitats to osmotic and matric stress. *Protoplasma* 243, 3–14. doi: 10.1007/s00709-009-0060-9
- Harholt, J., Moestrup, O., and Ulvskov, P. (2016). Why plants were terrestrial from the beginning. *Trends Plant Sci.* 21, 96–101. doi: 10.1016/j.tplants.2015.11.010
- Hawes, I. (1990). Effects of freezing and thawing on a species of *Zygnea* (Chlorophyta) from the Antarctic. *Phycologia* 29, 326–331. doi: 10.2216/10031-8884-29-3-326.1
- Herburger, K., and Holzinger, A. (2015). Localization and quantification of callose in the streptophyte green algae *Zygnea* and *Klebsormidium*: correlation with desiccation tolerance. *Plant Cell Physiol.* 56, 2259–2270. doi: 10.1093/pcp/pcv139

- Herburger, K., Karsten, U., and Holzinger, A. (2016a). *Entransia* and *Hormidiella*, sister lineages of *Klebsormidium* (Streptophyta), respond differently to light, temperature and desiccation stress. *Protoplasma* doi: 10.1007/s00709-015-0889-z [Epub ahead of print].
- Herburger, K., Remias, D., and Holzinger, A. (2016b). The green alga *Zygogonium ericetorum* (Zygnematophyceae, Charophyta) shows high iron and aluminium tolerance: protection mechanisms and photosynthetic performance. *FEMS Microbiol. Ecol.*
- Herburger, K., Lewis, L. A., and Holzinger, A. (2015). Photosynthetic efficiency, desiccation tolerance and ultrastructure in two phylogenetically distinct strains of alpine *Zygnuma* sp. (Zygnematophyceae, Streptophyta): role of pre-akinete formation. *Protoplasma* 252, 571–589. doi: 10.1007/s00709-014-0703-3
- Holzinger, A., and Becker, B. (2015). Desiccation tolerance in the streptophyte green alga *Klebsormidium*: the role of phytohormones. *Comm. Integr. Biol.* 8:e1059978. doi: 10.1080/19420889.2015.1059978
- Holzinger, A., Kaplan, F., Blaas, K., Zechmann, B., Komsic-Buchmann, K., and Becker, B. (2014). Transcriptomics of desiccation tolerance in the streptophyte green alga *Klebsormidium* reveal a land plant-like defense. *PLoS ONE* 9:e110630. doi: 10.1371/journal.pone.0110630
- Holzinger, A., and Karsten, U. (2013). Desiccation stress and tolerance in green algae: consequences for ultrastructure, physiological and molecular mechanisms. *Front. Plant Sci.* 4:327. doi: 10.3389/fpls.2013.00327
- Holzinger, A., and Lütz, C. (2006). Algae and UV irradiation: effects on ultrastructure and related metabolic functions. *Micron* 37, 190–207. doi: 10.1016/j.micron.2005.10.015
- Holzinger, A., Roleda, M. Y., and Lütz, C. (2009). The vegetative arctic green alga *Zygnuma* is insensitive to experimental UV exposure. *Micron* 40, 831–838. doi: 10.1016/j.micron.2009.06.008
- Holzinger, A., Tschaikner, A., and Remias, D. (2010). Cytoarchitecture of the desiccation-tolerant green alga *Zygogonium ericetorum*. *Protoplasma* 243, 15–24. doi: 10.1007/s00709-009-0048-5
- Hoppert, M., Reimer, R., Kemmling, A., Schröder, A., Günzl, B., and Heinenk, T. (2004). Structure and reactivity of a biological soil crust from a xeric sandy soil in central Europe. *Geomicrobiol. J.* 21, 183–191. doi: 10.1080/01490490275433
- Hori, K., Maruyama, F., Fujisawa, T., Togashi, T., Yamamoto, N., Seo, M., et al. (2014). *Klebsormidium flaccidum* genome reveals primary factors for plant terrestrial adaptation. *Nat. Comm.* 5:3978. doi: 10.1038/ncomms4978
- Ikegaya, H., Nakase, T., Iwata, K., Tsuchida, H., Sonobe, S., and Shimmen, T. (2012). Studies on conjugation of *Spirogyra* using monoclonal culture. *J. Plant Res.* 125, 457–464. doi: 10.1007/s10265-011-0457-3
- Ju, C., Van de Poel, B., Cooper, E. D., Thierer, J. H., Gibbons, T. R., Delwiche, C. F., et al. (2015). Conservation of ethylene as a plant hormone over 450 million years of evolution. *Nat. Plants* 1:14004. doi: 10.1038/nplants.2014.4
- Kadlubowska, J. Z. (1984). "Conjugatophyceae I: chlorophyta VIII: zygnemales," in *Süßwasserflora von Mitteleuropa, Band 16*, eds H. Ettr, J. Gerloff, H. Heyning, and D. Mollenhauer (Jena: Gustav Fisher), 1–532.
- Kaplan, F., Lewis, L. A., Herburger, K., and Holzinger, A. (2013). Osmotic stress in the arctic and antarctic green alga *Zygnuma* sp. (Zygnematales, Streptophyta): effects on photosynthesis and ultrastructure. *Micron* 44, 317–330. doi: 10.1016/j.micron.2012.08.004
- Kaplan, F., Lewis, L. A., Wastian, J., and Holzinger, A. (2012). Plasmolysis effects and osmotic potential of two phylogenetically distinct alpine strains of *Klebsormidium* (Streptophyta). *Protoplasma* 249, 789–804. doi: 10.1007/s00709-011-0324-z
- Karsten, U., Herburger, K., and Holzinger, A. (2014). Dehydration, temperature and light tolerance in members of the aeroterrestrial green algal genus *Interfilum* (Streptophyta) from biogeographically different temperate soils. *J. Phycol.* 50, 804–816. doi: 10.1111/jpy.12210
- Karsten, U., Herburger, K., and Holzinger, A. (2015). Living in biological soil crust communities of African deserts – physiological traits of green algal *Klebsormidium* species (Streptophyta) to cope with desiccation, light and temperature gradients. *J. Plant Physiol.* doi: 10.1016/j.jplph.2015.09.002 [Epub ahead of print].
- Karsten, U., and Holzinger, A. (2012). Light, temperature and desiccation effects on photosynthetic activity, and drought-induced ultrastructural changes in the green alga *Klebsormidium dissectum* (Streptophyta) from a high alpine soil crust. *Microp. Ecol.* 63, 51–63. doi: 10.1007/s00248-011-9924-6
- Karsten, U., and Holzinger, A. (2014). Green algae in alpine biological soil crust communities: acclimation strategies against ultraviolet radiation and dehydration. *Biodivers. Conserv.* 23, 1845–1858. doi: 10.1007/s10531-014-0653-2
- Karsten, U., Lütz, C., and Holzinger, A. (2010). Ecophysiological performance of the aeroterrestrial green alga *Klebsormidium crenulatum* (Klebsormidiophyceae, Streptophyta) isolated from an alpine soil crust with an emphasis on desiccation stress. *J. Phycol.* 46, 1187–1197. doi: 10.1111/j.1529-8817.2010.00921.x
- Karsten, U., Pröschold, T., Mikhaiyluk, T., and Holzinger, A. (2013). Photosynthetic performance of different genotypes of the green alga *Klebsormidium* sp. (Streptophyta) isolated from biological soil crusts of the Alps. *Algol. Stud.* 142, 45–62. doi: 10.1127/1864-1318/2013/0102
- Karsten, U., and Rindi, F. (2010). Ecophysiological performance of an urban strain of the aeroterrestrial green alga *Klebsormidium* sp. (Klebsormidiaceae, Klebsormidiophyceae). *Eur. J. Phycol.* 45, 426–435. doi: 10.1080/09670262.2010.498587
- Kim, G. H., Yoon, M., and Klochova, T. A. (2005). A moving mat: phototaxis in the filamentous green algae *Spirogyra* (Chlorophyta, Zygnemataceae). *J. Phycol.* 41, 232–237. doi: 10.1111/j.1529-8817.2005.03234.x
- Kitzing, C., and Karsten, U. (2015). UV-induced effects on optimum quantum yield and sunscreen contents in members of the genera *Interfilum*, *Klebsormidium*, *Hormidiella* and *Entransia* (Klebsormidiophyceae, Streptophyta). *Eur. J. Phycol.* 50, 279–287. doi: 10.1080/09670262.2015.1031190
- Kitzing, C., Pröschold, T., and Karsten, U. (2014). UV-induced effects on growth, photosynthetic performance and sunscreen contents in different populations of the green alga *Klebsormidium fluitans* (Streptophyta) from alpine soil crusts. *Microp. Ecol.* 67, 327–340. doi: 10.1007/s00248-013-0317-x
- Knack, J. J., Wilcox, L. W., Delaux, P.-M., Ané, J.-M., Piotrowski, M. J., Cook, M. E., et al. (2015). Microbiomes of streptophyte algae and bryophytes suggest that a functional suite of microbiota fostered plant colonization of land. *Int. J. Plant Sci.* 176, 405–420. doi: 10.1086/681161
- Kranner, I., Beckett, R., Hochman, A., and Nash, T. H. I. I. (2008). Desiccation-tolerance in lichens: a review. *Bryologist* 111, 576–593. doi: 10.1639/0007-2745-111.4.576
- Kroken, S. B., Graham, L. E., and Cook, M. E. (1996). Occurrence and evolutionary significance of resistant cell walls in charophytes and bryophytes. *Am. J. Bot.* 83, 1241–1254. doi: 10.2307/2446108
- Küster, A., Schaible, R., and Schubert, H. (2000). Light acclimation of the charophyte *Lamprothamnium papulosum*. *Aquat. Bot.* 68, 205–216. doi: 10.1016/S0304-3770(00)00122-4
- Lajos, K., Mayr, S., Buchner, O., and Holzinger, A. (2016). A new microscopic method to analyse desiccation induced volume changes in aeroterrestrial green algae. *J. Microsc.* doi: 10.1111/jmi.12409 [Epub ahead of print].
- Leliaert, F., Smith, D. R., Moreau, H., Herron, M. D., Verbruggen, H., Delchiche, C. F., et al. (2012). Phylogeny and molecular evolution of green algae. *Crit. Rev. Plant Sci.* 31, 1–46. doi: 10.1080/07352689.2011.615705
- Lewis, L. A., and McCourt, R. M. (2004). Green algae and the origin of land plants. *Am. J. Bot.* 91, 1535–1556. doi: 10.3732/ajb.91.10.1535
- Lütz, C., Seidlitz, H. K., and Meindl, U. (1997). Physiological and structural changes in the chloroplast of the green alga *Micrasterias denticulata* induced by UV-B simulation. *Plant Ecol.* 128, 54–64.
- Lütz-Meindl, U., Luckner, M., Andosch, A., and Wanner, G. (2015). Structural stress responses and degradation of dictyosomes in algae analysed by TEM and FIB-SEM tomography. *J. Microsc.* doi: 10.1111/jmi.12369 [Epub ahead of print].
- Meindl, U., and Lütz, C. (1996). Effects of UV irradiation on cell development and ultrastructure of the green alga *Micrasterias*. *J. Photochem. Photobiol. B Biol.* 36, 285–292. doi: 10.1016/S1011-1344(96)07395-2
- Meindl, U., Wittmann-Pinegger, D., and Kiermayer, O. (1989). Cell multiplication and ultrastructure of *Micrasterias denticulata* (Desmidiae) grown under salt stress. *Plant Syst. Evol.* 164, 197–208. doi: 10.1007/BF00940437
- Mikhailuk, T., Holzinger, A., Massalski, A., and Karsten, U. (2014). Morphology and ultrastructure of *Interfilum* and *Klebsormidium* (Klebsormidiaceae, Streptophyta) with special reference to cell division and thallus formation. *Eur. J. Phycol.* 49, 395–412. doi: 10.1080/09670262.2014.949308
- Mikkelsen, M. D., Harholt, J., Ulvskov, P., Johansen, I. E., Fangel, J. U., Doblin, M. S., et al. (2014). Evidence for land plant cell wall biosynthetic mechanisms in charophyte green algae. *Ann. Bot.* 114, 1217–1236. doi: 10.1093/aob/mcu171

- Morison, M., and Sheath, R. (1985). Response to desiccation stress by *Klebsormidium rivulare* (Ulotrichales, Chlorophyta) from a Rhode Island stream. *Phycologia* 24, 129–145. doi: 10.2216/10031-8884-24-2-129.1
- Nagao, M., Matsui, K., and Uemura, M. (2008). *Klebsormidium flaccidum*, a charophycean green alga, exhibits cold acclimation that is closely associated with compatible solute accumulation and ultrastructural changes. *Plant Cell Environ.* 31, 872–885. doi: 10.1111/j.1365-3040.2008.01804.x
- Nagao, M., and Uemura, M. (2012). Sucrose phosphate phosphatase in the green alga *Klebsormidium flaccidum* (Streptophyta) lacks an extensive C-terminal domain and differs from that of land plants. *Planta* 235, 851–861. doi: 10.1007/s00425-011-1550-5
- Neustupa, J., Eliáš, M., and Šejnohová, L. (2007). A taxonomic study of two *Stichococcus* species (Trebouxiophyceae, Chlorophyta) with a starch-enveloped pyrenoid. *Nova Hedwigia* 84, 51–63. doi: 10.1127/0029-5035/2007/0084-0051
- Newsome, A. G., Murphy, B. T., and van Breemen, R. B. (2013). Isolation and characterization of natural blue pigments from underexplored sources. *Phys. Method Food Anal.* 1138, 105–125. doi: 10.1021/bk-2013-1138.ch008
- Nishizawa, M., Yamagishi, T., Nonaka, G.-I., Nishioka, I., and Ragan, M. A. (1985). Gallotannins of the freshwater green alga *Spirogyra* sp. *Phytochemistry* 24, 2411–2413. doi: 10.1016/S0031-9422(00)83053-8
- Oertel, A., Aichinger, N., Hochreiter, R., Thalhammer, J., and Lütz-Meindl, U. (2004). Analysis of mucilage secretion and excretion in *Micrasterias* (Chlorophyta) by means of immunoelectron microscopy and digital time lapse video microscopy. *J. Phycol.* 40, 711–720. doi: 10.1111/j.1529-8817.2004.03222.x
- Oren, A. (2007). “Diversity of organic osmotic compounds and osmotic adaptation in cyanobacteria and algae,” in *Algae and Cyanobacteria in Extreme Environments*, ed. J. Seckbach (Berlin: Springer), 639–655.
- O’Rourke, C., Gregson, T., Murray, L., Sadler, I. H., and Fry, S. C. (2015). Sugar composition of the pectic polysaccharides of charophytes, the closest algal relatives of land-plants: presence of 3-O-methyl-D-galactose residues. *Ann. Bot.* 116, 225–236. doi: 10.1093/aob/mcv089
- Pichrtová, M., Arc, E., Stögg, W., Kranner, I., Hájek, T., Hackl, H., et al. (2016a). Formation of lipid bodies and fatty acid composition changes upon pre-akinetes formation in arctic and Antarctic *Zygnuma* (Zygnematophyceae, Streptophyta) strains. *FEMS Microbiol. Ecol.* doi: 10.1093/femsec/fiw096
- Pichrtová, M., Hájek, T., and Elster, J. (2014a). Osmotic stress and recovery in field populations of *Zygnuma* sp. (Zygnematophyceae, Streptophyta) on Svalbard (High Arctic) subjected to natural desiccation. *FEMS Microbiol. Ecol.* 89, 270–280. doi: 10.1111/1574-6941.12288
- Pichrtová, M., Hájek, T., and Elster, J. (2016b). Annual development of mat-forming conjugating green algae *Zygnuma* spp. in hydroterrestrial habitats in the Arctic. *Polar Biol.*
- Pichrtová, M., Kulichová, J., and Holzinger, A. (2014b). Nitrogen limitation and slow drying induce desiccation tolerance in conjugating green algae (Zygnematophyceae) from polar habitats. *PLoS ONE* 9:e113137. doi: 10.1371/journal.pone.0113137
- Pichrtová, M., Remias, D., Lewis, L., and Holzinger, A. (2013). Changes in phenolic compounds and cellular ultrastructure of Arctic and Antarctic strains of *Zygnuma* (Zygnematophyceae, Streptophyta) after exposure to experimentally enhanced UV to PAR ratio. *Micr. Ecol.* 65, 68–83. doi: 10.1007/s00248-012-0096-9
- Popper, Z. A., Michel, G., Herve, C., Domozych, D. S., Willats, W. G. T., Tuohy, M. G., et al. (2011). Evolution and diversity of plant cell walls: from algae to flowering plants. *Annu. Rev. Plant Biol.* 62, 567–590. doi: 10.1146/annurev-arplant-042110-103809
- Popper, Z. A., Ralet, M. C., and Domozych, D. S. (2014). Plant and algal cell walls: diversity and functionality. *Ann. Bot.* 114, 1043–1048. doi: 10.1093/aob/mcu214
- Popper, Z. A., and Tuohy, M. G. (2010). Beyond the green: understanding the evolutionary puzzle of plant and algal cell walls. *Plant Physiol.* 153, 373–383. doi: 10.1104/pp.110.158055
- Pouličková, A., Žižka, Z., Hašler, P., and Benada, O. (2007). Zygnematalean zygospores: morphological features and use in species identification. *Folia Microbiol.* 52, 135–145. doi: 10.1007/BF02932152
- Proctor, V. W. (1967). Storage and germination of *Chara* oospores. *J. Phycol.* 3, 90–92. doi: 10.1111/j.1529-8817.1967.tb04638.x
- Remias, D., Holzinger, A., Aigner, S., and Lütz, C. (2012a). Ecophysiology and ultrastructure of *Ancylonema nordenstkiöldii* (Zygnematales, Streptophyta), causing brown ice on glaciers in Svalbard (high arctic). *Polar Biol.* 35, 899–908. doi: 10.1007/s00300-011-1135-6
- Remias, D., Holzinger, A., and Lütz, C. (2009). Ultrastructure and physiological characterization of the ice alga *Mesotaenium berggrenii* (Zygnematophyceae, Chlorophyta) from glaciers in the European Alps. *Phycologia* 48, 302–312. doi: 10.2216/08-13.1
- Remias, D., Schwaiger, S., Aigner, S., Leya, T., Stuppner, H., and Lütz, C. (2012b). Characterization of an UV- and VIS-absorbing, purpurogallin-derived secondary pigment new to algae and highly abundant in *Mesotaenium berggrenii* (Zygnematophyceae, Chlorophyta), an extremophile living on glaciers. *FEMS Microbiol. Ecol.* 79, 638–648. doi: 10.1111/j.1574-6941.2011.01245.x
- Roach, T., and Krieger-Liszka, A. (2014). Regulation of photosynthetic electron transport and photoinhibition. *Curr. Prot. Pept. Sci.* 15, 351–362. doi: 10.2174/138920371566140327105143
- Ryšánek, D., Holzinger, A., and Škaloud, P. (2016). Influence of substrate and pH on the diversity of aeroterrrestrial alga *Klebsormidium* (Klebsormidales, Streptophyta): a potentially important factor for sympatric speciation. *Phycologia* doi: 10.2216/15-110.1
- Ryšánek, D., Hrèková, K., and Škaloud, P. (2015). Global ubiquity and local endemism of free-living terrestrial protists: phylogeographic assessment of the streptophyte alga *Klebsormidium*. *Environ. Microbiol.* 17, 689–698. doi: 10.1111/1462-2920.12501
- Sederias, J., and Colman, B. (2007). The interaction of light and low temperature on breaking the dormancy of *Chara vulgaris* oospores. *Aquat. Bot.* 87, 229–234. doi: 10.1016/j.aquabot.2007.06.008
- Sharma, N., Rai, A., Singh, S., and Brown, R. (2007). Airborne algae: their present status and relevance. *J. Phycol.* 43, 615–627. doi: 10.1111/j.1529-8817.2007.00373.x
- Shick, J. M., and Dunlap, W. C. (2002). Mycosporine-like amino acids and related gadusols: biosynthesis, accumulation, and UV-protective functions in aquatic organisms. *Ann. Rev. Physiol.* 64, 223–262. doi: 10.1146/annurev.physiol.64.081501.155802
- Škaloud, P. (2009). Species composition and diversity of aero-terrestrial algae and cyanobacteria of the Boreè Hill ventaroles. *Fottea* 9, 65–80.
- Škaloud, P., and Rindi, F. (2013). Ecological differentiation of cryptic species within an asexual protist morphospecies: case study of filamentous green alga *Klebsormidium* (Streptophyta). *J. Eukaryot. Microbiol.* 60, 350–362. doi: 10.1111/jeu.12040
- Sørensen, I., Pettolino, F. A., Bacic, A., Ralph, J., Lu, F., O’Neill, M. A., et al. (2011). The charophycean green algae provide insights into the early origins of plant cell walls. *Plant J.* 68, 201–211. doi: 10.1111/j.1365-313X.2011.04686.x
- Sørensen, I., Rose, J. K. C., Doyle, J. D., Domozych, D. S., and Willats, G. T. (2012). The charophycean green algae as model systems to study plant cell walls and other evolutionary adaptations that gave rise to land plants. *Plant Sign. Behav.* 7, 1–3. doi: 10.4161/psb.7.1.18574
- Stamenković, M., Bischof, K., and Hanelt, D. (2014). Xanthophyll cycle pool size and composition in several *Cosmarium* strains (Zygnematophyceae, Streptophyta) are related to their geographic distribution patterns. *Protoist* 165, 14–30. doi: 10.1016/j.protis.2013.10.002
- Stamenković, M., and Hanelt, D. (2011). Growth and photosynthetic characteristics of several *Cosmarium* strains (Zygnematophyceae, Streptophyta) isolated from various geographic regions under a constant light-temperature regime. *Aquat. Ecol.* 45, 455–472. doi: 10.1007/s10452-011-9367-7
- Stamenković, M., and Hanelt, D. (2014). Sensitivity of photosynthesis to UV radiation in sensitivity of photosynthesis to UV radiation in several *Cosmarium* strains (Zygnematophyceae, Streptophyta) is related to their geographic distribution. *Photochem. Photobiol. Sci.* 13, 1066–1081. doi: 10.1039/c3pp50192b
- Stancheva, R., Hall, J. D., Herburger, K., Lewis, L. A., McCourt, R. M., Sheath, R. G., et al. (2014). Phylogenetic position of *Zygogonium ericetorum* (Zygnematophyceae, Charophyta) from a high alpine habitat and ultrastructural characterization of unusual aplanospores. *J. Phycol.* 50, 790–803. doi: 10.1111/jpy.12229
- Stancheva, R., Hall, J. D., McCourt, R. M., and Sheath, R. G. (2013). Identity and phylogenetic placement of *Spirogyra* species (Zygnematophyceae,

- Charophyta) from California streams and elsewhere. *J. Phycol.* 49, 588–607. doi: 10.1111/jphy.12070
- Stancheva, R., Herburger, K., Sheath, R. G., and Holzinger, A. (2016). Conjugation morphology of *Zygogonium ericetorum* (Zygnematophyceae, Charophyta) from a high alpine habitat. *J. Phycol.* 52, 131–134. doi: 10.1111/jphy.12363
- Stancheva, R., Sheath, R. G., and Hall, J. D. (2012). Systematics of the genus *Zygnema* (Zygnematophyceae, Charophyta) from Californian watersheds. *J. Phycol.* 48, 409–422. doi: 10.1111/j.1529-8817.2012.01127.x
- Štástný, J. (2010). Desmids (Conjugatophyceae, Viridiplantae) from the Czech Republic; new and rare taxa, distribution, ecology. *Fottea* 10, 1–74.
- Stibal, M., Šabacká, M., and Žáráský, J. (2012). Biological processes on glacier and ice sheet surfaces. *Nature Geoscience* 5, 771–774. doi: 10.1038/ngeo1611
- Thangaraj, G. (2016). Antarctic strain of green filamentous alga *Zygnema* sp. shows a high resistance to photoinhibition under simulated polar conditions. *Czech Polar Rep.* 5, 176–184. doi: 10.5817/CPR2015-2-15
- Timme, R. E., Bachvaroff, T. R., and Delwiche, C. F. (2012). Broad phylogenomic sampling and the sister lineage of land plants. *PLoS ONE* 7:e29696. doi: 10.1371/journal.pone.0029696
- Timme, R. E., and Delwiche, C. F. (2010). Uncovering the evolutionary origin of plant molecular processes: comparison of *Coleochaete* (Coleochaetales) and *Spirogyra* (Zygnematales) transcriptomes. *BMC Plant Biol.* 10:96. doi: 10.1186/1471-2229-10-96
- Versteegh, G. J. M., and Blokker, P. (2004). Resistant macromolecules of extant and fossil microalgae. *Phycol. Res.* 52, 325–339. doi: 10.1111/j.1440-1835.2004.tb00342.x
- Vieira, J., and Necchi, O. (2003). Photosynthetic characteristics of charophytes from tropical lotic ecosystems. *Phycol. Res.* 51, 51–60. doi: 10.1111/j.1440-1835.2003.tb00170.x
- Vilumbrales, D. M., Skácelová, K., and Barták, M. (2013). Sensitivity of Antarctic freshwater algae to salt stress assessed by fast chlorophyll fluorescence transient. *Czech Polar Rep.* 3, 163–172. doi: 10.5817/CPR2013-2-17
- Wanner, G., Schäfer, T., and Lütz-Meindl, U. (2013). 3-D analysis of dictyosomes and multivesicular bodies in the green alga *Micrasterias denticulata* by FIB/SEM tomography. *J. Struct. Biol.* 184, 203–211. doi: 10.1016/j.jsb.2013.10.003
- Welsh, D. (2000). Ecological significance of compatible solute accumulation by micro organisms: from single cells to global climate. *FEMS Microbiol. Rev.* 24, 263–290. doi: 10.1111/j.1574-6976.2000.tb00542.x
- Weng, J.-K., and Chapple, C. (2010). The origin and evolution of lignin biosynthesis. *New Phytol.* 187, 273–285. doi: 10.1111/j.1469-8137.2010.03327.x
- Wickett, N. J., Mirarab, S., Nguyen, N., Warnow, T., Carpenter, E., Matasci, N., et al. (2014). Phylogenomic analysis of the origin and early diversification of land plants. *Proc. Natl. Acad. Sci. U.S.A.* 111, E4859–E4868. doi: 10.1073/pnas.1323926111
- Wodniok, S., Brinkmann, H., Glöckner, G., Heidel, A. J., Philippe, H., Melkonian, M., et al. (2011). Origin of land plants: do conjugating green algae hold the key? *BMC Evol. Biol.* 11:104. doi: 10.1186/1471-2148-11-104
- Yamada, S., Sonobe, S., and Shimmen, T. (2003). Synthesis of a callosic substance during rhizoid differentiation in *Spirogyra*. *Plant Cell Physiol.* 44, 1225–1228. doi: 10.1093/pcp/pcg152
- Yancey, P. (2005). Organic osmolytes as compatible, metabolic and counteracting cytoprotectants in high osmolarity and other stresses. *J. Exp. Biol.* 208, 2819–2830. doi: 10.1242/jeb.01730
- Yin, Y., John, M. A., Cao, H., and Rupani, M. (2014). A survey of plant and algal genomes and transcriptomes reveals new insights into the evolution and function of the cellulose synthase superfamily. *BMC Genomics* 15:260. doi: 10.1186/1471-2164-15-260
- Zhong, B., Sun, L., and Penny, D. (2015). The origin of land plants: a phylogenomic perspective. *Evol. Bioinform.* 11, 137–141. doi: 10.4137/EBO.S29089
- Zhong, B., Xi, Z., Goremykin, V. V., Fong, R., McLenahan, P. A., Novis, P. M., et al. (2014). Streptophyte algae and the origin of land plants revisited using heterogeneous models with three new algal chloroplast genomes. *Mol. Biol. Evol.* 31, 177–183. doi: 10.1093/molbev/mst200

Conflict of Interest Statement: The authors declare that the research was conducted in the absence of any commercial or financial relationships that could be construed as a potential conflict of interest.

Copyright © 2016 Holzinger and Pichrtová. This is an open-access article distributed under the terms of the Creative Commons Attribution License (CC BY). The use, distribution or reproduction in other forums is permitted, provided the original author(s) or licensor are credited and that the original publication in this journal is cited, in accordance with accepted academic practice. No use, distribution or reproduction is permitted which does not comply with these terms.



Multi-Scale Characean Experimental System: From Electrophysiology of Membrane Transporters to Cell-to-Cell Connectivity, Cytoplasmic Streaming and Auxin Metabolism

Mary J. Beilby*

School of Physics, The University of New South Wales, Sydney, NSW, Australia

OPEN ACCESS

Edited by:

David Domozych,
Skidmore College, USA

Reviewed by:

Tomomichi Fujita,
Hokkaido University, Japan

Sven B. Gould,
Heinrich Heine University Düsseldorf,
Germany

***Correspondence:**

Mary J. Beilby
m.j.beilby@unsw.edu.au

Specialty section:

This article was submitted to
Plant Evolution and Development,
a section of the journal
Frontiers in Plant Science

Received: 13 April 2016

Accepted: 05 July 2016

Published: 25 July 2016

Citation:

Beilby MJ (2016) Multi-Scale Characean Experimental System: From Electrophysiology of Membrane Transporters to Cell-to-Cell Connectivity, Cytoplasmic Streaming and Auxin Metabolism. *Front. Plant Sci.* 7:1052.
doi: 10.3389/fpls.2016.01052

The morphology of characean algae could be mistaken for a higher plant: stem-like axes with leaf-like branchlets anchored in the soil by root-like rhizoids. However, all of these structures are made up of giant multinucleate cells separated by multicellular nodal complexes. The excised internodal cells survive long enough for the nodes to give rise to new thallus. The size of the internodes and their thick cytoplasmic layer minimize impalement injury and allow specific micro-electrode placement. The cell structure can be manipulated by centrifugation, perfusion of cell contents or creation of cytoplasmic droplets, allowing access to both vacuolar and cytoplasmic compartments and both sides of the cell membranes. Thousands of electrical measurements on intact or altered cells and cytoplasmic droplets laid down basis to modern plant electrophysiology. Furthermore, the giant internodal cells and whole thalli facilitate research into many other plant properties. As nutrients have to be transported from rhizoids to growing parts of the thallus and hormonal signals need to pass from cell to cell, Characeae possess very fast cytoplasmic streaming. The mechanism was resolved in the characean model. Plasmodesmata between the internodal cells and nodal complexes facilitate transport of ions, nutrients and photosynthates across the nodes. The internal structure was found to be similar to those of higher plants. Recent experiments suggest a strong circadian influence on metabolic pathways producing indole-3-acetic acid (IAA) and serotonin/melatonin. The review will discuss the impact of the characean models arising from fragments of cells, single cells, cell-to-cell transport or whole thalli on understanding of plant evolution and physiology.

Keywords: Characeae, cell-to-cell transport, cytoplasmic droplets, cytoplasmic streaming, metabolic pathways, plasma membrane transporters, plasmodesmata, tonoplast transporters

INTRODUCTION

From all the charophytes, Characeae morphology appears most similar to embryophytes (land plants). The thallus consists of axial stem with leaf-like side branches and is anchored in the soil by root-like rhizoids. However, all these structures are made from large single cells with multiple nuclei, connected by nodal complexes consisting from small cells with single nuclei (**Figure 1**).

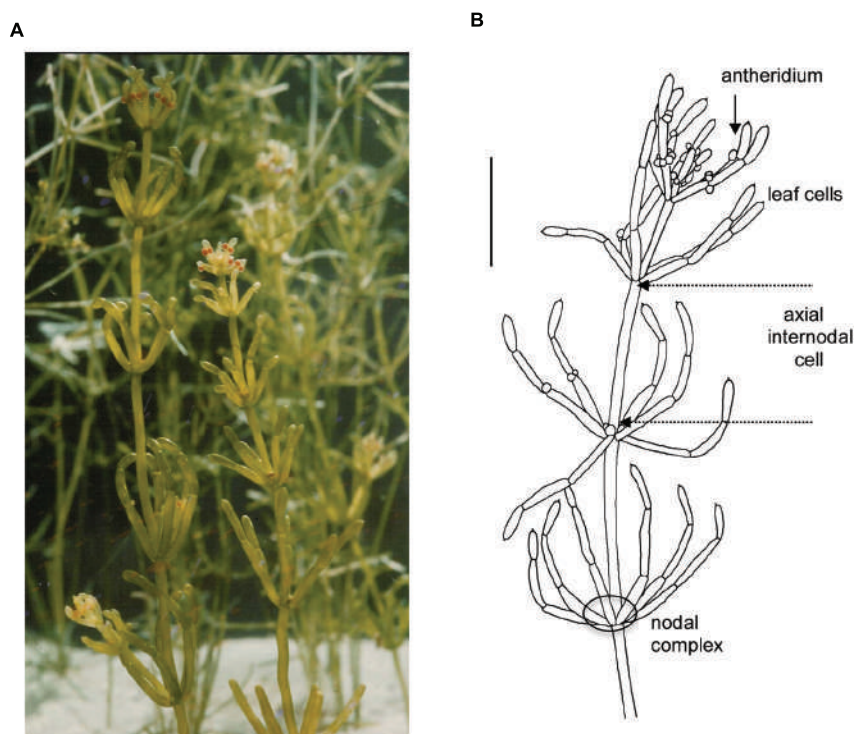


FIGURE 1 | General morphology of the characean plant. *Chara australis* is one of the most used characean experimental systems. **(A)** Plants are perennial and easily cultured in the lab setting for many years. **(B)** Male plant, identified by orange antheridia, with whorls of six branchelets. Multicellular nodes connect the axial internodes and the branchelets. The rhizoids (not shown) are also made up of large cells joined end to end. The scale bar is 10 mm. Part (B) is adapted from Beilby and Casanova (2013). For more details of Characeae morphology and variation between species see Beilby and Casanova (2013).

The axial internode cells grow up to diameter of 1 mm and up to half meter long in some species (see chapter 1 of Beilby and Casanova, 2013). New thalli regenerate from the nodal complexes.

Initially, Characeae seemed to be the closest streptophyte algal relatives to land plants (Karol et al., 2001), but recently Coleochaetophyceae or Zygnematophyceae moved into that position (Wodniok et al., 2011; Timme et al., 2012). Wickett et al. (2014) provide strong support for Zygnematophyceae to be the sister-group to land plants. This result is confirmed by plastid phylogenomics (Ruhfel et al., 2014) and plastid genome content (de Vries et al., 2016). Now that *Chara braunii* genome is in process of being sequenced and annotated and sequencing of the members from the other two classes is imminent, we can look forward to more complete solution to this puzzle.

The size of characean internodal cells makes it a good system for electrophysiology (for review see chapters 2 and 3 of Beilby and Casanova, 2013; Beilby, 2015). These cells fully recover after excision from the thallus and can be subjected to prolonged experiments (24 h and more) with multiple electrodes. For history of pioneering electrical and transport measurements on the characean plants see Walker (1955) and Hope and Walker (1975).

In this review, I will touch on electrophysiology, but mainly in context of exploring transporters at the tonoplast and plasma membrane often initially described in the Characeae. Some

of these transporters contribute to supplying the plant with chloride, nitrogen, phosphorus and potassium – elements vital to all plants (carbon transport is covered in another review: Beilby and Bisson, 2012). The movement of ions and nutrients through the characean thallus depends strongly on cytoplasmic streaming. The characean cell size and morphology facilitated the identification of the streaming mechanism. Plasmodesmata are another important element of cell-to-cell transport with some basic experiments made possible by the characean cell size and organization. Another aspect of plant physiology that can be studied in Characeae is metabolic pathways. Beilby et al. (2015) found circadian changes in endogenous concentration of indole-3-acetic acid (IAA) in *Chara australis*, confirming that the entanglement of this important hormone with the circadian clock pre-dates the emergence of plants on land.

ONE PLANT – MANY EXPERIMENTAL SYSTEMS

The morphology of Characeae facilitates creation of experimental systems on many different levels:

- Cytoplasmic droplets that allow patch clamp investigation of tonoplast channels.

- (ii) Perfusion and permeabilization that create access to both sides of plasma membrane and tonoplast in single cell context.
- (iii) Multi-compartmented cell holders that expose different parts of single cell to different media and tracer substances.
- (iv) Two or more tandem cells to measure cell-to-cell transport electrically and by tracers.
- (v) Whole thallus assays, where the results are dominated by contents of the large axial and leaf internodes with similar biochemistry and structure.

Perfusion, Permeabilized Plasma Membrane and Cytoplasmic Droplets: Tonoplast Transporters

The cylindrical symmetry of the large internodal cells allows perfusion of the vacuolar contents. The cell is put in a three-well holder (**Figure 2A**) with perfusion medium in pools A and C and the cell ends are cut. An inclination of the cell holder or higher fluid level in one of the wells creates pressure gradient to replace the vacuolar sap by artificial medium (**Figure 2B**, for the detailed technique description see Tazawa, 1964; Beilby,

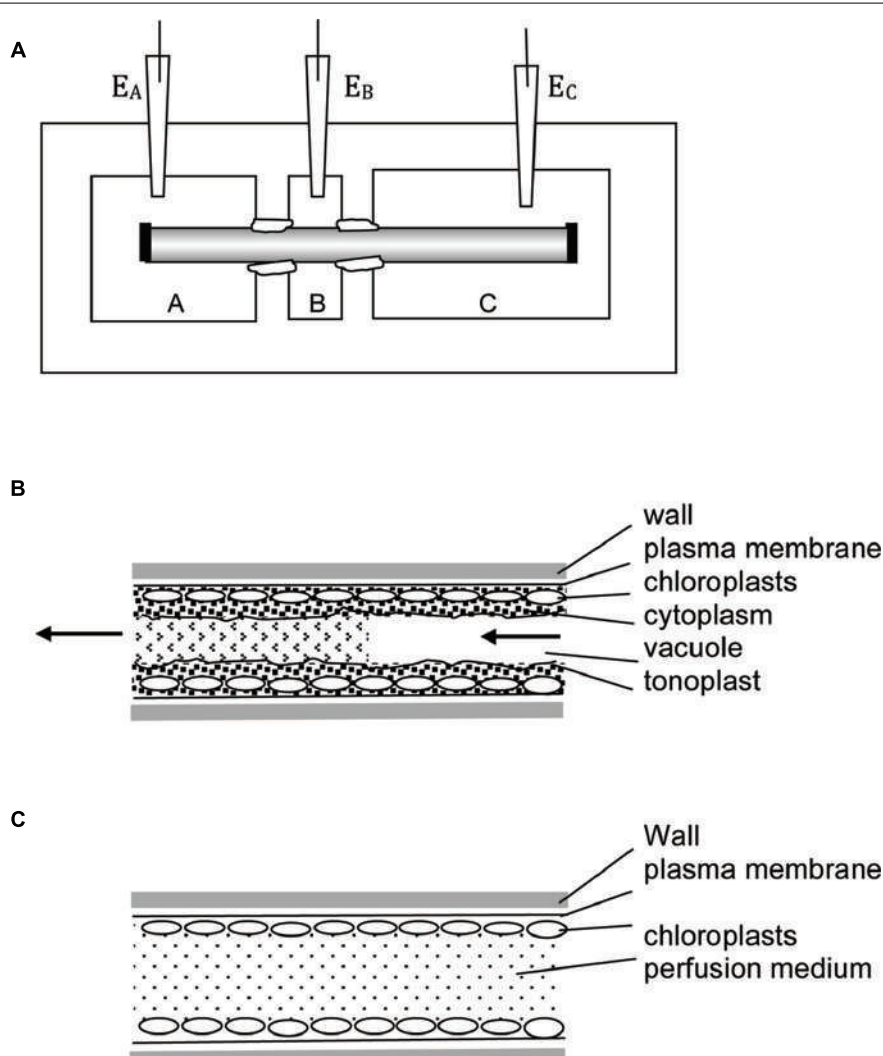


FIGURE 2 | Experimental techniques. **(A)** Multi-compartment Perspex or Lucite cell holder is employed in many types of experiments. The axial internodes grow to up to 30 cm, so more than three compartments can be introduced. The compartments are electrically insulated by applying silicon grease or Vaseline to the cells at each partition. In the three-compartment holder one compartment (e.g., B) can be filled with 50 – 100 mM KCl, reducing the membrane PD to zero due to activation of high conductance K⁺ channels (Beilby, 1985). The other compartments are filled with artificial pond water (APW) with osmolarity adjusted, so no water transport occurs between parts of the cell. The reading of electrodes E_A – E_B approximates the trans-membrane PD. In this technique no electrode insertion is necessary – very useful for wound and mechanical stress investigations. To perform vacuolar or cytoplasmic perfusion, chambers A and C are filled with perfusion medium, B with external medium. The nodes at the ends of the cell (shown as black rectangles) are cut and pressure gradient introduced, so that the vacuolar medium is replaced by artificial medium. In this case electrode E_A or E_C become the “internal” electrodes, while electrode E_B is the external electrode. The rate of perfusion and/or the perfusion medium composition determines if the cell retains tonoplast **(B)** or not **(C)**. For more details see text.

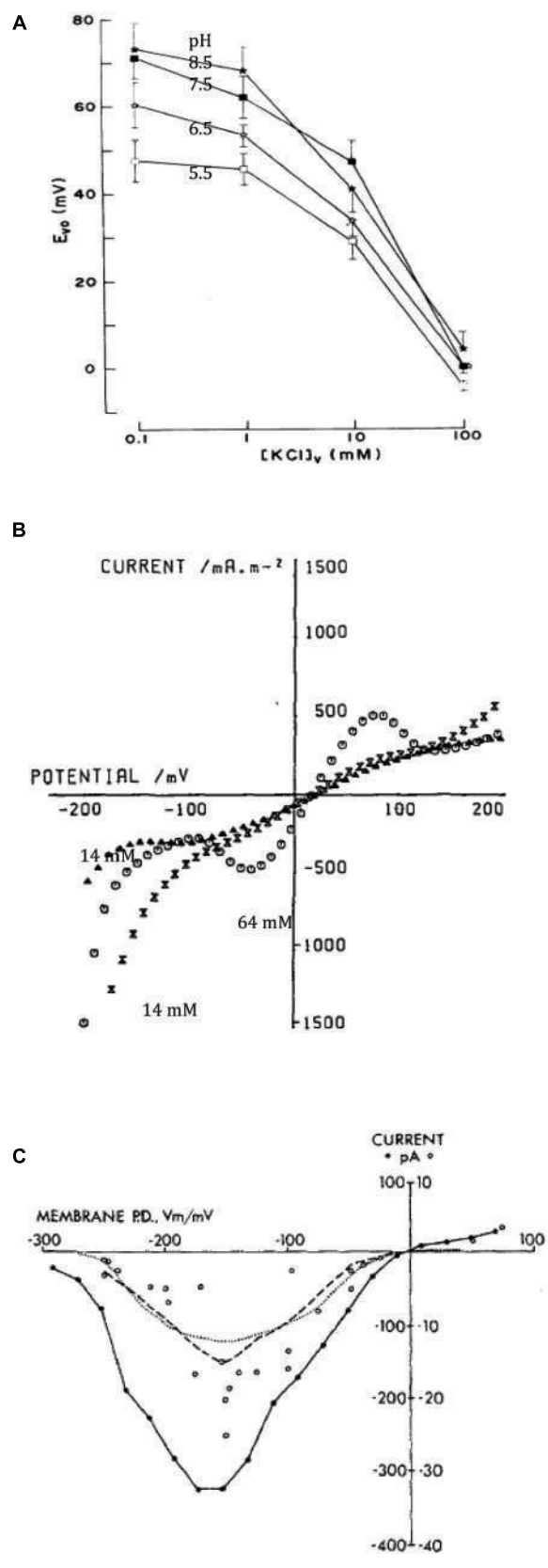


FIGURE 3 | Continued

FIGURE 3 | Tonoplast transporters. (A) Vacuolar PD (E_{V_o}) as function of vacuolar perfusion medium K^+ concentration and pH (for details see Moriyasu et al., 1984b). **(B)** I/V characteristics of the tonoplast with natural vacuolar sap and permeabilized plasma membrane with high (64 mM, empty circles) or low (14 mM, triangles before high concentration exposure and crossed triangles after) cytoplasmic Cl^- (Tester et al., 1987). **(C)** Time-averaged I/V characteristics of single tonoplast K^+ channels from several patches from cytoplasmic droplets (Laver and Walker, 1987).

1989). The perfusion can be repeated with different media, but cells are not turgid and survive only some hours. For electrical contact, the “internal electrode” is submerged into one of the outer compartments, and the “external electrode” into the middle compartment. The cell ends can be ligated with thread to ensure longer survival, but the composition of the medium changes with time.

Tonoplast Proton Pumps

Moriyasu et al. (1984a) demonstrated that the vacuolar pH is regulated close to 5, regardless of pH of the external medium. The perfused cells responded slowly to pH increase with inhibition by Dicyclohexylcarbodiimide (DCCD), while pH decrease was corrected quickly without inhibition, suggesting presence of ATP powered proton pump as well as H^+/OH^- channels in the tonoplast. To resolve tonoplast electrical characteristics Moriyasu et al. (1984b) increased the conductance of the plasma membrane by including 110 mM KCl in the external medium, opening large conductance K^+ channels. The potential difference (PD) across the tonoplast then dominated the combined PD across both membranes. Changing K^+ concentration in the perfusion medium revealed passive tonoplast PD due to potassium (Figure 3A). At low internal K^+ (0.1 mM) the PD generated by the proton pump, while regulating vacuolar pH, could be measured and increased up to +30 mV at high vacuolar pH (Figure 3A). As K^+ concentration in the perfusion medium approached the level of the sap (~100 mM), the pump PD was short-circuited (Figure 3A). So, there is an interesting difference between the two membranes: the plasma membrane H^+ ATPase shuts down, when the membrane conductance becomes dominated by K^+ channels (Beilby, 1985), while the tonoplast proton pump/s work against high K^+ conductance background with high K^+ concentrations (~100 mM) in the cytoplasm and vacuole.

Shimmen and MacRobbie (1987) employed the technique of permeabilization to disintegrate the plasma membrane by removing external and wall Ca^{2+} by ethylene glycol tetraacetic acid (EGTA). While the chloroplasts were disrupted, the tonoplast and the vacuolar compartment were largely unchanged. The cells were exposed to medium simulating the main features of the native cytoplasm (Shimmen and Tazawa, 1982) and ATP or Pyrophosphate (PPi) concentrations could be controlled. The cells were perfused and their ends ligated prior to permeabilization to control the vacuolar medium and to eliminate its buffering capacity. The H^+ pumping ability of the tonoplast was judged by accumulation of neutral red in the cell constructs. Shimmen and MacRobbie (1987) found two distinct types of proton pump in the tonoplast, energized either by ATP

or PPi. The PPase needs K^+ and Mg^{2+} , does not respond to NO_3^- and is less affected by DCCD. The ATPase needs Mg^{2+} but not K^+ , NO_3^- applied from the cytoplasmic side inhibits its activity and DCCD is a more powerful inhibitor. Both tonoplast pumps can be distinguished from the plasma membrane ATPase, as they are not affected by cytoplasmic vanadate.

I/V Characteristics of Pumps and Cl^- Channel

Tester et al. (1987) permeabilized young *Chara* leaf cells and measured I/V characteristics between -200 and $+200$ mV. With low cytoplasmic Cl^- , the sigmoid profile crossed the axis at slightly positive PD. A rise in cytoplasmic Cl^- concentration from 14 to 64 mM increased the conductance in PD-dependent manner, suggesting opening of Cl^- channels (**Figure 3B**). The equilibrium PD is positive in this preparation, as the reference electrode was placed in the cytoplasmic phase and the internal electrode in the vacuole. A drop in cytoplasmic K^+ concentration from 113 to 30 mM increased the tonoplast conductance in several experiments, somewhat contradictory to results of Moriyasu et al. (1984b).

K^+ Channels

To utilize new (then) technique of patch clamping, cytoplasmic droplet technique was developed by Luhring (1986) using results from Moriyasu et al. (1984a). A cut end of a slightly flaccid internodal cell was immersed in the vacuolar sap-like medium, producing droplets, which did not form cell walls. Sakano and Tazawa (1986) demonstrated the vacuolar origin of the membrane by fluorescence after perfusion with Concanavalin A/fluorescein isothiocyanate (FITC). The droplets were very stable and accessible to patch-clamp electrodes in both drop-attached and excised configurations.

Luhring (1986), Laver and Walker (1987) and Laver et al. (1989) made detailed studies of the conductive (170 pS) K^+ channel in the droplets. Laver and Walker (1987) formulated mathematical model with one fully open state and seven closed states. The average I/V characteristics exhibited a maximum between -100 and -200 mV, somewhat puzzling result, as tonoplast PD is usually positive (**Figure 3C**). Laver and Walker (1991) described channel activation by cytoplasmic Ca^{2+} concentration from 0.1 – 1 μM , with three bound calcium ions necessary for opening. However, for cytoplasmic Ca^{2+} concentrations above 10 μM , Ca^{2+} could act as a block. Laver (1992) distinguished two binding sites for Ca^{2+} in the vestibule to the vacuole and three binding sites for Ca^{2+} on the cytoplasmic side. Laver et al. (1997) observed that calmodulin inhibitors W-7 and trifluoperazine (TFP) affected the channel open state, with TFP promoting a new sub-state, but the channel was not Ca^{2+} -calmodulin activated. Homble and Fuks (1991) observed partial block by tetraethylammonium (TEA) on either side of the membrane. Bertl (1989) replaced K^+ by Na^+ , blocking the channel on either side of the tonoplast. The addition of Na^+ to K^+ resulted in regions of negative conductance. Tyerman et al. (1992) resolved conductance sub-states: a longer residency located near the main open state, while a “mid-state” occurred after fast transitions from the main state. Draber et al. (1993) and Schultze and Draber (1993) detected spontaneous cooperative

behavior of K^+ channels that might arise from channel clustering in the membrane. Katsuhara et al. (1989) suggested that Ca^{2+} -dependent K^+ currents across the tonoplast have an important role in hypotonic regulation in salt tolerant *Lamprothamnium succinatum*.

Another type of K^+ channel with smaller conductance (~ 90 pS) was also observed in tonoplast droplets (Tyerman and Findlay, 1989; Pottosin and Andjus, 1994). Pottosin and Andjus (1994) patch-clamped droplets of *C. gymnochilla* and classified these channels as slow delayed rectifier, activated by depolarization, not high Ca^{2+} and blocked by TEA, and Cs^+ . The authors suggested a role for repolarization after excitation event.

Cl^- Channels

The Cl^- channels with a conductance of ~ 21 pS were also detected in the droplets (Tyerman and Findlay, 1989). In droplet attached mode with media of 130 mM Cl^- outside and ~ 15 mM Cl^- inside the channel behaved as an outward rectifier. The rectification disappeared in symmetrical Cl^- concentrations in detached patches. Berecki et al. (1999) measured channel activation by increased cytoplasmic (but not vacuolar) Ca^{2+} concentration. $ZnCl_2$ (5 – 10 μM) acted as a block from cytoplasmic side. If the membrane PD was held negative of the reversal PD, larger negative currents were recorded, while pre-clamping to more positive PD produced larger positive currents. Low channel activity was observed at the normal cytoplasmic pH (7.2 – 7.4) with a half-maximal Ca^{2+} concentration of 100 – 200 μM (Berecki et al., 2001). At lower pH 6.0 the channel activity and mean open times became maximized at positive PDs and lower half-maximal activating Ca^{2+} concentration (5 μM), perhaps due to better calcium binding. Beilby et al. (1999) found more Cl^- channels in tonoplast of *Lamprothamnium* sp. as the external sulphated polysaccharide mucilage increased with cell age.

Comparison to Land Plant Tonoplast Transporters

The vacuolar ATPases were discovered in animal, fungi and land plant experimental systems. In land plants the proton pumping function was measured in late 1970 and early 1980s (see Beyenbach and Wieczorek, 2006 for historical account). The PPase was discovered in 1960s (see Hedrich and Schroeder, 1989 for review), but the proton pumping function was also realized later (Rea and Sanders, 1987). So, the elegant experiments of Moriyasu et al. (1984a,b) and Shimmen and MacRobbie (1987) confirmed results from isolated vacuoles and microsomes and placed it in evolutionary context. The sigmoid I/V characteristics observed for short periods in some experiments by Tester et al. (1987) may have been first recorded I/V characteristics of the vacuolar H^+ pumps (compare **Figure 3B** with simulations from OnGuard model, Blatt et al., 2014). While in many of their experiments the ATP or PPi was not supplied in the permeabilizing medium, small amounts could have been retained near the vacuolar membrane. This experimental system clearly needs revisiting. Nakanishi et al. (1999) found the cDNA sequence of the *C. corallina* PPase 71% identical to that of land plants and 46% identical to

that of chlorophyte *Acetabularia* and phototropic bacterium *Rhodospirillum rubrum*.

The vacuolar channels in land plants have been classified as slow activating (SV), fast activating (FV) and K⁺ selective (VK) (for review see Hedrich, 2012). The VK channel group includes two-pore channels (TPK). Patch clamp studies identified SV as non-selective cation channel, permeable to Na⁺ and under some conditions to Ca²⁺, which needs elevated cytoplasmic calcium level to open. In *Arabidopsis* genome TPC1 encodes the SV channel and loss of function mutants indicated that SV controls K⁺ homeostasis of the cell. Anion channels appear to be controlled by cell biochemistry and have been observed under elevated cytoplasmic calcium and in presence of kinases. CLC channels described in *Arabidopsis* genome operate as vacuolar anion channels or proton-Cl⁻ antiporters. Also in *Arabidopsis* the ALMT6 channels transport malate across the tonoplast. The SV channels seem to have appeared soon after plants came to land, as they were observed in patch clamp studies of *Physcomitrella patens* tonoplast (Koselski et al., 2013), but not in Characeae. In vascular land plants vacuoles have diversified to fulfill different functions in specialized tissues: for instance protein storage in a seed, storage of nitrogen in root tip, shrinking or swelling in stomata, storage of sulfate or storage of malate for crassulacean acid metabolism (CAM) photosynthesis (Martinoia et al., 2007). It will be interesting to compare sequences of K⁺, Cl⁻ and specialized channels in Characeae and land plants.

Cytoplasmic Perfusion, Combination of Flux and Electric Current Measurement, Increasing the Size of Cytoplasmic Layer: Plasma Membrane Transporters

The tonoplast can be swept away by increasing the rate of perfusion flow or including EGTA in the medium (Williamson, 1975; Tazawa et al., 1976; **Figure 2C**). The experimenter now has access to both sides of the plasma membrane. The cell can be repeatedly perfused if the ends are left open. Alternatively, the ends are ligated and electrical contact is made by impaled electrode. In each case the cells are fragile and live only for some hours.

Cl⁻/H⁺ Symporter

With the negative membrane PD across the plasma membrane, Cl⁻ needs active transport into the cell even with the low concentration in the cytoplasm. Cells concentrate Cl⁻ in the vacuoles as osmoticum and to keep electroneutrality. Sanders (1980a) found an increase in Cl⁻ influx following period of Cl⁻ “starvation.” Membrane PD transiently depolarized upon resupply of Cl⁻ in the medium (**Figure 4A**). Using perfused tonoplast-less cells he established that this flux stimulation resulted from drop of cytoplasmic Cl⁻ concentration. He also observed a strong dependence of Cl⁻ influx on cytoplasmic and external pH (**Figure 4B**; Sanders, 1980b). The control of the cytoplasmic phase facilitated resolution of the change in $\Delta_{\mu H}$, influence of external pH on cytoplasmic pH and the lack of influence of cation fluxes of K⁺ or Na⁺ (earlier

postulated salt pump – Findlay et al., 1969). Beilby and Walker (1981) demonstrated instantaneous manifestation of Cl⁻ influx by voltage-clamping the membrane PD of Cl⁻-starved *Chara* cell, challenging the cell with a range of low concentrations of Cl⁻ and recording an inward positive current (**Figure 4C**). Clamping the membrane PD prevented activation of other transporters by change in PD. The current amplitude leveled off with Michaelis-Menten kinetics ($V_m \sim 100 \text{ nmol/m}^2 \cdot \text{s}$, $K_m 10 - 20 \mu\text{M}$). Beilby and Walker (1981) modeled the data with the Hill-Whittingham equation, which is appropriate for processes with low K_m where an unstirred layer may be important. Sanders (1980b) and Beilby and Walker (1981) agreed that Cl⁻ is co-transported with 2H⁺, with net positive charge influx.

Sanders and Hansen (1981) formulated a kinetic model, where three reaction steps occur on either surface of the plasma membrane and loaded or unloaded carrier crosses the membrane. This scheme postulates that Cl⁻ binds on and leaves first and charge crosses membrane on loaded carrier. The model addresses the main features of the symporter: (i) Michaelis-Menten kinetics, (ii) cytoplasmic Cl⁻ concentration and pH effects on V_{max} but not K_m , and (iii) Cl⁻ concentration and pH interaction.

Amine Uniporter

Nitrogen is vital for many important plant biochemicals, such as chlorophyll, ATP, nucleic and amino acids. Smith and Walker (1978), Walker et al. (1979a,b) found that simple amines enter characean cells as cations, NH₄⁺ and CH₃NH₃⁺, at pH below their respective pK_a of 9.25 and 10.64. Using similar technique to Cl⁻ influx investigation, Walker et al. (1979a) challenged the cell with a range of amine concentrations and recorded clamp currents, also obtaining Michaelis-Menten relationship: V_m up to 200 mA/m², low K_m of $\sim 3 \mu\text{M}$ for NH₄⁺ and $200 \mu\text{M}$ CH₃NH₃⁺. Clamping at different membrane PDs established exponential PD dependence of both V_m and K_m . The Hill-Whittingham equation yielded unstirred layer of up to 150 μm in slow flowing media, which reduced to $\sim 40 \mu\text{m}$ in fast flowing media. The rate of transport fell rapidly with exposure to amines (At one time all Characeae cultures in the laboratory stopped reacting to amines and experiments could only be restarted after enthusiastic cleaning lady stopped mopping the lab floor with ammonium based cleaner!). The transporter was modeled as a uniport with a binding site inside the membrane and mid membrane potential energy barrier. Fairley and Walker (1987) concluded that increasingly substituted amines are transported in cationic form by the same porter. The stoichiometric ratio of the influx of charge and ¹⁴C methylamine was 0.9 mol/Faraday (pH 5.7 – 8.5). Above pH 9, the influx of amine increased with rising concentrations of the free bases (Walker et al., 1979b; **Figure 5A**). Ritchie (1987) measured permeabilities of ammonia, methylamine and ethylamine as $P_{\text{ammonia}} = (6.4 \pm 0.93) \times 10^{-6} \text{ m/s}$, $P_{\text{MA}} = (6.0 \pm 0.49) \times 10^{-6} \text{ m/s}$ and $P_{\text{EA}} = (8.4 \pm 1.2) \times 10^{-6} \text{ m/s}$ to $(14 \pm 1.2) \times 10^{-6} \text{ m/s}$. The pH_o in the alkaline bands is close to the pK_a of these amines (9.25 – 10.75), so the neutral amine transport is important. Ryan and Walker (1993) measured ammonium

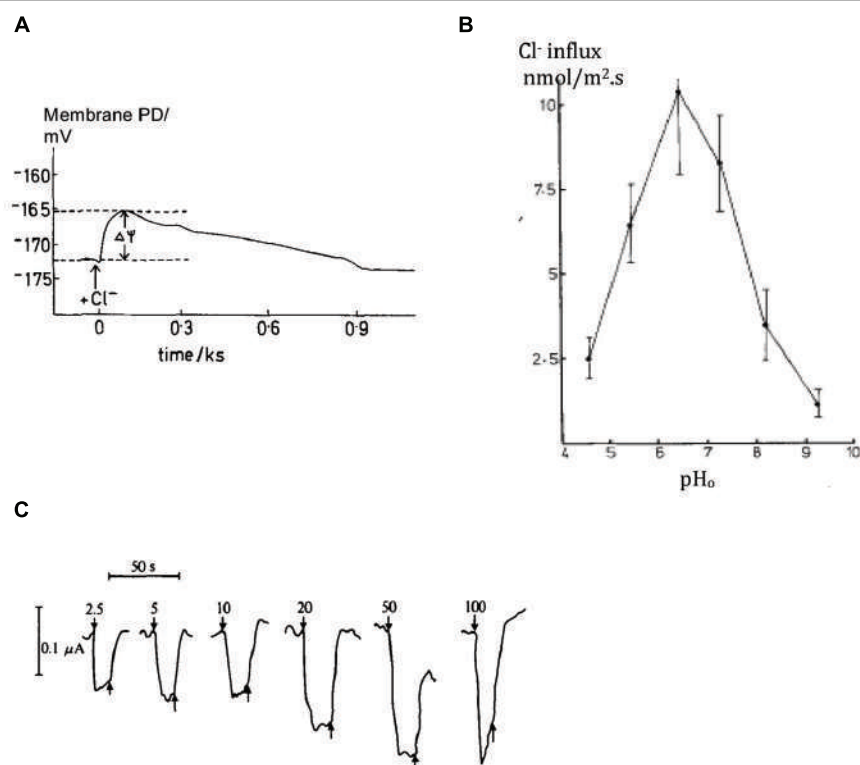


FIGURE 4 | Plasma membrane transporters: Cl^-/H^+ symporter. (A) Chara cell Membrane PD depolarization upon re-supplying Cl^- after overnight starvation, see arrow (Sanders, 1980b) **(B)** Chloride influx in intact cells as function of external medium pH, pH_o (Sanders, 1980b). **(C)** Positive inward currents observed in Chara cells with their resting PD voltage-clamped upon exposure to range of Cl^- concentrations shown next to each pulse in μM (Beilby and Walker, 1981).

concentration in *Chara* vacuole of up to 70 mM, mostly in protonated form due to low vacuolar pH. To preserve electroneutrality, cells exported K^+ and Na^+ and imported Cl^- or manufactured malate in Cl^- - free media. Ryan and Walker (1994) inhibited Glutamine synthase, enzyme involved in ammonia assimilation, by L-methionine-D, L-sulphoximine (MSX). An increased concentration of ammonia in the cell strongly inhibited amine uptake, suggesting kinetic regulation by the internal amine concentration or a concentration of an intermediate of nitrogen assimilation.

Phosphate Transport

Phosphorus is another vital element for building blocks of plant biochemistry: phospholipids in cell membranes, phosphate groups in DNA and RNA, ATP and other metabolic compounds in energy transduction. Inorganic phosphorus, Pi, forms phosphates: mainly H_2PO_4^- at pH 5, while HPO_4^{2-} dominates at pH 10. The observed Pi concentration of 5–10 mM in the cytoplasm must be maintained by active import, especially as the external concentration is in the micromolar range (Mimura, 1999). Even at this low external Pi, starvation of up to 10 days increased the influx transiently. In contrast to Cl^- concentration dynamics, the cytoplasmic Pi concentration did not change with starvation or when Pi was re-supplied, although the vacuolar concentration increased when Pi was available (Mimura et al., 1998). The membrane PD or the cytoplasmic pH was not affected

by Pi starvation. However, the rate of Pi influx increased for up to 7 days after Pi was re-supplied (Mimura et al., 2002). If the starvation medium contained small amount of Pi (0.5–1 μM) the response was greater, but more transient. The Pi influx showed two plateaus, as the Pi concentration increased and was modeled by a low affinity transporter with K_m of ~4 μM and a higher affinity transporter with K_m of ~220 μM (Mimura et al., 1998; Figure 5B). Pi and Na^+ uptakes were linked: Na^+ concentration with K_m of 300 μM , Pi concentration with K_m of 10 μM . In absence of external Na^+ induction and inactivation were abolished. Thus Na^+ is the main cotransported ion (Mimura et al., 1998; Reid et al., 2000). Combined tracer and voltage clamp experiments established the stoichiometry of Na:Pi of 5.68 at pH_o 6. The stoichiometry was confirmed by voltage-clamp experiments where the influx of positive charge exceeded the influx of ^{32}Pi by a factor of 6.26. The dependence of Pi influx on pH_o is consistent with the transported species being H_2PO_4^- . Interestingly, perfused cells required ATP in the perfusion medium to reach a similar influx of Pi to that of intact cells. It is possible that hyperpolarization is necessary for this symporter to function. While the electrochemical PD for H_2PO_4^- and Na^+ suggests that there is not enough energy at pH_o 5, a large influx was still observed. The authors suggest that the symporter might be able to utilize H^+ at low external pH, as observed in yeast and *Neurospora* (see Reid et al., 2000 for review).

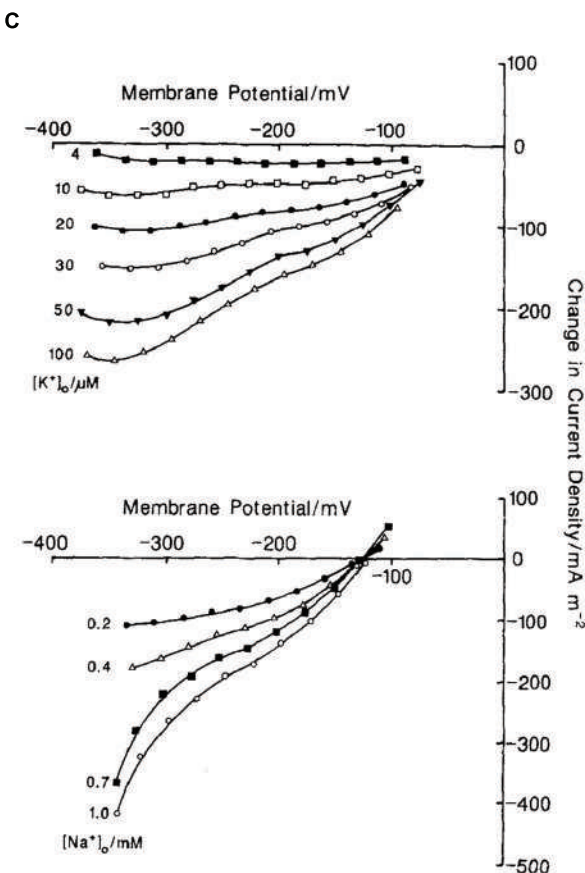
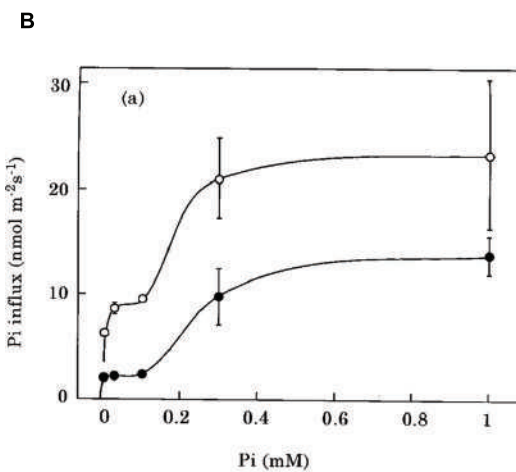
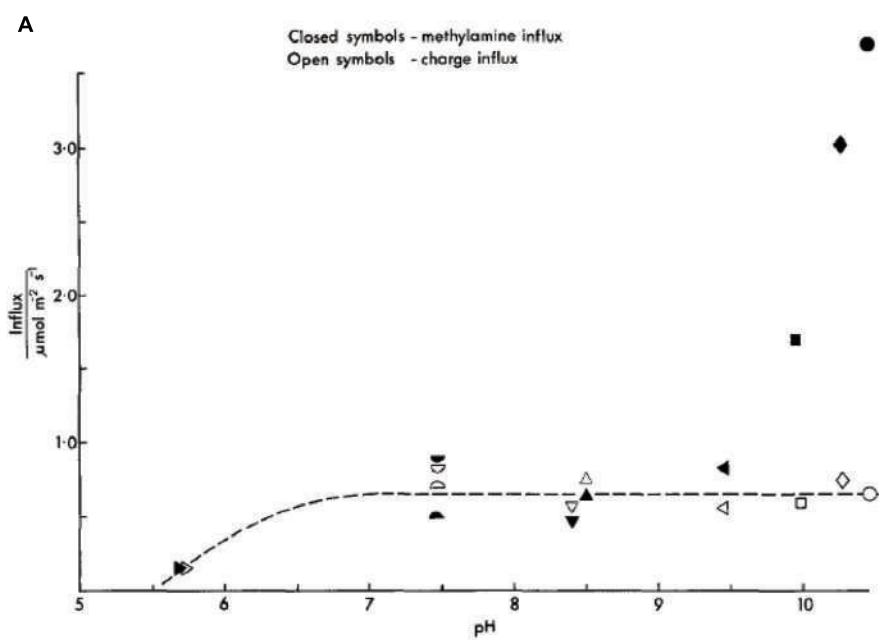


FIGURE 5 | Plasma membrane transporters. **(A)** Amine transport: comparison of influx of charge, empty symbols, and methylamine (neutral or charged form), filled symbols (Walker et al., 1979b). **(B)** Phosphate transport: The Pi influx as function of external Pi concentration: open circles, cells pretreated without Pi for 7 days; closed circles, cells pretreated with 0.1 mM Pi for 7 days (Mimura et al., 1998). **(C)** Na^+/K^+ symport: Difference current-voltage curves (calculated by subtracting the 1 mM Na^+ or 200 μM K^+ I/V characteristics) for range of K^+ concentrations with Na^+ at 1 mM (top) and Na^+ concentrations with K^+ at 200 μM (bottom) (McCulloch et al., 1990).

Na⁺/K⁺ Transport

Similar to phosphate, K⁺ is concentrated in both cytoplasm and vacuole (up to ~100 mM), but may be quite scarce in some ponds inhabited by freshwater Characeae. The K⁺ selective inward rectifier channels require very negative membrane PDs to open. The high conductance K⁺ channels open at less negative membrane PDs, but need external K⁺ concentrations above ~1 mM. After the cells were starved of K⁺, Smith and Walker (1989) measured electrogenic influx of K⁺, which was dependent on Na⁺ presence in the medium. The ratio of tracer and charge inflow confirmed symport of K⁺ with Na⁺ with a stoichiometry 1:1: K⁺ with K_m of ~30 μM and Na⁺ with K_m of ~470 μM. McCulloch et al. (1990) observed an exponential clamp current turnoff with short half times of ~50 s, even in low K⁺ concentrations. As K⁺ concentration in the cytoplasm is already high, Na⁺ was a more likely candidate for transport inhibition at ~5 mM (Tazawa et al., 1974). The authors used cytoplasm-enriched fragments to overcome current turnoff and gain more time for measurements. These cell constructs are prepared by slow centrifugation of long internodal cells creating cytoplasmic plug at one end, which is then tied off by a thread. With greater volume of cytoplasm for a given surface area, it was possible to obtain families of I/V characteristics at different K⁺ and Na⁺ concentrations (see **Figure 5C**). For K⁺ influx, K_m decreased as the PD became more negative, while V_{max} increased. For a Na⁺ influx both K_m and V_{max} increased with the negative going PD. These characteristics can be modeled either by simultaneous transit of K⁺ and Na⁺, or by the ions transiting in consecutive steps. Both models suggest a double negative charge on the unloaded carrier and extracellular binding of K⁺ followed by Na⁺. The charge transit process is the limiting step at more positive membrane PDs.

Comparison to Land Plant Plasma Membrane Transporters

The H⁺/Cl⁻ symporter in root hair cells of *Arabidopsis* relative mustard *Sinapis alba* was described by Felle (1994). Clearly, this transporter must be active in range of tissues of land plants, as Cl⁻ compartmentation is similar to Characeae: low in the cytoplasm and high in the vacuole to maintain turgor together with K⁺ and other inorganic and organic anions (Barbier-Bryggo et al., 2000). Teakle and Tyerman (2010) lament lack of data on Cl⁻ transport under salinity stress. They point out that the electrochemical potential for Cl⁻ changes as plants are exposed to saline environment and the Cl⁻ influx might become passive through channels. The salt tolerant Characeae *Lamprothamnium* increases its vacuolar Cl⁻ concentration from 200 – 800 mM as external salinity rises (Bisson and Kirst, 1980). This is a perfect system to study the nature of Cl⁻ inflow under salinity stress.

The ammonium ion transporters belong to the AMT/MEP/Rh family found in all domains of life and described in plants and fungi in 1990s (for reviews see Ludewig et al., 2007; McDonald et al., 2011). The detailed protein structures are being investigated and suggest charged NH₄⁺ is the transported molecule (Pantoja, 2012).

In phosphate transport, most land plants use H⁺ as the driver ion and Pi uptake causes cytoplasmic acidification (Mimura,

2001). The main family of Pi transporters are PHT1 (see Nussaume et al., 2011 for review). The Na⁺/Pi transporter in Characeae is similar to that in animal cells, which operate on Na⁺ economy. However, there are examples of Na⁺/Pi symport in some chlorophytes (Ullrich and Glasser, 1982; Ritchie et al., 1997).

Na⁺/K⁺ symport is limited to aquatic higher plants and was observed in *Egeria* and *Vallisneria* leaves, and in *Elodea* and *Egeria* roots. In land plants such as wheat, barley or *Arabidopsis*, the driver ion appears to be H⁺ (Maathuis et al., 1996). In Characeae the Na⁺ coupling is also implicated in the transport of urea, amino acids and sugars (Walker et al., 1993; Walker, 1994).

The detailed data on the control of the above transport systems by external and internal concentrations of driver and transported substances and pH were obtained utilizing the large size of characean cells and the ability to manipulate cellular compartments by perfusing the vacuole or the cytoplasm or concentrating the cytoplasm in the cytoplasm enriched cell constructs. Direct comparison of tracers and electrical currents in voltage clamped cells provided transport stoichiometries.

Cell to Cell Transport

Structure of Nodal Complex

The axial and branch internodes are separated by nodal complexes (see **Figure 6A**, Walker and Bostrom, 1973). Shepherd and Goodwin (1992b) describe how the new internode and the nodal architecture arise from the apical cell establishing the path of cytoplasmic streaming (see Streaming). The shortest path between two internodal cells is through two flat cells in the middle of the node (marked "C" in **Figure 6A**, Spanswick and Costerton, 1967).

Transport between internodal cells is mediated, and controlled, by plasmodesmata that connect the cytoplasm of neighboring cells (for review see Burch-Smith and Zambryski, 2012). Spanswick and Costerton (1967) found that in *Nitella translucens* the plasmodesmata between the nodal cells had uniform diameter, while plasmodesmata between nodal and internodal cells developed central cavities, sometimes with several openings. Young cells exhibited extensive connectivity with up to 14.7% of the wall occupied by plasmodesmata. Characeae form primary plasmodesmata containing endoplasmic reticulum (ER) with close similarity to higher plant plasmodesmata was established (Franceschi et al., 1994; Cook et al., 1997; Brecknock et al., 2011; **Figure 6B**).

Fluorescent Tracers

Shepherd and Goodwin (1992a,b) attached peptides of increasing molecular weight to fluorescein to establish molecular exclusion limit in cell to cell communication: 874 Da. They used young shoots of *C. corallina* and injected fluorescein by iontophoresis, sometime aided by pressure, into the cytoplasm of one of the cells in a lateral branch. In the winter months the lateral internode cells exhibited low resting PD of ~ -120 mV and restricted cell-to-cell communication of the internode and adjacent node. As the action potential inhibited cell-to-cell communication, the exposure to excitation inhibitor La³⁺ restored communication. In spring the branch cells with more negative resting PD (~

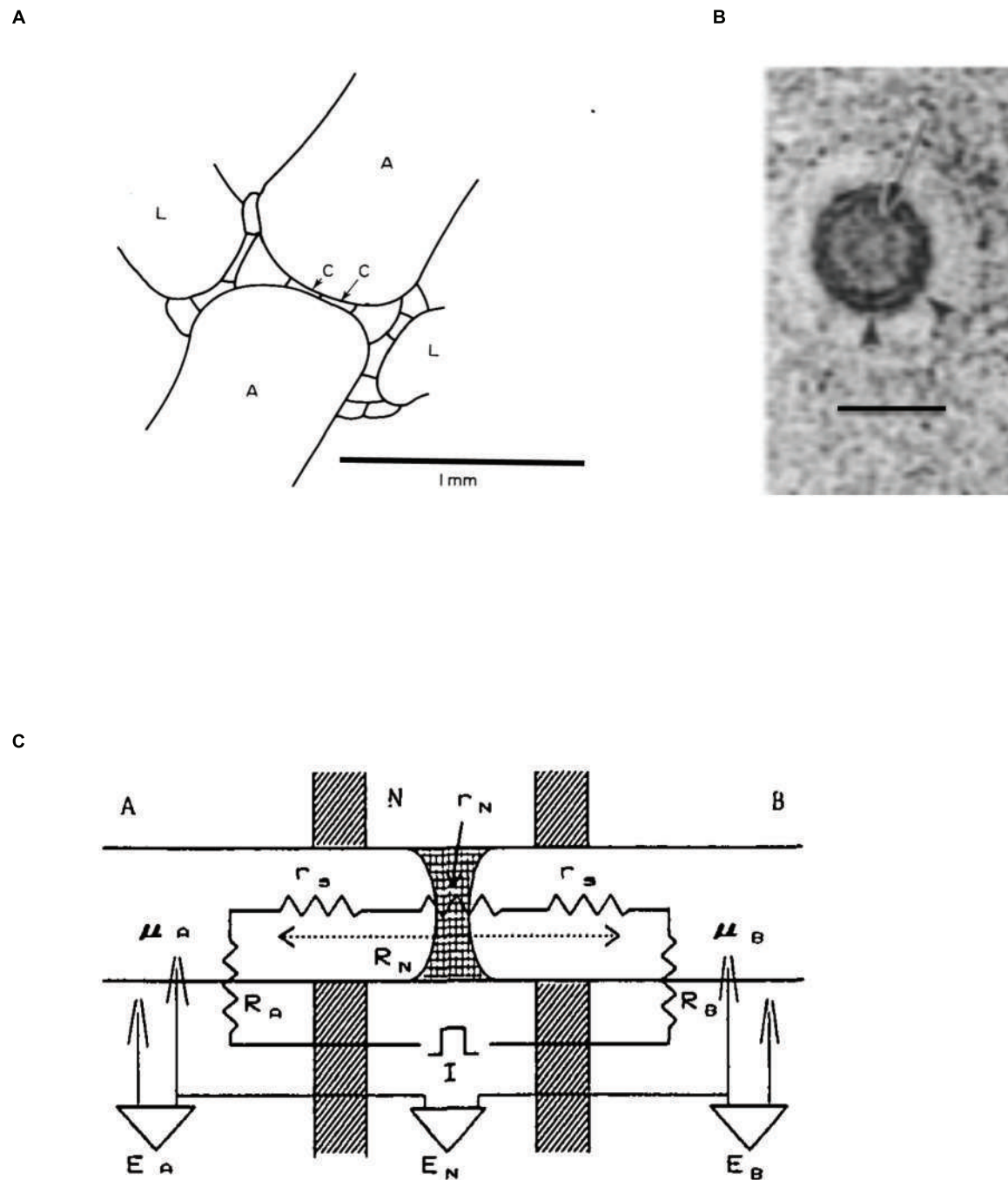


FIGURE 6 | Structure of the nodal complex. (A) In this diagram of longitudinal section through the node of *Chara* the axial internodes are marked “A,” the lateral (leaf) internodes are marked “L” and the two central nodal cells are labeled “C.” (adapted from Walker and Bostrom, 1973). **(B)** Electron microscopy of transverse view of plasmodesma in a branch node of *C. zeylanica*. Arrow marks the central desmatubule, small arrowheads indicate the spoke structures connecting it to plasma membrane. Bar is 50 nm (from Cook et al., 1997). **(C)** The electrical model of the node and its neighboring internodes (Ding and Tazawa, 1989): R_A is the membrane resistance of cell A, R_B is the membrane resistance of cell B, R_N is the resistance across the node, which is the sum of the node resistance r_N plus the resistances of the cell sap r_s . The PDs across cell A, cell B and the nodal region are E_A , E_B and E_N , respectively. The internal electrodes are labeled μ_A and μ_B .

–210 mV) increased transport of 6 carboxyfluorescein between nodes and internodes. As in winter cells, if cytoplasmic Ca^{2+} was increased due to action potential or exposure to ionophore A23187, cell-to-cell transport was inhibited.

The spring plants became fertile and formed male reproductive structures (antheridia) from the nodal cells located near the descending (internodal) cytoplasmic stream. While the molecular exclusion limit was smaller (between 750

and 874 Da), the young antheridia were easily reached by the fluorescent dye, while the mature antheridia lost connectivity from the rest of the plant (Shepherd and Goodwin, 1992b).

Kwiatkowska (2003) combined fluorescent dye Lucifer Yellow experiments with electron microscopy to study the development of the antheridia in *C. vulgaris* and *tomentosa*. Simple plasmodesmata connect the antheridium and supporting cells in early developmental stages. Gradually some plasmodesmata disappeared enforcing radial orientation of symplasmic routes through the antheridium. Simple plasmodesmata developed branching to provide pathway for gibberellins and nutrients. Then the plasmodesmata were selectively plugged, limiting the synchronization of cell divisions. Finally the plasmodesmata between the antheridium and the thallus were spontaneously broken, starving the antheridium of gibberellins and initiating spermiogenesis. ER penetrated into antheridial filament plasmodesmata at specific stage of spermiogenesis enabling exchange of nucleohistones into nucleoprotamines. These results confirm that the plasmodesmata are very dynamic structures under tight control of the plant.

Radioactive or Substitution Tracers

Bostrom and Walker (1975) employed two internodal cells in tandem to measure the intercellular transport of Cl^- . The cells were placed in three-compartment holder similar to that in **Figure 2A**. The node was positioned in the middle compartment (B) and compartments were insulated by silicone grease. The ^{36}Cl tracer was added to one compartment and the content of the tracer in both cells was monitored over time. The chloride was taken up and about two thirds remained in the vacuole of the exposed cell, while a third was transported to the other internode. No polarity was found, as the results were insensitive to swapping the basal and apical internodes as input cells. The rate of transport varied between 4 and 60 pmols.s $^{-1}$ and was consistent with diffusion through the plasmodesmata without invoking bulk flow or active transport. Bostrom and Walker (1976) controlled the speed of cytoplasmic streaming by cytochalasin B. The intercellular chloride flux was proportional to the streaming speed in the input internode but not the “sink” internode. Streaming speed did not affect the chloride influx in the input cell.

Chloride is not consumed in metabolism or complexed into compounds, but its distribution between cytoplasm and vacuole can be complicated by tonoplast action potentials elicited by handling the cells. MacRobbie (1969, 1975) initially postulated vesicle transport to explain the fast appearance of chloride tracer in the vacuole. Later she performed elegant experiments exposing only half of the internodal cell to radioactive label. A blockage of excitation diminished the fast “vesicle transport” phase.

Ding and Tazawa (1989) substituted Rb^+ for K^+ and exposed the input cell to 100 mM RbCl at 5°C. The low temperature inhibited the transnodal transport and 43 mM Rb^+ accumulated in the cytoplasm. Upon temperature increase to 25°C, ~12% was transported into the sink cell, suggesting diffusion process with coefficient $2.3 \times 10^{-11} \text{ m}^2.\text{s}^{-1}$ (plasmodesmata were assumed to occupy 10% of the nodal area). The rubidium transport was also strongly dependent on cytoplasmic streaming in either or

both internodes, regardless if the streaming speed was controlled by cytochalasin B or change in temperature. A turgor pressure gradient of 240 mOsm across the node decreased the nodal transport, suggesting the existence of valving system.

Zawadski and Fenson (1986a) measured intercellular transport of dissolved inorganic carbon (DIC) by supplying $\text{NaH}^{14}\text{CO}_3$ to the input cell. Their results were complicated by the complexity of DIC distribution in the medium as CO_2 or bicarbonate according to pH, the intricacy of the banding system (see Beilby and Bisson, 2012) and carbon fixation by photosynthesis. In this case low streaming rate in either cell resulted in diminished intercellular transport. In the winter the transport was more sensitive to anoxia and decrease in illumination. In the summer the cells have greater reserve of ATP, so it is possible that the DIC transport is active. The application of pressure gradients on the node confirmed this hypothesis. Zawadski and Fenson (1986b) found that trans-nodal transport of ^{14}C was independent of the direction of the pressure gradient (up to 2.5 bars). However, the rate of transport decreased with the increasing pressure gradient. The plasmodesmata are likely to contain pressure sensitive valving system. Similar pressure sensitivity was also found in plasmodesmata of higher plants (Oparka and Prior, 1992). Transports of ^{36}Cl , ^{32}P and ^{42}K were also affected by imposed pressure gradients: ^{42}K transport was consistent with diffusion, but active components were postulated in both ^{36}Cl and ^{32}P transport. Large portion of the ^{32}P in the input cell was metabolized, resulting in small feed into the sink cell. Working with whole plants of *C. hispida*, Box et al. (1984) measured the flux of ^{14}C from the rhizoids to the top of the plant. The rate of transport was reduced to 6% by exposure to cytochalasin B. However, transport of ^{32}P was somewhat slower than cytoplasmic streaming probably due to involvement in metabolism. Trebacz et al. (1988) found that blockers of photosystem I or II, such as 3-(3,4-Dichlorophenyl)-1,1-dymethylurea (DCMU), 2,6-Dichlorophenolindophenol (DCPIP) or uncouplers of phosphorylation Iodoacetamide (IAC) 2,4-Dinitriphenol (DNP), Diethyl stilbestrol (DES), NH_4^+ and citrate all diminished intake of DIC and reduced the transport across nodes. These findings suggest that the transport of carbon, chloride and phosphate compounds across the node is at least partially active.

Trebacz et al. (1988) identified pentoses, hexoses and disaccharides formed from the supplied $\text{NaH}^{14}\text{CO}_3$ by high performance liquid chromatography in the feed cell. These and small amino acids passed through the node into the adjacent cell. Ding et al. (1992) fed $\text{NaH}^{14}\text{CO}_3$ to a branchlet of *C. corallina* in a internode-branchlet complex and measured photoassimilates after 10 min in both the source branchlet and the sink internode, using thin-layer chromatography. The main photoassimilates transported were sucrose and amino acids. Transport was aided by downward concentration gradients of sucrose, serine and glutamic acid between the cytoplasm of the branchlet and the internodal cell, which decreased when the apex was detached.

Electrical Measurements

The insertion of electrodes into the internodes on each side of the node allows measurement of transnodal PD

and also the transmembrane PD of each internode (with appropriate reference electrodes in each compartment). It is also possible to pass current across the node to measure electrical resistance. The node resistance varied in different systems: $\sim 1.7 \text{ k}\Omega\cdot\text{cm}^2$ in *Nitella* (Spanswick and Costerton, 1967), $\sim 0.47 \text{ k}\Omega\cdot\text{cm}^2$ in *C. corallina* (Bostrom and Walker, 1975), $0.06 - 0.12 \text{ k}\Omega\cdot\text{cm}^2$ in the nodes between young branch *Chara* cells and $0.2 - 0.51 \text{ k}\Omega\cdot\text{cm}^2$ in the older branch cells (Reid and Overall, 1992). Ding and Tazawa (1989) measured the nodal resistance/conductance as a function of imposed pressure gradient. The pressure gradient of 180 mOsm diminished the conductance to $\sim 50\%$, but no further decrease was obtained with further pressure rise. The location of increased electrical resistance was found on the side of the node adjacent to the internode with reduced turgor. Thus the nodal cells deform by bulging out into the less turgid internode closing the valving mechanism. The rubidium trans-nodal flux diminished to 3% in such conditions. The authors formulated an electrical model of the node and adjacent internodes (see **Figure 6C**). In similar experiments the exposure of one of the tandem *Chara* internodes to 100 mM mannitol increased nodal resistance by 40% (Cote et al., 1987).

The metabolic inhibitor carbonyl cyanide m-chlorophenylhydrazone (CCCP) affected internodes by making the membrane PD less negative, increasing the membrane resistance and stopping the cytoplasmic streaming (Reid and Overall, 1992). The *trans*-nodal resistance greatly increased with the same time course. The exposure of one internode to 200 mM mannitol resulted in doubling of the nodal resistance. The fluxes of ^{14}C butyrate and ^{36}Cl were diminished both by CCCP and mannitol. The excision of one internode resulted in rapid resistance increase followed by further slow rise. The cytoplasmic pH changes induced by butyric acid, NH_4^+ or methylamine resulted in small effects on the *trans*-nodal resistance. On the other hand, the *trans*-nodal resistance was insensitive to changes in light intensity, cytoplasmic calcium concentration changes or *trans*-nodal PD manipulation.

Sibaoka and Tabata (1981) concentrated on action potential (AP) transmission across nodes of *C. braunii*. They inserted additional electrode in one of the large nodal cells. The whole nodal cell was not excitable, but the adjacent area of the nodal cell (end-membrane) displayed APs. At the time of AP conduction the stimulated internode produced greater electrotonic depolarization in the next internode without the end-membrane excitation, facilitating the internode-internode transmission. The authors modeled the internode with three resistances R_a (internode a), R_b (internode b) and nodal resistance R_n (compare to more complex model in **Figure 6C**). The coupling ratio for internode a was calculated as $R_b/(R_b + R_n)$. This ratio increases if $R_b > R_n$ or if APW (artificial pond water) in the nodal compartment was replaced by more conductive medium of 1 mM KCl or 10 mM NaCl. R_n was estimated as $1.2 \text{ k}\Omega\cdot\text{cm}^2$.

Conclusion

The early measurements of intercellular transport and electrical conductance provided basis to what is now a large field

mainly centered on structure and evolution of plasmodesmata (Burch-Smith and Zambryski, 2012; Evkaikina et al., 2014). In gymnosperms and angiosperms primary plasmodesmata develop at the time of cell division, while secondary plasmodesmata can form between any adjacent cells after cell division. Both primary and secondary plasmodesmata were observed in Characeae, but in different species of *Chara* (Franceschi et al., 1994; Cook et al., 1997; Brecknock et al., 2011). However, some early land plants such as Selaginellaceae and ferns seem to lack the ability to form secondary plasmodesmata (Evkaikina et al., 2014). Raven (2005) suggests complex evolutionary pathway: independent evolution of plasmodesmata in brown algae, in characean algae, and up to five times (!) in green algae, but not in red algae, haptophytes and dinoflagellates, despite multicellular morphology. In embryophytes plasmodesmata facilitate exchange of miRNA, proteins, and mRNA between adjacent cells in the course of plant development. The full role of characean plasmodesmata is yet to be investigated.

Streaming

Streaming and Morphology

The large size of characean cells makes observation of cytoplasmic streaming easy, requiring only low power microscope. The streaming pattern follows the orientation of the chloroplast rows, tracing a helical path around the cell, the upward and downward streams separated by a chloroplast-free “indifferent zone” (**Figure 7A**). As the chloroplast rows are fixed in the Characeae, the streaming direction is related to the whole plant development. The oldest leaf cell in each whorl and axillary new shoots grow below the descending cytoplasmic stream. The streams run in opposite directions on each side of the nodal complex (Hope and Walker, 1975). The velocity of streaming is comparatively steady given constant temperature and supply of ATP.

Mechanism: Actin and Myosin

The ribbon of cytoplasm ($\sim 10 \mu\text{m}$ thick) winds its way around the cell with the same speed, transferring some of the movement to the vacuole. This agitation drops off with the distance into vacuolar sap. Kamiya and Kuroda (1956) prepared cytoplasm-enriched cell constructs (see Na^+/K^+ Transport) with greater volume of flowing cytoplasm and observed similar speed decrease further away from the gel (static cytoplasm). The authors proposed the “sliding theory,” where the interactions of sol (flowing cytoplasm) and gel surfaces produce the shearing force that moves the sol along. Using light microscopy Kamitsubo (1966) observed rope-like structures on the cytoplasmic side of the chloroplasts. Nagai and Rebhun (1966) and Kersey and Wessells (1976) employed electron microscopy to resolve about 100 microfilaments making up each rope. Kamitsubo (1972) used strong illumination to detach chloroplasts and the cables on a small patch of the cell, strongly inhibiting the streaming. When the cables regenerated, streaming was restored. Palevitz et al. (1974) and Williamson (1974) observed arrowhead structure, found in animal systems with actin, when heavy mero-myosin (HMM) sub fragment S1

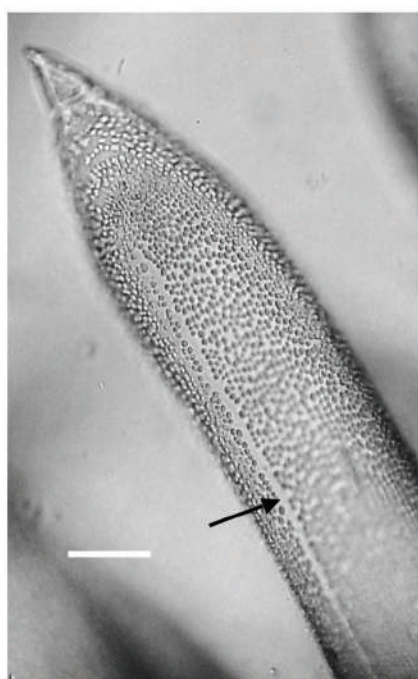
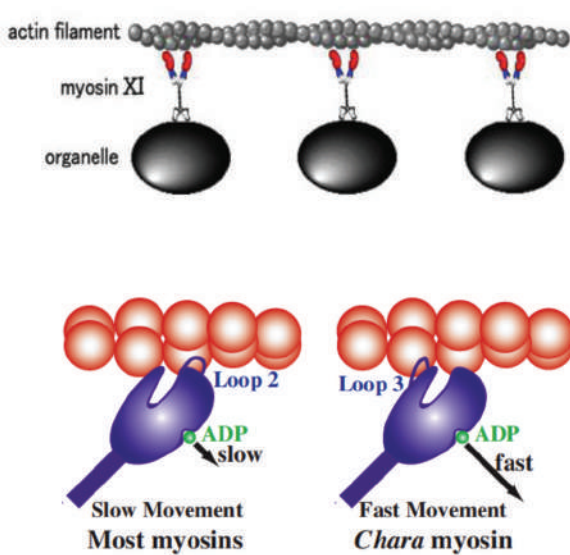
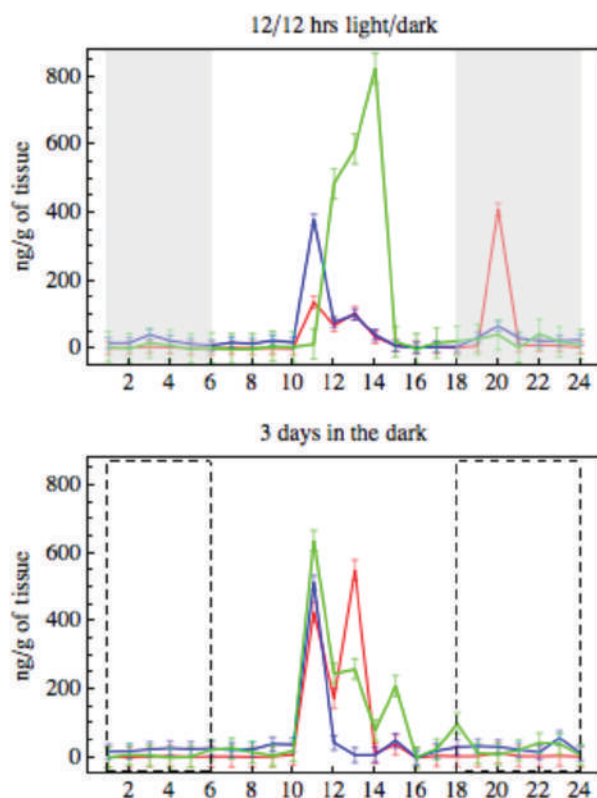
A**B****C****FIGURE 7 | Continued**

FIGURE 7 | (A) Cytoplasmic streaming Young leaf *Chara* cell showing the neutral zone between the two opposing cytoplasmic streams (black arrow), bar 500 μm (from Beilby and Casanova, 2013). **(B)** Model of cytoplasmic streaming (Shimmen, 2007): *Chara* myosin, which mediates the fast streaming speed, contacts actin via loop 3, with fast ADP release (most other myosins use loop 2, which slows ADP release). **(C)** Endogenous concentrations of auxin, melatonin and serotonin: changes over 24 h in IAA (green), melatonin (red) and serotonin (blue) in summer *Chara* thalli. Top graph: plants sampled straight from growth tank maintained on 12/12 light/dark cycle, darkness is indicated by gray rectangles. Bottom graph: explants were pretreated 3 days in darkness, the dashed line rectangles indicate where plants experienced dark in the 12/12 h regime (adapted from Beilby et al., 2015).

is applied. Nothnagel et al. (1981) confirmed actin presence by fluorescently labeled phalloidin, while Williamson and Toh (1979) used an antibody raised against actin. Williamson (1972) and Shimmen and Tazawa (1983) stopped streaming by applying the animal systems inhibitor of actin-based motility, cytochalasin.

In analogy to muscle movement it seemed likely that myosin also participates in cytoplasmic streaming. Kato and Tonomura (1977) purified myosin from *Nitella*. Chen and Kamiya (1975, 1981) located myosin in the cell by moving cytoplasm into one half of the cell by centrifugation. If the half without cytoplasm was treated by SH reagent *N*-ethylmaleimide (NEM), or heat of 47.5°C, the subsequent streaming was not affected. When the same treatments were applied to cytoplasm-containing half of the cell, the streaming was disrupted in the whole cell. Therefore, similar to muscle, characean myosin is more sensitive to NEM and heat than actin and is found in the cytoplasm (for references see Shimmen and Yokota, 1994). Williamson (1975) observed cytoplasmic organelles, which became strongly bound to actin cables, when ATP was removed from perfusion medium in tonoplast free cells. Using electron microscopy Nagai and Hayama (1979) observed horn-like shapes with small globules (~ 30 nm diameter) on endoplasmic organelles. Kachar and Reese (1988) agreed that myosin may be found in ER, to facilitate sliding along the actin cables.

In characean cells the streaming speed can reach 100 $\mu\text{m/sec}$, much greater than that in higher plants and actin-myosin sliding in skeletal muscle. In “mix and match” experiments, glass was coated with myosin. The fluorescent-labeled actin filaments were added and their movement could be observed (Kron and Spudich, 1986). Shimmen and Yokota (1994) combined myosin from characean cytoplasm and actin filaments from skeletal muscle to observe similar sliding speeds to those in characean cytoplasmic streaming. Shimmen and Yano (1984) set up tonoplast-free cell with characean actin and perfused it with latex beads coated with skeletal muscle myosin. The slow velocity of this combination indicated that the speed of characean streaming is due to the native myosin.

Genetically characean myosin is similar to that of land plants: myosin XI. The myosin molecule was resolved by electron microscopy, showing two head structures and a tail that mediates the binding process (Shimmen, 2007, **Figure 7B**). While myosins in other species have positive charge on loop 2 and several lysine residues, *Chara* myosin loop 2 is uncharged with no lysine cluster. Instead, the loop 3 is positively charged (Ito et al., 2009), which leads to high ATPase activity. The less charge on loop 2 enables higher velocity. The structure of myosin, altered accordingly, speeded up the sliding in *Dictyostelium*.

Energy Source: Adenylates and Mg^{2+}

Williamson (1975) and Tazawa et al. (1976) determined that ATP provides energy for the myosin head to release. Without ATP the organelles are connected to actin cables by rigor cross-bridges (Nagai and Hayama, 1979). Shimmen (1978) found that maximum streaming velocity was reached at ATP concentrations above 200 μM , well above the normal cytoplasmic concentration of 0.5 – 3.4 mM. The relationship between streaming velocity and ATP concentration is linear. Consequently, inhibitors that diminish ATP concentration also affect streaming (Reid and Walker, 1983). Reid and Walker (1983), Shimmen (1988) perfused tonoplast-free cells with cytoplasm-like medium containing 1.6 ATP, 0.6 ADP, 0.8 AMP, 14.7 Pi and 2 pyrophosphate (in mM) and obtained normal streaming speeds. If only ADP was included in the perfusion medium, it was converted to ATP by adenylate kinase and streaming started after a delay. This streaming recovery was abolished by addition of adenylate kinase inhibitor to ADP medium. If the Mg^{2+} concentration in the perfusion medium was decreased compared to that of ATP, streaming speed declined (Shimmen, 1978, 1988). Shimmen and Tazawa (1983) confirmed the importance of Mg^{2+} by including Mg^{2+} chelator in the media, inhibiting streaming in both tonoplast-free and permeabilized experimental preparations. As in muscle Mg^{2+} is necessary for myosin ATPase reaction and it also maintains the streaming system.

Temperature, pH, Light and Ca^{2+}

Shimmen and Yoshida (1993) made detailed measurements of sensitivity of cytoplasmic streaming to temperature (for historical temperature measurements see references in Shimmen and Yokota, 1994). With pH and Ca^{2+} concentration controlled in perfused cells, there is a linear relationship between streaming velocity and temperature decrease in the range 25 – 0.5°C. Some intact cells did show a steeper drop in streaming speed between 15 and 10°C.

Fujii et al. (1979), Tazawa and Shimmen (1982) employed the tonoplast-free system to explore the effect of pH, finding the greatest streaming velocity at neutral pH. Shimmen and Tazawa (1985) investigated the effect of carboxylic acid secreted by leaf-cutting ant, myrmicacin. At low pH, the undissociated form of the carboxylic acid penetrates the plasma membrane and acidifies the neutral cytoplasm by dissociation. Thus the cytoplasmic streaming is only affected if myrmicacin is applied at low external pH. Barr and Broyer (1964) reported higher velocity of streaming upon illumination, which was abolished by photosynthesis inhibitor DCMU (Plieth and Hansen, 1992). Miller and Sanders (1987) measured a decrease in cytoplasmic calcium concentration upon illumination,

possibly due to Ca^{2+} uptake by the photosynthesising chloroplasts.

The early experiments researching the effects of Ca^{2+} on streaming were done on cytoplasmic droplets, which contained rotating chloroplasts (Hayama and Tazawa, 1980). The authors assumed that same actin-myosin mechanism was involved as in cytoplasmic streaming. Iontophoretic injection of different ions into the droplet produced different effect on the chloroplast movement: K^+ and Mg^{2+} had no effect, Ca^{2+} stopped the movement transiently, Sr^{2+} and Ba^{2+} had similar effect to Ca^{2+} , Mn^{2+} and Cd^{2+} induced slow irreversible decline in motion. After Kikuyama and Tazawa (1982) stopped the streaming transiently by direct injection of CaCl_2 into intact *Nitella* cell, Williamson (1975), Hayama et al. (1979) turned to tonoplast-free cells and found that up to 1 mM Ca^{2+} was needed to stop the streaming with incomplete recovery. Tominaga and Tazawa (1981) monitored streaming with time after perfusion and found that it became more sensitive to Ca^{2+} concentration. However, compared to intact cells the Ca^{2+} concentration for streaming stoppage was too high: the data from the perfused cells was misleading! Using aequorin Williamson and Ashley (1982) monitored the Ca^{2+} concentration in the cytoplasm of intact characean cells at the time of excitation: the peak concentration was 43 μM in *Nitella* and only 6.7 μM in *Chara*. At the time of AP, the streaming cytoplasm appears to “freeze” completely, restarting slowly after some minutes. Shimmen and Tazawa (1983) employed the permeabilized cells to confirm that only 1 – 10 μM Ca^{2+} were needed to stop the streaming. In the tonoplast-free system the native cytoplasm is removed in the perfusion process, while during permeabilization the cytoplasm is not disrupted. Consequently, it is a component of the cytoplasm that is Ca^{2+} sensitive.

Shimmen and Yano (1986) perfused cells with beads coated by skeletal muscle myosin and, like in the muscle; the movement dependence on calcium concentration was lost. Myosin in skeletal muscle has no Ca^{2+} sensitivity. Further, the incorporation of muscle troponin-tropomyosin complex into characean actin filaments actually made higher calcium concentration necessary to start streaming. Consequently, the calcium sensitivity in the intact characean cell is associated with myosin. As most of native cytoplasm is removed in rapidly perfused cells, the calcium sensitivity changed. In animal and mold systems myosin produces sliding either in phosphorylated or de-phosphorylated state. Tominaga et al. (1987) introduced phosphatase-1 into perfusion medium and abolished the streaming stoppage at high Ca^{2+} concentrations. The inhibitors of phosphatase-1, on the other hand, totally inhibited streaming. As characean myosin only promotes streaming in de-phosphorylated state, ATP- γ -S irreversibly inhibited the recovery of streaming after it was stopped by high Ca^{2+} concentration (thio-phosphorylated proteins are not de-phosphorylated with phosphatases). The authors suggest that at the time of an AP the phosphatase is activated indirectly through Ca^{2+} binding to calmodulin, as Ca^{2+} concentration rises. Calmodulin inhibitors, indeed, prevent streaming recovery only following exposure to high Ca^{2+} concentration, while steady state streaming is not affected (Tominaga et al., 1985).

The Importance of Streaming

Cytoplasmic streaming can be observed in many eukaryotic organisms: algae, higher plants, fungi, slime molds, nematodes and flies. The cells that utilize cytoplasmic streaming tend to be larger than the usual 10–100 μm or have specialized functions (Goldstein and van de Meent, 2015). However, some cells of normal size, such as cells in stinging nettle, parenchymal cells in onion or leaf cells in *Elodea*, exhibit slow circulation streaming. Fountain streaming can be observed in root hairs and pollen tubes of various higher plants. The details of the actin-myosin driven streaming were elucidated in characean cells, because their cell compartments can be manipulated. In large celled characean thalli streaming is crucial for intercellular transport of both nutrients and organic compounds (see Radioactive or Substitution Tracers). The pH banding that aids carbon fixation does not occur without streaming. There may be further roles of streaming in cell metabolism and improving homeostasis by enhancing vacuolar mixing (Goldstein and van de Meent, 2015).

Evolution of Hormone Auxin and its Signaling Pathways

Polar Auxin Transport (PAT)

In land plants growth and development is directed by auxin indole-3-acetic acid (IAA) concentration minima, maxima and gradients. Young shoots of land plants produce IAA and transport it to roots by parenchyma cells which produce auxin influx- (AUX, LAX) and efflux- (PIN) supporting proteins (for review see Petrasek and Friml, 2009). 1-N-naphthylphthalamic acid (NPA) is an efficient inhibitor of the efflux PIN proteins. IAA research in Characeae can elucidate some of the developmental steps in auxin signaling and metabolic pathways from origins in chlorophyte algae (De Smet et al., 2011) to the complexity of extant land plants.

Hori et al. (2014) detected auxin in the basal branching charophyte *Klebsormidium*. In Characeae with more complex morphology, effects of external IAA and its transport through the thallus and rhizoids were investigated. Klammt et al. (1992) observed rhizoids developing in cuttings of *Chara globularis*. The polar growth of rhizoids was inhibited by explant decapitation or by addition of NPA. If IAA was added to the medium, the inhibition of growth was reversed. ^{14}C IAA was retained by the explants more strongly after treatment with NPA. Thus NPA seems to inhibit IAA efflux as it does in higher plants. The rhizoid development in mosses is also affected by IAA (Eklund et al., 2010). Clabeaux and Bisson (2009) decapitated *C. australis* explants or tied the second internode with a silk thread to prevent basipetal transport through streaming. Greater number of axillary branches was observed in decapitated explants and below the tied thread: clear demonstration of apical dominance. However, unlike higher plants, the tied explants also produced greater number of rhizoids and addition of IAA to the medium had no effect.

Boot et al. (2012) placed one or two adjacent internodes of *C. corallina* in three-compartment chamber. The middle chamber was labeled by addition of ^3H -IAA and the appearance of the label was then monitored in the outer chambers. After 1 hr

the shoot to rhizoid directed transport of IAA was 50-times greater than that in the opposite direction. The polarity was lost upon exposure to NPA. Initially, the IAA transport through the thallus was attributed to cytoplasmic streaming, as the rate was comparable. When no rate decrease resulted from streaming inhibition by cytochalasin, Raven (2013) proposed involvement of other mechano-chemical motors such as dynein-tubulin or kinesin-tubulin. If the label was added to one of the outer compartments, large amount of IAA was detected in the middle compartment. The cortication of *C. vulgaris* prevented some of the leakage. The authors concluded that the auxin influx carrier proteins of higher plants are probably lacking in Characeae. Bennett et al. (2014) made a detailed study of PIN protein evolution, finding that charophyte *Klebsormidium* PIN structure was substantially different to that of higher plants. Thus the IAA transport proteins evolved to their present forms in different types of tissues of land plants.

Circadian and Seasonal Effects on IAA and Melatonin/Serotonin Metabolic Pathways

Beilby et al. (2015) measured circadian concentrations of IAA, melatonin and serotonin in *C. australis* plants. The plants, which experienced summer day-length and temperatures, exhibited distinct concentration maxima about 4 h after subjective daybreak. Similar concentration distribution persisted in plants pre-treated for 3 days in the dark, confirming a circadian rhythm (**Figure 7C**). Plants pre-treated 3 days in the light exhibited more IAA concentration maxima, while melatonin and serotonin exhibited smaller concentrations changes, less synchronized with those of IAA. In the winter plants exhibited much smaller IAA concentration maxima in the subjective dark phase, which again persisted after dark pre-treatment. Melatonin and serotonin concentrations were also much smaller, compared to summer cells, with only a weak correlation to IAA concentration changes. The close synchronization between IAA and serotonin circadian cycling suggests IAA biosynthesis by the tryptamine pathway, which intersects with the serotonin/melatonin pathway (Mano and Nemoto, 2012; Ljung, 2013). The IAA synthesis was recently investigated in charophytes by searching for sequences of tryptophan aminotransferase (TAA) and flavin monooxygenase (YUCCA) enzymes that mediate the main synthesis pathway in model plant *Arabidopsis*. Wang et al. (2014) found homologs of

these enzymes in *Klebsormidium* and two Characeae, but Turnaev et al. (2015) argued that the differences are too large for the enzymes to be functional. Ke et al. (2015) suggested that the results are inconclusive. So, this is clearly a very active research area!

The data in this section indicate that polar auxin transport and circadian influence on IAA pre-dates emergence of plants on land. The advantage of using characean thalli for biochemical assays are (i) small number of large internodal cells (with their contents dominating over much smaller nodal complexes) in each sample and (ii) relatively small differentiation between axial and leaf internodes compared to variety of tissues encountered in vascular land plants. The seasonal and circadian nature of endogenous IAA concentration also highlights the importance of collecting plant samples in the right season and at the right part of day cycle.

CONCLUSION

The size of characean cells provides the experimentalist with many options not available in typical plant cells or tissue. Due to this unusual morphology, Characeae were initially regarded as “interesting,” but not representative of higher plants. In recent decades, however, many higher plant-like properties are starting to emerge. The different aspects of the Characeae research are now coming together: electrophysiology, nutrient acquisition, cell to cell transport, carbon concentrating mechanisms, cytoplasmic streaming, geotropism, metabolic pathways, circadian rhythms, plant evolution, wound healing, cytoskeleton organization, cell walls, phytoremediation, lake ecology – too many topics to be discussed in this review. On the other hand, the exceptional Characeae morphology is providing insights into physical limits of cell size, transport of nutrients, homeostasis and macromolecular targeting (Goldstein and van de Meent, 2015). The Characeae system is about to become even more valuable with sequencing of *C. braunii*.

AUTHOR CONTRIBUTIONS

The author confirms being the sole contributor of this work and approved it for publication.

REFERENCES

- Barbier-Brygoo, H., Vinauger, M., Colcombet, J., Ephritikhine, G., Frachisse, J.-M., and Maurel, C. (2000). Anion channels in higher plants: functional characterization, molecular structure and physiological role. *Biochim. Biophys. Acta* 1465, 199–218. doi: 10.1016/S0006-2736(00)00139-5
- Barr, C. E., and Broyer, T. (1964). Effect of light on sodium influx, membrane potential, and protoplasmic streaming in *Nitella*. *Plant Physiol.* 39, 48–52. doi: 10.1104/pp.39.1.48
- Beilby, M. J. (1985). Potassium channels at *Chara plasmalemma*. *J. Exp. Bot.* 36, 228–239. doi: 10.1093/jxb/36.2.228
- Beilby, M. J. (1989). “Electrophysiology of giant algal cells,” *Methods in Enzymology*, Vol. 174, eds S. Fleischer and B. Fleischer (San Diego, CA: Academic Press), 403–443.
- Beilby, M. J. (2015). Salt tolerance at single cell level in giant-celled Characeae. *Front. Plant Sci.* 6:226. doi: 10.3389/fpls.2015.00226
- Beilby, M. J., and Bisson, M. A. (2012). “pH banding in charophyte algae,” in *Plant Electrophysiology*, Chap. 11, ed. A. Volkov (Berlin: Springer-Verlag), 247–271.
- Beilby, M. J., and Casanova, M. T. (2013). *The Physiology of Characean Cells*. Berlin: Springer.
- Beilby, M. J., Cherry, C. A., and Shepherd, V. A. (1999). Dual regulation response to hypertonic stress in *Lamprothamnium papulosum*. *Plant Cell Environ.* 22, 347–359. doi: 10.1046/j.1365-3040.1999.00406.x
- Beilby, M. J., Turi, C. E., Baker, T. C., Tym, F. J. M., and Murch, S. J. (2015). Circadian changes in endogenous concentrations of indole-3-acetic acid, melatonin, serotonin, abscisic acid and jasmonic acid in Characeae (*Chara australis* Brown). *Plant Signal. Behav.* 10:e1082697. doi: 10.1080/15592324.2015.1082697

- Beilby, M. J., and Walker, N. A. (1981). Chloride transport in *Chara*: I. kinetics and current-voltage curves for a probable proton symport. *J. Exp. Bot.* 32, 43–54. doi: 10.1093/jxb/32.1.43
- Berecki, G., Eijken, M., Van Iren, F., and Van Duijn, B. (2001). Tonoplast anion channel activity modulation by pH in *Chara corallina*. *J. Membr. Biol.* 184, 131–141. doi: 10.1007/s00232-001-0081-6
- Berecki, G., Varga, Z., Van Iren, F., and Van Duijn, B. (1999). Anion channels in *Chara corallina* tonoplast membrane: calcium dependence and rectification. *J. Membr. Biol.* 172, 159–168. doi: 10.1007/s002329900593
- Bertl, A. (1989). Current-voltage relationships of sodium-sensitive potassium channel in the tonoplast of *Chara corallina*. *J. Membr. Biol.* 109, 9–19. doi: 10.1007/BF01870786
- Bennett, T. A., Liu, M. M., Aoyama, T., Bierfreund, N. M., Braun, M., Coudert, Y., et al. (2014). Plasma membrane-targeted PIN proteins drive shoot development in a moss. *Curr. Biol.* 24, 2776–2785 doi: 10.1016/j.cub.2014.09.054
- Beyenbach, K. W., and Wieczorek, H. (2006). The V-type H^+ ATPase: molecular structure and function, physiological roles and regulation. *J. Exp. Biol.* 209, 577–589. doi: 10.1242/jeb.02014
- Bisson, M. A., and Kirst, G. O. (1980). *Lamprothamnium*, a euryhaline charophyte II. Time course of turgor regulation. *J. Exp. Bot.* 31, 1237–1244. doi: 10.1093/jxb/31.5.1237
- Blatt, M. R., Wang, Y., Leonhardt, N., and Hills, A. (2014). Exploring emergent properties in cellular homeostasis using OnGuard to model K^+ and other ion transport in guard cells. *J. Plant Physiol.* 171, 770–778. doi: 10.1016/j.jplph.2013.09.014
- Boot, K., Libbenga, K. R., Hille, S. C., Offringa, R., and van Duijn, B. (2012). Polar auxin transport: an early invention. *J. Exp. Bot.* 63, 4213–4218. doi: 10.1093/jxb/ers106
- Bostrom, T. E., and Walker, N. A. (1975). Intercellular transport in plants. I. The rate of transport of chloride and the electric resistance. *J. Exp. Bot.* 26, 767–782. doi: 10.1093/jxb/26.6.767
- Bostrom, T. E., and Walker, N. A. (1976). Intercellular transport in plants. II. Cyclosis and the rate of intercellular transport of chloride in *Chara*. *J. Exp. Bot.* 27, 347–357. doi: 10.1093/jxb/27.2.347
- Box, R., Andrews, M., and Raven, J. A. (1984). Intercellular transport and cytoplasmic streaming in *Chara hispida*. *J. Exp. Bot.* 35, 1016–1021. doi: 10.1093/jxb/35.7.1016
- Brecknock, S., Dibbayawan, T. P., Veske, M., Veske, P. A., Faulkner, C., Barton, D. A., et al. (2011). High resolution scanning electron microscopy of plasmodesmata. *Planta* 234, 749–758. doi: 10.1007/s00425-011-1440-x
- Burch-Smith, T., and Zambryski, P. (2012). Plasmodesmata paradigm shift: regulation from without versus within. *Annu. Rev. Plant Biol.* 63, 239–260. doi: 10.1146/annurev-arplant-042811-105453
- Chen, J., and Kamiya, N. (1975). Localisation of myosin in the internodal cell of *Nitella* as suggested by differential treatment with N-ethylmaleimide. *Cell Struct. Funct.* 1, 1–9. doi: 10.1247/csf.1.1
- Chen, J., and Kamiya, N. (1981). Differential heat treatment of the *Nitella* internodal cell and its relation to cytoplasmic streaming. *Cell Struct. Funct.* 6, 201–207. doi: 10.1247/csf.6.201
- Clabeaux, B. L., and Bisson, M. A. (2009). Developmental patterns in *Chara australis* (Characeae, Charophyceae): apical dominance, pH and auxin. *Charophytes* 1, 68–72.
- Cook, M. E., Graham, L. E., Botha, C. E. J., and Lavin, C. A. (1997). Comparative ultrastructure of plasmodesmata of *Chara* and selected bryophytes: toward an elucidation of the evolutionary origin of plant plasmodesmata. *Am. J. Bot.* 84, 1169–1178. doi: 10.2307/2446040
- Cote, R., Thain, J. F., and Fenson, D. S. (1987). Increase in electrical resistance of plasmodesmata of *Chara* induced by an applied pressure gradient across nodes. *Can. J. Bot.* 65, 509–511. doi: 10.1139/b87-064
- De Smet, I., Voss, U., Lau, S., Wilson, M., Shao, N., Timme, R. E., et al. (2011). Unravelling the evolution of auxin signalling. *Plant Physiol.* 155, 209–221. doi: 10.1104/pp.110.168161
- de Vries, J., Stanton, A., Archibald, J. M., and Gould, S. B. (2016). Streptophyte terrestrialization in light of plastid evolution. *Trends Plant Sci.* 21, 467–476. doi: 10.1016/j.tplants.2016.01.021
- Ding, D., and Tazawa, M. (1989). Influence of cytoplasmic streaming and turgor pressure gradient on the transnodal transport of rubidium and electrical conductance in *Chara corallina*. *Plant Cell Physiol.* 30, 739–748.
- Ding, D. Q., Amino, S., Mimura, T., Sakano, K., Nagata, T., and Tazawa, M. (1992). Quantitative analysis of intercellularly transported photoassimilates in *Chara corallina*. *J. Exp. Bot.* 43, 1045–1051. doi: 10.1093/jxb/43.8.1045
- Draber, S., Schultze, R., and Hansen, U.-P. (1993). Cooperative behaviour of K^+ channels in the tonoplast of *Chara corallina*. *Biophys. J.* 65, 1553–1559. doi: 10.1016/S0006-3495(93)81194-9
- Eklund, D. M., Thelander, M., Landberg, K., Ståldal, V., Nilsson, A., Johansson, M., et al. (2010). Homologues of the *Arabidopsis thaliana* SHI/STY/LRP1 genes control auxin biosynthesis and affect growth and development in the moss *Physcomitrella patens*. *Development* 137, 1275–1284. doi: 10.1242/dev.039594
- Evkaikina, A. I., Romanova, M. A., and Voitsekhovskaja, O. V. (2014). Evolutionary aspects of non-cell-autonomous regulation in vascular plants: structural background and models to study. *Front. Plant Sci.* 5:31. doi: 10.3389/fpls.2014.00031
- Fairley, K. A., and Walker, N. A. (1987). Amine ion porter in *Chara australis*: effects of alkyl substitution and external pH. *J. Membr. Biol.* 98, 191–196. doi: 10.1007/BF01872130
- Felle, H. H. (1994). The H^+/Cl^- symporter in root-hair cells of *Sinapis alba*. An electrophysiological study using ion-selective microelectrodes. *Plant Physiol.* 106, 1131–1136.
- Findlay, G. P., Hope, A. B., Pitman, M. G., Smith, F. A., and Walker, N. A. (1969). Ion fluxes in cells of *Chara corallina*. *Biochim. Biophys. Acta* 183, 565–576. doi: 10.1016/0006-2736(69)90170-9
- Franceschi, V. R., Ding, B., and Lucas, W. J. (1994). Mechanism of plasmodesmata formation in characean algae in relation to evolution of intercellular communication in higher plants. *Planta* 192, 347–358. doi: 10.1007/BF00198570
- Fujii, S., Shimmen, T., and Tazawa, M. (1979). Effect of intracellular pH on the light-induced potential change and electrogenic activity in tonoplast-free cells of *Chara australis*. *Plant Cell Physiol.* 20, 1315–1328.
- Goldstein, R. E., and van de Meent, J.-W. (2015). A physical perspective on cytoplasmic streaming. *Interface Focus* 5:20150030. doi: 10.1098/rsfs.2015.0030
- Hayama, T., Shimmen, T., and Tazawa, M. (1979). Participation of Ca^{2+} in cessation of cytoplasmic streaming induced by membrane excitation in Characeae internodal cells. *Protoplasma* 99, 305–321. doi: 10.1007/BF01275803
- Hayama, T., and Tazawa, M. (1980). Ca^{2+} reversibly inhibits active rotation of chloroplasts in isolated cytoplasmic droplets of *Chara*. *Protoplasma* 102, 1–9. doi: 10.1007/BF01276943
- Hedrich, R. (2012). Ion channels in plants. *Physiol. Rev.* 92, 1777–1811. doi: 10.1152/physrev.00038.2011
- Hedrich, R., and Schroeder, J. I. (1989). The physiology of ion channels and electrogenic pumps in higher plants. *Annu. Rev. Plant Physiol.* 40, 539–569. doi: 10.1146/annurev.pp.40.060189.002543
- Homble, F., and Fuks, B. (1991). Quantitative analysis of single K^+ channels in the tonoplast of *Chara corallina*: selectivity and TEA blockade. *J. Plant Physiol.* 137, 729–733. doi: 10.1016/S0176-1617(11)81230-7
- Hope, A. B., and Walker, N. A. (1975). *The Physiology of Giant Algal Cells*. London: Cambridge University Press.
- Hori, K., Maruyama, F., Fujisawa, T., Togashi, T., Yamamoto, N., Seo, M., et al. (2014). *Klebsormidium flaccidum* genome reveals primary factors for plant terrestrial adaptation. *Nat. Commun.* 5:3978. doi: 10.1038/ncomms4978
- Ito, K., Yamaguchi, Y., Yanase, K., Ichikawa, Y., and Yamamoto, K. (2009). Unique charge distribution in surface loops confers high velocity on the fast motor protein *Chara* myosin. *Proc. Natl. Acad. Sci. U.S.A.* 106, 21585–21590. doi: 10.1073/pnas.0910787106
- Kachar, B., and Reese, T. (1988). The mechanism of cytoplasmic streaming in characean algal cells: sliding of endoplasmic reticulum along actin filaments. *J. Cell Biol.* 106, 1545–1552. doi: 10.1083/jcb.106.5.1545
- Kamitsubo, E. (1966). Motile protoplasmic fibrils in cells of Characeae. II. Linear fibrillar structure and its bearing on protoplasmic streaming. *Proc. Jpn. Acad.* 42, 640–643.
- Kamitsubo, E. (1972). A “window technique” for detailed observation of characean cytoplasmic streaming. *Exp. Cell Res.* 74, 613–616. doi: 10.1016/0014-4827(72)90430-2

- Kamiya, N., and Kuroda, K. (1956). Velocity distribution of the protoplasmic streaming in *Nitella* cells. *Bot. Magazine (Tokyo)* 69, 544–554. doi: 10.15281/jplantres1887.69.544
- Karol, K. G., McCourt, R. M., Cimino, M. T., and Delwiche, C. F. (2001). The closest living relatives of land plants. *Science* 294, 2351–2353. doi: 10.1126/science.1065156
- Kato, T., and Tonomura, Y. (1977). Identification of myosin in *Nitella flexilis*. *J. Biochem.* 82, 777–782.
- Katsuhara, M., Mimura, T., and Tazawa, M. (1989). Patch-clamp study on a Ca^{2+} -regulated K^+ channel in the tonoplast of the brackish characeae *Lamprothamnium succinctum*. *Plant Cell Physiol.* 30, 549–555.
- Ke, M., Zheng, Y., and Zhu, Z. (2015). Rethinking the origin of auxin biosynthesis in plants. *Front. Plant Sci.* 6:1093. doi: 10.3389/fpls.2015.01093
- Kersey, Y., and Wessells, N. (1976). Localisation of actin filaments in internodal cells of characean algae. *J. Cell Biol.* 68, 264–275. doi: 10.1083/jcb.68.2.264
- Kikuyama, M., and Tazawa, M. (1982). Ca^{2+} ion reversibly inhibits the cytoplasmic streaming of *Nitella*. *Protoplasma* 113, 241–243. doi: 10.1007/BF01280914
- Klambt, D., Knauth, B., and Dittmann, I. (1992). Auxin dependent growth of rhizoids of *Chara globularis*. *Physiol. Plant.* 85, 537–540. doi: 10.1111/j.1399-3054.1992.tb05823.x
- Koselski, M., Trebacz, K., and Dziubinska, H. (2013). Cation-permeable vacuolar ion channels in the moss *Physcomitrella patens*: a patch-clamp study. *Planta* 238, 357–367. doi: 10.1007/s00425-013-1902-4
- Kron, S., and Spudich, J. (1986). Fluorescent actin filaments move on myosin fixed to a glass surface. *Proc. Natl. Acad. Sci. U.S.A.* 83, 6272–6276. doi: 10.1073/pnas.83.17.6272
- Kwiatkowska, M. (2003). Plasmodesmal changes are related to different developmental stages of antheridia of *Chara* species. *Protoplasma* 222, 1–11. doi: 10.1007/s00709-003-0001-y
- Laver, D. R. (1992). Divalent cation block and competition between divalent and monovalent cations in the large-conductance K^+ channel from *Chara australis*. *J. Gen. Physiol.* 100, 269–300. doi: 10.1085/jgp.100.2.269
- Laver, D. R., Cherry, C. A., and Walker, N. A. (1997). The actions of calmodulin antagonists W-7 and TFP and of calcium on the gating kinetics of the calcium-activated large conductance potassium channel of the *Chara* protoplasmic drop: a substrate-sensitive analysis. *J. Membr. Biol.* 155, 263–274. doi: 10.1007/s002329900179
- Laver, D. R., Fairley, K. A., and Walker, N. A. (1989). Ion permeation in a K^+ channel in *Chara australis*: direct evidence for diffusion limitation of ion flow in a maxi-K channel. *J. Membr. Biol.* 108, 153–164. doi: 10.1007/BF01871026
- Laver, D. R., and Walker, N. A. (1987). Steady-state voltage-dependent gating and conduction kinetics of single K^+ channels in the membrane of cytoplasmic drops of *Chara australis*. *J. Membr. Biol.* 100, 31–42. doi: 10.1007/BF02290138
- Laver, D. R., and Walker, N. A. (1991). Activation by Ca^{2+} and block by divalent ions of the K^+ channel in the membrane of cytoplasmic drops from *Chara australis*. *J. Membr. Biol.* 120, 131–139. doi: 10.1007/BF01872396
- Ljung, K. (2013). Auxin metabolism and homeostasis during plant development. *Development* 140, 943–950. doi: 10.1242/dev.086363
- Ludewig, U., Neuhauser, B., and Dynowski, M. (2007). Molecular mechanisms of ammonium transport and accumulation in plants. *FEBS Lett.* 581, 2301–2308. doi: 10.1016/j.febslet.2007.03.034
- Luhring, H. (1986). Recording of single K^+ channels in the membrane of cytoplasmic drop of *Chara australis*. *Protoplasma* 133, 19–27. doi: 10.1007/BF01293183
- Maathuis, F. J. M., Verlin, D., Smith, F. A., Sanders, D., Fernandez, J. A., and Walker, N. A. (1996). The physiological relevance of Na^+ -coupled K^+ -transport. *Plant Physiol.* 112, 1609–1616.
- MacRobbie, E. A. C. (1969). Ion fluxes to the vacuole of *Nitella translucens*. *J. Exp. Bot.* 20, 236–256. doi: 10.1093/jxb/20.2.236
- MacRobbie, E. A. C. (1975). Intracellular kinetics of tracer chloride and bromide in *Nitella translucens*. *J. Exp. Bot.* 26, 489–507. doi: 10.1093/jxb/26.4.489
- Mano, Y., and Nemoto, K. (2012). The pathway of auxin biosynthesis in plants. *J. Exp. Bot.* 63, 2853–2872. doi: 10.1093/jxb/ers091
- Martinoia, E., Maeshima, M., and Neuhäus, H. E. (2007). Vacuolar transporters and their essential role in plant metabolism. *J. Exp. Bot.* 58, 83–102. doi: 10.1093/jxb/erl183
- McCulloch, S., Beilby, M. J., and Walker, N. A. (1990). Transport of potassium in *Chara australis*: II. Kinetics of a symport with sodium. *J. Membr. Biol.* 115, 129–143. doi: 10.1007/BF01869452
- McDonald, T. R., Dietrich, F. S., and Lutzoni, F. (2011). Multiple horizontal gene transfers of ammonium transporters/ammonia permeases from prokaryotes to eukaryotes: toward a new functional and evolutionary classification. *Mol. Biol. Evol.* 29, 51–60. doi: 10.1093/molbev/msr123
- Miller, A. J., and Sanders, D. (1987). Depletion of cytosolic calcium induced by photosynthesis. *Nature (Lond.)* 326, 397–400.
- Mimura, T. (1999). Regulation of phosphate transport and homeostasis in plant cells. *Int. Rev. Cytol.* 191, 149–200. doi: 10.1016/S0074-7696(08)60159-X
- Mimura, T. (2001). Physiological control of phosphate uptake and phosphate homeostasis in plant cells. *Aust. J. Plant Physiol.* 28, 655–660.
- Mimura, T., Reid, R. J., Ohsumi, Y., and Smith, F. A. (2002). Induction of the Na^+/Pi cotransport system in the plasma membrane of *Chara corallina* requires external Na^+ and low levels of Pi . *Plant Cell Environ.* 25, 1475–1481. doi: 10.1046/j.1365-3040.2002.00921.x
- Mimura, T., Reid, R. J., and Smith, F. A. (1998). Control of phosphate transport across the plasma membrane of *Chara corallina*. *J. Exp. Bot.* 49, 13–19. doi: 10.1093/jxb/49.318.13
- Moriyasu, Y., Shimmen, T., and Tazawa, M. (1984a). Vacuolar pH regulation in *Chara australis*. *Cell Struct. Funct.* 9, 225–234. doi: 10.1247/csf.9.235
- Moriyasu, Y., Shimmen, T., and Tazawa, M. (1984b). Electric characteristics of the vacuolar membrane of *Chara* in relation to pH regulation. *Cell Struct. Funct.* 9, 235–246. doi: 10.1247/csf.9.235
- Nagai, R., and Hayama, T. (1979). Ultrastructure of the endoplasmic factor responsible for cytoplasmic streaming in *Chara* internodal cells. *J. Cell Sci.* 36, 121–136.
- Nagai, R., and Rebhun, L. (1966). Cytoplasmic microfilaments in streaming *Nitella* cells. *J. Ultrastruct. Res.* 14, 571–589. doi: 10.1016/S0022-5320(66)80083-7
- Nakanishi, Y., Matsuda, N., Aizawa, K., Kashiyama, T., Yamamoto, K., Mimura, T., et al. (1999). Molecular cloning and sequencing of the cDNA for vacuolar H^+ -pyrophosphatase from *Chara corallina*. *Biochim. Biophys. Acta* 1418, 245–250. doi: 10.1016/S0005-2736(99)00037-1
- Nothnagel, E., Barak, L. S., Sanger, J. W., and Webb, W. W. (1981). Fluorescence studies on modes of cytochalasin and phalloidin action on cytoplasmic streaming in *Chara*. *J. Cell Biol.* 88, 364–372. doi: 10.1083/jcb.88.2.364
- Nussaume, N., Kanno, S., Javot, H., Marin, E., Pochon, N., Ayadi, A., et al. (2011). Phosphate import in plants: focus on the PHT1 transporters. *Front. Plant Sci.* 2:83. doi: 10.3389/fpls.2011.00083
- Oparka, K. J., and Prior, D. A. M. (1992). Direct evidence for pressure-generated closure of plasmodesmata. *Plant J.* 2, 741–750. doi: 10.1111/j.1365-313X.1992.tb00143.x
- Palevitz, B., Ash, J. F., and Hepler, P. K. (1974). Actin in the green alga, *Nitella*. *Proc. Natl. Acad. Sci. U.S.A.* 71, 363–366. doi: 10.1073/pnas.71.2.363
- Pantoja, O. (2012). High affinity ammonium transporters: molecular mechanism of action. *Front. Plant Sci.* 3:34. doi: 10.3389/fpls.2012.00034
- Petrasek, J., and Friml, J. (2009). Auxin transport routes in plant development. *Development* 136, 2675–2688. doi: 10.1242/dev.030355
- Plieth, C., and Hansen, U.-P. (1992). Light dependence of protoplasmic streaming in *Nitella flexilis* L. as measured by means of laser-velocimetry. *Plant* 188, 332–339. doi: 10.1007/BF00192799
- Pottosin, I., and Andujas, P. R. (1994). Depolarization-activated K^+ channel in *Chara* droplets. *Plant Physiol.* 106, 313–319.
- Raven, J. A. (2005). “Evolution of plasmodesmata,” in *Annual Plant Reviews, Plasmodesmata*, Vol. 18, ed. K. J. Oparka (Hoboken: Wiley-Blackwell), 33–53.
- Raven, J. A. (2013). Polar auxin transport in relation to long-distance transport of nutrients in the Charales. *J. Exp. Bot.* 64, 1–9. doi: 10.1093/jxb/ers358
- Rea, P. A., and Sanders, D. (1987). Tonoplast energization: two H^+ pumps, one membrane. *Physiol. Plant.* 71, 131–141. doi: 10.1111/j.1399-3054.1987.tb04630.x
- Reid, R. J., Mimura, T., Ohsumi, Y., Walker, N. A., and Smith, F. A. (2000). Phosphate uptake in *Chara*: membrane transport via Na/Pi cotransport. *Plant Cell Environ.* 23, 223–228. doi: 10.1046/j.1365-3040.2000.00524.x
- Reid, R. J., and Overall, R. L. (1992). Intercellular communication in *Chara*: factors affecting transnodal electrical resistance and solute fluxes. *Plant Cell Environ.* 15, 507–517. doi: 10.1111/j.1365-3040.1992.tb01484.x

- Reid, R. J., and Walker, N. A. (1983). Adenylate concentrations in *Chara*: variability, effects of inhibitors and relationship to protoplasmic streaming. *Aust. J. Plant Physiol.* 10, 373–383.
- Ritchie, R. J. (1987). The permeability of ammonia, methylamine and ethylamine in charophyte *Chara corallina* (C. australis). *J. Exp. Bot.* 38, 67–76. doi: 10.1093/jxb/38.1.67
- Ritchie, R. J., Trautman, D. A., and Larkum, A. W. D. (1997). Phosphate uptake in the cyanobacterium *Synechococcus* R-2 (*Anacystis nidulans*, S. leopoliensis) PCC 7942. *Plant Cell Physiol.* 38, 1232–1241. doi: 10.1093/oxfordjournals.pcp.a029110
- Ruhfel, B. R., Gitzendanner, M. A., Soltis, P. S., Soltis, D. E., and Burleigh, J. G. (2014). From algae to angiosperms – inferring the phylogeny of green plants (Viridiplantae) from 360 plastid genomes. *BMC Evol. Biol.* 14:23. doi: 10.1186/1471-2148-14-23
- Ryan, P. R., and Walker, N. A. (1993). Malate accumulates in the vacuole of *Chara australis* during uptake of ammonium from chloride-free solution. *J. Exp. Bot.* 44, 637–643. doi: 10.1093/jxb/44.3.637
- Ryan, P. R., and Walker, N. A. (1994). The regulation of ammonia uptake in *Chara australis*. *J. Exp. Bot.* 45, 1057–1067. doi: 10.1093/jxb/45.8.1057
- Sakano, K., and Tazawa, M. (1986). Tonoplast origin of the envelope membrane of cytoplasmic droplets prepared from *Chara* internodal cells. *Protoplasma* 131, 247–249. doi: 10.1007/BF01282988
- Sanders, D. (1980a). Control of Cl⁻ influx in *Chara* by cytoplasmic Cl⁻ concentration. *J. Membr. Biol.* 52, 51–60. doi: 10.1007/BF01869005
- Sanders, D. (1980b). The mechanism of Cl⁻ transport at the plasma membrane of *Chara corallina* I. Cotransport with H⁺. *J. Membr. Biol.* 53, 129–141. doi: 10.1007/BF01870581
- Sanders, D., and Hansen, U. P. (1981). Mechanism of Cl⁻ transport at the plasma membrane of *Chara corallina*: II. Transhibition and the determination of H⁺/Cl⁻ binding order from a reaction kinetic model. *J. Membr. Biol.* 58, 139–153. doi: 10.1007/BF01870976
- Schultze, R., and Draber, S. (1993). A nonlinear filter algorithm for the detection of jumps in patch-clamp data. *J. Membr. Biol.* 132, 41–52. doi: 10.1007/BF00233050
- Shepherd, V. A., and Goodwin, P. B. (1992a). Seasonal patterns of cell-to-cell communication in *Chara corallina* Klein ex Willd. I. Cell-to-cell communication in vegetative lateral branches during winter and spring. *Plant Cell Environ.* 15, 137–150. doi: 10.1111/j.1365-3040.1992.tb01468.x
- Shepherd, V. A., and Goodwin, P. B. (1992b). Seasonal patterns of cell-to-cell communication in *Chara corallina* Klein ex Willd. II. Cell-to-cell communication during the development of antheridia. *Plant Cell Environ.* 15, 151–162. doi: 10.1111/j.1365-3040.1992.tb01468.x
- Shimmen, T. (1978). Dependency of cytoplasmic streaming on intracellular ATP and Mg²⁺ concentrations. *Cell Struct. Funct.* 3, 113–121. doi: 10.1247/csf.3.113
- Shimmen, T. (1988). Cytoplasmic streaming regulated by adenine nucleotides and inorganic phosphates in Characeae. *Protoplasma Suppl.* 1, 3–9. doi: 10.1007/978-3-7091-9008-1_1
- Shimmen, T. (2007). The sliding theory of cytoplasmic streaming: fifty years of progress. *J. Plant Res.* 120, 31–43. doi: 10.1007/s10265-006-0061-0
- Shimmen, T., and MacRobbie, E. A. C. (1987). Characterisation of two proton transport systems in the tonoplast of plasmalemma-permeabilized *Nitella* cells. *Plant Cell Physiol.* 28, 1023–1031.
- Shimmen, T., and Tazawa, M. (1982). Reconstitution of cytoplasmic streaming in Characeae. *Protoplasma* 113, 127–131. doi: 10.1007/BF01282001
- Shimmen, T., and Tazawa, M. (1983). Control of cytoplasmic streaming by ATP, Mg²⁺ and cytochalasin B in permeabilized Characeae cell. *Protoplasma* 115, 18–24. doi: 10.1007/BF01293576
- Shimmen, T., and Tazawa, M. (1985). Mechanism of inhibition of cytoplasmic streaming by myrmicacin (β -Hydroxydecanoic acid) in *Chara* and *Spirogyra*. *Protoplasma* 127, 93–100. doi: 10.1007/BF01273705
- Shimmen, T., and Yano, M. (1984). Active sliding movement of latex beads coated coated with skeletal muscle myosin on *Chara* actin bundles. *Protoplasma* 121, 132–137. doi: 10.1007/BF01279760
- Shimmen, T., and Yano, M. (1986). Regulation of myosin sliding along *Chara* actin bundles by native skeletal muscle tropomyosin. *Protoplasma* 132, 129–136. doi: 10.1007/BF01276992
- Shimmen, T., and Yokota, E. (1994). Physiological and biochemical aspects of cytoplasmic streaming. *Int. Rev. Cytol.* 155, 97–139. doi: 10.1016/S0074-7696(08)62097-5
- Shimmen, T., and Yoshida, S. (1993). Analysis of temperture dependency of cytoplasmic streaming using tonoplast-free cells of Characeae. *Protoplasma* 176, 174–177. doi: 10.1007/BF01378954
- Sibaoka, T., and Tabata, T. (1981). Electrotonic coupling between adjacent internodal cells of *Chara braunii*: transmission of action potentials beyond the node. *Plant Cell Physiol.* 22, 397–411.
- Smith, F. A., and Walker, N. A. (1978). Entry of methylammonium and ammonium ions into *Chara* internodal cells. *J. Exp. Bot.* 29, 107–120. doi: 10.1093/jxb/29.1.107
- Smith, F. A., and Walker, N. A. (1989). Transport of potassium in *Chara australis*: I. A symport with sodium. *J. Membr. Biol.* 108, 125–137. doi: 10.1007/BF01871024
- Spanwick, R. M., and Costerton, J. (1967). Plasmodesmata in *Nitella translucens*: structure and electrical resistance. *J. Cell Sci.* 2, 451–464.
- Tazawa, M. (1964). Studies on *Nitella* having artificial cell sap. I. Replacement of the cell sap with artificial solutions. *Plant Cell Physiol.* 5, 33–43.
- Tazawa, M., Kikuyama, M., and Shimmen, T. (1976). Electric characteristics and cytoplasmic streaming of Characeae cells lacking tonoplast. *Cell Struct. Funct.* 1, 165–175. doi: 10.1247/csf.1.165
- Tazawa, M., Kishimoto, U., and Kikuyama, M. (1974). Potassium, sodium and chloride in the protoplasm of Characeae. *Plant Cell Physiol.* 15, 103–110.
- Tazawa, M., and Shimmen, T. (1982). Artificial control of cytoplasmic pH and its bearing on cytoplasmic streaming, electrogenesis and excitability of characeae cells. *J. Plant Res.* 95, 147–154. doi: 10.1007/BF02488581
- Teakle, N. L., and Tyerman, S. D. (2010). Mechanisms of Cl⁻ transport contributing to salt tolerance. *Plant Cell Environ.* 33, 566–589. doi: 10.1111/j.1365-3040.2009.02060.x
- Tester, M., Beilby, M. J., and Shimmen, T. (1987). Electrical characteristics of the tonoplast of *Chara corallina*: a study using permeabilised cells. *Plant Cell Physiol.* 28, 1555–1568.
- Timme, R. E., Bachvaro $\check{\text{d}}$, T. R., and Delwiche, C. H. F. (2012). Broad phylogenomic sampling and the sister lineage of land plants. *PLoS ONE* 7:e29696. doi: 10.1371/journal.pone.0029696
- Tominaga, Y., Muto, S., Shimmen, T., and Tazawa, M. (1985). Calmodulin and Ca²⁺ - controlled cytoplasmic streaming in characean cells. *Cell Struct. Funct.* 10, 315–325. doi: 10.1247/csf.10.315
- Tominaga, Y., and Tazawa, M. (1981). Reversible inhibition of cytoplasmic streaming by intracellular Ca²⁺ in tonoplast-free cells of *Chara australis*. *Protoplasma* 109, 103–111. doi: 10.1007/BF01287633
- Tominaga, Y., Wayne, R., Tung, H. Y. L., and Tazawa, M. (1987). Phosphorylation-dephosphorylation is involved in Ca²⁺-controlled cytoplasmic streaming of characean cells. *Protoplasma* 136, 161–169. doi: 10.1007/BF01276365
- Trebacz, K., Fenson, D. S., Harris, A., and Zawadski, T. (1988). Transnodal transport of ¹⁴C in *Nitella flexilis* III. Further studies on dissolved inorganic carbon movements in tandem cells. *J. Exp. Bot.* 39, 1561–1573. doi: 10.1093/jxb/39.11.1561
- Turnaev, I. I., Gunbin, K. V., and Afonnikov, D. A. (2015). Plant auxin biosynthesis did not originate in charophytes. *Trends Plant Sci.* 20, 463–465. doi: 10.1016/j.tplants.2015.06.004
- Tyerman, S. D., and Findlay, G. P. (1989). Current-voltage curves of single Cl⁻ channels which coexist with two types of K⁺ channel in the tonoplast of *Chara corallina*. *J. Exp. Bot.* 40, 105–117. doi: 10.1093/jxb/40.1.105
- Tyerman, S. D., Terry, B. R., and Findlay, G. P. (1992). Multiple conductances in the large K⁺ channel from *Chara corallina* shown by a transient analysis method. *Biophys. J.* 61, 736–749. doi: 10.1016/S0006-3495(92)81878-7
- Ullrich, W. R., and Glasser, E. (1982). Sodium-phosphate cotransport in the green alga *Ankistrodesmus braunii*. *Plant Sci. Lett.* 27, 155–161. doi: 10.1016/0304-4211(82)90144-4
- Walker, N. A. (1955). Microelectrode experiments on *Nitella*. *Aust. J. Biol. Sci.* 8, 476–489. doi: 10.1071/BI9550476
- Walker, N. A. (1994). “Sodium-coupled symports in the plasma membrane of plant cells,” in Proceedings of the Society for Experimental Biology Symposium XLVII: *Membrane Transport in Plants and Fungi: Molecular Mechanisms and Control*, eds M. R. Blatt, R. A. Leigh, and D. Sanders (Cambridge: The company of Biologists), 179–192.

- Walker, N. A., Beilby, M. J., and Smith, F. A. (1979a). Amine uniport at the plasmalemma of charophyte cells: I. Current - voltage curves, saturation kinetics, and effects of unstirred layers. *J. Membr. Biol.* 49, 21–55. doi: 10.1007/BF01871038
- Walker, N. A., and Bostrom, T. E. (1973). "Intercellular movement of chloride in *Chara* - a test of models for chloride influx," in *Ion Transport in Plants*, ed. W. P. Anderson (London: Academic Press), 447–461.
- Walker, N. A., Reid, R. J., and Smith, F. A. (1993). The uptake and metabolism of urea by *Chara australis*. IV. Symport with sodium – a slip model for the high and low affinity system. *J. Membr. Biol.* 136, 263–271. doi: 10.1007/BF00233665
- Walker, N. A., Smith, F. A., and Beilby, M. J. (1979b). Amine uniport at the plasmalemma of charophyte cells. II. Ratio of matter to charge transported and permeability of free base. *J. Membr. Biol.* 49, 283–296. doi: 10.1007/BF01871123
- Wang, C., Liu, Y., Li, S.-S., and Han, G.-Z. (2014). Origin of plant auxin biosynthesis in charophyte algae. *Trends Plant Sci.* 19, 741–743. doi: 10.1016/j.tplants.2014.10.004
- Wickett, N. J., Mirarab, S., Nguyen, N., Warnow, T., Carpenter, E., Matasci, N., et al. (2014). Phylogenomic analysis of the origin and early diversification of land plants. *Proc. Natl. Acad. Sci. U.S.A.* 111, E4859–E4868. doi: 10.1073/pnas.1323926111
- Williamson, R. E. (1972). A light-microscope study of the action of cytochalasin B on the cells and isolated cytoplasm of the characeae. *J. Cell Sci.* 10, 811–819.
- Williamson, R. E. (1974). Actin in the alga *Chara corallina*. *Nature (Lond.)* 248, 801–802. doi: 10.1038/248801a0
- Williamson, R. E. (1975). Cytoplasmic streaming in *Chara*: a cell model activated by ATP and inhibited by cytochalasin B. *J. Cell Sci.* 17, 655–668.
- Williamson, R. E., and Ashley, C. C. (1982). Free Ca^{2+} and cytoplasmic streaming in the alga *Chara*. *Nature* 296, 647–651. doi: 10.1038/296647a0
- Williamson, R. E., and Toh, B. (1979). "Motile models of plant cells and the immunofluorescence localisation of actin in a motile *Chara* cell model," in *Cell Motility: Molecules and Organisation*, eds H. I. S. Hatano and H. Sato (Tokyo: University of Tokyo Press).
- Wodniok, S., Brinkmann, H., Glockner, G., Heidel, A. J., Philippe, H., Melkonian, M., et al. (2011). Origin of land plants: do conjugating green algae 1776 hold the key? *BMC Evol. Biol.* 11:104. doi: 10.1186/1471-2148-11-104
- Zawadski, T., and Fenson, D. S. (1986a). Transnodal transport of ^{14}C in *Nitella flexilis*: I Tandem cells without applied pressure gradients. *J. Exp. Bot.* 37, 1341–1352. doi: 10.1093/jxb/37.9.1341
- Zawadski, T., and Fenson, D. S. (1986b). Transnodal transport of ^{14}C in *Nitella flexilis* II. Tandem cells with applied pressure gradients. *J. Exp. Bot.* 37, 1353–1363. doi: 10.1093/jxb/37.9.1353

Conflict of Interest Statement: The author declares that the research was conducted in the absence of any commercial or financial relationships that could be construed as a potential conflict of interest.

Copyright © 2016 Beilby. This is an open-access article distributed under the terms of the Creative Commons Attribution License (CC BY). The use, distribution or reproduction in other forums is permitted, provided the original author(s) or licensor are credited and that the original publication in this journal is cited, in accordance with accepted academic practice. No use, distribution or reproduction is permitted which does not comply with these terms.



Is Wortmannin-Induced Reorganization of the *trans*-Golgi Network the Key to Explain Charosome Formation?

Ilse Foissner^{*}, Aniela Sommer, Margit Hoeftberger, Marion C. Hoepflinger and Marketa Absolonova

Department of Cell Biology/Plant Physiology, University of Salzburg, Salzburg, Austria

OPEN ACCESS

Edited by:

David Domozych,
Skidmore College, USA

Reviewed by:

Yan Zhang,
Shandong Agricultural University,
China
Da Xing,
South China Normal University, China
Masa H. Sato,
Kyoto Prefectural University, Japan

***Correspondence:**

Ilse Foissner
ilse.foissner@sbg.ac.at

Specialty section:

This article was submitted to
Plant Evolution and Development,
a section of the journal
Frontiers in Plant Science

Received: 07 March 2016

Accepted: 17 May 2016

Published: 03 June 2016

Citation:

Foissner I, Sommer A, Hoeftberger M, Hoepflinger MC and Absolonova M (2016) Is Wortmannin-Induced Reorganization of the *trans*-Golgi Network the Key to Explain Charosome Formation? *Front. Plant Sci.* 7:756.
doi: 10.3389/fpls.2016.00756

Wortmannin, a fungal metabolite and an inhibitor of phosphatidylinositol-3 (PI3) and phosphatidylinositol-4 (PI4) kinases, is widely used for the investigation and dissection of vacuolar trafficking routes and for the identification of proteins located at multivesicular bodies (MVBs). In this study, we applied wortmannin on internodal cells of the characean green alga *Chara australis*. Wortmannin was used at concentrations of 25 and 50 μ M which, unlike in other cells, arrested neither constitutive, nor wounding-induced endocytosis via coated vesicles. Wortmannin caused the formation of “mixed compartments” consisting of MVBs and membranous tubules which were probably derived from the *trans*-Golgi network (TGN) and within these compartments MVBs fused into larger organelles. Most interestingly, wortmannin also caused pronounced changes in the morphology of the TGNs. After transient hypertrophy, the TGNs lost their coat and formed compact, three-dimensional meshworks of anastomosing tubules containing a central core. These meshworks had a size of up to 4 μ m and a striking resemblance to charasomes, which are convoluted plasma membrane domains, and which serve to increase the area available for transporters. Our findings indicate that similar mechanisms are responsible for the formation of charasomes and the wortmannin-induced reorganization of the TGN. We hypothesize that both organelles grow because of a disturbance of clathrin-dependent membrane retrieval due to inhibition of PI3 and/or PI4 kinases. This leads to local inhibition of clathrin-mediated endocytosis during charosome formation in untreated cells and to inhibition of vesicle release from the TGN in wortmannin-treated cells, respectively. The morphological resemblance between charasomes and wortmannin-modified TGN compartments suggests that homologous proteins are involved in membrane curvature and organelle architecture.

Keywords: *Chara australis*, wortmannin, *trans*-Golgi network, charosome, multivesicular body, endocytosis

INTRODUCTION

Wortmannin is a furanosteroid metabolite from the fungus *Penicillium funiculosum* which is widely used as a tool for the disruption and identification of vesicular trafficking routes and for defining endosomal compartments (Robinson et al., 2008). In plant cells, wortmannin interferes with protein trafficking to the plant vacuole (daSilva et al., 2005) and it causes homotypic fusion and

enlargement of multivesicular bodies (MVBs; Wang et al., 2009; Takáč et al., 2012). Wortmannin induces the fusion of vacuoles in guard cells where vacuoles are naturally fragmented after abscisic acid-induced stomata closure (Zheng et al., 2014), and on the other hand, wortmannin has been described to rescue vacuole fusion in a SNARE mutant of *Arabidopsis thaliana* (Zheng et al., 2014). In root meristems, wortmannin treatment results in the formation of abnormal vacuolar structures (Feraru et al., 2010), and in tobacco culture cells wortmannin inhibits autophagy (Takatsuka et al., 2004; Li and Vierstra, 2012). However, wortmannin also causes vacuolar cargo to be secreted to the apoplast (Pimpl et al., 2003), indicating that not only MVBs are affected, but also a compartment involved in exocytosis, e.g., the TGN (see Robinson et al., 2012). Indeed, mixed MVB/TGN compartments have been described in wortmannin-treated cells where SCAMP1, a marker of the TGN, was found to localize to the dilated, wortmannin-induced MVBs (Lam et al., 2007a). A proteomic study also confirmed the effect of wortmannin on TGNs (Takáč et al., 2012). Recently, wortmannin was found to suppress the V-ATPase activation in *A. thaliana* (Liu et al., 2016).

The huge internodes of the characean algae are useful models to study vesicular trafficking and lateral compartmentation of the plasma membrane (Foissner and Wasteneys, 2012, 2014). The cytoplasm of characean internodal cells consists of a stationary cortex in which helically oriented files of chloroplasts are anchored, and a mobile endoplasm which performs rotational streaming along actin filament bundles attached to the inner surface of the chloroplasts via interaction with myosin-coated organelles (Foissner and Wasteneys, 2014; Supplementary Figure 1). A conspicuous feature of *Chara* cells are convoluted plasma membrane domains, called charasomes. Charasomes can be stained in living cells by fluorescent plasma membrane dyes due to the increased signal caused by the superimposed plasma membrane infoldings (Schmoelzer et al., 2011; compare Figure 6A). Charasomes serve to accommodate a high number of H⁺-ATPases (Price and Whitecross, 1983; Schmoelzer et al., 2011), and probably also other transporters (Franceschi and Lucas, 1982; Keifer et al., 1982; Lucas et al., 1986). The H⁺-ATPases acidify the surroundings of the cell, so that the poorly membrane permeable hydrogen carbonate (HCO₃⁻, bicarbonate) is reduced to CO₂ which diffuses into the cell where it is used for photosynthesis (Lucas, 1983; Price et al., 1985).

The charasomes are not evenly distributed along the cell surface and extended regions with large, numerous charasomes alternate with smaller areas containing few, small charasomes, when cells have been exposed to standard light/dark conditions (16/8 h) for at least several days (Franceschi and Lucas, 1980; Bisson et al., 1991; Schmoelzer et al., 2011). In branchlet internodal cells of *C. australis* and under steady state conditions, the distribution of charasomes correlates with the pattern of acid and alkaline regions along the surface of cells, which can be visualized by phenol red (Schmoelzer et al., 2011). However, pH bands can also develop in the absence of charasomes, and the pH banding pattern readily changes upon disturbance of the cell (Franceschi and Lucas, 1980; Bulychev et al., 2004). These newly formed pH bands are probably due to differential activation of ion pumps and/or channels, and may explain the results of other

studies in which no correlation between pH bands and charosome density was found (Bisson et al., 1991).

Little is known about the formation and degradation of charasomes. Electron microscopy studies indicate that during charosome growth, vesicles derived from the TGN fuse with the plasma membrane in the absence of membrane recycling via coated vesicles (Lucas and Franceschi, 1981). The resulting tubules may again fuse with the plasma membrane and other tubules. In darkness, or in cells treated with inhibitors of photosynthesis, charasomes are degraded (e.g., Chau et al., 1994; Schmoelzer et al., 2011), probably via endocytosis. So far, it is unclear by which mechanism charosome membrane recycling is switched off or on.

The *trans*-Golgi network was first described as a “partially coated reticulum” in *Chara* internodal cells (Pesacreta and Lucas, 1984). Unlike as in many higher plant cells, the TGN of mature characean internodal cells is easy to distinguish from the Golgi body because of its distinct morphology and its location relative to the Golgi cisternae, at least in chemically fixed mature cells. Furthermore, TGN membranes are only slightly stained by zinc-iodide-osmium tetroxide in contrast to the membranes of the Golgi body (Pesacreta and Lucas, 1984). Based on these findings, the TGN was identified as an independent organelle (Pesacreta and Lucas, 1984). Later, the TGN has also been described in higher plant cells, and its identity as a separate organelle has been confirmed (e.g., Foresti and Denecke, 2008; Robinson et al., 2008 for references). The dual function of the TGN as an endocytic and secretory organelle has been proposed by localizing secretory and endocytic cargo (Viotti et al., 2010).

In an attempt to study vesicular trafficking in green algae, we treated internodal cells of *C. australis* with wortmannin. We found that wortmannin induced the fusion of MVBs with TGN-derived membranes, as described in other cells. More interestingly, wortmannin also inhibited the release of TGN vesicles, and caused a considerable reorganization of the loose TGN tubules into compact meshworks which had a stunning resemblance to charasomes. Our data indicate that similar mechanisms are involved in the formation of charasomes and wortmannin-modified TGNs, and that a similar set of proteins is involved in the development and maintenance of these complex tubular meshworks.

MATERIALS AND METHODS

Algal Material, Culture Conditions, and Inhibitor Treatments

Thalli of *Chara australis* were grown in a substrate of soil, peat and sand in 10–50 L aquaria filled with distilled water. The temperature was about 20°C and fluorescent lamps provided a 16/8 h light/dark cycle. The light intensity was low (about 5 $\mu\text{E} \cdot \text{m}^{-2} \cdot \text{s}^{-1}$) in order to prevent calcification and growth of epiphytes.

For our study, we used mature, non-growing internodal cells of the branchlets of *C. australis* collected from the 3rd and the 4th upper whorl of 1–2 month-old thalli. Each whorl consisted of 5 or 6 branchlets, and each branchlet consisted of 2–3 internodal

cells which varied in length between 5 and 30 mm. Prior to the experiments, the medial and distal internodal cells of the branchlets were isolated from the thallus with a small pair of scissors and incubated in artificial fresh water (10^{-4} M NaCl, 10^{-4} M KCl, 10^{-3} M CaCl₂) for at least 1 day. Cells were then incubated in wortmannin-containing AFW, or in the appropriate DMSO-containing solution (control).

Wortmannin (Enzo Life Sciences, Lausen, Switzerland) was dissolved in dimethyl sulfoxide (DMSO) at a concentration of 5 mM and diluted with AFW. During the course of this study we used 25 and 50 μ M working solutions. Controls contained the corresponding amounts of the solvent (up to 1%). For studying the internalization of FM/AM dyes, we additionally tested wortmannin solutions diluted from a 10 mM stock solution in order to decrease the DMSO content (maximal 0.5%) which could eventually lead to non-endocytotic uptake of the styryl dyes. The pH of the artificial fresh water was not significantly altered by the addition of DMSO or wortmannin.

The velocity of cytoplasmic streaming was measured in the light microscope using a 40x objective lens and a stop watch. The movement of at least two structures (organelles) in different regions of the bulk streaming mass was analyzed per cell and the highest value was used for statistical analysis.

pH Banding and *In vivo* Staining

The pH banding pattern of internodal cells was documented using phenol red (phenolsulfonphthalein; Sigma, St. Louis, USA) at a concentration of 4 μ M dissolved in AFW from a stock solution of 10 mM in distilled water.

For *in vivo* staining of charasomes and endosomes internodal cells were pulse labeled for 5 min with green fluorescent FM1-43FX (N-(3-triethylammoniumpropyl)-4-(4-(dibutylamino)styryl)pyridinium dibromide) (Invitrogen, Carlsbad, USA) and AM1-44 (Biotium, Hayward, USA), or with red fluorescent FM4-64 (N-(3-triethylammoniumpropyl)-4-(4-(diethylamino)phenyl)hexatrienyl)pyridinium dibromide) (Invitrogen) and AM4-65 (Biotium). All dyes were used at a concentration of 10 μ M.

The *in vivo* detection and counting of endosomal organelles stained by styryl dyes was hampered by the strong autofluorescence of the compact chloroplast files. Therefore, we applied the “window technique,” which is generally used for light microscopical observation of the endoplasm in characean cells (Kamitsubo, 1972). This method consists in local strong illumination of the cells which causes chloroplasts to bleach, swell and eventually detach from the irradiated area. *Chara* cells used in our experiments were locally irradiated with the blue light of a halide microscope lamp for 3 min at least 1 day prior to the experiments, which resulted in a chloroplast-free window with an area of about 30,000 μm^2 (ca. 200 \times 150 μm wide rectangle; compare Figure 1A). Data were collected from individual images and care was taken to analyze non-overlapping regions of endoplasm. Fluorescent particles were counted and analyzed using ImageJ (<http://imagej.nih.gov/ij>).

Immunofluorescence

Fixation and staining protocols for indirect immunofluorescence were as described by Schmoelzer et al. (2011). Primary antibodies

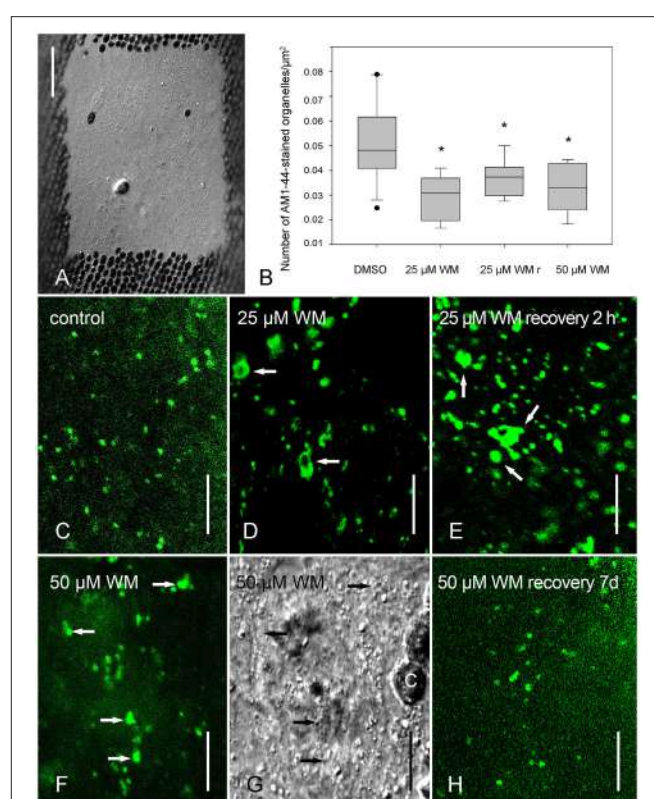


FIGURE 1 | Effect of wortmannin on internalization of AM1-44 in internodal cells of *Chara australis*. **(A)** Chloroplast-free window for imaging endosomal organelles (DIC). **(B)** Relative numbers of AM1-44-stained organelles in control cells, in cells treated with 25 μ M wortmannin (WM) for 2.5 h, in cells recovering from this treatment for 2 h in artificial fresh water (WMr) and in cells treated with 50 μ M wortmannin for 2.5 h are compared in box-and-whisker plots. Shown are median values with upper and lower quartiles (boxes), whiskers indicating the 10th and 90th percentiles, and outliers (dots) with $n =$ between 5 and 17. Differences between median values of control and treated cells are significant (asterisks; one way analysis of variance, $P = 0.001$). **(C–H)** AM1-44-stained organelles in cells treated with 0.5% DMSO **(C)**, with 25 μ M wortmannin for 2.5 h **(D)**, with 25 μ M wortmannin for 2.5 h followed by 2 h “recovery” in artificial fresh water **(E)**, with 50 μ M wortmannin for 2.5 h **(F,G** is the corresponding DIC image), and with 50 μ M wortmannin for 2.5 h, followed by 7 d recovery in artificial fresh water **(H**, compare with **F**). Arrows indicate enlarged organelles in response to wortmannin treatment; C, chloroplast. Bars are 50 μm **(A)** and 10 μm **(C–H)**.

used for this study were rabbit polyclonal anti-OsSCAMP1 (Lam et al., 2007a; generously provided by Liwen Jiang, University of Hongkong) used at a concentration of 40 μg per ml and rabbit polyclonal anti-CaARA7 which was used at a concentration of 3.6 μg per ml (Hoepflinger et al., 2015). Secondary antibodies were anti-rabbit IgG Alexa 488 (Invitrogen) diluted 2:1000, or anti rabbit IgG Alexa Fluor 546 (Invitrogen) diluted 3:1000. All antibodies were diluted in blocking buffer [1% (w/v) bovine serum albumin and 50 mM glycine in phosphate buffered saline (PBS), pH 7.2].

For double labeling experiments, we used basically the same fixing and staining protocol as above with some modifications because both primary antibodies were raised in rabbits. After incubation with the first primary antibody (rabbit polyclonal

anti-CaARA7), samples were incubated with a monovalent anti-rabbit Fab' fragment coupled to Alexa 488 (Nanoprobes, USA), then washed with PBS and subsequently post-fixed for 30 min in 1% (v/v) glutaraldehyde in PBS. Samples were rinsed overnight with PBS buffer and then blocked with 1% (w/v) bovine serum albumin and 50 mM glycine in PBS, followed by the incubation with the second primary antibody anti-OsSCAMP1. All subsequent steps were as described in Schmoelzer et al. (2011).

Confocal Laser Scanning Microscopy and Statistical Analysis

The confocal laser scanning microscopes used in this study were a Leica (Mannheim, Germany) TCS SP5 coupled to a DMI 6000B inverted microscope, and a Zeiss (Jena, Germany) LSM 510 coupled to a Zeiss Axiovert inverted microscope. For the excitation of Alexa 488, FM1-43, and AM1-44, we used the 488 nm line of the argon laser, and the emitted fluorescence was detected in the range 505–550 nm. For the excitation of the red fluorescent dyes FM4-64 and AM4-65, we used the 514 nm line of the argon laser and the detection of the fluorescent signal was between 660 and 720 nm. Alexa Fluor 546 was excited with the 561 nm line of a diode pumped solid state laser, and detected in the range 580–620 nm. For double-stained samples, we always used the sequential scanning mode. All images included in this study are single optical sections with a thickness of about 1.2 μm , and are positioned with vertical sides parallel to the long axes of the cells. Images were taken using a 40x water immersion objective with a numerical aperture of 1.2, or a 63x water immersion objective with a numerical aperture of 1.4. Statistical analysis of charosome area fraction and abundance of endocytic vesicles was performed using ImageJ and SigmaPlot (Systat Software, San Jose, USA). All experiments were repeated at least twice.

Electron Microscopy

Chemical fixation of branchlet internodal cells of *C. australis* was as described in Foissner (1991). Briefly, cells were fixed for 30 min at room temperature in 1% glutaraldehyde dissolved in phosphate buffer, pH 6.8. Following several washes in buffer, cells were postfixed overnight at 4°C in 2% OsO₄ dissolved in buffer. After dehydration in an ethanol series at 4°C, cells were embedded in Agar low viscosity resin (Agar Scientific, Essex, Great Britain). After staining with uranyl acetate and lead citrate, micrographs of ultrathin section were taken at elastic bright-field mode with a LEO 912 transmission electron microscope equipped with in-column energy filter (Zeiss, Oberkochen, Germany).

RESULTS

Wortmannin Does Not Arrest Endocytosis in Characean Internodal Cells

In order to get a first impression how wortmannin affected the branchlet internodal cells, we measured the rate of cytoplasmic streaming, which depends on the interaction of myosin-coated organelles with subcortical actin bundles attached to the inner

side of the stationary chloroplasts (Shimmen and Yokota, 2004 for review). We found that all concentrations and treatment times which had an effect on the fine structure of cells, also significantly decreased the rate of cytoplasmic streaming. The extent of streaming inhibition varied between cultures, and depended on the time period elapsing between isolation of individual cells and the beginning of the experiment. In general, cells from older cultures (2 months) were less affected by wortmannin than cells from young cultures (≤ 1 month), and cells which had been isolated for a longer time period were more resistant to the effect of wortmannin than cells freshly isolated from the thallus. Since cytoplasmic streaming is vital for most cellular processes, for further experiments we only used cells in which the streaming rate was above 70% of the control rate as shown in Table 1. Table 1 also shows that 25 and 50 μM wortmannin significantly decreased the number of pH bands per cell which were visualized by incubating cells in phenol red, a pH indicating dye. The pH banding activity depends on photosynthesis and on cytoplasmic streaming (Bulychev et al., 2001). The wortmannin-induced reduction in pH banding activity was therefore probably due to the lower streaming velocity, although we presently cannot exclude a possible effect on the rate of photosynthesis.

In a variety of cells, wortmannin has been reported to inhibit endocytosis probably via alterations of clathrin-coated domains (Ito et al., 2012 and references therein). We therefore investigated the effect of wortmannin on the internalization of styryl dyes, established markers for the plasma membrane and for organelles involved in endocytosis (Griffing, 2008). Cells were pretreated with solvent (control) or wortmannin for 2.5 h, and pulse labeled with AM4-65. After 30 min incubation in dye-free control, or wortmannin solution, time series were taken. Supplementary Video 1 shows AM4-65 stained charosomes in the cortex of a control cell. Between the stationary charosomes AM4-65-fluorescent, fast moving structures with a diameter of <250 nm (at the resolution limit) were occasionally seen (compare Klima and Foissner, 2008). To our surprise, such small mobile organelles, putative endosomes, were also present in wortmannin-treated cells (Supplementary Video 2). The cortex of wortmannin-treated cells additionally contained larger, mobile organelles which had a diameter of up to 700 nm. They performed saltatory movements along the plasma membrane, which alternated with periods of immobility (Supplementary Video 2). In order to quantify FM/AM internalization, a chloroplast free window was produced at least 1 day prior to the experiments, to get an undisturbed view into the endoplasm and to count the number of fluorescent organelles (Figures 1A,C–H). The endoplasm as well contained abundant FM/AM-fluorescent organelles, although their number was significantly lower than in solvent-treated cells (Figure 1B). The maximum size of fluorescent endoplasmic organelles in control internodes (Figure 1C) was 2.9 μm ($n = 625$), whereas in cells treated with wortmannin, enlarged organelles, including ring-like “wortmannin compartments,” and clusters of organelles with diameters of up to 4.2 μm ($n = 371$) were observed (Figures 1D,F). This suggests that the reduction in organelle number was at least partly due to the formation of wortmannin-induced compartments.

TABLE 1 | Effect of wortmannin on the velocity of cytoplasmic streaming and on the pH banding activity of branchlet internodal cells of *Chara australis*.

	DMSO 0.5%	25 μ M Wortmannin	50 μ M Wortmannin
v Streaming ($\mu\text{m.s}^{-1}$)	73.7 \pm 6.6 (15)	60.8 \pm 11.7 (13)*	53.6 \pm 4.3 (15)*
v Streaming ($\mu\text{m.s}^{-1}$), recovery 4 d	79.9 \pm 4.8 (15)	57.8 \pm 9.8 (13)*	62.7 \pm 9.5 (13)*
v Streaming ($\mu\text{m.s}^{-1}$), recovery 7 d	74.7 \pm 5.1 (15)	68.6 \pm 11.9 (13)+	67.7 \pm 10.6 (13)+
pH bands/cell	1.3 \pm 1.0 (15)	0 \pm 0 (13)*	0 \pm 0 (13)*
pH bands/cell; recovery 4 d	1.1 \pm 0.3 (15)	0.1 \pm 0.3 (13)*	0.1 \pm 0.3 (13)*
pH bands/cell; recovery 7 d	0.9 \pm 0.4 (15)	0.9 \pm 0.6 (13)	0.6 \pm 0.5 (13)+

Cells were treated with solutions containing wortmannin or DMSO and supplemented with 4 μ M phenol red. After 2 h treatment under room light, the number of alkaline bands was counted, and the velocity of streaming was measured. Following treatment, cells were allowed to recover in artificial fresh water supplemented with 4 μ M phenol red. Data are means \pm SD (number of cells). Significant differences between controls and treatments were calculated according to Students t-test and are indicated by *P \leq 0.01 and +P \leq 0.05.

With respect to size and number of fluorescent structures detected in wortmannin-treated cells, we could not see a concentration-dependent effect, namely there were no significant differences between 25 and 50 μ M. Size and number of fluorescent organelles in cells treated with 10 μ M wortmannin or less were not significantly different from those in control cells.

Largest AM1-44-stained particles with a size of up to 8 μ m were observed in cells “recovering” in artificial fresh water from a 30 min to 2.5 h treatment with 25 μ M wortmannin (Figure 1E). These data indicate that a “recovery” up to 2 h in fact reflects a prolonged treatment time because of the tight binding of wortmannin to its target enzyme(s) (see Section Discussion). Wortmannin-induced compartments were also observed when cells were first pulse-labeled with FM/AM dyes and subsequently incubated in wortmannin (not shown). The effects of wortmannin on cytoplasmic streaming and pH banding activity were reversible when cells were allowed to recover (Table 1). It took, however, several days in artificial fresh water until nearly normal streaming velocities and pH banding activities were regained. After 1 week recovery from wortmannin treatment (25 and 50 μ M), also the size of FM/AM-stained organelles was similar to that in control cells (Figure 1H).

Size, abundance and distribution of charosomes were not affected by wortmannin up to a concentration of 50 μ M and a treatment time of up to 3 h (data not shown).

Wortmannin Induces Clustering and Enlargement of Organelles Recognized by Markers for MVBs and TGNs

In order to identify the nature of wortmannin compartments, we applied immunofluorescence using antibodies against CaARA7 and OsSCAMP1 which are confident markers for MVBs and TGNs, respectively (Lee et al., 2004; Ueda et al., 2004; Lam et al., 2007a; Hoepflinger et al., 2015). In solvent treated control cells, the antibody against ARA7 labeled organelles (MVBs) with a size of up to 1.0 μ m (Figure 2A). Cells treated with 50 μ M wortmannin additionally contained up to 3.5 μ m large compartments (Figures 2B,C; see Hoepflinger et al., 2015 for size histograms). Organelles recognized by anti-OsSCAMP1 in control cells had a roundish shape and a size between 0.5 and 1.1 μ m (Figures 2D,G), corresponding to the shape and size

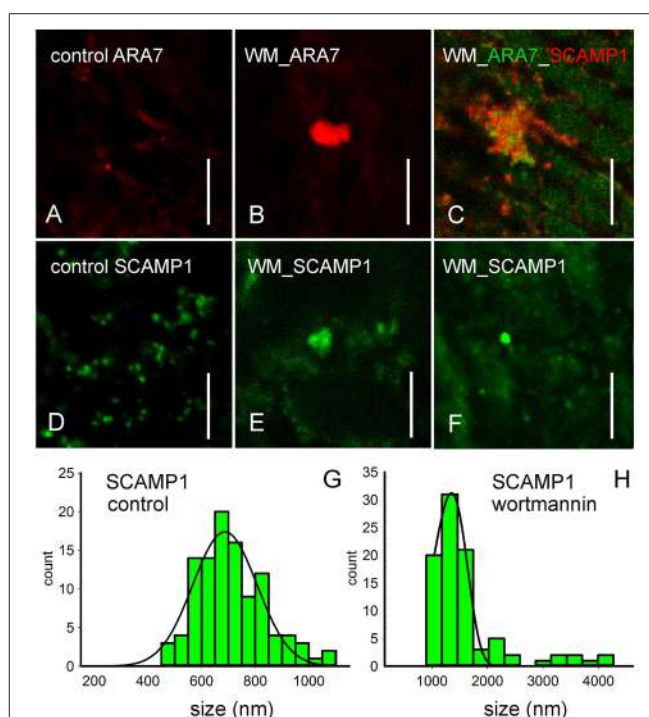


FIGURE 2 | Immunofluorescence with antibodies against endosomal markers of control cells (A,D), of internodal cells treated with 50 μ M wortmannin for 2 h (B,C,E,F) and corresponding histograms (G,H). (A,B) Immunofluorescence with an antibody against CaARA7, a marker for MVBs, shows small punctate organelles in untreated cells and larger compartments (B) in wortmannin-treated cells. (C) Double immunofluorescence with anti-CaARA7 and anti-OsSCAMP1, a marker of TGNs suggests that groups of small MVBs intermingle with TGN membranes. (D–F) Immunofluorescence with anti-OsSCAMP1. The antibody recognizes abundant small organelles with various shapes in the endoplasm of an untreated cell (D). In wortmannin-treated cells, large SCAMP1-positive aggregates (E) and large, globular organelles (F) are present. (G,H) The histograms show the size distributions of SCAMP1-positive organelles in solvent-treated cells, and in cells treated with 50 μ M wortmannin for 2 h. Bars are 10 μ m.

of TGNs seen on electron micrographs (e.g., Figure 3A). In wortmannin-treated cells the antibody against SCAMP1 labeled aggregates of smaller organelles which had a size of up to 4.3 μ m or large, globular organelles with a diameter of up

to $2.6 \mu\text{m}$ (**Figures 2E,F,H**). Immunolabeling of wortmannin-treated cells with both antibodies revealed that all large clusters carrying the ARA7 epitope were additionally recognized by anti-OsSCAMP1 although the fluorescent signals did not precisely overlap (**Figure 2C**). Unlike as in higher plant cells (Lam et al., 2008), the plasma membrane was not recognized by anti-OsSCAMP1. Secondary antibodies alone gave no staining (not shown).

Accumulation and Fusion of MVBs in *Chara* Internodal Cells Involves Participation of the TGN

To further verify the results obtained by immunolabeling, cells were fixed and processed for electron microscopy. The effect of wortmannin was investigated in cells exposed to $25 \mu\text{M}$ wortmannin for 30 min, in cells treated with $50 \mu\text{M}$ wortmannin for 2 h, and in cells recovering for 2 h from a 30 min treatment with $25 \mu\text{M}$ wortmannin. Because of the large size of the mature internodes, only chemical fixation could be applied. Wortmannin had no detectable effect on the fine structure of cortical chloroplasts and plasma membrane (**Figures 3A,B**). Smooth plasma membrane regions alternated with charasomes, where the plasma membrane formed complex labyrinths of anastomosing tubules (**Figure 3B**; Lucas and Franceschi, 1981; Chau et al., 1994). As in controls, coated pits (not shown) and coated vesicles were present at the smooth plasma membrane regions (**Figure 3B**), and less frequent at mature charasomes (compare Sommer et al., 2015). In the endoplasm, wortmannin modified the fine structure and distribution of MVBs and TGNs (see below) but the fine structure of other organelles like Golgi bodies, mitochondria (**Figure 3A**), nuclei (**Figure 4C**), and peroxisomes (not shown) were not affected. Just as in control cells, different kinds of vesicles were present between the numerous cisternae of the endoplasmic reticulum (**Figure 3A**). These observations indicate that wortmannin very specifically targeted the TGNs and the MVBs in *Chara* internodal cells.

The MVBs in the untreated, chemically fixed, mature branchlet internodal cells investigated in this study mostly had an irregular, flattened, or elongate shape and a mean length of $0.6 \pm 0.2 \mu\text{m}$ SD ($n = 24$; **Figures 3C,D**). Membranous tubules were occasionally seen to extend from their outer membrane (**Figure 3C**). Morphology and size of MVBs were similar in cells treated with $25 \mu\text{M}$ wortmannin for 30 min, but aggregates of MVBs were sometimes observed (not shown). Treatment with $50 \mu\text{M}$ wortmannin for 2 h had a stronger impact on distribution, shape, and morphology of these organelles. The cells contained huge clusters of roundish MVBs, which were surrounded by and continuous with membranous tubules (**Figure 3E**). The mean diameter of these MVBs ($0.5 \pm 0.1 \mu\text{m}$; $n = 39$) was similar to the size of MVBs in untreated cells (see above), but due to their roundish shape a higher volume can be assumed. Inside these clusters, MVBs fused into larger organelles (white arrow in **Figure 3E**). The MVBs in wortmannin-treated cells contained abundant tubules (**Figure 3E**), in contrast to the MVBs in control cells which predominantly contained vesicles (**Figures 3C,D**). The diameter of the tubules between and inside the MVBs and the

occasional presence of a central core (**Figure 3E**, inset), a typical structure of TGNs in *Chara* internodal cells (see below), suggest that these tubules were of TGN origin. Taken together, these data indicate that wortmannin-induced MVB clusters correspond to “mixed compartments.” This is consistent with our results of double immunofluorescence using anti-ARA7, a marker for MVBs, and anti-SCAMP1, a marker for TGNs (Lam et al., 2007a). Inside these clusters, MVBs fused with each other and with tubular membranes derived from TGNs. In contrast to TGNs, no single MVBs were observed outside the wortmannin-induced clusters.

Interestingly, the largest MVBs with a diameter of up to $1.2 \mu\text{m}$ were found in cells “recovering” for 2 h in artificial fresh water from 30 min treatment with $25 \mu\text{M}$ wortmannin (**Figure 3F**). Their MVBs had a roundish, cup-, or doughnut-like shape and their mean size (diameter; 0.8 ± 0.2 SD, $n = 24$) was significantly larger than the length of MVBs in control cells ($P \leq 0.0001$, Students *t*-test). These large MVBs were no longer surrounded by and continuous with membranous tubules, suggesting that these got used up during fusion.

Wortmannin Causes Reorganization of the TGNs into Charosome-Like Structures

In addition to the effect of wortmannin on MVBs, we found that this substance also profoundly altered the morphology of TGNs in *Chara* internodal cells. Interestingly, wortmannin did not affect all TGNs of a cell equally. TGNs with normal size and morphology, as well as TGN-derived glycosomes (polysaccharide-containing vesicles; (Franceschi and Lucas, 1981b); **Figure 3A**) were also present in the endoplasm of cells with a high number of compact wortmannin-modified TGNs (see below).

Figures 4A,B show a detail of a cell treated with $50 \mu\text{M}$ wortmannin for 2 h. The TGN visible in this area was enlarged, but its fine structure was similar to that in untreated cells. It consisted of a loose meshwork of smooth and coated tubules, which was often laterally associated with the Golgi bodies (Pesacreta and Lucas, 1984). The tubules alternated with enlarged regions which contained granular or amorphous material, and which probably gave rise to glycosomes (Pesacreta and Lucas, 1984). Coated and non-coated vesicles were present at the periphery of the TGN. Occasionally, a central core with a diameter of $8-10 \text{ nm}$ was seen within tubules or vesicles (**Figure 4B**).

A much stronger effect of wortmannin on the structure of TGNs is seen in **Figures 4C,D**. These organelles consisted of smooth tubules with a more uniform diameter, and neither coated vesicles, nor vesicles with a smooth membrane were seen at their periphery. However, even such strongly modified TGNs were still associated with Golgi bodies (**Figure 4C**). The most severe effect of wortmannin on TGNs is illustrated in **Figures 4E,F**. These TGNs consisted of smooth tubules, as described above, but formed a more roundish, compact organelle in which the distance between tubules was similar to the diameter of the tubules. All tubules contained a central core, which either had the shape of a filament, or appeared like a row of

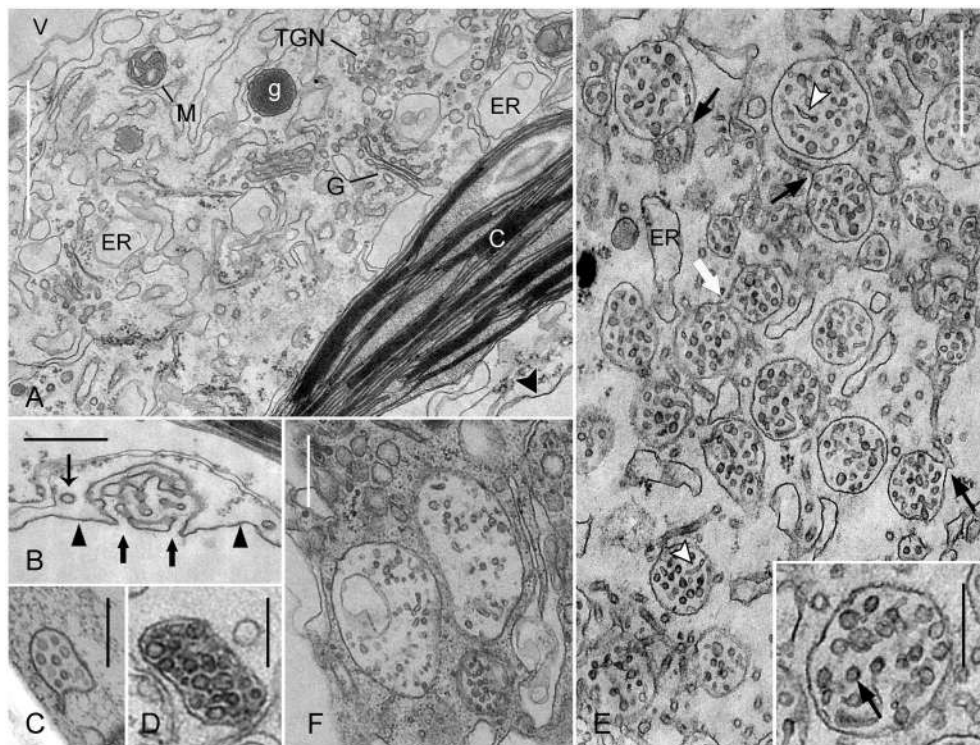


FIGURE 3 | Effect of wortmannin on MVBs in *Chara* internodal cells. Cells were treated with 50 μ M wortmannin for 2 h (**A,B,E**), and with 25 μ M for 30 min followed by 2 h recovery (**F**). Images of multivesicular bodies (**C,D**) are from untreated cells. (**A**) Cross-section through the chloroplast (C)-containing cortex near the plasma membrane (arrow head), and the endoplasm located between cortex and vacuole (V). Wortmannin does not affect the fine structure of chloroplasts, Golgi bodies (G), glycosomes (g), mitochondria (M), and endoplasmic reticulum (ER). Note also that the TGN visible in this area has a normal shape and morphology. (**B**) The charosome in a wortmannin-treated cell is similar to those in control cells. Thick arrows indicate the openings of charosome tubules to the cell wall space. The thin arrow points to a coated vesicle, probably released from the smooth plasma membrane (arrow heads). (**C,D**) MVBs in untreated branchlet internodal cells are small and variable in shape. (**E**) In wortmannin-treated cells, MVBs form large clusters with intertwining membrane tubules. The white arrow indicates fusion between two MVBs, and the black arrows point to continuities between MVBs and membrane tubules. Arrow heads indicate tubules within MVBs. The arrow in the inset points to a cross-sectioned tubule or vesicle with a central core. (**F**) Large MVBs in a cell recovering from wortmannin-treatment. Bars are 1 μ m (**A**), 500 nm (**E,B,F**), and 250 nm (**C,D** and inset in **E**).

dots (**Figures 4D,F**). In control cells, TGNs were predominantly located in the streaming endoplasm. Many of the compact wortmannin-modified TGNs, however, were found in the cortex (**Figures 4E,F**), and most probably corresponded to the mobile FM/AM-stained organelles visible in **Supplementary Video 2**. It is feasible that these compact TGNs move from the endoplasm toward the plasma membrane along actin filament bundles extending through the chloroplast layer (Foissner and Wasteneys, 2014), but we can also not exclude the possibility that these TGNs form *de novo* in the cortex.

Most interestingly, we found that the wortmannin-induced compact TGNs had a striking resemblance with charasomes. Electron microscopical images of both organelles typically showed three radiating tubules, and in addition, one or two arms extending toward regions outside the section (**Figure 4F**; compare Lucas and Smith, 1976; Franceschi and Lucas, 1980). The tubules were interconnected and formed a complex, three-dimensional structure. The diameter of charosome tubules described in previous studies varied between 20 and 40 nm (Franceschi and Lucas, 1980; Lucas et al., 1986; Chau et al.,

1994), and is obviously dependent on fixation and embedding protocol. The mean diameter of the tubules in our preparations measured at their narrowest region, was 69.8 ± 5.7 nm in charasomes, and 67.7 ± 7.6 nm in wortmannin-modified TGNs (no significant difference; 8 organelles from 3 different cells were measured). The charosome tubules, however, were less straight, and their diameter was not as uniform as the diameter of TGN tubules, because they were thicker at their base, i.e., at the site at which the tubules branched or anastomosed, respectively, at least after chemical fixation as used in our study. The tubules in wortmannin-modified TGNs contained a central core surrounded by electron lucent space (**Figures 4D,F**). Such a core is also present in the charosome tubules, although it is less distinct (**Figure 4F**). Both charasomes and wortmannin-modified TGNs are open to the surrounding cytoplasm, and the space between the tubules is thus cytosolic (arrows in **Figures 4E,G**). The cytosolic space between the charosome tubules often appears darker than that of compact TGNs, because it contains additional membrane material from uneven background tubules (Lucas and Franceschi, 1981). On the other hand, the lumen of

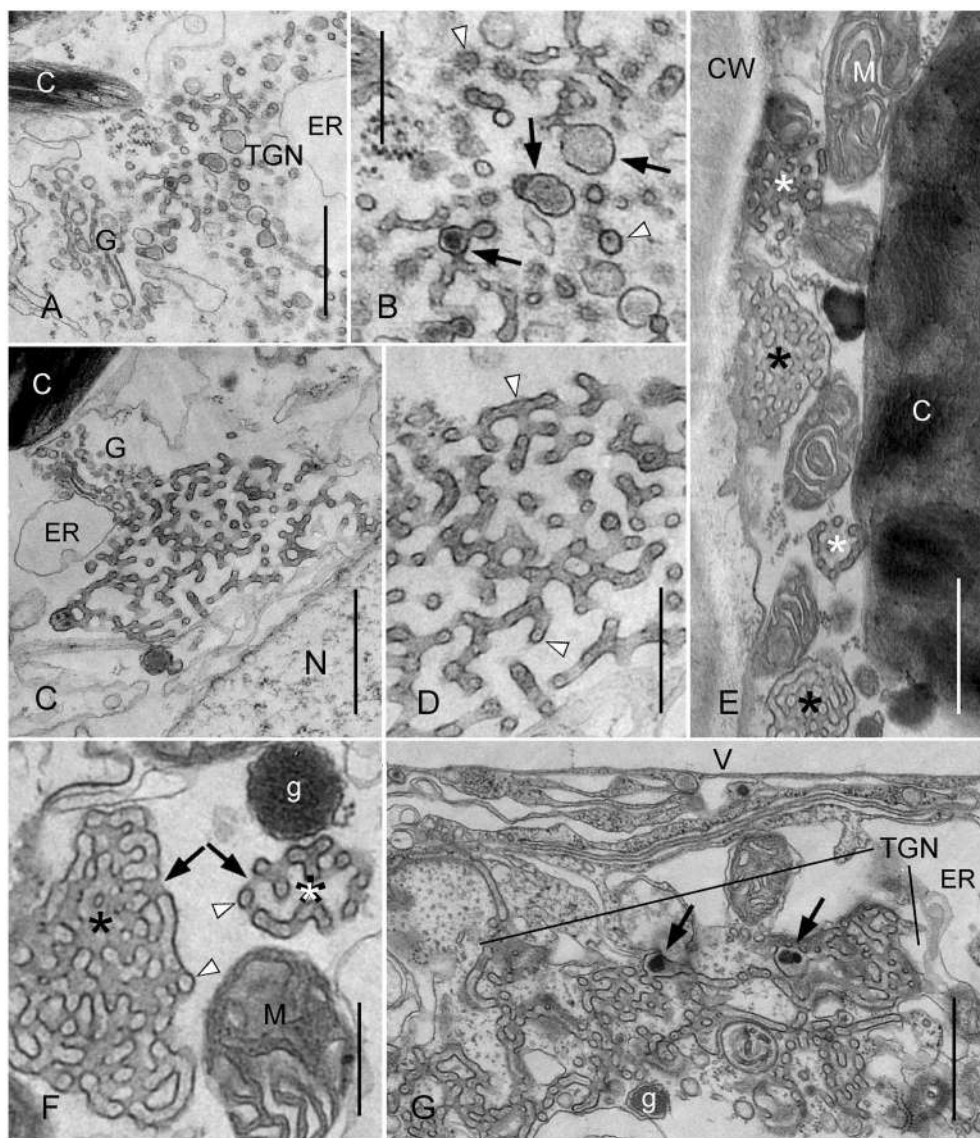


FIGURE 4 | Effect of wortmannin on TGNs in *Chara* internodal cells. Cells were treated with 50 μ M wortmannin for 2 h (**A–F**), and with 25 μ M for 30 min, followed by a recovery for 2 h (**G**). (**A,B**) Enlarged TGN near a Golgi body (G) in a wortmannin-treated cell (C, chloroplast; ER, endoplasmic reticulum). The higher magnification in (**B**) shows smooth and coated tubules, and vesicles which occasionally contain a central core (arrow heads). Enlarged regions with amorphous content are indicated by arrows. (**C,D**) Wortmannin-modified TGN located in the endoplasm between a Golgi body (G) and a nucleus (N). Arrow heads in the enlarged detail (**D**) indicate tubules with cross- or longitudinal sectioned central core. Note uniform diameter of tubules and absence of coated regions. (**E**) Charasomes (black asterisks), mitochondria (M), and wortmannin-modified TGNs (white asterisks) squeezed between cell wall (CW) and chloroplast (C). (**F**) Higher magnification of a charosome (black asterisk) and a wortmannin-modified compact TGN (white asterisk) in the cortex. Arrows indicate openings of the charosome and the TGN to the cytoplasmic space, respectively. Arrow heads indicate tubules or vesicles with central core. g, glycosome; M, mitochondrion. (**G**) Huge TGN complex in a cell recovering from wortmannin-treatment. g, glycosome; V, vacuole. Arrows point to enlarged areas with electron dense granular material. Bars are 1 μ m (**A,C,E,G**) and 500 nm (**B,D,F**).

wortmannin-modified TGN tubules appears slightly darker than those of the charosome tubules. As a result, images of the compact wortmannin-modified TGN complexes appear nearly as a negative of the images of the charosomes, when fixed and stained under identical conditions. The most important difference between charosomes and wortmannin-modified TGNs is, that the lumen of charosome tubules is open to the cell

wall space or periplasm (Figure 3B; Franceschi and Lucas, 1980), whereas wortmannin-modified TGN tubules seemed to be always closed, even when found near the plasma membrane (Figures 4E,F).

We also investigated cells which recovered from a 30 min treatment with 25 μ M wortmannin. After 2 h in artificial fresh water, these cells contained larger FM/AM-stained

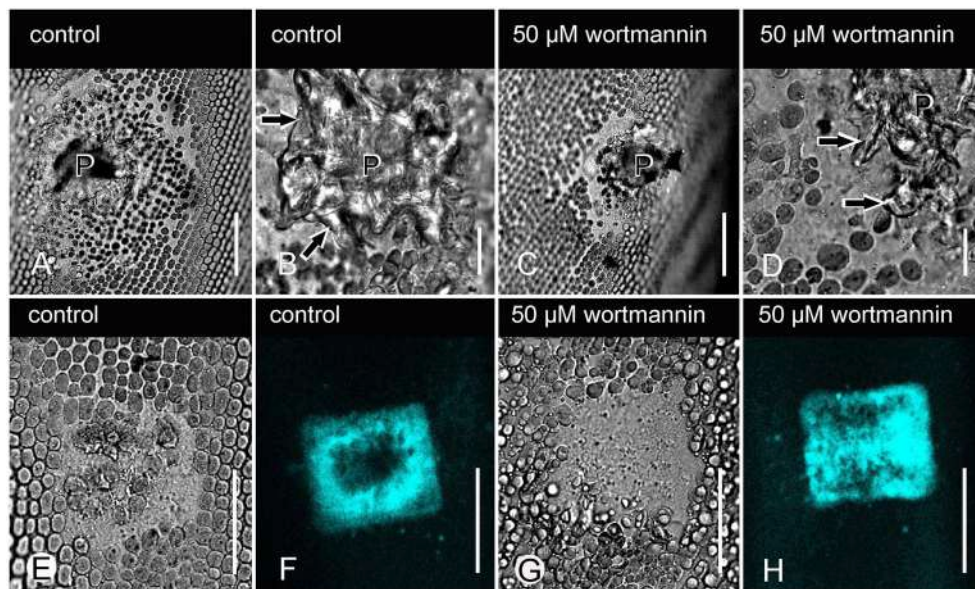


FIGURE 5 | Effect of wortmannin on wound response in *Chara* internodal cells. **(A–D)** DIC images of healed puncture wounds in a DMSO-treated cell (control; **A,B**), and in a cell treated with 50 μ M wortmannin (**C,D**). The wound plug (P), consisting of vacuolar inclusions, is covered by a cellulosic wound wall (arrows in **B,D**). **(E–H)** Healed UV-induced wounds in a control cell (**E,F**), and in a cell treated with 50 μ M wortmannin before and after wounding (**G,H**). **(E,G)** are DIC images and **(F,H)** are the corresponding images of callose visualized after staining with sirofluor. Bars are 50 μ m (**A,C,E–H**) and 10 μ m (**B,D**).

compartments than before recovery (see above). The compartments were also larger than those observed in cells treated with 50 μ M wortmannin for 2 h. The large compartments corresponded to huge clews of non-coated, loosely arranged TGN tubules (Figure 4G). All tubules contained a central core, but in addition, electron dense amorphous material and (clathrin-) coated pits (not shown) were present in some wider regions. They might represent TGN areas which were able to regenerate at least partly, or remnants of enlarged TGNs similar to that shown in Figure 4C. Compact charosome-like TGNs were also present although in lower numbers than in cells treated with 50 μ M wortmannin for 2 h.

Wortmannin Does Not Impair Wound Healing

We then wanted to know whether wortmannin interfered with the healing of wounds induced by puncturing and by UV irradiation, since the process of cell wall repair involves secretion as well as endocytic events. The two types of wound healing differed in the extent of plasma membrane recycling, and in the composition of the wound wall deposited, as described earlier (Foissner and Wasteneys, 2012). Before wounding, cells were treated with 50 μ M wortmannin for 2 h. After injuring the cell wall by puncturing with tungsten needles or by local irradiation with intense UV light (Klima and Foissner, 2011; Foissner and Wasteneys, 2012), cells were left in the wortmannin solution for 1 day. Control cells were wounded and recovered in AFW containing the adequate amount of solvent.

Puncturing internodal cells locally removed cortical chloroplasts, and after withdrawal of the needle, the cell

TABLE 2 | Effect of wortmannin on wound healing in branchlet internodal cells of *Chara australis*.

	DMSO 0.5%	50 μ M Wortmannin	P
Puncture wounds (diameter of injured cortical area in μ m)	153 \pm 58 (13)	154 \pm 55 (10)	0.9
UV-induced wounds (thickness of callose wound wall in μ m)	3.6 \pm 1.3 (7)	4.1 \pm 1.8 (7)	0.6

Before wounding, cells were treated with 50 μ M wortmannin or DMSO for 2 h. After injury, cells were left in the wortmannin or DMSO solution for 1 day. Data are means \pm SD (number of cells). Differences between controls and treatments were calculated according to Students t-test and were not significant.

wall hole became sealed by vacuolar inclusions (Figure 5A). Onto this wound plug, a cellulose-containing wound wall was deposited by fusion of wall forming vesicles and recycling of excess plasma membrane via coated vesicles (Figure 5B; Foissner and Wasteneys, 2012). A wound wall was also deposited onto the surrounding, damaged cortical region, and the diameter of this area was a suitable criterion for the efficacy of wound healing. Figures 5C,D show that the shape and morphology of healed puncture wounds in a wortmannin-treated cell were similar to those in a control cell, and the diameters of damaged cortical areas were not significantly different (Table 2). The survival rate was 100% in control cells and 90% in wortmannin-treated cells.

Local irradiation of the chloroplast-containing cell cortex with intense light caused the local accumulation of secretory vesicles (glycosomes) and FM/AM-stained putative endosomes between plasma membrane and chloroplasts (Klima and Foissner, 2011; Foissner and Wasteneys, 2012). Glycosomes and

endosomes fuse with the plasma membrane and with each other in the absence of membrane recycling, and callose is the characteristic polysaccharide of such wounds. Under the experimental conditions used during this investigation, AM1-44-stained organelles appeared in the cortex within 6 min, both in control and in cells treated with 25 (not shown) or 50 μM wortmannin. All injured cells survived until the following day and produced similar amounts of callose (Figures 5E–H; Table 2).

Effect of Wortmannin on Charosome Degradation and Charosome Formation

Charasomes form in the light and are degraded upon dark-incubation (Schmoelzer et al., 2011 and references therein). Formation requires fusion of TGN vesicles with the plasma membrane and local inhibition of endocytosis (Lucas and Franceschi, 1981; Franceschi and Lucas, 1982). Charosome degradation has not been studied so far, but most likely involves membrane recycling via coated vesicles. We were therefore interested to know whether wortmannin had an effect on light-induced charosome formation and darkness-induced charosome degradation.

For degradation studies, cells were isolated from the thallus and exposed to light (about 5 $\mu\text{E.m}^{-2}\cdot\text{s}^{-1}$, 16/8 h light/dark regime) for at least 1 week. These cells contained abundant charasomes similar to those illustrated in Figure 6A. Cells were then dark-incubated in various concentrations of wortmannin and in the corresponding amount of solvent (controls). After 8–13 days, charasomes were stained with FM/AM dyes and analyzed in the confocal laser scanning microscope, in order to determine the maximum charosome area fraction (% of cell surface area covered by charasomes) for each cell. Representative images for maximum charosome area fractions in a control cell and in a cell treated with 0.4 μM wortmannin are shown in Figures 6B,C. The statistical analysis confirmed a significant inhibitory effect of 0.4 μM wortmannin on charosome degradation (Figure 6D). Higher concentrations of wortmannin were lethal when applied for a longer time period, and even at 0.4 μM about 50% of the cells died (47% in the experiment illustrated in Figure 6E). Surviving cells, unlike the control cells and the cells treated with 0.2 μM wortmannin, did not develop acid and alkaline bands after 2 h exposure to light (Figure 6E). Although the ability to develop pH bands is not a prerequisite for charosome degradation (contrary to charosome formation; see below), the failure to do so may indicate a general, unspecific effect of wortmannin during long-time incubation, and the results therefore must be cautiously interpreted.

Charosome formation was studied in cells previously exposed to darkness for at least 10 days. These cells, which contained only few, small charasomes (Figure 7A), were then treated with solvent and wortmannin, respectively, and exposed to standard light-dark conditions for about 8 days. Significantly lower median values for charosome area fraction were obtained in cells treated with 0.2 μM wortmannin, in comparison to control cells, and to cells treated with lower concentrations (Figures 7B–D). Still, unlike charosome degradation, charosome formation strictly

depends on the development of acid and alkaline bands (Schmoelzer et al., 2011), and Figure 7E shows that pH banding was significantly disturbed at 0.2 μM wortmannin. Therefore, the inhibitory effect of wortmannin on charosome development was probably due to inhibition of pH banding.

DISCUSSION

The TGN Plays a Central Role in Wortmannin-Induced Fusion of MVBs in Characean Internodal Cells

Wortmannin causes the accumulation and enlargement of organelles which can be stained with endocytic markers, e.g., FM/AM dyes. These wortmannin-induced compartments were found to consist mainly of enlarged, homotypically fused MVBs, but some enlarged MVBs also contained proteins characteristic for the TGN (“mixed compartments”; e.g., Lam et al., 2007a,b; Wang et al., 2009; Takáč et al., 2012). During the course of this study we observed that fusion of MVBs in wortmannin-treated characean internodal cells occurred only in clusters where MVBs were surrounded by and continuous with tubular membranes. Electron microscopy and double immunofluorescence showing co-localization of ARA7 and SCAMP1 epitopes at wortmannin compartments indicate that these tubules were of TGN origin. These findings, as well as images of MVBs with tubular extensions in untreated characean internodal cells, and in the green alga *Botryococcus* (Noguchi and Kakami, 1999), are consistent with the idea of TGN-to-MVB maturation (Scheuring et al., 2011). Similar tubules are present within the enlarged MVBs. Therefore, in characean internodal cells, MVBs do not only fuse with each other, but also with tubular components of the TGN. In many other plant cells, only TGN vesicles have been described to fuse with the MVBs (Takáč et al., 2012).

Mature branchlet internodal cells contain only very few MVBs in the endoplasm. Hence, the chance to meet and fuse is low, as long as cytoplasmic mass streaming is continuous, so that organelles keep distance to each other. TGNs are much more abundant in characean internodal cells. We therefore speculate that MVBs in wortmannin-treated cells gather by means of TGN tubules. Of course, the mechanism by which this occurs remains to be elucidated, but this would explain why fusing MVBs were only observed in tubule-containing clusters.

Wortmannin Induces Reorganization of the TGN in *Chara* Internodal Cells

The TGN is a highly variable organelle and its size and morphology undergo considerable variation during the cell cycle (Kiermayer, 1981; Noguchi and Kakami, 1999). Here we describe that under the influence of wortmannin, some TGNs in *Chara* internodal cells greatly increase their size, lose their coat and the capacity to pinch off vesicles, and, finally, form compact three-dimensional structures consisting of branching/anastomosing membranous tubules, which have a striking resemblance with charasomes (see Figure 8 for a schematic summary). To our knowledge, this is the first description of extensive wortmannin-induced

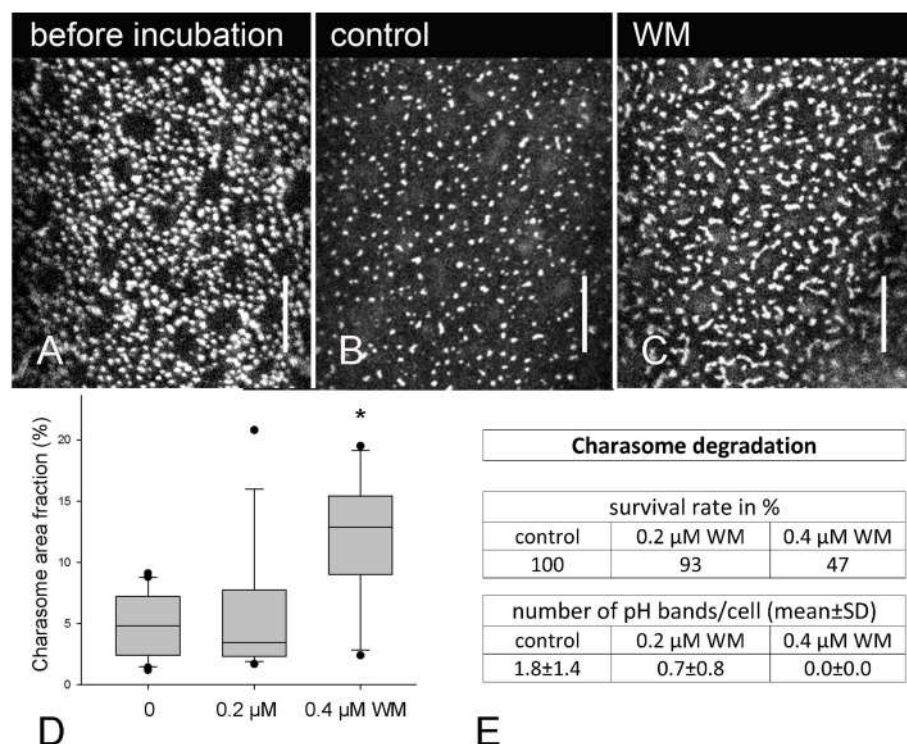


FIGURE 6 | Effect of wortmannin on charosome degradation in *Chara* internodal cells. **(A)** AM1-44 stained charosomes at the acid region of a cell exposed to standard light/dark conditions for 8 days (before treatment). **(B)** AM1-44 stained charosomes in a DMSO-treated cell after 8 days incubation in darkness (control). **(C)** AM1-44 stained charosomes in a wortmannin (WM)-treated cell after 8 days incubation in darkness. **(D)** Maximum charosome area fractions in control and wortmannin-treated cells are compared in box-and-whisker plots. Shown are median values with upper and lower quartiles (boxes), whiskers indicating the 10th and 90th percentiles and outliers (dots). Values are based on data obtained from 12 to 16 cells. Differences between median values of control and 0.4 μ M wortmannin treated cells are significant (asterisk; $P = 0.003$, Kruskal-Wallis one way analysis of variance on ranks). **(E)** Table showing the survival rate and pH banding activity of the cells analyzed in **(D)**. Bars are 10 μ m.

reorganization of TGNs. In other plant cells, TGNs have been described to be depleted during wortmannin-treatment (Takáč et al., 2012), or to be wortmannin-insensitive (Jaillais et al., 2008).

The effects of wortmannin on cellular organelles are due to the inhibition of phosphoinositide kinases. At low concentrations (up to 1 μ M) wortmannin has been reported to be a specific inhibitor of phosphoinositide 3 (PI3) kinases, but at higher concentrations other, PI3 kinase-related enzymes, and phosphatidylinositol 4 (PI4) kinases are also affected (Powis et al., 1994; Matsuoka et al., 1995; Krinke et al., 2007; Takáč et al., 2012 for references). Phosphatidylinositol kinases play an important role in cellular metabolism. They produce inositol phosphates which regulate vital cellular processes, including signal transduction and membrane trafficking. Phosphoinositides act as docking sites for proteins containing specific lipid-binding domains (van Leeuwen et al., 2004; Di Paolo and De Camilli, 2006; Krishnamoorthy et al., 2014). Different forms of phosphoinositides, regulated by the combined action of specific kinases and phosphatases, segregate on different intracellular membranes, thereby establishing an identity code of organelles involved in traffic, and enabling a fine tuned cargo delivery to the target membrane (Di Paolo and De Camilli, 2006;

Balla, 2013; Sekeres et al., 2015). PI3P has been shown to be enriched in late endosomes and in the tonoplast (Kim et al., 2001; Vermeer et al., 2006; Krishnamoorthy et al., 2014), which is consistent with the effect of wortmannin on MVBs and vacuoles. In contrast, PI4P has been reported to localize preferentially in the plasma membrane and in the Golgi bodies (Vermeer et al., 2009), but also in post Golgi, TGN, and recycling endosomes, respectively (Kang et al., 2011; Simon et al., 2014; Sekeres et al., 2015). Mutants that decrease PI4P levels at the TGN were found to slow, or uncouple coat assembly via interference with clathrin adaptor proteins (Daboussi et al., 2012). Whether this is a direct or indirect effect (e.g., via reduced V-ATPase activity; Liu et al., 2016) remains to be investigated. In any case, it is reasonable to conclude that the disappearance of vesicles from the TGN of *Chara* internodal cells is due to impaired coat assembly, caused by wortmannin-induced inhibition of PI4 kinase(s) (compare Bednarek and Backues, 2010). In this context, it is interesting to note that epsin, an amphipatic membrane protein that drives the curvature of the coated pits in conjunction with clathrin polymerization, has an absolute requirement for PI(4,5)P₂ (Ford et al., 2002; Boucrot et al., 2012). Another likely candidate for the observed changes is the small GTPase, RabA1d, which regulates vesicular trafficking at

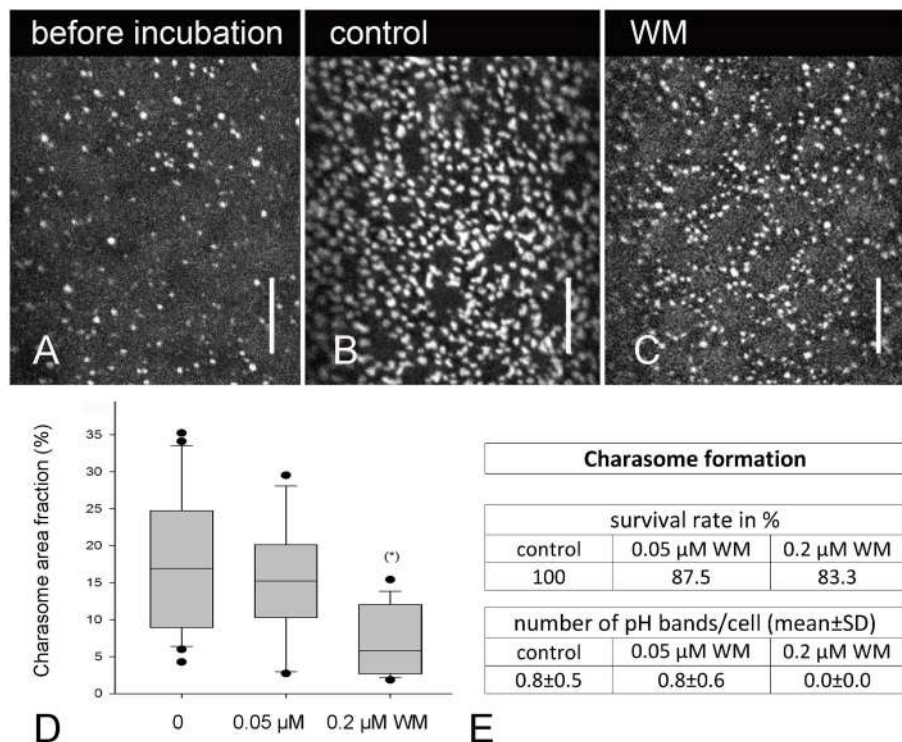


FIGURE 7 | Effect of wortmannin on charosome formation in *Chara* internodal cells. **(A)** AM1-44 stained charosomes in a cell which was dark-incubated for 2 weeks. **(B)** AM1-44 stained charosomes at the acid region of a control cell exposed to standard light conditions for 8 days. **(C)** AM1-44 stained charosomes in a cell treated with 0.2 μ M wortmannin (WM) under standard light conditions for 8 days. **(D)** Maximum charosome area fractions in control and in wortmannin-treated cells are compared in box-and-whisker plots. Shown are median values with upper and lower quartiles (boxes), whiskers indicating the 10th and 90th percentiles and outliers (dots). Values are based on data obtained from 15 to 17 cells. Differences between median values of control cells and cells treated with 0.2 μ M wortmannin are significant (asterisk; $P = 0.003$, Kruskal–Wallis one way analysis of variance on ranks). **(E)** Table showing the survival rate and pH banding activity of the cells analyzed in **(D)**. Bars are 10 μ m.

TGN, and was identified as a new protein negatively affected by wortmannin (Takáč et al., 2012). These known effects of wortmannin suggest that the TGNs in wortmannin-treated *Chara* internodal cells increase their size because of the failure to release vesicles via a PI4 kinase dependent and clathrin-mediated mechanism, and because of the ongoing supply of endocytic vesicles from the plasma membrane (see below). We speculate that this causes the accumulation of a protein involved in membrane curvature, which finally leads to the compactification of the organelle. Interestingly, however, TGN tubules in root cells of *Arabidopsis* PI4 kinase mutants appear to be blown up, but are still equipped with clathrin coats (Kang et al., 2011).

During the course of this study, we found a profound effect of wortmannin on the morphology of the TGNs in *Chara* internodal cells. However, not all TGNs were similarly affected. TGNs with normal size and morphology were always present in wortmannin-treated cells, even when they contained enlarged, vesicle-free, or compact TGNs. Therefore, the TGNs in wortmannin-treated *Chara* internodal cells can be present in three different forms, (1) as normal organelles (eventually enlarged), (2) as vesicle-free, loose, or compact meshworks

of uncoated tubules, and (3) as a component of mixed compartments together with MVBs. These findings may reflect the existence of different populations or “maturation stages” of TGNs, as described in *Arabidopsis* root and hypocotyl cells (e.g., Viotti et al., 2010; Kang et al., 2011; Uemura et al., 2014) and in yeast (Mogelsvang et al., 2003). It is possible that these populations differ in the PI3P/PI4P content of their membranes, which could explain the multiple effects of wortmannin.

Several authors have reported that treatment of cells with wortmannin is irreversible (e.g., Powis et al., 1994). In characean internodal cells, we found that the partial inhibition of cytoplasmic streaming and pH banding, as well as the formation of wortmannin-induced compartments, were reversible. The recovery took, however, several days, consistent with the strong covalent binding of wortmannin to the ATP-binding site of its target enzyme (Wymann et al., 1996; Walker et al., 2000; Yuan et al., 2007). This binding possibly also explains our observations that the size of wortmannin compartments (TGN as well as MVBs) transiently increased during recovery from treatment with 25 μ M wortmannin. Part of the recovery time can thus be considered as prolonged drug treatment.

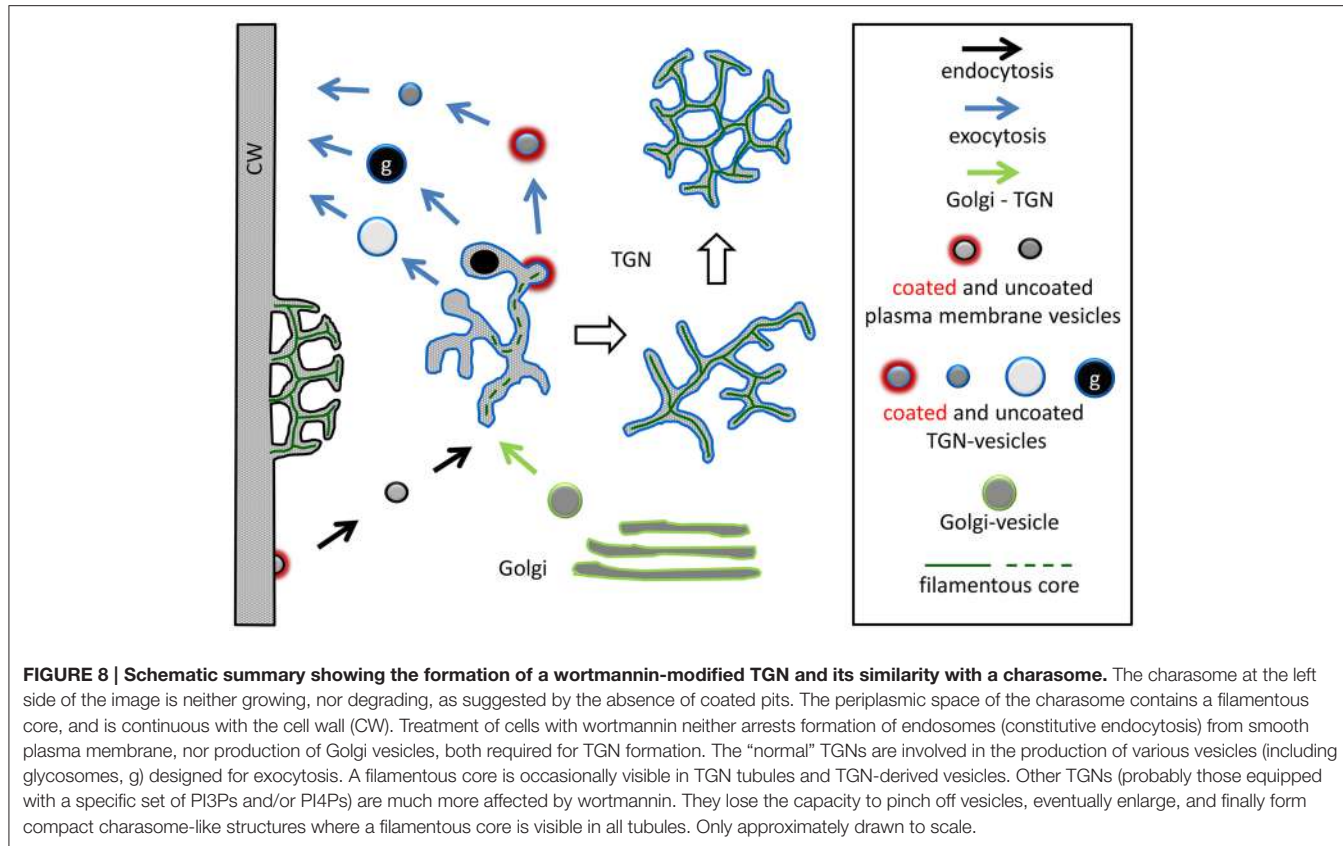


FIGURE 8 | Schematic summary showing the formation of a wortmannin-modified TGN and its similarity with a charosome. The charosome at the left side of the image is neither growing, nor degrading, as suggested by the absence of coated pits. The periplasmic space of the charosome contains a filamentous core, and is continuous with the cell wall (CW). Treatment of cells with wortmannin neither arrests formation of endosomes (constitutive endocytosis) from smooth plasma membrane, nor production of Golgi vesicles, both required for TGN formation. The “normal” TGNs are involved in the production of various vesicles (including glycosomes, g) designed for exocytosis. A filamentous core is occasionally visible in TGN tubules and TGN-derived vesicles. Other TGNs (probably those equipped with a specific set of PI3Ps and/or PI4Ps) are much more affected by wortmannin. They lose the capacity to pinch off vesicles, eventually enlarge, and finally form compact charosome-like structures where a filamentous core is visible in all tubules. Only approximately drawn to scale.

Are Similar Mechanisms Involved in the Formation of Charosomes and Wortmannin-Modified TGNs?

A characteristic feature of charosome tubules is a central core, which either appears as a filament, or as a row of dots, and which is surrounded by granular or fibrous material (Franceschi and Lucas, 1980). The granular or fibrous material is visible only after fixation with tannic acid-containing glutaraldehyde (Franceschi and Lucas, 1980). A central core (filamentous or row of dots) with a similar diameter is also seen in some, but not all regions of the TGN and in TGN-derived vesicles in untreated *Chara* internodal cells. In the non-coated, wortmannin-modified TGNs, the central core was always present. This finding possibly indicates that this structure is involved in the formation of membranous tubular meshworks, although its nature is completely unknown so far. It also does not correspond to the proteoglycan described in various studies to be present in the periplasmic space of charosome tubules (Franceschi and Lucas, 1981a; Beljanski et al., 1995; see above). In addition, membrane-localized proteins are likely to play a role in sensing and establishing membrane curvature, like BAR-domain-containing proteins, e.g., arfaptins, amphiphysin, or endophilin, which bind to the TGN membranes in a PI4P-dependent manner (Shin et al., 2012; Cruz-Garcia et al., 2013), and which are remarkably effective in promoting membrane tubulation (Peter et al., 2004; Boucrot et al., 2012; Cruz-Garcia et al., 2013; Simunovic et al., 2013). Future work will show

whether these or similar proteins are involved in the formation of charosomes and/or wortmannin-modified TGNs. In this respect, it is also important to note ARA6, an unconventional RAB5 GTPase residing in the plasma membrane, including charosomes, and in the TGN of *Chara* internodal cells (Hoepflinger et al., 2013). The exact function of this small GTPase is unknown so far, but it is likely involved in endocytosis and/or exocytosis (Ebine et al., 2012).

Scanning electron images suggest that during their development, charosomes undergo a transition from a loose network of long tubules to a complex anastomosing network of short tubules (Chau et al., 1994). The charosome tubules grow by fusion of TGN-derived vesicles with the plasma membrane, in the absence of membrane recycling (endocytosis; Franceschi and Lucas, 1980, 1982; Pesacreta and Lucas, 1984). Coated pits are abundant at the cytoplasmic surface of growing charosomes, and appear to fuse with each other, thereby forming the charosome tubules (Lucas and Franceschi, 1981). The cytoplasmic membrane (the inner surface) of charosomes in mature, untreated cells, however, is mostly uncoated (Franceschi and Lucas, 1980; Sommer et al., 2015). A similar sequence of events can be observed during formation of wortmannin-modified TGNs. Loose meshworks with clathrin-coated regions develop into compact, three-dimensional meshworks, which are devoid of a clathrin coat. The effect of wortmannin on the morphology of the TGNs in *Chara* internodal cells is likely to be

due to the inhibition of PI3 and/or PI4 kinases, which probably leads to a depletion of phosphoinositides by disturbing the fine balance existing between PI kinases and PI phosphatases, and to the inhibition of coat assembly required for the release of vesicles (see above). We therefore speculate that similar mechanisms and molecules are involved in formation of charasomes.

Clathrin-Dependent Constitutive and Wounding-Induced Endocytosis are Not Arrested by Wortmannin

It has been reported that wortmannin inhibits endocytosis (Bandmann and Homann, 2012; Ito et al., 2012 for references). In *Chara* internodal cells, wortmannin did not arrest the internalization of FM/AM dyes up to a concentration of 50 μM . FM/AM internalization in characean internodal cells has been shown to be active, and fluorescent organelles co-labeled with markers for the TGN and for MVBs, suggesting that these dyes can be used as endosomal markers (Klima and Foissner, 2008; Hoepflinger et al., 2013). In wortmannin-treated cells the number of FM/AM-stained endosomes was significantly lower as compared with the controls, but this is at least partly due to the formation of wortmannin-induced aggregates and ring-like compartments. In addition, electron micrographs show not only coated pits, but also coated vesicles at regions with smooth plasma membrane, i.e., between charasomes, which confirms that constitutive, clathrin-dependent endocytosis is not arrested by wortmannin in *Chara* internodal cells.

The deposition of a cellulosic wall beneath healing puncture wounds requires fusion of secretory vesicles with the plasma membrane and membrane recycling via coated vesicles, whereas the deposition of material in response to local irradiation occurs in the absence of membrane recycling (Klima and Foissner, 2011; Foissner and Wasteneys, 2012). Surprisingly, wortmannin neither had a detectable effect on healing of wounds induced by local irradiation (accumulation and fusion of organelles in the absence of membrane recycling), nor disturbed the healing of puncture wounds (fusion of vesicles with the plasma membrane and membrane recycling). This is in line with electron microscopical images showing that, even in cells treated with 50 μM wortmannin for 2 h, secretory vesicles required for wound healing were still present in sufficient number, and that wortmannin had only a small effect on clathrin-dependent plasma membrane retrieval. Wortmannin has therefore different effects on the release of coated vesicles from the plasma membrane and from (some of) the TGNs, respectively. This finding may reflect different membrane compositions regarding the type and amount of specific phosphoinositides (see above). Our data also show that wortmannin neither prevented local reorganization of actin cytoskeleton, nor significantly inhibited acto-myosin dependent transport, both required for delivery of secretory vesicles and other organelles toward the wound (Foissner and Wasteneys, 2012). This is consistent with our finding, that acto-myosin-dependent mass streaming of the endoplasm continued in the presence of 25 and 50 μM wortmannin for up to 2.5 h, although at lower rates, which may be due to the inhibition of a myosin light chain kinase

(e.g., Nakanishi et al., 1992; Powis et al., 1994; Burdyga and Wray, 1998). In the mesophyll of *Lemna*, wortmannin inhibited actin-dependent reorientation of chloroplasts at much lower concentrations than those used in our study, but this effect is likely to be due to the interruption of a light-induced signaling cascade (Grabalska and Malec, 2004).

Effect of Wortmannin on Charosome Degradation and Formation

The formation of wortmannin-induced compartments was studied with concentrations of 25 and 50 μM , which were lethal when applied for several days. Since the study of charosome formation and degradation requires a treatment time of at least 1 week, we had to use much lower concentrations (between 0.05 and 0.4 μM).

When *Chara* internodal cells are exposed to darkness, charasomes degrade via clathrin-dependent endocytosis (own, unpublished results). We are aware, that long-term treatment of cells with inhibitors must be cautiously interpreted because of unspecific side effects, and because of the rather low concentrations used, which had no significant effect on the size of FM/AM-stained organelles (data not shown). However, we assume that at these low concentrations wortmannin affects at least the activity of PI3 kinases (see Section Introduction) and retards the degradation of charasomes via an inhibitory effect on clathrin-dependent membrane retrieval. Charosome degradation was not totally inhibited, and this adds further support to the hypothesis that in *Chara*, plasma membrane recycling (at charasomes and at smooth plasma membrane regions) is less affected by wortmannin, than the release of coated vesicles from (at least some of) the TGNs.

So far, little can be said about the effect of wortmannin on charosome formation. Charosome formation is strictly dependent on the pH banding activity, which in turn requires photosynthesis and cytoplasmic streaming (e.g., Bulychev et al., 2001; Schmoelzer et al., 2011). The pH banding activity was significantly inhibited after long-time treatment with 0.2 μM wortmannin and this is probably the main reason why these cells contained significantly lower charosome area fractions.

AUTHOR CONTRIBUTIONS

IF acquired funding and conceived the study. IF, AS, MH, and MCH designed the research; IF, AS, MH, and MA performed the research; AS, MH, MCH, and MA analyzed the data; IF drafted the manuscript; IF, AS, MH, MCH, and MA contributed to the final manuscript. All authors approved the final version of the manuscript.

ACKNOWLEDGMENTS

This research was funded by the Austrian Science Fund (FWF project no. P 22957-B20 and FWF project no. P 27536-B16 to IF). The authors are grateful to Raimund Tenhaken (University of Salzburg) for support and valuable discussion and to Liwen Jiang (University of Hongkong) for antibodies against SCAMP1.

SUPPLEMENTARY MATERIAL

The Supplementary Material for this article can be found online at: <http://journal.frontiersin.org/article/10.3389/fpls.2016.00756>

Supplementary Video 1 | Cortex of a DMSO-treated, AM4-65-stained

Chara internodal cell. Only delicate mobile organelles are occasionally seen between charasomes (encircled area). Interval between consecutive frames is 3.7 s; playback rate of movie is 5 frames per second.

Supplementary Video 2 | Cortex of a Chara internodal cell treated with 50 μM wortmannin for 2 h and stained with AM4-65.

The starting point of a

large mobile organelle is indicated by an arrow, immobile organelles are charasomes. Interval between consecutive frames is 1 s; playback rate of movie is 5 frames per second.

Supplementary Figure 1 | Schematic longitudinal section through a characean internodal cell.

In the genus *Chara*, the plasma membrane (red line) adjacent to the cell wall (CW) may form convoluted domains (charasomes, arrows). Subcortical actin filament bundles (black lines) are present along the inner side of the cortical, stationary chloroplasts (C). Nuclei (N), Golgi bodies (G), trans-Golgi networks (TGNs), and multivesicular bodies (MVB) are predominantly located in the streaming endoplasm. Mitochondria (M), and various vesicles (v) may shuttle between cortex and endoplasm. V, small vacuole; cv, central vacuole. Organelles relevant for this study are shown in red. Only approximately drawn to scale.

REFERENCES

- Balla, T. (2013). Phosphoinositides: tiny lipids with giant impact on cell regulation. *Physiol. Rev.* 93, 1019–1137. doi: 10.1152/physrev.00028.2012
- Bandmann, V., and Homann, U. (2012). Clathrin-independent endocytosis contributes to uptake of glucose into BY-2 protoplasts. *Plant J.* 70, 578–584. doi: 10.1111/j.1365-313X.2011.04892.x
- Bednarek, S. Y., and Backus, S. K. (2010). Plant dynamin-related protein families DRP1 and DRP2 in plant development. *Biochem. Soc. Trans.* 38, 797–806. doi: 10.1042/BST0380797
- Beljanski, M., Zihnić, H., and Andjus, P. R. (1995). Evidence for the presence of the plasma membrane coat in the membrane fraction isolated from *Chara gymnotrichia*. *Plant Sci.* 110, 121–126. doi: 10.1016/0168-9452(95)04178-W
- Bisson, M. A., Siegel, A., Chau, R., Gelsomino, S. A., and Herdic, S. L. (1991). Distribution of charasomes in *Chara* – banding-pattern and effect of photosynthetic inhibitors. *Aust. J. Plant Physiol.* 18, 81–93. doi: 10.1071/PP9910081
- Boucrot, E., Pick, A., Camdere, G., Liska, N., Evergren, E., McMahon, H. T., et al. (2012). Membrane fission is promoted by insertion of amphipathic helices and is restricted by crescent BAR domains. *Cell* 149, 124–136. doi: 10.1016/j.cell.2012.01.047
- Bulychev, A. A., Kamzolkina, N. A., Luengviriya, J., Rubin, A. B., and Müller, S. C. (2004). Effect of a single excitation stimulus on photosynthetic activity and light-dependent pH banding in *Chara* cells. *J. Membr. Biol.* 202, 11–19. doi: 10.1007/s00232-004-0716-5
- Bulychev, A. A., Polezhaev, A. A., Zykov, S. V., Pljusnina, T. Y., Riznichenko, G. Y., Rubin, A. B., et al. (2001). Light-triggered pH banding profile in *Chara* cells revealed with a scanning pH microprobe and its relation to self-organization phenomena. *J. Theor. Biol.* 212, 275–294. doi: 10.1006/jtbi.2001.2375
- Burdyga, T. V., and Wray, S. (1998). The effect of inhibition of myosin light chain kinase by wortmannin on intracellular $[Ca^{2+}]$, electrical activity and force in phasic smooth muscle. *Pflugers Arch.* 436, 801–803. doi: 10.1007/s004240050705
- Chau, R., Bisson, M. A., Siegel, A., Elkin, G., Klim, P., and Straubinger, R. M. (1994). Distribution of charasomes in *Chara* – Reestablishment and loss in darkness and correlation with banding and inorganic carbon uptake. *Aust. J. Plant Physiol.* 21, 113–123. doi: 10.1071/PP9940113
- Cruz-Garcia, D., Ortega-Bellido, M., Scarpa, M., Villeneuve, J., Jovic, M., Porzner, M., et al. (2013). Recruitment of arfaptins to the *trans*-Golgi network by PI(4)P and their involvement in cargo export. *EMBO J.* 32, 1717–1729. doi: 10.1038/embj.2013.116
- Daboussi, L., Costaguta, G., and Payne, G. S. (2012). Phosphoinositide-mediated clathrin adaptor progression at the *trans*-Golgi network. *Nat. Cell Biol.* 14, 239–248. doi: 10.1038/ncb2427
- daSilva, L. L., Taylor, J. P., Hadlington, J. L., Hanton, S. L., Snowden, C. J., Fox, S. J., et al. (2005). Receptor salvage from the prevacuolar compartment is essential for efficient vacuolar protein targeting. *Plant Cell* 17, 132–148. doi: 10.1105/tpc.104.026351
- Di Paolo, G., and De Camilli, P. (2006). Phosphoinositides in cell regulation and membrane dynamics. *Nature* 443, 651–657. doi: 10.1038/nature05185
- Ebine, K., Miyakawa, N., Fujimoto, M., Uemura, T., Nakano, A., and Ueda, T. (2012). Endosomal trafficking pathway regulated by ARA6, a RAB5 GTPase unique to plants. *Small GTPases* 3, 23–27. doi: 10.4161/sgt.18299
- Feraru, E., Paciorek, T., Feraru, M. I., Zwiewka, M., De Groodt, R., De Rycke, R., et al. (2010). The AP-3 beta adaptin mediates the biogenesis and function of lytic vacuoles in *Arabidopsis*. *Plant Cell* 22, 2812–2824. doi: 10.1105/tpc.110.075424
- Foissner, I. (1991). Induction of exocytosis in characean internodal cells by locally restricted application of chlortetracycline and the effect of cytochalasin B, depolarizing and hyperpolarizing agents. *Plant Cell Environ.* 14, 907–915. doi: 10.1111/j.1365-3040.1991.tb00959.x
- Foissner, I., and Wasteneys, G. O. (2012). The characean internodal cell as a model system for studying wound healing. *J. Microsc.* 247, 10–22. doi: 10.1111/j.1365-2818.2011.03572.x
- Foissner, I., and Wasteneys, G. O. (2014). “Characean internodal cells as a model system for the study of cell organization,” in *International Review of Cell and Molecular Biology*, ed W. J. Kwang (Burlington: Academic Press), 307–364.
- Ford, M. G., Mills, I. G., Peter, B. J., Vallis, Y., Praefcke, G. J., Evans, P. R., et al. (2002). Curvature of clathrin-coated pits driven by epsin. *Nature* 419, 361–366. doi: 10.1038/nature01020
- Foresti, O., and Denecke, J. (2008). Intermediate organelles of the plant secretory pathway: identity and function. *Traffic* 9, 1599–1612. doi: 10.1111/j.1600-0854.2008.00791.x
- Franceschi, V. R., and Lucas, W. J. (1980). Structure and possible function(s) of charasomes; complex plasmalemma-cell wall elaborations present in some characean species. *Protoplasma* 104, 253–271. doi: 10.1007/BF01279771
- Franceschi, V. R., and Lucas, W. J. (1981a). The charosome periplasmic space. *Protoplasma* 107, 269–284. doi: 10.1007/BF01276830
- Franceschi, V. R., and Lucas, W. J. (1981b). The glycosome of *Chara*: ultrastructure, development, and composition. *J. Ultrastr. Res.* 75, 218–228. doi: 10.1016/S0022-5320(81)80137-2
- Franceschi, V. R., and Lucas, W. J. (1982). The relationship of the charosome to chloride uptake in *Chara corallina*: physiological and histochemical investigations. *Planta* 154, 525–537. doi: 10.1007/BF00402996
- Grabska, M., and Malec, P. (2004). Blue light-induced chloroplast reorientations in *Lemna trisulca* L. (Duckweed) are controlled by two separable cellular mechanisms as suggested by different sensitivity to wortmannin. *Photochem. Photobiol.* 79, 343–348. doi: 10.1562/LE-03-16.1
- Griffing, L. R. (2008). FRET analysis of transmembrane flipping of FM4-64 in plant cells: is FM4-64 a robust marker for endocytosis? *J. Microsc.* 231, 291–298. doi: 10.1111/j.1365-2818.2008.02042.x
- Hoepflinger, M. C., Geretschlaeger, A., Sommer, A., Hoeftberger, M., Hametner, C., Ueda, T., et al. (2015). Molecular analysis and localization of CaARA7 a conventional RAB5 GTPase from characean algae. *Traffic* 16, 534–554. doi: 10.1111/tra.12267
- Hoepflinger, M. C., Geretschlaeger, A., Sommer, A., Hoeftberger, M., Nishiyama, T., Sakayama, H., et al. (2013). Molecular and biochemical analysis of the first ARA6 homologue, a RAB5 GTPase, from green algae. *J. Exp. Bot.* 64, 5553–5568. doi: 10.1093/jxb/ert322
- Ito, E., Fujimoto, M., Ebine, K., Uemura, T., Ueda, T., and Nakano, A. (2012). Dynamic behavior of clathrin in *Arabidopsis thaliana* unveiled by live imaging. *Plant J.* 69, 204–216. doi: 10.1111/j.1365-313X.2011.04782.x

- Jaillais, Y., Fobis-Loisy, I., Miege, C., and Gaude, T. (2008). Evidence for a sorting endosome in *Arabidopsis* root cells. *Plant J.* 53, 237–247. doi: 10.1111/j.1365-313X.2007.03338.x
- Kamitsubo, E. (1972). A “window technique” for detailed observation of characean cytoplasmic streaming. *Exp. Cell Res.* 74, 613–616. doi: 10.1016/0014-4827(72)90430-2
- Kang, B. H., Nielsen, E., Preuss, M. L., Mastronarde, D., and Staehelin, L. A. (2011). Electron tomography of RabA4b- and PI-4Kbeta1-labeled *trans*-Golgi network compartments in *Arabidopsis*. *Traffic* 12, 313–329. doi: 10.1111/j.1600-0854.2010.01146.x
- Keifer, D. W., Franceschi, V. R., and Lucas, W. J. (1982). Plasmalemma chloride transport in *Chara corallina* - inhibition by 4,4'-diisothiocyanato-2,2'-disulfonic acid stilbene. *Plant Physiol.* 70, 1327–1334. doi: 10.1104/pp.70.5.1327
- Kiermayer, O. (1981). Cytoplasmic basis of morphogenesis in *Micrasterias*. *Cell Biol. Monogr.* 8, 147–190. doi: 10.1007/978-3-7091-8602-2_6
- Kim, D. H., Eu, Y. J., Yoo, C. M., Kim, Y. W., Pih, K. T., Jin, J. B., et al. (2001). Trafficking of phosphatidylinositol 3-phosphate from the *trans*-Golgi network to the lumen of the central vacuole in plant cells. *Plant Cell* 13, 287–301. doi: 10.1105/tpc.13.2.287
- Klima, A., and Foissner, I. (2008). FM dyes label sterol-rich plasma membrane domains and are internalized independently of the cytoskeleton in characean internodal cells. *Plant Cell Physiol.* 49, 1508–1521. doi: 10.1093/pcp/pcn122
- Klima, A., and Foissner, I. (2011). Actin-dependent deposition of putative endosomes and endoplasmic reticulum during early stages of wound healing in characean internodal cells. *Plant Biol.* 13, 590–601. doi: 10.1111/j.1438-8677.2010.00413.x
- Krinke, O., Ruelland, E., Valentová, O., Vergnolle, C., Renou, J.-P., Taconnat, L., et al. (2007). Phosphatidylinositol 4-kinase activation is an early response to salicylic acid in *Arabidopsis* suspension cells. *Plant Physiol.* 144, 1347–1359. doi: 10.1104/pp.107.100842
- Krishnamoorthy, P., Sanchez-Rodriguez, C., Heilmann, I., and Persson, S. (2014). Regulatory roles of phosphoinositides in membrane trafficking and their potential impact on cell-wall synthesis and re-modelling. *Ann. Bot.* 114, 1049–1057. doi: 10.1093/aob/mcu055
- Lam, S. K., Cai, Y., Hillmer, S., Robinson, D. G., and Jiang, L. W. (2008). SCAMPs highlight the developing cell plate during cytokinesis in tobacco BY-2 cells. *Plant Physiol.* 147, 1637–1645. doi: 10.1104/pp.108.119925
- Lam, S. K., Siu, C. L., Hillmer, S., Jang, S., An, G. H., Robinson, D. G., et al. (2007a). Rice SCAMP1 defines clathrin-coated, *trans*-Golgi-located tubular-vesicular structures as an early endosome in tobacco BY-2 cells. *Plant Cell* 19, 296–319. doi: 10.1105/tpc.106.045708
- Lam, S. K., Tse, Y. C., Miao, Y. S., Li, H., Wang, J., Lo, S. W., et al. (2007b). Molecular characterization of plant prevacuolar and endosomal compartments. *J. Integr. Plant Biol.* 49, 1119–1128. doi: 10.1111/j.1672-9072.2007.00517.x
- Lee, G. J., Sohn, E. J., Lee, M. H., and Hwang, I. (2004). The *Arabidopsis* Rab5 homologs Rha1 and Ara7 localize to the prevacuolar compartment. *Plant Cell Physiol.* 45, 1211–1220. doi: 10.1093/pcp/pch142
- Li, F., and Vierstra, R. D. (2012). Autophagy: a multifaceted intracellular system for bulk and selective recycling. *Trends Plant Sci.* 17, 526–537. doi: 10.1016/j.tplants.2012.05.006
- Liu, J., Ji, X., Zhou, J., and Xing, D. (2016). Phosphatidylinositol 3-kinase promotes V-ATPase activation and vacuolar acidification and delays methyl jasmonate-induced leaf senescence. *Plant Physiol.* 170, 1714–1731. doi: 10.1104/pp.15.00744
- Lucas, W. J. (1983). Photosynthetic assimilation of exogenous HCO_3^- by aquatic plants. *Annu. Rev. Plant Physiol.* 34, 71–104. doi: 10.1146/annurev.pp.34.060183.000443
- Lucas, W. J., and Franceschi, V. R. (1981). Characean charosome-complex and plasmalemma vesicle development. *Protoplasma* 107, 255–267. doi: 10.1007/BF01276829
- Lucas, W. J., Keifer, D. W., and Pesacreta, T. C. (1986). Influence of culture-medium pH on charosome development and chloride transport in *Chara corallina*. *Protoplasma* 130, 5–11. doi: 10.1007/BF01283326
- Lucas, W. J., and Smith, F. A. (1976). Influence of irradiance on H^+ efflux and Cl^- influx in *Chara corallina*: an investigation aimed at testing two Cl^- transport models. *Aust. J. Plant Physiol.* 3, 443–456.
- Matsuoka, K., Bassham, D. C., Raikhel, N. V., and Nakamura, K. (1995). Different sensitivity to wortmannin of two vacuolar sorting signals indicates the presence of distinct sorting machineries in tobacco cells. *J. Cell Biol.* 130, 1307–1318. doi: 10.1083/jcb.130.6.1307
- Mogelsvang, S., Gomez-Ospina, N., Soderholm, J., Glick, B. S., and Staehelin, L. A. (2003). Tomographic evidence for continuous turnover of Golgi cisternae in *Pichia pastoris*. *Mol. Biol. Cell* 14, 2277–2291. doi: 10.1091/mbc.E02-0-0697
- Nakanishi, S., Kakita, S., Takahashi, I., Kawahara, K., Tsukuda, E., Sano, T., et al. (1992). Wortmannin, a microbial product inhibitor of myosin light chain kinase. *J. Biol. Chem.* 267, 2157–2163.
- Noguchi, T., and Kakami, F. (1999). Transformation of *trans*-Golgi network during the cell cycle in a green Alga, *Botryococcus braunii*. *J. Plant Res.* 112, 175–186. doi: 10.1007/PL00013871
- Pesacreta, T. C., and Lucas, W. J. (1984). Plasma-membrane coat and a coated vesicle-associated reticulum of membranes - their structure and possible interrelationship in *Chara corallina*. *J. Cell Biol.* 98, 1537–1545. doi: 10.1083/jcb.98.4.1537
- Peter, B. J., Kent, H. M., Mills, I. G., Vallis, Y., Butler, P. J., Evans, P. R., et al. (2004). BAR domains as sensors of membrane curvature: the amphiphysin BAR structure. *Science* 303, 495–499. doi: 10.1126/science.1092586
- Pimpl, P., Hanton, S. L., Taylor, J. P., Pinto-daSilva, L. L., and Denecke, J. (2003). The GTPase ARF1p controls the sequence-specific vacuolar sorting route to the lytic vacuole. *Plant Cell* 15, 1242–1256. doi: 10.1105/tpc.010140
- Powis, G., Bonjouklian, R., Berggren, M. M., Gallegos, A., Abraham, R., Ashendel, C., et al. (1994). Wortmannin, a potent and selective inhibitor of phosphatidylinositol-3-kinase. *Cancer Res.* 54, 2419–2423.
- Price, G. D., Badger, M. R., Bassett, M. E., and Whitecross, M. I. (1985). Involvement of plasmalemmasomes and carbonic anhydrase in photosynthetic utilization of bicarbonate in *Chara corallina*. *Aust. J. Plant Physiol.* 12, 241–256. doi: 10.1071/PP9850241
- Price, G. D., and Whitecross, M. I. (1983). Cytochemical localization of ATPase activity on the plasmalemma of *Chara corallina*. *Protoplasma* 116, 65–74. doi: 10.1007/BF01294232
- Robinson, D. G., Jiang, L., and Schumacher, K. (2008). The endosomal system of plants: charting new and familiar Territories. *Plant Physiol.* 147, 1482–1492. doi: 10.1104/pp.108.120105
- Robinson, D. G., Pimpl, P., Scheuring, D., Stierhof, Y. D., Sturm, S., and Viotti, C. (2012). Trying to make sense of retromer. *Trends Plant Sci.* 17, 431–439. doi: 10.1016/j.tplants.2012.03.005
- Scheuring, D., Viotti, C., Kräger, F., Känzl, F., Sturm, S., Bubeck, J., et al. (2011). Multivesicular bodies mature from the *trans*-Golgi network/early endosome in *Arabidopsis*. *Plant Cell* 23, 3463–3481. doi: 10.1105/tpc.111.086918
- Schmoelzer, P. M., Hoeflberger, M., and Foissner, I. (2011). Plasma membrane domains participate in pH banding of *Chara* internodal cells. *Plant Cell Physiol.* 52, 1274–1288. doi: 10.1093/pcp/pcr074
- Sekeres, J., Pleskot, R., Pejchar, P., Zarsky, V., and Potocky, M. (2015). The song of lipids and proteins: dynamic lipid-protein interfaces in the regulation of plant cell polarity at different scales. *J. Exp. Bot.* 66, 1587–1598. doi: 10.1093/jxb/erv052
- Shimmen, T., and Yokota, E. (2004). Cytoplasmic streaming in plants. *Curr. Opin. Cell Biol.* 16, 68–72. doi: 10.1016/j.cub.2003.11.009
- Shin, H. W., Takatsu, H., and Nakayama, K. (2012). Mechanisms of membrane curvature generation in membrane traffic. *Membranes* 2, 118–133. doi: 10.3390/membranes2010118
- Simon, M. L. A., Platres, M. P., Assil, S., van Wijk, R., Chen, W. Y., Chory, J., et al. (2014). A multi-colour/multi-affinity marker set to visualize phosphoinositide dynamics in *Arabidopsis*. *Plant J.* 77, 322–337. doi: 10.1111/tpj.12358
- Simunovic, M., Srivastava, A., and Voth, G. A. (2013). Linear aggregation of proteins on the membrane as a prelude to membrane remodeling. *Proc. Natl. Acad. Sci. U.S.A.* 110, 20396–20401. doi: 10.1073/pnas.1309819110
- Sommer, A., Hoeflberger, M., Hoepflinger, M. C., Schmalbrock, S., Bulychev, A., and Foissner, I. (2015). Convoluted plasma membrane domains in the green alga *Chara* are depleted of microtubules and actin filaments. *Plant Cell Physiol.* 56, 1981–1996. doi: 10.1093/pcp/pcv119
- Takáč, T., Pechan, T., Šamajová, O., Ovečka, M., Richter, H., Eck, C., et al. (2012). Wortmannin treatment induces changes in *Arabidopsis* root proteome and post-Golgi compartments. *J. Proteome Res.* 11, 3127–3142. doi: 10.1021/pr201111n

- Takatsuka, C., Inoue, Y., Matsuoka, K., and Moriyasu, Y. (2004). 3-Methyladenine inhibits autophagy in tobacco culture cells under sucrose starvation conditions. *Plant Cell Physiol.* 45, 265–274. doi: 10.1093/pcp/pch031
- Ueda, T., Uemura, T., Sato, M. H., and Nakano, A. (2004). Functional differentiation of endosomes in *Arabidopsis* cells. *Plant J.* 40, 783–789. doi: 10.1111/j.1365-313X.2004.02249.x
- Uemura, T., Suda, Y., Ueda, T., and Nakano, A. (2014). Dynamic behavior of the *trans*-Golgi network in root tissues of *Arabidopsis* revealed by super-resolution live imaging. *Plant Cell Physiol.* 55, 694–703. doi: 10.1093/pcp/pcu010
- van Leeuwen, W., Ökrész, L., Bögrel, L., and Munnik, T. (2004). Learning the lipid language of plant signalling. *Trends Plant Sci.* 9, 378–384. doi: 10.1016/j.tplants.2004.06.008
- Vermeer, J. E. M., Thole, J. M., Goedhart, J., Nielsen, E., Munnik, T., and Gadella, T. W. (2009). Imaging phosphatidylinositol 4-phosphate dynamics in living plant cells. *Plant J.* 57, 356–372. doi: 10.1111/j.1365-313X.2008.03679.x
- Vermeer, J. E. M., van Leeuwen, W., Tobena-Santamaria, R., Laxalt, A. M., Jones, D. R., Divecha, N., et al. (2006). Visualization of PtdIns3P dynamics in living plant cells. *Plant J.* 47, 687–700. doi: 10.1111/j.1365-313X.2006.02830.x
- Viotti, C., Bubeck, J., Stierhof, Y. D., Krebs, M., Langhans, M., van den Berg, W., et al. (2010). Endocytic and secretory traffic in *Arabidopsis* merge in the *trans*-Golgi network/early endosome, an independent and highly dynamic organelle. *Plant Cell* 22, 1344–1357. doi: 10.1105/tpc.109.072637
- Walker, E. H., Pacold, M. E., Perisic, O., Stephens, L., Hawkins, P. T., Wymann, M. P., et al. (2000). Structural determinants of phosphoinositide 3-kinase inhibition by wortmannin, LY294002, quercetin, myricetin, and staurosporine. *Mol. Cell* 6, 909–919. doi: 10.1016/S1097-2765(05)00089-4
- Wang, J. Q., Cai, Y., Miao, Y. S., Lam, S. K., and Jiang, L. W. (2009). Wortmannin induces homotypic fusion of plant prevacuolar compartments. *J. Exp. Bot.* 60, 3075–3083. doi: 10.1093/jxb/erp136
- Wymann, M. P., Bulgarelli-Leva, G., Zvelebil, M. J., Pirola, L., Vanhaesebroeck, B., Waterfield, M. D., et al. (1996). Wortmannin inactivates phosphoinositide 3-kinase by covalent modification of Lys-802, a residue involved in the phosphate transfer reaction. *Mol. Cell Biol.* 16, 1722–1733. doi: 10.1128/MCB.16.4.1722
- Yuan, H., Barnes, K. R., Weissleder, R., Cantley, L., and Josephson, L. (2007). Covalent reactions of wortmannin under physiological conditions. *Chem. Biol.* 14, 321–328. doi: 10.1016/j.chembiol.2007.02.007
- Zheng, J. M., Han, S. W., Rodriguez-Welsh, M. F., and Rojas-Pierce, M. (2014). Homotypic vacuole fusion requires VTI11 and is regulated by phosphoinositides. *Mol. Plant* 7, 1026–1040. doi: 10.1093/mp/ssu019

Conflict of Interest Statement: The authors declare that the research was conducted in the absence of any commercial or financial relationships that could be construed as a potential conflict of interest.

Copyright © 2016 Foissner, Sommer, Hoeftberger, Hoepflinger and Absolonova. This is an open-access article distributed under the terms of the Creative Commons Attribution License (CC BY). The use, distribution or reproduction in other forums is permitted, provided the original author(s) or licensor are credited and that the original publication in this journal is cited, in accordance with accepted academic practice. No use, distribution or reproduction is permitted which does not comply with these terms.



Concanavalin A Disrupts the Release of Fibrous Material Necessary for Zygote Formation of a Unicellular Charophycean Alga, *Closterium peracerosum-strigosum-littorale* Complex

OPEN ACCESS

Edited by:

Iben Sorensen,
Cornell University, USA

Reviewed by:

Andrew Charles Cuming,
The University of Leeds, UK

Mary Jane Beilby,
The University of New South Wales,
Australia

***Correspondence:**

Jun Abe
junabe@kc.chuo-u.ac.jp
Hiroyuki Sekimoto
sekimoto@fc.jwu.ac.jp

†Present address:

Jun Abe,
Department of Biological Sciences,
Faculty of Science and Engineering,
Chuo University, 1-13-27
Kasuga, Bunkyo-ku,
Tokyo, Japan

[‡]These authors have contributed
equally to this work.

Specialty section:

This article was submitted to
Plant Evolution and Development,
a section of the journal
Frontiers in Plant Science

Received: 22 March 2016

Accepted: 01 July 2016

Published: 13 July 2016

Citation:

Abe J, Hori S, Sato M and
Sekimoto H (2016) Concanavalin
A Disrupts the Release of Fibrous
Material Necessary for Zygote
Formation of a Unicellular
Charophycean Alga, *Closterium*
peracerosum-strigosum-littorale
Complex. *Front. Plant Sci.* 7:1040.
doi: 10.3389/fpls.2016.01040

Jun Abe^{1*†‡}, Sachie Hori^{2‡}, Mamiko Sato³ and Hiroyuki Sekimoto^{1,2*}

¹ Department of Chemical and Biological Sciences, Faculty of Science, Japan Women's University, Tokyo, Japan, ² Division of Material and Biological Sciences, Graduate School of Science, Japan Women's University, Tokyo, Japan, ³ Laboratory of Electron Microscopy, Japan Women's University, Tokyo, Japan

The *Closterium peracerosum-strigosum-littorale* (*C. psl.*) complex is the best characterized charophycean alga with respect to the processes of sexual reproduction. We examined the effect of concanavalin A (Con A) on physiological and ultrastructural changes during the conjugation of the *C. psl.* complex. Two heterothallic gametangial cells formed a sexual pair as usual; however, the release of gametes was completely blocked by the addition of Con A. Fluorescein isothiocyanate-labeled Con A bound to the outermost layer of the conjugation papillae of paired cells. In the absence of Con A, the disruption of outer cell walls on the conjugation papillae and the secretion of fibrous materials from the conjugation papillae were observed using a transmission electron microscope, but Con A-treated cells did not show these changes. Instead, a highly electron-dense layer was observed in the outermost papillae, and the excess fibrous materials remained at the inside of the layer. These results suggest that an unknown molecule(s) recognized by Con A is essential for the diffusion of fibrous materials at the conjugation papillae, which is an indispensable step for gamete release during conjugation of the *C. psl.* complex.

Keywords: charophycean, *Closterium*, conjugation, gamete, Concanavalin A (Con A), sexual reproduction

INTRODUCTION

Land plants (embryophyta) are believed to have evolved from ancestral charophycean algae (Karol et al., 2001). The charophyceans comprise five lineages (orders) of freshwater green algae: Charales, Coleochaetales, Zygnematales, Klebsormidiales, and Chlorokybales. Based on phylogenetic analyses, Zygnematales – or a clade consisting of the Zygnematales and the Coleochaetales – has been proposed as a sister group of land plants (Turmel et al., 2006; Wodniok et al., 2011).

The desmid *Closterium*, which belongs to Zygnematales, is the most successfully studied unicellular charophycean alga in terms of the maintenance of strains and sexual reproduction (Sekimoto et al., 2012, 2014a,b). Heterothallic strains of the *Closterium peracerosum-strigosum-littorale* complex (*C. psl.* complex) have two sexes: mating type plus (*mt*⁺) and mating type

minus (mt^-). Sexual reproduction readily occurs when cells of these two sexes are cultured together in nitrogen-depleted medium under light conditions. Recently, a technique for achieving reverse genetics in this complex has been developed (Abe et al., 2011; Hirano et al., 2015) and its genome project is now underway (Sekimoto et al., personal communication).

Two sex pheromones are essential for regulating the processes of sexual reproduction: protoplast-release-inducing protein (PR-IP) and PR-IP Inducer (Sekimoto et al., 1990, 1993). PR-IP is secreted from mt^+ cells and induces the secretion of mucilage, sexual cell division for differentiation into gametangial cells (Akatsuka et al., 2006), and the release of protoplasts (gametes) from the gametangial cells (Sekimoto et al., 1990), whereas PR-IP Inducer is secreted from mt^- cells and induces the secretion of mucilage (Akatsuka et al., 2003), sexual cell division (Tsuchikane et al., 2003, 2005), and the expression of genes encoding two subunits of PR-IP (Sekimoto et al., 1994). Both gametangial cells make a sexual pair, form conjugation papillae, release their gametes, and form a zygote by the fusion of the gametes (Sekimoto et al., 2012); however, the mechanisms behind the pairing for zygote formation remain unclear.

From the results of cDNA microarray analyses, we identified 88 pheromone-inducible, conjugation-related, and/or sex-specific genes (Sekimoto et al., 2006). Among them, the function of the *CpRLK1* gene encoding receptor-like protein kinase was characterized (Hirano et al., 2015). *CpRLK1* localized at conjugation papilla and the knockdown mt^+ transformants of *CpRLK1* showed reduced competence for sexual reproduction and formed an abnormally enlarged conjugation papilla after pairing with the mt^- cells. Because *CpRLK1* shares phylogenetic features with the CrRLK1L-1 subfamily, which is thought to act as a cell wall integrity sensor in higher plants, it is proposed that *CpRLK1* is an ancient cell wall sensor and regulates the osmotic pressure of the cell for appropriate gamete release, a process required for successful conjugation.

To elucidate further the mechanisms of conjugation, especially the release and fusion of gametes in the *C. psl.* complex, we have focused on the lectins, carbohydrate-binding proteins. Generally, carbohydrate plays important roles in biological organization on the cell surface and cell-cell recognition phenomena. Hori et al. (2012) examined whether some lectins affected the conjugation processes of the *C. psl.* complex. Among 20 lectins tested, we conclude that a concanavalin A (Con A), which bind to mannose and glucose residues in carbohydrates and in *N*-linked glycan moieties of glycoproteins, is a certain candidate to understand the phenomena during fusion of gametes in *C. psl.* complex. Hori et al. (2012) reported that fluorescein isothiocyanate (FITC)-labeled Con A weakly bound to the surface of vegetative and nitrogen-deprived cells, however, binding of FITC-labeled Con A at conjugation papillae is quite remarkable and the addition of Con A completely inhibited zygote formation, indicating binding molecule(s) of Con A localized on the conjugation papillae is specifically involved in zygote formation and plays important roles during the process of conjugation in the *C. psl.* complex. However, the precise details of Con A inhibition during conjugation remain unclear.

In this study, we thus investigated the physiological and ultrastructural changes caused by Con A during the conjugation in the *C. psl.* complex. The results indicate that the Con A binding molecule(s) on conjugation papillae acts to disperse uncharacterized fibrous materials, which is indispensable for the release of gametes in the *C. psl.* complex.

MATERIALS AND METHODS

Strains, Culture Conditions, and Preparation of Sexually Differentiated Cells

The strains of the heterothallic *C. psl.* complex used in this work were NIES-67 (mt^+) and NIES-68 (mt^-), obtained from the National Institute for Environmental Studies (Ibaraki, Japan). Cells were grown in 300-mL Erlenmeyer flasks containing 150 mL of nitrogen-supplemented medium (C medium¹) at 23°C under a 16:8-h light:dark regime. Light from fluorescent lamps (FL40SSD; Toshiba, Tokyo, Japan) was adjusted to 28 $\mu\text{mol m}^{-2} \text{s}^{-1}$ at the surface of the culture medium. To obtain sexually differentiated cells, mt^+ and mt^- vegetative cells in mid-logarithmic phase (10 days of culture) were separately harvested by centrifugation and washed three times with nitrogen-depleted mating-inducing (MI) medium (Ichimura, 1971). Then, 7.2×10^5 cells were inoculated into 72 mL of MI medium in a 300-mL Erlenmeyer flask and incubated for 24 h in continuous light (28 $\mu\text{mol m}^{-2} \text{s}^{-1}$) (Sekimoto and Fujii, 1992).

Inhibition of the Conjugation Processes by the Addition of Con A during Mating Culture

Cells at conjugation stages were obtained by mixing the respective sexually differentiated cells (5.0×10^3 cells each in 1 mL of MI medium) in a test tube (1.75 cm in diameter, 13 cm long) and then incubated for 48 h under continuous light (28 $\mu\text{mol m}^{-2} \text{s}^{-1}$). FITC-labeled Con A (Vector Laboratories, Burlingame, CA, USA) was added to cells at a final concentration of 7 $\mu\text{g mL}^{-1}$ at each of 0, 8, 16, and 24 h after mixing of the cells. In parallel, mixed cells in the absence of Con A were also prepared and fixed using 0.6% (w/v) glutaraldehyde (Wako, Japan, Osaka) at these different periods of Con A addition. The population of sexual reproductive cells (conjugation pairs, gamete-releasing cells, and zygotes) was counted 48 h after the mixing.

Localization of FITC-Labeled Con A

To monitor the developmental changes on conjugation papillae, 2.0×10^4 cells mL^{-1} of sexually differentiated mt^+ and mt^- cells were stained separately by Calcofluor White ST (American Cyanamid Co., Wayne, NJ, USA) at a final concentration of 0.1% (w/v) for 1 h under dark conditions. They were then harvested, washed three times with MI medium, and mixed together at a cell density of 5.0×10^3 cells each in 1 mL of MI medium. After

¹<http://mcc.nies.go.jp/02medium-e.html#>

16 h of incubation under continuous light, cells were harvested, washed three times with MI medium, and incubated in MI medium containing FITC-labeled Con A at a final concentration of $10 \mu\text{g mL}^{-1}$ for 1 h under dark conditions. Then, cells were washed three times with MI medium and fluorescence of the cells was observed using a fluorescent microscope (BX60; Olympus, Tokyo, Japan).

The localization of FITC-labeled Con A on conjugation papillae was detected as follows: cells at pairing stages (16 h after the mixing) were harvested, washed three times with MI medium, and resuspended in the same medium at a final density of $1 \times 10^4 \text{ cells mL}^{-1}$. Then, both FITC-labeled Con A (final concentration: $10 \mu\text{g mL}^{-1}$) and Calcofluor White ST (final concentration: 0.1%) were added to the cells simultaneously. After 1 h of incubation under dark conditions, the fluorescence of the cells was detected using a confocal laser scanning microscope (FV500; Olympus).

Transmission Electron Microscopy

Fluorescein isothiocyanate-labeled Con A was added to the cells at the pairing stage (16 h after the mixing) at a final concentration of $10 \mu\text{g mL}^{-1}$, followed by incubation for 4 h under continuous light. The cells were then harvested by centrifugation, prefixed in 2% glutaraldehyde in 0.1 M phosphate buffer or 0.05 M Cacodylate buffer (pH 7.2), and kept at room temperature for 2 h. Next, they were gently centrifuged, washed three times in this buffer, and postfixed in 1% OsO₄ with the same buffer at 4°C overnight. After washing with the buffer, 1×10^5 cells were collected by filtration using SUPREC-01 (Takara, Shiga, Japan). They were embedded in 2% low-melting-point agarose, dehydrated through an ethanol series, and passed through QY-2 (methyl glycidyl ether; Nissin EM, Tokyo, Japan) and embedded in Quetol-812 mixture (Nissin EM), followed by polymerization at 60°C for 48 h. Ultrathin sections of 60–70 nm were cut with an ultramicrotome, Ultracut S (Reichert-Nissei, Tokyo, Japan), stained with 4% uranyl acetate and 0.4% lead citrate, and observed with a TEM, JEM-1200EXS (JEOL, Tokyo, Japan), at 80 kV.

RESULTS

Con A Inhibits the Process of Gamete Release or Later Stages in the *C. psl.* Complex

When both mt⁺ and mt⁻ cells of the *C. psl.* complex are mixed in nitrogen-depleted medium, the following processes of sexual reproduction are observed: (i) mucilage secretion, (ii) sexual cell division to form gametangial cells, (iii) pair formation between opposite mating type gametangial cells, (iv) formation of conjugation papillae, (v) release of protoplasts (gametes) from the cells, and (vi) fusion of the gametes to form a zygote (Ichimura, 1971; Sekimoto et al., 2012). We previously reported that Con A completely inhibits the zygote formation (Hori et al., 2012). Even though the results indicated that the target molecule(s) of Con A plays important roles in zygote formation, the details of the stage influenced by Con A have not been clarified.

First, we confirmed the temporal changes during the conjugation process in the *C. psl.* complex. Equal numbers of mt⁺ and mt⁻ cells, which had been separately induced in advance to undergo sexual differentiation in nitrogen-depleted medium, were mixed and then monitored for changes in the ratio of sexually reproductive cells at three developmental stages: conjugating pairs, gametes, and zygotes. As shown in **Figure 1A**, the mixed cells did not exhibit signs of sexual reproduction within the first 8 h; however, some of them had begun to form conjugating pairs by 16 h, followed by an increase in the release of gametes and zygote formation from 24 to 48 h.

Concanavalin A was added to samples at 0, 8, 16, and 24 h after the initial mixing and then comparisons to the proportion of sexually reproducing cells at 48 h were performed. The experimental procedure is outlined in **Figure 1B**, and the results are shown in **Figures 1C,D**. In the absence of Con A, about 66% of cells exhibited signs of sexual reproduction at 48 h after the mixing: 7, 44, and 14% of the cells formed conjugating pairs, released gametes, and formed zygotes, respectively (**Figures 1C,D4**).

When mixed cells, to which Con A had been added at 0, 8, and 16 h after the mixing, were incubated for 48 h (**Figure 1B**), they showed signs of sexual reproduction at rates of 19, 53, and 58%, respectively (**Figure 1C1–C3**), although the cells were mostly in the conjugating pair stage. Moreover, the conjugating pairs in the presence of Con A abundantly extruded conjugation papillae, but the release of gametes was markedly absent (**Figure 1D3**). These results clearly indicate that Con A affects the release of gametes, which is a prerequisite for cell fusion. In addition, no released gametes were observed in Con A-treated mixed cells by 16 h after extending incubation for 10 days (data not shown). This indicates that the addition of Con A does not delay the progression of gamete release, but instead completely inhibits it.

By comparison with the cells prior to Con A addition (0, 8, and 16 h after mixing), the proportion of conjugating pairs after 48 h of incubation increased from 0 to 18%, 0 to 51%, and 26 to 58%, respectively (**Figure 1C1–C3**). This indicates that Con A does not fully inhibit early processes of conjugation leading up to the formation of conjugating pairs. However, cells treated with Con A at 0 h exhibited reduced sexual reproduction compared with those at 8 and 16 h (**Figure 1C1**). Although this suggests that Con A exerts some effects on mixed cells during the early stages, this will be further elucidated in Section “Discussion.” Reduced zygote formation was also observed (**Figure 1C4**) when Con A was added at 24 h after the mixing, suggesting that it might affect cellular processes after gamete release.

Behavior and Subcellular Localization of Con A-Target Molecules

In a previous study, we demonstrated that target molecule(s) of Con A mainly localized on the conjugation papillae during conjugation processes in the *C. psl.* complex (Hori et al., 2012). To monitor the developmental changes on conjugation papillae, Calcofluor White, which stains β-D-glucopyranose polysaccharides in cell walls, was used as a vital staining reagent. Both mating type cells were separately pulse-labeled by

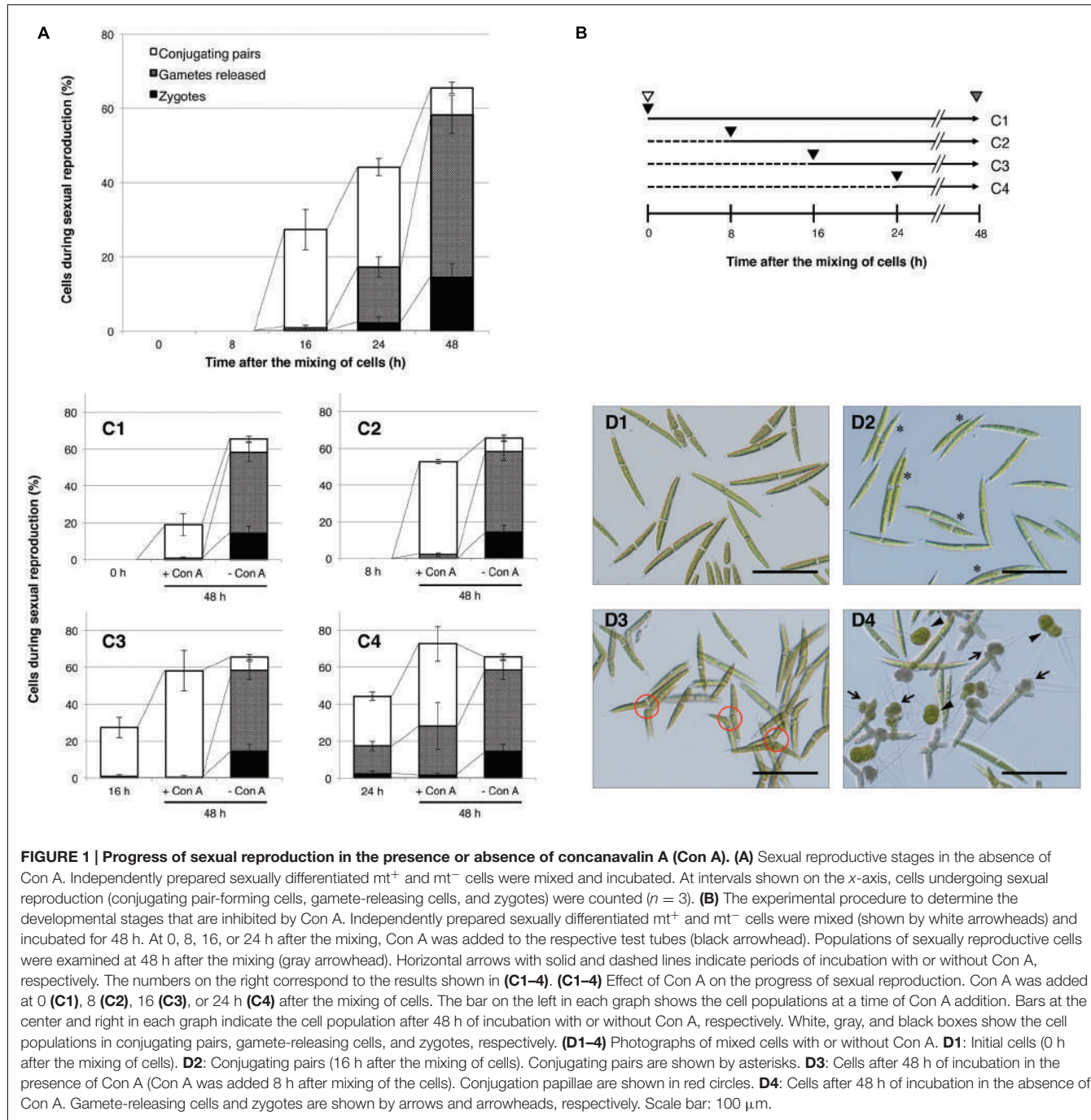


FIGURE 1 | Progress of sexual reproduction in the presence or absence of concanavalin A (Con A). (A) Sexual reproductive stages in the absence of Con A. Independently prepared sexually differentiated mt⁺ and mt⁻ cells were mixed and incubated. At intervals shown on the x-axis, cells undergoing sexual reproduction (conjugating pair-forming cells, gamete-releasing cells, and zygotes) were counted ($n = 3$). (B) The experimental procedure to determine the developmental stages that are inhibited by Con A. Independently prepared sexually differentiated mt⁺ and mt⁻ cells were mixed (shown by white arrowheads) and incubated for 48 h. At 0, 8, 16, or 24 h after the mixing, Con A was added to the respective test tubes (black arrowhead). Populations of sexually reproductive cells were examined at 48 h after the mixing (gray arrowhead). Horizontal arrows with solid and dashed lines indicate periods of incubation with or without Con A, respectively. The numbers on the right correspond to the results shown in (C1–4). (C1–4) Effect of Con A on the progress of sexual reproduction. Con A was added at 0 (C1), 8 (C2), 16 (C3), or 24 h (C4) after the mixing of cells. The bar on the left in each graph shows the cell populations at a time of Con A addition. Bars at the center and right in each graph indicate the cell populations after 48 h of incubation with or without Con A, respectively. White, gray, and black boxes show the cell populations in conjugating pairs, gamete-releasing cells, and zygotes, respectively. (D1–4) Photographs of mixed cells with or without Con A. D1: Initial cells (0 h after the mixing of cells). D2: Conjugating pairs (16 h after the mixing of cells). Conjugating pairs are shown by asterisks. D3: Cells after 48 h of incubation in the presence of Con A (Con A was added 8 h after mixing of the cells). Conjugation papillae are shown in red circles. D4: Cells after 48 h of incubation in the absence of Con A. Gamete-releasing cells and zygotes are shown by arrows and arrowheads, respectively. Scale bar: 100 μ m.

Calcofluor White and then mixed. Fluorescence on the whole cell surface and the central area was clearly detected before formation of the pair (Figure 2A4). After physical contact of the cells, narrow slit-like bands, which did not emit fluorescence signals, appeared near the base of the semi-cells (Figure 2A5, arrowhead). Upon enlargement of these bands, conjugation papillae appeared (Figure 2A6, arrowhead), namely, the conjugation papillae were synthesized *de novo* after pair formation. When FITC-labeled Con A was added to the mixed cells just before pair formation, the signals were first detected at the point of adhesion of the

cells (Figure 2A7), then on the edge of developing papillae (Figure 2A8), and finally on conjugation papillae with a ring-like shape (Figure 2A9). These results indicated that the Con A binding molecule(s) was synthesized prior to papilla formation and accumulated around developing papillae.

Next, we investigated the exact localization of Con A binding molecules on conjugation papillae by confocal laser scanning microscopy. Calcofluor White and FITC-labeled Con A were simultaneously added at the time of conjugation papilla formation. As shown in Figure 2B2, Calcofluor White fluoresced

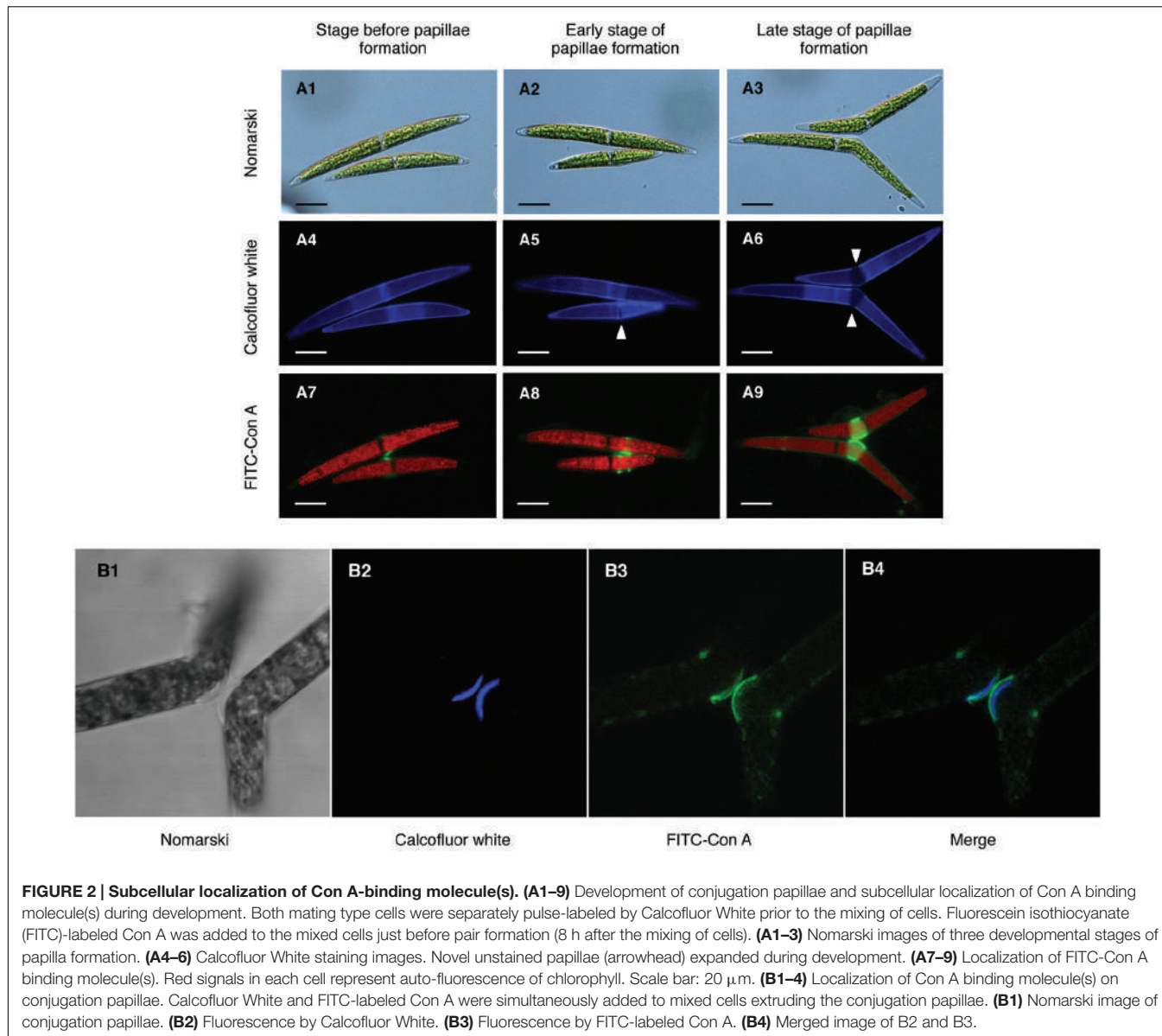


FIGURE 2 | Subcellular localization of Con A-binding molecule(s). **(A1–9)** Development of conjugation papillae and subcellular localization of Con A binding molecule(s) during development. Both mating type cells were separately pulse-labeled by Calcofluor White prior to the mixing of cells. Fluorescein isothiocyanate (FITC)-labeled Con A was added to the mixed cells just before pair formation (8 h after the mixing of cells). **(A1–3)** Nomarski images of three developmental stages of papilla formation. **(A4–6)** Calcofluor White staining images. Novel unstained papillae (arrowhead) expanded during development. **(A7–9)** Localization of FITC-Con A binding molecule(s). Red signals in each cell represent auto-fluorescence of chlorophyll. Scale bar: 20 μ m. **(B1–4)** Localization of Con A binding molecule(s) on conjugation papillae. Calcofluor White and FITC-labeled Con A were simultaneously added to mixed cells extruding the conjugation papillae. **(B1)** Nomarski image of conjugation papillae. **(B2)** Fluorescence by Calcofluor White. **(B3)** Fluorescence by FITC-labeled Con A. **(B4)** Merged image of B2 and B3.

intensively on the outer layers of conjugation papillae, indicating that the conjugation papillae consist of cell wall materials such as cellulose. Interestingly, fluorescence detected in the papillae did not exhibit contact between adhesion points in each mating type cell (Figure 2B2). Furthermore, signals derived from FITC-labeled Con A were detected on the outermost layer of the papilla (Figure 2B3), where the signals were not co-localized but contacted at adhesion points between the two mating type cells (Figure 2B4).

Con A Inhibits the Release of Fibrous-Like Materials from Conjugation Papillae

As shown in Figure 1C, Con A inhibited the release of gametes from paired cells. To investigate the intracellular changes caused

by Con A, we compared the ultrastructures in conjugation papillae with and without Con A.

Sections obtained in the experiments are shown in Figure 3A. In the absence of Con A, two layers of cell wall showing different electron densities, high electron density (outer cell wall, OCW) and low electron density (inner cell wall, ICW), were observed in horizontal sections at the intermediate region of semi-cells (Figure 3B). At the basal regions of the conjugation papillae, disruption of the OCW and the release of fibrous-like materials from the ICW (or further inside the ICW) were detected (Figure 3C). Numerous vesicles of various sizes were detected in the cytoplasmic portion of the papillae, suggesting the active supply of unknown materials into the intercellular space (Figure 3D). The fibrous-like materials spread densely and subsequently filled the area between the papillae of the pairing cells. On the other hand, the fibrous-like materials did

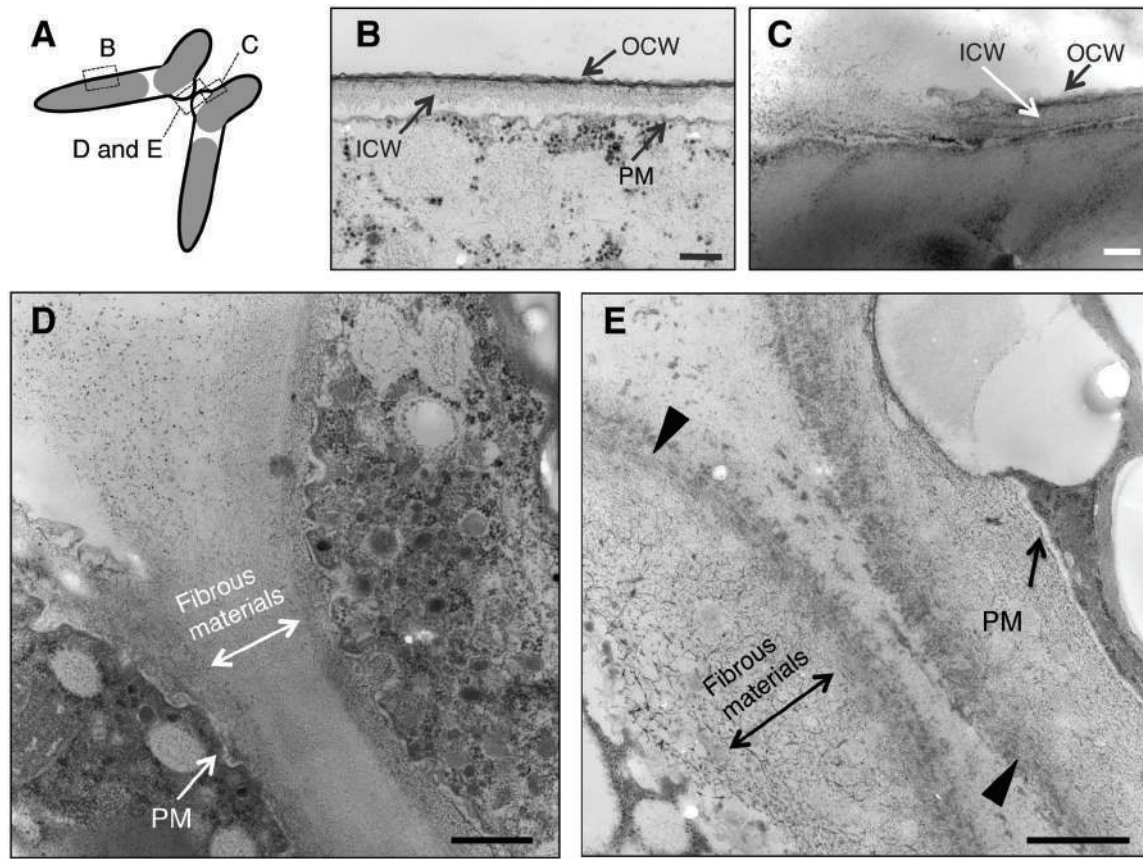


FIGURE 3 | Ultrastructural observations of paired cells using a transmission electron microscope (TEM). (A) Illustration of TEM sections observed in this study. (B) *Closterium* cell wall consists of two layers: outer cell wall (OCW) and inner cell wall (ICW). Around the conjugation papillae, the OCW was disrupted (C) and fibrous-like materials were released from the papillae (D). When Con A was added prior to cell fusion (16 h after the mixing), the fibrous-like materials accumulated in the conjugation papillae of respective paired cells. Increased electron density at the outermost layer was also observed (arrowhead) (E). PM, plasma membrane. Bars: 250 nm (B), 200 nm (C), and 500 nm (D,E).

not accumulate in the intercellular space in the presence of Con A. Distinct highly electron-dense layer on the outermost papillae and accumulation of fibrous-like materials within the conjugation papillae were observed (**Figure 3E**).

From the aforementioned ultrastructural comparisons, it was indicated that the disruption of OCWs and the subsequent release of fibrous-like materials in conjugation papillae were indispensable for the release of gametes and that Con A binding molecules were possibly involved in the dispersion of such fibrous materials in the *C. psl.* complex.

DISCUSSION

We previously showed that Con A completely inhibited the zygote formation of the *C. psl.* complex (Hori et al., 2012). In the present study, we investigated the physiological and ultrastructural changes caused by Con A during conjugation processes in the *C. psl.* complex.

Normally, cells of both mating types form conjugation pairs by 16 h after mixing and then gamete release and zygote

formation can subsequently be observed (**Figure 1A**). As shown in **Figure 1C1–C3**, mixed cells, to which Con A had been added by 16 h after the mixing, formed a sexual pair and conjugation papillae; however, subsequent processes were almost completely blocked. These results indicate that Con A does not affect the formation of sexual pairs and conjugation papillae but completely inhibits the later process of gamete release. However, we detected partial inhibition of the formation of conjugation pairs when Con A was added at the time of cell mixing (0 h). Hori et al. (2012) showed that Con A bound abundantly on conjugation papillae, but also slightly on the surface of vegetative and nitrogen-deprived cells. Indeed, both vegetative and sexual cell divisions were partially inhibited in the presence of Con A (data not shown). Therefore, we consider that Con A also binds to a molecule(s) that is essential for sexual cell division, and inhibits the pairing partly by inhibiting the formation of sexually competent gametangial cells.

On the other hand, the addition of Con A completely inhibited the processes after the formation of conjugation papillae (**Figure 1C1–C3**) and the FITC-Con A bound to the conjugation papillae remarkably (**Figure 2**), suggesting that Con A-binding

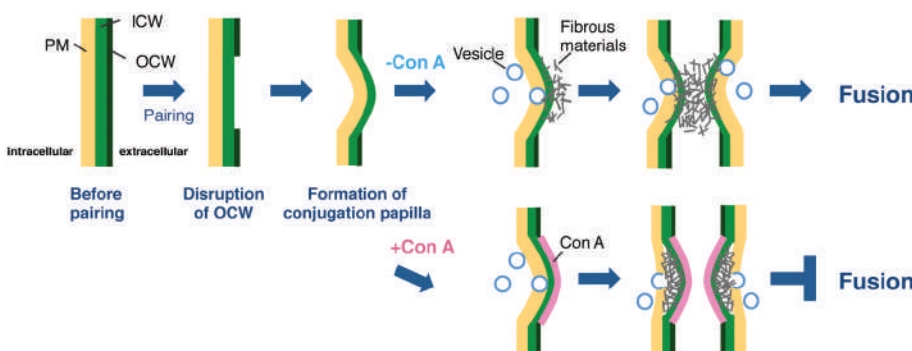


FIGURE 4 | Possible model for cell fusion in the *C. psl.* Complex. Once mt^+ and mt^- cells have formed a conjugation pair, the OCWs (OCW) at the point of adhesion of the two cells are disrupted. The cytoplasm of both paired cells is extruded from the thin wall area to form papillae by osmotic pressure. In parallel, fibrous materials, which are indispensable for gamete release, diffuse from the ICW to the tip of papillae with the supply of materials by vesicle transport. The target molecule of Con A is synthesized at adhesion sites prior to the formation of papillae and finally acts to unfold or refold the fibrous materials on the surface of papillae. In the presence of Con A, the highly electron-dense layer at the outermost papillae is appeared and the unfolding or refolding by the target molecule is inhibited; therefore, paired cells cannot complete gamete release and cell fusion.

molecule(s) on the conjugation papillae is critically responsible for the gamete release during the conjugation processes. In the absence of Con A, the disruption of OCWs and the diffusion of fibrous materials from the conjugation papillae were clearly observed (Figures 3C,D). In contrast, Con A-treated cells exhibited the highly electron-dense layer at the outermost papillae, and the excess fibrous materials remained at the inside of the layer (Figure 3E). These results clearly indicate that Con A blocks diffusion of the fibrous materials from the papillae.

From the fluorescence in the papillae stained by Calcofluor White (Figure 2B2), which recognizes β -D-glucopyranose polysaccharides, it was apparent that the conjugation papillae contained cell wall materials such as cellulose. Using a TEM, Pickett-Heaps and Fowke (1971) also reported that the conjugation papillae in *Closterium littorale*, a species related to the *C. psl.* complex, contained cell wall materials (Pickett-Heaps and Fowke, 1971). We also observed numerous vesicles in the cytoplasm inside the papillae (Figure 3D), probably due to active transport of the materials for papilla formation. These results suggest that the papillae are formed by rapid and considerable deposition of cell wall materials, accompanied by the rapid synthesis of cellulose microfibrils on the surface of the plasma membrane. Because of the co-localization of the fluorescence of Calcofluor White (Figure 2B2) and fibrous materials in the papillae (Figure 3E), the fibrous materials may be cell wall components. In addition, we also observed that the mutual contact area of two papillae is filled with fibrous materials in the absence of Con A (Figure 3D), suggesting the crossing of fibrous materials between the cells may be essential for cell fusion. In the case of Con A-treated cells, however, the diffusion of fibrous materials could not be observed (Figure 3E), suggesting that the diffusion is indispensable for the release of gametes and cell fusion. From these discussions, we consider that an unknown molecule(s) recognized by Con A may be involved in the unfolding or refolding of fibrous materials on the surface of conjugation papillae to achieve gamete release and cell fusion (Figure 4). At present, however, we have no

information whether the binding of Con A might be a general obstruction to fibrous material release and such obstruction might be seen in the other life stage, such as vegetative cell division, or the obstruction is specific event and is only triggered on the conjugation papillae. Alternatively, the molecule may be an unknown signaling molecule for gamete release. In the *C. psl.* complex, a sex pheromone, PR-IP (Sekimoto et al., 1990), is known to be involved in gamete release from mt^- cells; however, no binding of Con A to PR-IP was confirmed by Western blotting (data not shown).

To identify the Con A-target molecules, two-dimensional polyacrylamide gel electrophoresis and western blotting with biotin-labeled Con A have been performed. In preliminary experiments, several spots have been abundantly detected in pairing-induced samples, comparing to the non-pairing samples (Supplementary Figure S1). One of them, having molecular mass of 75 kDa (red arrow), showed most apparent difference between two samples. These ConA-binding polypeptide species, that appear specific to induction of sexual pair formation, represent candidates for the mediation of the release of fibrous material. It will be necessary to identify these molecules in order to test this proposed function, for example by using our established knockdown procedure (Hirano et al., 2015).

AUTHOR CONTRIBUTIONS

JA, SH, and HS conceived of and designed the research. SH performed all experimental work. MS provided essential support for the TEM experiments. JA and HS wrote the manuscript.

FUNDING

This work was partly supported by Grants-in-Aid for Scientific Research (nos. 23657161, 24370038, 24247042, 25304012, 26650147, and 15H05237 to HS and no. 23770277 to JA)

from the Japan Society for the Promotion of Science and Grants-in-Aid for Scientific Research on Innovative Areas “Elucidating common mechanisms of allogenic authentication” (nos. 22112521 and 24112713 to HS) from the Ministry of Education, Culture, Sports, Science and Technology, Japan.

REFERENCES

- Abe, J., Hori, S., Tsuchikane, Y., Kitao, N., Kato, M., and Sekimoto, H. (2011). Stable nuclear transformation of the *Closterium peracerosum-strigosum-littorale* complex. *Plant Cell Physiol.* 52, 1676–1685. doi: 10.1093/pcp/pcr103
- Akatsuka, S., Sekimoto, H., Iwai, H., Fukumoto, R., and Fujii, T. (2003). Mucilage secretion regulated by sex pheromones in *Closterium peracerosum-strigosum-littorale* complex. *Plant Cell Physiol.* 44, 1081–1087. doi: 10.1093/pcp/pcg131
- Akatsuka, S., Tsuchikane, Y., Fukumoto, R., Fujii, T., and Sekimoto, H. (2006). Physiological characterization of the sex pheromone protoplast-release-inducing protein from the *Closterium peracerosum-strigosum-littorale* complex (Charophyta). *Phycol. Res.* 54, 116–121. doi: 10.1111/j.1440-1835.2006.00418.x
- Hirano, N., Marukawa, Y., Abe, J., Hashiba, S., Ichikawa, M., Tanabe, Y., et al. (2015). A Receptor-like kinase, related with cell wall sensor of higher plants, is required for sexual reproduction in the unicellular charophycean alga, *Closterium peracerosum-strigosum-littorale* complex. *Plant Cell Physiol.* 56, 1456–1462. doi: 10.1093/pcp/pcv065
- Hori, S., Sekimoto, H., and Abe, J. (2012). Properties of cell surface carbohydrates in sexual reproduction of the *Closterium peracerosum-strigosum-littorale* complex (Zygnematophyceae, Charophyta). *Phycol. Res.* 60, 254–260. doi: 10.1111/j.1440-1835.2012.00656.x
- Ichimura, T. (1971). “Sexual cell division and conjugation-papilla formation in sexual reproduction of *Closterium strigosum*,” in *Proceedings of the 7th International Seaweed Symposium*, ed. K. Nishizawa (Tokyo: University of Tokyo Press), 208–214.
- Karol, K. G., McCourt, R. M., Cimino, M. T., and Delwiche, C. F. (2001). The closest living relatives of land plants. *Science* 294, 2351–2353. doi: 10.1126/science.1065156
- Pickett-Heaps, J. D., and Fowke, L. C. (1971). Conjugation in the desmid *Closterium littorale*. *J. Phycol.* 7, 37–50. doi: 10.1111/j.1529-8817.1971.tb01476.x
- Sekimoto, H., Abe, J., and Tsuchikane, Y. (2012). New insights into the regulation of sexual reproduction in *Closterium*. *Int. Rev. Cell Mol. Biol.* 297, 309–338. doi: 10.1016/B978-0-12-394308-8.00014-5
- Sekimoto, H., Abe, J., and Tsuchikane, Y. (2014a). “Mechanism of sexual reproduction in fresh water microalgae,” in *Reproductive Biology of Plants*, eds K. G. Ramawat, J. M. Merillon, and K. R. Shivanna (Boca Raton, FL: CRC Press), 29–56.
- Sekimoto, H., and Fujii, T. (1992). Analysis of gametic protoplast release in *Closterium peracerosum-strigosum-littorale* complex (Chlorophyta). *J. Phycol.* 28, 615–619. doi: 10.1111/j.0022-3646.1992.00615.x
- Sekimoto, H., Inoki, Y., and Fujii, T. (1993). Detection and evaluation of an inducer of diffusible mating pheromone of heterothallic *Closterium peracerosum-strigosum-littorale* complex. *Plant Cell Physiol.* 37, 991–996.
- Sekimoto, H., Satoh, S., and Fujii, T. (1990). Biochemical and physiological properties of a protein inducing protoplast release during conjugation in the *Closterium peracerosum-strigosum-littorale* complex. *Planta* 182, 348–354. doi: 10.1007/BF02411384
- Sekimoto, H., Sone, Y., and Fujii, T. (1994). Regulation of expression of the genes for a sex pheromone by an inducer of the sex pheromone in the *Closterium peracerosum-strigosum-littorale* complex. *Planta* 193, 137–144. doi: 10.1007/BF00191617
- Sekimoto, H., Tanabe, Y., Tsuchikane, Y., Shiroasaki, H., Fukuda, H., Demura, T., et al. (2006). Gene expression profiling using cDNA microarray analysis of the sexual reproduction stage of the unicellular charophycean alga *Closterium peracerosum-strigosum-littorale* complex. *Plant Physiol.* 141, 271–279. doi: 10.1104/pp.106.078048
- Sekimoto, H., Tsuchikane, Y., and Abe, J. (2014b). “Sexual reproduction of a unicellular charophycean alga, *Closterium peracerosum-strigosum-littorale* complex,” in *Sexual Reproduction in Animals and Plants*, eds H. Sawada, N. Inoue, and M. Iwano (Tokyo: Springer), 345–357.
- Tsuchikane, Y., Fukumoto, R., Akatsuka, S., Fujii, T., and Sekimoto, H. (2003). Sex pheromones that induce sexual cell division in the *Closterium peracerosum-strigosum-littorale* complex (Charophyta). *J. Phycol.* 39, 303–309. doi: 10.1046/j.1529-8817.2003.02062.x
- Tsuchikane, Y., Ito, M., Fujii, T., and Sekimoto, H. (2005). A sex pheromone, protoplast-release-inducing protein (PR-IP) Inducer, induces sexual cell division and production of PR-IP in *Closterium*. *Plant Cell Physiol.* 46, 1472–1476. doi: 10.1093/pcp/pci158
- Turmel, M., Otis, C., and Lemieux, C. (2006). The chloroplast genome sequence of *Chara vulgaris* sheds new light into the closest green algal relatives of land plants. *Mol. Biol. Evol.* 23, 1324–1338. doi: 10.1093/molbev/msk018
- Wodniok, S., Brinkmann, H., Glockner, G., Heidel, A. J., Philippe, H., Melkonian, M., et al. (2011). Origin of land plants: do conjugating green algae hold the key? *BMC Evol. Biol.* 11, 104. doi: 10.1186/1471-2148-11-104

SUPPLEMENTARY MATERIAL

The Supplementary Material for this article can be found online at: <http://journal.frontiersin.org/article/10.3389/fpls.2016.01040>

Copyright © 2016 Abe, Hori, Sato and Sekimoto. This is an open-access article distributed under the terms of the Creative Commons Attribution License (CC BY). The use, distribution or reproduction in other forums is permitted, provided the original author(s) or licensor are credited and that the original publication in this journal is cited, in accordance with accepted academic practice. No use, distribution or reproduction is permitted which does not comply with these terms.



Enzyme-Less Growth in *Chara* and Terrestrial Plants

John S. Boyer*

Division of Plant Sciences, College of Agriculture, Food and Natural Resources, University of Missouri, Columbia, MO, USA

Enzyme-less chemistry appears to control the growth rate of the green alga *Chara corallina*. The chemistry occurs in the wall where a calcium pectate cycle determines both the rate of wall enlargement and the rate of pectate deposition into the wall. The process is the first to indicate that a wall polymer can control how a plant cell enlarges after exocytosis releases the polymer to the wall. This raises the question of whether other species use a similar mechanism. *Chara* is one of the closest relatives of the progenitors of terrestrial plants and during the course of evolution, new wall features evolved while pectate remained one of the most conserved components. In addition, charophytes contain auxin which affects *Chara* in ways resembling its action in terrestrial plants. Therefore, this review considers whether more recently acquired wall features require different mechanisms to explain cell expansion.

OPEN ACCESS

Edited by:

David Domozych,
Skidmore College, USA

Reviewed by:

Charles T. Anderson,
The Pennsylvania State University,
USA

Herman Höfte,
Institut National de la Recherche
Agronomique, France

Philip Lintilhac,
University of Vermont, USA

*Correspondence:

John S. Boyer
boyerjs@missouri.edu

Specialty section:

This article was submitted to
Plant Evolution and Development,
a section of the journal
Frontiers in Plant Science

Received: 26 February 2016

Accepted: 02 June 2016

Published: 21 June 2016

Citation:

Boyer JS (2016) Enzyme-Less
Growth in *Chara* and Terrestrial
Plants. *Front. Plant Sci.* 7:866.
doi: 10.3389/fpls.2016.00866

INTRODUCTION

Chara corallina is a favorable model for studying how plants enlarge. Their cells contain no xylem, and phloem is absent in this particular species. There are no secondary walls characteristic of terrestrial plants, so lignin chemistry is at a minimum. Nevertheless, the walls contain cellulose, hemicellulose, and pectins like the primary walls of vascular plants (see discussion below). This review considers whether the growth mechanism in *Chara* might also be present in terrestrial plants.

Calcium complexing with pectin will be a prominent feature of the discussion and we will follow the practice of referring to Ca^{2+} when it is clearly ionized but spelling out calcium when it is complexed. This is because the complexes involve chelation whose coordination bonds do not conform to the valence state of the ion. The exact nature of the coordination bonds is debated and appears to involve stereochemical interactions with oxygen in the pectin that replace water in hydration shells around the Ca^{2+} , typically estimated to be about eightfold bonding (Braccini and Perez, 2001).

The central feature of the growth mechanism is that *C. corallina* appears to enlarge its cell wall without the mediation of enzymes and instead in a strictly chemical fashion. This is based on three kinds of evidence. First, irreversible turgor-driven enlargement occurs in isolated walls (no cytoplasm). Second, the enlargement is observed after boiling the isolated walls for 10 min (no enzyme activity). Third, an enzyme-less chemistry can be demonstrated to produce the same enlargement in the isolated walls as in the living cells (chemical mechanism). As part of this process, new wall material is deposited and allows the strength of the wall to be maintained while it enlarges. All of these tests were made without removing the cells from the medium in which they were grown. Importantly, although enzymes produce wall constituents and deliver them to the wall, the enzyme-less portion begins after delivery by exocytosis.

The focus is on the wall because it is the tough outer covering controlling the rate at which plant cells enlarge. The enlargement in turn controls most plant size and thus plant growth. The wall chemistry in *Chara* was treated in an earlier review (Boyer, 2009), but experiments with terrestrial species cannot use the same methods as with *Chara* for various reasons. Despite this drawback, certain features of growth are apparent both in the alga and in various terrestrial species, and these will be compared.

Because the charophytes are the closest extant algal relatives of the progenitors of land plants, *Chara* walls accordingly lack a few constituents thought to have evolved later (and described below, but see Popper and Tuohy, 2010; Popper et al., 2011; Leliaert et al., 2012; O'Rourke et al., 2015 for details). The new constituents add new dimensions to the process and make it necessary to consider whether growth occurs by newly evolved and intrinsically different mechanisms.

BACKGROUND

The enlargement of multicellular plants relies mostly on the rapid and irreversible enlargement of cells localized in or derived from meristems. After cells divide, water moves down a gradient in water potential and into each cell, expanding the tough, elastic cell wall irreversibly (Boyer and Silk, 2004). The wall first becomes soft enough to yield to turgor and prevent turgor pressure from becoming as high as it otherwise would. This creates a growth-induced water potential low enough to bring water into the enlarging cells, while turgor remains high enough to continue extending the walls irreversibly (Boyer, 1985). The entering water fills the newly extended volume.

But much of this hydraulic complexity can be avoided if individual cells are surrounded with water. The cells then have abundant water instead of having to rely on hydraulic transport through intervening small cells. In an early attempt at a study of this kind, Green et al. (1971) explored the relationship between turgor pressure and enlargement in *Nitella* internodes. *Nitella* is a charophyte alga with single-cell internodes large enough to measure pressure and growth simultaneously. Despite having to use primitive methods, this remarkable work suggested there might be factors that kept growth fairly constant when turgor changes were small. The control of this system and whether it was enzymatic was not further explored.

Eventually, Proseus and Boyer (2006b) showed that it was possible to isolate the internode walls of a similar large-celled alga *C. corallina* without removing the cell from the culture medium. Artificial turgor pressures were developed by injecting oil into the wall lumen vacated by the cytoplasm. Pressures were comparable to those in the living cell. The oil did not leak through the wall because it was held by the same hydrophobic forces that hold the plasma membrane in place. Any substance could be injected into the lumen at any pressure.

As long as turgor was at normal levels for the intact cell (about 0.5 MPa or 5 bar), the isolated walls grew at a normal rate for 1 or 2 h whether they had been boiled or not (Proseus and Boyer, 2006b). During this time, growth was irreversible and

rapid, just like that in the intact cell when attached to the plant. After 1 or 2 h, most growth stopped while it continued in the live cells. Although growth seemed to be enzyme-less, something was missing from the isolated wall. There are many ingredients produced in the cytoplasm that could be missing from isolated walls. What specific molecules allowed growth for 1 or 2 h, then were depleted or missing when walls were isolated from the cytoplasm?

WALL STRUCTURE

In order to answer this question, it is first necessary to consider the structure of the wall. The internode cells of *Chara* and *Nitella* surround a large coenocytic cytoplasm and the walls appear to be dense gels about 5 μm thick in which cellulose microfibrils are embedded. Growing walls have a longitudinal elastic modulus of about 70 MPa that increases to 200 MPa as the cells mature, indicating the wall is tough and strong (Proseus et al., 1999). Elongation occurs evenly over the entire internode.

According to Morrison et al. (1993) and O'Rourke et al. (2015), the walls contain 45–50% pectin, 15–25% hemicellulose, and 30–35% cellulose, which is similar to the composition of the primary walls in dicotyledonous land plants. The pectins have sugar compositions suggesting homogalacturonans (polygalacturonic acid or PGA), i.e., linear unbranched polymers of α -1,4-D-galacturonic acid sometimes with a small amount of rhamnose (usually 1–2%; Ralet et al., 2001; Fraeye et al., 2009, 2010). The pectins also include rhamnogalacturonans (RGI) but not the boron-containing rhamnogalacturonan II (RGII) of terrestrial species (Matsunaga et al., 2004). The carboxyl groups of the PGA show little esterification and are mostly free to deprotonate to form a carboxylate anion (Anderson and King, 1961a,b; Morrison et al., 1993). The lack of esterification was detected by chemical means.

Recent genomic analysis indicates that genes for pectin synthesis diversified as plants acquired the land habit (Yin et al., 2010; Yang et al., 2013; McCarthy et al., 2014). For example, only a few homogalacturonan biosynthesis genes (α -galacturonosyltransferases (GAUTs) or GAUT-like) were detected in green algae but 10 were present in the moss *Physcomitrella patens*, 26 in sorghum (*Sorghum bicolor*), and 55 in soybean (*Glycine max*; Yin et al., 2010). Many genes related to pectin modification appeared to have diverged before genes for cellulose biosynthesis (McCarthy et al., 2014). Recently evolved walls of some grasses differ in pectin composition from those of dicotyledonous species mostly by containing less pectin and instead substantial amounts of glucuronylarabinoxylans and mixed linkage glucans (β 1,3- and β 1,4-linked glucose; (Vogel, 2008). It should be noted that glucuronylarabinoxylans might have pectin-like properties that could complement the low pectin contents of these grass walls. Levesque-Tremblay et al. (2015) review pectin modifications and point out some of the tissue-specific roles for them.

Among matrix polysaccharides other than pectins, *Chara* internode walls contain galacturonans, glucans, mannans, and xyloglucans but none of the xyloglucans prevalent in terrestrial species

(Popper and Fry, 2003), although xyloglucans were detected in the antheridia (Domozych et al., 2009). It seems likely that some of the matrix polymers have xyloglucan-like properties. In addition to these matrix polysaccharides, the cellulose in *Chara* is laid down in microfibrils mostly perpendicular to the long axis of the cell. The cells tend to elongate cylindrically (Baskin, 2001, 2005). These basic features are similar to those in land plants and because wall evolution in charophytes appears to have occurred monophyletically (Popper et al., 2011), growing *Chara* walls are likely to be primitive versions of their terrestrial counterparts.

BASIC CHEMISTRY OF CALCIUM PECTATE

As described more fully below, the growth ingredient missing from isolated walls of *Chara* appeared to be newly secreted pectate. It combines with calcium that is the main inorganic constituent of the wall although smaller amounts of magnesium are also present (B, Na, K, Fe, Zn, and Cu could not be detected; Proseus and Boyer, 2006c). It is important to note that calcium forms pectate gels but magnesium does not.

This gelling activity is the basis for industrial applications of calcium pectate. Industrial quantities of PGA are obtained from citrus peel or apple pomace usually in an esterified form. Fraeye et al. (2009, 2010) point out that PGA from these sources contains methyl esterified galacturonic acid or occasionally in sugar beet or potato tuber acetyl esterified galacturonic acid. If the pectin is highly methoxylated, acid conditions cause a gel to form in the presence of a high concentration of sucrose. These conditions reduce electrostatic repulsion between polymers and decrease the water activity to form weak gels of jams and jellies. If the pectin is less methoxylated and Ca^{2+} is present, stronger gels form with calcium cross-bridges between pectin polymers.

Fraeye et al. (2009, 2010) also indicate that PGA can be demethoxylated either by chemical methods or enzymatically with various pectin methylesterases. The pectin methylesterases from terrestrial plants create clusters of galacturonic acid in blocks along the polymer backbone. Those blocks with 6–14 galacturonic acid units have an “egg-box” structure with calcium held in each box, cross-bridging anti-parallel PGA chains with sufficient strength to form the junction zones of a gel. Greater demethoxylation creates a stronger gel. When the demethoxylation is kept constant, gel strength increases with PGA concentration and/or Ca^{2+} concentration.

Basically, PGA acts as a chelator to hold divalent cations with coordination bonds. In order to form cross-bridges with calcium, the carboxyl groups need to be dissociated, and galacturonic acid in PGA has a pKa of about 3.5 indicating a weak acid. The acid weakens further as the degree of dissociation of the carboxyl groups increases (Ralet et al., 2001). Greater methoxylation tends to return the pKa toward 3.5.

The pH has a moderate effect. Above 4.5, the gel properties are relatively independent of pH. Below 4.5, dissociation decreases and the affinity for Ca^{2+} decreases.

BASIC CHEMISTRY OF PECTATES IN CHAROPHYTES

Like charophytes, the primary cell walls of angiosperms include cellulose microfibrils synthesized by rosettes in the plasma membrane (Delmer and Amor, 1995; Sarkar et al., 2009; Gu et al., 2010). The microfibrils strengthen the composite wall structure but have crystalline diameters of only around 2–4 nm (Davies and Harris, 2003; Sarkar et al., 2009). These diameters are smaller than the water-filled interstices of the matrix embedding the microfibrils. The interstices are typically 3.5–8.6 nm in a range of species (Read and Bacic, 1996) including *Chara* (4.6–4.7 nm, Proseus and Boyer, 2005). It seems that without hemicelluloses, the microfibrils would be unable to remain in place. In effect, hydrogen bonding of xyloglucans (or their equivalent) to the microfibrils converts them to macrofibrils and anchors them in the matrix.

In contrast to cellulose biosynthesis, matrix polysaccharides (pectins and hemicelluloses) are released to the wall in vesicles matured from Golgi bodies (Zhang and Staehelin, 1992). The exocytosis is not influenced by turgor pressure because the release creates a thin “periplasm” or “cushion” separating the vesicles from the load-bearing part of the wall (Proseus and Boyer, 2006a). Pressures would be uniform across the vesicles as they release their contents to the wall. At normal turgor pressures in *Chara* (0.5 MPa), the periplasm is quite thin and the polymers are concentrated against the inner wall face (Proseus and Boyer, 2005). At these concentrations, pectins spontaneously form weak gels and if Ca^{2+} is present, make strong gels. At lower pressures, the periplasm is thicker because its osmotic properties cause water to be absorbed and thus dilute the periplasm.

The pressure causes the carbohydrates to enter wall interstices depending on their molecular weight. Dextrans (α -1,6-glucans) applied to the inside of the wall and mimicking the cytoplasmic delivery of matrix polysaccharides such as PGA (α -1,4-galacturonans) did not move into the wall unless driven by a pressure differential (Proseus and Boyer, 2005). The polysaccharide end (having the diameter of a sugar) appeared to start and the rest of the polymer reptated through in snake-like fashion. Small polymers (40 kDa) entered more readily than large ones (500 kDa), placing the small ones in intimate contact with polymers of the existing wall. This allows the polymers to bind to the existing wall and probably accounts for its general assembly.

Domozych et al. (2014) explored wall assembly in the charophyte *Penium margaritaceum* that constructs its wall in layers starting midway along the length of the cell. They report that a cellulose layer is deposited first and that pectin (homogalacturonan and RGI) is extruded through the layer onto the surface where it binds to Ca^{2+} to form a reticulated outer layer. They suggest that a similar process might account for the position of the middle lamella, with large carbohydrates percolating through the cellulose layer. The middle lamella is the primary cement holding plant cells together in a tissue. Perhaps like *Chara*, a turgor-dependence and reptation exists for pectin extrusion in *P. margaritaceum* and might be detected by varying

the osmoticum around the cells (assuming osmotic adjustment is negligible).

The strength of the calcium cross-bridging and gelling activity varies with the number of cross-bridges. In the *Penium* system, calcium binding to pectin was enhanced by pectin methylesterase that increased the availability of carboxyl groups. The pectin lattice in the outer layer was more clearly reticulated at higher Ca^{2+} concentrations, indicating that calcium increasingly bound to the pectins in the layer. In the *Chara* culture medium containing 0.6 mM Ca^{2+} , the walls had a moderate number of cross-bridges, allowing the walls to elongate. Increasing the Ca^{2+} to 50 mM decreased the rate of growth slightly (Proseus and Boyer, 2006c). If new pectate was then supplied to the culture medium containing 50 mM Ca^{2+} , it combined with the calcium and immediately gelled, encasing the wall. The gel was so strong that it prevented further growth (Proseus and Boyer, 2006c).

The strength of these coordination bonds in cell walls is fertile ground for further work. So far, it appears that gel strength depends on the number of bonds in each local site and is somewhere between the strength of covalent bonds and van der Waals forces, i.e., in the range where the activation energy of enzymatic reactions also occurs in biology. This suggests that enzyme-mediated growth would be difficult to distinguish from enzyme-less growth unless stringent tests are made as described above.

UNIQUE CYCLIC CHEMISTRY OCCURS IN THE WALL

Figure 1 shows the basic structure of PGA (Ridley et al., 2001) and it is obvious that tension on the ends of the polymer will move the carboxyls apart, changing the strength of their coordination bonds with calcium. Morikawa and Senda (1974) and Morikawa et al. (1974) measured infrared spectra in *Nitella* cell walls under tension and found that the tension caused changes in the spectra of carboxyl groups. Similarly, turgor pressure puts wall polymers under tension in the plane of the walls, potentially distorting some of them. Clearly, those tensile elements bearing most of the load will be the most severely distorted and therefore the most susceptible to new PGA that is not distorted. Thermodynamically, this suggests that the egg-box structure in calcium pectate in the wall will lose its calcium to undistorted PGA whose bonds with calcium may be stronger. In this way, the new PGA from exocytosis can target the load-bearing population of calcium pectate in the wall. There is evidence that less than 5% of the calcium pectate in the wall is load bearing, distorted, and thus a target for new PGA (Proseus and Boyer, 2006c).

Of course below the minimum turgor pressure for distortion, there is no preferential targeting of the calcium pectate in the wall by the newly released PGA. Although the new PGA still removes some calcium from the wall, it has little effect on the extension of the wall (shown by Proseus and Boyer, 2007). The new pectate has growth activity only if the turgor pressure is above a minimum, i.e., creates enough tension to distort load-bearing wall pectate

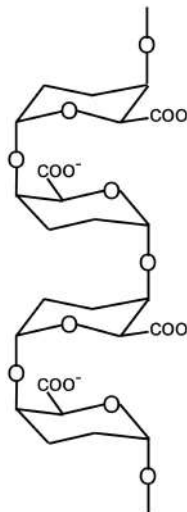


FIGURE 1 | Structure of PGA showing two egg boxes. For simplicity, only oxygenic bonds and carboxyls are indicated.

and creates a thermodynamic difference in bond strength with calcium.

The distortion starts a sequence of reactions resulting in a cycle summarized in **Figure 2** (see Boyer, 2009 for more details). Starting on the left, turgor pressure above a threshold distorts the egg box for the load-bearing fraction of the pectate in the wall (**Figure 2**, left member of the pair). Exocytosis delivers new pectate to the wall. Because the new molecules are not under tension and are not distorted, they bind calcium more tightly than the distorted load-bearing pectate in the wall (**Figure 2**, step 1, red). This thermodynamic difference causes the new pectate to remove calcium from the distorted pectate preferentially. The vacated pectate in the wall relaxes and the wall elongates until other pectate takes the load and distorts (**Figure 2**, step 1, right member of the pair). The new pectate with its calcium can enter the wall and bind to the relaxed pectate (**Figure 2**, step 2, blue). This replaces the number of cross-bridges originally present but does not further strengthen the lengthened and thinner wall. Additional pectate from the cytoplasm plus Ca^{2+} from the medium is needed and binds to the rest of the vacated pectate (**Figure 2**, step 3, green). The deposition of this new calcium pectate re-establishes the original strength and thickness of the wall. However, this re-establishment creates the distorted pectate (step 1) and wall strength (step 3) to allow the reactions to repeat, completing the cycle (**Figure 2**, step 4, black). Each step in **Figure 2** has been verified experimentally (Boyer, 2009).

Tension is the key to this cycle sequence, and tests done without sufficient tension are unlikely to detect the sequence. But when the tension is above the minimum and cytoplasm releases new PGA to the wall, wall extension accelerates to the rate in intact plants. PGA of various molecular weights and from different sources has the same accelerating action. Pectic material is then deposited while the cell is growing (Proseus and Boyer, 2006a).

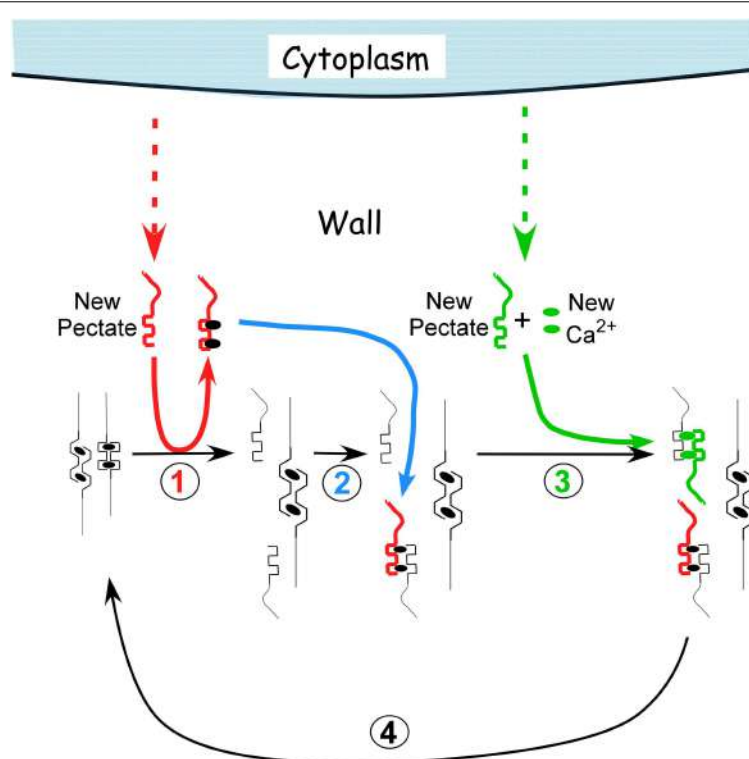


FIGURE 2 | Calcium pectate cycle. Only two calcium pectate cross-links are shown (ovals in anti-parallel pectate molecules, left side of figure in black), but the same principles apply to larger numbers of calcium pectate cross-links in the wall. Turgor pressure is high enough to distort the egg box in one of the pair, weakening its bonds with calcium (left pectate in pair). New pectate from the cytoplasm (dashed red arrow) is undistorted and preferentially removes calcium from the distorted pectate (step 1, red). The load-bearing pectate relaxes after its cross-bridging calcium is removed. The wall elongates incrementally, shifting the load to the other member of the pectate pair, which distorts. The remaining steps 2–4 follow (see text) and result in a cycle. Additional calcium pectate is deposited in the wall as part of the cycle (step 3, green). The net result is elongation plus wall deposition. Note that in *Chara* the cycle occurs in the medium in which the cells are grown (0.6 mM Ca^{2+}). Also note that the rate of growth depends on the rate of pectate release from cytoplasm to wall by exocytosis (red and green dashed arrows).

It is also important that cell enlargement without step 3 (Figure 2) would eventually result in a wall too weak to withstand turgor. Proseus and Boyer (2012a,b) tested this possibility and reported that the walls eventually burst when the cycle occurred without step 3. Bursting was abrupt and lethal for live cells.

The cycle shows that calcium chelation is dynamic, with bonds breaking and re-forming continually in the wall. In effect, the calcium pectate in the wall is in equilibrium with free Ca^{2+} in the interstices of the wall, and the calcium pectate gel continually re-structures whether new PGA is present or not. Above the minimum turgor pressure for growth but without new PGA, the wall may only “creep” slowly (distorted wall PGA gives up its calcium to a non-distorted wall PGA nearby). This auto-propagation probably accounts for any slow changes in length of isolated *Chara* walls after 1 or 2 h, i.e., in isolated walls no longer growing. Below the minimum turgor pressure for growth, auto-propagation is less likely and may not occur at all.

It is also worth mentioning that new PGA delivered by exocytosis is coming from a cytoplasm low in Ca^{2+} (concentration of less than 1 μM as a secondary signaling molecule). The newly released PGA is encountering the first substantial Ca^{2+} it has seen. Accordingly, Ca^{2+}

migrates to the newly arrived PGA ultimately driving the elongation/deposition process. Because of the turgor pressure, PGA (now calcium pectate) supplied by the cytoplasm also can enter the wall and might cause growth in part by occupying space between the existing wall polymers, i.e., spreading the wall polymers apart by intussusception. This would cause wall pectin to distribute throughout the wall. Matrix polysaccharides distribute in this way in walls of rapidly growing tissues of terrestrial species (*Avena* and *Pisum*; Ray, 1967).

TERRESTRIAL PLANTS

One of the arguments favoring an enzyme-based growth process is the reaction to metabolic inhibitors, which decrease rates of expansion. However, many chemical inhibitors cause turgor loss in *Chara* (Proseus and Boyer, 2006b) and a better one may be low temperature, which inhibits growth with only a slight turgor loss due to its effect on the osmotic potential of the cell. At 0.1°C, *Chara* growth was zero but revived when turgor was raised above that normally in the cell (Proseus et al., 2000). It seems possible that the wall was capable of elongating but was not receiving

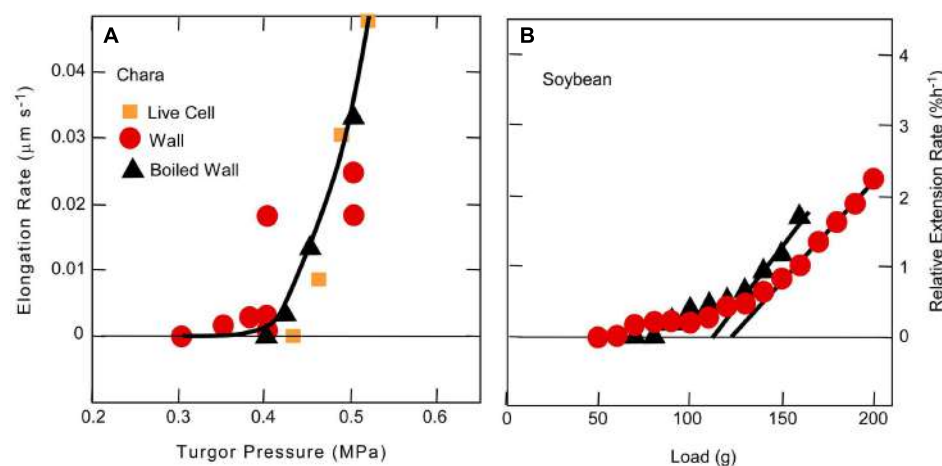


FIGURE 3 | Cell elongation in single *Chara corallina* internodes (A) or single soybean hypocotyls (B) when tension on the wall was varied. In (A), tension was varied with turgor pressure and in (B) with an extensometer. Data in (A) are for live cells, isolated walls, or isolated walls after boiling and in (B) for dead tissue or dead tissue after boiling. Although there was a slight difference in boiled and non-boiled tissue in (B), it was not statistically significant. Note in both experiments that tension had to be above a minimum before irreversible extension was observed. (A) from Proseus and Boyer (2006b) and (B) from Ezaki et al. (2005).

new pectate from the cytoplasm because of the cold, as shown by Proseus and Boyer (2008). In this situation, the calcium pectate cycle would operate only slowly thus requiring higher turgor.

Tissues of most land plants do not have large cells as easily accessible to experimental manipulation as those of *Chara*. Furthermore, each cell may have its own turgor. Coleoptiles or intercalary meristems of hypocotyls tend to be more uniform and help minimize some of this complexity but, as mentioned above, the turgor must be high enough to expand the wall while still being low enough to bring water into the expanding cells. Turgor may thus increase or decrease depending on the treatment. Moreover, inappropriate turgor in only a few cells can change water potential gradients rapidly and thus availability of water to all the other cells, affecting growth (Passioura and Boyer, 2003; Boyer and Silk, 2004).

In order to avoid this ambiguity, tissues may be killed. A unidirectional force is then applied in a direction the tissue would grow when alive, using an extensometer like that of Cosgrove (1989) that allows the extension to be monitored while the force is present. Above a minimum force, the tissue elongates irreversibly in proportion to the applied force just as in *Chara* internodes exposed to various turgor pressures (Figure 3). Ezaki et al. (2005) used this system to detect the minimum force for irreversible wall extension of soybean hypocotyls and found no statistical difference between dead tissue before or after boiling when the pH was 6 (Figure 3B). This result resembles that in *Chara*. But at pH 4–5.5, Ezaki et al. (2005) observed significant differences. Glutarate buffer was used for these latter experiments, and it is difficult to be certain but glutarate chelates calcium weakly and in the concentrations used (10 mM) at low pH, probably removed considerable calcium from the tissue. In this situation protons might more easily displace load-bearing calcium cross-bridges, accounting for the differences at low pH (see discussion of calcium pectate chemistry above).

In the same study, Ezaki et al. (2005) removed wall calcium with the chelator Quin 2 and observed an increased rate of irreversible extension. Addition of Ca^{2+} quenched the chelator activity. They could not observe the effect unless tension was above a threshold. Although Ezaki et al. (2005) did not expose the killed tissues to PGA or explore the effects in live tissues, they concluded that calcium cross-bridging of wall pectins accounted for their results. Essentially their results agree with the calcium pectate cycle of Figure 2 except that Ezaki et al. (2005) also include a possible involvement of enzymes.

ROLE OF XYLOGLUCANS, PROTEINS, AND ENZYMES

Xyloglucans have been proposed to bind cellulose microfibrils by hydrogen bonding, thereby controlling the expansion of cells (Passioura and Fry, 1992; Passioura, 1994). In effect, the xyloglucans were considered to be the main load-bearing wall components and the protein expansin was considered to release the xyloglucan bonds bearing the load (McQueen-Mason et al., 1992; McQueen-Mason and Cosgrove, 1995).

Zhao et al. (2008) found that cucumber hypocotyls lost their sensitivity to expansins as the hypocotyls matured. Zhao et al. (2008) were able to restore it with various hydrolytic enzymes targeting pectins (pectin lyase, pectate lyase, and polygalacturonase). Other enzymes had little effect (endoglucanases, xylanases, and protease). The sensitivity could be restored by treatment with the calcium chelator EGTA to remove wall calcium. They found more calcium in basal tissues than elongating tissues and conclude that calcium cross-bridging of pectates caused the loss of expansin activity in the basal tissues.

In *Arabidopsis*, Dick-Perez et al. (2011) used advanced NMR methods to study cell wall components and reported that xyloglucans seem less important as tethers of cellulose than

are the pectins. They used double and triple mutants lacking xyloglucans that were developed by Cavalier et al. (2008) and Zabotina et al. (2012). The mutant plants showed morphological changes and grew a little less rapidly than the wild-type plants (Xiao et al., 2016). However, it is important that they did grow – and with no detectable xyloglucan. The authors concluded that other matrix polysaccharides may control the growth of the cells. When wall properties were examined in these mutants, the results were incompatible with a load-bearing xyloglucan (Park and Cosgrove, 2012a,b). Although Passioura and Fry (1992) and Passioura (1994) had suggested that load-bearing xyloglucan-cellulose tethers might control growth rate, the tethers might be replaced by calcium pectate cross-bridging with the same effect. Peaucelle et al. (2012) recognized this possibility and included calcium pectate in their model of wall expansion, suggesting it might act as in **Figure 2**. In this regard, it is of interest that *Chara* internodes grow without benefit of xyloglucans (Popper and Fry, 2003) or expansins (Cosgrove, 2000; Popper et al., 2011). Expansins are thought to have evolved after plants colonized the land (Popper et al., 2011).

According to **Figure 2** for *Chara*, growth rate is controlled by the secretion rate for PGA. Evidence for this concept also was found in *Arabidopsis* mutants impaired in secretion of PGA that displayed stunted growth (Mouille et al., 2007). Because the remaining PGA was methyl esterified, the authors propose that PGA synthesis was linked to methoxylation of the PGA, and the mutants disrupted this part of the synthesis and thus exocytosis. Gendre et al. (2013) found mutants inhibiting Golgi secretion of matrix polysaccharides and observed severe dwarfism in shoots and roots. Moreover, Zhu et al. (2015) found major losses in pectin deposition that led to decreased growth. Caffall et al. (2009) report not only decreased growth but also lethal effects of some pectin mutants of *Arabidopsis*. In another test, Kong et al. (2015) modified xyloglucans in an *Arabidopsis* mutant by deleting galactose. They observed inhibited rates of secretion resulting in slower growth, i.e., dwarfism. With an additional mutation to eliminate xyloglucans altogether, vesicle secretion reverted nearly to the wild type and so did growth rate. The authors concluded that altered xyloglucan was more inhibitory to secretion than elimination of the xyloglucan. But the experiment was also a test for the rate of secretion of matrix polysaccharides. It thus appears that the exocytosis of matrix polysaccharides is a central feature of the growth rate of this plant.

Instead of xyloglucans, Derbyshire et al. (2007) focused directly on pectins and recognized that decreasing methyl esterification of PGA might increase the calcium cross-bridging in the walls, strengthening them and decreasing their extensibility. They expressed a fungal pectin methylesterase in *Arabidopsis* to lower the degree of methyl esterification and reported slower growth presumably from the stiffened walls. In the reverse experiment, pectin methylesterase mutants of *Arabidopsis* unable to remove the methyl esters caused the walls to weaken (Hongo et al., 2012). Also, maintaining high levels of methylesterification in transgenic *Arabidopsis* increased the size of the plants as expected if the walls were highly extensible, i.e., had few calcium pectate cross-links (Lionetti et al., 2010). Interestingly, Xiao et al. (2014) found polygalacturonase in the

apoplast of *Arabidopsis* and conclude that it aids cell expansion in hypocotyls when over-expressed. Each of these papers suggest the fundamental control of cell enlargement involved the pectins.

AUXIN

In general, growth regulators affect cell enlargement but most are beyond the scope of this review. However, in evolutionary terms, auxin is an ancient regulator of plant development (Cooke et al., 2002) and it mediates many of the processes in charophytes also seen in terrestrial species. In *Chara*, internodes etiolate in low light. Growing plants also show apical dominance, develop rhizoids more rapidly if auxin is present (Klambt et al., 1992), and display rapid basipetal transport of the hormone (Boot et al., 2012; Zabka et al., 2016). Charophytes appear to control auxin concentrations by a balance of biosynthesis and degradation rather than by conjugation with other molecules as in many terrestrial species (Cooke et al., 2002). Some but not all of the auxin signaling pathways have been detected in algae, suggesting that additional auxin functions may have evolved as plants moved onto land (De Smet et al., 2011).

ACID GROWTH

Auxin accelerates cell elongation and is most obvious in certain susceptible tissues such as coleoptiles and hypocotyls. A prominent theory is that proton ATPases in the plasma membrane are stimulated by auxin, creating a low pH at the inner wall face and causing “acid growth”. The increased acidity was proposed to enhance the growth rate of the tissue, and low pH did so transiently (Rayle and Cleland, 1972, 1992). The concept was easily tested in *Chara* because the culture medium had enough intrinsic buffering capacity to hold pH nearly constant while cell elongation was measured without additional buffers. Efforts to demonstrate an acid effect failed (pH as low as 3.5, Proseus and Boyer, 2006c).

Virk and Cleland (1988, 1990) studied growth in soybean hypocotyls and concluded that there were acid labile, load-bearing bonds in the wall, but Ezaki et al. (2005) questioned whether applied tensions were high enough to cause irreversible wall extension. Nevertheless, it is worth noting that methoxylated pectate is less acidic than pectate without methoxy groups (see above description of pectate chemistry). Peaucelle et al. (2008) report that localized de-methylesterification and thus acidification is required for organ formation in *Arabidopsis* meristems. By placing beads with pectin methylesterase on the meristem, floral primordia could be induced where none would ordinarily exist. Growth of the stems was not affected, so the local acidification did not extend to the whole meristem. In addition, Peaucelle et al. (2015) found that local acidification controlled growth anisotropy in *Arabidopsis* hypocotyls. The idea that de-methylesterification increases extensibility is the opposite of the usual interpretation that de-methylesterification increases calcium cross-bridging and decreases extensibility. Instead, Peaucelle et al. (2008) suggest more extensible walls might be caused by too little Ca^{2+} available locally.

Braybrook and Peaucelle (2013) have evidence that local auxin triggers local cell wall softening in meristems, initiating organ development. However, auxin is also required for general extension of the primordium. This implies that there is a transition from a local effect to a general one as the organ develops, oriented around cell wall properties. The concept that a patterned signal transitions to a general one deserves further attention.

PEROXIDASE AND HYDROXYL RADICALS

A totally different view of growth control by auxin involves breakage of covalent bonds by reactive oxygen intermediates, specifically hydroxyl radicals (Schopfer, 2001; Schopfer et al., 2002; Liszkay et al., 2004). There is no doubt that these intermediates could break covalent bonds in the wall because of their high reactivity (Fry, 1998). An obstacle is the absence of oxidases necessary to form the intermediates, such as superoxide dismutase, oxalate oxidase, ascorbate peroxidase, glutaredoxin, and most peroxidases that are not present in root tips of maize (Zhu et al., 2007). On the other hand, reactive oxygen intermediates have been implicated in the formation of lignins (Passardi et al., 2004) and since maturing tissues of terrestrial species generally have some lignin-containing cells, the associated chemistry is likely to be present (Schopfer, 1994; Voothuluru and Sharp, 2013). Reactive oxygen might signal developmental changes that trigger lignification. Incidentally, *Chara* and *Nitella* do not develop secondary walls like those of terrestrial plants, and peroxidase chemistry is less prominent (Passardi et al., 2004). As land was invaded by plants, lignins and other forms of secondary wall thickening evolved depending on the species. This probably occurred because the colonization of land made gravitational force a larger feature than in the algae, and secondary thickening became necessary to strengthen the walls after the primary cell walls had expanded.

Tagawa and Bonner (1957) took a different view of the auxin mechanism of growth control and tested the effects of Ca^{2+} , Mg^{2+} , and K^+ on auxin-accelerated elongation of *Avena* coleoptiles that contained mostly primary walls. The authors observed large effects of Ca^{2+} and were among the first to suggest pectins could be involved. In related work about the same time, Heath and Clark (1956) exposed wheat coleoptiles to chelators or auxin and found similar effects for both types of molecule. In fact, chelators sometimes were considered to have hormonal properties (Heath and Clark, 1956; Weinstein et al., 1956). Consistent with these papers, the accelerating action of 10 μM auxin was inhibited by Ca^{2+} in maize coleoptiles (Siemieniuk and Karcz, 2015). No chelators were used and instead the authors measured membrane polarization which changed with auxin and Ca^{2+} and K^+ treatment. They propose that the changes in polarization were attributable to H^+ -ATPase activity in the plasma membrane, linking coleoptile growth to auxin action by acid growth. Although the polarization was correlated with auxin effects, no causation could be assigned

and instead the authors indicated that Ca^{2+} might have altered K^+ -channel activity sufficient to change the polarization and growth rate. However, it seems possible that an alternate explanation could be the pectin one of Tagawa and Bonner (1957). Further work with this coleoptile system would be valuable.

The sensitivity to auxin differs between shoots and roots. In maize, an auxin concentration of 10 μM that accelerated the growth of coleoptiles (Siemieniuk and Karcz, 2015) inhibited the growth of roots (Hasenstein and Evans, 1986). When the auxin-inhibited roots were exposed to EGTA, the inhibitory action of auxin was reversed (Figure 4). Ca^{2+} quenched the EGTA effect, restoring the auxin-induced inhibition. The authors interpreted these effects in terms of a secondary messenger role of calcium in the cytoplasm but the similarity to enzyme-less growth in Figure 2 is striking.

Auxin accelerates both the elongation of coleoptiles and the delivery of pectin and other matrix polysaccharides to cell walls (Albersheim and Bonner, 1959; Baker and Ray, 1965; Ray and Baker, 1965). Consequently, it would be predicted that, at turgor pressures low enough to inhibit auxin-induced elongation, the deposition of new wall material would also be inhibited. This is indeed found in *Chara* as shown in Figures 5A,B (Proseus and Boyer, 2006a), but *Avena* coleoptiles also display a similar turgor dependence for the two processes (Cleland, 1967) (Figures 5C,D). This turgor dependence suggests a similar link might exist between wall deposition and growth in *Chara* and *Avena*.

The existence of this link is one of the stronger tests of the calcium pectate cycle. That the exocytosis of matrix polysaccharides, including pectins, was affected by auxin suggests a key role for the cycle in auxin-stimulated tissues. However, no reports are known to this author that include auxin-treated tissue exposed to PGA. The calcium chelator EGTA is perhaps the closest analogy (Hasenstein and Evans, 1986). The molecule is small enough to enter the interstices of the wall in most tissues while externally supplied PGA may be excluded because of its size (e.g., 170 kDa sometimes used by Proseus and Boyer, 2006c). When PGA is externally supplied, it is exposed only to atmospheric pressure instead of the higher pressure needed for molecular entry into the wall (Proseus and Boyer, 2005). But in the *Chara* experiments, even though externally supplied PGA might not enter the wall, the immediacy of its action suggests that wall calcium was removed instead. The Ca^{2+} ion would readily move through the wall to the PGA outside. External PGA of 170 kDa removed about 60% of the wall calcium in *Chara* (Proseus and Boyer, 2006c). Similar removal might be expected in terrestrial tissues exposed to PGA.

TIP GROWTH

In contrast to *Chara* and many tissues of terrestrial plants, pollen tubes and root hairs grow at the tip rather than along the entire cell. In fact, pollen tubes grow more rapidly and for greater distances than any other cell. An example is maize, whose pollen

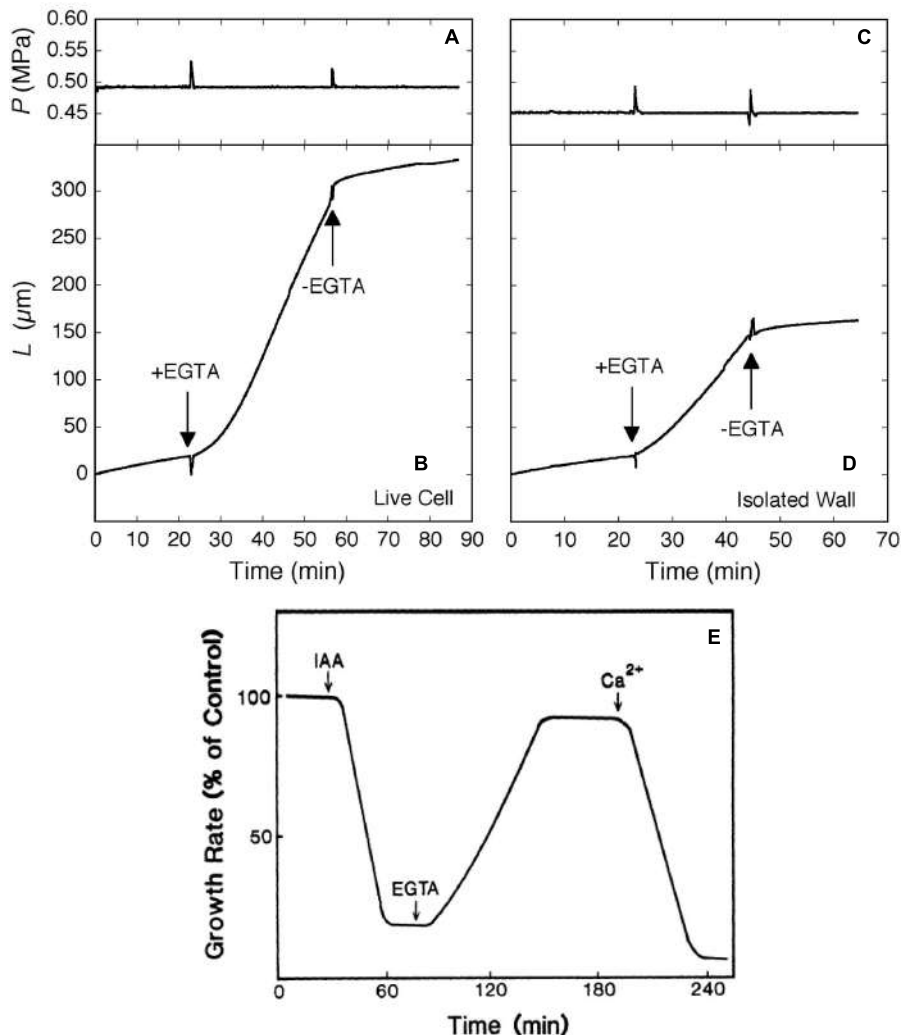


FIGURE 4 | Elongation in *Chara corallina* internodes (A–D) and maize roots (E) exposed to the Ca^{2+} chelator EGTA (downward arrows). In *Chara*, the EGTA (2.5 mM, pH 7) removed 95% of Ca and 100% of Mg from the wall. Ca^{2+} (0.6 mM) was resupplied when EGTA was removed with fresh culture medium (upward arrows). Turgor pressure (P) is shown in (A) and (C), change in length of internodes (L) in (B) and (D) for live *Chara* cells and isolated walls, respectively. In maize (E), roots were exposed to a growth-inhibiting concentration of IAA (10 μM) and subsequently to EGTA (1 mM), then to Ca^{2+} (0.5 mM). Root growth is shown as % of control rate. (A–D) from Proseus and Boyer (2006c) and (E) from Hasenstein and Evans (1986) by permission from www.plantphysiol.org, Copyright American Society of Plant Biologists.

tube travels about 10 mm per hour for about 300–400 mm. Calcium is necessary for pollen tube growth and below 10 μM , the cell bursts. Above 10 mM, the cell stops growing. Between these extremes, growth is rapid but may not be continuous because in lily the rate oscillates with a period of 15–50 s (see review by Hepler et al., 2013). The oscillation has been used to determine which events precede or follow the maximum rate.

The wall of the pollen tube is rich in pectins and in order to deliver the pectate to the tip, Golgi-derived vesicles containing methoxylated pectate are carried along actin cables that appear to oscillate in their delivery rate, possibly under the control of a tip-focused gradient in cytoplasmic Ca^{2+} where sub- μM concentrations act as a second messenger (Hepler et al., 2013).

The vesicles fuse with the plasma membrane and release their contents to the wall by exocytosis. If maximum growth rates are used as a reference condition, the highly methoxylated pectate is released a few seconds before maximum growth occurs. This may be because the esterification blocks many of the carboxyls and only a few cross-bridges form when exposed to Ca^{2+} . This causes a highly extensible tip and accounts for the maximum rate (McKenna et al., 2009).

On the other hand, maximum Ca^{2+} uptake occurs a few seconds after the maximum growth (Hepler et al., 2013). At the tip, pectin methylesterases are also secreted and fail to be active for a few seconds. They are secreted as a pro-enzyme, and proteases in the wall act on the pro-enzyme to create the active form. Also, an inhibitor at the tip is

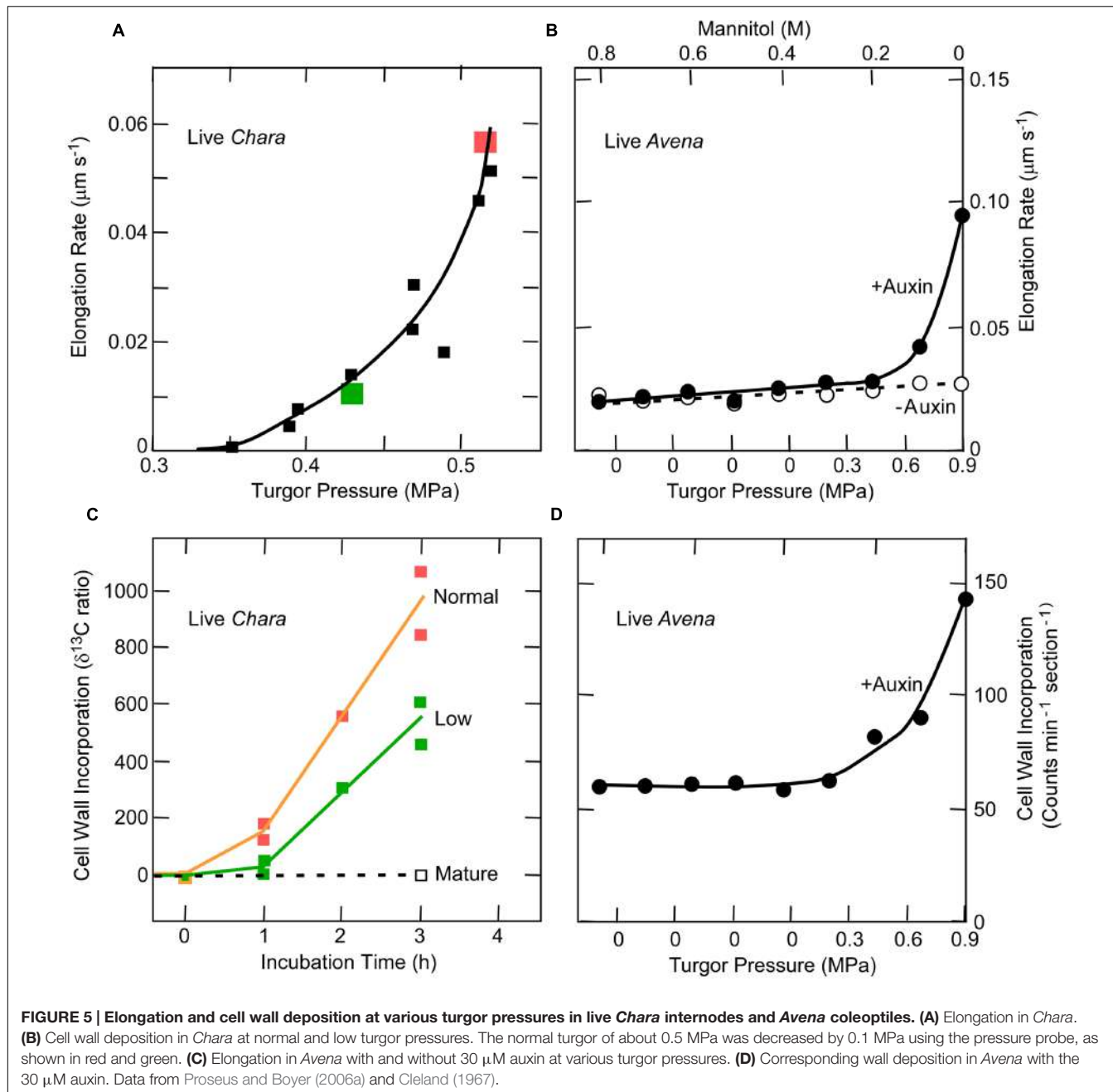


FIGURE 5 | Elongation and cell wall deposition at various turgor pressures in live *Chara* internodes and *Avena* coleoptiles. **(A)** Elongation in *Chara*. **(B)** Cell wall deposition in *Chara* at normal and low turgor pressures. The normal turgor of about 0.5 MPa was decreased by 0.1 MPa using the pressure probe, as shown in red and green. **(C)** Elongation in *Avena* with and without 30 μM auxin at various turgor pressures. **(D)** Corresponding wall deposition in *Avena* with the 30 μM auxin. Data from Proseus and Boyer (2006a) and Cleland (1967).

retrieved by endocytosis behind the tip. Both of these actions delay the esterase activity until after the peak growth rate. As a result, most newly freed carboxyl groups are in the shank of the pollen tube. They bind calcium and stiffen the wall, as measured by micro-indentation (Parre and Geitmann, 2005; for alternate view, see Vogler et al., 2012). **Figure 6** shows how this oscillating action might relate to the *Chara*-type calcium pectate cycle of **Figure 2**. Rojas et al. (2011) also propose that a similar cycle controls pollen tube growth. They tested a physical model using rheological principles and conclude that the fit with calcium pectate chemistry is quite good.

OTHER FORMS OF TARGETED WALL DELIVERY

Another example of targeted wall delivery is seen in transfer cells. These cells develop specialized wall ingrowths that expand the area of the plasma membrane and allow more transporters to be present in the expanded area, enhancing transport across the membrane. The cells are particularly obvious between parent plants and their embryos, which require rapid transport as the seed develops. The ingrowths form from wall constituents delivered to the inner surface of specific areas of the primary wall. McCurdy et al. (2008) report that the ingrowths consist mostly of

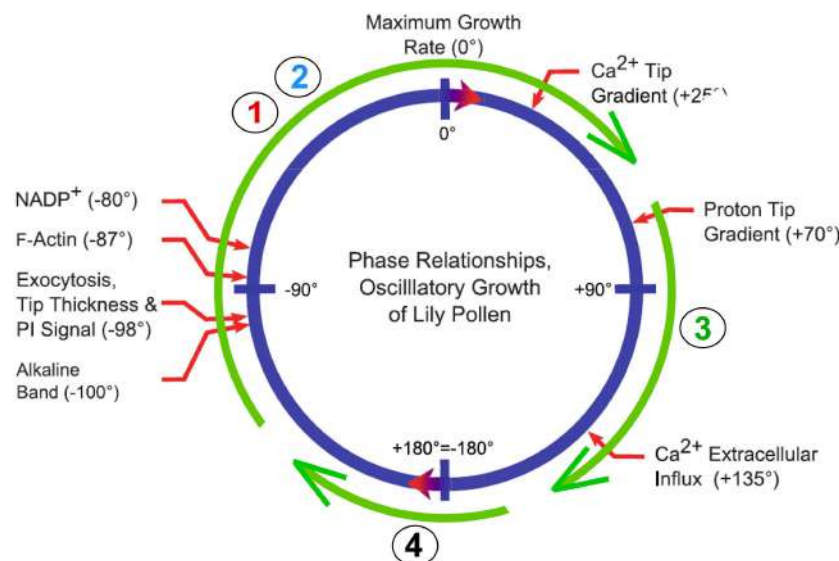


FIGURE 6 | Possible relation of calcium pectate cycle to oscillatory growth of a pollen tube. Blue circle shows phase angles and thus sequence of events for pollen tube growth of lily from Figure 3 of Hepler et al. (2013). Green circle shows Steps 1–4 of calcium pectate cycle from **Figure 2**.

cellulose and matrix polysaccharides that resemble those already present in the primary wall. Their development seems similar to the mechanism of tip growth in pollen tubes, but with targets at specific areas of the inner face instead of being localized at a growing tip. Recent work indicates that Ca^{2+} plumes can be seen extending from the cell exterior into the cytoplasm at each targeted locus (Zhang et al., 2015a,b). It seems possible that the plumes expose PGA to Ca^{2+} before the PGA extracts calcium from the wall. Consequently the new pectate might be deposited immediately rather than act to remove wall calcium. This suggests that only step 3 of **Figure 2** might operate, accounting for the unusual anatomy of the transfer cell walls.

CONCLUSION

The primitive walls of *Chara* and *Nitella* allow certain features of cell expansion to stand out, particularly pectin chemistry. The properties of pectin also are important for terrestrial plants but the evidence is arguably less direct than in the charophytes. Nevertheless, there are hints that the calcium pectate cycle may occur in both kinds of plants. Cell expansion is linked to wall deposition in both, and the two processes require turgor pressure above a minimum, rely on the rate of exocytosis, respond to pectin methoxylation, are affected by Ca^{2+} , and share certain auxin features. Although *Chara* internodes expand more slowly than the cells of terrestrial species, expansion continues longer (weeks), and the final cell length equals or exceeds that of many terrestrial cells. Wall synthesis must keep up and emphasizes the important of the linkage between expansion and deposition.

In *Chara*, a unique aspect of calcium pectate chemistry is the distortion by turgor that leads to a cycle of reactions. If

turgor diminishes slightly, the cycle can cease and the ensuing reactions also cease even though the plants appear moderately turgid. When normal turgor returns, the cycle can resume. It is tempting to explore this behavior more fully in terrestrial plants because it may be a tool for controlling or testing the presence of the cycle.

The evidence so far, while still fragmentary, suggests that the process in *Chara*, being chemical, could be widespread in green plants. Wherever the chemicals are present and turgor can distort the pectate, the reactions should occur. Pectins particularly homogalacturonans seem to be among the most conserved wall components in green plants (Ridley et al., 2001; Popper and Fry, 2003; O'Rourke et al., 2015). With adequate water, the cells should be able to generate enough turgor to run the cycle. Fueling this speculation is the cross-bridging of the pectate as part of its chemistry. This structural feature immediately suggests a means to loosen or tighten a wall.

In turn, it seems that methoxylation may be a means to control the cross-bridging, usually acting as a growth accelerator when enhanced but a decelerant when diminished. The evidence is strong in pollen tubes but the opposite has been reported when organs are initiated in *Arabidopsis* meristems. This suggests that pectin has roles beyond the calcium pectate cycle, and recently evolved pectin modifications probably reflect this.

Methoxylation is minimal in *Chara* perhaps because the single large wall must have high strength to bear the tension of turgor pressure (pressure is force/area and the larger the area the larger the force). Plants with small cells are found among the charophytes and these show evidence of methoxylation (e.g., Domozych et al., 2014). In tissues of terrestrial species, small cells are the rule and many walls share the tension. Perhaps methoxylation evolved to control cross-bridging and thus the rate of growth in these plants.

Later evolutionary arrivals such as RGII complexed with boron may play a role in growth. Boron deficiency can be especially obvious in meristems of terrestrial species and a mutant for a B transporter causes deformed meristems that alter the development of reproductive and vegetative tissues in maize (Durbak et al., 2014). Although RGII is a pectin, no direct tests have been made of its possible growth effects. This leaves open the possibility that later-evolved features of wall pectins could participate in meristem function as well as wall biomechanics.

Because the calcium pectate cycle links elongation and wall deposition of pectins automatically without special regulatory metabolism, it would be useful to know whether the link is similar in terrestrial plants. If so, it may be unnecessary to invoke recently evolved but fundamentally different mechanisms for cell enlargement.

This link indicates that prolonged intervals of low turgor necessarily must signal metabolism. Otherwise, wall constituents would accumulate unused in the cytoplasm or wall. In *Chara*, the feedback requires 23–53 min after which biosynthesis is brought into balance with the lower rate of deposition of matrix polysaccharide (Proseus and Boyer, 2008). The

signals controlling this process are intriguing and need further identification.

AUTHOR CONTRIBUTIONS

The author confirms being the sole contributor of this work and approved it for publication.

ACKNOWLEDGMENTS

I thank the Department of Energy, Office of Science, Energy Biosciences for funding the early part of this research. I am grateful to Carolyn A. Thoroughgood, past dean of the College of Marine Studies, University of Delaware for creative financing of the rest of it. I am also grateful to the University of Missouri for financial support during the writing of this review and Dr. Priyamvada Voothuluru for suggestions on an early version of it. I am greatly indebted to three reviewers whose suggestions were exceptionally valuable. This work is dedicated to Timothy E. (Ted) Proseus who spent 10 years in my lab on this project and is now employed elsewhere.

REFERENCES

- Albersheim, P., and Bonner, J. (1959). Metabolism and hormonal control of pectic substances. *J. Biol. Chem.* 234, 3105–3108.
- Anderson, D. M. W., and King, N. J. (1961a). Polysaccharides of the Characeae. III. The carbohydrate content of *Chara australis*. *Biochim. Biophys. Acta* 52, 449–454. doi: 10.1016/0006-3002(61)90402-4
- Anderson, D. M. W., and King, N. J. (1961b). Polysaccharides of the Characeae. II. The carbohydrate content of *Nitella translucens*. *Biochim. Biophys. Acta* 52, 441–449. doi: 10.1016/0006-3002(61)90401-2
- Baker, D. B., and Ray, P. M. (1965). Relation between effects of auxin on cell wall synthesis and cell elongation. *Plant Physiol.* 40, 360–368. doi: 10.1104/pp.40.2.360
- Baskin, T. I. (2001). On the alignment of cellulose microfibrils by cortical microtubules: a review and a model. *Protoplasma* 215, 150–171. doi: 10.1007/BF01280311
- Baskin, T. I. (2005). Anisotropic expansion of the plant cell wall. *Annu. Rev. Cell Dev. Biol.* 21, 203–222. doi: 10.1146/annurev.cellbio.20.082503.103053
- Boot, K. J. M., Libbenga, K. R., Hille, S. C., Offringa, R., and van Duijn, B. (2012). Polar auxin transport: an early invention. *J. Exp. Bot.* 63, 4213–4218. doi: 10.1093/jxb/ers106
- Boyer, J. S. (1985). Water transport. *Annu. Rev. Plant Physiol.* 36, 473–516. doi: 10.1146/annurev.pp.36.061805.002353
- Boyer, J. S. (2009). Cell wall biosynthesis and the molecular mechanism of plant enlargement. *Funct. Plant Biol.* 36, 383–394. doi: 10.1071/FP09048
- Boyer, J. S., and Silk, W. K. (2004). Hydraulics of plant growth. *Funct. Plant Biol.* 31, 761–773. doi: 10.1071/FP04062
- Braccini, I., and Perez, S. (2001). Molecular basis of Ca^{2+} -induced gelation in alginates and pectins: the egg-box model revisited. *Biomacromolecules* 2, 1089–1096. doi: 10.1021/bm010008g
- Braybrook, S. A., and Peaucelle, A. (2013). Mechano-chemical aspects of organ formation in *Arabidopsis thaliana*: the relation between auxin and pectin. *PLoS ONE* 8:e57813. doi: 10.1371/journal.pone.0057813
- Caffall, K. H., Patahil, S., Phillips, S. E., Hahn, M. G., and Mohnen, D. (2009). *Arabidopsis thaliana* T-DNA mutants implicate GAUT genes in the biosynthesis of pectin and xylan in cell walls and seed testa. *Mol. Plant* 2, 1000–1014. doi: 10.1093/mp/ssp062
- Cavalier, D. M., Lerouxel, O., Neumetzler, L., Yamauchi, K., Reinecke, A., Freshour, G., et al. (2008). Disrupting two *Arabidopsis thaliana* xylosyltransferase genes results in plants deficient in xyloglucan, a major primary cell wall component. *Plant Cell* 20, 1519–1537. doi: 10.1105/tpc.108.059873
- Cleland, R. E. (1967). A dual role of turgor pressure in auxin-induced cell elongation in *Avena coleoptiles*. *Planta* 77, 182–191. doi: 10.1007/BF00387455
- Cooke, T. J., Poli, D. B., Sztein, A. E., and Cohen, J. D. (2002). Evolutionary patterns in auxin action. *Plant Mol. Biol.* 49, 319–338. doi: 10.1023/A:1015242627321
- Cosgrove, D. J. (1989). Characterization of long-term extension of isolated cell walls from growing cucumber hypocotyls. *Planta* 177, 121–130. doi: 10.1007/BF00392162
- Cosgrove, D. J. (2000). Expansive growth of plant cell walls. *Plant Physiol. Biochem.* 38, 109–124. doi: 10.1016/S0981-9428(00)00164-9
- Davies, L. M., and Harris, P. J. (2003). Atomic force microscopy of microfibrils in primary cell walls. *Planta* 217, 283–289.
- De Smet, I., Voss, U., Lau, S., Wilson, M., Shao, N., Timme, R. E., et al. (2011). Unraveling the evolution of auxin signaling. *Plant Physiol.* 155, 209–221. doi: 10.1104/pp.110.168161
- Delmer, D. P., and Amor, Y. (1995). Cellulose biosynthesis. *Plant Cell* 7, 987–1000. doi: 10.1105/tpc.7.7.987
- Derbyshire, P., McCann, M. C., and Roberts, K. (2007). Restricted cell elongation in *Arabidopsis* hypocotyls is associated with a reduced average pectin esterification level. *BMC Plant Biol.* 7:31. doi: 10.1186/1471-2229-7-31
- Dick-Perez, M., Zhang, Y., Hayes, J., Salazar, A., Zabotina, O. A., and Hong, M. (2011). Structure and interactions of plant cell-wall polysaccharides by two- and three-dimensional magic-angle-spinning solid-state NMR. *Biochemistry* 50, 989–1000. doi: 10.1021/bi101795q
- Domozych, D., Sørensen, I., Popper, Z. A., Ochs, J., Andreas, A., Fangel, J. U., et al. (2014). Pectin metabolism and assembly in the cell wall of the charophyte green alga *Penium margaritaceum*. *Plant Physiol.* 165, 105–118. doi: 10.1104/pp.114.236257
- Domozych, D. S., Sørensen, I., and Willats, W. G. T. (2009). The distribution of cell wall polymers during antheridium development and spermatogenesis in the Charophycean green alga, *Chara corallina*. *Ann. Bot.* 104, 1045–1056. doi: 10.1093/aob/mcp193
- Durbak, A. R., Phillips, K. A., Pike, S., O'Neill, M. A., Mares, J., Gallavotti, A., et al. (2014). Transport of boron by the tassel-less1 aquaporin is critical for

- vegetative and reproductive development in maize. *Plant Cell* 26, 2978–2995. doi: 10.1105/tpc.114.125898
- Ezaki, N., Kido, N., Takahashi, K., and Katou, K. (2005). The role of wall Ca^{2+} in the regulation of wall extensibility during the acid-induced extension of soybean hypocotyl cell walls. *Plant Cell Physiol.* 46, 1831–1838. doi: 10.1093/pcp/pci199
- Fraeye, I., Doungla, E., Duvetter, T., Moldenaers, P., Van Loey, A., and Hendrickx, M. (2009). Influence of intrinsic and extrinsic factors on rheology of pectin-calcium gels. *Food Hydrocoll.* 23, 2069–2077. doi: 10.1016/j.foodhyd.2009.03.022
- Fraeye, I., Duvetter, T., Doungla, E., Van Loey, A., and Hendrickx, M. (2010). Fine tuning the properties of pectin-calcium gels by control of pectin fine structure, gel composition and environmental conditions. *Trends Food Sci. Technol.* 21, 219–228. doi: 10.1016/j.tifs.2010.02.001
- Fry, S. C. (1998). Oxidative scission of plant cell wall polysaccharides by ascorbate-induced hydroxyl radicals. *Biochem. J.* 332, 507–515. doi: 10.1042/bj3320507
- Gendre, D., McFarlane, H. E., Johnson, E., Mouille, G., Sjödin, A., Oh, J., et al. (2013). Trans-Golgi network localized ECHIDNA/Ypt interacting protein complex is required for the secretion of cell wall polysaccharides in *Arabidopsis*. *Plant Cell* 25, 2633–2646. doi: 10.1105/tpc.113.112482
- Green, P. B., Erickson, R. O., and Buggy, J. (1971). Metabolic and physical control of cell elongation rate. *Plant Physiol.* 47, 423–430. doi: 10.1104/pp.47.3.423
- Gu, Y., Kaplinsky, N., Bringmann, M., Cobb, A., Carroll, A., Sampathkumar, A., et al. (2010). Identification of a cellulose synthase-associated protein required for cellulose biosynthesis. *Proc. Nat. Acad. Sci. U.S.A.* 107, 12866–12871. doi: 10.1073/pnas.1007092107
- Hasenstein, K.-H., and Evans, M. L. (1986). Calcium dependence of rapid auxin action in maize roots. *Plant Physiol.* 81, 439–443. doi: 10.1104/pp.81.2.439
- Heath, O. V. S., and Clark, J. E. (1956). Chelating agents as plant growth substances. A possible clue to the mode of action of auxin. *Nature* 177, 1118–1121. doi: 10.1038/1771118a0
- Hepler, P. K., Rounds, C. M., and Winship, L. J. (2013). Control of cell wall extensibility during pollen tube growth. *Mol. Plant* 6, 998–1017. doi: 10.1093/mp/sst103
- Hongo, S., Sato, K., Yokoyama, R., and Nishitani, K. (2012). Demethylesterification of the primary wall by PECTIN METHYLESTERASE35 provides mechanical support to the *Arabidopsis* stem. *Plant Cell* 24, 2624–2634. doi: 10.1105/tpc.112.099325
- Klambt, D., Knauth, B., and Dittmann, I. (1992). Auxin dependent growth of rhizoids of *Chara globularis*. *Physiol. Plant.* 85, 537–540. doi: 10.1111/j.1399-3054.1992.tb05823.x
- Kong, Y., Pena, M. J., Renna, L., Avci, U., Pattathil, S., Tuomivaara, S. T., et al. (2015). Galactose-depleted xyloglucan is dysfunctional and leads to dwarfism in *Arabidopsis*. *Plant Physiol.* 167, 1296–1306. doi: 10.1104/pp.114.255943
- Leliaert, F., Smith, D. R., Moreau, H., Herron, M. D., Verbruggen, H., Delwiche, C. F., et al. (2012). Phylogeny and molecular evolution of the green algae. *Crit. Rev. Plant Sci.* 31, 1–46. doi: 10.1080/07352689.2011.615705
- Levesque-Tremblay, G., Pelloux, J., Braybrook, S. A., and Müller, K. (2015). Tuning of pectin methylesterification: consequences for cell wall biomechanics and development. *Planta* 242, 791–811. doi: 10.1007/s00425-015-2358-5
- Lionetti, V., Francocci, F., Ferrari, S., Volpi, C., Bellincampi, D., Galletti, R., et al. (2010). Engineering the cell wall by reducing the de-methyl-esterified homogalacturonan improves saccharification of plant tissues for bioconversion. *Proc. Nat. Acad. Sci. U.S.A.* 107, 616–621. doi: 10.1073/pnas.0907549107
- Liszkay, A., van der Zalm, E., and Schopfer, P. (2004). Production of reactive oxygen intermediates (O_2^- , H_2O_2 , and $\cdot\text{OH}$) by maize roots and their role in wall loosening and elongation growth. *Plant Physiol.* 136, 3114–3123. doi: 10.1104/pp.104.044784
- Matsunaga, T., Ishii, T., Matsumoto, S., Higuchi, M., Darvill, A., Albersheim, P., et al. (2004). Occurrence of the primary cell wall polysaccharide rhamnogalacturonan II in pteridophytes, lycophytes, and bryophytes. Implications for the evolution of vascular plants. *Plant Physiol.* 134, 339–351. doi: 10.1104/pp.103.030072
- McCarthy, T. W., Der, J. P., Honaas, L. A., dePamphilis, C. W., and Anderson, C. T. (2014). Phylogenetic analysis of pectin-related gene families in *Physcomitrella patens* and nine other plant species yields evolutionary insights into cell walls. *BMC Plant Biol.* 14:79. doi: 10.1186/1471-2229-14-79
- McCurdy, D. W., Patrick, J. W., and Offler, C. E. (2008). Wall ingrowth formation in transfer cells: novel examples of localized wall deposition in plant cells. *Curr. Opin. Plant Biol.* 11, 653–661. doi: 10.1016/j.pbi.2008.08.005
- McKenna, S., Kunkel, J. G., Bosch, M., Rounds, C. M., Vidai, L., Winship, L. J., et al. (2009). Exocytosis precedes and predicts the increase in growth in oscillating pollen tubes. *Plant Cell* 21, 3026–3040. doi: 10.1105/tpc.109.069260
- McQueen-Mason, S., Durachko, D. M., and Cosgrove, D. J. (1992). Two endogenous proteins that induce wall elongation in plants. *Plant Cell* 4, 1425–1433. doi: 10.1105/tpc.4.11.1425
- McQueen-Mason, S. J., and Cosgrove, D. J. (1995). Expansin mode of action on cell walls. *Plant Physiol.* 107, 87–100.
- Morikawa, H., and Senda, M. (1974). Oriented structure of matrix polysaccharides in and extension growth of *Nitella* cell wall. *Plant Cell Physiol.* 15, 1139–1142.
- Morikawa, H., Tanizawa, K., and Senda, M. (1974). Infrared spectra of *Nitella* cell walls and orientation of carboxylate ions in the walls. *Agric. Biol. Chem.* 38, 343–348. doi: 10.1271/bbb1961.38.343
- Morrison, J. C., Greve, L. C., and Richmond, P. A. (1993). Cell wall synthesis during growth and maturation of *Nitella* internodal cells. *Planta* 189, 321–328. doi: 10.1007/BF00194428
- Mouille, G., Ralet, M.-C., Cavelier, C., Eland, C., Effroy, D., Hématy, K., et al. (2007). Homogalacturonan synthesis in *Arabidopsis thaliana* requires a Golgi-localized protein with a putative methyltransferase domain. *Plant J.* 50, 605–614. doi: 10.1111/j.1365-313X.2007.03086.x
- O'Rourke, C., Gregson, T., Murray, L., Sadler, I. H., and Fry, S. C. (2015). Sugar composition of the pectic polysaccharides of charophytes, the closest algal relatives of land-plants: presence of 3-O-methyl-D-galactose residues. *Ann. Bot.* 116, 225–236. doi: 10.1093/aob/mcv089
- Park, Y. B., and Cosgrove, D. J. (2012a). Changes in cell wall biomechanical properties in the xyloglucan-deficient xxt1/xxt2 mutant of *Arabidopsis*. *Plant Physiol.* 158, 465–475. doi: 10.1104/pp.111.189779
- Park, Y. B., and Cosgrove, D. J. (2012b). A revised architecture of primary cell walls based on biomechanical changes induced by substrate-specific endoglucanases. *Plant Physiol.* 158, 1933–1943. doi: 10.1104/pp.111.192880
- Parre, E., and Geitmann, A. (2005). Pectin and the role of the physical properties of the cell wall in pollen tube growth of *Solanum chacoense*. *Planta* 220, 582–592. doi: 10.1007/s00425-004-1368-5
- Passardi, F., Penel, C., and Dunand, C. (2004). Performing the paradoxical: how plant peroxidases modify the cell wall. *Trends Plant Sci.* 9, 534–540. doi: 10.1016/j.tplants.2004.09.002
- Passioura, J. B. (1994). The physical chemistry of the primary cell wall: implications for the control of expansion rate. *J. Exp. Bot.* 45, 1675–1682.
- Passioura, J. B., and Boyer, J. S. (2003). Tissue stresses and resistance to water flow conspire to uncouple the water potential of the epidermis from that of the xylem of elongating plant stems. *Funct. Plant Biol.* 30, 325–334. doi: 10.1071/FP02202
- Passioura, J. B., and Fry, S. C. (1992). Turgor and cell expansion: beyond the Lockhart equation. *Aust. J. Plant Physiol.* 19, 565–576. doi: 10.1071/PP9920565
- Peaucelle, A., Braybrook, S., and Höfte, H. (2012). Cell wall mechanics and growth control in plants: the role of pectins revisited. *Front. Plant Sci.* 3:121. doi: 10.3389/fpls.2012.00121
- Peaucelle, A., Louvet, R., Johansen, J. N., Höfte, H., Laufs, P., Pelloux, J., et al. (2008). *Arabidopsis* phyllotaxis is controlled by the methyl-esterification status of cell wall pectins. *Curr. Biol.* 18, 1943–1948. doi: 10.1016/j.cub.2008.10.065
- Peaucelle, A., Wightman, A., and Höfte, H. (2015). The control of growth symmetry breaking in the *Arabidopsis* hypocotyl. *Curr. Biol.* 25, 1746–1752. doi: 10.1016/j.cub.2015.05.022
- Popper, Z. A., and Fry, S. C. (2003). Primary cell wall composition of bryophytes and charophytes. *Ann. Bot.* 91, 1–12. doi: 10.1093/aob/mcg013
- Popper, Z. A., Michel, G., Herve, C., Domozych, D. S., Willats, W. G. T., Tuohy, M. G., et al. (2011). Evolution and diversity of plant cell walls: from algae to flowering plants. *Ann. Rev. Plant Biol.* 62, 567–590. doi: 10.1146/annurev-arplant-042110-103809
- Popper, Z. A., and Tuohy, M. G. (2010). Beyond the green: understanding the evolutionary puzzle of plant and algal cell walls. *Plant Physiol.* 153, 373–383. doi: 10.1104/pp.110.158055

- Proseus, T. E., and Boyer, J. S. (2005). Turgor pressure moves polysaccharides into growing cell walls of *Chara corallina*. *Ann. Bot.* 95, 967–979. doi: 10.1093/aob/mci113
- Proseus, T. E., and Boyer, J. S. (2006a). Periplasm turgor pressure controls wall deposition and assembly in growing *Chara corallina* cells. *Ann. Bot.* 98, 93–105. doi: 10.1093/aob/mcl098
- Proseus, T. E., and Boyer, J. S. (2006b). Identifying cytoplasmic input to the cell wall of growing *Chara corallina*. *J. Exp. Bot.* 57, 3231–3242. doi: 10.1093/jxb/erl087
- Proseus, T. E., and Boyer, J. S. (2006c). Calcium pectate chemistry controls growth rate of *Chara corallina*. *J. Exp. Bot.* 57, 3989–4002. doi: 10.1093/jxb/erl166
- Proseus, T. E., and Boyer, J. S. (2007). Tension required for pectate chemistry to control growth in *Chara corallina*. *J. Exp. Bot.* 58, 4283–4292. doi: 10.1093/jxb/erm318
- Proseus, T. E., and Boyer, J. S. (2008). Calcium pectate chemistry causes growth to be stored in *Chara corallina*: a test of the pectate cycle. *Plant Cell Environ.* 31, 1147–1155. doi: 10.1111/j.1365-3040.2008.01829.x
- Proseus, T. E., and Boyer, J. S. (2012a). Calcium deprivation disrupts enlargement of *Chara corallina* cells: further evidence for the calcium pectate cycle. *J. Exp. Bot.* 63, 3953–3958. doi: 10.1093/jxb/ers089
- Proseus, T. E., and Boyer, J. S. (2012b). Pectate chemistry links cell expansion to wall deposition in *Chara corallina*. *Plant Signal. Behav.* 7, 1490–1492. doi: 10.4161/psb.21777
- Proseus, T. E., Ortega, J. K. E., and Boyer, J. S. (1999). Separating growth from elastic deformation during cell enlargement. *Plant Physiol.* 119, 775–784. doi: 10.1104/pp.119.2.775
- Proseus, T. E., Zhu, G.-L., and Boyer, J. S. (2000). Turgor, temperature, and the growth of plant cells: using *Chara corallina* as a model system. *J. Exp. Bot.* 51, 1481–1494. doi: 10.1093/jexbot/51.350.1481
- Ralet, M.-C., Dronnet, V., Buchholt, H. C., and Thibault, J.-F. (2001). Enzymatically and chemically de-esterified lime pectins: characterization, polyelectrolyte behavior and calcium binding properties. *Carbohydr. Res.* 336, 117–125. doi: 10.1016/S0008-6215(01)00248-8
- Ray, P. M. (1967). Radioautographic study of cell wall deposition in growing plant cells. *J. Cell Biol.* 35, 659–674. doi: 10.1083/jcb.35.3.659
- Ray, P. M., and Baker, D. B. (1965). The effect of auxin on synthesis of oat coleoptile cell wall constituents. *Plant Physiol.* 40, 353–360. doi: 10.1104/pp.40.2.353
- Rayle, D. L., and Cleland, R. E. (1972). The in-vitro acid-growth response: relation to in-vivo growth responses, and auxin action. *Planta* 104, 282–296. doi: 10.1007/BF00386312
- Rayle, D. L., and Cleland, R. E. (1992). The acid growth theory of auxin-induced cell elongation is alive and well. *Plant Physiol.* 99, 1271–1274. doi: 10.1104/pp.99.4.1271
- Read, S. M., and Bacic, A. (1996). Cell wall porosity and its determination. *Modern Methods Plant Anal.* 17, 63–80. doi: 10.1007/978-3-642-60989-3_4
- Ridley, B. L., O'Neill, M. A., and Mohnen, D. (2001). Pectins: structure, biosynthesis, and oligogalacturonide-related signaling. *Phytochemistry* 57, 929–967. doi: 10.1016/S0031-9422(01)00113-3
- Rojas, E. R., Hotton, S., and Dumais, J. (2011). Chemically mediated mechanical expansion of the pollen tube cell wall. *Biophys. J.* 101, 1844–1853. doi: 10.1016/j.bpj.2011.08.016
- Sarkar, P., Bosneaga, E., and Auer, M. (2009). Plant cell walls throughout evolution: towards a molecular understanding of their design principles. *J. Exp. Bot.* 60, 3615–3635. doi: 10.1093/jxb/erp245
- Schopfer, P. (1994). Histochemical demonstration and localization of H₂O₂ in organs of higher plants by tissue printing on nitrocellulose paper. *Plant Physiol.* 104, 1269–1275.
- Schopfer, P. (2001). Hydroxyl radical-induced cell-wall loosening *in vitro* and *in vivo*: implications for the control of elongation growth. *Plant J.* 28, 679–688. doi: 10.1046/j.1365-313x.2001.01187.x
- Schopfer, P., Liszkay, A., Bechtold, M., Frahry, G., and Wagner, A. (2002). Evidence that hydroxyl radicals mediate auxin-induced extension growth. *Planta* 214, 821–828. doi: 10.1007/s00425-001-0699-8
- Siemieniuk, A., and Karcz, W. (2015). Effect of K⁺ and Ca²⁺ on the indole-3-acetic acid- and fusicoccin-induced growth and membrane potential in maize coleoptile cells. *AoB Plants* 7:lv070. doi: 10.1093/aobpla/plv070
- Tagawa, T., and Bonner, J. (1957). Mechanical properties of the *Avena coleoptile* as related to auxin and ionic interactions. *Plant Physiol.* 33, 207–212. doi: 10.1104/pp.32.3.207
- Virk, S. S., and Cleland, R. E. (1988). Calcium and the mechanical properties of soybean hypocotyl cell walls: possible role of calcium and protons in cell-wall loosening. *Planta* 176, 60–67. doi: 10.1007/BF00392480
- Virk, S. S., and Cleland, R. E. (1990). The role of wall calcium in the extension of cell walls of soybean hypocotyls. *Planta* 182, 559–564. doi: 10.1007/BF02341032
- Vogel, J. (2008). Unique aspects of the grass cell wall. *Curr. Opin. Plant Biol.* 11, 301–307. doi: 10.1016/j.pbi.2008.03.002
- Vogler, H., Draeger, C., Weber, A., Felekis, D., Eichenberger, C., Routier-Kierzkowska, A.-L., et al. (2012). The pollen tube: a soft shell with a hard core. *Plant J.* 73, 617–627. doi: 10.1111/tpj.12061
- Voothuluru, P., and Sharp, R. E. (2013). Apoplastic hydrogen peroxide in the growth zone of the maize primary root under water stress. I. Increased levels are specific to the apical region of growth maintenance. *J. Exp. Bot.* 64, 1223–1233. doi: 10.1093/jxb/ers277
- Weinstein, L. H., Meiss, A. N., Uhler, R. L., and Purvis, E. R. (1956). Growth-promotive effects of ethylene-diamine tetra-acetic acid. *Nature* 178, 1188. doi: 10.1038/1781188a0
- Xiao, C., Somerville, C., and Anderson, D. T. (2014). POLYGALACTURONASE INVOLVED IN EXPANSION1 functions in cell elongation and flower development in *Arabidopsis*. *Plant Cell* 26, 1018–1035. doi: 10.1105/tpc.114.123968
- Xiao, C., Zhang, T., Zheng, Y., Cosgrove, D. J., and Anderson, C. T. (2016). Xyloglucan deficiency disrupts microtubule stability and cellulose biosynthesis in *Arabidopsis*, altering cell growth and morphogenesis. *Plant Physiol.* 170, 234–249. doi: 10.1104/pp.15.01395
- Yang, Z.-L., Liu, H.-J., Wang, X.-R., and Zeng, Q.-Y. (2013). Molecular evolution and expression divergence of the *Populus* polygalacturonase supergene family shed light on the evolution of increasingly complex organs in plants. *New Phytol.* 197, 1353–1365. doi: 10.1111/nph.12107
- Yin, Y., Chen, H., Hahn, M. G., Mohnen, D., and Xu, Y. (2010). Evolution and function of the plant cell wall synthesis-related Glycosyltransferase Family 8. *Plant Physiol.* 153, 1729–1746. doi: 10.1104/pp.110.154229
- Zabka, A., Polit, J. T., Winnicki, K., Paciorek, P., Juszczak, J., Nowak, M., et al. (2016). PIN2-like proteins may contribute to the regulation of morphogenetic processes during spermatogenesis in *Chara vulgaris*. *Plant Cell Rep.* doi: 10.1007/s00299-016-1979-x [Epub ahead of print].
- Zabotina, O. A., Avci, U., Cavalier, D., Pattathil, S., Chou, Y. H., Eberhard, S., et al. (2012). Mutations in multiple XXT genes of *Arabidopsis* reveal the complexity of xyloglucan biosynthesis. *Plant Physiol.* 159, 1367–1384. doi: 10.1104/pp.112.19819
- Zhang, G. F., and Staehelin, L. A. (1992). Functional compartmentation of the Golgi apparatus of plant cells: immunocytochemical analysis of high-pressure frozen- and freeze-substituted sycamore maple suspension culture cells. *Plant Physiol.* 99, 1070–1083. doi: 10.1104/pp.99.3.1070
- Zhang, H.-M., Imtiaz, M. S., Laver, D. R., McCurdy, D. W., Offler, C. E., van Helden, D. F., et al. (2015a). Polarized and persistent Ca²⁺ plumes define loci for formation of wall ingrowth papillae in transfer cells. *J. Exp. Bot.* 66, 1179–1190. doi: 10.1093/jxb/eru460
- Zhang, H.-M., van Helden, D. F., McCurdy, D. W., Offler, C. E., and Patrick, J. W. (2015b). Plasma membrane Ca²⁺-permeable channels are differentially regulated by ethylene and hydrogen peroxide to generate persistent plumes of elevated cytosolic Ca²⁺ during transfer cell trans-differentiation. *Plant Cell Physiol.* 56, 1711–1720. doi: 10.1093/pcp/pcv100
- Zhao, Q., Yuan, S., Wang, X., Zhang, Y., Zhu, H., and Lu, C. (2008). Restoration of mature etiolated cucumber hypocotyl cell wall susceptibility to expansin by pretreatment with fungal pectinases and EGTA *in vitro*. *Plant Physiol.* 147, 1874–1885. doi: 10.1104/pp.108.116962
- Zhu, C., Ganguly, A., Baskin, T. I., McClosky, D. D., Anderson, C. T., Foster, C., et al. (2015). The Fragile Fiber1 kinesin contributes to cortical microtubule-mediated trafficking of cell wall components. *Plant Physiol.* 167, 780–792. doi: 10.1104/pp.114.251462
- Zhu, J., Alvarez, S., March, E. L., LeNoble, M. E., Cho, I.-J., Sivaguru, M., et al. (2007). Cell wall proteome in the maize primary root elongation zone. II. Region-specific changes in water soluble and lightly ionically bound

proteins under water deficit. *Plant Physiol.* 145, 1533–1548. doi: 10.1104/pp.107.107250

Conflict of Interest Statement: The author declares that the research was conducted in the absence of any commercial or financial relationships that could be construed as a potential conflict of interest.

Copyright © 2016 Boyer. This is an open-access article distributed under the terms of the Creative Commons Attribution License (CC BY). The use, distribution or reproduction in other forums is permitted, provided the original author(s) or licensor are credited and that the original publication in this journal is cited, in accordance with accepted academic practice. No use, distribution or reproduction is permitted which does not comply with these terms.

Advantages of publishing in Frontiers



OPEN ACCESS

Articles are free to read,
for greatest visibility



COLLABORATIVE PEER-REVIEW

Designed to be rigorous
– yet also collaborative,
fair and constructive



FAST PUBLICATION

Average 85 days from
submission to publication
(across all journals)



COPYRIGHT TO AUTHORS

No limit to article
distribution and re-use



TRANSPARENT

Editors and reviewers
acknowledged by name
on published articles



SUPPORT

By our Swiss-based
editorial team



IMPACT METRICS

Advanced metrics
track your article's impact



GLOBAL SPREAD

5'100'000+ monthly
article views
and downloads



LOOP RESEARCH NETWORK

Our network
increases readership
for your article

Frontiers

EPFL Innovation Park, Building I • 1015 Lausanne • Switzerland
Tel +41 21 510 17 00 • Fax +41 21 510 17 01 • info@frontiersin.org
www.frontiersin.org

Find us on

